U.PORTO

DOUTORAMENTO EM CIÊNCIAS FARMACÊUTICAS

ESPECIALIDADE EM TOXICOLOGIA

Development of new chemical entities based on natural scaffolds with therapeutic potential towards age-related disorders

Daniel Freitas Chavarria

D

2020

Daniel Freitas Chavarria

Development of new chemical entities based on natural scaffolds with therapeutic potential towards age-related disorders

Thesis for Doctor degree in Pharmaceutical Sciences
Toxicology Speciality

Work performed under the supervision of
Professor Doctor Paulo Jorge Gouveia Simões da Silva Oliveira

And co-supervision of
Professor Doctor Maria Fernanda Martins Borges
Professor Doctor Fernando Manuel Gomes Remião

January 2020

“Yesterday is History.
Tomorrow is a mystery.
Today is a gift.
That’s why it is called the present.”

Alice Morse Earle in *Sundials and Roses of Yesterday*

The financial support was provided by “Fundação para a Ciência e a Tecnologia” (FCT) (SFRH/BD/108119/2015), under the POPH – QREN – Type 4.1 – Advanced Training, funded by the European Social Fund and by National funds from the “Ministério da Educação e Ciência”, and FCT/FEDER/COMPETE funds (Grants UID/QUI/00081/2015, POCI-01-0145-FEDER-006980, NORTE-01-0145-FEDER-000028, POCI-COMPETE 016659 and FCT, IP PTDC/DTP-FTO/2433/2014).



ACCORDING TO THE APPLICABLE LEGISLATION, THE REPRODUCTION OF ANY PART OF THIS THESIS IS NOT PERMITTED.

PUBLICATIONS

The data contained in the following publications are contained in this Thesis.

Manuscripts in International Peer-Review Journals

1. **Daniel Chavarria**, Fernando Cagide, Miguel Pinto, Lígia R. Gomes, John N. Low and Fernanda Borges. “Development of piperic acid-based monoamine oxidase inhibitors: synthesis, structural characterization and biological evaluation”. *J. Mol. Struct*., **2019**, 1182: 298-307. DOI: 10.1016/j.molstruc.2019.01.060.

2. **Daniel Chavarria**, Carlos Fernandes, Vera Silva, Cátia Silva, Eva Gil-Martins, Pedro Soares, Tiago Silva, Renata Silva, Fernando Remião, Paulo J. Oliveira and Fernanda Borges. “Design of novel monoamine oxidase-B inhibitors based on piperine scaffold: structure-activity-toxicity, drug-likeness and efflux transport studies”. *Eur. J. Med. Chem.*, **2020**, 185:111770. DOI: 10.1016/j.ejmech.2019.111770.

3. **Daniel Chavarria**, Carlos Fernandes, Tiago Silva, Jorge Garrido, Fernando Remião, Paulo J. Oliveira and Fernanda Borges. “Bioisosteric OH- to SH-replacement changes the antioxidant profile of ferulic acid”. *Org. Biomol. Chem.*, **2019**, 17: 9646-9654. DOI: 10.1039/C9OB01875A.

4. **Daniel Chavarria**, Carlos Fernandes, Brandon Aguiar, Tiago Silva, Jorge Garrido, Fernando Remião, Paulo J. Oliveira, Eugenio Uriarte and Fernanda Borges. “Insights into the discovery of novel neuroprotective agents: a comparative study between sulfanylcinnamic acid derivatives and related phenolic analogues”, *Molecules*, **2019**, 24(23): E4405. DOI: 10.3390/molecules24234405.

5. **Daniel Chavarria**, Sofia Benfeito, Tiago Silva, Cátia Silva, Pedro Soares, Jorge Garrido, Paula Serrão, Patrício Soares-da-Silva, Fernando Remião and Fernanda Borges. “Boosting caffeic acid performance as antioxidant and monoamine oxidase/catechol-*O*-methyltransferase inhibitor”, to be submitted.

6. **Daniel Chavarria**, Carlos Fernandes, José Teixeira, Fernando Cagide, Fernando Remião, Paulo Jorge Oliveira and Fernanda Borges. “Development of piperine-based mitochondria-targeted agents as antioxidants and monoamine oxidase/cholinesterase inhibitors”, to be submitted.

Reviews

1. **Daniel Chavarria**, Tiago Silva, Diogo Magalhães e Silva, Fernando Remião, Fernanda Borges. "Lessons from black pepper: piperine and derivatives thereof". *Expert Opin. Ther. Pat.*, **2016**, 26 (2): 245-264. **DOI:** 10.1517/13543776.2016.1118057.

2. Francesco Mesiti, **Daniel Chavarria**, Alexandra Gaspar, Stefano Alcaro and Fernanda Borges. "The chemistry toolbox of multitarget-directed ligands for Alzheimer's disease". *Eur. J. Med. Chem.*, **2019**, 181, 111572

Poster Communications in Scientific Meetings

1. **Daniel Chavarria**, Tiago Silva, Jorge Garrido, Fernando Remião and Fernanda Borges. Insights on the development of novel neuroprotective agents: a comparative study between ferulic acid and related sulfanyl derivatives. *6th Meeting of the Paul Ehrlich MedChem Euro-PhD Network and Mutalig COST Action, 1st WG meeting/ Poly-pharmacology expanding Paul Ehrlich's magic bullet concept*, **2016**, November 18th-20th, Budapest, Hungary.

2. **Daniel Chavarria**, Tiago Silva, Carlos Fernandes, Jorge Garrido, Fernando Remião and Fernanda Borges. Effect of the acid strength on the antioxidant profile of natural and synthetic antioxidants. *37th Edition of the European School of Medicinal Chemistry (ESMEC)*, **2017**, July 2nd-6th, Urbino, Italy.

3. **Daniel Chavarria**, Tiago Silva, Carlos Fernandes, Jorge Garrido, Fernando Remião and Fernanda Borges. Design, synthesis and neuroprotective properties of new hydroxycinnamic acid-based antioxidants. *7th meeting of Paul Ehrlich MedChem EuroPhD Network*, **2017**, August 25th-27th, Vienna, Austria.

4. **Daniel Chavarria**, Tiago Silva, Carlos Fernandes, Jorge Garrido, Fernando Remião and Fernanda Borges. Natural products in drug discovery: enhancing the antioxidant profile of hydroxycinnamic acids. *EpiChemBio (CM1406) and MuTaLig COST (CA15135) actions joint meeting*, **2017**, September 22nd-24th, Porto, Portugal.

5. **Daniel Chavarria**, Tiago Silva, Carlos Fernandes, Jorge Garrido, Fernando Remião and Fernanda Borges. Hydroxycinnamic acid derivatives and sulfured analogues: from synthesis to antioxidant properties. *2nd WG meeting – Status of WG activities of the MuTaLig COST Action (CA15135)*, **2018**, March 15th-16th, Tenerife, Spain.

6. **Daniel Chavarria**, Tiago Silva, Carlos Fernandes, Jorge Garrido, Fernando Remião and Fernanda Borges. Development of Novel Phenolic and Thiophenolic Antioxidants based on Hydroxycinnamic Acid Scaffold. *8th meeting of Paul Ehrlich MedChem EuroPhD Network,* **2018**, July 12th-14th, Porto, Portugal.

7. **Daniel Chavarria**, Carlos Fernandes, Fernando Cagide, Fernando Remião, Paulo Jorge Oliveira and Fernanda Borges. Development of piperine-based triphenylphosphonium conjugates as a therapeutic solution for Alzheimer's disease. *3rd Annual meeting - MuTaLig COST ACTION (CA15135),* **2018**, October 18th-19th, Valletta, Malta.

8. **Daniel Chavarria**, Carlos Fernandes, Fernando Cagide, Fernando Remião, Paulo Jorge Oliveira and Fernanda Borges. Searching for New Neuroprotective Agents: Design, Synthesis and Biological Evaluation of Piperine-derived Cationic Compounds. 26th Young Research Fellows Meeting (YRFM), **2019**, February 20th-22nd, Paris, France.

Oral Communications in Scientific Meetings

1. **Daniel Chavarria**, Carlos Fernandes, Fernando Cagide, Fernando Remião, Paulo Jorge Oliveira and Fernanda Borges. Development of Dual-Target Agents Based on Piperine Scaffold. 3rd WG meeting – Activities of young investigators within the WG MuTaLig COST Action (*CA15135),* **2019**, February 23rd-24th, Paris, France.

2. **Daniel Chavarria**, Carlos Fernandes, Fernando Remião, Paulo Jorge Oliveira and Fernanda Borges. Lessons from black pepper: moving from one to multitarget-directed ligands by diversity-oriented synthesis. IX Meeting of the Paul Ehrlich Euro-PhD Network & 4th Annual meeting – MuTaLig COST Action meeting*,* **2019**, June 13th-15th, Catanzaro, Italy.

AGRADECIMENTOS/ACKNOWLEDGEMENTS

Although English is considered the universal language, Portuguese is the official language of my heart. Therefore, my profound gratitude to all the people involved in this project can only be expressed in Portuguese.

À Fundação para a Ciência e a Tecnologia (FCT) pela bolsa de doutoramento (SFRH/BD/108119/2015) e pelo suporte financeiro.

Começo por agradecer à **Prof. Dra. Fernanda Borges**. Corria o ano de 2011 quando me acolheu como aluno de projeto de licenciatura (sim, já passaram 8 anos!). Desde então transmitiu tantos valiosos conhecimentos e proporcionou inúmeras oportunidades que permitiam que crescesse a nível pessoal e profissional. Muito obrigado por todas as palavras de incentivo, principalmente nos (vários) momentos pouco otimistas, e pela inabalável e contagiante boa disposição!

Ao **Prof. Dr Paulo Oliveira**, meu orientador, agradeço toda a disponibilidade e apoio dados durante os últimos 4 anos na orientação deste projeto.

Ao **Prof. Dr. Fernando Remião**, obrigado pela oportunidade de trabalhar no ramo da Toxicologia. A minha passagem por esta área foi relativamente curta, mas foi o suficiente para me deixar fascinado e com vontade de desenvolver novos projetos. Agradeço também todo o apoio demonstrado na orientação desta Tese.

Ao **Prof. Dr Eugenio Uriarte**, por permitir a caracterização de todos os compostos por espectrometria de massa. Obrigado por toda a disponibilidade demonstrada e pelos momentos de alegria e boa disposição.

Ao **Dr. Carlos Fernandes**, de cognome “o maridão”. Não tenho palavras para agradecer o forte apoio dado durante o doutoramento, os fins-de-semana investidos na execução de trabalho experimental, as inúmeras trocas de emails e de telefonemas, mas, acima de tudo, o companheirismo e as palavras de apoio. Mais do que um colega de trabalho, considero-te um grande amigo! Deixo também um agradecimento especial à **Dra. Sofia Benfeito**, “a esposa”. O “eterno caloirinho” cresceu e está a tornar-se um homem!

Ao **Dr. Tiago Silva**, tenho a agradecer todo o criticismo construtivo e a ajuda preciosa na construção dos artigos. Prometo que um dia conseguirei escrever um artigo com frases curtas! Mesmo tendo-me transmitido conhecimentos fundamentais durante o projeto de mestrado, penso que ainda hoje tenho muito a aprender contigo.

Ao **Prof. Dr. Jorge Garrido**, agradeço toda a disponibilidade na execução dos estudos eletroquímicos.

À **Dra Renata Silva** e doutorandas associadas – **Vera Silva** e **Eva Gil Martins** –, agradeço a disponibilidade na execução dos estudos relacionados com a glicoproteína P, bem como o auxílio na discussão dos resultados obtidos.

Ao **Dr José Teixeira**, pela disponibilidade imediata na avaliação da toxicidade mitocondrial dos "Mito-peppers" (o nome talvez precise de ser trabalhado!).

Ao **Prof. Dr. Patrício Soares-da-Silva** e à **Dra. Paula Serrão**, pela colaboração nos ensaios de inibição da COMT.

Deixo também um muito obrigado à *muy bella* e formosa gente do Laboratório 2.26, pelo espírito de camaradagem, pelos almoços animados, pelas diversas aventuras nos intervalos dos congressos, pela guerra silenciosa na escolha da estação de rádio. O grupo de investigação está em constante expansão, por isso espero não me esquecer de ninguém: **Dra Catarina Oliveira**, **Dr. Fernando Cagide**, **Dra Alexandra Gaspar**, **Dr. Pedro Soares**, **Cátia Soares**, **Miguel Pinto**, **Daniel Martins**, **Lisa Sequeira**, **Francesco Mesiti**, **Brandon Aguiar**. Agradeço também aos jovens doutorados com os quais partilhei bons momentos, mas que neste momento desenvolvem os seus projetos noutros grupos de investigação: **Dra. Joana Reis** e **Dr. André Fonseca**.

A investigação em geral traz momentos muito gratificantes, mas também é repleta de dias onde reinam a frustração e irritação. Assim sendo, não poderia deixar de agradecer a todos os meus "companheiros de porrada" da equipa **Norte Forte** e aos mestres **Filipe Albergaria** e **Ricardo Quintela**. A troca de golpes nos treinos da manhã são uma ótima forma de começar o dia e ajudam-me a manter um espírito zen!

Por último, deixo um enorme obrigado aos meus **pais** e **irmão**, não pelos últimos quatro anos, mas sim pelos vários projetos que tive durante a minha (curta) vida. O homem que sou e tudo o que alcancei até hoje deve-se a vocês! Obrigado por compreenderem o meu silêncio quase infinito que se equipara ao de um monge budista. Obrigado pelos múltiplos tupperwares de comida que, aos olhos de uma mãe, nunca são suficientes. Obrigado pelo apoio incondicional durante os meus 28 anos de vida. Também não posso deixar de agradecer à **Luna**, a cadela da família, pelas receções calorosas em todas as visitas à "terrinha". Não há dúvida de que se consegue um amigo para a vida com meia-dúzia de festas.

Muito Obrigado!

ABSTRACT

Neurodegenerative diseases represent a set of chronic, progressive and incurable diseases whose clinical symptoms are commonly associated with the decline of cognitive and/or motor functions. Although the etiology of NDs is not fully clarified, it is accepted that neurodegeneration results from the interplay of multiple pathological mechanisms. The selective neuronal loss and consequent neurotransmitter depletion are recognized as pathological hallmarks of NDs. Based on these findings, inhibitors of acetylcholinesterase (AChE), butyrylcholinesterase (BChE), monoamine oxidase (MAO) and catechol-*O*-methyltransferase (COMT) were developed to increase brain acetylcholine (ACh) and dopamine (DA) levels. However, the available single-target treatments for NDs only provide symptomatic relief but fail to modify the disease progression. Other factors, such as oxidative stress and mitochondrial dysfunction, also contribute to neurodegeneration. In this context, recent efforts have been focused on developing multitarget-directed ligands (MTDLs) able to interact with multiple targets involved in the pathogenesis of NDs.

Natural-based scaffolds are considered important sources of inspiration in drug design and discovery. In particular, ferulic acid (FA), caffeic acid (CA) and piperine are recognized as privileged scaffolds in central nervous system (CNS) drug discovery since they present biological activities with potential therapeutic interest, namely antioxidant activity and MAO inhibition. With the aim of developing new chemical entities able to target oxidative stress and/or neurotransmitter depletion, three libraries based on the chemical scaffolds of FA, CA and piperine were developed in this Thesis.

Ferulic acid-based thiophenols were designed to boost the antioxidant activity of the natural compound. The data obtained clearly showed marked differences between FA-based thiophenols and the corresponding phenols. Thiophenols reacted faster and more efficiently with synthetic radicals, displayed lower oxidation potential (E_p) values and were more acidic than the corresponding phenols. However, unlike phenols, thiophenols were unable to scavenge peroxyl ($ROO^{\bullet}$) radicals in the ORAC-FL assay. While the insertion of 5-methoxy and 5-phenyl groups did not significantly improve the antioxidant properties of thiophenols, the carboxylic acid amidation with lipophilic groups was proven to be a beneficial structural modification, since it preserved the antioxidant profile of the parent acids while improving the drug-like properties. The cytotoxicity of cinnamic acid derivatives in differentiated SH-SY5Y cells was not increased with the OH to SH replacement. Compounds **2**, **3** and **10** presented mild cytoprotective effects against hydrogen peroxide (H_2O_2), iron(III) and *tert*-butyl hydroperoxide (*t*-BHP).

In addition, piperine and CA bioisosteres were developed and, based on the results obtained, new structure-activity relationships were established. Both potency and selectivity towards MAO-B were increased with the presence of a benzodioxole ring, and α-CN and benzyl ester groups. Compound **36**, the most potent MAO-B inhibitor of the series, presented a competitive and reversible inhibition profile. The antioxidant properties of CA were improved with the insertion of an additional double bond and decreased with the presence of an α-CN. Carboxylic acid amidation of CA derivatives reduced the reactivity towards $ROO^{\bullet}$ radicals in the ORAC-FL assay but maintained E_p values. In general, CA derivatives at 10 μM did not exhibit cytotoxic effects in differentiated SH-SY5Y cells, although mild cytotoxicity was observed at 50 μM. Catechols **20** and **21** at 10 μM protected differentiated SH-SY5Y cells from *t*-BHP-induced damage. With the exception of compound **27**, piperine derivatives did not display cytotoxicity in both differentiated SH-SY5Y cells and Caco-2 cells. Compound **31** demonstrated potential for P-glicoprotein (P-gp) activation in Caco-2 cells while compounds **36** and **37** acted as mild P-gp inhibitors.

Finally, CA- and piperine derivatives were conjugated with triphenylphosphonium (TPP) cations to target them to mitochondria. From the data obtained in enzyme inhibition studies, it was concluded that lipophilic TPP conjugates were potent BChE inhibitors and moderate AChE, MAO-A and MAO-B inhibitors. In addition, the best BChE inhibitors presented a mixed-type BChE inhibition profile. Compounds **40** and **41** shared similar antioxidant properties to other structurally related catechols. Cytotoxicity studies in differentiated SH-SY5Y cells showed that lipophilic TPP conjugates were not cytotoxic at concentrations up to 12.5 μM, although they may affect cellular metabolic activity at higher concentrations. These compounds accumulated in the mitochondrial matrix of energized mouse liver mitochondria, with compound **41** showing the highest mitochondria accumulation ratio. Catechols at non-toxic concentrations presented favourable mitochondrial toxicity profiles, while benzodioxole derivatives significantly decreased maximal respiration and spare respiratory capacity in differentiated SH-SY5Y cells.

The most promising compounds were predicted to have favourable drug-like properties to exert their biological effects in the CNS. Based on the data gathered from all experiments, compounds **20**, **36** and **41** were proposed as leads for future optimization and development of neuroprotective agents.

Keywords: neurodegenerative diseases, hydroxycinnamic acids, piperine, thiophenols, mitochondria-targeted agents

RESUMO

As doenças neurodegenerativas (DNs) representam um conjunto de doenças crónicas, progressivas e incuráveis com sintomas clínicos relacionados com o declínio das funções cognitivas e/ou motoras. Apesar da etiologia das DNs não estar totalmente elucidada, é aceite que a neurodegeneração resulta da combinação de vários mecanismos patológicos. A morte neuronal seletiva e a resultante depleção de neurotransmissores são marcas patológicas das DNs. Com base nestas observações, desenvolveram-se inibidores da acetilcolinesterase (AChE), butirilcolinesterase (BChE), monoamina oxidase (MAO) e catecol-*O*-metiltransferase (COMT), com o objetivo de aumentar os níveis de acetilcolina (ACh) e de dopamina (DA) no cérebro. No entanto, os fármacos aprovados para o tratamento de DNs atuam num único alvo e apenas oferecem alívio sintomático, não alterando a progressão das doenças. Outros fatores, como a disfunção mitocondrial e o stress oxidativo, também contribuem para a morte neuronal. Neste sentido, têm sido desenvolvidos fármacos multialvo capazes de atuar em vários alvos envolvidos na patogénese das DNs.

As estruturas baseadas em compostos naturais são consideradas uma fonte importante de inspiração no desenvolvimento e descoberta de novos fármacos. Os ácidos ferúlico (AF) e cafeico (AC) e a piperina são reconhecidos como estruturas privilegiadas na descoberta de fármacos para o sistema nervoso central (SNC), uma vez que que exibem atividades biológicas com interesse terapêutico, nomeadamente atividade antioxidante e inibição da MAO. Com o objetivo de desenvolver novas entidades químicas capazes de reduzir o stress oxidativo e aumentar os níveis de neurotransmissores, desenvolveram-se nesta Tese três bibliotecas de compostos baseadas nas estruturas do AF, AC e piperina.

Foram sintetizados tiofenóis baseados no AF para aumentar a atividade antioxidante do composto natural. Os resultados obtidos mostraram diferenças notórias entre os tiofenóis e os fenóis correspondentes. Os tiofenóis reagiram com radicais sintéticos de forma mais rápida e eficaz, e apresentaram potenciais de oxidação (E_p) mais baixos e maior acidez do que os fenóis correspondentes. No entanto, ao contrário dos fenóis, os tiofenóis não neutralizaram radicais peroxilo ($ROO^{\bullet}$) no ensaio do ORAC-FL. A introdução de grupos 5-metoxi e 5-fenil não melhorou significativamente as propriedades antioxidantes dos tiofenóis. Por outro lado, a amidação do ácido carboxílico com grupos lipofílicos foi benéfica, dado que manteve o perfil antioxidante do ácido correspondente e melhorou as suas propriedades físico-quimicas. A substituição do grupo OH pelo SH não aumentou a citotoxicidade dos compostos em células SH-SY5Y diferenciadas. Os

compostos **2**, **3** e **10** exibiram efeitos citoprotetores moderados contra o peróxido de hidrogénio (H_2O_2), ferro(III) e *tert*-butil hidroperóxido (t-BHP).

Também foram desenvolvidos bioisósteros da piperina e do AC e, com base nos resultados obtidos, estabeleceram-se novas relações estrutura-atividade. A presença de um anel benzodioxole e de grupos α-CN e benzil éster aumentaram a potência e seletividade para a MAO-B. O composto **36**, o inibidor mais potente da série, apresentou um perfil de inibição competitivo e reversível. As propriedades antioxidantes do AC melhoraram com a inserção de um grupo etilénico e diminuíram com a presença de um α-CN. A amidação do ácido carboxílico dos derivados do CA reduziu a reatividade para os radicais $ROO^{\bullet}$ mas manteve os valores de E_p. De um modo geral, os derivados do AC a 10 μM não apresentaram citotoxicidade em células SH-SY5Y diferenciadas, apesar de se terem observado efeitos citotóxicos moderados a 50 μM. Os catecóis **20** e **21** a 10 μM protegeram as células SH-SY5Y diferenciadas contra danos causados pelo *t*-BHP. Excetuando o composto **27**, os derivados da piperina não exibiram citotoxicidade em células SH-SY5Y diferenciadas e Caco-2. O composto **31** demonstrou potencial para atuar como ativador da glicoproteína P (P-gp), enquanto os compostos **36** e **37** apresentaram atividade inibitória ligeira da P-gp.

Por último, derivados a piperina e do AC foram conjugados com catiões trifenilfosfónio (TFF) com o intuito de direcioná-los para a mitocôndria. Os compostos conjugados com o TFF atuaram como inibidores potentes da BChE e como inibidores moderados da AChE, MAO-A e MAO-B. O mecanismo de inibição da BChE dos compostos mais promissores foi do tipo misto. As propriedades antioxidantes dos compostos **40** e **41** foram idênticas à de outros catecóis com estrutura química semelhante. Os compostos conjugados com a TFF não apresentaram citotoxicidade a concentrações inferiores a 12.5 μM, mas podem afetar a atividade metabólica das células a concentrações mais elevadas. Estes compostos acumularam na matriz mitocondrial de mitocôndrias de fígado de rato energizadas, destacando-se o composto **41** que apresentou a maior acumulação. Os catecóis exibiram perfis de toxicidade mitocondrial favoráveis, enquanto os derivados com um anel benzodioxole diminuíram significativamente a respiração máxima e a capacidade respiratória de reserva em células SH-SY5Y diferenciadas.

Os compostos mais promissores apresentaram propriedades físico-químicas adequadas para exercer os seus efeitos biológicos no SNC. Com base em todos os resultados reunidos, os compostos **20**, **36** e **41** foram propostos como compostos líder para otimização futura e desenvolvimento de fármacos neuroprotetores.

Palavras-chave: doenças neurodegenerativas, ácidos hidroxicinâmicos, piperina, tiofenóis, fármacos dirigidos à mitocôndria

THESIS OUTLINE

The Thesis is organized in five main chapters:

Chapter I: Introduction

Chapter I provides a brief literature review on pathophysiological and pharmacological aspects of neurodegenerative diseases. It also includes a summary of the main approaches and key aspects of central nervous system drug design, and the significance of natural scaffolds as templates for the development of neuroprotective agents. Finally, the main goals of this Thesis are set at the end of this chapter.

Chapter II: Introduction complement

Chapter II includes two scientific article reviews prepared within the scope of the Thesis. It is a complement to Chapter I, since it contains additional information. Accordingly, **Manuscript IA** summarizes the synthetic strategies used over the last 5 years to develop multitarget-directed ligands based on drugs approved for AD. **Manuscript IB** provides an overview of recent developments in patented processes and applications involving piperine and derivatives thereof.

Chapter III: Experimental section

Chapter III encloses the scientific articles prepared within the scope of the Thesis.

Chapter IV: Integrated discussion, conclusions and future perspectives

Chapter IV comprises a general discussion of the experimental data and the respective conclusions, highlighting the most relevant results and providing new ideas for future projects.

Chapter IV: References

Chapter V lists all the references used in the previous chapters.

Annex

The annex includes the chemical structures of natural scaffolds and related derivatives used in pharmacological and toxicological studies.

TABLE OF CONTENTS

PUBLICATIONS ..... **xi**

AGRADECIMENTOS/ACKNOWLEDGEMENTS ..... **xv**

ABSTRACT ..... **xvii**

RESUMO ..... **xix**

THESIS OUTLINE ..... **xxi**

TABLE OF CONTENTS ..... **xxiii**

LIST OF FIGURES ..... **xxvii**

LIST OF TABLES ..... **xxx**

LIST OF ABBREVIATIONS ..... **xxxi**

CHAPTER I **1**

1.1. Neurodegenerative diseases 3

1.1.1. Alzheimer's disease: major hallmarks 4

1.1.2. Parkinson's disease: major hallmarks 7

1.2. Pharmacotherapy of Alzheimer's and Parkinson's diseases 9

1.2.1. Targeting neurotransmitter depletion 9

1.2.1.1. Cholinergic transmission and Alzheimer's disease 9

1.2.1.1.1. Acetylcholinesterase and Butyrylcholinesterase 11

1.2.1.1.2. Cholinesterase inhibitors 13

1.2.1.2. Dopaminergic transmission and Parkinson's disease 14

1.2.1.2.1. Monoamine oxidases 16

1.2.1.2.2. Monoamine oxidase B inhibitors 18

1.2.1.2.3. Catechol-*O*-methyltransferase 20

1.2.1.2.4. Catechol-*O*-methyltransferase inhibitors 21

1.2.2. Targeting oxidative and nitrosative stress 22

1.2.2.1. Oxidative and nitrosative stress 22

1.2.2.2. Antioxidant defences 25

1.2.2.3. Oxidative stress in Alzheimer's and Parkinson's diseases.....28
1.2.2.4. Antioxidant therapy for neurodegenerative diseases: an overview.....33
1.3. Drug discovery and neurodegenerative diseases.....35
1.3.1. Single-target and multitarget-based approaches.....35
1.3.2. Blood-brain barrier in CNS drug discovery.....36
1.3.3. Natural scaffolds in CNS drug discovery.....39
1.4. Thesis objectives.....42

CHAPTER II.....47

2.1. Manuscript IA.....51
2.2. Manuscript IB.....69

CHAPTER III.....105

3.1. Manuscript II.....107
3.2. Manuscript III.....123
3.3. Manuscript IV.....153
3.4. Manuscript V.....195
3.5. Manuscript VI.....217
3.6. Manuscript VII.....273

CHAPTER IV.....311

4.1. Design and development of new chemical entities based on natural scaffolds.....314
4.1.1. Synthesis of ferulic acid-based thiophenols.....315
4.1.2. Synthesis of ferulic acid derivatives.....317
4.1.3. Synthesis of piperine and caffeic acid derivatives.....318
4.1.4. Synthesis of α-cyano compounds based on piperine and caffeic acid.....320
4.1.5. Synthesis of piperine-based triphenylphosphonium conjugates.....322
4.2. Biological and toxicological profiles of compound libraries.....324
4.2.1. Boosting the antioxidant activity of ferulic acid.....324
4.2.1.1. Antioxidant profile in cell-free systems.....325
4.2.1.2. Cytotoxicity and antioxidant activity in differentiated SH-SY5Y cells.....327

4.2.2. Fine-tuning the pharmacological profile of caffeic acid and piperine 329

4.2.2.1. Biological effects in cell-free systems.....330

4.2.2.2. Cytotoxicity in differentiated SH-SY5Y cells and Caco-2 cells.....334

4.2.2.3. Antioxidant activity of caffeic acid derivatives in SH-SY5Y cells 336

4.2.2.4. Modulation of P-glycoprotein transport activity by piperine derivatives in Caco-2 cells.....337

4.2.3. Targeting piperine and caffeic acid derivatives to michochondria.....339

4.2.3.1. Biological effects in cell-free systems.....340

4.2.3.2. Cytotoxicity in differentiated SH-SY5Y cells.....342

4.2.3.3. Mitochondrial accumulation, and glycolytic and mitochondrial oxidative phosphorylation fluxes.....344

4.3. Evaluation of drug-like properties.....347

4.4. Selection of drug candidates for lead optimization 351

4.5. Conclusions and future perspectives 352

CHAPTER V 357

ANNEX.....381

LIST OF FIGURES

Figure 1.1: Primary brain regions affected in the most common neurodegenerative diseases. Adapted from (15). 4
Figure 1.2: Major hallmarks of AD. (A) Degeneration of cholinergic neurons in the basal forebrain. (B) Formation of senile plaques and neurofibrillary tangles. Adapted from (33) .5
Figure 1.3: Formation of amyloid β (A) and tau (B) aggregates in the human brain. Adapted from (41)....6
Figure 1.4: Major hallmarks of Parkinson's disease. (A) Degeneration of nigrostriatal dopaminergic neurons. (B) Formation of Lewy inclusions. Adapted from (62, 63). 8
Figure 1.5: Formation of α-synuclein aggregates in the human brain. Adapted from (41). 9
Figure 1.6: Enzymes and transporters involved in the synthesis, storage and metabolism of acetylcholine. Adapted from (88, 89) 11
Figure 1.7: Schematic representation of active site gorge of cholinesterases. Adapted from (94, 103).....12
Figure 1.8: FDA-approved cholinesterase inhibitors for Alzheimer's disease. Adapted from (19). 13
Figure 1.9: Enzymes and transporters involved in the synthesis, storage and metabolism of dopamine. Adapted from (126, 127). 15
Figure 1.10: Schematic representation of the oxidative deamination reaction catalysed by MAOs. Adapted from (135).....16
Figure 1.11: Ribbon diagrams of monomeric units of human MAO-A (PDB ID: 2BXS) and MAO-B (PDB ID: 1GOS). Adapted from (143). 17
Figure 1.12: FDA-approved MAO-B inhibitors for Parkinson's disease. Adapted from (57). 18
Figure 1.13: (A) Schematic representation of COMT-catalysed methyl group transfer to a catechol substrate. (B) Crystal structure of soluble COMT (PDB ID: 108V). Adapted from (163, 165).....20
Figure 1.14: FDA-approved MAO-B inhibitors for Parkinson's disease. Adapted from (57). 21
Figure 1.15: Formation of ROS (red) and RNS (purple) and their elimination by enzymatic antioxidant systems (dashed line). Adapted from (198). 24
Figure 1.16: Representative examples of endogenous (blue) and exogenous (orange) non-enzymatic antioxidants. 26
Figure 1.17: Pathological events of neurodegenerative diseases associated with increased oxidative stress. 29
Figure 1.18: Formation of ROS in mitochondria. Adapted from (244, 249).....30

Figure 1.19: Generation of ROS during enzymatic (dashed line) and non-enzymatic (plain line) DA decomposition. Adapted from (258). 31
Figure 1.20: Mitochondrial uptake of lipophilic triphenylphosphonium cations. Adapted from (287, 292). 34
Figure 1.21: Cellular components of the blood-brain barrier (A) and the main routes of molecular trafficking (B). Adapted from (319, 322) 37
Figure 1.22: Chemical structures of hydroxycinnamic acids and piperine. 40
Figure 1.23: Design strategies followed to obtain a series of derivatives based on ferulic acid, caffeic acid and piperine scaffolds. 43

Figure 4.1: compound libraries developed in this Thesis based on the chemical scaffolds of ferulic acid (FA), caffeic acid (CA) and piperine. 313
Figure 4.2: general overview of the starting materials and the resulting final compounds. 315
Figure 4.3: Synthetic strategy pursued to obtain ferulic acid-based thiophenols **2-6**.....316
Figure 4.4: Synthetic strategy pursued to obtain compounds **7**, **8** and **10** 318
Figure 4.5: Synthetic strategy pursued to obtain compounds **12-16** and **23-29**.....319
Figure 4.6: Synthetic strategy pursued to obtain α-CN derivatives **17-21** and **30-37**.....320
Figure 4.7: Synthetic strategy pursued to obtain mitochondria-targeted agents **38-41**. .323
Figure 4.8: Drug design strategy used to improve the antioxidant activity of FA. 325
Figure 4.9: Representative results obtained with FA **1** and compound **2** (radical scavenging activity, redox potentials (E_p) and kinetic curves obtained in DPPH$^\bullet$ assay).....326
Figure 4.10: Cellular viability of differentiated SH-SY5Y neuroblastoma cells after a 24 h treatment with FA (compound **1**, red) and compound **2** at eight different concentrations (1.6 µM – 200 µM).. 327
Figure 4.11: Protection against H_2O_2-induced damage in differentiated SH-SY5Y neuroblastoma cells by thiophenols **2-6** and phenols **1**, **7-10**.....328
Figure 4.12: Protection against FeNTA-induced damage in differentiated SH-SY5Y neuroblastoma cells by thiophenols **2-6** and phenols **1**, **7-10**.....328
Figure 4.13: Drug design strategy used to obtain piperine-based MAO-B inhibitors. 329
Figure 4.14: Drug design strategy used to obtain CA-based derivatives **12-21**. 330
Figure 4.15: Preliminary structure-activity relationships obtained from *h*MAO-B inhibition studies with piperine- and CA-based libraries. 332
Figure 4.16: (**A**) Representative double reciprocal plot of the initial velocity of *h*MAO-B at increasing substrate concentrations (10-100 µM) in the absence or the presence of compound **36**. (**B**) Time-dependent inhibition of recombinant *h*MAO-B by reference drugs rasagiline and safinamide, and compound **36**.....333

Figure 4.17: Preliminary structure-activity relationships obtained from ORAC assay and electrochemical assays with caffeic acid **11** and derivatives **12-21**. 334
Figure 4.18: Cellular viability of differentiated SH-SY5Y cells after incubation with CA (compound **11**) and compounds 1**2, 13**, **17-21** at two concentrations (10 and 50 µM) for 24 h.. 335
Figure 4.19: cellular viability of differentiated SH-SY5Y cells (**A**) and Caco-2 cells (**B**) after incubation with piperine (**22**) and compounds **27**, **28**, **31**, **36** and **37** at two different concentrations (10 µM and 50 µM) for 24 h. 336
Figure 4.20: chemical structures and biological effects of caffeic acid derivatives **20** and **21**. 337
Figure 4.21: Neuroprotection against *t*-BHP-induced damage in differentiated SH-SY5Y cells by α-CN derivatives 1**7**, **20** and **21**.....337
Figure 4.22: chemical structures and biological effects of piperine (compound **22**) and compounds **28, 31, 36** and **37**. 338
Figure 4.23: Evaluation of P-gp activity in Caco-2 cells exposed to compounds **22**, **28**, **31, 36** and **37** (10 µM) only during the incubation period with the fluorescent substrate (RHO 123, 5 µM). 338
Figure 4.24: Drug design strategy used to obtain mitochondria-targeted agents based on the chemical scaffolds of piperine and caffeic acid. 340
Figure 4.25: Representative double reciprocal plot of the initial velocity of *eq*BChE at increasing substrate concentrations (0.063 – 1.3 mM), in the absence or the presence of compound **41**. 341
Figure 4.26: Cellular viability of differentiated SH-SY5Y neuroblastoma cells after a 24 h treatment with increasing concentrations of compounds **38-41** (0.20-100 µM). 343
Figure 4.27: (A) Evaluation of intracellular oxidative stress levels in differentiated SH-SY5Y cells using the DCF fluorescence assay, after incubation for 24 h with compounds **38-41** at 10 and 50 µM. 344
Figure 4.28: Effect of piperine (compound **22**) and TPP conjugates **38-41** at non-toxic concentrations on mitochondrial oxygen consumption.. 346
Figure 4.29: chemical structures and biological data of lead candidates. 351

LIST OF TABLES

Table 4.1: chemical structures and reaction yields of ferulic acid-based thiophenols **2-6** and related intermediates. 317
Table 4.2: chemical structures and reaction yields of compounds **7**, **8** and **10**. 318
Table 4.3: chemical structures and reaction yields of compounds **12-16** and **30-37**.....319
Table 4.4: chemical structures and reaction yields of α-CN derivatives **17-21** and **30-37** and related intermediates. 321
Table 4.5: chemical structures and reaction yields of alkyl triphenylphosphonium conjugates **38-41** and related intermediates. 323
Table 4.6: *h*MAO inhibitory activities of compounds **12-16**, **23-29** and reference inhibitors. 331
Table 4.7: *h*MAO inhibitory activities of α-CN derivatives **17-21**, **30-37**. 331
Table 4.8: ChE (*ee*AChE and *eq*BChE) and *h*MAOs (*h*MAO-A and *h*MAO-B) inhibitory activities of piperine (compound **22**), compounds **38-41** and reference inhibitors. 341
Table 4.9: Retention times (t_R) obtained by LC/UV at pH 2.3 and 7.4 and calculated CHI parameters of CA (compound 11), CA derivatives **12**, **17**, **20**, **21**, piperine (compound 22), piperine derivatives **28**, **36** and **37**, and mitochondria-targeted antioxidants **40** and **41**..348
Table 4.10: Predicted drug-like properties of FA derivatives **2**, **3** and **10**, CA derivatives **12**, **17**, **20**, **21**, piperine (compound **22**), piperine derivatives **28**, **36** and **37**, and mitochondria-targeted antioxidants **40** and **41**. 349

LIST OF ABBREVIATIONS

AADC: Aromatic amino acid decarboxylase

$ABTS^{\bullet+}$: 2,2′-azinobis-(3-ethylbenzothiazoline-6-sulfonic acid) radical cation

ACh: Acetylcholine

Acetyl-CoA: Acetylcoenzyme A

AD: Alzheimer's disease

AChE: Acetylcholinesterase

ADMET: Absorption, distribution, metabolism, excretion and toxicology

APP: Amyloid Precursor Protein

ATP: Adenosine triphosphate

Aβ: Amyloid β

BBB: Blood-brain barrier

BChE: Butyrylcholinesterase

BDNF: Brain-derived neurotrophic factor

CA: Caffeic acid

CAPE: Caffeic acid phenethyl ester

CAS: Catalytic active site

CAT: Catalase

ChAT: Choline acetyltransferase

ChE: Cholinesterase

CHI: Chromatographic hydrophobicity index

ChT1: Choline transporter

cLogP: Calculated logarithm of octanol/water partition coefficient

COMT: Catechol-O-methyltransferase

COSY: Correlation spectroscopy

COX: Cyclooxygenase

CNS: Central nervous system

CV: Cyclic voltammetry

DA: Dopamine

DAT: Dopamine transporter

DCF: 2',7'-Dichlorofluorescein

DPV: Differential pulse voltammetry

$DPPH^{\bullet}$: 2,2'-Diphenyl-1-picrylhydrazyl radical

ECAR: Extracellular acidification rates

EI-MS: Electron impact mass spectrometry

ETC: Electron transport chain

ESI-MS: Electrospray ionization mass spectrometry

FA: Ferulic acid

FAD: Flavin adenine dinucleotide

FDA: Food and Drug Administration

G6PDH: Glutathione-6-phosphate dehydrogenase

GO$^{\bullet}$: Galvinoxyl radical

GPx: Glutathione peroxidase

GR: Glutathione reductase

GSH: Reduced glutathione

GST: Glutathione-S-transferase

GSSG: Oxidized glutathione

HBA: Hydrogen atom acceptor

HBD: Hydrogen atom donor

HCA: Hydroxycinnamic acid

HSQC: Heteronuclear single quantum coherence spectroscopy

HMBC: Heteronuclear multiple bond correlation

IRL/MA: Ratio between the intracellular RS levels and metabolic activity

K_i: Inhibition constant

K_M: Michaelis constant

LogBB: the logarithm of the ratio of the concentration of the compound in the brain and in the blood

MAO: Monoamine oxidase

MB-COMT: membrane-bond COMT

MCI: Mild cognitive impairment

MLM: Mouse liver mitochondria

MTDL: Multitarget-directed ligand

MTT: 3-(4,5-dimethylthiazol-2-yl)-2,5-diphenyltetrazolium

MW: Molecular weight

NADH: Nicotinamide adenine dinucleotide

NADPH: Nicotinamide adenine dinucleotide phosphate

ND: Neurodegenerative disease

NTF: Neurofibrillary tangle

NMR: Nuclear magnetic resonance

NOX: NADPH oxidase

NOS: Nitric oxide synthase

NR: Neutral Red

ORAC: oxygen radical absorbance capacity

OCR: Oxygen consumption rate

OLIG: oligomycin

PD: Parkinson's disease

PAS: Peripheral anionic site

P-gp: P-glycoprotein

pK_a: acid dissociation constant

PSEN1: presenilin 1

PSEN2: presenilin 2

RHO 123: rhodamine 123

RNS: Reactive nitrogen species

$ROO^{\bullet}$: Peroxyl radical

ROT/AA: Rotenone and antimicyn A

ROS: Reactive oxygen species

RS: Reactive species

RB: Rotatable bonds

SAH: S-adenosyl-L-homocysteine

SAM: S-adenosyl-L-methionine

S-COMT: soluble COMT

SNpc: S*ubstantia nigra pars compacta*

SOD: Superoxide dismutase

SP: Senile plaques

SRB: Sulphorhodamine B

TH: Tyrosine hydroxylase

TPP: Triphenylphosphonium

tPSA: Topological polar surface area

t_R: retention time

VAL: Valinomycin

VAT: Vesicular acetylcholine transporter

VMAT2: Vesicular monoamine transporter

V_{max}: Maximum velocity

XO: Xanthine oxidase

CHAPTER I

Introduction

1.1. Neurodegenerative diseases

The average human life expectancy of the worldwide populations has been rising in the last decades (1). Several factors seem to contribute to this achievement, namely the cumulative improvements in sanitation and medical care, rising living standards and the decline in child mortality (1, 2). Although the increased life span is to be celebrated, the prevalence of the common chronic and fatal diseases (cancer and metabolic, cardiovascular and neurodegenerative diseases (NDs)) grows dramatically with advanced aging (1). Therefore, the rise of elderly populations has been soaring the increased incidence of age-related degenerative diseases, reaching epidemic proportions in the high-income countries (3).

Neurodegenerative diseases are a set of progressive, chronic and incurable disorders. They represent an enormous disease burden both in terms of human suffering and economic cost (4), being the major contributors to disability and dependence in the word due to their debilitating nature (5). In general, NDs are characterized by the progressive loss of specific neuronal populations (6, 7), which contributes to the development of clinical symptoms commonly related with motor disability, cognitive impairment and dementia (8). The most common NDs include Alzheimer's disease (AD), Parkinson's disease (PD), Huntington's disease and amyotrophic lateral sclerosis (9).

The etiology of NDs is not completely understood (10, 11) and the onset of neurodegeneration may precede the clinical symptoms by many years (12). However, it is widely accepted that the pathogenesis of NDs is multifactorial involving a complex combination of genetic, environmental and endogenous factors acting cooperatively or independently (10, 11, 13, 14). Although each disease presents its own molecular mechanisms and clinical manifestations (**Figure 1.1**), NDs share common pathogenic events (15).

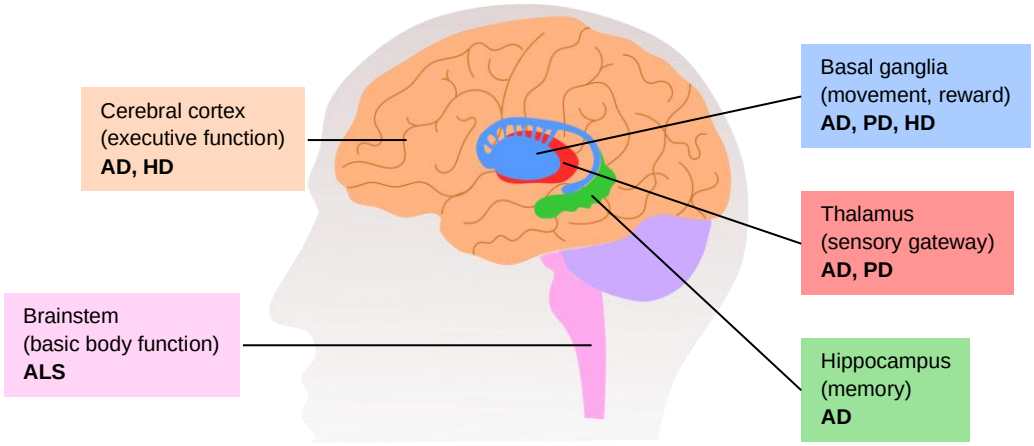


Figure 1.1: Primary brain regions affected in the most common neurodegenerative diseases. Adapted from (15).

The available treatments for NDs only provide symptomatic relief for a limited period of time (16) and are unable to modify the disease progression (17). Therefore, the development of disease-modifying drugs able to halt or reverse the progression of NDs remains an unmet clinical need (18). The discovery of effective treatments is progressively more urgent due to the increase in life expectancy of the global population and the increasing prevalence of NDs (19).

1.1.1. Alzheimer's disease: major hallmarks

Originally described by Alois Alzheimer in 1906 (20), AD is the most common ND worldwide (21) and accounts for 50 to 70 % of all dementia cases (20). The most common form of AD is sporadic and with a late onset age (late onset AD, > 65 years), representing approximately 95 % of all cases (20). Late onset AD results from a complex combination of genetic, environmental and stochastic factors (16). Early-onset AD may also occur, accounting for up to 5 % of all cases and with an onset from 30 to 65 years (20, 22). Early-onset AD cases are predominantly familial forms and are caused by rare mutations in one of three main genes (amyloid precursor protein (*APP*), presenilin 1 (*PSEN1*), or presenilin 2 (*PSEN2*) genes) (20, 22).

Clinically, AD is characterized by a devastating, irreversible and progressive decline of cognitive functions, including memory and language, and motor skills (23-25). Clinical symptoms may evolve as the disease progresses, from normal cognition to mild cognitive impairment (MCI) at early stages of AD, followed by advanced dementia at later stages (24, 26). Although the time course of AD progression is not fully elucidated, it is believed that

pathological mechanisms begin a decade or more before the clinical detection of dementia (24).

The progressive cognitive impairment can be associated with the significant reduction of brain size observed in AD patients (27). The brain atrophy arises from the loss of synapses and from the selective neuronal death in the hippocampus and in the cerebral cortex (21, 27-29). The most prominent losses are observed in neurons with long projections, such as cholinergic neurons in the basal forebrain (**Figure 1.2**) (30). These neurons innervate the hippocampus, thalamus, amygdala and neocortex, and play key roles in attention, cognitive flexibility and learning (31). Although the neurons that degenerate in AD are mostly cholinergic (32), glutamatergic neurons are also affected (11).

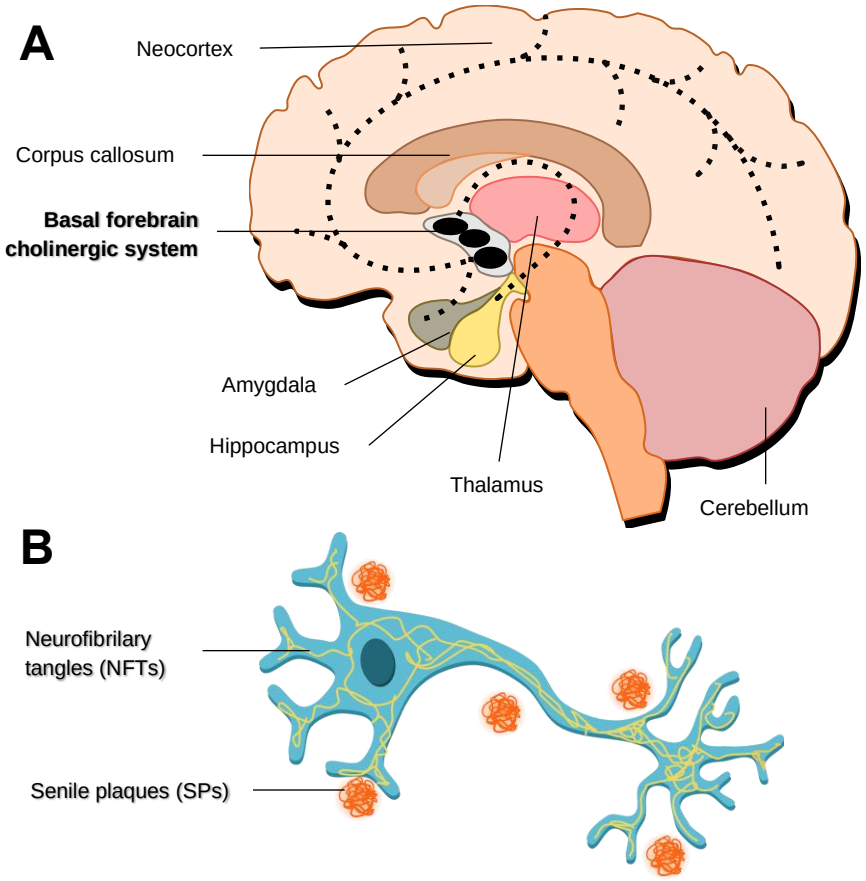


Figure 1.2: Major hallmarks of AD. (A) Degeneration of cholinergic neurons in the basal forebrain. (B) Formation of senile plaques and neurofibrillary tangles. Adapted from (33)

The brain of AD patients also presents extracellular senile plaques (SPs) and intracellular neurofibrillary tangles (NFTs) (16, 34). One of the major components of SPs is the amyloid β (Aβ) peptide, generated from the sequential cleavage APP by β- and γ-secretases (35). The resulting peptide may contain either 40 or 42 amino acids in length (36), with the longer form being more neurotoxic and the major constituent of SPs (36, 37).

The propensity of Aβ peptides to interact with one another leads to the spontaneous formation of oligomeric species (38). Then, Aβ oligomers reorganize into protofibrils and fibrils, which accumulate in the brain parenchyma in the cerebral blood vessels where they form SPs (28, 39, 40). In the human brain, SPs initially appear in basal temporal and orbitofrontal neocortex (**Figure 1.3A**) (41). Later, they are found throughout the neocortex, hippocampus, diencephalon and basal ganglia (41). The brain areas with SPs present a decreased number of synapses and damaged neurites (27). Moreover, the accumulation of Aβ peptides and deposits induces oxidative stress and mitochondrial dysfunction, promotes the formation of hyperphosphorylated tau protein and contributes to neuroinflammation, leading to neuronal cell death (8, 40, 42).

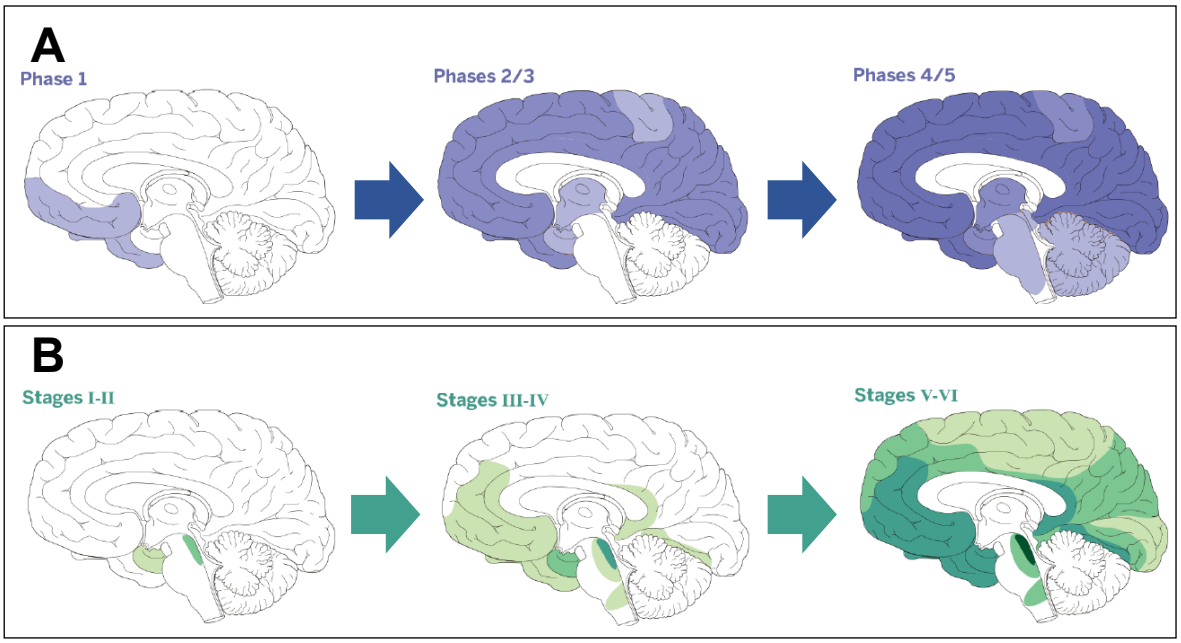


Figure 1.3: Formation of amyloid β (A) and tau (B) aggregates in the human brain. Adapted from (41).

The intracellular NFTs are composed of paired helical filaments sometimes admixed with straight filaments (43). In AD brains, NTFs progressively accumulate in the entorhinal cortex, followed by hippocampus and neocortex (**Figure 1.3B**) (44). The main component of NTFs is the hyperphosphorylated tau protein (45), the major microtubule associated protein predominantly found in the axons of mature neurons (46, 47). The functions of tau include promotion of microtubule self-assembly and stabilization of their structure (47, 48), and regulation of motor-driven axonal transport (47). Tau hyperphosphorylation induces a loss-of function that hampers its ability to bind to microtubules, leading to microtubule depolymerization that compromises the axonal trafficking and the dendrite structure (19).

The formation of toxic NTFs together with the loss of microtubule-associated tau functions compromise neuronal survival (44, 45).

1.1.2. Parkinson's disease: major hallmarks

Initially described by James Parkinson in 1817, PD is the second most common ND after AD and the most common movement disorder (49). Parkinson's disease is mostly sporadic, resulting from a complex interplay between genetic susceptibility and environmental factors (50-52). However, approximately 5-10 % of PD cases are caused by familiar genetic mutations (52, 53) that usually result in early-onset PD (54). Mutations in *SNCA*, *LRRK2* and *VPS35* genes were associated with autosomal dominant PD, while mutations in *PINK1*, *PARK7/DJ-1*, *PARK2/PARKIN*, *PLA2G6*, *ATP13A2*, and *FBXO7* cause autosomal recessive PD and/or parkinsonism (55).

Clinical manifestations of PD include four cardinal motor symptoms: bradykinesia, resting tremor, rigidity and postural instability (51). Patients with PD may also experience numerous non-motor symptoms, such as autonomic deficiency, cognitive impairment and sleep disorders (16, 56, 57). Non-motor symptoms are common in the early stages of PD (pre-motor/prodromal phase) and frequently precede the onset of motor symptoms (56, 57). Motor dysfunction worsens with the disease progression and are managed with symptomatic treatments (57). However, long-term therapy is associated with gradual loss of efficacy and the emergence of adverse effects such as motor fluctuations, dyskinesia and psychosis (57, 58). Late-stage PD is characterized by treatment-resistant motor and non-motor symptoms that substantially contribute to the patients' disability (57). The median age of onset of PD is 60 years, and the mean duration from diagnosis to death is 15 years (59).

The motor dysfunction observed in PD is linked to the loss of dopaminergic neurons in the *substantia nigra pars compacta* (SNpc), which contributes to severe dopamine (DA) deficiency in the putamen and the caudate nucleus (60). The cell bodies of nigrostriatal neurons are in the SNpc and their axon terminals project to the dorsal striatum (i.e., putamen and caudate nucleus) (**Figure 1.4**) (53, 61). Symptoms only develop after the loss of 50-60 % of nigral neurons and the depletion of 80-85 % of DA levels (10). Although the neuropathology of PD is primarily characterized by dopaminergic neuron loss, neurodegeneration also extends to other neurotransmitter systems (56). Indeed, cholinergic (nucleus basalis of Meynert, dorsal nucleus of vagus), serotonergic (raphe) and noradrenergic (locus coeruleus) neurons are also affected (61).

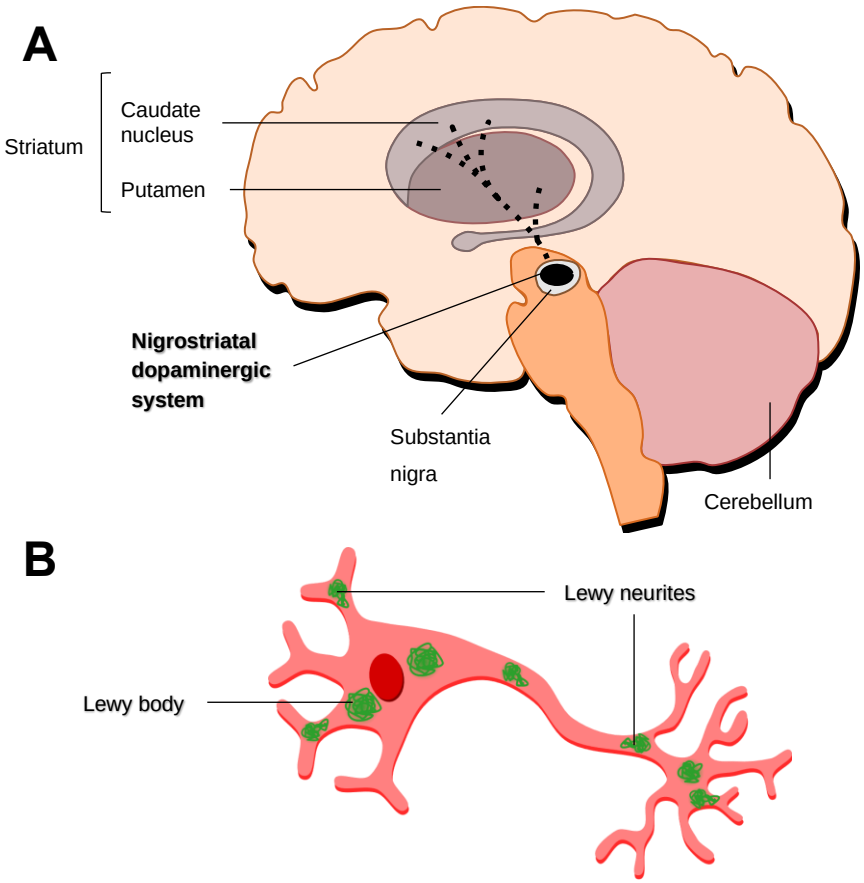


Figure 1.4: Major hallmarks of Parkinson's disease. (A) Degeneration of nigrostriatal dopaminergic neurons. (B) Formation of Lewy inclusions. Adapted from (62, 63).

Another neuropathological hallmark of PD is the presence of neuronal inclusions in the surviving neurons whose main component is α-synuclein (10, 64), a protein involved in the modulation of vesicular trafficking (49). In dopaminergic neurons, α-synuclein regulates the synthesis, storage and release of DA (49). Alpha-synuclein is prone to form oligomeric and fibrillar species in the cytosol or associated to the cellular membrane (65). The formation of α-synuclein inclusions begins in the lower brainstem nuclei (41, 66), spreads through the pons to the midbrain and basal forebrain and reaches the neocortex (**Figure 1.5**) (41). These inclusions may accumulate in neuronal perikarya (Lewy bodies) and in neuronal processes (Lewy neurites) (64, 67). The presence of these aggregates is associated with the accumulation of synaptic vesicles, decreased DA release, impairment of degradation pathways and increased oxidative stress (49).

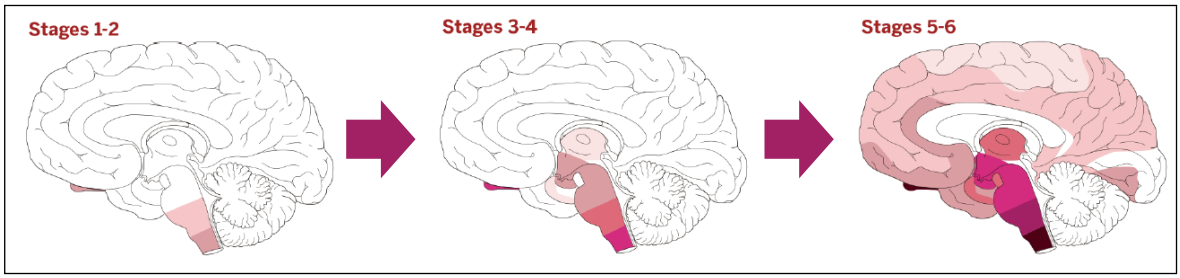


Figure 1.5: Formation of α-synuclein aggregates in the human brain. Adapted from (41).

1.2. Pharmacotherapy of Alzheimer's and Parkinson's diseases

Neurodegeneration is a complex process resulting from multiple defects or insults. (68). The most obvious pathological features of AD and PD include the selective loss of neuronal populations with consequent decrease of neurotransmitter levels, and the formation of protein aggregates (51, 69). These observations led to the identification of the primary targets (e.g.: cholinesterases (ChEs), monoamine oxidases (MAOs), catechol-*O*-methyltransferase (COMT)) (68) and to the subsequent development of the currently available therapeutic agents (6, 70).

However, with a more detailed understanding of the mechanisms involved in neurodegeneration, other pathogenic events were identified (71). Elevated oxidative and nitrosative stress, mitochondrial dysfunction, calcium dyshomeostasis, accumulation of transition metals, neuroinflammation and aberrant axonal transport emerged as major determinants in the development and progression of NDs (72-74). These mechanisms may cause neuronal loss, affect neurotransmitter levels and impair signal transduction, thus accelerating the progressive decline of cognitive and motor functions (19).

Despite the extensive research performed to understand the molecular mechanisms involved in neurodegeneration, researchers continue to investigate new therapeutic strategies, molecular mechanisms and druggable targets (75).

1.2.1. Targeting neurotransmitter depletion

1.2.1.1. Cholinergic transmission and Alzheimer's disease

Cholinergic neurons are widely distributed in both the central and the peripheral nervous system (CNS and PNS, respectively) (31). Although they represent less than 1 % of neurons in the nervous system, almost every brain region and peripheral target receives cholinergic innervation (76). Cholinergic neurons in the basal forebrain contain extensive

cortical projections that are involved in the modulation of other neurotransmitter systems (77). The damage or the presence of abnormalities in cholinergic pathways, especially in the basal forebrain neurons, was correlated with the level of cognitive decline in late-stage AD patients (78). Together with the loss of cholinergic markers, such as choline acetyltransferase (ChAT, EC 2.3.1.6) and acetylcholinesterase (AChE, EC 3.1.1.7), these observations led to the formulation of the cholinergic hypothesis (79), which states that the dysfunction of the cholinergic system contributes to the cognitive deficits in AD (80).

Acetylcholine (ACh) was the first neurotransmitter to be identified (81) and plays important functional roles in attention, memory, learning, stress response, wakefulness and sleep, and sensory information (82). In fact, the hippocampal and cortical levels of ACh in the brain of AD patients are decreased in approximately 90 % (83).

The synthesis of ACh is catalysed by ChAT in the cytosol of presynaptic cholinergic neurons in a single step reaction, in which choline (Ch) and acetyl-coenzyme A (acetyl-CoA) are used as substrates (**Figure 1.6**) (84). While acetyl-CoA is synthesized by mitochondria (85), Ch is taken up from the extracellular space since it is not synthesized in neurons (85). The rate-limiting step for the synthesis of ACh is the uptake of Ch by the Na^+-dependent, high-affinity choline transporter (ChT1) (86). The neurotransmitter ACh is then accumulated in synaptic vesicles by the vesicular acetylcholine transporter (VAT). This transporter uses an electrochemical gradient generated by a proton adenosine triphosphate (ATP)ase to perform the uptake of one ACh molecule in exchange of two protons (85-87). During neurotransmission, ACh is released from the pre-synaptic neuron into the synaptic cleft, where it binds to cholinergic receptors (muscarinic or nicotinic) in the post-synaptic and pre-synaptic membranes (84, 88).

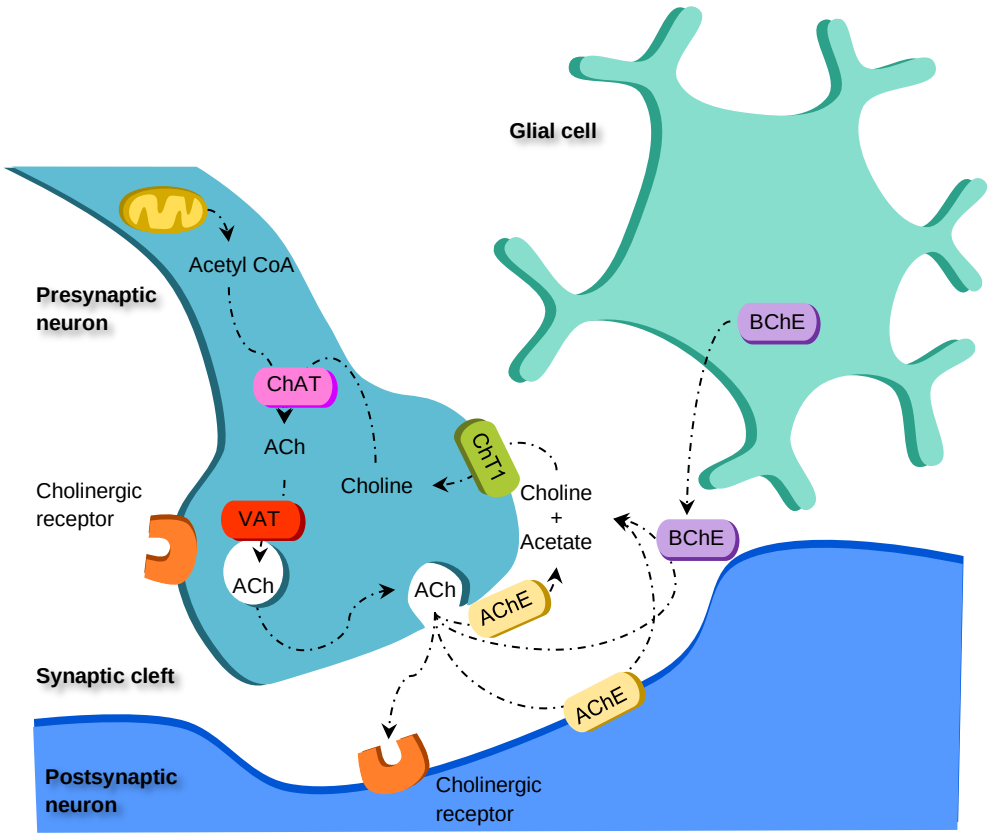


Figure 1.6: Enzymes and transporters involved in the synthesis, storage and metabolism of acetylcholine. Adapted from (88, 89)

The action of ACh may persist for a long time due to the chemical stability of the neurotransmitter (90). Therefore, the rapid hydrolysis of ACh by cholinesterases (ChEs) prevents cholinergic overactivation (91). Two ChEs are present in mammals: AChE and butyrylcholinesterase (BChE, EC 3.1.1.8) (79). While the Ch obtained from ACh inactivation is taken up by pre-synaptic neuron via ChT1 (84, 90), acetic acid is further decomposed (90).

1.2.1.1.1. Acetylcholinesterase and Butyrylcholinesterase

Acetylcholinesterase is a substrate-specific ChE that selectively hydrolyses ACh (92) and is mainly localized in the CNS, neuromuscular junctions and erythrocytes (93). The main function of AChE is the regulation of ACh levels in cholinergic synapses (94). On the other hand, BChE is a non-specific ChE, catalyzing the breakdown of ACh and other esters (95). This enzyme is predominantly found in peripheral tissues, although it is present in the brain in very small amounts (96). The physiological role of BChE is not completely understood (79). However, it has been proposed that, in addition to the minor function in

the regulation of brain ACh levels (97), BChE activity is important in drug metabolism and detoxification and in lipid metabolism (98).

In the CNS, AChE is primarily present in neurons, while BChE is mainly found in glial cells and endothelial cells (**Figure 1.6**) (99). The proximity of glial BChE to cholinergic neurons enables a synergistic BChE-mediated hydrolysis, thereby assisting on the regulation of ACh levels (100).

Although AChE and BChE are encoded by different genes in chromosomes 7 and 3, respectively, they share 65 % of structural homology (101). Both ChEs contain a catalytic active site (CAS), a deep gorge and a peripheral anionic site (PAS) (**Figure 1.7**) (97). The active site contains a catalytic triad consisting of three conserved amino acids (Ser203, His447, Glu334 in human AChE, *h*AChE; Ser198, His438, Glu325 in human BChE, *h*BChE) and a choline binding site (97). The main structural differences between AChE and BChE are especially found in the acyl binding pocket, which accommodates the acyl group (101, 102). While *h*AChE contains two bulky amino acids (Phe295 and Phe297), *h*BChE presents two smaller amino acids (Leu286 and Val288) (97). The aliphatic amino acids of *h*BChE enable the accommodation and subsequent hydrolysis of larger substrates than ACh (102).

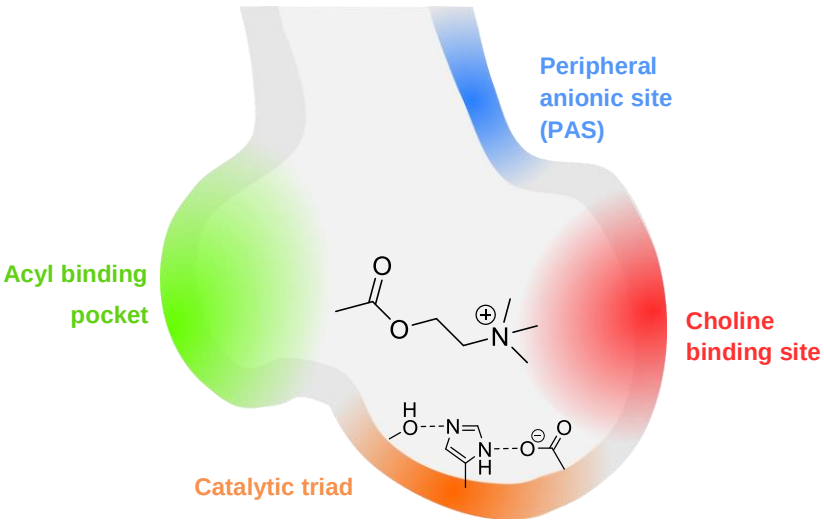


Figure 1.7: Schematic representation of active site gorge of cholinesterases. Adapted from (94, 103).

The kinetic responses of AChE and BChE to the concentrations of ACh are also different (92, 100). At low concentrations of the neurotransmitter, AChE is highly efficient while BChE is less efficient (92, 100). On the other hand, at higher ACh concentrations, AChE is inhibited by the substrate while BChE becomes more efficient in the decomposition of ACh (92, 100).

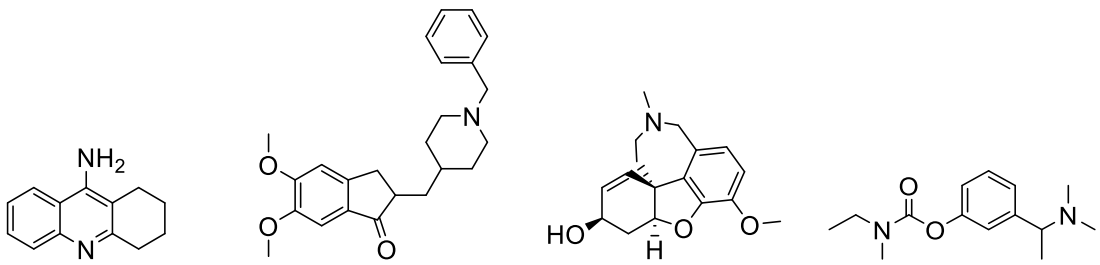
In healthy human brains, AChE represents 80 % of the ChEs activity, while BChE plays a supporting role (103). Over the progression of AD, AChE levels decrease as much

of 85 % in specific brain areas (77), while BChE levels increase possibly as a result of glial cell proliferation (89). As a result, the ratio of BChE to AChE in cortical areas of the brain shifts from 0.2 to as much as 11 (77). In AD, the elevated BChE levels is a compensatory mechanism for ACh metabolism (89). Therefore, the inhibition of both AChE and BChE is considered desirable for the effective management of AD (68, 96).

1.2.1.1.2. Cholinesterase inhibitors

Given the cholinergic deficits observed in AD, the mainstay of AD pharmacotherapy is mainly focused on restoring the cholinergic neurotransmission through the inhibition of ChEs (70, 104). The use of ChE inhibitors prevents ACh decomposition, increasing the synaptic levels of the neurotransmitter and prolonging its action (95, 101). Cholinesterase inhibitors significantly ameliorate cognition, memory, communication and some behavioural manifestations of AD, making an important contribution for the management and well-being of AD patients (105, 106).

At present, only four ChE inhibitors have been approved by the Food and Drug Administration for AD treatment (107). **Tacrine** (**Figure 1.8**) was the first AChE inhibitor approved, but it was soon withdrawn from the market due to its hepatotoxicity (69). However, three other ChE inhibitors were further approved for AD treatment: **dopenezil, rivastigmine and galantamine** (**Figure 1.8**) (106).



Tacrine Donepezil Galantamine Rivastigmine

Figure 1.8: FDA-approved cholinesterase inhibitors for Alzheimer's disease. Adapted from (19).

Donepezil (trade name Aricept®, **Figure 1.8**) is a reversible, highly selective piperidine-based AChE inhibitor (108, 109). Due to its elongated structure, donepezil spans the entire cavity of the AChE active site gorge, interacting with residues present in both the CAS and the PAS through aromatic interactions (110). In addition to AChE inhibition, donepezil may counteract the glutamate-induced excitotoxicity and attenuate Aβ formation and neurotoxicity (109). Donepezil is the most widely drug prescribed for the treatment for

AD (111). It was approved to manage mild to moderate AD and, at higher doses, to manage moderate to severe AD (111, 112). Treatment of AD patients with donepezil has been associated with improvement in cognitive function and in daily functioning (111). Donepezil is considered safe at therapeutic dosages, but AD patients may experience side effects associated with increased cholinergic activity, such as gastrointestinal disturbances (nausea, diarrhoea, vomiting), bradycardia and behavioural disturbances (agitation, hallucinations and delusions) (84, 109, 113). The incidence of these adverse reactions is increased in patients treated with higher dosages (114).

Rivastigmine (trade name Exelon®, **Figure 1.8**) is a slow-reversible carbamate inhibitor that covalently bind to the active site of both AChE and BChE, being slowly hydrolysed by these enzymes (70, 105). Rivastigmine was approved by the FDA in 2000 for the treatment of mild to moderate AD (115, 116), and in 2006 for the treatment of mild to moderate dementia associated with PD (105). The adverse effects of rivastigmine include nausea, vomiting, diarrhoea and anorexia (84, 116). Rivastigmine is available in both oral and transdermal patch formulations (117). In comparison to oral delivery, the use of transdermal patches enables a smoother, continuous and controlled delivery of rivastigmine, resulting in fewer side effects (116).

Galantamine (trade name Razadine®, **Figure 1.8**) is a tertiary phenanthrene alkaloid that has been isolated from several species of the *Amaryllidaceae* family (118). It was approved for the treatment of mild to moderate AD in 2001 (115). Galantamine is a reversible and competitive AChE inhibitor, interacting with both the choline- and acyl binding sites located at the base of the active site gorge (105, 119). Galantamine also enhances cholinergic activation acting as a positive allosteric modulator of nicotinic ACh receptors (118, 120). In the hippocampus, this modulatory activity facilitates glutamatergic transmission providing beneficial effects on learning and memory (119, 121). The side effects of galantamine are similar to dopenezil and rivastigmine, being mainly associated with gastrointestinal disturbances (84).

1.2.1.2. Dopaminergic transmission and Parkinson's disease

DA is a catecholamine neurotransmitter present in the CNS and in some peripheral areas (122). In the brain, DA transmission is associated with the control of fine motor movements and with cognitive functions that include learning, reward, attention and decision-making (122, 123). More particularly, the DA released in the nigrostriatal pathway is linked to the performance of voluntary movements, as well as the selection and initiation of suitable motor actions (124).

In the cytoplasm of the presynaptic dopaminergic neuron, DA biosynthesis occurs in two steps (**Figure 1.9**) (63, 125). The first step involves the hydroxylation of tyrosine into L-3,4-dihydroxyphenylalanine (L-DOPA) by tyrosine hydroxylase (TH, EC 1.14.16.2), which is followed by a decarboxylation reaction catalysed by aromatic amino acid decarboxylase (AADC, EC 4.1.1.28) to afford DA (63, 125). The neurotransmitter is then transported into synaptic vesicles by the vesicular monoamine transporter (VMAT2) or metabolized by intraneuronal monoamine oxidase A (MAO-A, EC 1.4.3.4) (126). Following the release into the synaptic cleft, DA binds to the dopaminergic receptors present in the post-synaptic neuron (125). The transport of the released DA into the presynaptic neuron occurs via DA transporter (DAT), and is followed by DA recycling into the synaptic vesicles or by DA deamination by MAO-A (126). Alternatively, the DA transported into non-dopaminergic post-synaptic neurons and glial cells is metabolized by monoamine oxidase B (MAO-B, EC 1.4.3.4) and catechol-*O*-methyltransferase (COMT, EC 2.1.1.6) (126).

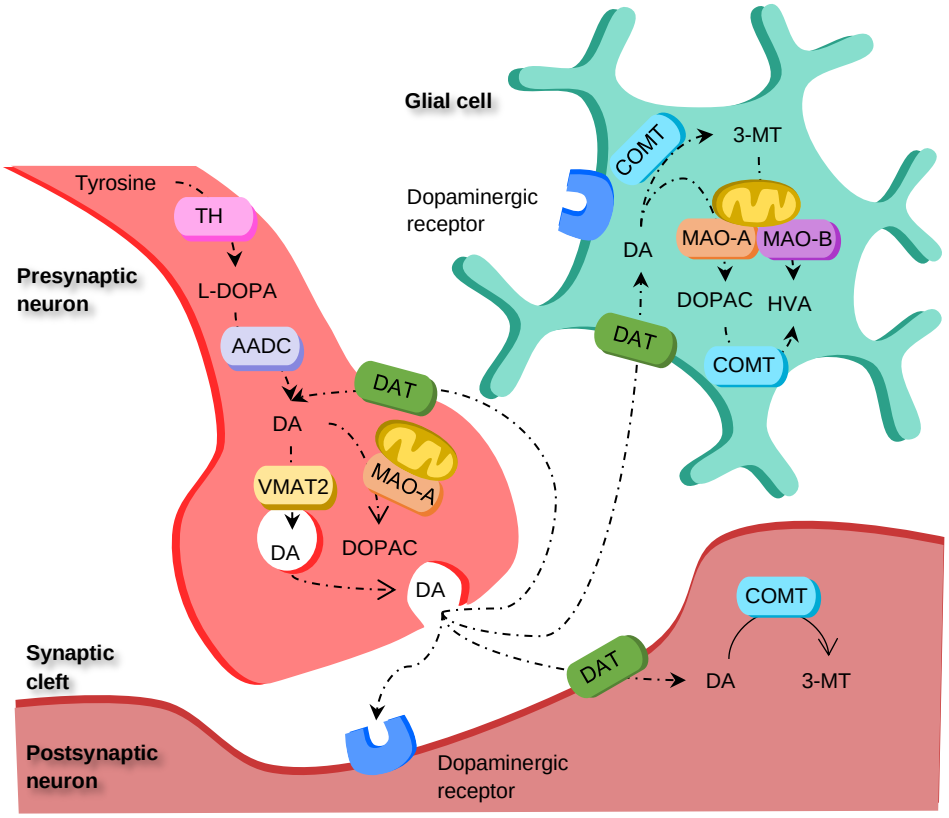


Figure 1.9: Enzymes and transporters involved in the synthesis, storage and metabolism of dopamine. Adapted from (126, 127).

The loss of nigrostriatal dopaminergic neurons is associated with the development of motor symptoms of PD, namely difficulty in initiating and terminating movements, gait disturbance and muscular rigidity (124). Therefore, to reduce the severity of motor handicap, most PD therapies are based on enhancing the dopaminergic signalling (6, 59).

The use of the DA precursor L-DOPA remains the gold-standard treatment for PD (128). Unlike DA, L-DOPA can cross the blood-brain barrier (BBB) and increase DA synthesis in the brain (125). To prevent the peripheral metabolic activation to DA, L-DOPA is commonly administered with decarboxylase inhibitors (e.g.: carbidopa, benserazide) (50). Despite the efficacy of L-DOPA in ameliorating motor symptoms, its long-term use is associated with progressive loss of efficacy together with motor fluctuations and dyskinesia (58, 129).

In addition to L-DOPA, other therapeutic approaches involve the inhibition of DA metabolism with MAO and COMT inhibitors, inhibition of DA reuptake, or the use of agonists of post-synaptic DA receptors (130, 131).

1.2.1.2.1. Monoamine oxidases

Monoamine oxidases are flavin-containing enzymes bound to the outer mitochondrial membrane (132). They catalyse the oxidative deamination of monoaminergic neurotransmitters, dietary amines and hormones (133), which occurs in two half reactions (**Figure 1.10**) (75, 134). First, two hydrogen atoms are transferred from the substrate to the flavin adenine dinucleotide (FAD) cofactor (reductive half-reaction) (75, 134). The resulting imine is hydrolysed into the corresponding aldehyde and ammonia in a non-enzymatic reaction (135, 136). Then, the reduced FAD is reoxidized by molecular oxygen (oxidative half-reaction) yielding hydrogen peroxide (H_2O_2) (75, 134).

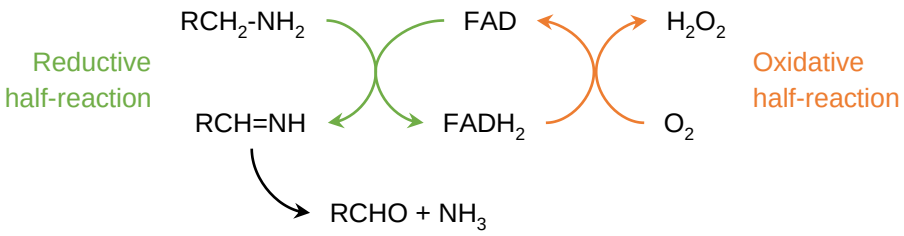


Figure 1.10: Schematic representation of the oxidative deamination reaction catalysed by MAOs. Adapted from (135).

Monoamine oxidases are widely expressed in the brain (137) and in peripheral tissues such as placenta, duodenum, liver, kidney, spleen and heart (138). In the brain, MAOs are involved in the regulation of monoamine neurotransmitters levels and in the inactivation of amines able to act as false neurotransmitters (139). In peripheral tissues, MAOs terminate paracrine or autocrine actions of monoaminergic hormones (139). In

addition, MAOs have a central role in the metabolism of xenobiotics taking place in the liver and intestine (139).

Two isoforms of MAO (MAO-A and MAO-B) were identified in humans, which differ in the substrate selectivity, inhibitor specificity, tissue and brain regional distribution, and clinical significance (140).

Although MAO-A and MAO-B are encoded by separate but adjacent genes in the X chromosome, they share approximately 70 % of amino acid sequence identity (137, 141). Furthermore, both MAO-A and MAO-B contain a flavin-binding domain, a substrate-binding domain and a membrane-binding domain (**Figure 1.11**) (142). However, differences in the cavity size and in specific amino acids of the substrate-binding site contribute to the substrate and inhibitor selectivity of MAO-A and MAO-B (142). Monoamine oxidase A has a single substrate cavity of approximately 550 $Å^3$ in size close to the membrane surface (143). On the other hand, MAO-B contains bipartite elongated cavity consisting of a smaller hydrophobic entrance cavity and the substrate binding site (143). The entrance cavity and the substrate binding site are separated by an isoleucine residue, whose rotation after binding of the appropriate substrate enables the fusion of the two chambers into a larger 700 $Å^3$ cavity (144). The small entrance cavity allows the binding of small hydrophobic molecules (e.g. benzylamine, β-phenylethylamine) and restricts the access of large hydroxylated amines (e.g. 5-HT) (144).

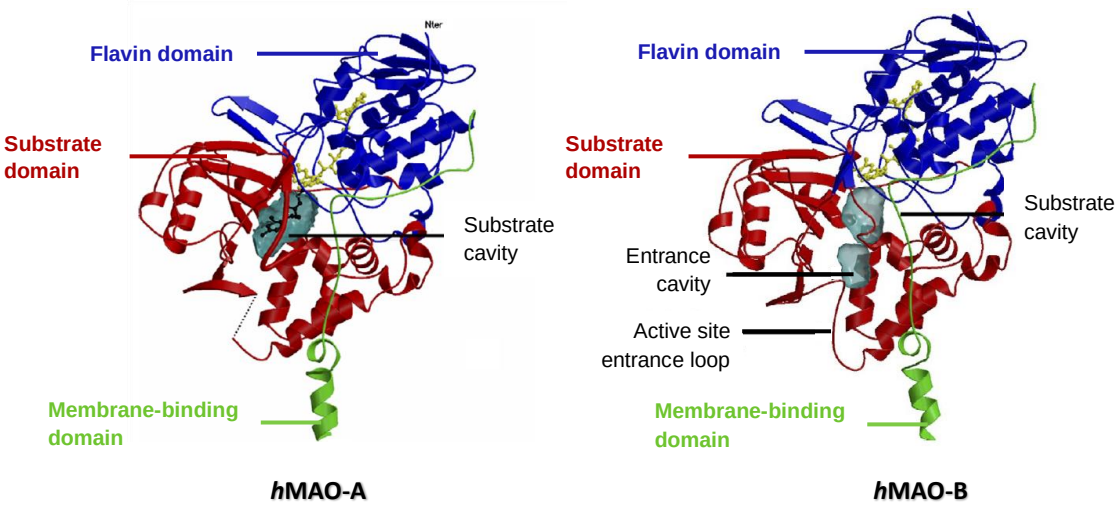


Figure 1.11: Ribbon diagrams of monomeric units of human MAO-A (PDB ID: 2BXS) and MAO-B (PDB ID: 1GOS). Adapted from (143).

In the brain, MAO-A is predominantly found in catecholaminergic neurons (145) and preferably deaminates adrenaline and serotonin (5-hydroxytryptamine, 5-HT) (146). On the

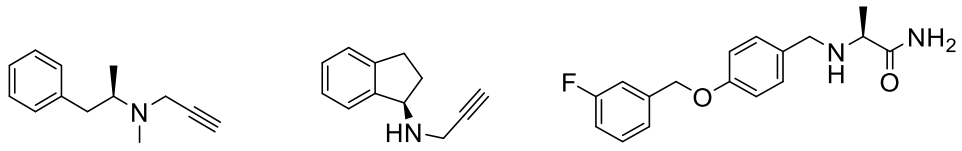
other hand, MAO-B is commonly located in histaminergic and serotonergic neurons (145), and in glial cells (126). Monoamine oxidase B presents higher affinity for non-hydroxylated amines such as benzylamine and β-phenylethylamine (141). Dopamine is a common substrate of both isoforms (146).

Due to their pivotal role in neurotransmitter catabolism and their affinity for specific neurotransmitters, MAOs are considered attractive drug targets in the therapeutic treatment of depression and NDs (147, 148). In particular, MAO-B is the main isozyme involved in DA metabolism in the aged parkinsonian brain (146). In fact, while MAO-A activity is maintained with aging, the activity and expression of MAO-B in the human brain increases approximately 4-fold in most brain areas such as the basal ganglia (146, 149), possibly as a result of glial cell proliferation and the concomitant loss of neuronal cells (75). The increased MAO-B activity leads to nigrostriatal DA depletion and to a higher production of H_2O_2 and toxic aldehydes, which contribute to increased oxidative stress and neuronal degeneration (146, 149).

Monoamine oxidase B inhibitors are currently used in PD therapies to prevent DA catabolism and prolong the action of DA in the basal ganglia (150). The inhibition of MAO-B may also decrease the formation of dopamine-derived oxidative products and thereby delay the disease progression (151). Usually, MAO-B inhibitors are prescribed either as monotherapy or in combination with L-DOPA (152). Their use in monotherapy is more effective at the early stages of PD and may delay the use of L-DOPA (152). When combined with L-DOPA, MAO-B inhibitors prolong the therapeutic effects of L-DOPA, decrease the dose of L-DOPA required to control the symptoms and reduce the occurrence of L-DOPA-associated side effects (146, 152).

1.2.1.2.2. Monoamine oxidase B inhibitors

Currently, three MAO-B inhibitors are used in PD pharmacotherapies: selegiline, rasagiline and safinamide (**Figure 1.12**).



(R)-(−)-deprenyl (Selegiline) Rasagiline Safinamide

Figure 1.12: FDA-approved MAO-B inhibitors for Parkinson's disease. Adapted from (57).

Selegiline (trade name Eldepryl®, **Figure 1.12**) was the first irreversible, propargylamine-based MAO-B inhibitor approved by the FDA for the management of PD (150). Its mechanism of action involves the irreversible and covalent binding to the N-5 position of the isoalloxazine moiety of FAD (153). However, selegiline is an L-amphetamine derivative, and its metabolism into L-methamphetamine and L-amphetamine leads to amphetamine-like sympathomimetic side effects (150, 153).

Based on the studies performed with selegiline, **rasagiline** (trade name Azilect®, **Figure 1.12**) was developed as an antiparkinsonian drug (153). Rasagiline, a second-generation irreversible MAO-B inhibitor approved by the FDA in 2006 (154), presents the same mechanism of action of selegiline (155). The therapeutic use of rasagiline is advantageous in comparison to selegiline (154, 155). Unlike selegiline, rasagiline is not metabolized into amphetamine-like compounds, and its main metabolite (1-aminoindan) presents neuroprotective effects (155, 156).

Although selegiline and rasagiline have been extensive used on the treatment of PD, these drugs present the drawbacks associated with irreversible enzyme inhibition. These include the loss of isoform selectivity due to repeated drug administration, potential immunogenicity associated to the formation of N(5)-flavocyanine adducts, and inhibition independent of variations in the substrate concentration (148, 157, 158). Moreover, the recovery of irreversible enzyme inhibition after drug withdrawal is slow, requiring *de novo* biosynthesis of the enzyme (157-159). In the human brain, the turnover rate for the biosynthesis of MAO-B is close to 40 days (157, 158).

On the other hand, reversible inhibition allows the enzyme recovery with inhibitor elimination, decreases the risk of selectivity loss due to the shorter duration of action and, in the case of competitive inhibitors, the enzyme inhibition is relieved as the substrate concentration increases (157-159). Therefore, reversible MAO-B inhibitors have been developed to avoid the disadvantages associated with irreversible inhibition (148).

Safinamide (trade name Xadago®, **Figure 1.12**), a reversible and selective MAO-B inhibitor, was recently approved as an add-on therapy to L-DOPA alone or in combination with other antiparkinsonian drugs in mid- to late-stage PD patients (58, 160, 161). In addition to MAO-B inhibition, safinamide blocks dopamine reuptake, and inhibits excessive glutamate release through the blockade of voltage-dependent sodium channels and the modulation of *N*-type calcium channels (147, 149, 160). Therefore, safinamide is a multitarget drug, acting in multiple pharmacological targets present in both dopaminergic and glutamatergic systems (161, 162).

1.2.1.2.3. Catechol-O-methyltransferase

Catechol-*O*-methyl transferase, a magnesium-dependent enzyme, catalyses the regioselective transfer of an activated methyl group from S-adenosyl-L-methionine (SAM) on one hydroxyl of the catechol substrate (**Figure 1.13**) (163, 164). The corresponding mono-*O*-methyl ether of the catechol substrate and S-adenosyl-L-homocysteine (SAH) are the end-products of this reaction (163).

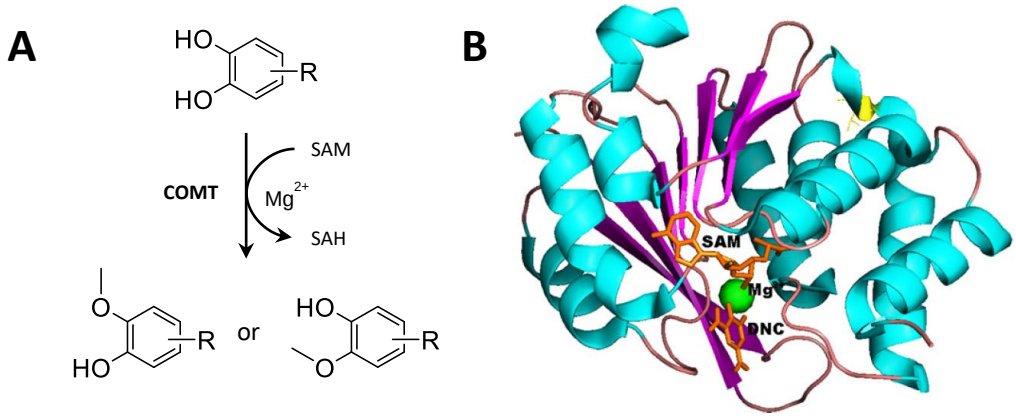


Figure 1.13: (A) Schematic representation of COMT-catalysed methyl group transfer to a catechol substrate. (B) Crystal structure of soluble COMT (PDB ID: 108V). Adapted from (163, 165).

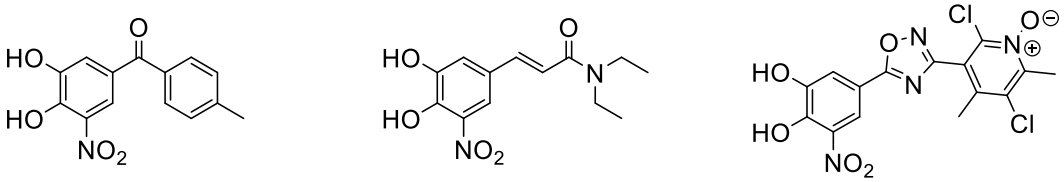
Catechol-*O*-methyl transferase exists in two forms, soluble COMT (S-COMT) and membrane-bond COMT (MB-COMT), both of which are encoded by the same gene located on chromosome 22q11.2 (165, 166). Soluble COMT is present in the cytosol, while MB-COMT is anchored to the rough endoplasmic reticulum (167). The only structural difference between the two forms is the inclusion of additional 50 hydrophobic amino acids at the *N*-terminus of MB-COMT for membrane anchoring (165). The dominant form in most tissues is the S-COMT, with the highest levels found in the liver and kidney (167), with the only exception being the human brain, in which 70 % is MB-COMT (166). Although these isozymes exhibit identical amino acid sequences at the catalytic site, they show marked differences in their kinetic behaviour that determine their physiological role (168). In particular, MB-COMT displays a higher substrate affinity (low K_M) than S-COMT and is primarily involved in the termination of catecholaminergic neurotransmission at low physiological levels of catecholamines (169). On the other hand, S-COMT presents a higher capacity (high V_{max}) than MB-COMT, and is more relevant when a higher metabolic rate is required, such as when the concentrations of endogenous and exogenous catechols suddenly increase (169, 170).

Catechol-*O*-methyl transferase has received considerable attention due to its involvement in the metabolism of L-DOPA (171). Given adjunctively with L-DOPA, COMT inhibitors decrease L-DOPA premature inactivation, prolonging its half-life and improving its delivery to the brain (171, 172). In addition, COMT inhibitors enable a decrease in both dose and administration frequency of L-DOPA, reducing "off" time and increasing "on" time, thereby improving and prolonging the clinical response to L-DOPA (172). Inhibitors of peripheral and cerebral COMT were developed and are available for the adjunctive treatment of PD (126). Peripheral COMT inhibition decreases the systemic decomposition of L-DOPA, but COMT inhibition in the CNS has the additional advantage of decreasing the metabolism of both L-DOPA and DA in the brain (126).

1.2.1.2.4. Catechol-O-methyltransferase inhibitors

Following the first purification and characterization of COMT in the late 1950s, several classes of COMT inhibitors were identified. "First generation" COMT inhibitors were mainly based on catechol or a pyrogallol motifs and presented moderate potency (173), poor bioavailability and short duration of action (174). In the search for new COMT inhibitors, "second generation" inhibitors were developed, showing improved pharmacokinetic profiles compared to those of the first-generation inhibitors. Second generation COMT inhibitors remain useful drugs in adjunctive treatments of PD (168).

Clinically relevant COMT inhibitors include tolcapone, entacapone and opicapone (**Figure 1.14**), all of which share a nitrocatechol pharmacophore (168). Nitrocatechols are poor enzyme substrates despite the presence of the same catechol binding motif of COMT substrates (171, 173). The electron-withdrawing nitro group significantly decreases the pK_a value of the neighbouring hydroxyl group, thereby reducing the extent of *O*-methylation of the resulting phenolate (167, 168, 171). Nitrocatechols are reversible tight-binding inhibitors, acting competitively with respect to the catechol substrate and uncompetitively with respect to the co-substrate SAM (173).



Tolcapone Entacapone Opicapone

Figure 1.14: FDA-approved MAO-B inhibitors for Parkinson's disease. Adapted from (57).

Tolcapone (trade name Tasmar®, **Figure 1.14**) is a non-selective COMT inhibitor acting in both cerebral and peripheral COMT, although it presents limited brain penetration (brain to plasma ratio up to 0.01) (164, 175, 176). Tolcapone is more potent and has a longer duration of action than entacapone, but it has been associated with severe hepatotoxicity (173, 176, 177). As a result, its clinical use requires careful monitoring of liver function and is restricted to patients who failed to respond to peripherally acting inhibitors (126, 175).

Entacapone (trade name Comtan®, **Figure 1.14**) is a selective, peripherally acting COMT inhibitor (178). Unlike tolcapone, entacapone is not associated with hepatotoxicity and represents the drug of choice due to its satisfactory safety and tolerability (172, 179). However, entacapone requires frequent administrations, as a result of its short half-life and its low-to moderate oral bioavailability that decrease its clinical efficacy (172, 180-182).

Recently, **opicapone** (trade name Ongentys®, **Figure 1.14**) was approved as adjunctive therapy to L-DOPA in PD patients with end-of-dose motor fluctuations (183). Opicapone is a long-acting, peripherally selective COMT inhibitor (179) that presents a more sustained enzyme inhibition than tolcapone and entacapone (184). Opicapone also presented favorable safety and tolerability profiles, with no dose relationship for most of the treatment-emergent adverse events (179, 183, 185).

The inhibition of peripheral COMT has been associated with gastrointestinal and hepatic adverse effect (177, 186). Therefore, considerable efforts have been made to develop safer CNS-active COMT inhibitors, which may have great therapeutic potential towards neurological disorders resulting from catecholamine depletion (170, 182).

1.2.2. Targeting oxidative and nitrosative stress

1.2.2.1. Oxidative and nitrosative stress

The preservation of the cellular redox homeostasis is imperative to maintain the normal cellular functions and the cell survival (25). In living organisms, redox homeostasis is maintained as a balance between the levels of pro-oxidants and antioxidants (187). However, age, genetic and environmental factors contribute to a transient and sustained imbalance between oxidants and antioxidants at tissue, cell or organelle level, with consequent molecular damage and/or disturbance of redox signalling. The deregulation of redox homeostasis in favour to the pro-oxidants, commonly known as oxidative stress (188, 189), has been associated with the development of numerous pathological conditions such as diabetes, cancer, atherosclerosis, cardiovascular diseases and NDs (190).

Reactive species (RS) such as reactive oxygen species (ROS) and reactive nitrogen species (RNS) are oxidants generated in biological systems as by-products of aerobic metabolism, and through enzymatic (e.g. nicotinamide adenine dinucleotide phosphate (NADPH) oxidase (NOX), cytochrome P450, xanthine oxidase (XO), cyclooxygenase (COX), MAOs) and non-enzymatic processes (e.g.: autoxidation of endogenous and exogenous molecules) (191-193).

The biological effects of RS are dependent of their concentrations (194). On the one hand, they fulfil crucial regulatory functions at low and carefully controlled concentrations, such as cell signalling, immune responses, smooth muscle relaxation, cell differentiation, cell proliferation, and regulation of blood pressure (187, 194). On the other hand, an uncontrolled elevation of RS levels increases the risk of cellular damage due to their high reactivity towards biological molecules (proteins, lipids, carbohydrates, nucleic acids) (195).

Common RS known to participate in the redox state comprise both free radicals (e.g.: superoxide ($O_2^{\bullet-}$), hydroxyl radical ($HO^{\bullet}$), nitric oxide ($NO^{\bullet}$)) and non-free radical molecules (e.g.: hydrogen peroxide (H_2O_2) and peroxynitrite (NO_3^-)) (190).

Reactive oxygen species are generated from the partial reduction of molecular oxygen (O_2) (196) (**Figure 1.15**). Superoxide ($O_2^{\bullet-}$) may be formed by several oxidases (e.g. NOX, XO, COX) or during the oxidative phosphorylation that occur in mitochondria (197). Although $O_2^{\bullet-}$ is not considered a strong oxidizing agent, it presents potential toxicity (198). For instance, $O_2^{\bullet-}$ can oxidize iron-sulfur clusters in proteins, leading to cluster degradation and loss of the catalytic iron and hence enzymatic activity (198). However, $O_2^{\bullet-}$ is unable to cross cell membranes due to the negative charge and has a relatively short half-life; therefore, $O_2^{\bullet-}$ acts at the site of its generation (25, 198). Considered the “primary” ROS, $O_2^{\bullet-}$ generates “secondary” RS after interacting with other molecules (191, 199).

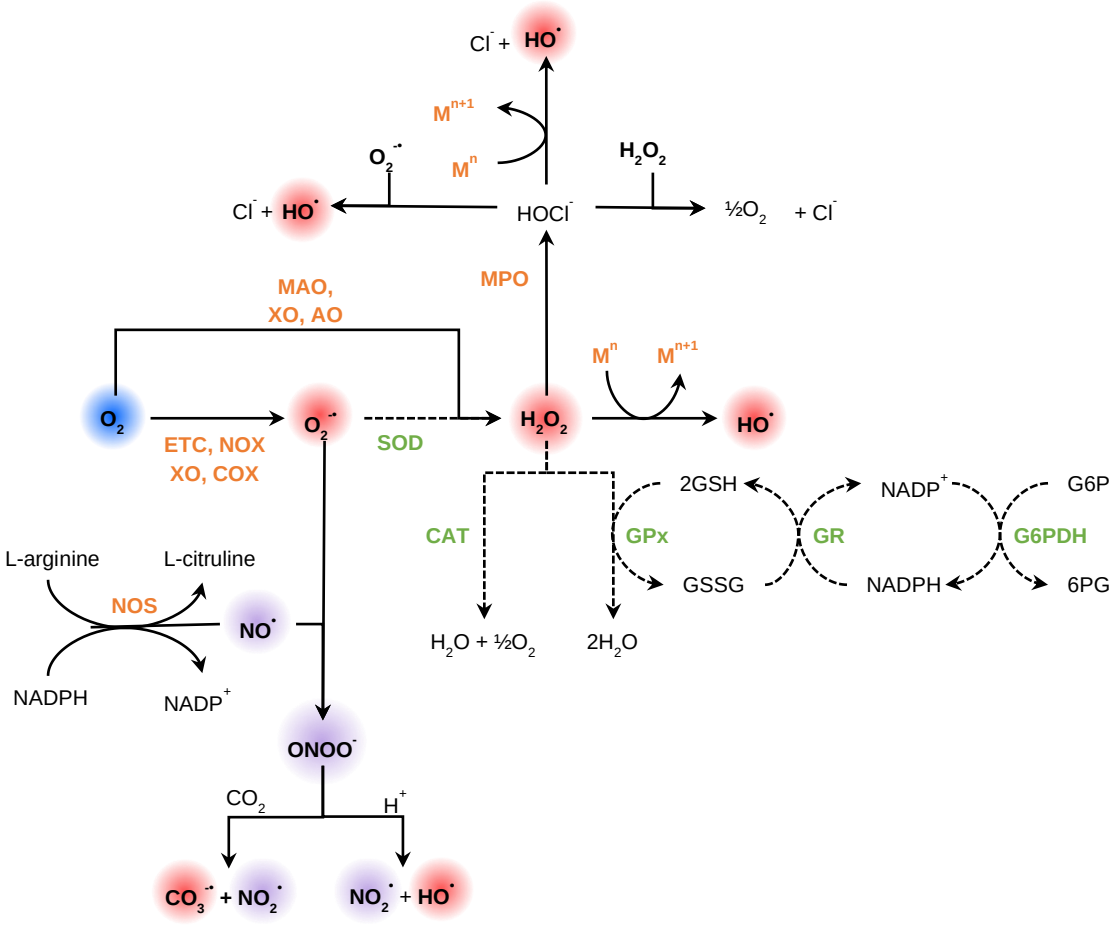


Figure 1.15: Formation of ROS (red) and RNS (purple) and their elimination by enzymatic antioxidant systems (dashed line). Adapted from (195).

Hydrogen peroxide may be produced by dismutation of $O_2^{\bullet-}$ that may occur either spontaneously or catalysed by superoxide dismutases (SODs) (**Figure 1.15**) (200, 201). Moreover, H_2O_2 is generated by two electron transfer to molecular oxygen mediated by oxidoreductases (e.g.: MAOs, aldehyde oxidase, XO) (197, 201, 202). Contrary to $O_2^{\bullet-}$, H_2O_2 can cross biological membranes and reach other cellular compartments (198). Hydrogen peroxide may react with transition metals (copper, iron) via Fenton reaction yielding the highly reactive $HO^{\bullet}$ radical (199). This radical is considered the main instigator of oxidative damage, reacting non-discriminately at the site of its generation with biomolecules (nucleic acids, proteins, lipids, carbohydrates) (197, 203).

Neuronal, endothelial and inducible isoforms of nitric oxide synthase (NOS) catalyse the formation of $NO^{\bullet}$ from L-arginine (**Figure 1.15**) (204). This RNS is an important biological signalling molecule, playing crucial roles in neurotransmission, vasodilation, smooth muscle relaxation and regulation of the immune response (187, 205). Most of toxic effects of $NO^{\bullet}$ are not directly associated to $NO^{\bullet}$ itself but rather to $ONOO^-$, the product of

the reaction between $O_2^{\bullet-}$ and $NO^{\bullet}$ (206). Peroxynitrite is a strong oxidant that covalently interacts with all biological molecules (197). For instance, $ONOO^-$ induces lipid peroxidation, protein oxidation and nitration, and DNA oxidation and fragmentation (206, 207). Since both $NO^{\bullet}$ and $ONOO^-$ are relatively long-lived diffusible RNS, the oxidative damage may occur at relatively long distances (71). The decomposition of $ONOO^-$ also leads to the formation of other RS (71, 198).

1.2.2.2. Antioxidant defences

The exposure of biological systems to the deleterious effects of RS triggers the activation of the antioxidant defence system (208). To control the cellular levels of RS, antioxidants may act in three different lines of defence through diverse mechanisms (187, 206, 209). Preventative antioxidants constitute the first line of defence by preventing the formation of new RS without being consumed in the reaction. These include enzymes such as SODs, catalase (CAT) and glutathione peroxidase (GPx), and proteins that sequester transition metal ions (e.g.: ferritin, ceruloplasmin, transferrin and albumin) (197, 208, 210). On the other hand, the second line of defence includes antioxidants that are consumed in the reaction following the inactivation of RS and oxidants, thus preventing chain initiation reactions and/or terminating chain propagation reactions. These include chain-breaking antioxidants, iron chelators and singlet oxygen quenchers such as vitamins C and E, glutathione and phenolic compounds (197, 208). Finally, the third line of defence is composed of enzymes that repair or remove damaged biomolecules following oxidative damage, such as lipases, proteases, DNA repair enzymes and transferases (208-210).

The antioxidant defence system consists of endogenous and exogenous antioxidants. Endogenous antioxidants are produced in the human body and are classified as enzymatic (e.g.: SODs, CAT, GPx) or non-enzymatic (e.g.: coenzyme Q10, biothiols such as glutathione and α-lipoic acid, proteins such as albumin, ceruloplasmin an transferrin) (211) (**Figure 1.16**). Exogenous antioxidants are obtained from dietary sources or supplements and include, among others, vitamins (e.g.: Vitamin C, Vitamin E), phenolic compounds and synthetic antioxidant drugs (211). Endogenous and exogenous antioxidants act synergistically to preserve or restore the cellular redox homeostasis (208).

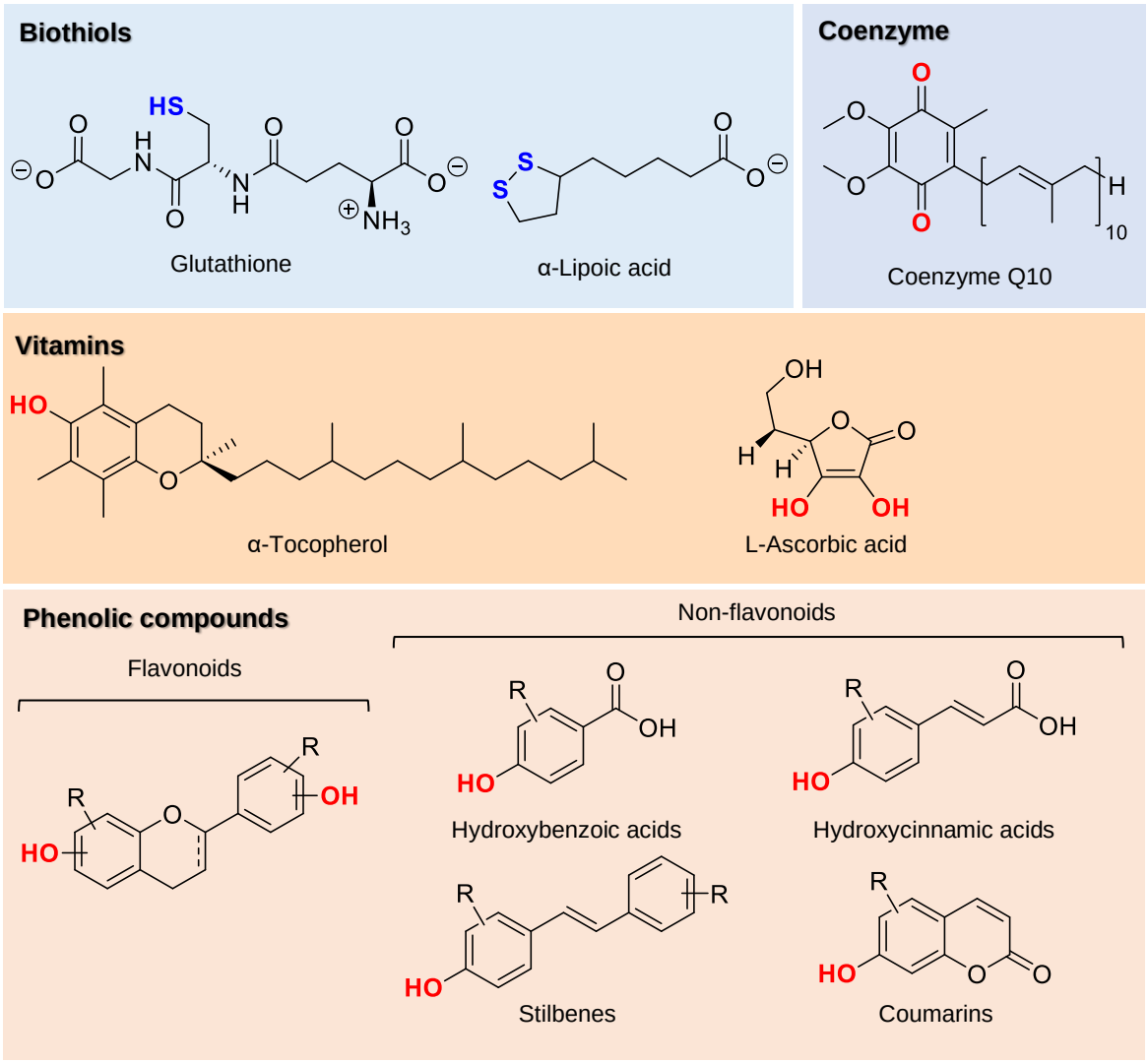


Figure 1.16: Representative examples of endogenous (blue) and exogenous (orange) non-enzymatic antioxidants.

The first-line enzymatic defences comprise three important enzymes that act together to prevent the formation or neutralize RS: SODs, CAT and GPx (**Figure 1.15**) (208, 212). First, SOD catalyses the dismutation of $O_2^{\bullet-}$ into H_2O_2 and O_2 mitigating the deleterious effects of $O_2^{\bullet-}$ (213). Then, CAT mediates the conversion of H_2O_2 into water and O_2 preventing the formation of $HO^{\bullet}$ radicals (212). Glutathione peroxidase catalyses the reduction of peroxides into non-toxic molecules using reduced glutathione (GSH) as a reducing agent (212, 213). Other enzymes do not directly neutralize RS, but may provide co-substrates to the first-line enzymes (e.g.: glutathione reductase (GR), glucose-6-phosphate dehydrogenase (G6PDH)) (211) or may be involved in the detoxification of RS (e.g.: glutathione-S-transferase (GST)) (212).

Biologically-derived thiols, or **biothiols**, represent a class of organic sulfur derivatives having a sulfhydryl (SH) functional group (214) ubiquitously distributed in

biological systems (215). Common biothiols found in living organisms include glutathione, cysteine, homocysteine, α-lipoic acid and coenzyme A (216). Since biothiols have negative standard reduction potentials (e.g.: $E^0_{GSSG,\ GSH}$ = -0.23 V; $E^0_{CYSS,\ CYS}$ = -0.34 V), they act as reducing agents (217). In fact, they have a pivotal role in redox homeostasis, due to their ability to neutralize reactive species under oxidative stress conditions (217). The resulting thyil radicals ($RS^{\bullet}$) recombine to form the corresponding disulphide (R-S-S-R) (217). Biothiols also participate in other redox-mediated or redox-regulated processes in cells, such as protein synthesis, redox-sensitive signal transduction, cell growth and proliferation, regulation of programmed cell death, xenobiotic metabolism, and immune regulation (215).

Glutathione (**Figure 1.16**), a tripeptide composed of glutamate, cysteine and glycine (214, 216), is the most common biothiol and is found in high concentrations in prokaryotic and eukaryotic cells (216). Glutathione can directly scavenge ROS and regenerate tocopherol and ascorbic acid into their active forms. Glutathione is also a cofactor of several antioxidant enzymes (e.g.: GPx, GST) (206). The ratio of reduced (GSH) and oxidized (GSSG) glutathione is an indicator of cellular health (218, 219). Under normal conditions, the concentration of the GSH redox couple in mammalian cells range between 1 and 10 mM (218). The most prevalent form is the reduced form (GSH), with GSH/GSSG exceeding 100:1 (218, 219). However, this ratio decreases with aging and is considerably reduced in NDs such as AD and PD (219).

Alpha-lipoic acid (**Figure 1.16**) is a disulphide derivative of octanoic acid (199). Due to its solubility in both water and lipophilic systems, α-lipoic acid is widely distributed in cellular membranes, cytosol and extracellular space (220). Aside from its role as a cofactor of mitochondrial enzymes (e.g.: α-ketoglutarate dehydrogenase, pyruvate dehydrogenase) (199, 221), α-lipoic acid and its reduced form (dihydrolipoic acid) act as antioxidants by scavenging RS, chelating transition metals and directly or indirectly regenerating other antioxidants into their reduced form (e.g.: glutathione, ubiquinol, and vitamins C and E) (220, 222).

Coenzyme Q10 (**Figure 1.16**) is an endogenously produced lipid-soluble benzoquinone, which contains a hydrophobic polyisoprenoid side chain that provides stability to the molecule inside the phospholipid membranes (223, 224). It is an essential component of the mitochondrial electron transport chain (ETC) and protects cell membranes and plasma lipoproteins from oxidative damage (223, 224). The reduced form of coenzyme Q10 (ubiquinol) acts by scavenging lipid radicals and lipid peroxyl radicals and by regenerating tocopheroxyl radicals into tocopherol (197, 225).

Vitamin E is a general term representing chemically related compounds classified into tocopherols and tocotrienols (226). Structurally, they contain a chromanol head group

with antioxidant activity and a long saturated (tocopherols) or unsaturated (tocotrienols) side chain (227, 228). Alpha-tocopherol (**Figure 1.16**) is the most important form of vitamin E in humans (229). Vitamin E is considered the most potent hydrophobic antioxidant *in vivo* and protects lipidic structures (e.g.: cell membranes, lipoproteins) from oxidative damage (225, 229). It acts as a chain-breaking antioxidant by donating its phenolic hydrogen to peroxyl radical, leading to the formation of tocopheroxyl radicals that are unable to continue the lipid peroxidation (225, 226).

Vitamin C (L-ascorbic acid, **Figure 1.16**) is an important hydrophilic antioxidant that scavenges a diverse array of RS in biological media, such as $O_2^{\bullet-}$, H_2O_2, $HO^{\bullet}$ and $NO^{\bullet}$ (230). Moreover, it acts synergistically with vitamin E in the protection of lipidic structures from peroxidation. L-ascorbic acid regenerates the membrane-bound tocopheroxyl radicals into the reduced form, thus restoring its antioxidant properties (231). In cells, L-ascorbic acid is maintained in the reduced form by glutathione (227).

Phenolic compounds (**Figure 1.16**) are one of the most important groups of exogenous antioxidants obtained from the human diet, being commonly found in fruits, vegetables, grains, cereals and other plant-derived products (221, 232). Phenolic compounds represent a heterogeneous group of phytochemicals containing at least one hydroxyl group (233), being currently classified according to their structure into and flavonoids and nonflavonoids (e.g.: hydroxybenzoic acids, hydroxycinnamic acids (HCAs), stilbenes and coumarins) (221, 234). The antioxidant properties of phenolic compounds are associated with different mechanism of action, namely direct scavenging of RS, chelation of redox-active transition metals (e.g.: copper, iron), enhancement of the production of endogenous antioxidants (e.g.: SOD, glutathione), and inhibition or RS-generating enzymes (e.g.: NOX, COX) (233, 234).

1.2.2.3. Oxidative stress in Alzheimer's and Parkinson's diseases

Oxidative stress is one of the major contributors to the pathogenic cascade that leads to neurodegeneration in AD and PD (235, 236). Constant evidences of RS-mediated injury were observed in AD and PD brains. For instance, increased levels of oxidative markers and damaged cell components were detected in patients with AD and PD (188). A decline on the pool of endogenous antioxidants and a decrease on the activity of antioxidant enzymes were also reported (29, 237).

The brain is particularly prone to oxidative stress-induced damage. Although the brain constitutes only ~ 2 % of the total body weight, it is responsible for more than 20 % of the body oxygen consumption, with a significant amount of oxygen being converted into ROS (236, 238, 239). Despite this massive oxygen consumption, the brain presents a lower

content in endogenous antioxidants (e.g: glutathione, catalase) in comparison to other tissues, thus being more sensitive to cellular redox dyshomeostasis (238, 240). In addition, redox-active metals (e.g.: iron, copper) accumulate in specific regions of the brain and catalyse the formation of RS (236, 241). Finally, the high levels in polyunsaturated fatty acids in the brain increases the susceptibility to lipid peroxidation and subsequent formation of toxic compounds (236, 238).

The increased oxidative and nitrosative stress in NDs is strictly connected to other pathological events, namely mitochondrial dysfunction, dopamine oxidation, neuroinflammation and Aβ production and accumulation (**Figure 1.17**) (19).

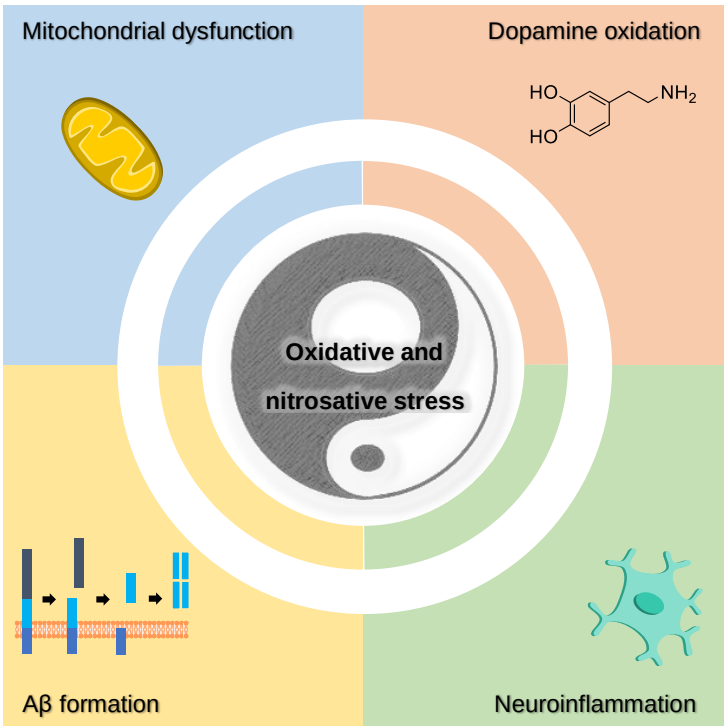


Figure 1.17: Pathological events of neurodegenerative diseases associated with increased oxidative stress.

Although RS are generated in several cellular compartments, **mitochondria** is one of the main sources of ROS in the majority of cell types (242). In fact, the formation of ROS in mitochondria occurs primarily at the ETC present in the inner mitochondrial membrane (**Figure 1.18**) (236, 243). The mitochondrial ETC consists of a series of membrane-bound complexes (complexes I, II, III and IV) (244), which generate a proton gradient across the inner mitochondrial membrane through electron transfers, leading to the production of ATP by ATP synthase (complex V) (236). Metabolic intermediates formed during the Krebs cycle are used for the oxidative phosphorylation (245). During the ETC, a small proportion of electrons occasionally leak and directly reduce O_2 to $O_2^{\bullet-}$ (245, 246), which in turn is

converted into other ROS such as H_2O_2 and $HO^{\bullet}$ (242). The formation of $O_2^{\bullet -}$ occurs mainly in complexes I and III (246, 247). Enzymes from the Krebs cycle (e.g.: α-ketoglutarate dehydrogenase, pyruvate dehydrogenase, aconitase) may also generate ROS (247, 248).

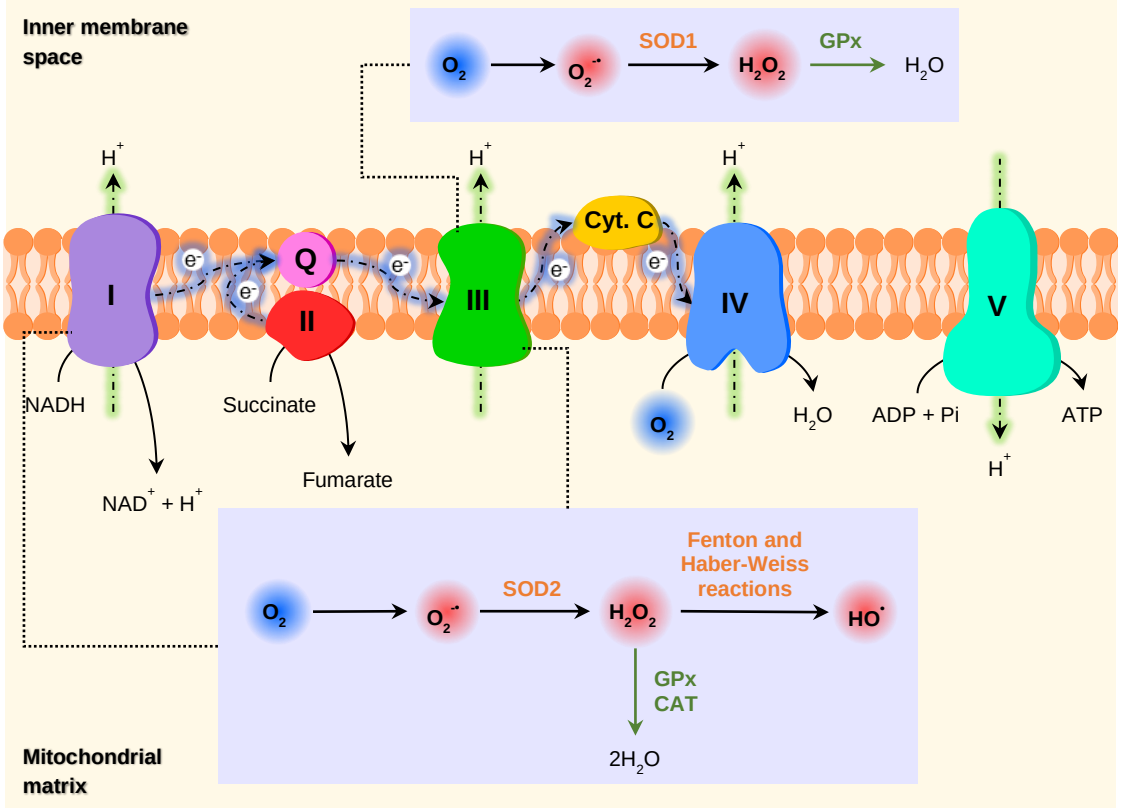


Figure 1.18: Formation of ROS in mitochondria. Adapted from (244, 249).

Mitochondrial ETC is one of the primary targets of the harmful effects of ROS (244, 250). The oxidative damage of the mitochondrial ETC leads to the inhibition of ATP synthesis and to the increased production of ROS in a vicious and detrimental cycle, contributing for cell dysfunction and cell death (243, 250, 251). Mitochondria contain other components susceptible to oxidative damage, namely several iron-sulfur centers, proteins and unsaturated fatty acids in the inner membrane, and mitochondrial DNA (mtDNA), all of which are important for proper mitochondrial function (243). Considering that mtDNA encodes the some of the subunits of the complexes that constitute the ETC, the oxidative damage of mtDNA leads to the defective production of these proteins and subsequent mitochondrial dysfunction (250).

Since neurons have limited glycolytic capacity, they are particularly dependent of mitochondrial oxidative phosphorylation to meet their high energy requirements (251-253). In addition to ATP synthesis, mitochondria are involved in other crucial cellular functions

such as the synthesis of amino acids and steroids, β-oxidation of fatty acids, Ca^{2+} homeostasis and regulation of apoptotic cell death (254). Therefore, improper mitochondrial function compromises neuronal survival and contribute to neurodegeneration (248, 254)

In PD, **DA oxidation** is associated to the selective vulnerability of dopaminergic neurons to oxidative stress (249). Despite the essential role of DA in neurotransmission, DA contains a catechol group that may participate in the generation of ROS and metal chelation (255). Dopamine is normally stored into monoaminergic vesicles under a low pH environment that prevents its oxidation (256). However, DA may undergo enzymatic and non-enzymatic decomposition in the cytosol, which is accompanied by the formation of ROS (**Figure 1.19**) (257).

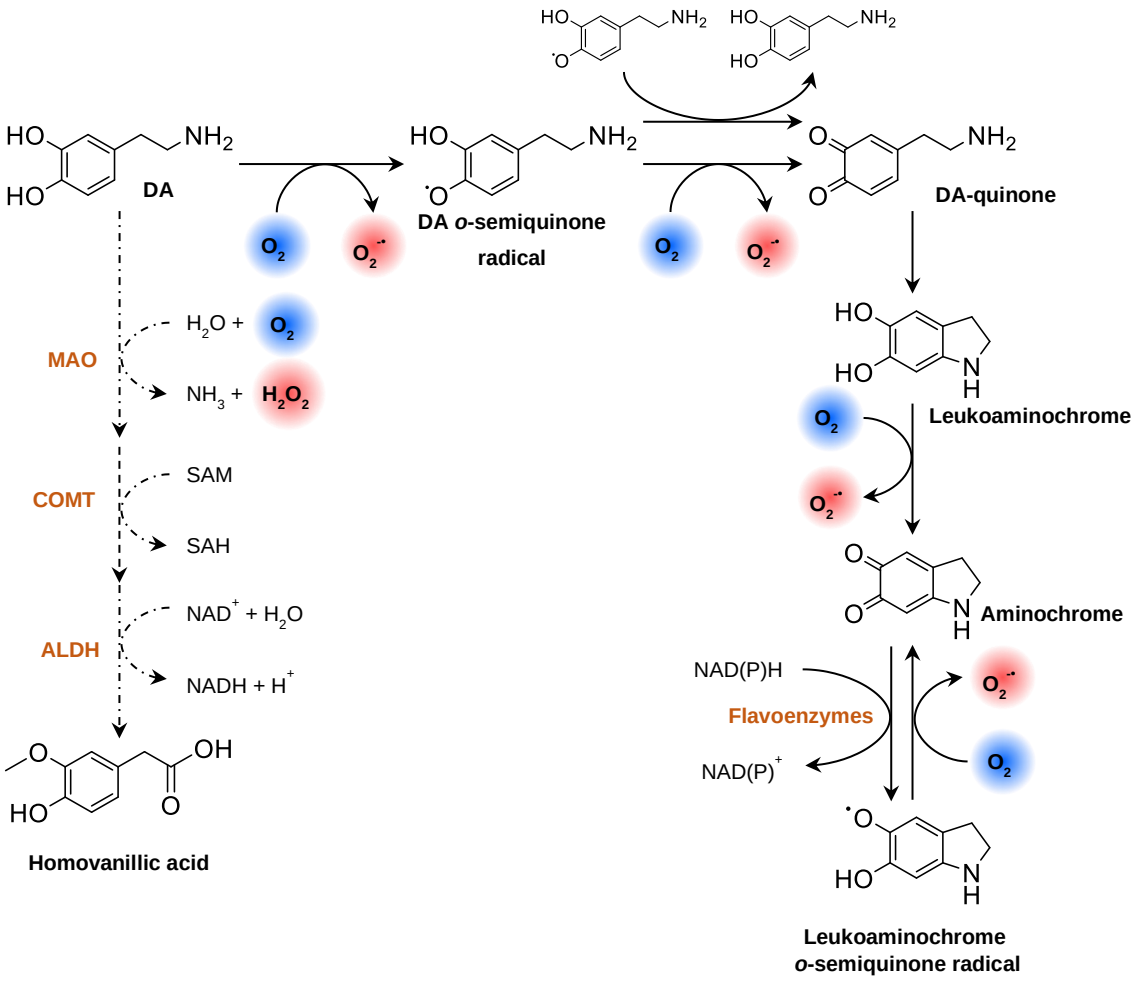


Figure 1.19: Generation of ROS during enzymatic (dashed line) and non-enzymatic (plain line) DA decomposition. Adapted from (258).

In the presence of O_2, DA generates $O_2^{\bullet-}$ and electron-deficient DA semiquinones and DA quinones (**Figure 1.19**) (257, 259, 260). The reaction rate of DA semiquinone

formation is slow, but it is accelerated by redox-active transition metals (240). The spontaneous cyclization of DA quinone yields leucoaminochrome whose further autoxidation forms aminochrome and $O_2^{\bullet-}$ (259). Aminochrome participates in redox-cycling reactions that results in the formation of $O_2^{\bullet-}$ and in the depletion of cellular nicotinamide adenine dinucleotide (NADH) and NADPH (261). Dopamine quinone and aminochrome also form adducts with cellular nucleophiles modifying their function (262, 263). These include DNA, biothiols (e.g.: glutathione), α-synuclein and proteins involved in ATP synthesis (complexes I, III and V of the ETC), proteasomal degradation (parkin), microtubule stabilization (α- and β-tubulin) and axonal transport (actin) (258). Therefore, the formation of these adducts contributes to mitochondrial dysfunction, impairment of the axonal transport, inhibition of the proteasomal system, disruption of cytoskeleton architecture and formation of α-synuclein aggregates (258, 261). Aminochrome also polymerizes into neuromelanin, a brain pigment that contributes to neurodegeneration by triggering neuroinflammatory processes (236).

The oxidative deamination of DA by MAOs uses O_2 and generates H_2O_2 and ammonia as by-products (**Figure 1.19**) (264). Due to the increased expression with age in neuronal tissue (148, 265), MAO-B becomes the predominant isoform involved in DA metabolism (236). Monoamine oxidase B is mainly found in glial cells (151, 266), but the H_2O_2 produced during DA deamination can permeate cell membranes and induce toxic effects in the neighbouring neurons (236). In fact, compared with astrocytes, neurons are more vulnerable to H_2O_2 due to the lower content in antioxidants involved in its detoxification (e.g.: GPx and glutathione) (266). The H_2O_2 generated from MAO-B activity in astrocytes is also associated with increased amyloid plaque deposition (158).

Neuroinflammation represents a set of inflammatory processes occurring in the central nervous system that involve the action of glial cells in CNS (microglia, oligodendrocytes, astrocytes), non-glial resident myeloid cells (macrophages and dendritic cells) and peripheral leukocytes (267, 268). Neuroinflammation plays an important role in the progression of NDs (257). For instance, in AD, microglia are activated by the presence of Aβ and co-localize with the plaques (269). However, instead of efficiently remove the Aβ deposits, microglia releases pro-inflammatory mediators that lead to neuronal damage (270). In NDs, the expression of NOX and inducible NOS in activated microglia and reactive astrocytes is increased, resulting in the excessive formation of $O_2^{\bullet-}$ and $NO^{\bullet}$ (257, 271). The activation of RS-producing enzymes in glial cells is associated to neurotoxic effects, which arise not only from the direct oxidative damage in neurons, but also from the intracellular redox signalling that exacerbate the pro-inflammatory response (271, 272).

The formation of **Aβ peptides** is also associated with increased oxidative stress (35). Following the amyloidogenic processing of APP, the generated Aβ can be incorporated as small oligomers into the lipid bilayer adopting an α-helical conformation (273, 274). This conformation enables the interaction between the sulfur atom of Met-35 and the carbonyl oxygen of Ile-31, which increases the vulnerability of Met-35 to one-electron oxidation and subsequent formation of sulfaranyl radicals ($MetS^{\bullet}$) (273, 274). The generated $MetS^{\bullet}$ can in turn abstract an allylic hydrogen atom from the unsaturated acyl chains of lipid molecules, thus initiating lipid peroxidation processes (35, 222).

In addition to the extracellular formation, Aβ accumulate within the cells after the amyloidogenic processing of APP at the organellar membrane where the APP is localized (38, 275). Intracellular Aβ binds to mitochondrial membranes and affects mitochondrial function and dynamics, leading to an increased formation of ROS, impairment of the ETC chain, decreased ATP synthesis, dysregulation of Ca^{2+} homeostasis and loss of synaptic functions (27, 38, 275).

Amyloid beta also coordinates with redox-active transition metals such as copper and iron (28). The resulting complexes may generate H_2O_2 and $HO^{\bullet}$ through Fenton-like reactions and oxidized, cross-linked forms of Aβ with higher tendency to aggregate (28, 199, 271).

1.2.2.4. Antioxidant therapy for neurodegenerative diseases: an overview

Considering the involvement of oxidative and nitrosative stress in the pathophysiology of NDs, the rationale of using exogenous antioxidants to delay, prevent or remove the oxidative damage is clear (222, 239). In fact, several antioxidants showed promising results in animal and cellular models (238, 239). However, the results obtained in clinical trials were inconclusive, negative or showed little benefit in NDs (211). Numerous factors contribute to the discrepancy between pre-clinical and clinical results. In addition to aspects associated to the design of clinical trials (e.g.: posology, duration of treatment, age and disease stage of the patients), most of known dietary antioxidants display poor bioavailability and are unable to cross the BBB, affecting their delivery into the brain (211, 238, 239, 276).

A common strategy used to overcome these pharmacokinetic limitations is the introduction of minor structural modifications on the antioxidant scaffold. The resulting derivatives may improve the drug-like properties while preserving or enhancing the antioxidant profile of the parent compounds (277-280).

Aside from the pharmacokinetic constraints, the lack of clinical efficacy of antioxidants may also result from the uniform distribution of antioxidants across all tissues and organs following administration, with only a small fraction being taken up by mitochondria (211, 281, 282), the main source and the target of ROS. Therefore, the development of antioxidants that selectively accumulate within mitochondria and tackle the oxidative damage is of particular interest (283, 284). Compounds lacking mitochondriotropism but with relevant biological activities towards mitochondrial targets usually need to be directed to mitochondria (285). In this sense, several approaches were developed to deliver antioxidants and other bioactive molecules to mitochondria, but one of the most widely used is their conjugation with lipophilic cations such as triphenylphosphonium (TPP) (243, 284, 286).

Lipophilic TPP cations can diffuse across phospholipid bilayers because their positive charge is surrounded and dispersed over a large hydrophobic surface area, which decreases the activation energy for membrane permeation (287-289). In response to the plasma and mitochondrial membrane potentials ($\Delta\Psi_{plasma}$ and $\Delta\Psi_{mitochondria}$, respectively), these compounds accumulate within the mitochondrial matrix against the concentration gradient (289, 290) (**Figure 1.20**). Assuming a Nernstian behaviour, the accumulation of lipophilic TPP cations increases ten-fold for every ~60 mV increase in membrane potential (291). Accordingly, the $\Delta\Psi_{plasma}$ enables a 3 to 10-fold accumulation of the compounds in the cytosol ($\Delta\Psi_{plasma}$= -30 to -60 mV) (249, 288). Then, TPP conjugates are taken up from the intracellular space to the mitochondrial matrix in response to the $\Delta\Psi_{mitochondria}$ (-140 to -160 mV), leading to 100 to 500-fold accumulation within the mitochondrial matrix (249, 288).

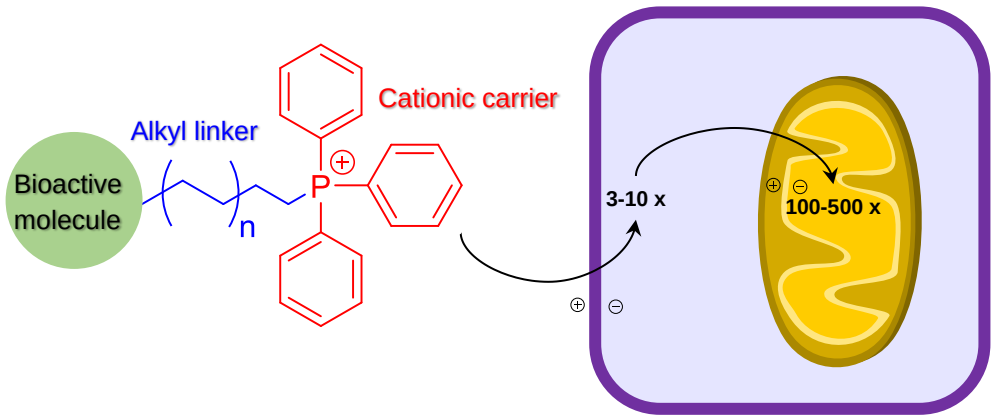


Figure 1.20: Mitochondrial uptake of lipophilic triphenylphosphonium cations. Adapted from (287, 292).

The increased accumulation of lipophilic TPP conjugates enhances the compounds' potency and decreases the external dose required, limiting extramitochondrial metabolism that result in inactivation, excretion or toxicity (243, 293). However, the extensive accumulation of these compounds within the mitochondrial matrix can disrupt membrane integrity and thereby compromise cellular respiration and ATP production (281, 294).

Over the last decades, low molecular weight antioxidants such as coenzyme Q10, vitamin E and phenolic acids served as basis for the development of mitochondria-targeted antioxidants (295-300). These compounds can diffuse across the biological membranes and concentrate within mitochondria more easily than the non-targeted analogues, thus protecting mitochondrial more efficiently against oxidative damage (249, 296). Following oral or intravenous administration, lipophilic TPP conjugates are rapidly taken up by the organs most affected by mitochondrial dysfunction (e.g.: liver, heart, brain) (289, 301). Therefore, targeting antioxidants to mitochondria stands out as a promising strategy in the discovery of new therapies for oxidative stress-related disorders.

1.3. Drug discovery and neurodegenerative diseases

1.3.1. Single-target and multitarget-based approaches

The available treatments for AD and PD provide valuable symptomatic relief, but only reduce the symptoms for a short period of time before the cognitive or motor functions continue to deteriorate (19). Given the lack of therapeutic efficacy of the current treatments, the use of single-target drugs may be insufficient to address the multiple pathological aspects of NDs (302, 303). Treatment of AD and PD may thus require the manipulation of several targets to restore the physiological balance and thereby attain significant therapeutic efficacy (304).

Traditionally, the "one-drug, one-target" paradigm is the mainstay drug discovery concept in the pharmaceutical industry (69, 305). This paradigm is mainly focused on generating drugs that selectively bind to single biological target, avoiding potential adverse side effects associated to mistargeting other biological entities (305, 306). However, despite the extensive research efforts, single-target drugs are insufficient to achieve satisfactory therapeutic efficacy in multifactorial diseases (306, 307). Therefore, therapeutics that simultaneously manipulate multiple targets may provide therapeutic benefits in diseases where single-target drugs failed (308).

Multitarget therapy may be attained using two approaches (308). The first approach consists in the mixture of multiple drugs acting on single targets (307, 308). This strategy enables better dose flexibility and reduced treatment costs (307). However, it may present

drawbacks associated with poor patient compliance, adverse effects resulting from drug-drug interactions, and complex and unpredictable pharmacokinetic/pharmacodynamic profiles (309). Combination drugs have been used in the symptomatic treatment of NDs and include memantine/donepezil (trade name Nazmaric®) for AD (302), and L-DOPA/carbidopa (trade name Sinemet®), L-DOPA/benserazide (trade name Madopar®) and L-DOPA/carbidopa/entacapone (trade name Stalevo®) for PD (172).

The second approach consists on use of multitarget-directed ligands (MTDLs), in which a single drug simultaneously interacts with multiple biological targets involved in the disease pathogenesis (307, 308). Multitarget-directed ligands may provide superior efficacy against advanced stage diseases compared with highly selective single-target agents (310). Well-designed MTDLs may also replace therapies based on drug combination and thereby reduce polypharmacy, leading to a more predictable pharmacokinetic profile and to decreases in treatment complexity, drug-drug interactions and drug side effects (304, 310).

Currently, NDs are in the focus of multitarget drug discovery due to their multifactorial pathophysiology (304). The most common synthetic strategies used to develop new MTDLs for NDs, with a particular emphasis in AD, were reviewed in **Manuscript IA**.

1.3.2. Blood-brain barrier in CNS drug discovery

The discovery of novel drugs for NDs remain a huge unmet medical need (311). The development of novel CNS drugs is a long and difficult process (312), presenting numerous challenges from both biological and chemical perspectives (313). The attrition rate of CNS drug is considerably high compared to other areas of drug discovery (314). This may be due to the inability of failed drugs to overcome the hurdles required to obtain viable CNS drugs, which include appropriate safety, pharmacokinetics, BBB penetration, pharmacological activity, and efficacy (312).

One of the major challenges for effective drug delivery into the brain is the BBB, the primary interface between the brain and the circulatory system (315, 316). Indeed, more than 98 % of small molecule drugs and all large-molecule therapeutics are unable to cross the BBB (316).

The BBB is a neurovascular unit consisting of capillary endothelial cells, pericytes, astrocytic foot processes, neurons, mast cells, microglia and circulating immune cells (**Figure 1.21A**) (317, 318). It has a crucial role in brain homeostasis, providing protection against harmful toxins from the blood and supplying the brain with nutrients for functioning (319). Tight junctions and adherent junctions connect the highly polarized endothelial cells and prevent paracellular diffusion (317, 318). Only small-water soluble molecules cross the

BBB through paracellular diffusion, but not at great extent (318, 320). Therefore, the exchange of molecules between the blood and the brain occurs via transcellular routes (**Figure 1.21B**) (317, 318, 321). Small lipophilic molecules and gaseous molecules (e.g.: O_2, CO_2) cross the luminal (blood-facing) and abluminal (brain-facing) membranes of endothelial cells through passive diffusion (320, 321). Capillary endothelial cells also contain specific transporter proteins involved in the influx of nutrients into the brain (e.g.: influx carriers for glucose and amino acids) or in the efflux of waste products and xenobiotics (e.g.: P-glycoprotein (P-gp)) (320, 321). Large molecules such as proteins and peptides may cross the endothelium through vesicular routes, either by receptor-mediated transcytosis or adsorptive-mediated transcytosis (320, 321).

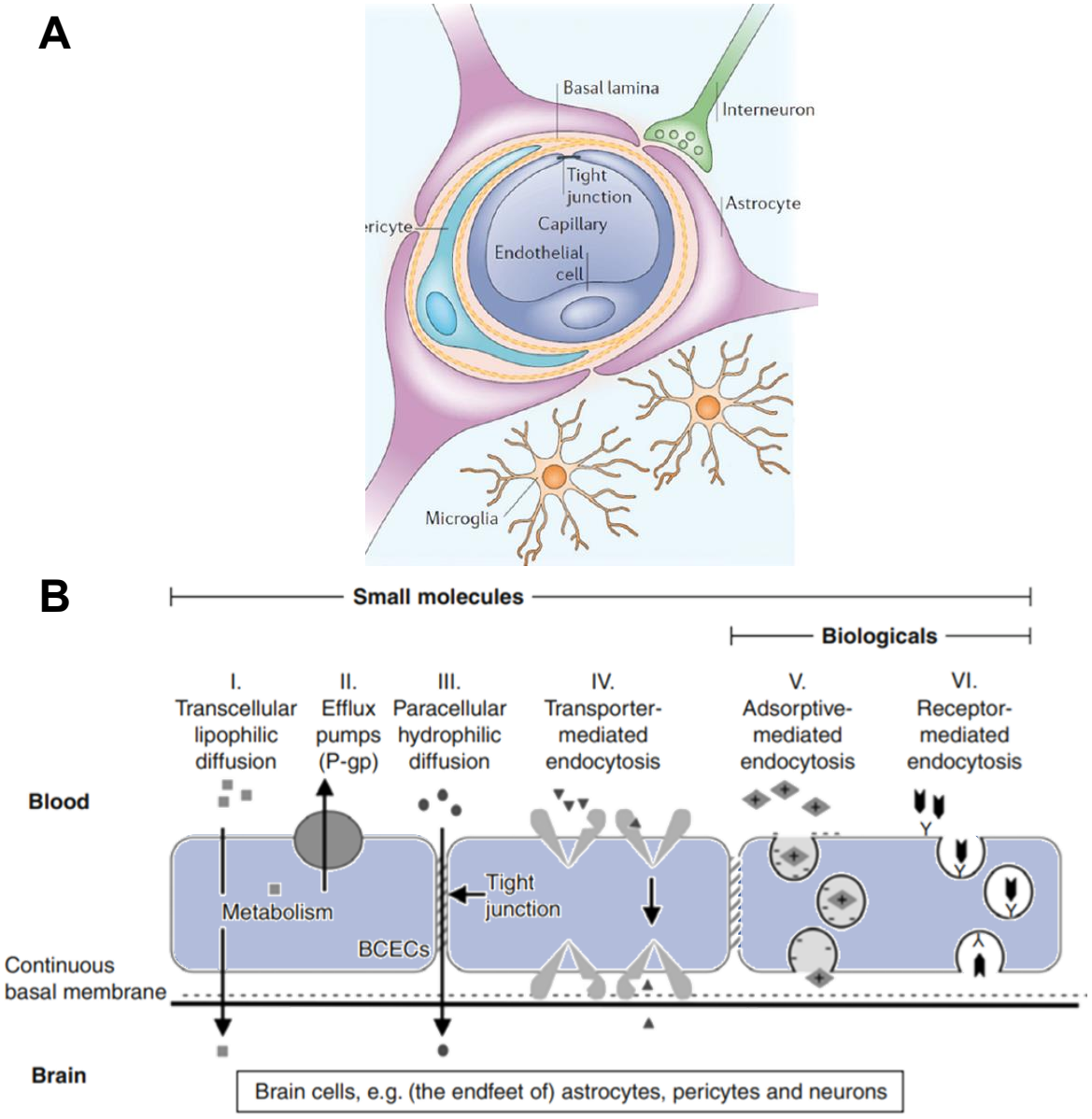


Figure 1.21: Cellular components of the blood-brain barrier (A) and the main routes of molecular trafficking (B). Adapted from (319, 322)

In CNS drug discovery, most drug candidates are small molecules designed to penetrate the BBB through transcellular passive diffusion (323). The ability of a molecule to move across the BBB is influenced by its physicochemical properties (324). Multiple key physicochemical properties were identified as important for optimal brain exposure, namely lipophilicity, molecular weight (MW), number of hydrogen-bond donors (HBD) and acceptors (HBA), topological polar surface area (tPSA), ionization state and number of rotatable bonds (RB) (325). Over the last years, numerous studies were performed to define the optimal characteristics of successful drugs and drug candidates (326-329).

Lipophilicity, commonly represented by octanol/water partition coefficients (LogP or LogD), is widely considered one of the most important physicochemical properties in drug discovery (325, 330). Lipophilicity contributes for the absorption, distribution, metabolism, excretion and toxicology (ADMET) properties of drugs, modulating their solubility and membrane permeability, potency, selectivity and promiscuity (330, 331). For instance, low lipophilicity is associated with poor bioavailability, while high lipophilicity can contribute for increased promiscuity and toxicity, as well as poor solubility and metabolic stability (325, 331). Moderate lipophilicity of CNS drugs (cLogP: 2-5; cLogD (pH 7.4): 2-5) facilitate transport through the BBB (328).

Molecular weight (MW) may influence numerous events such as absorption, bile elimination rate, BBB penetration and interaction with targets (155). The MW of CNS drugs is usually lower than other therapeutics; the mean MW of marketed CNS drugs is 310, while the mean MW for all oral drugs is 377 (327). Most drugs in clinical use present a MW lower than 500 Da (315).

Hydrogen bonds donors (HBD) and **HBAs** reflect the compounds' polarity and permeability (155). A high number of HBA and HBD is associated with lower BBB permeability (327). Reducing the number of HBD and HBA (HBD < 3; HBA < 7) (327, 328) of a drug is a strategy applied to optimize drug brain exposure (306).

The **tPSA**, currently defined as the surface sum of all polar atoms, is another descriptor for hydrogen bonding and is important for permeability, specially the BBB (332). The suggested upper limit of tPSA for CNS drug candidates is around 90 $Å^2$ (328), although more stringent cut-offs have been proposed (60-70 $Å^2$) (327, 333).

The **number of RB** expresses the conformational flexibility of a molecule and influences the compounds' bioavailability. High conformational flexibility decreases the rate transport across cell membranes and restricts the binding of molecules to their pharmacological targets (334). The number of RB is significantly lower in CNS drugs than in other drug classes, suggesting that the conformational range is limited in CNS drugs. The proposed number of RB of a successful CNS drug is < 8 (327).

Another parameter used to describe the permeability across the BBB is the logarithm of the ratio of the steady-state concentrations of the compound in the brain and in the blood **(logBB)** (335). It was concluded from experimental data that compounds with logBB > 0.3 can cross the BBB readily, while compounds with logBB < −1 have low distribution into the brain and thus are unlikely to act as CNS drugs (335, 336). Since the experimental determination of logBB is usually time-consuming, laborious and expensive, logBB is frequently estimated using computational approaches (337).

In addition to the ability to move across the BBB, CNS drugs need to remain in the brain long enough to exert their therapeutic effect (338). Therefore, CNS drugs must avoid being a substrate of transport proteins that extrude compounds from the brain (338). Brain capillary endothelial cells contain multiple drug transporters, with most of them positioned to play a gatekeeper function in the BBB (**Figure 1.21**) (339, 340). One of the most important transporters present at the BBB is P-gp, a 170-kDa member of the ATP-binding cassette superfamily of membrane transporters encoded by the multidrug resistance gene 1 (338, 340). P-glycoprotein is mainly located at the luminal membrane and uses ATP to actively extrude drugs against the concentration gradient (339, 341). P-glycoprotein can extrude a wide variety of structurally and functionally unrelated compounds with mass between 300-4000 Da (341), contributing for the high attrition of CNS drug candidates and to the variable response to CNS pharmacotherapy between patients (339).

Several antiparkinsonian drugs, such as L-DOPA and dopaminergic agonists (e.g.: pergolide, pramipexole, bromocriptine) were found to be P-gp substrates. Therefore, P-gp limits their entry into the brain and reduces the effectiveness of their therapeutic effect (342). In this context, rapid and reversible P-gp inhibition in capillary endothelial cells could provide enough time to deliver P-gp substrates to the brain with a minimal disruption of protection (339).

1.3.3. Natural scaffolds in CNS drug discovery

Natural compounds have been looked as an invaluable source of inspiration in drug design and development (343), offering a wide variety of biologically relevant scaffolds and pharmacophore patterns (344). Natural compounds can be viewed as “privileged structures” that evolved in nature to interact with several biological targets for specific purposes (345, 346). This view is reinforced by the fact that natural compounds are used as effective drugs in numerous therapeutic indications (345). However, the clinical application of natural compounds can be restricted by their unfavourable pharmacokinetics, toxicity and structural complexity. In this case, structural modification is commonly required (343).

In the drug discovery process, the structure of natural compounds has been served as basis to design new analogues with the desired pharmacokinetic profile, efficacy and safety (347, 348). Several approaches can be used to assist the library design and hit-to-lead expansion, which include diversity-oriented synthesis and biology-oriented synthesis (349). In particular, biology-oriented synthesis is an approach that employs biological relevance and scaffold pre-validation as the main criteria for the selection of compound classes (350).

Hydroxycinnamic acids (HCAs) and piperine (**Figure 1.22**) present relevant biological activities, and therefore they can be viewed as privileged scaffolds for the development of bioactive molecules with therapeutic potential.

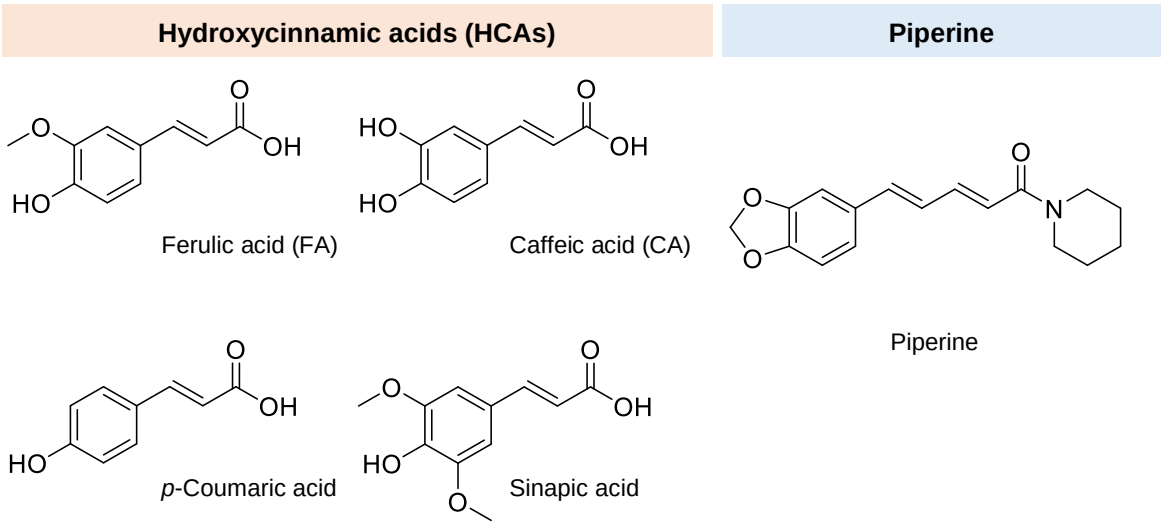


Figure 1.22: Chemical structures of hydroxycinnamic acids and piperine.

Hydroxycinnamic acids are an important subclass of phenolic compounds and are ubiquitously distributed in the plant kingdom (351). They are secondary metabolites derived from L-phenylalanine and L-tyrosine (352, 353). All HCAs contain a C6-C3 carbon chain, consisting of an aromatic ring bearing one or more hydroxyl groups and an α,β-unsaturated carboxylic acid (353, 354). Although *E* and *Z* forms may occur in plants, the *E* form is predominant and more stable (355).

Hydroxycinnamic acids are well-known for their antioxidant activity, which has been associated with numerous biological effects (e.g.: anti-inflammatory, antimutagenic, antibacterial, anticancer and neuroprotective activities) (356, 357). In fact, HCAs and other phenolic compounds may act as chain breaking antioxidants (358), an activity that is related to the hydrogen atom or electron-donating ability of the phenolic group (232, 359, 360). The resulting phenoxyl radical is then stabilized by resonance across the conjugated system

comprising the aromatic ring and the ethylenic side chain (358, 361, 362). The antioxidant activity of HCAs is also associated with indirect and long-lasting mechanisms, namely chelation of redox-active transition metals, inhibition of pro-oxidant enzymes, induction of cytoprotective pathways (e.g. NRF2-ARE) and regeneration of reduced forms of endogenous antioxidants (280, 363, 364). The antioxidant activity of HCAs is influenced by the number and position of hydroxyl groups and the substitution pattern of the aromatic ring (362, 365, 366). *Para*-coumaric acid, ferulic acid (FA), caffeic acid (CA) and sinapic acid are the most representative HCAs (**Figure 1.22**) (362).

Ferulic acid, the most abundant HCA, was first isolated in 1866 from *Ferula foetida*, the plant from which its name was derived (367, 368). Ferulic acid contains an electron-donating methoxy group at the *ortho* position to the hydroxyl group, which provides additional stabilization of the phenoxyl radical formed in the reaction with free radicals (369, 370). Numerous studies explored the potential of FA and derivatives thereof as neuroprotective agents. For instance, FA prevented protein oxidation and lipid peroxidation in neuronal cells and in synaptosomal membranes (371). In a rotenone-induced PD rat model, FA (50 mg/kg bodyweight) restored the levels of antioxidant enzymes (SOD, CAT), prevented glutathione depletion and lipid peroxidation, and decreased the expression of cyclooxygenase 2 (COX-2) and inducible NOS (372). In addition, FA and derivatives thereof may prevent Aβ oligomerization (373), destabilize pre-formed Aβ fibrils (374) and protect against Aβ-induced oxidative stress (375, 376).

Caffeic acid is an HCA containing a catechol group that is responsible for its potent antioxidant activity (377). Indeed, the presence of the *ortho*-hydroxyl group decreases the O-H dissociation enthalpy enhancing the compounds' radical scavenging activity (378). Caffeic acid is also capable of chelating pro-oxidant transition metals and thereby inhibit the formation and propagation of RS (379-381). The neuroprotective properties of CA and derivatives thereof have been studied over the last decades. Caffeic acid protected against Aβ-induced toxicity in PC12 cells by attenuating the increased oxidative stress, calcium influx and tau hyperphosphorylation (382). Caffeic acid phenethyl ester (CAPE), a CA derivative, reduced microglial activation and the expression of pro-oxidant enzymes (inducible NOS, COX) in BV-2 murine microglial cells (383). Moreover, CAPE (10 µmol/kg body weight) prevented 6-hydroxydopamine-induced loss of dopaminergic neurons in male Wistar rats. This neuroprotective effect was associated with radical scavenging and metal chelating activities of CAPE and to its ability to inhibit the formation of the mitochondrial permeability transition pore (384).

Piperine (**Figure 1.22**) is the main pungent alkaloid present in the fruits of black pepper (*Piper nigrum*), long pepper (*Piper longum*) and other piper species belonging to the

plant family *Piperaceae* (385). The recent advances in patented processes and applications involving piperine and derivatives thereof were reviewed in **Manuscript IB**.

Several studies indicate that piperine have beneficial effects in the CNS. For instance, piperine displayed neuroprotective effects against corticosterone-induced neurotoxicity in PC12 cells, at least partially, by increasing glutathione levels, SOD activity and brain-derived neurotrophic factor (BDNF) mRNA levels (386). In a rotenone-induced PD mouse model, treatment with piperine (25 and 50 mg/kg body weight) improved motor performance, attenuated the loss of dopaminergic neurons in the striatum and decreased the rotenone-induced mitochondrial damage (387). Piperine (5-20 mg/kg body weight) also improved cognitive dysfunction and decreased neurodegeneration in the hippocampus in adult male Winstar rats treated with AF64A (a cholinotoxin), which was partially associated to the decreased lipid peroxidation and AChE activity (388). Finally, piperine was identified as a reversible and competitive MAO inhibitor (389). Therefore, piperine represents a valid scaffold for the development of neuroprotective agents.

1.4. Thesis objectives

The mainstay of AD and PD management is based on monotherapy or combination therapy using single-target agents. The available therapies address the diseases' symptomatology but are unable to stop or delay the disease progression. The limited clinical efficacy and the lack of disease-modifying effects of the available drugs shifted the research focus from single-target agents to MTDLs. Natural scaffolds are privileged and versatile starting points for the development of MTDLs, since they provide a diverse array scaffolds and pharmacophores with relevant biological activities.

With this in mind, the main goal of this thesis is the **rational design of new chemical entities based on natural scaffolds and the evaluation of their pharmacological and toxicological effects towards oxidative stress and/or neurotransmitter depletion.** Accordingly, three sets of compounds were designed and synthesized (**Figure 1.23**). Inspired on the redox properties of biothiols, FA-based thiophenols with enhanced antioxidant activity were developed (**Figure 1.23A**). Moreover, a small library of piperine and CA bioisosteres were prepared and, based on their biological activities, structure-activity relationships were established (**Figure 1.23B**). Finally, to obtain a series of compounds that selectively accumulate within mitochondria, piperine- and CA-based scaffolds were conjugated with TPP (**Figure 1.23C**).

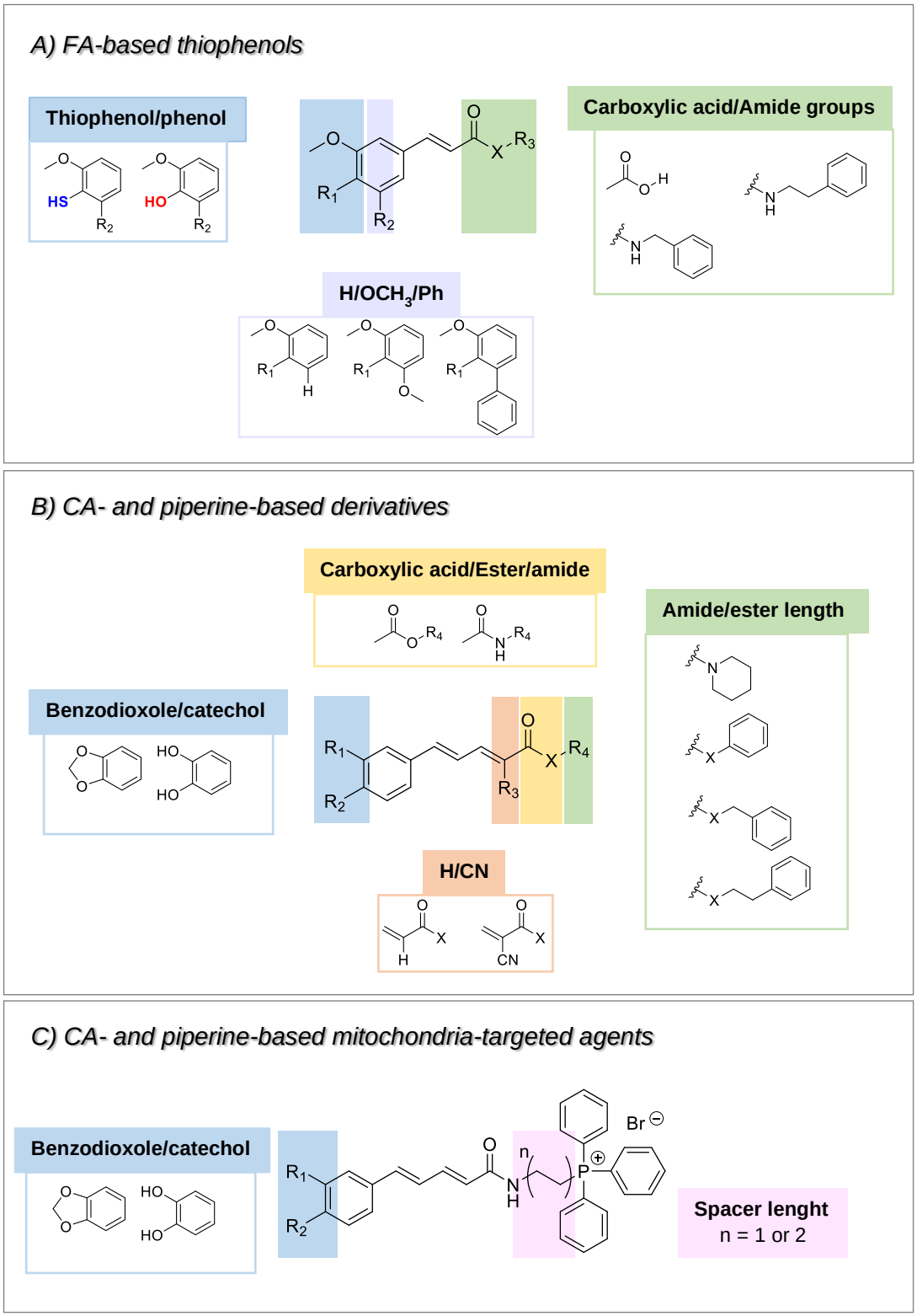


Figure 1.23: Design strategies followed to obtain a series of derivatives based on ferulic acid, caffeic acid and piperine scaffolds.

The following specific goals were established for the present study:

1. **Rational design and development of new chemical entities based on piperine, FA and CA scaffolds**. The main structural modifications included the replacement of phenolic hydroxyl groups with sulfhydryl groups, elongation of the ethylenic side chain of HCAs, incorporation of an α-CN group, introduction of lipophilic substituents connected with ester or amide bonds, and conjugation of bioactive moieties with TPP. Structural elucidation was performed using NMR (^{1}H NMR, ^{13}C NMR, DEPT135, COSY, HSQC and HMBC) and mass spectrometry (EI-MS and ESI-MS) techniques and X-ray diffraction.

2. ***In vitro* evaluation of the antioxidant profile of compounds bearing a phenol or thiophenol function in cell-based and cell-free systems**. The antioxidant profile was studied using spectrophotometric (DPPH$^{\bullet}$, ABTS$^{\bullet+}$ and GO$^{\bullet}$ assays), fluorometric (ORAC-FL) and voltammetric (DPV and CV) assays. In addition, human neuroblastoma (SH-SY5Y) cells were used to evaluate the protective properties against oxidative stress induced by *tert*-butyl hydroperoxide (*t*-BHP), iron (III) and H_2O_2.

3. **Evaluation of *in vitro* inhibition of neurotransmitter-metabolizing enzymes.** Compound libraries were screened towards AChE, BChE, MAOs and COMT. Moreover, the reversibility and the mechanism of enzyme inhibition of the most promising compounds were assessed.

4. **Evaluation of cytotoxicity profile in two different cell lines**. Cytotoxicity of compounds with relevant biological activities was evaluated in differentiated SH-SY5Y cells and in colon adenocarcinoma (Caco-2) cells using the MTT reduction, resazurin reduction and NR uptake assays.

5. **Evaluation of intracellular oxidative stress levels.** The effects of compounds with relevant biological activities on intracellular RS formation were studied in differentiated SH-SY5Y cells by the DCF fluorescence assay.

6. **Evaluation of P-gp transport activity**. The effect of compounds with relevant biological activities on P-gp transport activity was assessed in Caco-2 cells, using Rhodamine 123 as a P-gp substrate and zosuquidar as a specific third-generation P-gp inhibitor

7. **Measurement of mitochondrial accumulation.** Isolated rat liver mitochondria were used to study the accumulation of mitochondria-targeted agents in the mitochondrial matrix.

8. **Evaluation of mitochondrial (dys)function parameters.** The effect of mitochondria-targeted agents in mitochondrial and glycolytic functions was studied in differentiated SH-SY5Y cells using the Seahorse XF96 Extracellular Flux Analyzer-based Mito Stress Test.

9. **Evaluation of drug-like properties**. Chromatographic hydrophobicity indexes (CHIs) of the most promising candidates were determined as a measure of the compounds' lipophilicity. Other drug-like properties were also be estimated and used as a criterion for lead selection.

10. **Proposal of a lead multitarget candidate**. The compounds with the most relevant pharmacological and toxicological profiles were selected as potential multitarget lead candidates for further optimization.

CHAPTER II

Introduction complement

Chapters II and II are composed by the manuscripts prepared within the scope of this Thesis. According to the recommendations of the Ethics Committee, the author **D. Chavarria** declares his contributions to each manuscript as follows:

MANUSCRIPT IA: The author was responsible for the review of contents related with the synthetic strategies used to obtain donepezil-based multitarget-directed ligands;

MANUSCRIPT IA: The author was responsible for the review of contents related with the synthesis and pharmacological activities of piperine derivatives;

MANUSCRIPT II: The author was responsible for the design, synthesis and structural elucidation of the test compounds; stability studies; evaluation of antioxidant activity; data analysis and the redaction of the manuscript;

MANUSCRIPT III: The author was responsible for the design, synthesis and structural elucidation of the test compounds; evaluation of antioxidant activity; evaluation of cytotoxicity in differentiated SH-SY5Y cells; estimation of drug-like properties; data analysis and the redaction of the manuscript;

MANUSCRIPT IV: The author was responsible for the design, synthesis and structural elucidation of the test compounds; evaluation of antioxidant activity and *h*MAO inhibitory activities; estimation of drug-like properties; data analysis and the redaction of the manuscript;

MANUSCRIPT V: The author was responsible for the design, synthesis and structural elucidation of the test compounds by nuclear magnetic resonance; evaluation of *h*MAO inhibitory activities; estimation of drug-like properties; data analysis and the redaction of the manuscript;

MANUSCRIPT VI: The author was responsible for the design, synthesis and structural elucidation of the test compounds; evaluation of *h*MAO inhibitory activities and mechanisms of *h*MAO-B inhibition; data analysis and the redaction of the manuscript;

MANUSCRIPT VII: The author was responsible for the design, synthesis and structural elucidation of the test compounds; evaluation of *h*MAO inhibitory activities and mechanisms of *h*MAO-B inhibition; assessment of *ee*AChE and *eq*BChE inhibitory activities and mechanisms of *eq*BChE inhibition; estimation of drug-like properties; data analysis and the redaction of the manuscript;

2.1. Manuscript IA

The chemistry toolbox of multitarget-directed ligands for Alzheimer's disease

European Journal of Medicinal Chemistry, **2019**, 181: 111572.
DOI: 10.1016/j.ejmech.2019.111572.

European Journal of Medicinal Chemistry 181 (2019) 111572

Contents lists available at ScienceDirect

European Journal of Medicinal Chemistry

journal homepage: http://www.elsevier.com/locate/ejmech

Research paper

The chemistry toolbox of multitarget-directed ligands for Alzheimer's disease

Francesco Mesiti [a, b, c, 1], Daniel Chavarria [a, d, 1], Alexandra Gaspar [a, **], Stefano Alcaro [b, c], Fernanda Borges [a, *]

[a] *CIQUP/Department of Chemistry and Biochemistry, Faculty of Sciences, University of Porto, Porto, Portugal*
[b] *Department of "Scienze della Vita", University "Magna Græcia" of Catanzaro, Catanzaro, Italy*
[c] *Net4Science Srl, University Magna Græcia, Viale Europa, Catanzaro, Italy*
[d] *CNC - Center for Neuroscience and Cell Biology, University of Coimbra, UC Biotech, Biocant Park, Cantanhede, Portugal*

ARTICLE INFO

Article history:
Received 30 June 2019
Received in revised form
26 July 2019
Accepted 29 July 2019
Available online 1 August 2019

Keywords:
Multitarget-directed ligands
Alzheimer's disease
Synthetic strategies contents

ABSTRACT

The discovery and development of multitarget-directed ligands (MTDLs) is a promising strategy to find new therapeutic solutions for neurodegenerative diseases (NDs), in particular for Alzheimer's disease (AD).

Currently approved drugs for the clinical management of AD are based on a single-target strategy and focus on restoring neurotransmitter homeostasis. Finding disease-modifying therapies AD and other NDs remains an urgent unmet clinical need.

The growing consensus that AD is a multifactorial disease, with several interconnected and deregulated pathological pathways, boosted an intensive research in the design of MTDLs. Due to this scientific boom, the knowledge behind the development of MTDLs remains diffuse and lacks balanced guidelines. To rationalize the large amount of data obtained in this field, we herein revise the progress made over the last 5 years on the development of MTDLs inspired by drugs approved for AD. Due to their putative therapeutic benefit in AD, MTDLs based on MAO-B inhibitors will also be discussed in this review.

© 2019 Elsevier Masson SAS. All rights reserved.

1. Introduction

Neurodegenerative diseases (NDs) such as Alzheimer's disease (AD) are a group of progressive, chronic and incurable neurological disorders that affect millions of people worldwide. The incidence of NDs has been increasing to epidemic proportions, whose disabling effects may continue for years or even decades, representing a growing health and socioeconomic burden [1–3].

Current treatments for NDs are mainly focused on symptomatic relief and rely on mono- or combination therapies [1]. In particular, the mainstay of AD pharmacological therapy is the treatment with acetylcholinesterase inhibitors (AChEI) and with *N*-methyl-D-aspartate receptor (NMDAR) antagonists [4]. Examples of ACHEI and NMDAR antagonists that reached the market are donepezil, rivastigmine, tacrine (THA), galantamine, memantine (MEM) and amantadine (AMA) (Fig. 1) [5].

Over the past decades, major advances have been made to understand the etiopathology of NDs, but the mechanisms and the cascade of events that lead to neurodegeneration remain unknown. Nevertheless, it is generally accepted that AD and other NDs are multifactorial and share common mechanisms [6].

The knowledge of the complex multifactorial nature of NDs triggered a change on the drug discovery rational design paradigm from one target to multitarget [7–9]. Taking as an example one can mention rasagiline and safinamide (Fig. 1), the last two drugs approved by the Food and Drug Administration (FDA) as adjunctive treatment for Parkinson's disease (PD). Although they were approved as selective monoaminoxidase B (MAO-B) inhibitors, the neuroprotective properties of rasagiline and the ability of safinamide to block Na^+ and Ca^{2+} channels has been also reported [10]. In point of fact, these evidences were an inspiration for the development of new multitarget-directed ligands (MTDLs) [10].

* Corresponding author. CIQUP/Department of Chemistry and Biochemistry, Faculty of Sciences, University of Porto, Porto, 4169-007, Portugal.
** Corresponding author. CIQUP/Department of Chemistry and Biochemistry, Faculty of Sciences, University of Porto, Porto, 4169-007, Portugal.
E-mail addresses: alexandra.gaspar@fc.up.pt (A. Gaspar), fborges@fc.up.pt (F. Borges).
[1] These authors contributed equally.

https://doi.org/10.1016/j.ejmech.2019.111572
0223-5234/© 2019 Elsevier Masson SAS. All rights reserved.

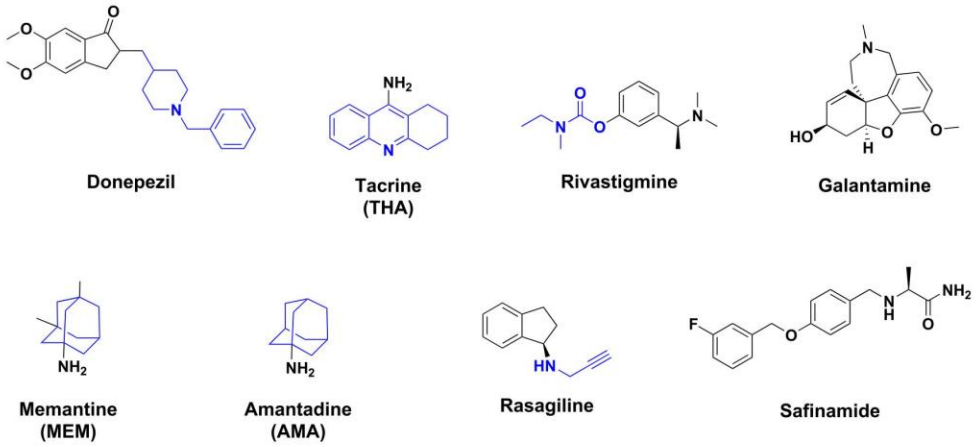


Fig. 1. Drugs used to treat neurodegenerative diseases: **ACHEIs**: donepezil, tacrine (THA), (*S*)-rivastigmine, and galantamine (4); **NMDAR antagonists**: memantine (MEM), and amantadine (AMA); **MAO-B inhibitors**: rasagiline and safinamide.

The multitarget approach has been applied to find new therapeutic solutions for NDs [11,12]. Multitarget-directed ligands can be obtained by combining pharmacophores of one target ligands into a single molecule. The pharmacophores can be connected by stable and lengthy linkers (linking), attached directly (fusing) or overlapped (merging) (Fig. 2) [13]. The choice of the strategy is driven by the nature of the targets, the availability of the starting materials and the synthetic feasibility [14,15]. The chemical synthesis is considered a rate-limiting factor to obtain MTDLs. In fact, the selection of robust, scalable and safe synthetic strategies is of utmost importance not only to obtain the desired hybrids but also to face the iterative cycles of lead optimization [16–18].

As a contribute to pull ahead the process herein we review the synthetic strategies used in the development of MTDLs for AD inspired on acetylcholinesterase inhibitors (donepezil, tacrine and rivastigmine) and on NMDAR antagonists (memantine and amantadine). Considering the increasing importance of the use of MAO-B inhibitors for AD therapy (Fig. 1) the revision was extended to rasagiline-based hybrids.

2. Donepezil-based multitarget-directed ligands

Donepezil (1-benzyl-4-[5,6-dimethoxy-(1-indanone)-2-yl] methyl piperidine, Fig. 1) was approved by the FDA in 1996 [19] and it is widely prescribed for the palliative treatment of mild to moderate AD [5,20]. Since donepezil has been considered the most effective drug among the AChEI, a long work has been done toward the optimization of its synthetic strategies. For instance, Reddy

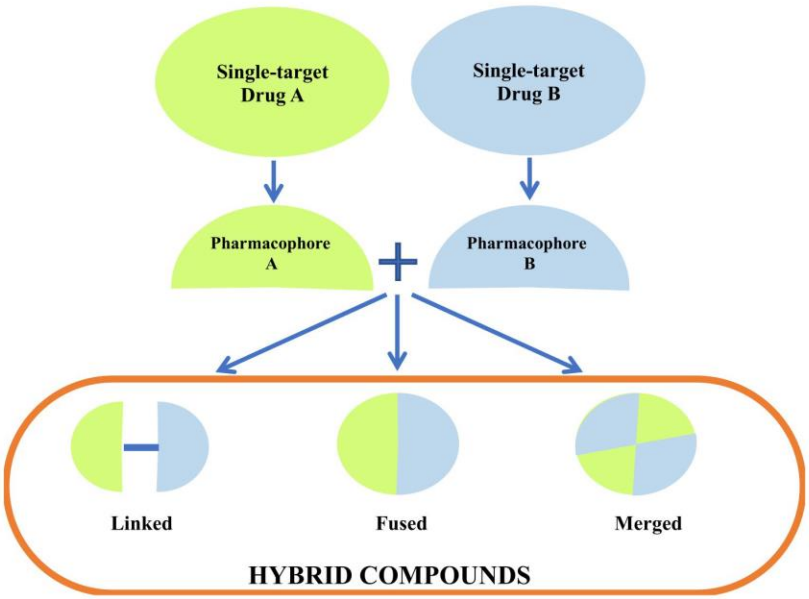
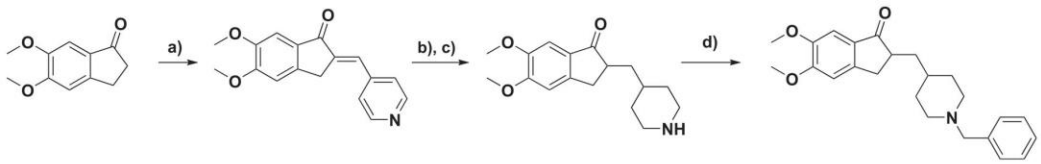
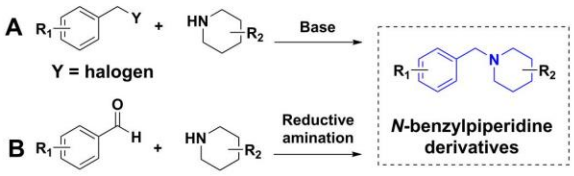


Fig. 2. Rational design of multitarget-directed ligands.



Scheme 1. Synthesis of donepezil. a) isonicotinaldehyde, *p*-TSA, toluene, reflux, b) Pd/C, H_2, MeOH, N_2, c) base (aq), d) benzyl bromide, Na_2CO_3, EtOH.



Scheme 2. Classic reactions used to obtain *N*-benzylpiperidine derivatives.

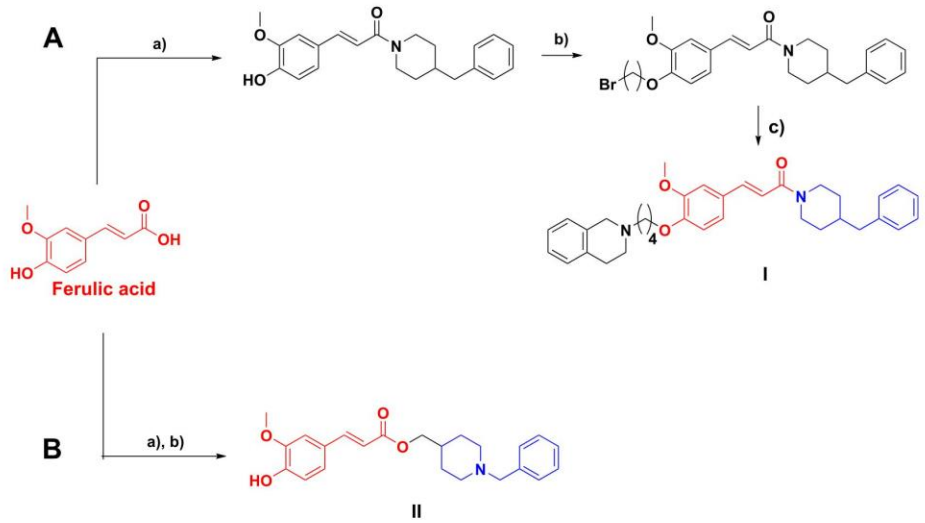
et al. [21] developed an effective synthetic strategy (Scheme 1) in which the first step enclosed an aldol condensation of 5,6-dimethoxyindanone with pyridine-4-carboxaldehyde to yield 5,6-dimethoxy-2-(pyridin-4-yl)methyleneindan-1-one (Scheme 1, step a). After hydrogenation (Scheme 1, step b), pH adjustment (Scheme 1, step c) and N-alkylation (Scheme 1, step d) donepezil was obtained in an overall yield of 83% [21].

The high potency *versus* the safety profile make donepezil pharmacophore a popular scaffold for the design of new MTDLs [22]. Within this strategy the *N*-benzylpiperidine fragment of donepezil has been hybridized with other scaffolds endowed with relevant pharmacological properties. The *N*-benzylpiperidine fragment was commonly attached through amine [23–25], amide [26], ester [22], ether [27–29], ketone [30] or acyl hydrazone [31] functions. Generally, linking [32,33] and merging [31,34] MTDLs strategies were reported.

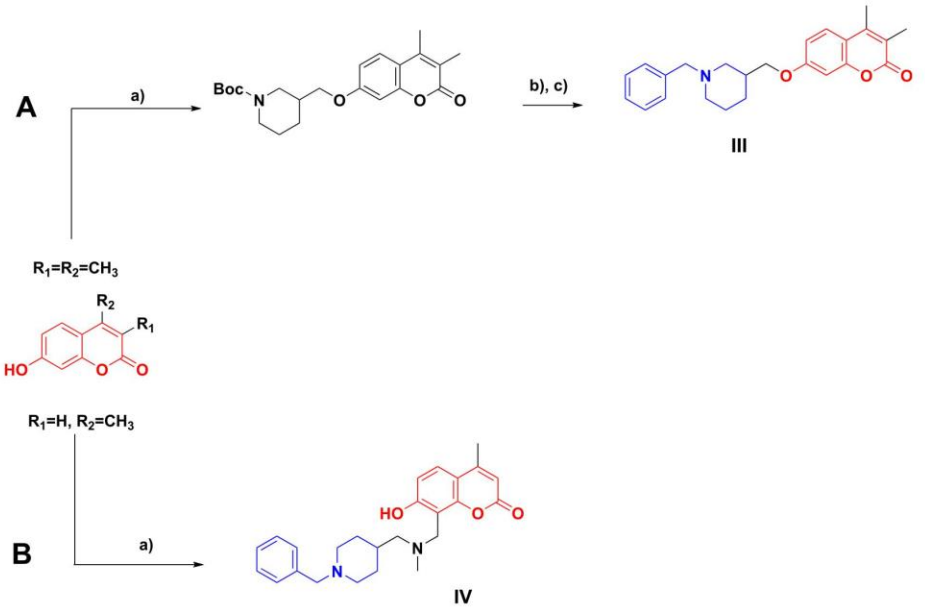
Several donepezil-based MTDLs were obtained by hybridization of the *N*-benzylpiperidine fragment with privileged structures, such as flavonoids [32], cinnamic acids [22,28], coumarins [24,27], and quinolones [23]. Usually, two classic methods were used to synthetize the *N*-benzylpiperidine fragment: a) *N*-alkylation of piperidine, or its derivatives, with benzyl halides under alkaline conditions (Scheme 2A) [23,25,27] or b) reductive amination of benzaldehyde, or its derivatives, in the presence of piperidine, or its derivatives, and a reducing reagent, such as $NaBH_3CN/ZnCl_2$ and $NaBH(OAc)_3$ (Scheme 2B) [22,27,31].

Sang et al. [28] reported the synthesis and biological evaluation of ferulic acid-O-alkylamines linked to the *N*-benzylpiperidine fragment (Scheme 3A) [28]. Compound **I**, which synthesis is depicted in Scheme 3A, is highlighted as MTDL as it acts as cholinesterase and Aβ-aggregation inhibitor, metal chelator and neuroprotector. Ferulic acid was also used as scaffold by Dias et al. [22]. Feruloyl-*N*-benzylpiperidine hybrid **II** (Scheme 3B) was reported as an MTDL compound, showing acetylcholinesterase (AChE) inhibitory activity and anti-inflammatory, metal chelating and neuroprotective properties [22]. The synthetic strategy encompasses ferulic acid activation with $SOCl_2$ and the linking of the *N*-benzylpiperidine fragment through an ester bond (Scheme 3B, steps a and b) [22].

The *N*-benzylpiperidine moiety was also linked to a coumarin scaffold to develop dual AChE/MAO-B inhibitors [24,27]. Pisani et al. [27] designed a series of coumarin-based MTDLs and compound **III** was found to be the best of the series. This compound was obtained using a four-step synthetic strategy (Scheme 4A) [27]. Briefly, 3,4-dimethyl-7-hydroxycoumarin was coupled with Boc-3-piperidinemethanol by a Mitsunobu etherification reaction (Scheme 4A, step a). After the removal of the



Scheme 3. Synthesis of multitarget-directed ligands based on ferulic acid. **A**: a) 4-benzylpiperidine, THF, EDC.HCl, HOBT, b) $Br(CH_2)_4Br$, CH_3CN, c) 1,2,3,4-tetrahydroisoquinoline, K_2CO_3, CH_3CN. **B**: a) $SOCl_2$, DMF, CH_2Cl_2, b) (1-benzylpiperidin-4-yl)methanol, CH_2Cl_2.



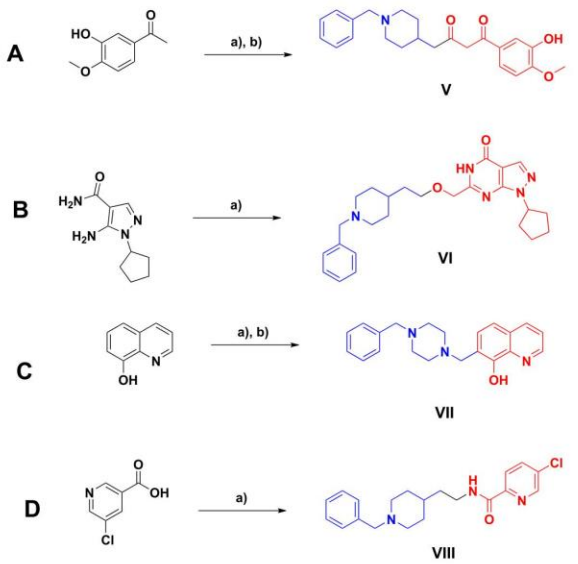
Scheme 4. Synthesis of multitarget-directed ligands based on coumarin **A**: a) 1-Boc-3-methanesulfonyloxymethyl-piperidine, Et_3N, Cs_2CO_3, dry DMF, b) TFA, CH_2Cl_2, c) benzyl bromide, anhydrous K_2CO_3, CH_3COCH_3. **B**: a) 1-benzyl-4-(methylamino)piperidine, formaldehyde, EtOH.

protecting group (Scheme 4A, step b), the piperidinyl intermediate was *N*-alkylated with benzyl bromide under microwave (MW) irradiation to yield compound **III** (Scheme 4A, step c) [27]. Within the same scope, Domínguez et al. [24] reported the synthesis of coumaroyl-*N*-benzylpiperidine hybrids. Compound **IV** (Scheme 4B), a dual AChE/MAO-B inhibitor, was synthesized by a Mannich reaction between 7-hydroxy-4-methylcoumarin and the *N*-benzylpiperidine derivative (Scheme 4B) [24].

Other research groups reported the synthesis of hybrids constructed by the linkage of *N*-benzylpiperidine fragment with curcumin and purine based scaffolds, such as compounds **V** [30] and **VI** [29], respectively (Scheme 5A and 5B). Yan et al. [30] described compound **V** (Scheme 5A) as an antioxidant with ChE and Aβ self-aggregation inhibitory activities. Compound **V** was synthesized by a Claisen condensation between the *N*-benzylpiperidine ester derivative and a protected acetophenone (Scheme 5A, step a). The removal of the protecting group under acidic conditions afforded final compound (Scheme 5A, step b) [30]. Hu and coworkers [29] obtained a MTDL (compound **VI**) displaying a dual AChE/phosphodiesterase-9 (PDE9A) inhibitor profile by reacting the appropriate pyrazole derivative with an *N*-benzylpiperidine intermediate (Scheme 5B, step a) [29].

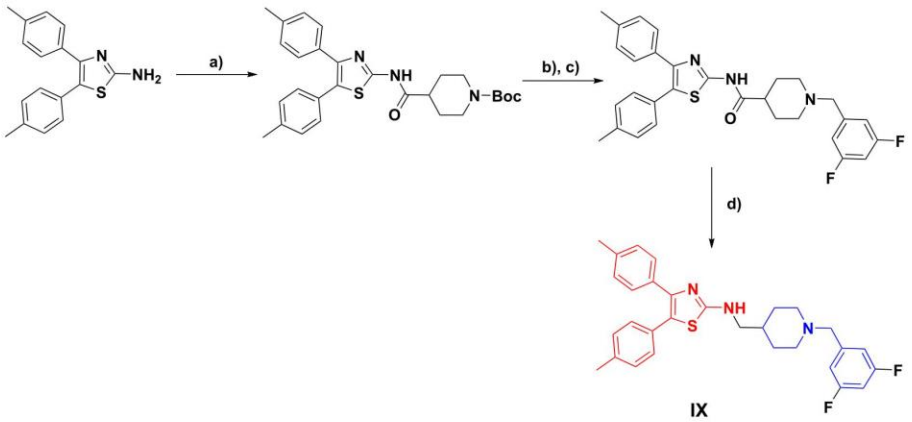
By linking *N*-benzylpiperazine with 8-hydroxyquinoline, Prati and coworkers [23] synthesized compound **VII**. Briefly, 7-(piperazin-1-ylmethyl)-8-hydroxyquinoline was obtained by a microwave assisted Mannich reaction between piperazine and 8-hydroxyquinoline (Scheme 5C, step a) that then reacted with benzyl chloride to afford compound **VII** (Scheme 5C, step b). This hybrid showed anti-Aβ self-aggregating and human butyrylcholinesterase (BuChE) inhibitory activities [23].

Li and coworkers [26] synthesized a series of *N*-benzylpiperidine-nicotinic acid hybrids, in which compound **VIII** (Scheme 5D) stood out as the best dual ChE/MAO inhibitor [26]. This compound was obtained through an amide bond linkage using 1,1′-carbonyldiimidazole (CDI) as coupling reagent [26].



Scheme 5. Synthesis of the multitarget-directed ligands **V**, **VI, VII,** and **VIII**. **A:** a) ethyl 2-(1-benzylpiperidin-4-yl)acetate, $NaNH_2$, THF, b) HCl, EtOH. **B:** a) *tert*-butyl 2-(2-(1-benzylpiperidin-4-yl)ethoxy)acetate, t-BuOK, THF. **C:** a) piperazine, paraformaldehyde, EtOH, b) DIPEA, DMF. **D:** (a) 2-(1-benzylpiperidin-4-yl)ethanamine, CDI, CH_2Cl_2.

Shidore and coworkers [25] synthesized a series of *N*-benzylpiperidine-diarylthiazol hybrids able to interact with both PAS (peripheral anionic site) and catalytic anionic site (CAS) of AChE. Compound **IX** was considered the best of the series and its synthesis is outlined in Scheme 6 [25]. Briefly, the *N*-Boc intermediate



Scheme 6. Synthesis of the *N*-benzylpiperidine-diaryltriazine hybrid **IX**. a) *N*-Boc-piperidine-4-carboxylic acid, BOP, DIPEA, dry CH_3CN, b) TFA/CH_2Cl_2, c) K_2CO_3, dry DMF, 3,5-difluorobenzyl bromide, d) BH_3–DMS, dry THF.

was obtained by an amidation reaction using (benzotriazol-1-yloxy)tris(dimethylamino)phosphonium hexafluorophosphate (BOP) as coupling agent (Scheme 6, step a). After deprotection and subsequent reaction with 3,5-difluorobenzyl bromide via S_N2 nucleophilic reaction an intermediate (Scheme 6, steps b and c) containing a carbonyl group was obtained. Its reduction with borane-dimethyl sulfide complex (BH_3-DMS) afford compound **IX** (Scheme 6, step d) [25].

A series of MTDLs based on the molecular hybridization of *N*-acylhydrazone and *N*-benzylpiperidine fragments were designed by Viegas et al. [31]. Compound **X** (Scheme 7) was the best among the series, displaying AChE inhibitory activity and anti-inflammatory/neuroprotective properties [31]. This compound was synthesized according to the strategy shown in Scheme 7. In brief, after the activation of *p*-formyl benzoic acid with $SOCl_2$ and subsequent reaction with an amine the intermediate was reduced (Scheme 7, steps a and b). Then, the ester derivative reacted with hydrazine (Scheme 7, step c) and the amination of the resulting intermediate afforded compound **X** (Scheme 7, step d) [31].

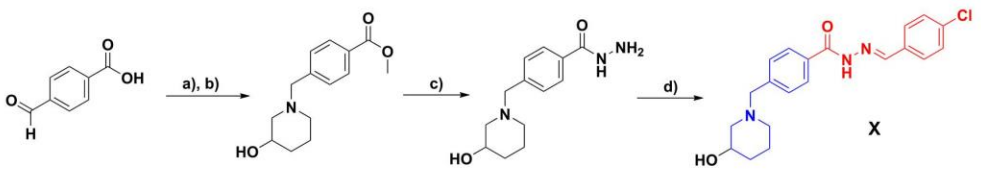
Lecoutey and coworkers [34] obtained donecopride (compound **XI**, Scheme 8), a compound that showed a dual activity profile as *h*5-HT_4R partial agonist/AChE inhibitor [34]. The synthetic strategy started with the carboxylic acid group activation of 4-amino-5-chloro-2-methoxybenzoic acid with CDI and subsequent reaction with monoethyl malonate potassium salt to yield a β-ketoester (Scheme 8, step a). Then, the β-ketoester reacted with *N*-Boc-4-iodomethylpiperidine under basic conditions, followed by a saponification-decarboxylation reaction with hydroalcoholic potassium hydroxide. (Scheme 8, step b). After, *N*-Boc protecting group cleavage with trifluoroacetic acid (TFA) (Scheme 8, step c), and reaction with bromomethylcyclohexane compound **XI** was obtained (Scheme 8, step d) [34].

3. Tacrine -based multitarget-directed ligands

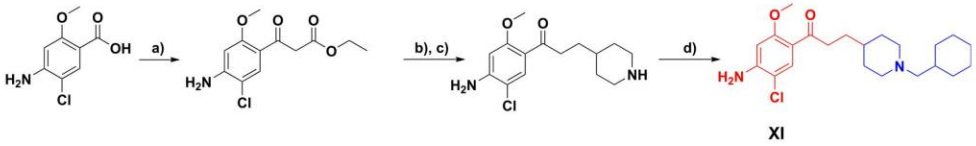
Tacrine (1,2,3,4-tetrahydroacridin-9-amine, THA, Fig. 1) was approved in 1993 by the FDA for the palliative treatment of AD. However, it was withdrawn from the market due to its hepatotoxicity [35]. Nevertheless, due to its relevant AChE inhibitory activity THA scaffold has been used on the development of new MTDLs [36–38].

The synthesis of THA was first reported in 1945. Since then, several synthetic strategies have been developed. Tacrine can be synthesized by the Friedlander method (Scheme 9A), which involves the condensation of anthranilonitrile and cyclohexanone in the presence of a Lewis acid, such as $ZnCl_2$, $AlCl_3$, *p*-toluenesulfonic acid (*p*-TSA) or BF_3/Et_2O (Scheme 9A, step a) [39]. However, due to Friedlander drastic reaction conditions [40,41], it has been modified and improved. For instance, Khalilzadeh et al. [40] reported the synthesis of THA using solid catalyst *p*-TSA/silica gel under MW irradiation. A similar synthetic strategy was reported by Hasaninejad et al. [41], in which sulfuric acid-modified PEG-6000 was used as an efficient, green, inexpensive and biodegradable polymeric catalyst. Another classic method used to synthetize THA is by the Hu reaction (Scheme 9B), in which anthranilic acid was refluxed with cyclohexanone and phosphoryl chloride ($POCl_3$) (Scheme 9B, step a) and then the formed intermediate was treated with concentrated ammonium hydroxide (NH_4OH) (Scheme 9B, step b) [42,43].

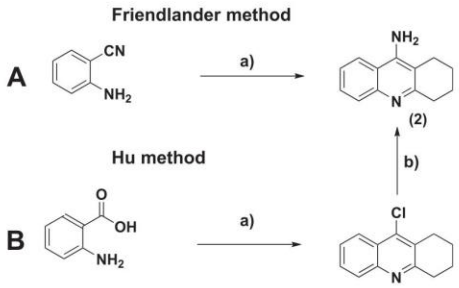
Over the last years, several hybrids were obtained by linking THA, or its derivatives, with a diversity of scaffolds [44–46]. For instance, Quintanova et al. [46] synthesized a novel class of MTDLs by linking THA with cinnamic acid derivatives. Compound **XII** (Scheme 10), the most active compound of the series, showed AChE and Aβ aggregation inhibitory activity along with antioxidant



Scheme 7. Synthesis of the *N*-benzylpiperidine -*N*-acylhydrazone hybrid **X**. a) 1. $SOCl_2$, DMF, CH_2Cl_2, 2. MeOH, b) $NaBH_3CN/ZnCl_2$, MeOH, N_2; c) $N_2H_4 \cdot H_2O$, EtOH, d) 4-chlorobenzaldehyde, HCl.



Scheme 8. Synthesis of the multitarget-directed ligand donecopride. a) 1. CDI, THF; 2. $KO_2CCH_2CO_2Et$, $MgCl_2$, THF, b) 1. *N*-Boc-4-iodomethylpiperidine, K_2CO_3, DMF; 2. KOH, EtOH/H2O, c) TFA, CH_2Cl_2, d) (bromomethyl) cyclohexane, K_2CO_3, DMF.



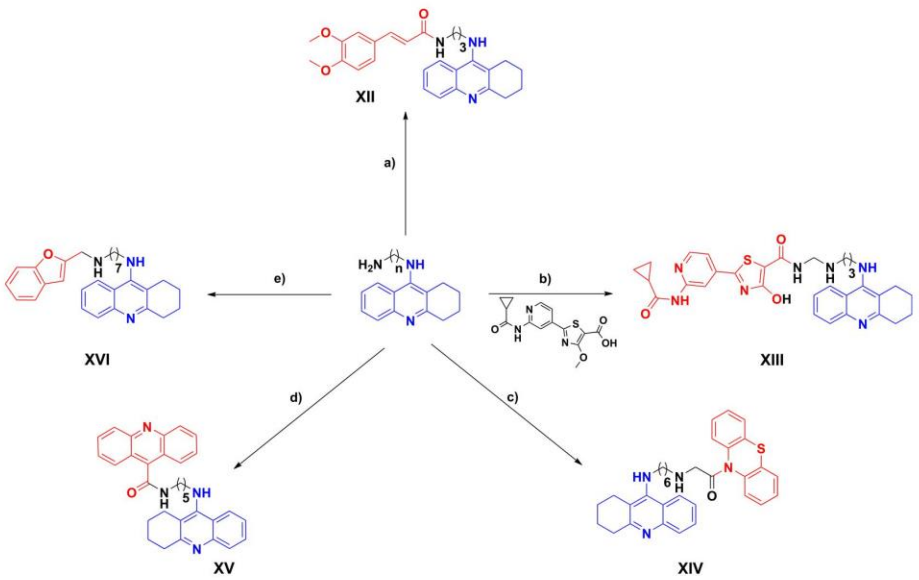
Scheme 9. Synthesis of tacrine by Friendlander and Hu methods. **A:** a) cyclohexanone, Lewis acid. **B:** a) cyclohexanone, $POCl_3$, b) NH_4OH.

properties. Compound **XII** was obtained by an amidation reaction between 3,4-dimethoxycinnamic acid and the suitable 9-aminoalkyltacrine derivative (Scheme 10, step a) [46]. Following the same strategy and using 1-[bis(dimethylamino)methylene]-1H-1,2,3-triazolo[4,5-*b*]pyridinium 3-oxid hexafluorophosphate (HATU) as coupling agent, Jiang et al. [44] synthesized compound **XIII** as a dual glycogen synthase kinase (GSK)-3β/AChE inhibitor (Scheme 10, step b).

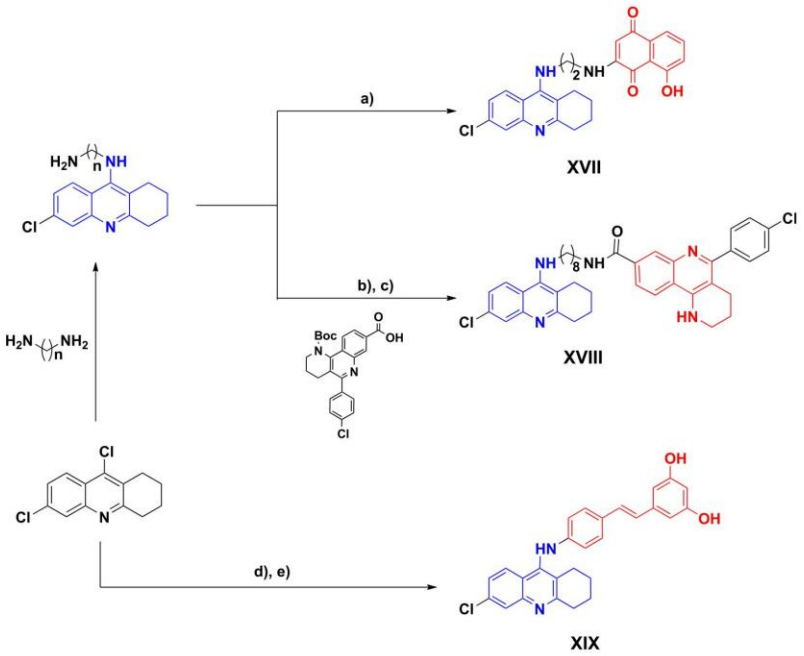
Another THA-phenothiazine hybrid **XIV** was obtained by a nucleophilic substitution using the appropriate chloroacetyl phenothiazine (Scheme 10, step c) [45]. Compound **XIV** is an inhibitor of AChE and tau hyperphosphorylation and Aβ fibrils [45]. With the same endeavour, Chufarova et al. [47] designed new THA-acridine hybrids as cholinesterase inhibitors with anti-Aβ aggregation activity. The most active molecule, compound **XV**, was synthetized by reacting the appropriate 9-aminoalkyltacrine derivative with 9-acridinecarboxylic acid using 2-chloro-4,6-dimethoxy-1,3,5-triazine (CDMT) as coupling reagent (Scheme 10, step d) [47]. In other work, a library of novel THA-benzofuran derivatives was obtained [48]. Compound **XVI** (Scheme 10) presented the best biological profile, displaying human AChE, human β-secretase-1 (BACE-1) and Aβ aggregation inhibitory activities. Compound **XVI** was obtained by N-alkylation of a 9-aminoalkyltacrine derivative with indole bromide (Scheme 10, step e) [48]. Other THA hybrids were obtained using 6-chloro-9-aminoalkyltacrine and 6,9-dichloro-1,2,3,4-tetrahydroacridine derivatives [49–51].

Linked THA-naphthoquinone hybrids were designed as a new class of ChE and Aβ aggregation inhibitors by Nepovimova et al. [49]. Among all hybrids, compound **XVII** (Scheme 11) displayed the most promising biological outline [49]. This compound was synthesized by connecting the appropriate 6-chloro-9-aminoalkyltacrine with 5-hydroxy-1,4-naphthoquinone under MW irradiation (Scheme 11, step a) [49].

New tetrahydrobenzo[*h*] [1,6]naphthyridine-6-chlorotacrine hybrids were reported by Di Pietro et al. [51] as new MTDLs compounds able to target ChEs and Aβ plaques and tau tangles.



Scheme 10. Synthesis of the tacrine-based multitarget-directed ligands **XII-XVI**. a) 3,4-dimethoxycinnamic acid, T3P, *N*-methylmorpholine, CH_2Cl_2, b) HATU, DIPEA, DMF, c) 10-(chloroacetyl)-10H-phenothiazine, K_2CO_3, CH_2Cl_2, d) 9-acridinecarboxylic acid CDMT, *N*-methylmorpholine, THF, e) 2-(bromomethyl)benzofuran, KI, K_2CO_3 in dry CH_2Cl_2.



Scheme 11. Synthesis of tacrine-based multitarget-directed ligands **XVII-XIX**. a) juglone, CH_2Cl_2, b) HOBt/EDC, Et_3N, EtOAc/DMF, c) HCl/dioxane, d) (E)-4-(3, 5-dimethoxystyryl) aniline, phenol, MW, e) BBr_3.

Compound **XVIII** (Scheme 11), the hybrid with the most interesting multitarget profile, was obtained following the synthetic route depicted in the Scheme 11 [51]. In this case, a 6-chloro-9-aminoalkyltacrine was coupled with the appropriated carboxylic acid by an amidation reaction, using 1-hydroxybenzotriazole hydrate/*N*-(3-dimethylaminopropyl)-*N*′-ethylcarbodiimide (HOBt/EDC) as coupling agent, followed by *N*-Boc deprotection with HCl/dioxane (Scheme 11, steps b and c) [51].

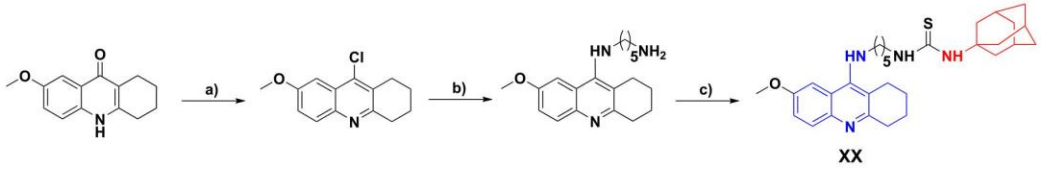
Jeřábek et al. [50] synthesized a series of THA-resveratrol fused hybrids with AChE inhibitory activity, and anti-Aβ self-aggregation and antioxidant properties (Scheme 11). Compound **XIX**, identified as the most promising derivative, was obtained by coupling 6,9-dichloro-1,2,3,4-tetrahydroacridine with the appropriate aminostilbene in the presence of phenol, under MW irradiation and solvent free conditions (Scheme 11, step d), followed by an *O*-demethylation reaction (Scheme 11, step e) [50].

Spilovska and co-workers [52] synthesized THA-adamantine heterodimers acting as ChEs inhibitors and NMDAR antagonists. Compound **XX** (Scheme 12) was the most promising hybrid. The synthesis of compound **XX** is outlined in Scheme 12. Briefly, it encompasses the reaction of the tetrahydroacridinone derivative with $POCl_3$ (Scheme 12, step a) and subsequent N-alkylation reaction with the appropriate diamine yielded a 7-methoxy-9-aminoalkyltacrine derivative (Scheme 12, step b), which in turn react with 1-adamantyl isothiocyanate to afford the final compound (Scheme 12, step c) [52].

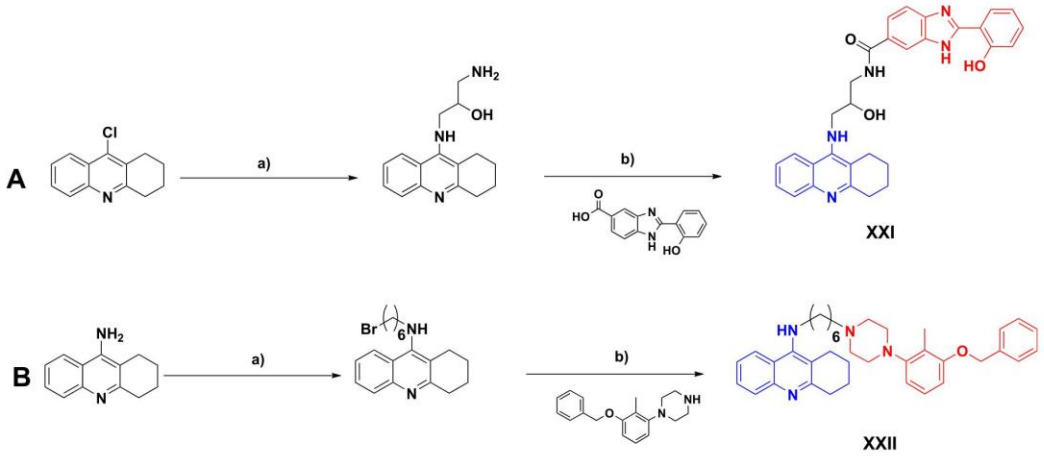
Based on a similar approach, Hiremathad and co-workers [53] synthesized THA benzimidazole derivatives. Compound **XXI** (Scheme 13A) was the best of the series, displaying AChE and self and Cu-induced Aβ aggregation inhibitory activities and antioxidant properties [53]. Compound **XXI** (Scheme 13A) was obtained after the coupling of a tetrahydroacridine intermediate (Scheme 13A, step a) with 2-(2-hydroxyphenyl)-1*H*-benzo[*d*]imidazole-5-carboxylic acid (Scheme 13A, step b) [53].

Tacrine hybrids acting as cholinesterase inhibitors and 5-HT_6 receptor antagonists were also described by Wieckowska and co-workers [54]. Among them, the most promising was compound **XXII** (Scheme 13B), which was obtained by N-alkylation of THA with the appropriate dibromoalkane (Scheme 13B, step a) and subsequent reaction with (1-(3-(benzyloxy)-2-methylphenyl) piperazine (Scheme 13B, step b) [54].

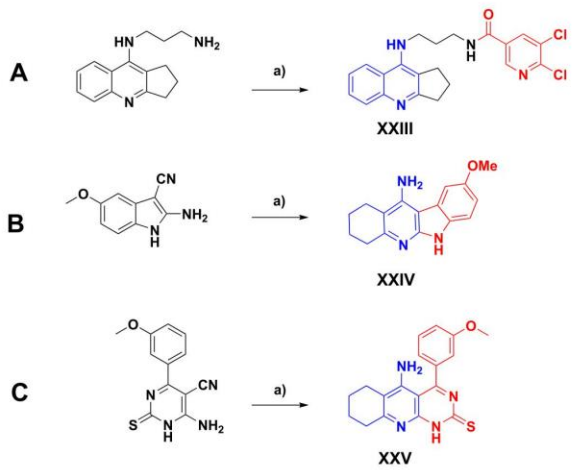
Inspired on THA scaffold, Czarnecka et al. [55] designed and synthesized a library of quinoline derivatives by linking 2,3-dihydro-*1H*-cyclopenta[*b*]quinoline to 5,6-dichloronicotinic acid (Scheme 14A). Compound **XXIII** was the most promising ChE inhibitor with Aβ anti-aggregating activity [55].



Scheme 12. Synthesis of the tacrine/amantadine hybrid **XX**. a) $POCl_3$, b) 1,5-diaminopentane, phenol, c) 1-isothiocyanatoadamantane, $CHCl_3$.



Scheme 13. Synthesis of the tacrine hybrids **XXI** and **XXII**. **A:** a) 1,3-diamino-2-propanol, KI, phenol b) DCC, NHS. **B:** a) 1,6-dibromohexane, KOH, dry DMSO, b) K_2CO_3, KI, ACN.



Scheme 14. Synthesis of the tacrine-inspired hybrids **XXIII-XXV**. **A:** a) 5,6-dichloronicotinic acid, CDMT, *N*-methylmorpholine. **B:** a) cyclohexanone, $AlCl_3$, 1,2-dichloroethane, MW. **C:** a) $AlCl_3$, CH_2Cl_2, MW.

In addition to linking strategies, THA was also merged with different scaffolds [56,57]. For instance, Benek et al. [56] obtained new indolotacrine analogues by coupling 2-aminoindole-3-carbonitrile with THA (Scheme 14B). Compound **XXIV** (Scheme 14B) emerged as the best ChE and MAO inhibitor [56]. The synthesis of compound **XXIV** is outlined in Scheme 14B [56].

Chioua et al. [57] synthesized tacripyrimidines by merging 3,4-dihydropyrimidin-2(*1H*)-thione, an efficient calcium channel blocker (CCB), with THA. Compound **XXV** (Scheme 14C) showed the most favourable biological outline [57]. The synthetic procedure followed to obtain compound **XXV** is depicted in Scheme 14C [57]. The starting material (Scheme 14C) was obtained by a Biginelli reaction between arylidenemalonitrile and thiourea (Scheme 14C) [57].

4. Rivastigmine-based multitarget-directed ligands

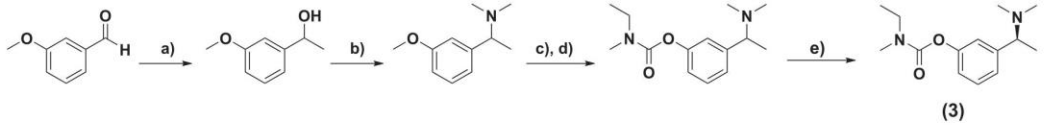
Rivastigmine ((*S*)-3-[1-(dimethylamino)ethyl]phenyl-ethyl(methyl) carbamate, Fig. 1), was approved in 2000 by the FDA for palliative treatment of AD [58]. Studies showed that the (*S*)-enantiomer display the most potent AChE activity [59].

The synthesis of rivastigmine was first reported in 1986 by Weinstock-Rosin and is depicted in Scheme 15 [60,61]. A Grignard reaction between 3-methoxybenzaldehyde and methyl magnesium iodide (CH_3MgI) (Scheme 15, step a) was followed by an N-alkylation reaction (Scheme 15, step b), yielding a 3-methoxybenzylamine derivative. This intermediate was demethylated via Stedman procedure (Scheme 15, step c), and the resulting phenol reacted with *N*-ethyl-*N*-methylcarbamoyl chloride to afford the racemic mixture of rivastigmine (Scheme 15, step d). The enantiomeric resolution was performed using *p*-toluoyl-*D*-tartrate (DTTA) (Scheme 15, step e) [60,61].

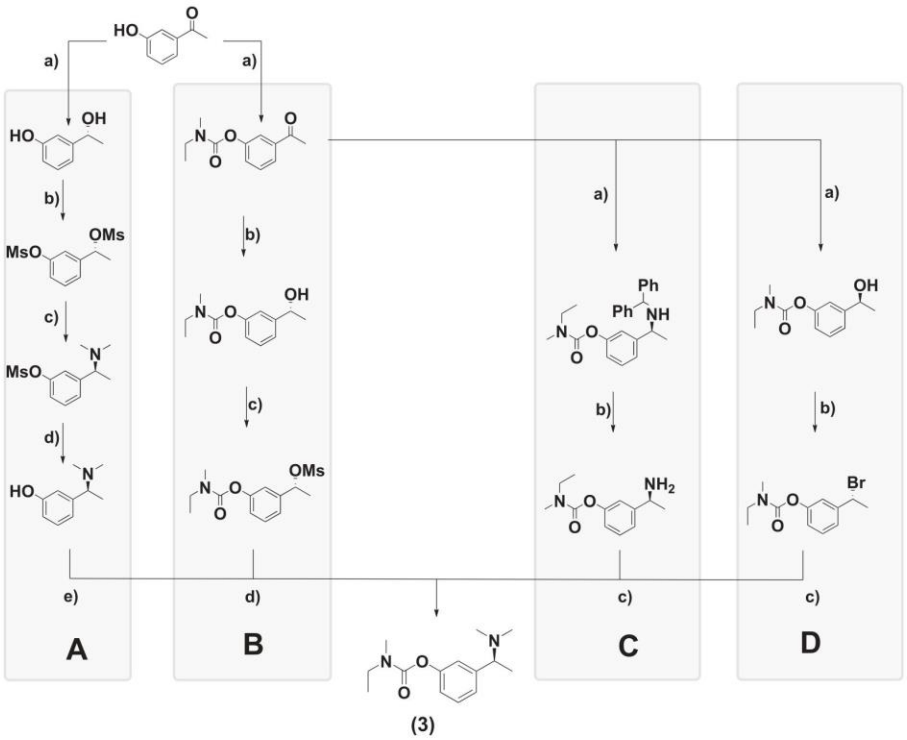
Over the last years, several methods were developed to obtain (*S*)-rivastigmine without relying on the resolution of racemic mixtures [62]. The synthetic methods described so far to obtain (*S*)-rivastigmine are summarized in Scheme 16 [62–64].

As *N,N*-dialkylcarbamate is the fragment responsible for interaction of rivastigmine with the active site of AChE it has been used to obtain new MTDLs [65].

Montanari et al. [66] synthesized a series of coumarin derivatives containing a carbamate group targeted to fatty acid amide hydrolase and ChE (Scheme 17). The best MTDLs were compounds



Scheme 15. Synthesis of rivastigmine by Weinstock-Rosin reaction. a) 1. CH_3MgI, diethyl ether, 2. HBr, benzene, b) dimethylamine, benzene, c) HBr, d) *N*-ethyl-*N*-methylcarbamoyl chloride, NaH, e) DTTA.



Scheme 16. Synthesis of (*S*)-rivastigmine: **A:** a) H_2, Ir-(*S*)-SpiroPAP-3-CH_3, *t*-BuONa, EtOH, b) MsCl, Et_3N, THF c) dimethylamine, THF, d) NaOH, e) *N*-ethyl-*N*-methylcarbamoyl chloride, K_2CO_3, EtOAc. **B:** a) *N*-ethyl-*N*-methylcarbamoyl chloride, K_2CO_3 or Et_3N, EtOAc or acetone or CH_2Cl_2, b) H_2, Ir-(*S*)-SpiroPAP-3-CH_3, t-BuONa, EtOH, c) MsCl, Et_3N, THF, d) dimethylamine, THF. **C:** a) $NH_2(Ph)_2$, CH_2Cl_2, TFA, $Ti(OiPr)_4$, b) Pd/C, MeOH, c) CH_2O, $NaBH(OAc)_3$, CH_2Cl_2. **D:** a) ketoreductase b) PBr_3, Na_2CO_3, CH_2Cl_2, c) dimethylamine hydrochloride.

XXVI and **XXVII**. The synthetic strategy pursued to obtain these compounds is depicted in Scheme 17 [66]. Initially, 7-hydroxycoumarin was *O*-alkylated to obtain the coumarin intermediates (Scheme 17, steps a and e). One intermediate, 7-(3-iodopropyloxy)coumarin, reacted with *N*-(3-hydroxybenzyl)-methylamine by a nucleophilic substitution (Scheme 17, step c), and the resulting product reacted with the appropriate isocyanate in the presence of NaH to afford compound **XXVI** (Scheme 17, step d) [66]. The other intermediate, *O*-propargyl coumarin, reacted with 1-(azidomethyl)-3-methoxybenzene, via Huisgen 1,3-dipolar cycloaddition, to afford a 1,2,3-triazole derivative (Scheme 17, step f), After *O*-demethylation (Scheme 17, step g) and reaction with the appropriate isothiocyanate (Scheme 17, step h) compound **XXVII** was obtained [66].

The *N,N*-dialkylcarbamate fragment was also used to obtain hybrids based on scutellarein [67] and curcumin [68]. The most promising scutellarein-rivastigmine hybrid (compound **XXVIII**, Fig. 3) showed cholinergic, antioxidant, metal chelating and neuroprotective properties. Compound **XXVIII** was obtained by reacting the appropriate flavonoid derivative with *N,N*-diethylcarbamoyl chloride under alkaline conditions using 4-dimethylaminopyridine (4-DMAP) as catalyst [67]. The best curcumin-rivastigmine hybrid **XXIX** (Fig. 3) displayed relevant AChE and Aβ aggregation inhibitory activities. The synthesis of compound **XXIX** started with the reaction of vanillin with *N,N*-dimethylcarbamoyl chloride in the presence of NaH, and subsequent reduction of the product formed with $NaBH_4$ [68]. After, reaction with $SOCl_2$ and subsequent nucleophilic substitution with piperidine compound **XXIX** was obtained (Fig. 3) [68].

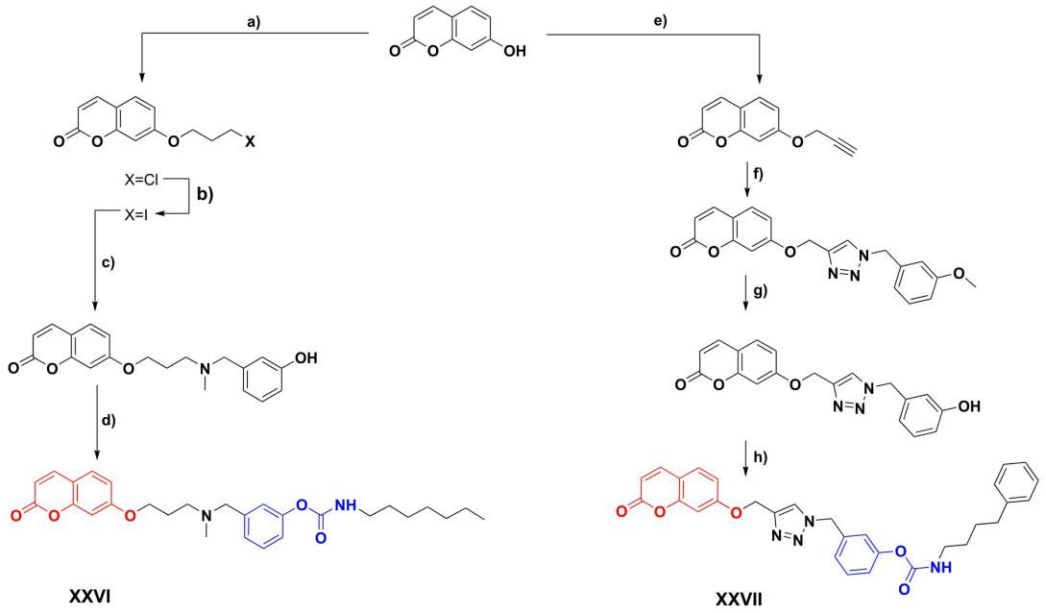
Yu and co-workers [69] reported the synthesis of pyrazolopyrimidinone-rivastigmine hybrids as potential PDE9A and BuChE inhibitors. Among the derivatives, compound **XXX** (Scheme 18) showed the best dual inhibitor profile [69]. The tracked synthetic route outlined in Scheme 18 used a dichloropurine derivative as starting material that after alkaline hydrolysis afford the corresponding carbonyl compound (Scheme 18, step a). After N-alkylation (Scheme 18, step b) and reaction with *N,N*-dimethylcarbamoyl chloride in the presence of NaH compound **XXX** was obtained (Scheme 18, step c) [69].

5. Memantine/amantadine-based multitarget-directed ligands

Memantine (3,5-dimethyladamantan-1-amine, MEM, Fig. 1) and amantadine (adamantan-1-amine, AMA, Fig. 1) are two drugs that have an adamantane moiety. These drugs are uncompetitive NMDAR antagonists approved for the treatment of NDs as monotherapy or administrated in combination with AChEI [70,71].

Memantine was first synthesized by Eli Lilly & Co. as an antidiabetic drug but it was ineffective in lowering elevated blood sugar [72]. The repurposing of this drug led to its approval for AD in 2003 by the European Medicines Agency (EMEA) and the FDA [73].

Amantadine was firstly described as a preventive agent for Asian influenza and influenza A but in 1969 it was reported that AMA ameliorated the symptoms of Parkinson's disease (PD) such as akinesia, rigidity and tremors [74]. After a long path FDA approved



Scheme 17. Synthesis of the coumarin-rivastigmine based hybrids **XXVI** and **XXVII**. a) 1- bromo-3-chloro-propane, K_2CO_3, acetone b) NaI, MeCOEt, c) *N*-(3-hydroxybenzyl)-methylamine, Et_3N, toluene, d) isocyanate, NaH, toluene e) propargyl bromide, K_2CO_3, acetone, f) 1-(azidomethyl)-3-methoxybenzene, Et_3N, $CuSO_4$, sodium ascorbate, DMSO, g) BBr_3, CH_2Cl_2, h) isocyanate, NaH, toluene.

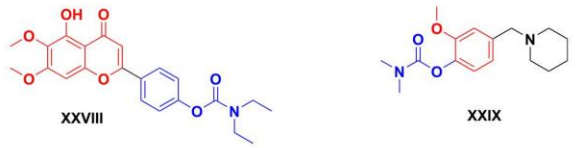
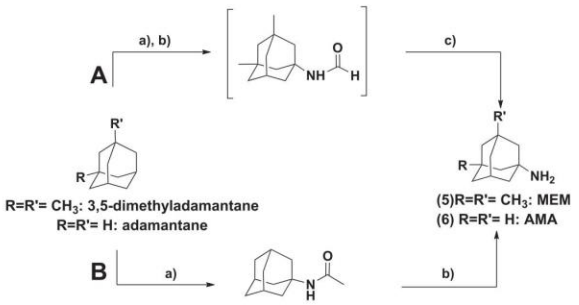


Fig. 3. Scutellarein-rivastigmine (**XXVIII**) and curcumin-rivastigmine based hybrids (**XXIX**).

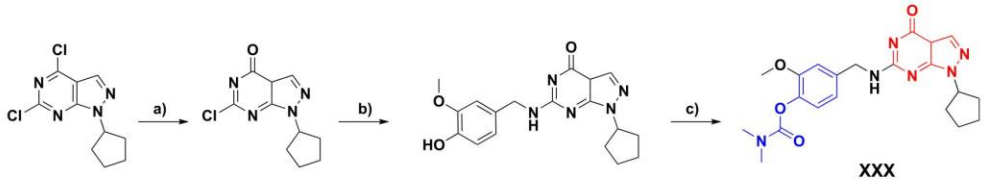
in 2017 AMA in association with L-Dopa for the treatment of the early stage of PD [75].

The development of new and effective synthetic strategies to obtain MEM and AMA is still an active area [76–78]. In this context, one-step procedures were developed to circumvent the time-consuming and expensive purification steps and thereby save time and increase the reaction yield [79]. For instance, Ivleva and Klimochkin reported an one-pot method to synthesize MEM (Scheme 19A) [80]. in which the tertiary carbon of 3,5-dimethyladamantane was firstly activated using HNO_3 (Scheme 19A, step a) and then the adamantylamide intermediate, obtained via Ritter reaction (Scheme 19A, step b) [81], was treated with aqueous solution of NH_3 to afford MEM (Scheme 19A, step c) [80].



Scheme 19. Synthesis of memantine (MEM), and amantadine (AMA). **A:** a) HNO_3, b) HCN, c) NH_3 aq. **B:** a) H_2SO_4, CH_3CN, b) KOH, PG, H_2O.

With the same endeavor Vu et al. [82] optimized the synthesis of AMA using a two-step synthetic strategy (Scheme 19B) and adamantane as starting material. After reaction with sulfuric acid and acetonitrile the amide derivative (Scheme 19B, step a) was hydrolyzed, with a mixture of KOH, propylene glycol (PG) and water, yielding AMA (Scheme 19B, step b) [82].



Scheme 18. Synthesis of the pyrazolopyrimidinone-rivastigmine based hybrid **XXX**. a) KOH, b) 4-(aminomethyl)-2-methoxyphenol, *i*-PrOH, Et_3N, c) *N*-ethyl-*N*-methylcarbamoyl chloride, NaH, DMF.

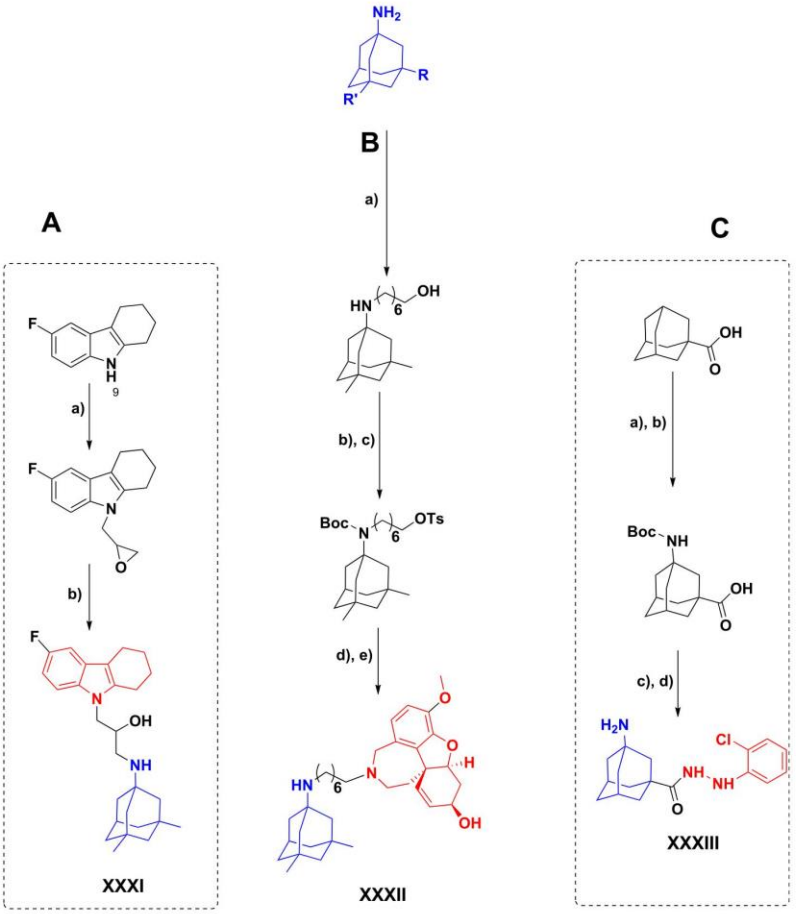
Currently, several research groups designed MEM- and AMA-based hybrids to obtain compounds able to modulate different targets [83–86]. Bachurin and co-workers [83,84] linked amino-adamantane to a carbazole scaffold to obtain compounds acting as BuChE inhibitors and NMDAR antagonists (Scheme 20A). The synthesis of the best compound is depicted in the Scheme 20A [83,84]. Compound **XXXI** was obtained by N-alkylation of the fluorocarbazole derivative with epibromohydrin in the presence of KOH (Scheme 20A, step a) and subsequent reaction with MEM (Scheme 20A, step b) [83,84].

Galantamine (Fig. 1) and MEM were combined by Simoni et al. [85] to obtain dual target compounds, specifically as AChE inhibitors and NMDAR antagonists (Scheme 20B). Compound **XXXII** was the best hybrid of the series. Its synthesis started with the N-alkylation of MEM with the appropriate bromoalkylalcohol in the presence of K_2CO_3 (Scheme 20B, step a). After *N*-Boc protection (Scheme 20B, step b) and hydroxyl group activation with TsCl (Scheme 20B, step c), the tosyl intermediate reacted with *O*-desmethyl galantamine to afford compound **XXXII** (Scheme 20B, steps d and e) [85].

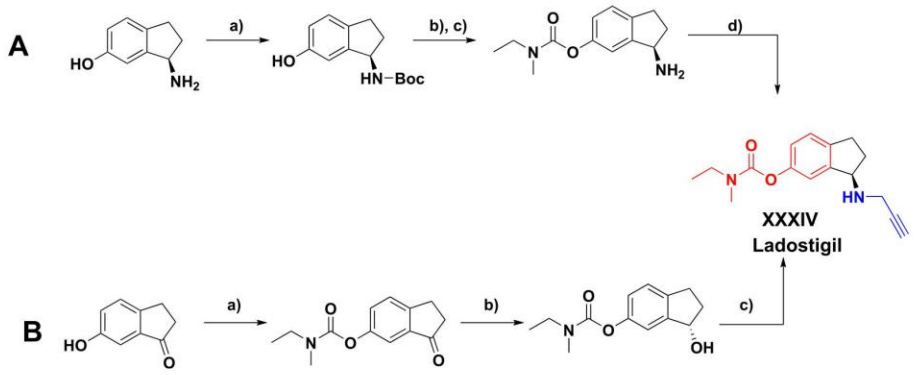
Karoutzou et al. [86] reported the synthesis of AMA derivatives acting as dual ATP-gated P2X7 receptors/NMDAR antagonists (Scheme 20C). Compound **XXXIII** was obtained following the synthetic route depicted in Scheme 20C [86]. 1-Adamantanecarboxylic acid was treated with HNO_3/H_2SO_4 and refluxed with HCl to afford the amine derivative, which in turn was protected withBoc anhydride (Scheme 20C, steps a and b). The coupling the resulting intermediate with (2-chlorophenyl)hydrazine, and subsequent *N*-Boc deprotection, afforded compound **XXXIII** (Scheme 20C, steps c and d) [86].

6. Rasagiline-based multitarget-directed ligands

Over the last few decades, the propargylamine fragment present in MAO-B inhibitors such as rasagiline (Fig. 1) has received increasing interest as it is associated with neuronal and mitochondrial protective properties [87,88], antiapoptotic and anti-Aβ aggregation activities [87–89].



Scheme 20. Synthesis of the memantine and amantadine -based hybrids **XXXI**-**XXXIII**: **A:** a) epibromohydrin, KOH, DMF, b) MEM, *i*-PrOH. **B:** a) 6-bromohexan-1-ol, K_2CO_3, DMF, b) Boc_2O, Na_2CO_3, THF/H_2O, c) TsCl, Et_3N, DMAP, CH_2Cl_2, d) desmethyl galantamine, Et_3N, MeCN, e) HCl, dioxane. **C:** a) 1. HNO_3, H_2SO_4, ACN, 2. HCl, H_2O, b) Boc_2O, NaOH, THF, c) (2-chlorophenyl)hydrazine, HOBt, EDC, CH_2Cl_2, d) HCl, 1,4-dioxane.

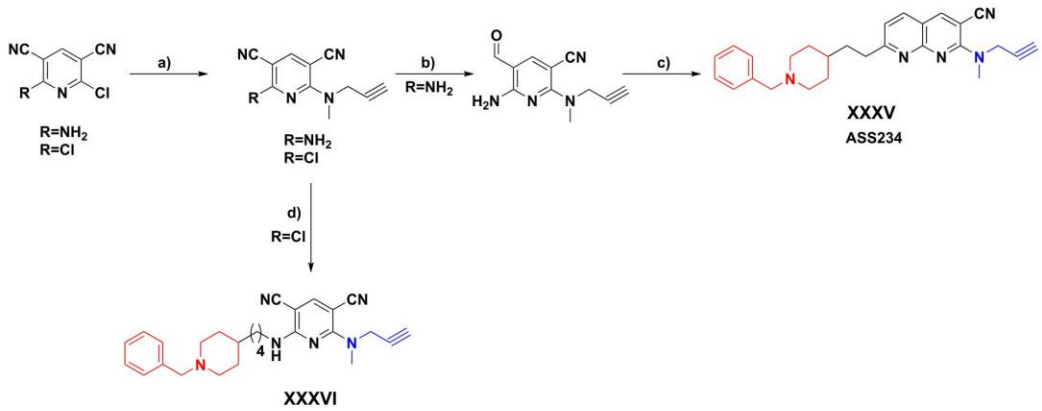


Scheme 21. Synthesis of ladostigil. **A:** a) Boc_2O, di-*t*-butyl decarbonate, Et_3N, THF, b) *N*-ethyl-*N*-methylcarbamoyl chloride, NaH, ACN c) HCl, dioxane d) propargyl bromide, K_2CO_3, ACN. **B:** a) *N*-ethyl-*N*-methylcarbamoyl chloride, K_2CO_3, ACN, b) formic acid, *(S,S)*-TsDPEN Ru(*p*-cymene)C1, Et_3N, CH_2Cl_2 c) propargylamine, CH_3SO_2Cl anhydride, CH_2Cl_2.

In this respect, the propargylamine fragment has been incorporated into structures of diverse scaffolds to obtain new MTDLs [90]. For instance, ladostigil ((*R*)-(+)-6-(*N*-methyl-*N*-ethylcarbamoyloxy)-*N*′-propargyl-1-aminoindan, compound **XXXIV**, Scheme 21), a dual ChE/MAO inhibitor was obtained by merging the carbamate moiety of rivastigmine (Fig. 1) with the propargyl group [91]. Ladostigil was first synthesized by Sterling and coworkers (Scheme 21A) [91]. The synthesis involved a four-step sequence using *(S)*-6-hydroxy-1-aminoindan as starting material (Scheme 21A) [91]. The synthesis started with a *N*-Boc protection of the staring material (Scheme 21A, step a) followed by the carbamylation of the resulting intermediate (Scheme 21A, step b). After, *N*-Boc deprotection (Scheme 21A, step c) and propargylation ladostigil was obtained (Scheme 21A, step d) [91]. In 2006, Teva Pharmaceutical Industries Ltd [92] patented a new synthetic strategy to scale-up the process for industrial production (Scheme 21B). Briefly, 1-indanone was carbamylated (Scheme 21B, step a) and reduced to *(S)*-indanol in the presence of an optically active catalyst or by hydrogenation (Scheme 21B, step b). The hydroxyl group was then changed into a good leaving group to introduce by an S_N2 reaction the propargylamine group (Scheme 21B, step c) [92].

In an attempt to obtain new MTDLs, Samadi et al. [93] designed a small library of compounds containing the propargylamine fragment of rasagiline (Fig. 1) and the *N*-benzyl piperidine moiety of donepezil (Fig. 1) and pyridine or naphthyridine rings as scaffolds. Compound **XXXV** (Scheme 22) was the most promising of the series [93]. To obtain this compound [93,94], 2-amino-6-chloropyridine-3,5-dicarbonitrile and *N*-methylprop-2-yn-1-amine were refluxed in a mixture of THF/EtOH (Scheme 22, step a). Then, the aldehyde obtained by reducing the nitrile group of the propargylamine derivative (Scheme 22, step b) was used in a Friedländer reaction with 4-(1-benzylpiperidin-4-yl)butan-2-one to afford the final compound (Scheme 22, step c) [93,94]. Compound **XXXV**, also known as **ASS234**, is a MTDL with potent ChE/MAO inhibitory activities, and is still under study to develop a drug candidate for AD [90]. Along this framework Bautista-Aguilera et al. [95] designed and developed potent and selective dual AChE/MAO-B inhibitors based on **ASS234** (Scheme 22, compound **XXXVI**). In this case, 2,6-dichloropyridine-3,5-dicarbonitrile reacted with propargylamine to obtain 2-chloro-6-(prop-2-yn-1-yl)amino-pyridine-3,5-dicarbonitrile (Scheme 22, step a), which in turn was coupled with 3-(1-benzylpiperidin-4-yl)propan-1-amine to yield compound **XXXVI** (Scheme 22, step d) [95]. The synthetic strategy followed to fit in the *N*-benzylpiperidine and propargylamine moieties were similar to the described by Samadi et al. [93].

The design and synthesis of new propargylamine-based MTDLs was not only focused on dual ChE/MAO inhibitors. Several target combinations have been looked, namely with oxidative stress,



Scheme 22. Synthesis of the rasagiline-based hybrids **XXXV** and **XXXVI**. a) *N*-methylpropargylamine, Et_3N, THF/EtOH, b) $LiAlH_4$, THF, c) 4-(*N*-benzylpiperidin)-butanone, pyrrolidine CH_2Cl_2/MeOH d) 4-(*N*-benzylpiperidin)-butanamine, Et_3N, THF, EtOH.

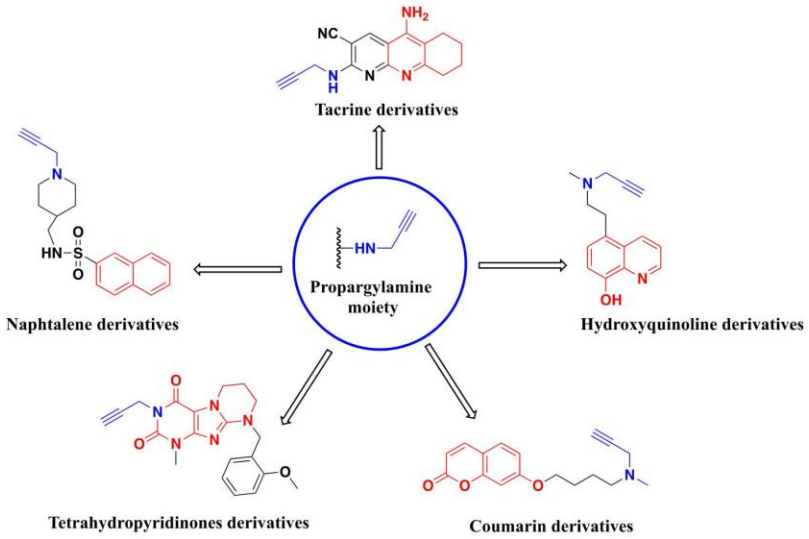


Fig. 4. Chemical diversity of rasagiline -based multitarget-directed ligands.

NMDAR and adenosine, serotonin or dopamine receptor [90]. The scaffolds used were quite diverse and included THA [96], tetrahydropyridinone [97], naphthalene [98], hydroxyquinoline [99–101], and coumarin derivatives (Fig. 4) [102].

7. Concluding remarks

The design and development of new MTDLs is a hot topic in drug discovery programs for multifactorial diseases such as AD. While MTLDs can be designed by linking, merging or fusing pharmacophores different bioactive compounds, our query clearly disclosed a continuing dependence on the synthesis of hybrids of the first type.

The chemistry toolbox used in the development of MTDLs for AD includes classic synthetic organic reactions. This was also the case for linked pharmacophores, where amide linking reactions dominated the synthetic strategies. Overall, the use of innovative, versatile and green synthetic strategies is still largely absent in this field.

At the same time, we noticed a clear lack of focus on physicochemical properties associated with absorption, distribution, metabolism, and excretion – toxicity (ADME-Tox), which are often disregarded over parameters like pharmacological potency. In our opinion, particular attention should be given to the overall quality of the developed MTLDs, namely related to the optimum lipophilicity range and efficiency indexes. Future strategies to obtain MTDLs should be normalized to encompass these key parameters of drug design.

Although NDs are genetically distinct and have specific pathological hallmarks, accumulating evidence suggests that crosstalk mechanisms can occur between two or more NDs. It is thus our opinion that the MTLD approach will provide a valuable strategy to feed the pipeline of innovative and disease-modifying drugs for currently incurable NDs.

Acknowledgements

This work was funded by FEDER funds through the Operational Programme Competitiveness Factors-COMPETE and national funds by FCT – Foundation for Science and Technology under research grants (UID/QUI/00081, NORTE-01-0145-FEDER-000028, POCI-01-0145-FEDER-029164). D. Chavarria grant (SFRH/BD/108119/2015) is supported by FCT, POPH and QREN. This article is based upon work from COST Action CA15135.

Conflicts of interest

No conflict of interest is declared.

References

[1] J.Y.Y. Szeto, S.J.G. Lewis, Current treatment options for Alzheimer's disease and Parkinson's disease dementia, Curr. Neuropharmacol. 14 (2016) 326–338.
[2] H. Shah, E. Albanese, C. Duggan, I. Rudan, K.M. Langa, M.C. Carrillo, K.Y. Chan, Y. Joanette, M. Prince, M. Rossor, S. Saxena, H.M. Snyder, R. Sperling, M. Varghese, H. Wang, M. Wortmann, T. Dua, Research priorities to reduce the global burden of dementia by 2025, Lancet Neurol. 15 (2016) 1285–1294.
[3] M. Prince, R. Bryce, E. Albanese, A. Wimo, W. Ribeiro, C.P. Ferri, The global prevalence of dementia: a systematic review and metaanalysis, Alzheimer's Dementia 9 (2013) 63–75.
[4] C.G. Parsons, W. Danysz, A. Dekundy, I. Pulte, Memantine and cholinesterase inhibitors: complementary mechanisms in the treatment of Alzheimer's disease, Neurotox. Res. 24 (2013) 358–369.
[5] M.B. Colović, D.Z. Krstić, T.D. Lazarević-Pašti, A.M. Bondžić, V.M. Vasić, Acetylcholinesterase inhibitors: pharmacology and toxicology, Curr. Neuropharmacol. 11 (2013) 315–335.
[6] L. Gan, M.R. Cookson, L. Petrucelli, A.R. La Spada, Converging pathways in neurodegeneration, from genetics to mechanisms, Nat. Neurosci. 21 (2018) 1300–1309.
[7] A. Cavalli, M.L. Bolognesi, A. Minarini, M. Rosini, V. Tumiatti, M. Recanatini, C. Melchiorre, Multi-target-Directed ligands to combat neurodegenerative diseases, J. Med. Chem. 51 (2008) 347–372.
[8] J.L. Medina Franco, M.A. Giulianotti, G.S. Welmaker, R.A. Houghten, Shifting from the single to the multitarget paradigm in drug discovery, Drug Discov. Today 18 (2013) 495–501.
[9] Y. Bansal, O. Silakari, Multifunctional compounds: smart molecules for multifactorial diseases, Eur. J. Med. Chem. 76 (2014) 31–42.
[10] R.R. Ramsay, M.R. Popovic Nikolic, K. Nikolic, E. Uliassi, M.L. Bolognesi, A perspective on multi-target drug discovery and design for complex diseases, Clin. Transl. Med. 7 (2018) 1–14.
[11] M.B. Youdim, L. Kupershmidt, T. Amit, O. Weinreb, Promises of novel multitarget neuroprotective and neurorestorative drugs for Parkinson's disease, Park. Relat. Disord. 20 (2014) S132–S136.
[12] M. Benchekroun, S. Maramai, Multitarget-directed ligands for neurodegenerative diseases: real opportunity or blurry mirage? Future Med. Chem. 11 (2019) 261–263.

[13] J. Zhou, X. Jiang, S. He, H. Jiang, F. Feng, W. Liu, W. Qu, H. Sun, Rational design of multitarget-directed ligands: strategies and emerging paradigms, J. Med. Chem. 15 (6) (2009) 587–600.
[14] R. Morphy, Z. Rankovic, Designing multiple ligands - medicinal chemistry strategies and challenges, Curr. Pharmaceut. Des. 15 (2009) 587–600.
[15] E. Uliassi, F. Prati, S. Bongarzone, M.L. Bolognesi, Medicinal chemistry of hybrids for neurodegenerative diseases, in: Michael Decker (Ed.), Design of Hybrid Molecules for Drug Development, Elsevier Inc., 2017, pp. 259–277.
[16] D.C. Blakemore, L. Castro, I. Churcher, D.C. Rees, A.W. Thomas, D.M. Wilson, A. Wood, Organic synthesis provides opportunities to transform drug discovery, Nat. Chem. 10 (2018) 383–394.
[17] J. Boström, D.G. Brown, R.J. Young, G.M. Keserü, Expanding the medicinal chemistry synthetic toolbox, Nat. Rev. Drug Discov. 17 (2018) 709–727.
[18] D.G. Brown, J. Boström, Analysis of past and present synthetic methodologies on medicinal chemistry: where have all the new reactions gone? J. Med. Chem. 59 (2016) 4443–4458.
[19] M.C. Rodrigues Simões, F.P. Dias Viegas, M.S. Moreira, M. de Freitas Silva, M.M. Riquiel, P.M. da Rosa, M.R. Castelli, M.H. dos Santos, M.G. Soares, C. Viegas Jr., Donepezil: an important prototype to the design of new drug candidates for Alzheimer's disease, Mini Rev. Med. Chem. 14 (2014) 2–19.
[20] B. Seltzer, Donepezil: a review, Expert Opin. Drug Metabol. Toxicol. 1 (2005) 527–536.
[21] M.S. Reddy, S. Eswaraiah, M.V. Thippannachar, E.R.R. Chandrashekar, P.A. Kumar, K.N. Kumar, US Pat. US 2004/0143121 A1 (2004).
[22] K.S. Dias, C.T. de Paula, T. Dos Santos, I.N. Souza, M.S. Boni, M.J. Guimarães, F.M. da Silva, N.G. Castro, G.A. Neves, C.C. Veloso, M.M. Coelho, I.S. de Melo, F.C. Giusti, A. Giusti-Paiva, M.L. da Silva, L.E. Dardenne, I.A. Guedes, L. Pruccoli, F. Morroni, A. Tarozzi, C. Viegas Jr., Design, synthesis and evaluation of novel feruloyl-donepezil hybrids as potential multitarget drugs for the treatment of Alzheimer's disease, Eur. J. Med. Chem. 130 (2017) 440–457.
[23] F. Prati, C. Bergamini, R. Fato, O. Soukup, J. Korabecny, V. Andrisano, M. Bartolini, M.L. Bolognesi, Novel 8-hydroxyquinoline derivatives as multitarget compounds for the treatment of Alzheimer's disease, ChemMedChem 11 (2016) 1284–1295.
[24] J.L. Domínguez, F. Fernández-Nieto, J.M. Brea, M. Catto, M.R. Paleo, S. Porto, F.J. Sardina, M. Castro, L. Pisani, A. Carotti, R. Soto-Otero, E. Méndez-Alvarez, M.C. Villaverde, F. Sussman, 8-Aminomethyl-7-hydroxy-4-methylcoumarins as multitarget leads for Alzheimer's disease, ChemistrySelect 1 (2016) 2742–2749.
[25] M. Shidore, J. Machhi, K. Shingala, P. Murumkar, M.K. Sharma, N. Agrawal, A. Tripathi, Z. Parikh, P. Pillai, M.R. Yadav, Benzylpiperidine-linked diarylthiazoles as potential anti-alzheimer's agents: synthesis and biological evaluation, J. Med. Chem. 59 (2016) 5823–5846.
[26] F. Li, Z.M. Wang, J.J. Wu, J. Wang, S.S. Xie, J.S. Lan, W. Xu, L.Y. Kong, X.B. Wang, Synthesis and pharmacological evaluation of donepezil-based agents as new cholinesterase/monoamine oxidase inhibitors for the potential application against Alzheimer's disease, J. Enzym. Inhib. Med. Chem. 31 (2016) 41–53.
[27] L. Pisani, R. Farina, M. Catto, R.M. Iacobazzi, O. Nicolotti, S. Cellamare, G.F. Mangiatordi, N. Denora, R. Soto-Otero, L. Siragusa, C.D. Altomare, A. Carotti, Exploring basic tail modifications of coumarin-based dual acetylcholinesterase-monoamine oxidase B inhibitors: identification of water-soluble, brain-permeant neuroprotective multitarget agents, J. Med. Chem. 59 (2016) 6791–6806.
[28] Z. Sang, W. Pan, K. Wang, Q. Ma, L. Yu, Y. Yang, P. Bai, C. Leng, Q. Xu, X. Li, Z. Tan, W. Liu, Design, synthesis and evaluation of novel ferulic acid-*O*-alkylamine derivatives as potential multifunctional agents for the treatment of Alzheimer's disease, Eur. J. Med. Chem. 130 (2017) 379–392.
[29] J. Hu, Y.D. Huang, T. Pan, T. Zhang, T. Su, X. Li, H.B. Luo, L. Huang, Design, synthesis, and biological evaluation of dual-target inhibitors of acetylcholinesterase (AChE) and phosphodiesterase 9A (PDE9A) for the treatment of Alzheimer's disease, ACS Chem. Neurosci. 10 (2019) 537–551.
[30] J. Yan, J. Hu, A. Liu, L. He, X. Li, H. Wei, Design, synthesis, and evaluation of multitarget-directed ligands against Alzheimer's disease based on the fusion of donepezil and curcumin, Bioorg. Med. Chem. 25 (2017) 2946–2955.
[31] F.P. Dias Viegas, M. de Freitas Silva, M. Divino da Rocha, M.R. Castelli, M.M. Riquiel, R.P. Machado, S.M. Vaz, L.M. Simões de Lima, K.C. Mancini, P.C. Marques de Oliveira, E.P. Morais, V.S. Gontijo, F.M.R. da Silva, D. D'Alincourt da Fonseca Pecanha, N.G. Castro, G.A. Neves, A. Giusti-Paiva, F.C. Vilela, L. Orlandi, I. Camps, M.P. Veloso, L.F. Leomil Coelho, M. Ionta, G.A. Ferreira-Silva, R.M. Pereira, L.E. Dardenne, I.A. Guedes, W. de Oliveira Carneiro Junior, P.M. Quaglio Bellozi, A.C. Pinheiro de Oliveira, F.F. Ferreira, L. Pruccoli, A. Tarozzi, C. Viegas Jr., Design, synthesis and pharmacological evaluation of N-benzyl-piperidinyl-aryl-acylhydrazone derivatives as donepezil hybrids: discovery of novel multi-target anti-alzheimer prototype drug candidates, Eur. J. Med. Chem. 147 (2018) 48–65.
[32] Z. Sang, X. Qiang, Y. Li, R. Xu, Z. Cao, Q. Song, T. Wang, X. Zhang, H. Liu, Z. Tan, Y. Deng, Design, synthesis and evaluation of scutellarein-O-acetamidoalkylbenzylamines as potential multifunctional agents for the treatment of Alzheimer's disease, Eur. J. Med. Chem. 135 (2017) 307–323.
[33] A. Pau, M. Catto, G. Pinna, S. Frau, G. Murineddu, B. Asproni, M.M. Curzu, L. Pisani, F. Leonetti, M.I. Loza, J. Brea, G.A. Pinna, A. Carotti, Multitarget-directed tricyclic pyridazinones as G protein-coupled receptor ligands and cholinesterase inhibitors, ChemMedChem 10 (2015) 1054–1470.
[34] C. Lecoutey, D. Hedou, T. Freret, P. Giannoni, F. Gaven, M. Since, V. Bouet, C. Ballandonne, S. Corvaisier, A. Malzert Freon, S. Mignani, T. Cresteil, M. Boulouard, S. Claeysen, C. Rochais, P. Dallemagne, Design of donecopride, a dual serotonin subtype 4 receptor agonist/acetylcholinesterase inhibitor with potential interest for Alzheimer's disease treatment, Proc. Natl. Acad. Sci. U.S.A. 111 (2014) E3825–E3830.
[35] M. Girek, P. Szymański, Tacrine hybrids as multi-target-directed ligands in Alzheimer's disease: influence of chemical structures on biological activities, Chem. Pap. 73 (2019) 269–289.
[36] A. Romero, R. Cacabelos, M.J. Oset-Gasque, A. Samadi, J. Marco-Contelles, Novel tacrine-related drugs as potential candidates for the treatment of Alzheimer's disease, Bioorg. Med. Chem. Lett 23 (2013) 1916–1922.
[37] A. Minarini, A. Milelli, E. Simoni, M. Rosini, M.L. Bolognesi, C. Marchetti, V. Tumiatti, Multifunctional tacrine derivatives in Alzheimer's disease, Curr. Top. Med. Chem. 13 (2013) 1771–1786.
[38] A. Musial, M. Bajda, B. Malawska, Recent developments in cholinesterases inhibitors for Alzheimer's disease treatment, Curr. Med. Chem. 14 (2007) 2654–2679.
[39] S.S. Xie, X.B. Wang, J.Y. Li, L. Yang, L.Y. Kong, Design, synthesis and evaluation of novel tacrine-coumarin hybrids as multifunctional cholinesterase inhibitors against Alzheimer's disease, Eur. J. Med. Chem. 64 (2013) 540–553.
[40] M. Khalilzadeh, A. Hosseini, M. Tajbakhsh, Synthesis of tacrine derivatives under solventless conditions, J. Heterocycl. Chem. 44 (2007) 535–538.
[41] A. Hasaninejad, A. Zare, M. Shekouhy, J. Ameri-Rad, Sulfuric acid-modified PEG-6000 (PEG-OSO3H): an efficient, bio-degradable and reusable polymeric catalyst for the solvent-free synthesis of poly-substituted quinolines under microwave irradiation, Green Chem. 13 (2011) 958–964.
[42] M.K. Hu, L.J. Wu, G. Hsiao, M.H. Yen, Homodimeric tacrine congeners as acetylcholinesterase inhibitors, J. Med. Chem. 45 (2002) 2277–2282.
[43] Q.P. Qin, S.L. Wang, M.X. Tan, Z.F. Wang, D.M. Luo, B.Q. Zou, Y.C. Liu, P.F. Yao, H. Liang, Novel tacrine platinum(II) complexes display high anticancer activity via inhibition of telomerase activity, dysfunction of mitochondria, and activation of the p53 signaling pathway, Eur. J. Med. Chem. 158 (2018) 106–122.
[44] X.Y. Jiang, T.K. Chen, J.T. Zhou, S.Y. He, H.Y. Yang, Y. Chen, W. Qu, F. Feng, H.P. Sun, Dual GSK-3β/AChE inhibitors as a new strategy for multitargeting anti-alzheimer's disease drug discovery, ACS Med. Chem. Lett. 9 (2018) 171–176.
[45] A.l. Hui, Y. Chen, S.j. Zhu, C.s. Gan, J. Pan, A. Zhou, Design and synthesis of tacrine-phenothiazine hybrids as multitarget drugs for Alzheimer's disease, Med. Chem. Res. 23 (2014) 3546–3557.
[46] C. Quintanova, R.S. Keri, S.M. Marques, M. G-Fernandes, S.M. Cardoso, M.L. Serralheiro, M.A. Santos, Design, synthesis and bioevaluation of tacrine hybrids with cinnamate and cinnamylidene acetate derivatives as potential anti-Alzheimer drugs, Med. Chem. Comm. 6 (2015) 1969–1977.
[47] N. Chufarova, K. Czarnecka, R. Skibinski, M. Cuchra, I. Majsterek, P. Szymanski, New tacrine-acridine hybrids as promising multifunctional drugs for potential treatment of Alzheimer's disease, Arch. Pharm. 351 (2018) 1–11.
[48] X. Zha, D. Lamba, L. Zhang, Y. Lou, C. Xu, D. Kang, L. Chen, Y. Xu, L. Zhang, A. De Simone, S. Samez, A. Pesaresi, J. Stojan, M.G. Lopez, J. Egea, V. Andrisano, M. Bartolini, Novel tacrine-benzofuran hybrids as potent multitarget-directed ligands for the treatment of Alzheimer's disease: design, synthesis, biological evaluation, and X-ray crystallography, J. Med. Chem. 59 (2016) 114–131.
[49] E. Nepovimova, E. Uliassi, J. Korabecny, L.E. Peña-Altamira, S. Samez, A. Pesaresi, G.E. Garcia, M. Bartolini, V. Andrisano, C. Bergamini, R. Fato, D. Lamba, M. Roberti, K. Kuca, B. Monti, M.L. Bolognesi, Multitarget drug design strategy: quinone–tacrine hybrids designed to block Amyloid-β aggregation and to exert anticholinesterase and antioxidant effects, J. Med. Chem. 57 (2014) 8576–8589.
[50] J. Jerabek, E. Uliassi, L. Guidotti, J. Korabecny, O. Soukup, V. Sepsova, M. Hrabinova, K. Kuca, M. Bartolini, L.E. Pena-Altamira, S. Petralla, B. Monti, M. Roberti, M.L. Bolognesi, Tacrine-resveratrol fused hybrids as multi-target-directed ligands against Alzheimer's disease, Eur. J. Med. Chem. 127 (2017) 250–262.
[51] O. Di Pietro, F.J. Perez-Areales, J. Juarez-Jimenez, A. Espargaro, M.V. Clos, B. Perez, R. Lavilla, R. Sabate, F.J. Luque, D. Munoz-Torrero, Tetrahydrobenzo[h][1,6]naphthyridine-6-chlorotacrine hybrids as a new family of anti-Alzheimer agents targeting beta-amyloid, tau, and cholinesterase pathologies, Eur. J. Med. Chem. 84 (2014) 107–117.
[52] K. Spilovska, J. Korabecny, J. Kral, A. Horova, K. Musilek, O. Soukup, L. Drtinova, Z. Gazova, K. Siposova, K. Kuca, 7-Methoxytacrine-adamantylamine heterodimers as cholinesterase inhibitors in Alzheimer's disease treatment-synthesis, biological evaluation and molecular modeling studies, Molecules 18 (2013) 2397–2418.
[53] A. Hiremathad, R.S. Keri, A.R. Esteves, S.M. Cardoso, S. Chaves, M.A. Santos, Novel Tacrine-Hydroxyphenylbenzimidazole hybrids as potential multitarget drug candidates for Alzheimer's disease, Eur. J. Med. Chem. 148 (2018) 255–267.
[54] A. Wieckowska, T. Wichur, J. Godyn, A. Bucki, M. Marcinkowska, A. Siwek, K. Wieckowski, P. Zareba, D. Knez, M. Gluch-Lutwin, G. Kazek, G. Latacz, K. Mika, M. Kolaczkowski, J. Korabecny, O. Soukup, M. Benkova, K. Kiec-Kononowicz, S. Gobec, B. Malawska, Novel multitarget-directed ligands aiming at symptoms and causes of alzheimer's disease, ACS Chem. Neurosci. 9 (2018) 1195–1214.

[55] K. Czarnecka, M. Girek, K. Maciejewska, R. Skibiński, J. Jończyk, M. Bajda, J. Kabziński, P. Sołowiej, I. Majsterek, P. Szymański, New cyclopentaquinoline hybrids with multifunctional capacities for the treatment of Alzheimer's disease, J. Enzym. Inhib. Med. Chem. 33 (2018) 158–170.
[56] O. Benek, O. Soukup, M. Pasdiorova, L. Hroch, V. Sepsova, P. Jost, M. Hrabinova, D. Jun, K. Kuca, D. Zala, R.R. Ramsay, J. Marco-Contelles, K. Musilek, Design, synthesis and in vitro evaluation of indolotacrine analogues as multitarget-directed ligands for the treatment of Alzheimer's disease, ChemMedChem 11 (2016) 1264–1269.
[57] M. Chioua, E. Buzzi, I. Moraleda, I. Iriepa, M. Maj, A. Wnorowski, C. Giovannini, A. Tramarin, F. Portali, L. Ismaili, P. Lopez-Alvarado, M.L. Bolognesi, K. Jozwiak, J.C. Menendez, J. Marco-Contelles, M. Bartolini, Tacripyrimidines, the first tacrine-dihydropyrimidine hybrids, as multitarget-directed ligands for Alzheimer's disease, Eur. J. Med. Chem. 155 (2018) 839–846.
[58] M.L. Onor, M. Trevisiol, E. Aguglia, Rivastigmine in the treatment of Alzheimer's disease: an update, Clin. Interv. Aging 2 (2007) 17–32.
[59] A. Enz, German Pat. DE 3805744, 1988.
[60] M. Weinstock, M. Razin, M. Chorev, Z. Tashma, Pharmacological activity of novel anticholinesterase agents of potential use in the treatment of Alzheimer's disease, in: Abraham Fisher, Israel Hanin, Chaim Lachman (Eds.), Alzheimer's and Parkinson's Disease: Strategies for Research and Development, Springer US, Boston, MA, 1986, pp. 539–549.
[61] M. Weinstock Rosin, M. Chorev, Z. Tashma, European Pat. EP 0193926B3, 1986.
[62] P.C. Yan, G.L. Zhu, J.H. Xie, X.D. Zhang, Q.L. Zhou, Y.Q. Li, W.H. Shen, D.Q. Che, Industrial scale-up of enantioselective hydrogenation for the asymmetric synthesis of rivastigmine, Org. Process Res. Dev. 17 (2013) 307–312.
[63] G. Gao, S. Du, Y. Yang, X. Lei, H. Huang, M. Chang, Direct asymmetric reductive amination for the synthesis of (S)-Rivastigmine, Molecules 23 (2018) 1–8.
[64] M.K. Sethi, S.R. Bhandya, N. Maddur, R. Shukla, A. Kumar, V.S.N.J. Mittapalli, Asymmetric synthesis of an enantiomerically pure rivastigmine intermediate using ketoreductase, Tetrahedron Asymmetry 24 (2013) 374–379.
[65] P. Bar On, C.B. Millard, M. Harel, H. Dvir, A. Enz, J.L. Sussman, I. Silman, Kinetic and structural studies on the interaction of cholinesterases with the anti-Alzheimer drug rivastigmine, Biochemistry 41 (2002) 3555–3564.
[66] S. Montanari, L. Scalvini, M. Bartolini, F. Belluti, S. Gobbi, V. Andrisano, A. Ligresti, V. Di Marzo, S. Rivara, M. Mor, A. Bisi, A. Rampa, Fatty acid amide hydrolase (FAAH), acetylcholinesterase (AChE), and butyrylcholinesterase (BuChE): networked targets for the development of carbamates as potential anti-Alzheimer's disease agents, J. Med. Chem. 59 (2016) 6387–6406.
[67] Z. Sang, Y. Li, X. Qiang, G. Xiao, Q. Liu, Z. Tan, Y. Deng, Multifunctional scutellarin-rivastigmine hybrids with cholinergic, antioxidant, biometal chelating and neuroprotective properties for the treatment of Alzheimer's disease, Bioorg. Med. Chem. Lett 23 (2015) 668–680.
[68] Y. Li, P. Peng, L. Tang, Y. Hu, Y. Hu, R. Sheng, Design, synthesis and evaluation of rivastigmine and curcumin hybrids as site-activated multitarget-directed ligands for Alzheimer's disease therapy, Bioorg. Med. Chem. 22 (2014) 4717–4725.
[69] Y.F. Yu, Y.D. Huang, C. Zhang, X.N. Wu, Q. Zhou, D. Wu, Y. Wu, H.B. Luo, Discovery of novel pyrazolopyrimidinone derivatives as phosphodiesterase 9A inhibitors capable of inhibiting butyrylcholinesterase for treatment of alzheimer's disease, ACS Chem. Neurosci. 8 (2017) 2522–2534.
[70] J. Folch, O. Busquets, M. Ettcheto, E. Sanchez-Lopez, R.D. Castro-Torres, E. Verdaguer, M.L. Garcia, J. Olloquequi, G. Casadesus, C. Beas-Zarate, C. Pelegri, J. Vilaplana, C. Auladell, A. Camins, Memantine for the treatment of dementia: a review on its current and future applications, J. Alzheimer's Dis. 62 (2018) 1223–1240.
[71] H. Sawada, T. Oeda, S. Kuno, M. Nomoto, K. Yamamoto, M. Yamamoto, K. Hisanaga, T. Kawamura, G. Amantadine Study, Amantadine for dyskinesias in Parkinson's disease: a randomized controlled trial, PLoS One 5 (2010), e15298.
[72] M.W. Akhtar, S. Sanz-Blasco, N. Dolatabadi, J. Parker, K. Chon, M.S. Lee, W. Soussou, S.R. McKercher, R. Ambasudhan, T. Nakamura, S.A. Lipton, Elevated glucose and oligomeric beta-amyloid disrupt synapses via a common pathway of aberrant protein S-nitrosylation, Nat. Commun. 7 (2016) 1–11.
[73] S.H. Ferris, Evaluation of memantine for the treatment of Alzheimer's disease, Expert Opin. Pharmacother. 4 (2003) 2305–2313.
[74] R.S. Schwab, A.C. England, D.C. Poskanzer, R.R. Young, Amantadine in the treatment of Parkinson's disease, J. Am. Med. Assoc. 208 (1969) 1168–1170.
[75] D. Charvin, R. Medori, R.A. Hauser, O. Rascol, Therapeutic strategies for Parkinson disease: beyond dopaminergic drugs, Nat. Rev. Drug Discov. 17 (2018) 804–822.
[76] Markus-Rene Gold, Aigars Jirgensons, F.A.M. Huber, Pat. WO2010069555A1, 2010.
[77] Bandi Parthasaradhi Reddy, Kura Rathnakar Reddy, Dasari Muralidhara Reddy, Rapolu Raji Reddy, Matta Ramakrishna Reddy, Bandi Vamsi Krishna, Pat. WO2011125062A1, 2011.
[78] Jambula Mukunda Reddy, Ganji Prasad, Veeramalla Raju, Mylavarapu Ravikumar, Vurumidi Himabindu, Ghanta Mahesh Reddy, An improved synthesis of memantine Hydrochloride: anti-alzheimer's drug, Org. Process Res. Dev. 11 (2007) 268–269.
[79] Y. Hayashi, Pot economy and one-pot synthesis, Chem. Sci. 7 (2016) 866–880.
[80] E.A. Ivleva, Y.N. Klimochkin, Convenient synthesis of memantine hydrochloride, Org. Prep. Proced. Int. 49 (2017) 155–162.
[81] J.J. Ritter, J. Kalish, A new reaction of nitriles. II. Synthesis of t-carbinamines, J. Am. Chem. Soc. 70 (1948) 4048–4050.
[82] D.B. Vu, T.V. Nguyen, S.T. Le, C.D. Phan, An improved synthesis of amantadine hydrochloride, Org. Process Res. Dev. 21 (2017) 1758–1760.
[83] S.O. Bachurin, E.F. Shevtsova, G.F. Makhaeva, V.V. Grigoriev, N.P. Boltneva, N.V. Kovaleva, S.V. Lushchekina, P.N. Shevtsov, M.E. Neganova, O.M. Redkozubova, E.V. Bovina, A.V. Gabrelyan, V.P. Fisenko, V.B. Sokolov, A.Y. Aksinenko, V. Echeverria, G.E. Barreto, G. Aliev, Novel conjugates of aminoadamantanes with carbazole derivatives as potential multitarget agents for AD treatment, Sci. Rep. 7 (2017) 1–15.
[84] V.B. Sokolov, A.Y. Aksinenko, T.V. Goreva, T.A. Epishina, V.V. Grigoŕev, A.V. Gabrelyan, D.V. Vinogradova, M.E. Neganova, E.F. Shevtsova, S.O. Bachurin, Molecular design of multitarget neuroprotectors 3. Synthesis and bioactivity of tetrahydrocarbazole—aminoadamantane conjugates, Russ. Chem. Bull. 65 (2016) 1354–1359.
[85] E. Simoni, S. Daniele, G. Bottegoni, D. Pizzirani, M.L. Trincavelli, L. Goldoni, G. Tarozzo, A. Reggiani, C. Martini, D. Piomelli, C. Melchiorre, M. Rosini, A. Cavalli, Combining galantamine and memantine in multitargeted, new chemical entities potentially useful in Alzheimer's disease, J. Med. Chem. 55 (2012) 9708–9721.
[86] O. Karoutzou, S.H. Kwak, S.D. Lee, D. Martínez Falguera, F.X. Sureda, S. Vázquez, Y.C. Kim, M. Barniol-Xicota, Towards a novel class of multitarget-directed ligands: dual P2X7–NMDA receptor antagonists, Molecules 23 (2018) 1–13.
[87] J. Sterling, Y. Herzig, T. Goren, N. Finkelstein, D. Lerner, W. Goldenberg, I. Miskolczi, S. Molnar, F. Rantal, T. Tamas, G. Toth, A. Zagyva, A. Zekany, G. Lavian, A. Gross, R. Friedman, M. Razin, W. Huang, B. Krais, M. Chorev, M.B. Youdim, M. Weinstock, Novel dual inhibitors of AChE and MAO derived from hydroxy aminoindan and phenethylamine as potential treatment for Alzheimer's disease, J. Med. Chem. 45 (2002) 5260–5279.
[88] M. Yogev-Falach, O. Bar Am, T. Amit, O. Weinreb, M.B. Youdim, A multifunctional, neuroprotective drug, ladostigil (TV3326), regulates holo-APP translation and processing, FASEB J. 20 (2006) 2177–2179.
[89] O. Bar Am, T. Amit, O. Weinreb, M.B. Youdim, S. Mandel, Propargylamine containing compounds as modulators of proteolytic cleavage of amyloid-beta protein precursor: involvement of MAPK and PKC activation, J. Alzheimer's Dis. 21 (2010) 361–371.
[90] F.T. Zindo, J. Joubert, S.F. Malan, Propargylamine as functional moiety in the design of multifunctional drugs for neurodegenerative disorders: MAO inhibition and beyond, Future Med. Chem. 7 (2015) 609–629.
[91] J. Sterling, Y. Herzig, T. Goren, N. Finkelstein, D. Lerner, W. Goldenberg, I. Miskolczi, S. Molnar, F. Rantal, T. Tamas, G. Toth, A. Zagyva, A. Zekany, G. Lavian, A. Gross, R. Friedman, M. Razin, W. Huang, B. Krais, M. Chorev, M.B. Youdim, M. Weinstock, Novel dual inhibitors of AChE and MAO derived from hydroxy aminoindan and phenethylamine as potential treatment for Alzheimer's disease, J. Med. Chem. 45 (2002) 5260–5279.
[92] L.T. Boulton, I.C. Lennon, E. Bahar, US Pat. US 2006O199974A1, 2006.
[93] A. Samadi, M. Chioua, I. Bolea, C. de Los Rios, I. Iriepa, I. Moraleda, A. Bastida, G. Esteban, M. Unzeta, E. Galvez, J. Marco-Contelles, Synthesis, biological assessment and molecular modeling of new multipotent MAO and cholinesterase inhibitors as potential drugs for the treatment of Alzheimer's disease, Eur. J. Med. Chem. 46 (2011) 4665–4668.
[94] Z. Luo, F. Qin, S. Yan, X. Li, An efficient and promising method to prepare Ladostigil (TV3326) via asymmetric transfer hydrogenation catalyzed by Ru–Cs-DPEN in an HCOONa–H2O–surfactant system, Tetrahedron Asymmetry 23 (2012) 333–338.
[95] O.M. Bautista-Aguilera, G. Esteban, M. Chioua, K. Nikolic, D. Agbaba, I. Moraleda, I. Iriepa, E. Soriano, A. Samadi, M. Unzeta, J. Marco-Contelles, Multipotent cholinesterase/monoamine oxidase inhibitors for the treatment of Alzheimer's disease: design, synthesis, biochemical evaluation, ADMET, molecular modeling, and QSAR analysis of novel donepezil-pyridyl hybrids, Drug Des. Dev. Ther. 8 (2014) 1893–1910.
[96] A. Samadi, C. Valderas, C. de los Rios, A. Bastida, M. Chioua, L. Gonzalez-Lafuente, I. Colmena, L. Gandia, A. Romero, L. Del Barrio, M.D. Martin-de-Saavedra, M.G. Lopez, M. Villarroya, J. Marco-Contelles, Cholinergic and neuroprotective drugs for the treatment of Alzheimer and neuronal vascular diseases. II. Synthesis, biological assessment, and molecular modelling of new tacrine analogues from highly substituted 2-aminopyridine-3-carbonitriles, Bioorg. Med. Chem. 19 (2011) 122–133.
[97] P. Koch, R. Akkari, A. Brunschweiger, T. Borrmann, M. Schlenk, P. Kuppers, M. Kose, H. Radjainia, J. Hockemeyer, A. Drabczynska, K. Kiec-Kononowicz, C.E. Muller, 1,3-Dialkyl-substituted tetrahydropyrimido[1,2-f]purine-2,4-diones as multiple target drugs for the potential treatment of neurodegenerative diseases, Bioorg. Med. Chem. 21 (2013) 7435–7452.
[98] U. Kosak, D. Knez, N. Coquelle, B. Brus, A. Pislar, F. Nachon, X. Brazzolotto, J. Kos, J.P. Colletier, S. Gobec, N-Propargylpiperidines with naphthalene-2-carboxamide or naphthalene-2-sulfonamide moieties: potential multifunctional anti-Alzheimer's agents, Bioorg. Med. Chem. 25 (2017) 633–645.
[99] L. Wang, G. Esteban, M. Ojima, O.M. Bautista-Aguilera, T. Inokuchi, I. Moraleda, I. Iriepa, A. Samadi, M.B. Youdim, A. Romero, E. Soriano, R. Herrero, A.P. Fernandez Fernandez, M. Ricardo Martinez, J. Marco-Contelles, M. Unzeta, Donepezil + propargylamine + 8-hydroxyquinoline

2.2. Manuscript IB

Lessons from black pepper: piperine and derivatives thereof

Expert Opinion on Therapeutic patents, **2016**, 26(2):245-264.
DOI: 10.1517/13543776.2016.1118057

Lessons from black pepper: piperine and derivatives thereof

D. Chavarria[1ǂ], T. Silva[1ǂ], D. Magalhães e Silva[1], F. Remião[2] and F. Borges[1*]

[1]CIQUP/Department of Chemistry and Biochemistry, Faculty of Sciences, University of Porto, Rua do Campo Alegre s/n, 4169-007, Porto, Portugal.
[2]UCIBIO-REQUIMTE, Laboratory of Toxicology, Department of Biological Sciences, Faculty of Pharmacy, University of Porto, Rua de Jorge Viterbo Ferreira, 4050-313, Porto, Portugal

ǂ These authors contributed equally to this work.
*Corresponding author:
Fernanda Borges, CIQUP/Department of Chemistry and Biochemistry, Faculty of Sciences, University of Porto, Porto 4169-007, Portugal. E-mail: fborges@fc.up.pt

Abstract

Introduction: Piperine is a simple and pungent alkaloid found in the fruits of black pepper (*Piper nigrum*). Following its isolation and full characterization, the biological properties of piperine have been extensively studied, and piperine-like derivatives have shown an interesting range of pharmacological activities. In this context, significant advances have been made in the discovery of new chemical entities, based on the piperine scaffold, endowed with therapeutic potential.

Areas covered: The aim of this review is to provide a thorough inquiry on the therapeutic potential of piperine and related derivatives. It provides an overview of recent developments in patented processes and applications thereof between 2000 and 2015.

Expert opinion: Cumulative evidence shows that piperine is currently paving its way to become a privileged scaffold for the development of bioactive compounds with therapeutic application in multiple human diseases. In particular, piperine derivatives were shown to modulate the activity of several targets related to neurological disorders, including epilepsy, Parkinson's disease, depression and pain related disorders. Moreover, the efflux pump inhibitory ability of piperine and its analogues tackles important drug resistance mechanisms and may improve the clinical efficacy of antibiotic and anticancer drugs. Although the use of piperine as a scaffold for bioactive compounds is still in its early stages, the continuous exploration of this structure may lead to remarkable advances in drug discovery programs.

Keywords: Piperine; piperine-like derivatives; privileged scaffold; therapeutic applications.

1. Introduction

Piperine (1-[5-[1,3-benzodioxol-5-yl]-1-oxo-2,4-pentadienyl]piperidine, compound (**1)**, **Figure 1**) is the main alkaloid of black pepper (*Piper nigrum* L.) and is responsible for its biting pungent flavor. Piperine and its stereoisomer chavicine (compound **(2)**, **Figure 1**) can be found in the fruits of *P. nigrum* and *P. longum*, among other species belonging to the genus Piper. [1] Piperine was first isolated in 1820 by the Danish chemist Hans Christian Oersted and occurs as a yellow crystalline solid (MW = 285.33 $g.mol^{-1}$, m.p. = [128-130°C]) poorly soluble in water and presenting weak base properties. [1]. Structurally, piperine is constituted by a benzo[1,3]dioxol moiety connected to a piperidine ring by an amide bond and a (*E*,*E*)-diene tether. [2] Black pepper (*P. nigrum*) contains 5-9% of piperine and a daily consumption of 0.33g of black pepper by a 60 kg person would result in a piperine intake of 16.5-29.7 mg. [1]

Piperine is a secondary metabolite biosynthetically derived from *L*-lysine and a cinnamoyl-CoA precursor (**Figure 2**). Decarboxylation of *L*-lysine by lysine decarboxylase (LDC, EC 4.1.1.18) yields cadaverine, which undergoes oxidative deamination by copper amine oxidase (CuAO, EC 1.4.3.22) originating 5-aminopentanal. This compound is rapidly cyclized into Δ^1-piperideine Schiff base and subsequently reduced to form piperidine. In parallel, piperonyl-CoA is generated from a cinnamoyl –CoA precursor; this precursor undergoes chain elongation with malonyl-CoA in a Claisen-like reaction, generating a keto-ester that is reduced by NADPH and then dehydrated to afford piperonyl-CoA. The piperine unit reacts with piperonyl-CoA affording piperine (**Figure 2**). [3, 4]

Bioavailability studies in mice showed that piperine is rapidly absorbed across the gut wall and that the kidneys are the major excretion route for piperine metabolites, including piperonylic acid, piperonyl alcohol, piperonal, vanilic acid, as well as conjugates coming from the metabolite obtained after hydrolysis of the methylenedioxy moiety. [4] Piperine is widely recognized as a bioavailability enhancer, which is due to its ability to inhibit human CYP3A4 and *P*-glycoprotein (*P*-gp), two key regulators of xenobiotic metabolism [1, 2, 4–6]. By inhibiting metabolism and efflux, piperine enhances the bioavailability of xenobiotics. In this context, piperine has been shown to enhance the bioavailability of several drugs and nutraceuticals, including antioxidants [7–9], non-steroidal anti-inflammatory drugs [10, 11], antidiabetics [12, 13], antihistamines [14], anti-epiletics [15, 16], antiretrovirals [17] and others [18]. The bioavailability enhancing properties of piperine may have a significant clinical impact on the treatment of highly prevalent human diseases, and this line of research is currently a hot topic within the field of biomedical and pharmaceutical sciences. Nevertheless, other important pharmacological activities have been reported for piperine, including anticancer [19–25], anti-inflammatory [26]–[32] and antimicrobial activity [33–38]. Due to its promising therapeutic potential, this naturally occurring compound is being increasingly used as a template for the development of new chemical entities in drug discovery programs. Herein, we review recent advances in patent reports involving piperine and its derivatives, and therapeutic applications thereof. *Piper nigrum* extracts have a complex chemical composition and their pharmacological and toxic effects, which have been discussed elsewhere [1, 18, 39] fall out of the scope of the present review.

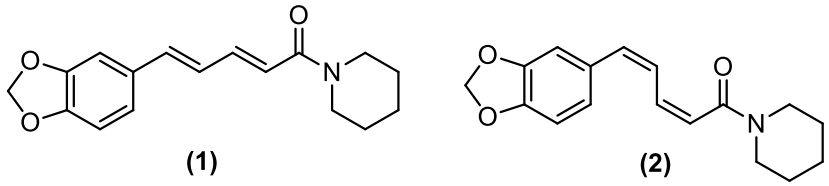


Figure 1. Chemical structure of piperine **(1)** and its stereoisomer chavicine **(2).**

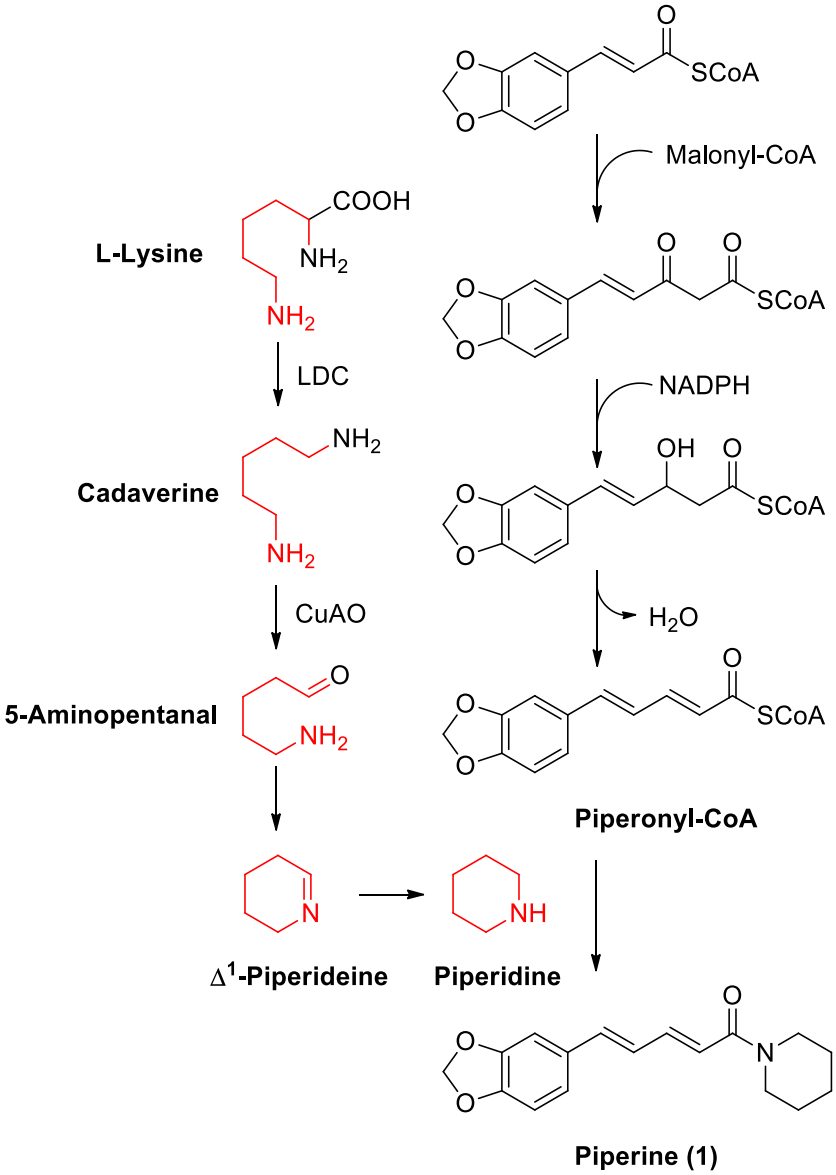


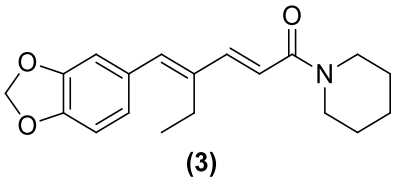
Figure 2. Biosynthesis of piperine. LDC: Lysine decarboxylase, CuAO: copper amine oxidase, NADPH: nicotinamide adenine dinucleotide phosphate, CoA: coenzyme A.

2. Patent Review

2.1. Efflux pump inhibition

Efflux pumps are present in all organisms and play an important role on the extrusion of structurally heterogeneous xenobiotics. [40] The reduction of their intracellular concentration derived from the activity of overexpressed efflux pumps provides a multidrug resistance phenotype with special relevance in oncology and in infectious diseases. [41] In particular, drug efflux pumps have physiological functions during the adaptation, development, pathogenesis and virulence of bacteria. [42] These include the extrusion of antimicrobial agents,[43] intercellular communication via quorum sensing mechanism and biofilm formation. [42] Therefore, the development of novel efflux pump inhibitors (EPIs) can potentially improve the clinical efficacy of antibiotics and simultaneously decrease the selection of resistant strains. [44] In cancer cells, the overexpression of efflux pumps such as *P*-gp reduces the accumulation of chemotherapeutic drugs inside the tumor and the ability of those agents to reach their target. [45, 46] The concomitant administration of chemotherapeutic agents with EPIs can limit the transporter mediated efflux and increase the drug sensitivity. [46]

In this context, Koul. *et al.* [47] described the preparation of a piperine derivative (compound **(3)**, **Figure 3**) and subsequent application as a bioavailability enhancer of antimicrobial and anticancer drugs.



(3)

Figure 3. Chemical structure of the efflux pump inhibitor **(3)**.

2.1.1. Chemistry

Compound **(3)** was obtained following the synthetic strategy depicted in **Figure 4**. The synthesis began with the reaction of piperonal **(4)** with propyl magnesium iodide at room temperature in an anhydrous ether or tetrahydrofuran (THF) to produce the corresponding substituted phenyl alkanol **(5)** (step (*i)*, **Figure 4**). The treatment of **(5)** with a mixture of dimethylformamide (DMF) and phosphorus oxychloride ($POCl_3$) led to the formation of (*E*)-2-(benzo[d][1,3]dioxol-5-ylmethylene)butanal **(6)** (step (*ii)*, **Figure 4**). Compound **(7)** was obtained by the reaction of compound **(6)** with a Wittig reagent prepared from triphenyl phosphine and bromoalkyl acetate in the presence of a base (*e.g.* NaH), followed by isolation of the crude pentadienoic ester and subsequent hydrolysis in alkaline solution (step (*iii)*, **Figure 4**). Compound **(7)** was converted to the corresponding acid chloride using tionyl chloride ($SOCl_2$). The subsequent condensation of the acyl chloride with the appropriate amine led to the formation of compound **(3)** (step (*iv)*, **Figure 4**). [47]

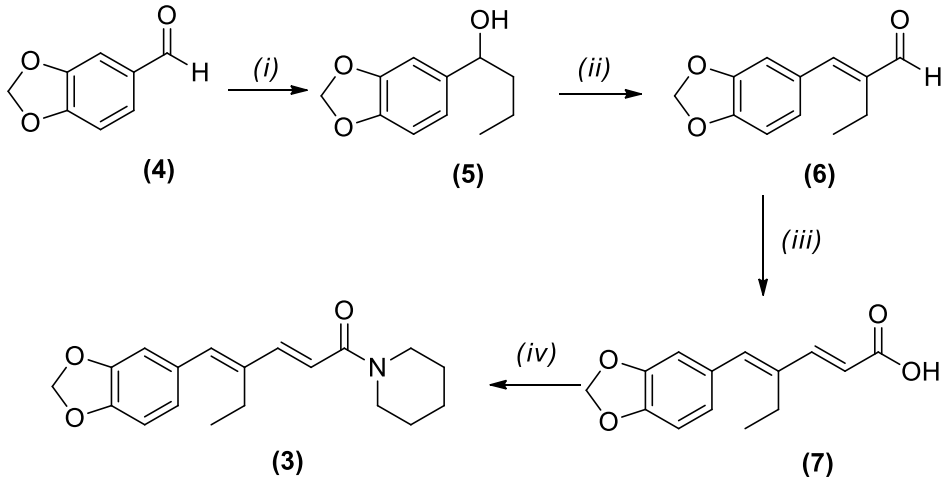


Figure 4. Synthetic strategy used for the obtention of piperine derivative **(3)**. *(i)* $CH_3CH_2CH_2MgI$, anhydrous ether or THF, *(ii)* DMF-$POCl_3$, *(iii)* 1. PPh_3-CHCOOEt/NaH; 2. OH^-, *(iv)* 1. $SOCl_2$; 2. piperidine.

2.1.2. Pharmacological activity

The potentiation/synergism properties of compound **(3)** (**Figure 3**) were assessed by the checkerboard method, a procedure that is widely used to evaluate antimicrobial combinations *in vitro*. Using a sequential dilution layout across the wells of a microtiter plate, this method enables the evaluation of several combinations of two compounds at different concentrations. [47] The activity of 4 standard antibiotics (amikacin, ciprofloxacin, rifampicin and mupirocin) in the presence and absence of compound **(3)** was evaluated against *Staphylococcus aureus*, *Staphylococcus epidermidis* and *Mycobacterium* sp. [47] Results were expressed as minimum inhibitory concentration (MIC) (**Tables 1a-b)**, defined as the lowest concentration of the antimicrobial agents that prevents visible growth of a microorganism under defined conditions. [48] Overall, significant reductions in the MIC values for all the standard antibiotics against the tested bacteria were observed. For instance, a 4-fold reduction on the MIC of amikacin against *S. aureus* and *S. epidermidis* was observed. Interestingly, maximum synergic effect was often reached for low concentrations of compound **(3)** (*e.g.* rifampicin + 0.09 µg/mL of compound **(3)** against *M. tuberculosis*, **Table 1b**). [47]

To evaluate if the observed effect was related with the inhibition of efflux pumps, the ethidium bromide accumulation and efflux method was used. Ethidium bromide is fluorescencent only when bound to nucleic acids inside the cells, and its extrusion mediated by efflux pumps results in a rapid decrease in fluorescence.[49] Briefly, bacterial suspensions of *S. aureus* ATCC 29213 (wild strain) and CIP^r-1 (ciprofloxacin-selected mutant) were exposed to ethidium bromide (2 µg/mL) in the absence (control) and presence of the compound **(3)** (25 µg/mL) for 30 minutes at 37º C. The cells were pelleted by centrifugation, resuspended in fresh uptake buffer, and the fluorescence was measured. The control cells extruded the ethidium bromide (loss of fluorescence), while the treatment with compound **(3)** blocked the extrusion. [47] These results suggested that the inhibition of bacterial efflux pumps may be the mechanism underlying the potentiation of antibiotics' efficacy when combined with compound **(3).**

Table 1. MICs of (a) Amikacin, Ciprofloxacin, Mupirocin and (b) Rifampicin, alone and in combination with compound **(3)**, against multiple bacterial species.

Antibiotic	Cmpnd 3 (μg/ml)	MIC (μg/ml)			
		S. aureus			*S. epidermidis*
		ATCC 29213	MRSA 33	MRSA 450	ATCC 12228
Amikacin	—	2.0	8.0	16	1.0
	6.25	1.0	8.0	**8.0**	**0.5**
	12.5	1.0	8.0	**8.0**	**0.5**
	25.0	**0.5**	**4.0**	**4.0**	**0.25**
	50.0	**0.25**	**2.0**	**4.0**	**0.25**
Ciprofloxacin	—	0.25	32	32	0.12
	6.25	0.12	32	32	0.12
	12.5	**0.06**	**16**	**16**	**0.06**
	25.0	**0.06**	**16**	**16**	**0.03**
	50.0	**0.06**	**16**	**16**	**0.03**
Mupirocin	—	0.12	0.12	0.25	—
	3.12	0.12	0.12	0.25	—
	6.25	0.12	0.12	0.25	—
	12.5	**0.06**	**0.06**	**0.12**	—
	25.0	**0.06**	**0.03**	**0.12**	—
	50.0	**0.03**	**0.03**	**0.06**	—

(a)

Cmpnd 3 (μg/ml)	MIC (μg/ml) of Rifampicin				
	M. tuberculosis			*M. avium*	*M. intracellure*
	H37Rv	611	615	ATCC 49601	ATCC 13950
—	0.12	0.06	0.06	2.0	2.0
0.09	**0.03**	**0.03**	**0.03**	2.0	2.0
0.78	**0.03**	**0.03**	**0.03**	2.0	1.0
6.25	**0.03**	**0.03**	**0.03**	**1.0**	**1.0**
50.0	**0.03**	**0.03**	**0.03**	**1.0**	**1.0**

(b)

The *in vivo* activity of ciprofloxacin in combination with compound **(3)** was evaluated in Swiss albino mice infected intravenously with *S. aureus* ATCC 29213 (10^7 CFU/mouse). The mice were divided in groups of six mice and each group was treated with different doses immediately after the infection and after 6 hours. The mice were observed for seven days and the median effective dose (ED_{50}) was determined after the referred period. The results showed that ED_{50} of ciprofloxacin was 9.2 mg/kg and in combination with compound **(3)** was reduced to 5.86 mg/kg. [47]

Recently, the bioavailability enhancement properties of compound **(3)** were studied in combination with etoposide [50], an anticancer agent with poor and variable bioavailability after oral dosing. Swiss mice were divided into five different groups: I (etoposide (20 mg/kg)), II (etoposide (20 mg/kg)) + compound **(3)** (1.25 to 40 mg/kg)), III (compound **(3)** (20 mg/kg)), IV (etoposide (20 mg/kg) + compound **(3)** (20 mg/kg) premixed) and V (etoposide (20 mg/kg) intravenously). Blood samples were collected at different intervals post-dosing: 0 to 16 h from animals in groups I, III, IV and V and 0.5 h from mice in group II. After separation of the plasma by centrifugation, etoposide and compound **(3)** were recovered by solid phase extraction and analyzed in an ultra-performance liquid chromatography – quadrupole time of flight mass spectrometer system. The dose-dependent effect of compound **(3)** on etoposide plasma levels at 0.5 h (group II) was firstly studied. Etoposide levels were amplified with the increasing doses of compound **(3)**, showing a maximum of 93.2 % increase in the peak plasma concentration (C_{max}) at 20 mg/kg. Plasma concentration-time curves were established for each analyte from the treated mice (groups I, III, IV and V) and used for the determination of pharmacokinetic parameters. The results revealed an increase of the extent of absorption (AUC) and the half-life ($t_{1/2}$) of etoposide in the presence of compound **(3)**, while the volume of distribution (V_d) and the clearance was decreased. The oral bioavailability of etoposide in the presence of compound **(3)** was enhanced by 2.32-fold. [50]

Further studies were performed to explore the mechanism of action of compound **(3)**. [51] The absorption of etoposide (100 µM) in everted gut sacs was found to increase by 41 % in groups treated with compound **(3)**. [51] The possible involvement of compound **(3)** in the modulation of *P*-gp was studied by Rhodamide-123 (Rho-123) efflux inhibition in everted jejunal sacs. The efflux of Rho-123 decreased 55 % in jejunal sacs treated with compound **(3)**. [51] A subsequent experiment on rat jejunal membrane preparations showed that compound **(3)** inhibited *P*-gp ATPase activity by 18-22% in a concentration range of 12.5-100 µM. [51] A parallel artificial membrane permeability assay was also carried out to clarify whether the compound affects non-carried mediated transport absorption in the intestine. The results showed that compound **(3)** (25, 50 and 100 µM) did not affect significantly the passive transport of etoposide. [51]

Finally, to assess the effect of compound **(3)** on CYP3A4, microsomes were isolated from treated rat liver and used for CYP-catalyzed enzyme activities. Erythromycin, 7-methoxycoumarin and 7-ethoxyresorufin were used as substrates. Compound **(3)** was shown to inhibit NADPH-assisted *O*-demethylation and *O*-deethylation in a concentration-dependent manner. The inhibition of *N*-demethylation was also recorded. [51]

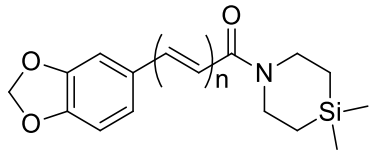
In summary, the mechanisms underlying the compound **(3)**-mediated enhancement in the oral bioavailability of etoposide could possibly result from modulation of *P*-gp and CYP3A4 disposition mechanisms. [51]

2.2. Antimicrobial activity

2.2.1. Antitubercular activity

Tuberculosis (TB), an infectious disease caused by *Mycobacterium tuberculosis*, is typically transmitted through the respiratory route. The infection results from inhalation of particles containing the bacteria from patients with active TB. [52, 53] Currently, the main drugs used in first-line of anti-TB therapy are rifampicin, isoniazid, ethambutol and pyrazinamide. [53, 54] Despite the large number of antibiotics available for TB therapy, both as first and second line therapies, the mortality rate remains high. This is due to the increase of multi-drug resistant strains and the suboptimal safety profiles of currently available anti-infective drugs. In this sense, the development of new antitubercular agents with different mechanisms of action and enhanced tolerability is presently a pressing and unmet clinical need.[55, 56]

Inspired by the broad range of applications of piperine, Reddy *et al.* [57] developed piperine silicon analogues (Compounds **(8-9)**, **Figure 5**) and evaluated the potential application on the treatment of TB.

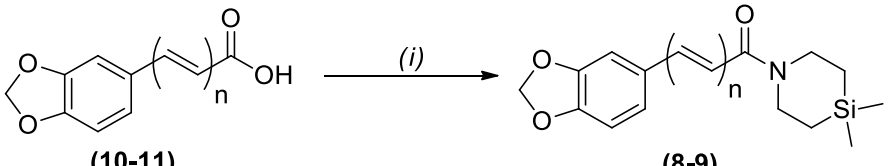


(8) n=1
(9) n=2

Figure 5. Chemical structure of piperine silicon analogues with antitubercular activity **(8, 9)**.

2.2.1.1. Chemistry

The piperine silicon analogues (compounds **(8)** and **(9), Figure 5**) were obtained according to the synthetic strategy depicted in **Figure 6**. Briefly, the amide derivatives were obtained by treating carboxylic acids **(10)** and **(11)** with 4,4-dimethyl-1,4-azasilinane hydrochloride using *N*-(3-dimethylaminopropyl)-*N′*-ethylcarbodiimide hydrochloride (EDC·HCl) as coupling reagent. [57]



(10-11)

(8, 10) n=1
(9, 11) n=2

(8-9)

Figure 6. General synthetic strategy to obtain silyl analogues of piperine **(8, 9)**. *(i)* 1. DCM, EDC.HCl, HOBt, DIPEA, 0º C; 2. 4,4-dimethyl-1,4-azasilinane hydrochloride, room temperature, 8h.

2.2.1.2. Pharmacological activity

The antitubercular activity of compounds **(8)** and **(9)** (**Figure 5**) was evaluated by growth inhibition of the virulent strain of *M. tuberculosis* H37Rv. The MIC values of compounds **(8)** and **(9)** against H37Rv were determined using the colorimetric resazurin microtiter assay. Growth was measured by visual readout and

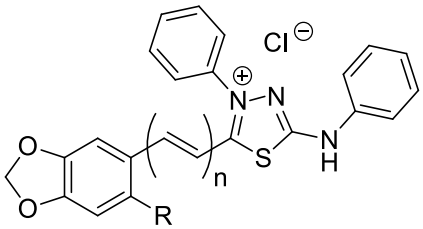
rifampicin was used as a positive control. The results showed lower MIC values for compounds **(8)** and **(9**) when compared to piperine (compound **(8)**, MIC = 50 µg/mL; compound **(9)**, MIC = 50 µg/mL; piperine, MIC = 100 µg/mL). [57] This modification may also lead to the improvement the pharmacokinetic profile when compared to piperine. [57]

2.2.2. Antitrypanosomal activity

Trypanosoma cruzi is the ethiological agent of Chagas disease. The life cycle of this hemoflagelatte protozoan includes obligatory passages through invertebrates (triatomine bugs) and vertebrate (mammals, including man) hosts. [58] The non-infectious epimastigote form of *T. cruzi* passes through the digestive tract of the invertebrate toward the rectum to transform into the infectious, non-replicative metacyclic trypomastigote form. [59] After contagion by contact with insect feces, [60] trypomastigotes penetrate in various tissues of the vertebrate and differentiate into amastigotes by binary fission. The further transformation of amastigote back into trypomastigote bursts the host cell, releases the infectious form to the bloodstream and continues to invade other nucleated cells, amplifying the infection. [61]

Nifurtimox and benzdiazole are nitroheterocyclic drugs currently used for the treatment of Chagas disease during the acute and short-term chronic phases. However, these therapeutic approaches are limited by severe side effects, low effectiveness and poorly understood drug resistance mechanisms. [58, 61] The discovery of new drugs with high selectivity and minimum side effects is urgently needed. [61]

Previous studies have shown that 1,3,4-thiadiazolium-2-phenylamine derivatives based on cinnamic acid scaffold displayed a relevant activity against promastigote and amastigote forms of *Leishmania amazonensis*. [62] Inspired by the antitrypanosomal activity of piperine and some analogues, and considering that the genera *Leishmania* and *Trypanosoma* belong to the same family (Trypanosomatidae), Ferreira *et al.* synthesized new mesoionic 1,3,4-thiadiazolium-2-phenylamine derivatives based on piperine framework and evaluated their antitrypanosomal activity (compounds **(12-14)**, **Figure 7**). [37, 62]



(12) n=2, R=H,
(13) n=1, R=H
(14) n=1, R=NO_2

Figure 7. Chemical structure of mesoionic compounds **(12-14)** with trypanocydal activity **(12-14)**.

2.2.2.1. Chemistry

The synthesis of mesoionic derivatives (compounds **(12-14)**, **Figure 7)** is outlined on **Figure 8**. Piperic acid **(11)** was prepared by basic hydrolysis of piperine **(1)** (step *(i)*, **Figure 8)**. The cinnamic acid derivatives **(16)** and **(17)** were obtained by a Knoevenagel reaction using piperonal **(4)** or its nitrated derivative (**15)** (step *(ii)*, **Figure 8**) as starting materials (step *(iii)*, **Figure 8**). Carboxylic acids **(11)**, **(16)** and **(17)** were then treated

with $(COCl)_2$ to obtain the corresponding acyl chloride (compounds **(18-20)**, step *(iv)*, **Figure 8**). The reaction of these acyl intermediates with 1,4-diphenylthiosemicarbazide afforded the final compounds **(12-14)**, (step *(v)*, **Figure 8**).[62]

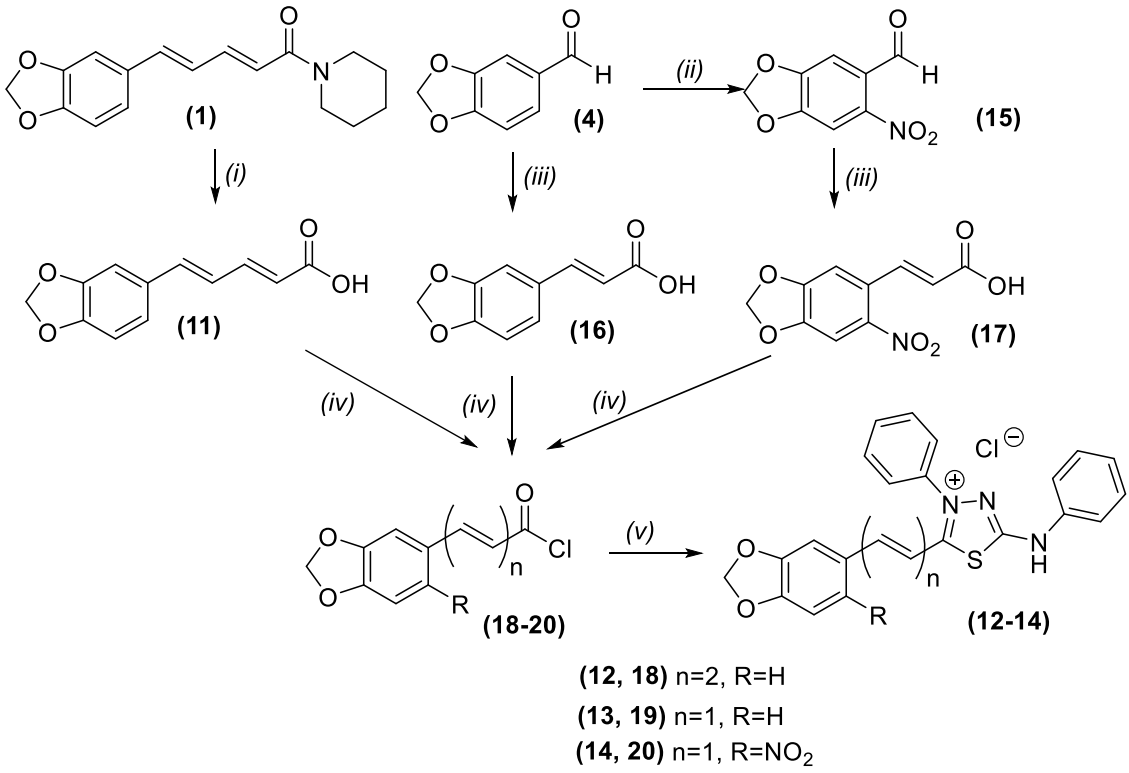


Figure 8. General synthetic strategy to obtain 1,3,4-thiadiazolium-2-phenylamine chloride piperine derivatives **(12**– **14)**. *(i)* 1. KOH, ethanol, reflux, 24h; 2. HCl, 0º C; *(ii)* CH_3COOH (glacial), HNO_3 (concd), 3h; *(iii)* 1. malonic acid, pyridine, piperidine, reflux, 8h; 2. HCl, 0º C; *(iv)* $(COCl)_2$, 25º C, 2h; *(v)* 1,4-diphenylthiosemicarbazide, 1,4-dioxane, 25º C, 24–48 h.

2.2.2.2. Pharmacological activity

The activity of mesoionic compounds **(12-14)** (**Figure 7**), piperine and benznidazole was first evaluated against epimastigotes of *T. cruzi* (Y strain). A high antiproliferative effect on epimastigotes was detected (compound **(12)**, IC_{50} = 10.83 ± 2.2 µM; compound **(13)**, IC_{50} = 4.13 ± 1.2 µM; compound **(14)**, IC_{50} = 0.64 ± 0.14 µM), with some showing higher activity than piperine (IC_{50} = 7.31 ± 1.5 µM) and benznidazole (IC_{50} = 2.21 ± 0.85 µM). [62] The toxic effect of the compounds against the host cells (murine macrophages) was also assessed and expressed as LD_{50} values. Even though a significant activity against epimastigote forms of *T. cruzi* was observed for compounds **(13)** and **(14)**, they were toxic for host cells (compound **(13)**, LD_{50} = 1.95 ± 0.5 µM; compound **(14)**, LD_{50} = 1.08 ± 0.23 µM). Compound **(12)** was the least toxic derivative (compound **(12)**, LD_{50} = 38.56 ± 4.6 µM). [62]

The activity of compounds **(12-14)**, piperine and benznidazole against trypomastigote form of *T. cruzi* was evaluated at non-toxic concentrations to macrophages. Compounds **(13)** and **(14)** displayed higher IC_{50} values than the toxic dosage for host cells.[62] In contrast, compound **(12)** exhibited an interesting activity

profile against the trypomastigote form (compound **(12)**, IC_{50} = 6.70 ± 1.7 µM). This derivative was more effective than the natural alkaloid piperine. [62]

Finally, the activity of compound **(12)**, piperine and benznidazole against the amastigote form of *T. cruzi* was studied. Compound **(12)** was more active against the intracellular amastigote form than piperine and the reference drug benznidazole (Compound **(12)**, IC_{50} = 1.35 ± 0.95 µM; piperine, IC_{50} = 4.91 ± 1.1 µM; benznidazole, IC_{50} = 2.51 ± 0.7 µM). [62]

2.2.3. Antileishmanial activity

Leishmaniosis comprise a spectrum of infectious diseases resulting from the transmission of protozoa of the genus *Leishmania*. The parasite develops as promastigotes in the gut of the phlebotomine sand flies and as amastigotes in the macrophages of vertebrate hosts. [63] Some *Leishmania* species, such as *Leishmania major*, remain mainly in the skin and cause permanent scarring and disfiguration (cutaneous leishmaniosis). Other species, like *Leishmania donovani*, infect visceral organs (spleen and liver). Visceral leishmaniosis is often fatal due to the failure of the host immune system. [64, 65]

Pentavalent antimonials (*e.g.* sodium stibogluconate, meglumine antimoniate) remain as the primary line of treatment. However, they are usually toxic, their administration is painful and require long treatment regiments. Over the last decade, safer therapeutics were developed (*e.g.* lipid formulations of amphotericin B, miltefosine, and paromomycin), but the side effects are still significant and the resistance is emerging and increasing in some endemic areas. Thus, the need for new antileishmanial drugs remains high. [64, 66, 67]

Previous studies reported the potential of aminoacid esters and amides as inhibitors of intracellular and isolated amastigotes of *L. amazonensis* and *L. mexicana*. Based on this hypothesis, Singh *et al.* synthesized and evaluated the antileishmanial activity of piperonyl-amino acid conjugates (Compounds **(21-35)**, **Figure 9**). [67]

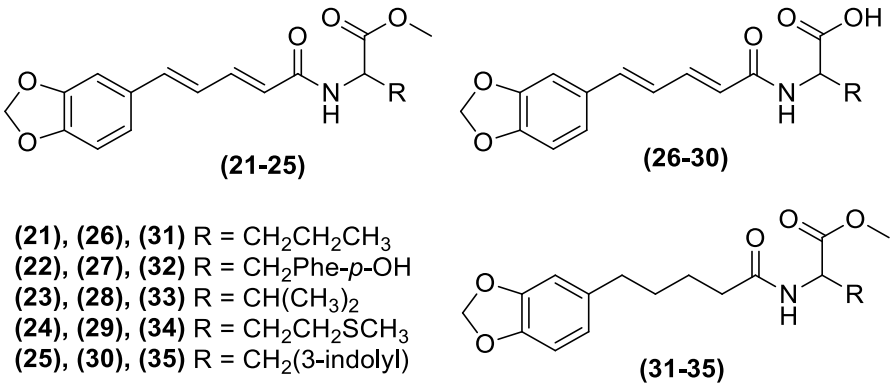


Figure 9. Chemical structure of piperonyl-amino acid conjugates with antileishmanial activity (**21-35)**.

2.2.3.1. Chemistry

Compounds **(21-35)** were prepared according to the synthetic strategy described on **Figure 10**. The synthesis started with the alkaline hydrolysis of piperine **(1)** (step *(i)*, **Figure 10**). The resulting piperic acid **(11)** was treated with methanesulfonyl chloride (CH_3SO_2Cl) in dry dichloromethane to afford the piperic acid mesilate (step *(ii)*, **Figure 10**), which in turn reacted with diverse amino acid methyl esters to yield the piperonyl-amino acid methyl ester conjugates **(21-25)**, (step *(iii)*, **Figure 10**). Deprotection of the carboxyl

group by microwave assisted solid phase reaction with Al_2O_3 afforded compounds **(26-30)** (step *(vi)*, **Figure 10**). Two routes were envisaged to obtain the saturated analogues. Compounds **(31-33)** and **(35)** were synthesized by catalytic hydrogenation of compounds **(21-23)** and **(25)** (step *(v)*, **Figure 10**). Alternatively, tetrahydropiperic acid (compound **(36)**, **Figure 10**) was prepared by catalytic hydrogenation of piperic acid (**11**) and coupled with methionine methyl ether to give compound **(34)**. [67]

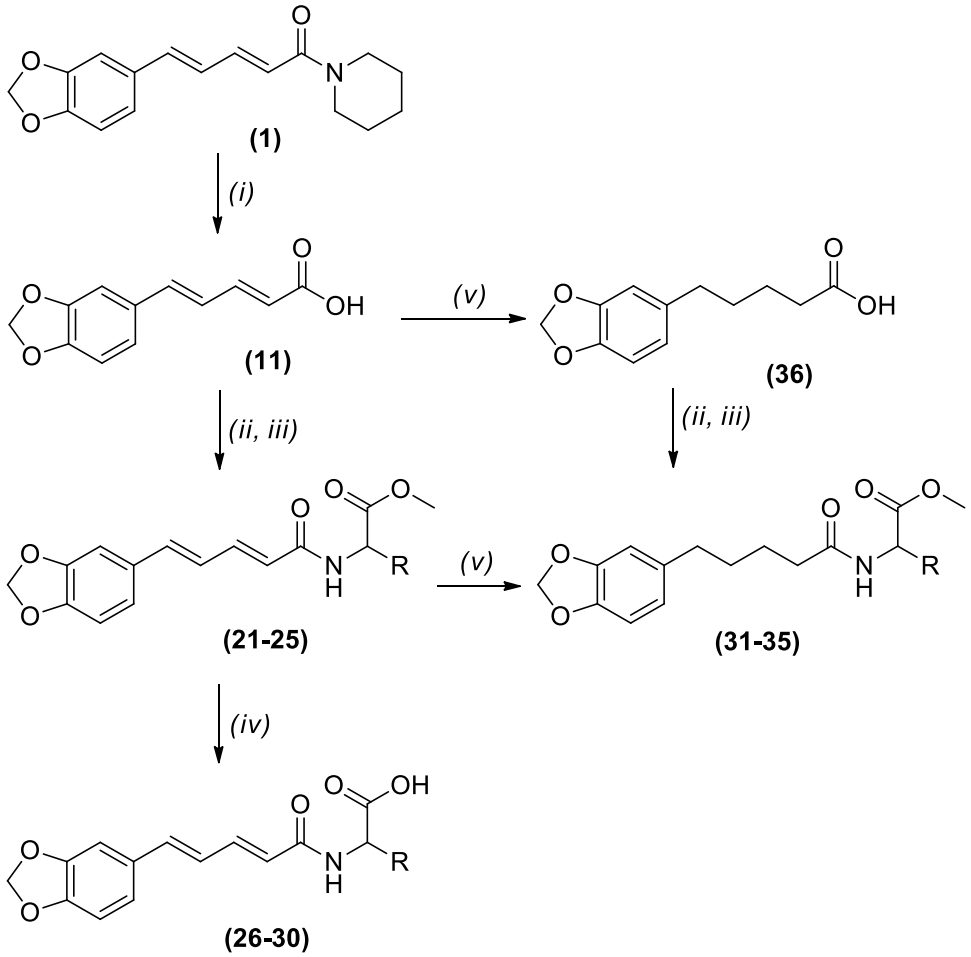


Figure 10. General synthetic strategy to obtain piperonyl-amino acid conjugates **(21**– **35)**. *(i)* 20 % KOH, CH_3OH 80º C, 3 days; *(ii)* CH_3SOCl_2, Et_3N, DCM, 0º C, 30 min; *(iii)* amino acid methyl ester , Et_3N, DCM, room temperature; *(iv)* KF-Al_2O_3, microwave, 1000 W, 3-4 min; *(v)* 5 % Pd/C, H, MeOH, 30 min.

2.2.3.2. Pharmacological activity

The *in vitro* antileishmanial activity of the synthesized compounds **(21-35) (Figure 9)** was evaluated against amastigote and promastigote forms of *L. donovani* and results are expressed as IC_{50} (**Table 2**). In general, the leishmanicidal effect of the compounds under study was higher than piperine. Piperonyl-amino acid methyl ester conjugates (compounds **(22-25)**) were found to be more efficient against the amastigote form. In particular, the valine based derivative **(23)** showed an IC_{50} of 0.075 nM. Interestingly, the removal of the methyl group from the amino acid moiety (compounds **(27-30)**) decreased the antileishmanial activity against the amastigote form. On the other hand, the saturation of the linker double bonds (compounds **(31-35)**) increased the antileishmanial activity against promastigotes and decreased against amastigotes. [67]

Table 2. Leishmanicidal activity and cytotoxicity of piperonyl-amino acid conjugates **(21-35)**.

R	Compound	IC_{50} (mM)		Cytotoxicity (%)
		Amastigotes	Promastigotes	At 2xIC_{50}
	(21)	1.97	0.834	7
$CH_2CH_2CH_3$	**(26)**	0.256	0.927	8.5
	(31)	0.212	0.669	7.2
	(22)	0.210	0.791	6
CH_2Phe-*p*-OH	**(27)**	0.249	0.761	6
	(32)	0.202	0.536	7.6
	(23)	0.075	0.875	3.8
$CH(CH_3)_2$	**(28)**	0.310	1.030	9
	(33)	0.240	0.722	7.7
	(24)	0.168	0.823	7.5
$CH_2CH_2SCH_3$	**(29)**	0.237	1.312	7.7
	(34)	0.221	0.607	5
	(25)	0.119	0.855	5.2
CH_2(3-indolyl)	**(30)**	0.236	1.025	10
	(35)	0.176	0.473	5
___	Piperine **(1)**	0.752	2.558	10
___	Miltefosine	0.018	0.033	35

The cytotoxicity of all synthesized compounds was assessed against peripheral blood mononuclear cells. None of the compounds displayed more than 10% loss of cellular viability at the maximum tested concentration. [67]

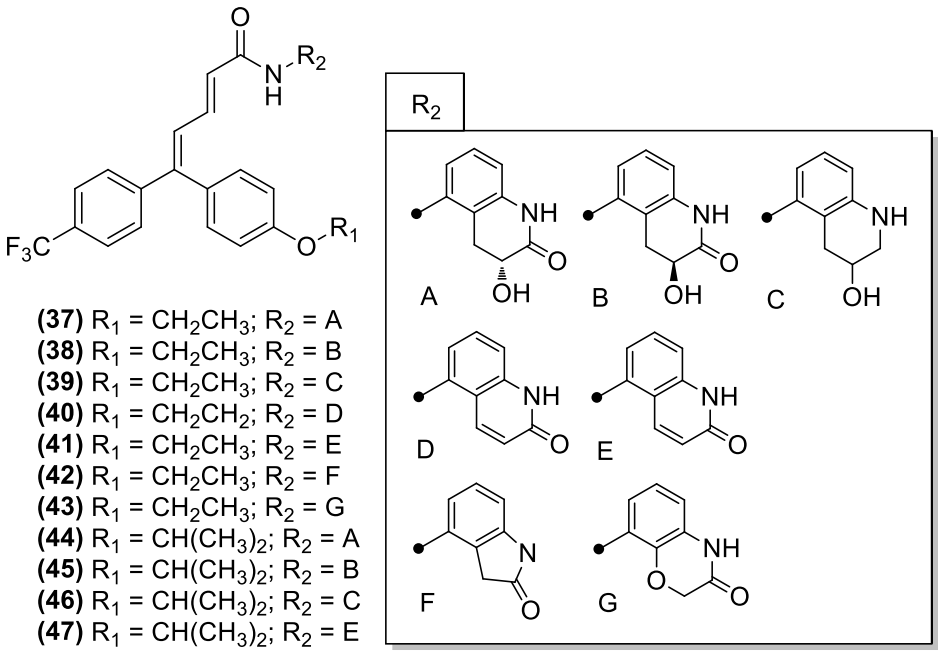
The leishmanicidal activity of compound **(23)** was also assessed in Male Golden Syrian Hamsters infected with *L. donovani*. Miltefosine was used as standard antileishmanial drug. After intraperitoneal injection of **(23)** or miltefosine at 250 mg/kg for a period of ten days, the hamsters were sacrificed and both spleen weight and spleen parasitic burden were determined. Compound **(23)** displayed a significant reduction

in spleen parasitic burden (35 %) and spleen weight (30 %), although the effect of miltefosine was even more marked. [67]

2.3. TRPV1 antagonism

Sensory functions such as touch, pain, taste and thermosensation are mediated by members of the transient receptor potential (TRP) superfamily. [68] Structurally, these ionic channels have six transmembrane domains with a pore region between segments 5 and 6. [69,70] The oldest and best characterized member of TRP family receptors is the transient receptor potential vanilloid type 1 (TRPV1). TRPV1 is a non-selective cation channel with a preference for calcium ion that is activated by various unrelated stimuli, including exogenous and endogenous ligands (*e.g.* capsaicin, anandamide, products of lipoxygenase, venoms from spiders and jellyfish), protons, G-protein coupled receptor signaling and physical stimuli such as heat (> 42º C).[68, 71] Currently, the development of TRPV1 antagonists represents a new strategy for pain relief on the central nervous system, skin and musculo-skeletal, gastrointestinal, urinary and respiratory systems (reviewed in Szallasi *et a.l* [70]).

Piperine was identified in 2005 as an agonist of the human TRPV1 receptor. [72] Based on this discovery, Saku *et al.* [73] developed a library of 5,5-diarylpentadienamides with potential TRPV1 antagonist activity. Among the synthesized compounds, 5-(4-alkoxyphenyl)-5-(4-(trifluoromethyl)phenyl)penta-2,4-dienamides (compounds **(37-47)**, **Figure 11**) were shown to display a promising antagonist effect.



(37) $R_1 = CH_2CH_3$; R_2 = A
(38) $R_1 = CH_2CH_3$; R_2 = B
(39) $R_1 = CH_2CH_3$; R_2 = C
(40) $R_1 = CH_2CH_2$; R_2 = D
(41) $R_1 = CH_2CH_3$; R_2 = E
(42) $R_1 = CH_2CH_3$; R_2 = F
(43) $R_1 = CH_2CH_3$; R_2 = G
(44) $R_1 = CH(CH_3)_2$; R_2 = A
(45) $R_1 = CH(CH_3)_2$; R_2 = B
(46) $R_1 = CH(CH_3)_2$; R_2 = C
(47) $R_1 = CH(CH_3)_2$; R_2 = E

Figure 11. Chemical structure of piperine derivatives with TRPV1 antagonist activity **(37-47)**.

2.3.1. Chemistry

The synthetic sequence depicted in **Figure 12** was used to obtain compounds **(37-47)**. Briefly, compound **(49)** was obtained by treating the aldehyde **(48)** with triphenylphosphine and carbon tetrabromide (*step (i)*, **Figure 12**). A subsequent series of two Pd-catalyzed Suzuki cross-coupling reactions afforded the

(2*E*,4*Z*) isomer **(50)** and subsequently compound **(51)** (*steps (ii)* and *(iii)*, **Figure 12**). The introduction of alkyl substituents on the hydroxyl function, by a Mitsubonu reaction, yielded compounds (**52)** and **(53)** (*step (iv)*, **Figure 12**). Final products **(37-47)** were obtained after ester hydrolysis of compounds (**52-53)** (*step (v)*, **Figure 12**) and subsequent amidation of the resulting 5,5-diarylpentadienoic acids **(54-55)** with the appropriate amine (*step (vi)*, **Figure 12**). [73]

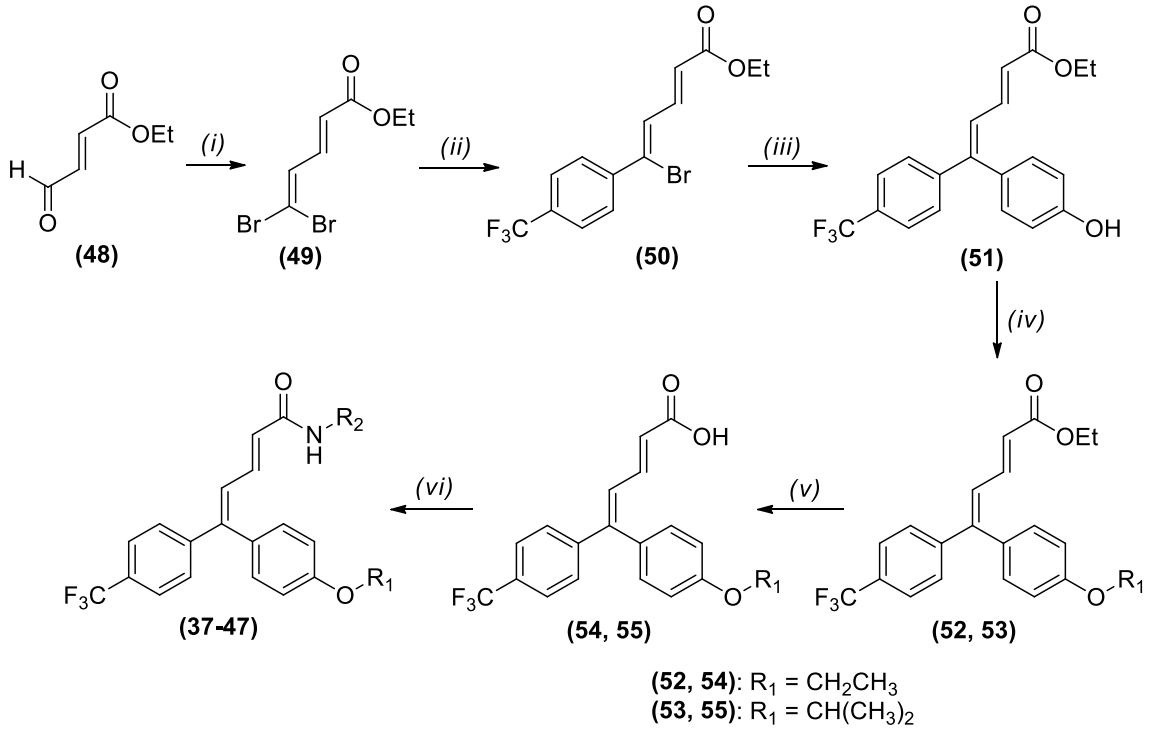


Figure 12. General synthetic strategy for the synthesis of 5,5-diphenylpentadienamides **(37– 47)**. *(i)* CBr_4, PPh_3, CH_2Cl_2; *(ii)* $FC_3PheB(OH)_2$, $Pd(PPh_3)_4$, aq Na_2CO_3, THF; *(iii)* 4-(4,4,5,5-tetramethyl-1,3,2-dioxaborolan-2-yl)phenol, $Pd_2(dba)_3$, TFP, aqueous Na_2CO_3, dioxane; *(iv)* CH_3CH_2OH or $(CH_3)_2CHOH$, Diethyl azodicarboxylate solution (DEAD), PPh_3, toluene; *(v)* $LiOH{\cdot}H_2O$, MeOH, H_2O, THF; *(vi)* R_2NH_2, *N*-(3-Dimethylaminopropyl)-*N′*-ethylcarbodiimide hydrochloride (WSC·HCl), $HOBt{\cdot}H_2O$, DMF.

2.3.2. Pharmacological activity

Compounds **(37-41)** and **(44-47)** exhibited excellent *in vitro* inhibition of capsaicin-induced influx of Ca^{2+} in human or rat TRPV1-expressing 293 EBNA cells (ED_{50} below 1 nM). [73] On the other hand, compounds **(42)** and **(43)** showed decreased activity, although the ED_{50} remained within the nanomolar range. The pharmacokinetic parameters of the most promising compounds were evaluated in male Sprague-Dawley rats. In general, the derivatives showed similar pharmacokinetic profiles and displayed moderate oral bioavailability and central nervous system permeability (brain-to-plasma concentration ratio, K_p = 0.18-0.91), as well as long half-life ($t_{1/2}$ =4.7-47 h). [73] Compared to other derivatives, compound **(44)** showed improved peak plasma concentration (C_{max} = 225 ng/mL) and increased absorption (AUC = 12000 ng.h/mL). Further pharmacokinetic data of compound **(44)** obtained in other animal models (dogs and monkeys) showed low clearance, acceptable volume of distribution, good bioavailability and long half-life [73]

Based on the potent *in vitro* activity towards TRPV1 and the satisfactory pharmacokinetic profile, the efficacy of compound **(44)** on the treatment of neuropathic pain in two *in vivo* models was evaluated.

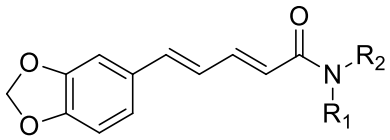
Compound **(44)** was orally administered to male Sprague-Dawley rats 18-21 days after the production of sciatic nerve constriction injury. The reversal of established mechanical allodynia was evaluated with von Frey filaments. The treatment with compound **(44)** showed a dose-dependent blockage of mechanical allodynia. [73]

The ability of compound **(44)** to block thermal hyperalgesia was also assessed in rats with sciatic nerve injury. In this model, the hind paw withdrawal latencies on a hot plate at 48º C was measured hourly after drug and placebo administration. Compound **(44)** reversed the thermal hyperalgesia at 3 and 10 mg/kg. The magnitude of the effect at 10 mg/kg was greater than that observed on rats treated with a standard drug used to relieve neuropathic pain (gabapentin, 100 mg/kg). [73]

2.4. $GABA_A$ receptor modulation

The ionotropic γ-aminobutyric acid type A ($GABA_A$) receptors are the major inhibitory neurotransmitter receptors in the mammalian brain. The activation of these postsynaptic heteropentamers by the endogenous ligand γ-aminobutyric acid induces the inward flux of chloride that transiently decreases the local membrane excitability. [74, 75] Compounds that enhance chloride currents through $GABA_A$ receptors (*e.g.* benzodiazepines) are widely used in the treatment of anxiety, panic disorders, sleep disturbances and epilepsy. [76]

In 2010, piperine was described as a positive allosteric modulator of $GABA_A$ receptors targeting a benzodiazepine-independent binding site. [75] However, as previously mentioned, piperine acts as a TRPV1 receptor agonist and the simultaneous activation of this receptor may be an obstacle to its therapeutic application due to unwanted side effects (*e.g.* changes in pain sensation and body temperature). [77] In this sense, Herring *et al.* used the piperine scaffold to develop highly potent $GABA_A$ receptor modulators that do not interact with TRPV1 receptors (compounds **(56-58)**, **Figure 13**).[78]



(56) $R_1 = R_2 = (CH_2)_3CH_3$
(57) $R_1 = R_2 = (CH_2)_2CH_3$
(58) $R_1 = R_2 = CH_2CH(CH_3)_2$

Figure 13. Chemical structure of piperine derivatives with $GABA_A$ receptor modulatory activity **(56-58)**.

2.4.1. Chemistry

The synthetic strategy used to obtain the piperine analogues described by Herring *et al.* [59] is summarized in **Figure 14**. The first step involved the piperine **(1)** hydrolysis in alkaline conditions (step *(i)*, **Figure 14**) with the obtention of piperic acid **(11)**. Subsequent treatment of **(11)** with thionyl chloride afforded the acyl chloride **(18)** (step *(ii)*, **Figure 14)**, which was used as starting material for the preparation of diverse amide derivatives **(56-58)** (step *(iii)*, **Figure 14)**. [78]

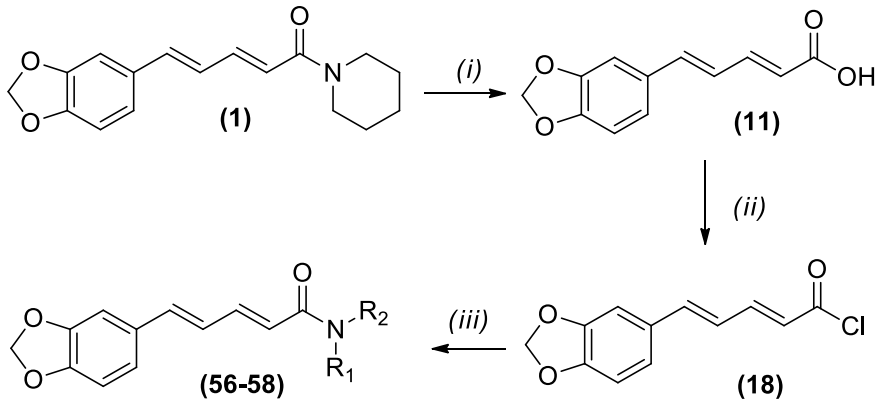


Figure 14. General synthetic strategy used to obtain amides structurally related to piperine **(56-58)**. *(i)* ethanolic KOH 2 N, reflux; *(ii)* dry THF, $SOCl_2$, reflux; *(iii)* dry THF, NHR_1R_2.

2.4.2. Pharmacological activity

The $GABA_A$ modulatory properties of piperine and its derivatives **(**compounds **(56-58)**, **Figure 13)** were first assessed on recombinant $GABA_A$ receptors composed by $\alpha_1\beta_2\gamma_2$ subunits expressed on *Xenopus laevis* oocytes. The modulation of GABA-induced chloride currents (I_{GABA}) was studied using the two-microelectrode-voltage-clamp technique and fast perfusion. All the derivatives were shown to be positive allosteric modulators by enhancing I_{GABA}. [78] The TRPV1 receptor activation was also evaluated using a similar procedure. In opposition to piperine, none of the referred analogues induced cation currents through TRPV1 receptors at a concentration of 300 μM. [78]

Further behavioral and seizure threshold studies in mice were performed to analyze the anxiolytic, sedative and anticonvulsant effects of piperine and its analogues [78] The anxiety-related behavior was tested in the Elevated Plus Maze test (EPM) 30 minutes after intra-peritoneal injection of the test compounds. When compared to control (treated with saline), treated mice (0.3 and 1 mg piperine/kg bodyweight) spent more time in the open arms. Mice treated with a dose > 1 mg/kg bodyweight also covered a slightly reduced distance compared to control, which is indicative of a sedative effect of piperine. [78] In the EPM test, the time spent in the open arms at a dose of 0.3 mg/kg was significantly increased with compounds **(57)** and **(58)**. However, at the tested doses the same behavior was not statistically significant for compound **(56)**. [75] The test was repeated with higher concentrations of compounds **(57)** and **(58)**. Compound **(57)** increased the time spent in the open arms of the EPM, an effect that was dose dependent and reached a maximum at a dose of 10 mg/kg. The dose-response behavior of compound **(58)** was similar, reaching a maximum effect at 3 mg/kg bodyweight. These data suggested that piperine analogues **(56-58)** enhanced the anxiolytic effect. [75]

The sedative effect at higher doses was evaluated by the open field (OF) test. In this test, reduction in ambulation is associated with sedation. The injection of piperine reduced the travelled distance in a dose-dependent manner. A dose of 30 mg/kg bodyweight reduced mice ambulation more than 50%. [78] The OF test was also applied to study their sedative effects. In contrast with piperine, none of the analogues affected the ambulation at a concentration of 10 mg/kg bodyweight. Compounds **(57)** and **(58)** reduced the total distance at 30 mg/kg bodyweight, while compound **(56)** lacked this sedative effect. However, compounds **(57)** and **(58)** showed a weaker effect on ambulation, when compared to piperine. The data suggest that, under these experimental conditions, piperine analogues exhibited reduced sedative properties. [78]

Anticonvulsant effects were determined through analysis of seizure threshold. After intra-peritoneal injection of piperine (0.1 to 30 mg/kg bodyweight) or 10 % dimethylsulfoxide in saline containing 3 % Tween 80 (control), seizure threshold was assessed by pentylenetetrazole (PTZ) tail vein injection on freely moving animals at a rate of 100 µL/min (100 g/mL saline, pH 7.4). When animals displayed generalized chronic seizures, the infusion was stopped and mice were immediately sacrificed. The seizure threshold dose was calculated from the infused volume relative to the bodyweight. The results revealed a biphasic dose response behavior on PTZ induced seizure threshold, indicating the activation of other receptor besides $GABA_A$ (*e.g.* TRPV1). [78]. Compounds **(56-58)** exhibited strong antiepileptic effects, but at different dosages: while compounds **(56)** and **(57)** significantly increased the seizure threshold at doses between 0.1 and 3 mg/kg bodyweight, the same behavior was recorded for compound **(58)** at doses > 10 mg/kg bodyweight. [78]

A subsequent study explored the effect of piperine and compound **(58)** on nine different $GABA_A$ receptor subtypes expressed in oocytes from *Xenopus laevis* ($\alpha_1\beta_2$, $\alpha_2\beta_2$, $\alpha_1\beta_3$, $\alpha_2\beta_3$, $\alpha_3\beta_2$, $\alpha_5\beta_2$, $\alpha_1\beta_2\gamma_{2s}$, $\alpha_2\beta_2\gamma_{2s}$, $\alpha_3\beta_2\gamma_{2s}$, $\alpha_5\beta_2\gamma_{2s}$). The highest efficacy of piperine was observed for receptors containing α_3, β_2 and β_3 receptors. The omission of γ_{2s} subunit had no effect on efficacy or potency of piperine, suggesting its interaction with a binding site located on α and/or β subunits or on the α/β interface. Interestingly, the replacement of piperidine ring of piperine by a *N,N*-diisobutyl moiety (compound **(58)**) led to a significant increment in potency and efficacy (1.2 to 6.5 fold) and affected the subunit dependence. For instance, compound **(58)** displayed equal efficacy on activation of receptors containing β_1, β_2 and β_3 subunits. [77]

These findings encouraged the development of library of structurally heterogeneous piperine derivatives (**Figure 15**) that were screened towards $GABA_A$ receptors. The establishment of structure-activity relationships (SAR) led to the identification of structural elements essential for efficiency and efficacy. First, several modifications on the amide function (**Figure 15A**) were performed. The SAR data showed that noncyclic *N,N*-dialkyl and cyclic methylpiperidinyl substituents increased both efficacy and potency. In contrast, compounds containing dimethylpiperinyl, morpholinyl or *N*-alkyl piperazinyl groups, as well as secondary amides and the thioamide, showed no modulatory activity. The diene conjugated region of piperine was also modified by shortening and rigidification processes (**Figure 15B**). Linker shortening significantly reduced the I_{GABA} enhancement, while rigidification did not have a substantial effect on GABA receptor modulation. [79]

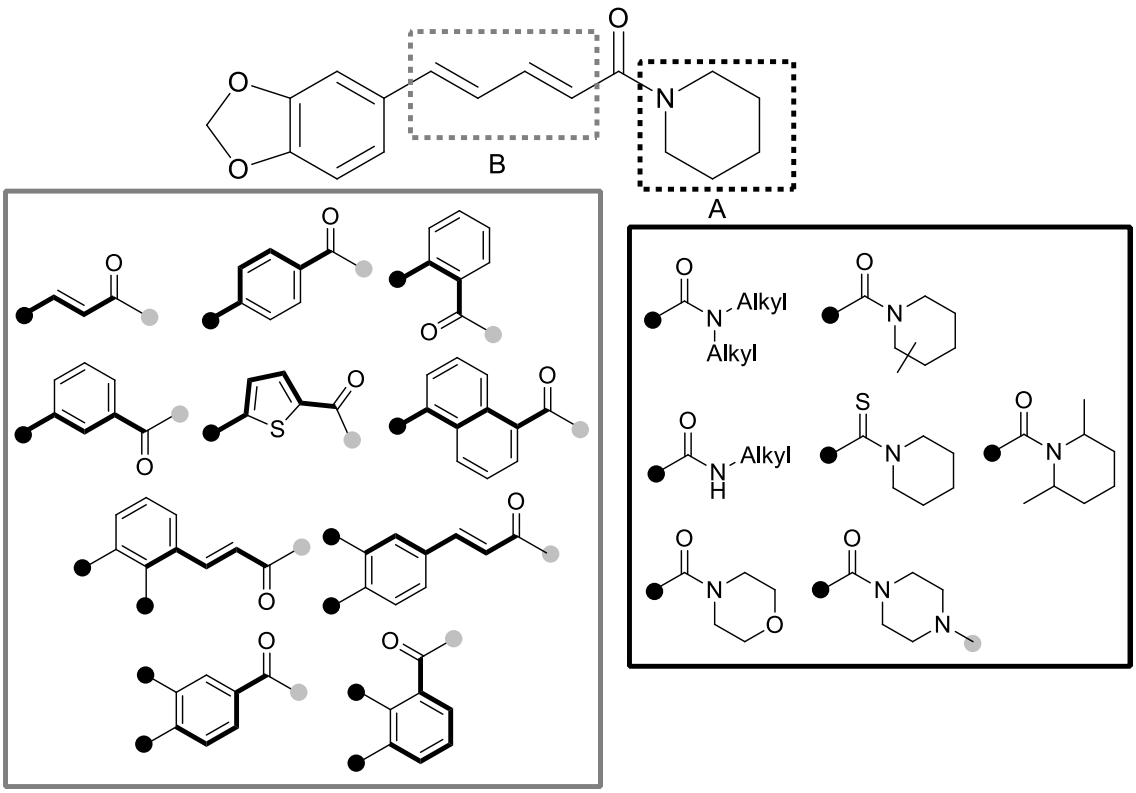


Figure 15. General modifications of amide function (**A**) and diene conjugated chain (**B**) performed on piperine scaffold.

2.5. Modulation of targets associated with neurodegenerative diseases

Monoamine oxidase (MAO, EC 1.4.3.4), an enzyme that catalyzes the oxidative deamination of monoamine neurotransmitters, has been divided into two subtypes (MAO-A and MAO-B) according to their amino acid sequence, substrate and inhibitor selectivity, and tissue distribution. While MAO-A inhibitors are useful for the treatment of anxiety and depression, MAO-B has special relevance on Alzheimer's and Parkinson's diseases.[80, 81] In this context, studies were run to evaluate the effect of piperine on MAO activity. The results showed that this alkaloid had more selectivity for MAO-A isolated from rat [82] while it was more selective for MAO-B isolated from mouse. [83] Based on this preliminary knowledge, Li-Hua Mua *et al.* developed a library of piperine derivatives and assessed their MAO inhibitory profile (compounds **(11, 59-71), Figure 16**). [81]

Recently, A_{2A} adenosine receptors have been considered important targets for the development of new drugs for neurodegenerative disorders, namely Parkinson's disease. These G-protein coupled receptors are predominantly expressed in dopamine rich areas of the central nervous system where they colocalize with dopamine D2 receptors.[84, 85] A_{2A} receptor stimulation has been shown to exert an antagonistic effect on D2 receptors with concomitant decrease of dopamine affinity. Thus, A_{2A} receptor antagonists may be used alone or as an enhancer of the effect of dopamine receptor agonists. In this context, Pretorius *et al.* synthesized (*E,E*)-8-(4-phenylbutadien-1-yl)caffeinyl analogues (compounds **(72-78)**, **Figure 17**) and screened the potential adenosine 2A receptor antagonism and MAO-B inhibition. [86] Dual target-directed drugs may have enhanced therapeutic potential, not only due to the benefits of addressing two pharmacological targets, but also because they reduce the risk of side effects in comparison to the combination of two drugs. [87]

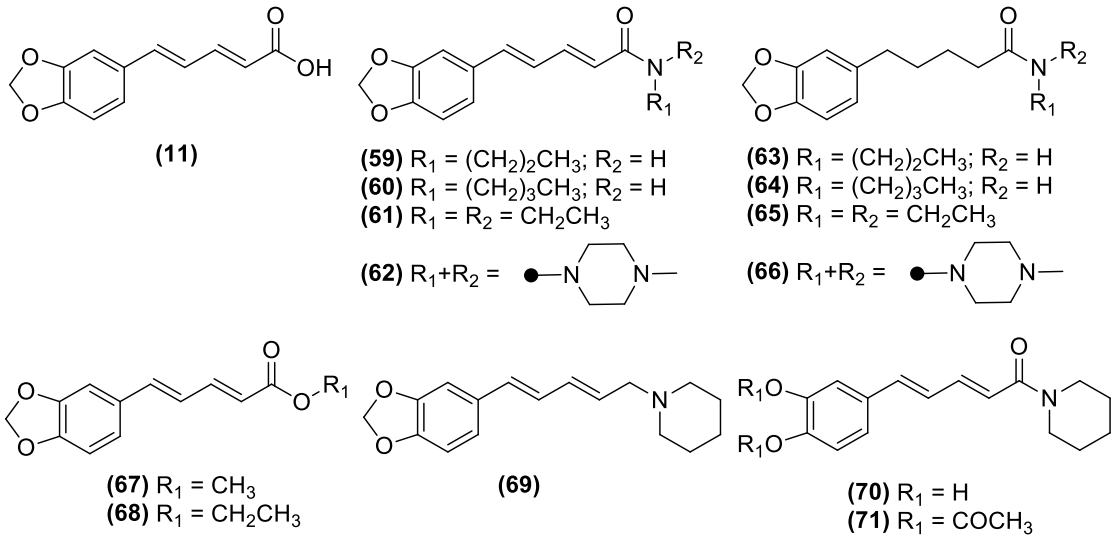


Figure 16. Chemical structure of piperine derivatives studied towards MAO **(11, 59-71)**.

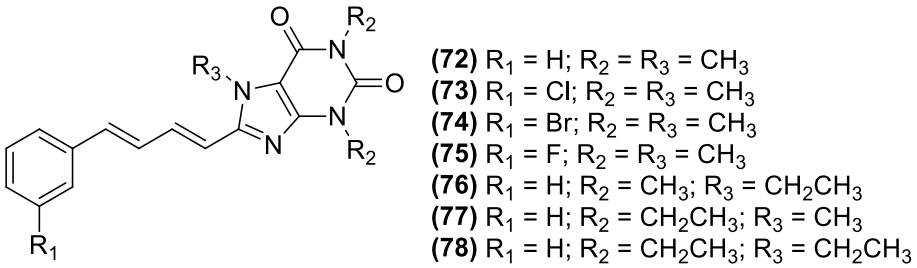


Figure 17. Chemical structure of (*E*,*E*)-8-(4-phenylbutadien-1-yl)caffeinyl analogues with MAO-B inhibitory and adenosine A_{2A} antagonist activities **(72-78)**.

2.5.1. Chemistry

Piperine derivatives **(59-71)** were synthesized as depicted in **Figure 18**. General changes of piperine scaffold included the derivatization of the amide function (compound **(59-62)**, **Figure 18**), hydrogenation of the aliphatic chain (compound **(63-66)**, **Figure 18**), replacement of the amide for an ester group (compound **(67-68)**, **Figure 18**), carbonyl group removal (compound **(69)**, **Figure 18)** and modifications on methylenedioxyphenyl (MDP) ring (compounds **(70)** and **(71)**, **Figure 18**). [81]

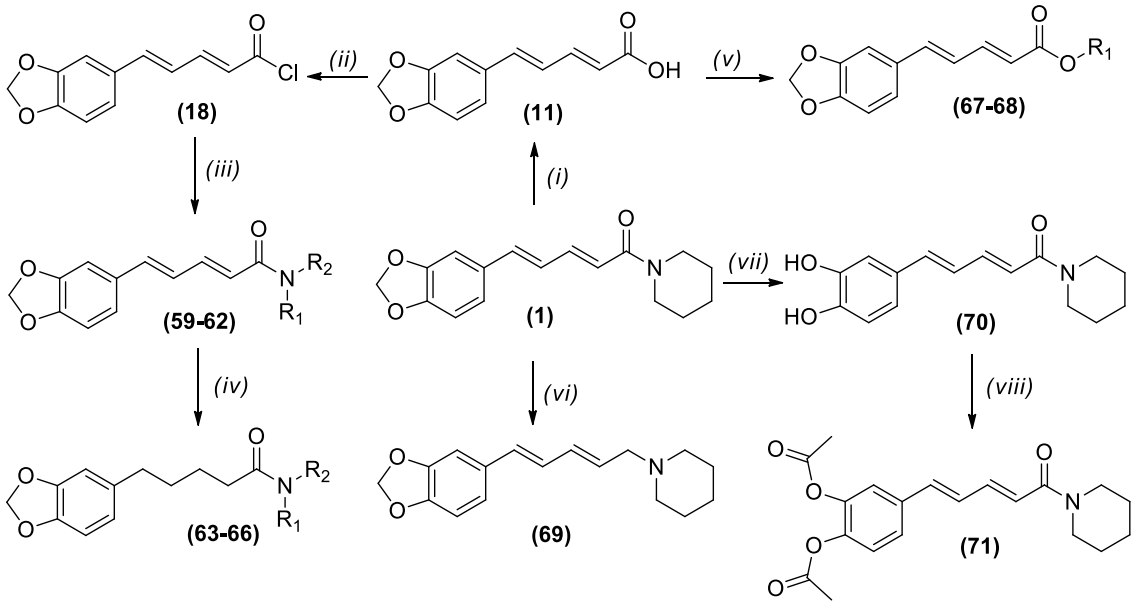


Figure 18. General synthetic strategy used for the obtention of structurally related piperine analogues **(59-71)**. *(i)* KOH; *(ii)* $SOCl_2$ in CH_2Cl_2, reflux, 1 h; *(iii)* R_2R_3NH, room temperature, 30 minutes; *(iv)* H_2, Pd/C, 2 h; *(v)* MeOH or EtOH, H_2SO_4, reflux, 6 h; *(vi)* $NaBH_4/I_2$, THF, 0º C, nitrogen atmosphere, 48 h; *(vii)* BBr_3 in CH_2Cl_2, rt, 48 h; *(viii)* Ac_2O/pyridine.

The general strategy for the synthesis of (*E*,*E*)-8-(4-phenylbutadien-1-yl)caffeinyl analogues **(72-78)** (**Figure 17**) is depicted on **Figure 19**. Briefly, the first step involved an aldol condensation between the substituted benzaldehydes **(79-82)** and acetaldehyde under basic conditions (step *(i)* and *(ii)*, **Figure 19**) affording cinnamaldehydes **(83-86)**, which were then treated with malonic acid in pyridine to yield cinnamylidenemalonic acids **(87-90)** (step *(iii)*, **Figure 19**). The reaction of this intermediate with acetic anhydride (step *(iv)*, **Figure 19**), followed by a photochemical reaction in a chloroform solution of iodine (step *(v)*, **Figure 19**), led to the obtention of the (*E*,*E*)-5-phenyl-2,4-pentadienoic acids **(91-94)**. These intermediates were coupled with different 1,3-substituted-5,6-diaminouracil heterocycles in the presence of a carbodiimide activating reagent (*N*-(3-dimethylaminopropyl)-*N'*-ethylcarbodiimide hydrochloride, EDAC). The resulting amidyl intermediates underwent ring closing under reflux in aqueous sodium hydroxide to render the corresponding 1,3-dialkyl-8-sustituted-7*H*-xanthinyl analogues **(95-100)** (step *(vi)* and *(vii)*, **Figure 19**). A subsequent reaction of *N*-alkylation at the N7 position of xanthinyl intermediates (**95-100),** with an excess of iodomethane or iodoethane yielded the desired compounds **(72-78)** (step *(viii)*, **Figure 19**).[86]

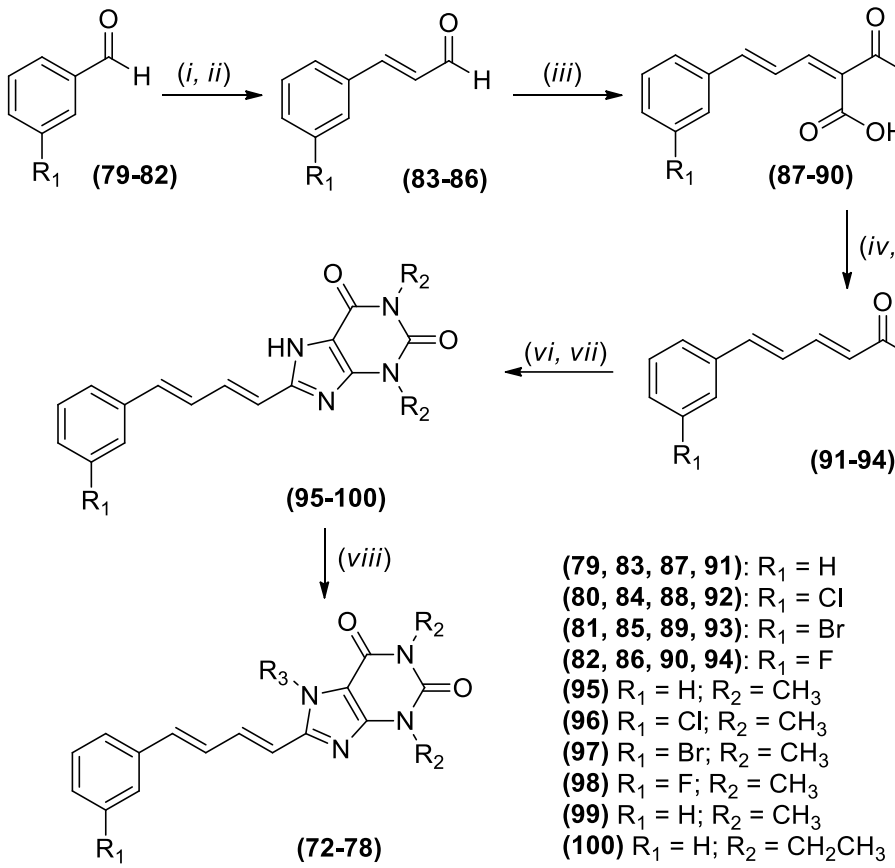


Figure 19. General synthetic strategy for the obtainment of (*E*,*E*)-8-(4-phenylbutadien-1-yl)caffeinyl analogues **(72-78)** *(i)* NaOH, CH_3CHO; *(ii)* Ac_2O, 120º C; *(iii)* $CH_2(CO_2H)_2$, pyridine, 100º C; *(iv)* Ac_2O, CH_3CO_2H, reflux; *(v)* $CHCl_3$, I_2, light; *(vi)* 1,3-substituted-5,6-diaminouracil, EDAC, dioxane/H_2O; *(vii)* NaOH, reflux; *(vii)* CH_3I or C_2H_5I, K_2CO_3, DMF.

2.5.2. Pharmacological activity

Compounds **(1, 11, 59-71) (Figure 16)** were screened toward MAO by a fluorometic assay using rat brain mitochondria isolated from Sprague–Dawley rats. In this method, kynuramine was the substrate and selegiline and clorgyline (1μM) were used as specific inhibitors of MAO-A and MAO-B, respectively. The results are presented in **Table 3** and expressed as IC_{50} values. Compounds bearing a secondary (compounds **(59)** and **(60)**, **Figure 16**) or tertiary amide (compounds **(61-62)**, **Figure 16**) or an ester (compounds **(67)** and **(68)**, **Figure 16**) inhibited both isoforms, although with more selectivity for MAO-B. [81] The hydrogenated analogues (compounds **(63-66)**, **Figure 16**) and the derivative lacking the carbonyl group (compound **(69)**, **Figure 16**) showed poor or no inhibition of both MAO isoforms. Derivative **(70)** displayed selective MAO-A inhibition and the inhibitory activity of compound **(71)** was lower when compared to piperine. Interestingly, all compounds lacking the piperidine moiety (compounds **(11)**, **(59-61)**, **(63-65)**, **(67-68)**, **Figure 16**, **Table 3**) showed a significant loss of MAO-A inhibitory activity, when compared to piperine. In particular, compounds **(59)** and **(61)** showed high MAO-B inhibitory activity and selectivity. These results enabled the establishment of a preliminary SAR summarized in **Figure 20**: a) the substitution of piperidine ring is likely to improve MAO-B inhibitory activity and selectivity; b) the double bonds and the carbonyl group seem to be structurally important for MAO inhibition; c) modifications of MDP ring seem to decrease MAO-B inhibitory activity. [81]

Table 3. MAO-A and MAO-B inhibition by piperine **(1)** and related derivatives **(11, 59-71).**

Compound	IC_{50} (μM)		SI*
	MAO-A	MAO-B	
Piperine **(1)**	0.404	0.26	1.55
Piperic acid **(11)**	18.34	13.59	1.35
(59)	3.66	0.045	81.5
(60)	>100	0.33	___
(61)	3.82	0.078	49.0
(62)	2.04	0.96	2.12
(63)	>100	>100	___
(64)	16.08	3.50	4.59
(65)	5.21	1.75	2.98
(66)	>100	>100	___
(67)	2.74	0.23	11.9
(68)	7.55	0.33	22.8
(69)	>100	>100	___
(70)	0.80	1.57	0.51
(71)	1.28	0.75	1.71
Selegiline	>100	13.91×10^{-3}	___
Clorgyline	0.42×10^{-3}	0.26	1.62×10^{-3}

SI* = IC_{50} of MAO-A/IC_{50} of MAO-B.

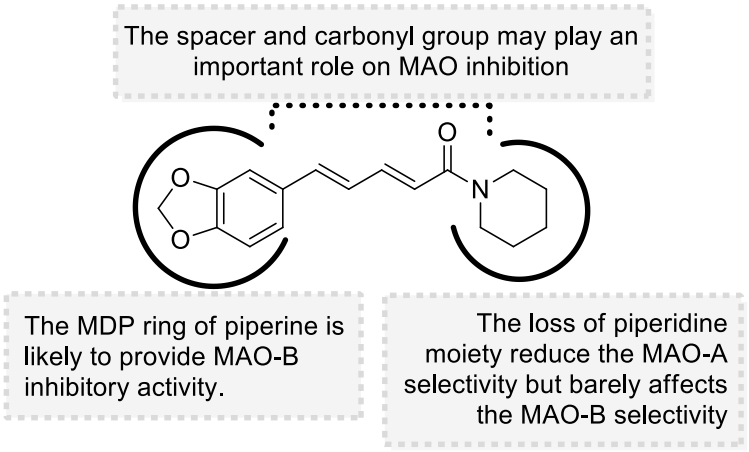


Figure 20. Structure-activity relationship of MAO-B inhibitors based on piperine scaffold.

The MAO-B inhibitory activity of (*E*,*E*)-8-(4-phenylbutadien-1-yl)caffeinyl analogues **(72-78)** **(Figure 17)** was evaluated using mitochondrial fractions of baboon liver. The oxidation of the substrate 1-methyl-4-(1-methylpyrrol-2-yl)-1,2,3,6-tetrahydropyridine to the corresponding dihydropyridinium metabolite in the presence of the test inhibitors was monitored spectrophotometrically at 420 nm. The derivatives bearing different substituents on the phenyl ring (compounds **(73-75)**, **Table 4**) showed the best results, with a competitive MAO-B inhibition mechanism and enzyme-inhibitor dissociation constants (K_i values) ranging from 17 to 46.4 nM. [86] The effect of the structural modification of caffeinyl ring on MAO-B inhibition was studied by expanding the series to include compounds **(76-79)**. Ethyl derivatives were much weaker MAO-B inhibitors than compounds **(72-75)**. For instance, compounds **(77)** and **(78)** exhibited only 32.7% and 14.6% MAO-B inhibition at 30 µM, respectively. [86]

Table 4. MAO-B and A_{2A} inhibition by (*E*,*E*)-8-(4-phenylbutadien-1-yl)caffeinyl analogues **(72-78)**.

Compound	Substituents			MAO-B	A_{2A}
	R_1	R_2	R_3	K_i (nM)	K_i (nM)
(72)	H	CH_3	CH_3	148.6	153 ± 5.40
(73)	Cl	CH_3	CH_3	42.1	104 ± 1.50
(74)	Br	CH_3	CH_3	17.2	59.1 ± 15.8
(75)	F	CH_3	CH_3	46.4	114 ± 14.2
(76)	H	CH_3	C_2H_5	1712	13.5 ± 4.87
(77)	H	C_2H_5	CH_3	___	2.74 ± 0.35
(78)	H	C_2H_5	C_2H_5	___	7.73 ± 2.80

The potential antagonist effect of compounds **(72-78)** on A_{2A} adenosine receptor was further explored by competitive inhibition of *N*-[^{3}H]ethyladenosin-5'-uronamide radioligand binding in rat striatal membranes. All the (*E*,*E*)-8-(4-phenylbutadien-1-yl)caffeinyl analogues were shown to be potent A_{2A} adenosine receptor antagonists (**Table 4**). However, in contrast to MAO-B inhibition, ethyl substituents on the caffeinyl ring had a positive effect on the potency of the A_{2A} antagonism (compounds **(72-75)**: K_i = 59.1-153 nM; compounds **(76-78)**: K_i = 7.73-13.5 nM). [86]

3. Conclusion

Over the last decade, the development of new compounds based on piperine scaffold has increased and promising data on multiple areas of biomedical and pharmaceutical research have been attained. In general, piperine derivatives displayed improved biological activities when compared to the parent alkaloid. Piperine and derivatives thereof have shown encouraging results and may have potential therapeutic applicability in the pharmaceutical industry. Moreover, their extended array of biological activities makes them promising candidates as drugs and/or coadjuvant therapies in highly prevalent human diseases, such neurodegenerative, infectious and inflammatory diseases and cancer. The pioneering chemical and pharmacological artwork currently being developed around this scaffold may result in new drug candidates in a foreseeable future.

4. Expert Opinion

Although the discovery and development of piperine based derivatives is still in early stage, the diverse array of biological activities makes piperine an appealing template for the development of new chemical entities and the therapeutic areas of application seem almost limitless.

The bioenhancing properties of piperine have been the most explored; in fact, piperine has been used in several pharmaceutical compositions containing nonsteroidal anti-inflammatory drugs (NSAIDs), [88] antitubercular drugs [89, 90] and chemosensitizing agents. [91] Piperine analogues were shown to effectively improve the bioefficacy of antibacterial and chemotherapeutic agents. The resulting decrease of the dose is beneficial since it reduces the costs of treatment and the side effects associated to the use of higher doses of the drugs alone.

Antimicrobial agents used in current therapies are quite efficient. Nonetheless, the toxicity of these compounds to the host is common and the number of multi-drug resistant strains is increasing. The introduction of new antimicrobial agents with reduced side effects is an urgent quest. The validation of piperine as a suitable template for the development of new drugs with leishmanicidal and trypanocydal activity was recently performed. [36, 37] Further modifications of piperine framework provided compounds with promising antimicrobial effect and reduced toxicity.

Piperine was shown to exhibit neuroprotective activity in 6-hydroxydopamine-induced Parkinson's rat model through antioxidant, anti-inflammatory and antiapoptotic mechanisms. [92] Piperine improved memory impairment and neurodegeneration in hippocampus of adult male Wistar rats, possibly via reduction of lipid peroxidation and acetylcholinesterase activity. Furthermore, a neurotrophic effect was also observed. [93] Piperine exerted neuroprotection against corticosterone-induced neurotoxicity in PC12 cells, at least partially, through the inhibition of oxidative stress and the upregulation of brain-derived neurotrophic factor (BDNF) mRNA expression. [94] Additionally, piperine showed antidepressant-like effect in corticosterone-treated

mice. The upregulation of BDNF expression seemed to be mechanism underlying this activity. [95] Therefore, and considering that piperine is likely to penetrate the blood-brain barrier, [96] the development of piperine analogues may result in the discovery of lead compounds with potential application on therapies of neurological disorders. Indeed, several piperine derivatives were shown to interact with a wide range of central nervous system targets ($GABA_A$, TRPV1 and adenosine A_{2A} receptors and MAO-B) involved in human diseases with high social and economic impact, including neurodegenerative diseases and other neurological disorders.

Natural products provide valuable scaffolds for multitarget directed drugs (MTDD). The structural refinement enables the improvement of the affinity when the pathways relevant for the disease are identified. [97] In this review, we reported the development of piperine-based compounds and their biological outline. Overall, the pharmacological activity was multivalent and diverse. In this sense, piperine may provide a promising framework for the design of new MTDDs.

Another important issue is the fact that piperine undergoes isomerization and exists as four distinct geometric isomers: (*E*,*E*)-piperine (piperine), (*Z*,*E*)-piperine (isopiperine), (*E*,*Z*)-isochavicine and (*Z*,*Z*)-piperine (chavicine). [98] The rate and extent of isomerization is variable. For instance, no piperine isomers were detected in human plasma samples spiked with different concentrations of piperine and in plasma of healthy volunteers after oral ingestion of piperine (50 mg). [99] Contrarily, all isomers were detected in egg yolks and blood plasma of hens fed daily with 80 mg piperine/100g feed stuff. [100] Although piperine has been identified as the main isomer in *Piper* sp, enzymatic-catalyzed and/or photo-induced isomerization may have different dietary, pharmacological and toxicological properties and the same observation applies to piperine-based derivatives. For instance, UV-induced isomerization of piperine led to a loss of its ability to stimulate melanocyte proliferation and to bind to human serum albumin *in vitro*. [101] Further studies are needed to fully understand the impact of isomerization on piperine's biological activity and safety profile.

Finally, the piperine scaffold can be a valuable starting point to build new drug candidates. The patents reported in this review showed that, depending on the structural modifications and substitution patterns introduced, new effective agents with multiple therapeutic applications can be developed. Naturally occurring scaffolds like piperine are still valuable assets, providing helpful and inspiring starting points in drug discovery programs.

5. Declaration of interest

The authors were supported by the Foundation for Science and Technology (FCT), Portugal, under grant number QUI/UI0081/2015 and by Quadro de Referência Estratégica Nacional (QREN) under project number FCUP-CIQ-UP-NORTE-07-0124-FEDER-000065. D Chavarria is in receipt of FCT grant number SFRH/BD/108119/2015. T Silva is in receipt of FCT grant number SFRH/BD/79671/2011. The Chemistry Research Center University of Porto (CIQUP) and the Research Unit on Applied Molecular Biosciences/Rede de Química e Tecnologia (UCIBIO/REQUIMTE), with which the authors are affiliated, are non-profit scientific organizations confined within the University of Porto. The authors have no other relevant affiliations or financial involvement with any organization or entity with a financial interest in or financial conflict with the subject matter or materials discussed in the manuscript apart from those disclosed.

6. References

1 MS Butt, I Pasha, MT Sultan, et al., Black pepper and health claims: a comprehensive treatise. *Crit. Rev. Food Sci. Nutr.* 2013; 53: 875–886.

•• Review of chemical and biological background.

2 II Koleva, TA van Beek, AEMF Soffers, et al., Alkaloids in the human food chain - natural occurrence and possible adverse effects. *Mol. Nutr. Food Res.* 2012; 56: 30–52.

3 S Bunsupa, M Yamazaki, and K Saito, Quinolizidine alkaloid biosynthesis: recent advances and future prospects. *Front. Plant Sci.* 2012; 3: 1–7.

4 K Srinivasan, Black pepper and its pungent principle-piperine: a review of diverse physiological effects. *Crit. Rev. Food Sci. Nutr.* 2007; 47: 735–748.

•• Review of chemical and biological background.

5 V Alugolu, S Rentala, a L Komarraju, et al., Docking studies of piperine - iron conjugate with human CYP450 3A4. *Bioinformation* 2013; 9: 334–338.

6 RK Bhardwaj, H Glaeser, L Becquemont, et al., Piperine, a major constituent of black pepper, inhibits human P-glycoprotein and CYP3A4. *J. Pharmacol. Exp. Ther.* 2002; 302: 645–650.

• Influence of piperine on drug metabolism and efflux regulators.

7 JJ Johnson, M Nihal, I a Siddiqui, et al., Enhancing the bioavailability of resveratrol by combining it with piperine. *Mol Nutr Food Res.* 2012; 55: 1169–1176.

8 M Bishnoi, K Chopra, L Rongzhu, et al., Protective effect of curcumin and its combination with piperine (bioavailability enhancer) against haloperidol-associated neurotoxicity: Cellular and neurochemical evidence. *Neurotox. Res.* 2011; 20: 215–225.

9 P Rinwa and A Kumar, Quercetin along with piperine prevents cognitive dysfunction, oxidative stress and neuro-inflammation associated with mouse model of chronic unpredictable stress. *Arch. Pharm. Res.* 2013; 1–10: published online 16 July 2013, doi: 10.1007/s12272-013-0205-4.

10 S Verkantesh, K Durga, Y Padmavathi, et al., Influence of piperine on ibuprofen induced antinociception and its pharmacokinetics. *Arzneimittelforschung* 2011; 61: 506–509.

11 SK Gupta, P Bansal, RK Bhardwaj, et al., Comparative anti-nociceptive, anti-inflammatory and toxicity profile of nimesulide vs nimesulide and piperine combination. *Pharmacol. Res.* 2000; 41: 657–662.

12 V Sama, M Nadipelli, P Yenumula, et al., Effect of piperine on antihyperglycemic activity and pharmacokinetic profile of nateglinide. *Arzneimittelforschung.* 2012; 62: 384–388.

13 C Veeresham, S Sujatha, and T Rani, Effect of piperine on the pharmacokinetics and pharmacodynamics of glimepiride in normal and streptozotocin-induced diabetic rats. *Nat Prod Commun.* 2012; 7: 1283–286.

14 MJ Jin and HK Han, Effect of piperine, a major component of black pepper, on the intestinal absorption of fexofenadine and its implication on food-drug interaction. *J. Food Sci.* 2010; 75: H93–H96.

15 T Velpandian, R Jasuja, RK Bhardwaj, et al., Piperine in food: interference in the pharmacokinetics of phenytoin. *Eur. J. Drug Metab. Pharmacokinet.* 2001; 26: 241–247.

16 S Pattanaik, D Hota, S Prabhakar, et al., Effect of Piperine on the Steady-state Pharmacokinetics of Phenytoin in Patients with Epilepsy. *Phyther. Res.* 2006; 20: 683–686.

17 R Kashibhata and M Naidu, Influence of piperine on the pharmacokinetics of nevirapine under fasting conditions: a randomised, crossover, placebo-controlled study. *Drugs R D.* 2007; 8: 383–391.

18 H-K Han, The effects of black pepper on the intestinal absorption and hepatic metabolism of drugs. *Expert Opin. Drug Metab. Toxicol.* 2011; 7: 721–729.

19 N Tharmalingam, S Kim, M Park, et al., Inhibitory effect of piperine on Helicobacter pylori growth and adhesion to gastric adenocarcinoma cells. *Infect. Agent. Cancer* 2014; 9: 1–10.

20 J Zhang, X Zhu, H Li, et al., Piperine inhibits proliferation of human osteosarcoma cells via G2/M phase arrest and metastasis by suppressing MMP-2/-9 expression. *Int. Immunopharmacol.* 2015; 24: 50–58.

21 PB Yaffe, MR Power Coombs, CD Doucette, et al., Piperine, an alkaloid from black pepper, inhibits growth of human colon cancer cells via G1 arrest and apoptosis triggered by endoplasmic reticulum stress. *Mol. Carcinog.* 2014; 54: 1070–1085.

22 AL Greenshields, CD Doucette, KM Sutton, et al., Piperine inhibits the growth and motility of triple-negative breast cancer cells. *Cancer Lett.* 2015; 357: 129–140.

23 Y Xia, PN Khoi, HJ Yoon, et al., Piperine inhibits IL-1β-induced IL-6 expression by suppressing p38 MAPK and STAT3 activation in gastric cancer cells. *Mol. Cell. Biochem.* 2014; 398: 147–156.

24 L Lai, Q Fu, Y Liu, et al., Piperine suppresses tumor growth and metastasis in vitro and in vivo in a 4T1 murine breast cancer model. *Acta Pharmacol. Sin.* 2012; 33: 523–530.

25 NM Fofaria, SH Kim, and SK Srivastava, Piperine causes G1 phase cell cycle arrest and apoptosis in melanoma cells through checkpoint kinase-1 activation. *PLoS One* 2014; 9: 1–10.

26 X-F Hou, H Pan, L-H Xu, et al., Piperine Suppresses the Expression of CXCL8 in Lipopolysaccharide-Activated SW480 and HT-29 Cells via Downregulating the Mitogen-Activated Protein Kinase Pathways. *Inflammation* 2014; 38: 1093–1102.

27 RA Gupta, MN Motiwala, NG Dumore, et al., Effect of piperine on inhibition of FFA induced TLR4 mediated inflammation and amelioration of acetic acid induced ulcerative colitis in mice. *J. Ethnopharmacol.* 2015; 164: 239–246.

28 Y Dong, Z Huihui, and C Li, Piperine inhibit inflammation, alveolar bone loss and collagen fibers breakdown in a rat periodontitis model. *J. Periodontal Res.* 2015; 1–8: published online 2 March 2015, doi: 10.1111/jre.12262.

29 N Bojjireddy, RK Sinha, and G Subrahmanyam, Piperine inhibits type II phosphatidylinositol 4-kinases: A key component in phosphoinositides turnover. *Mol. Cell. Biochem.* 2014; 393: 9–15.

30 X Ying, K Yu, X Chen, et al., Piperine inhibits LPS induced expression of inflammatory mediators in RAW 264.7 cells. *Cell. Immunol.* 2013; 285: 49–54.

31 S Umar, AHM Golam Sarwar, K Umar, et al., Piperine ameliorates oxidative stress, inflammation and histological outcome in collagen induced arthritis. *Cell. Immunol.* 2013; 284: 51–59.

32 X Ying, X Chen, S Cheng, et al., Piperine inhibits IL-β induced expression of inflammatory mediators in human osteoarthritis chondrocyte. *Int. Immunopharmacol.* 2013; 17: 293–299.

33 ZY Jiang, WF Liu, XM Zhang, et al., Anti-HBV active constituents from Piper longum. *Bioorganic Med. Chem. Lett.* 2013; 23: 2123–2127.

34 A Kumar, RP Raman, K Kumar, et al., Antiparasitic efficacy of piperine against Argulus spp. on

Carassius auratus (Linn. 1758): In vitro and in vivo study. *Parasitol. Res.* 2012; 111: 2071–2076.

35 S Sharma, NP Kalia, P Suden, et al., Protective efficacy of piperine against Mycobacterium tuberculosis. *Tuberculosis* 2014; 94: 389–396.

36 C Ferreira, DC Soares, CB Barreto-Junior, et al., Leishmanicidal effects of piperine, its derivatives, and analogues on Leishmania amazonensis. *Phytochemistry* 2011; 72: 2155–2164.

37 L Freire-De-Lima, TS Ribeiro, GM Rocha, et al., The toxic effects of piperine against Trypanosoma cruzi: Ultrastructural alterations and reversible blockage of cytokinesis in epimastigote forms. *Parasitol. Res.* 2008; 102: 1059–1067.

38 M Mohtar, SA Johari, AR Li, et al., Inhibitory and resistance-modifying potential of plant-based alkaloids against methicillin-resistant Staphylococcus aureus (MRSA). *Curr. Microbiol.* 2009; 59: 181–186.

39 M Meghwal and TK Goswami, Piper nigrum and piperine: An update. *Phyther. Res.* 2013; 27: 1121–1130.

40 JP Brincat, F Broccatelli, S Sabatini, et al., Ligand promiscuity between the efflux pumps human p-glycoprotein and s. aureus NorA. *ACS Med. Chem. Lett.* 2012; 3: 248–251.

41 ML Cuestas, AI Castillo, A Sosnik, et al., Downregulation of mdr1 and abcg2 genes is a mechanism of inhibition of efflux pumps mediated by polymeric amphiphiles. *Bioorganic Med. Chem. Lett.* 2012; 22: 6577–6579.

42 J Sun, Z Deng, and A Yan, Bacterial multidrug efflux pumps: Mechanisms, physiology and pharmacological exploitations. *Biochem. Biophys. Res. Commun.* 2014; 453: 254–267.

43 C Ramalhete, G Spengler, A Martins, et al., Inhibition of efflux pumps in meticillin-resistant Staphylococcus aureus and Enterococcus faecalis resistant strains by triterpenoids from Momordica balsamina. *Int. J. Antimicrob. Agents* 2011; 37: 70–74.

44 A Kumar, IA Khan, S Koul, et al., Novel structural analogues of piperine as inhibitors of the NorA efflux pump of Staphylococcus aureus. *J. Antimicrob. Chemother.* 2008; 61: 1270–1276.

45 L Amin, P-glycoprotein Inhibition for Optimal Drug Delivery. *Drug Target Insights* 2013; 7: 27–34.

46 MK DeGorter, CQ Xia, JJ Yang, et al., Drug transporters in drug efficacy and toxicity. *Annu Rev Pharmacol Toxicol* 2012; 52: 249–273.

47 GQ Surrinder Koul, Jawahir Koul, Subhash Taneja, Pankaj Gupta, Inshad Khan, Zahid Mirza, Ashwani Kumar, Rakesh Johri, Monika Pandita, Anita Khosa, Ashok Tikoo, Subhash Sharma, Vijeshwar Verma, Aromatic amides as potentiators of bioefficacy of anti-infective drugs, US 20070004645 A1, 2007.

• Patent with multiple strategies to obtain piperine derivatives modified on the alkene spacer and the amide moiety.

48 I Wiegand, K Hilpert, and REW Hancock, Agar and broth dilution methods to determine the minimal inhibitory concentration (MIC) of antimicrobial substances. *Nat. Protoc.* 2008; 3: 163–175.

49 PL Sangwan, JL Koul, S Koul, et al., Piperine analogs as potent Staphylococcus aureus NorA efflux pump inhibitors. *Bioorganic Med. Chem.* 2008; 16: 9847–9857.

50 BS Sachin, IA Najar, SC Sharma, et al., Simultaneous determination of etoposide and a piperine analogue (PA-1) by UPLC-qTOF-MS: Evidence that PA-1 enhances the oral bioavailability of

etoposide in mice. *J. Chromatogr. B* 2010; 878: 823–830.

51 IA Najar, SC Sharma, GD Singh, et al., Involvement of P-glycoprotein and CYP 3A4 in the enhancement of etoposide bioavailability by a piperine analogue. *Chem. Biol. Interact.* 2011; 190: 84–90.

52 D Evangelopoulos, J Diniz, and SJ Waddell, Understanding anti-tuberculosis drug efficacy : rethinking bacterial populations and how we model them. *Int. J. Infect. Dis.* 2015; 32: 76–80.

53 D-D Pham, E Fattal, and N Tsapis, Pulmonary drug delivery systems for the treatment of tuberculosis. *Int. J. Pharm.* 2015; 478: 517–529.

54 S Sharma, M Kumar, S Sharma, et al., Piperine as an inhibitor of Rv1258c, a putative multidrug efflux pump of Mycobacterium tuberculosis. *J. Antimicrob. Chemother.* 2010; 65: 1694–1701.

55 A Zhou, J Ni, Z Xu, et al., Application of 1H NMR spectroscopy-based metabolomics to sera of tuberculosis patients. *J. Proteome Res.* 2013; 12: 4642–4649.

56 M Naik, S Ghorpade, LK Jena, et al., 2-Phenylindole and Arylsulphonamide: Novel Scaffolds Bactericidal against Mycobacterium tuberculosis. *ACS Med. Chem. Lett.* 2014; 5: 1005–1009.

57 DS Reddi and R Ramesh, Antitubercular compounds and process for the preparation thereof, WO2014128724 A1, 2014.

58 RFS Menna-Barreto, K Salomão, AP Dantas, et al., Different cell death pathways induced by drugs in Trypanosoma cruzi: an ultrastructural study. *Micron* 2009; 40: 157–168.

59 L Osorio, I Ríos, B Gutiérrez, et al., Virulence factors of Trypanosoma cruzi: Who is who? *Microbes Infect.* 2012; 14: 1390–1402.

60 W da Silva Ferreira, L Freire-de-Lima, VB Saraiva, et al., Novel 1,3,4-thiadiazolium-2-phenylamine chlorides derived from natural piperine as trypanocidal agents: Chemical and biological studies. *Bioorganic Med. Chem.* 2008; 16: 2984–2991.

61 JC Aponte, M Verástegui, E Málaga, et al., Synthesis, cytotoxicity, and anti-Trypanosoma cruzi activity of new chalcones. *J. Med. Chem.* 2008; 51: 6230–6234.

62 EF Da Silva, MM Canto-Cavalheiro, VR Braz, et al., Synthesis, and biological evaluation of new 1,3,4-thiadiazolium-2-phenylamine derivatives against Leishmania amazonensis promastigotes and amastigotes. *Eur. J. Med. Chem.* 2002; 37: 979–984.

63 P Leprohon, C Fernandez-Prada, É Gazanion, et al., Drug resistance analysis by next generation sequencing in Leishmania. *Int. J. Parasitol. Drugs Drug Resist.* 2015; 5: 26–35.

64 JA Hutton, V Goncalves, JA Brannigan, et al., Structure-Based Design of Potent and Selective Leishmania N−Myristoyltransferase Inhibitors. *J. Med. Chem.* 2014; 57: 8664−8670.

65 L Syrjänen, AB Vermelho, I De Almeida Rodrigues, et al., Cloning, characterization, and inhibition studies of a β-carbonic anhydrase from Leishmania donovani chagasi, the protozoan parasite responsible for leishmaniasis. *J. Med. Chem.* 2013; 56: 7372–7381.

66 A Yadav, A Amit, R Chaudhary, et al., Leishmania donovani: impairment of the cellular immune response against recombinant ornithine decarboxylase protein as a possible evasion strategy of Leishmania in visceral leishmaniasis. *Int. J. Parasitol.* 2015; 45: 33–42.

67 IP Singh, SK Jain, A Kaur, et al., Synthesis and Antileishmanial activity of Piperoyl-Amino Acid Conjugates. *Eur. J. Med. Chem.* 2010; 45: 3439–3445.

68 NR Gavva, AW Bannon, S Surapaneni, et al., The vanilloid receptor TRPV1 is tonically activated in vivo and involved in body temperature regulation. *J. Neurosci.* 2007; 27: 3366–3374.

69 J Peng and YJ Li, The vanilloid receptor TRPV1: Role in cardiovascular and gastrointestinal protection. *Eur. J. Pharmacol.* 2010; 627: 1–7.

70 A Szallasi, DN Cortright, CA Blum, et al., The vanilloid receptor TRPV1: 10 years from channel cloning to antagonist proof-of-concept. *Nat. Rev. Drug Discov.* 2007; 6: 357–372.

71 N Khairatkar-Joshi and A Szallasi, TRPV1 antagonists: the challenges for therapeutic targeting. *Trends Mol. Med.* 2009; 15: 14–22.

72 FN McNamara, A Randall, and MJ Gunthorpe, Effects of piperine, the pungent component of black pepper, at the human vanilloid receptor (TRPV1). *Br. J. Pharmacol.* 2005; 144: 781–790.

73 O Saku, H Ishida, E Atsumi, et al., Discovery of novel 5,5-diarylpentadienamides as orally available transient receptor potential vanilloid 1 (TRPV1) antagonists. *J. Med. Chem.* 2012; 55: 3436–3451.

74 EI Charych, F Liu, SJ Moss, et al., GABAA receptors and their associated proteins: Implications in the etiology and treatment of schizophrenia and related disorders. *Neuropharmacology* 2009; 57: 481–495.

75 J Zaugg, I Baburin, B Strommer, et al., HPLC-based activity profiling: discovery of piperine as a positive GABAA receptor modulator targeting a benzodiazepine-independent binding site. *J. Nat. Prod.* 2010; 73: 185–191.

76 L Wimmer, D Schönbauer, P Pakfeifer, et al., Developing piperine towards TRPV1 and GABAA via Heck-coupling of conjugated dienes. *Org. Biomol. Chem.* 2015; 13: 990–994.

77 S Khom, B Strommer, A Schöffmann, et al., GABAA receptor modulation by piperine and a non-TRPV1 activating derivative. *Biochem. Pharmacol.* 2013; 85: 1827–1836.

78 DS Steffen Hering, Thomas Erker, Thomas Schwarz, Igor Baburin, Novel piperine derivatives as GABAA receptors modulators, WO2011080313 A1, 2011.

79 A Schöffmann, L Wimmer, D Goldmann, et al., Efficient modulation of γ-aminobutyric acid type a receptors by piperine derivatives. *J. Med. Chem.* 2014; 57: 5602–5619.

• **Original article with diverse strategies to integrate aryl cores on the alkene spacer of piperine derivatives.**

80 L Legoabe, J Kruger, A Petzer, et al., Monoamine oxidase inhibition by selected anilide derivatives. *Eur. J. Med. Chem.* 2011; 46: 5162–5174.

81 LH Mu, B Wang, HY Ren, et al., Synthesis and inhibitory effect of piperine derivates on monoamine oxidase. *Bioorganic Med. Chem. Lett.* 2012; 22: 3343–3348.

82 LD Kong, CHK Cheng, and RX Tan, Inhibition of MAO A and B by some plant-derived alkaloids, phenols and anthraquinones. *J. Ethnopharmacol.* 2004; 91: 351–355.

83 S a Lee, SS Hong, XH Han, et al., Piperine from the fruits of Piper longum with inhibitory effect on monoamine oxidase and antidepressant-like activity. *Chem. Pharm. Bull. (Tokyo).* 2005; 53: 832–835.

84 JP Petzer, N Castagnoli, M a Schwarzschild, et al., Dual-Target – Directed Drugs that Block Monoamine Oxidase B and Adenosine A2A Receptors for Parkinson's Disease. *Neurotherapeutics* 2009; 6: 141–151.

85 P Jenner, a. Mori, R Hauser, et al., Adenosine, adenosine A2A antagonists, and Parkinson's disease. *Park. Relat. Disord.* 2009; 15: 406–413.

86 J Pretorius, SF Malan, N Castagnoli, et al., Dual inhibition of monoamine oxidase B and antagonism of the adenosine A2A receptor by (E,E)-8-(4-phenylbutadien-1-yl)caffeine analogues. *Bioorganic Med. Chem.* 2008; 16: 8676–8684.

87 A Stößel, M Schlenk, S Hinz, et al., Dual Targeting of Adenosine A2A Receptors and Monoamine Oxidase B by 4H-3,1-Benzothiazin-4-ones. *J. Med. Chem.* 2013; 56: 4580–4596.

88 R Jain and A Singh, Pharmaceutical compositions containing NSAIDs and piperine, EP 0935964 A1, 1999.

89 DD Bhatt, MR Trivedi, IA Modi, et al., Pharmaceutical composition of isoniazid, WO 2011012987 A1, 2011.

90 KL Bedi, SK Dhar, RK Johri, et al., Pharmaceutical compositions containing piperine and an antituberculosis or antileprosydrug, EP 0650728 B1, 2002.

91 PF Di, Compositions containing a phospholipid-curcumin complex and piperine as chemosensitizing agent, EP 2228062 A1, 2010.

92 P Shrivastava, K Vaibhav, R Tabassum, et al., Anti-apoptotic and Anti-inflammatory effect of Piperine on 6-OHDA induced Parkinson's Rat model. *J. Nutr. Biochem.* 2013; 24: 680–687.

93 P Chonpathompikunlert, J Wattanathorn, and S Muchimapura, Piperine, the main alkaloid of Thai black pepper, protects against neurodegeneration and cognitive impairment in animal model of cognitive deficit like condition of Alzheimer's disease. *Food Chem. Toxicol.* 2010; 48: 798–802.

94 QQ Mao, Z Huang, SP Ip, et al., Protective effects of piperine against corticosterone-induced neurotoxicity in PC12 cells. *Cell. Mol. Neurobiol.* 2012; 32: 531–537.

95 QQ Mao, Z Huang, XM Zhong, et al., Piperine reverses the effects of corticosterone on behavior and hippocampal BDNF expression in mice. *Neurochem. Int.* 2014; 74: 36–41.

96 OB Al-Baghdadi, NI Prater, CJ Van Der Schyf, et al., Inhibition of monoamine oxidase by derivatives of piperine, an alkaloid from the pepper plant Piper nigrum, for possible use in Parkinson's disease. *Bioorganic Med. Chem. Lett.* 2012; 22: 7183–7188.

97 A Koeberle and O Werz, Multi-target approach for natural products in inflammation. *Drug Discov. Today* 2014; 19: 1871–1882.

98 N Kozukue, MS Park, SH Choi, et al., Kinetics of light-induced cis-trans isomerization of four piperines and their levels in ground black peppers as determined by HPLC and LC/MS. *J. Agric. Food Chem.* 2007; 55: 7131–7139.

99 M Kakarala, SK Dubey, M Tarnowski, et al., Ultra-low flow liquid chromatography assay with ultraviolet (UV) detection for piperine quantitation in human plasma. *J. Agric. Food Chem.* 2010; 58: 6594–6599.

100 W Ternes and EL Krause, Characterization and determination of piperine and piperine isomers in eggs. *Anal. Bioanal. Chem.* 2002; 374: 155–160.

101 A Soumyanath, R Venkatasamy, M Joshi, et al., UV irradiation affects melanocyte stimulatory activity and protein binding of piperine. *Photochem. Photobiol.* 2006; 82: 1541–1548.

CHAPTER III

Experimental section

3.1. Manuscript II

Bioisosteric OH- to SH- replacement changes the antioxidant profile of ferulic acid

Organic and Biomolecular Chemistry, **2019**, 17: 9646-9654.
DOI: 10.1039/C9OB01875A

ARTICLE

Bioisosteric OH- to SH- replacement changes the antioxidant profile of ferulic acid

Received 00th January 20xx,
Accepted 00th January 20xx

DOI: 10.1039/x0xx00000x

Daniel Chavarria,[a,b†] Carlos Fernandes,[a†] Tiago Silva,[a,b] Jorge Garrido,[c] Fernando Remião,[d] Paulo J. Oliveira[b] and Fernanda Borges[a*]

We report the synthesis of 4-thioferulic acid (TFA), a new ferulic acid (FA) derivative, and highlight the differences between the two compounds concerning rate and mechanism of radical scavenging activity, redox potential, acidity of the phenol/thiophenol moieties, cytotoxicity in differentiated SH-SY5Y cells, and neuroprotection against hydrogen peroxide (H_2O_2) and *tert*-butyl hydroperoxide (*t*-BHP) in the same cellular model.

Introduction

Ferulic acid (3-(4-hydroxy-3-methoxyphenyl)-2-propenoic acid, FA, **Fig. 1**) is a phytochemical widely distributed in the plant kingdom and in plant-derived products.[1] FA and other hydroxycinnamic acids (HCAs) are well-known for their antioxidant activity, which has been associated with numerous health benefits (*e.g.* anticarcinogenic, neuroprotective and cardioprotective).[2] The mechanisms underlying the antioxidant activity of HCAs include direct free radical scavenging and/or indirect actions, such as metal chelation, inhibition of pro-oxidant enzymes and upregulation of the expression of antioxidant enzymes.[3-5] HCAs scavenge free radicals by hydrogen atom or electron transfer mechanisms,[4, 6] and the resulting phenoxyl radical is stabilized by resonance across the conjugated system.[7, 8] Although the antioxidant activity of FA has been documented,[9, 10] it is usually outperformed by other HCAs, like caffeic and sinapic acids.[11-14] Moreover, in opposition to FA, caffeic acid also operates as a transition metal chelator.[15]

Biothiols such as glutathione and cysteine (**Fig. 1**) are members of the physiological antioxidant defence system, playing a pivotal role on protecting cells against the harmful effects inflicted by reactive species under oxidative stress.[16] In particular, biothiols participate in redox-mediated or redox-regulated processes in cells by acting as reducing agents.[17] Taking inspiration from biothiols, the replacement of the hydroxyl group (OH) by a sulfhydryl group (SH) in cinnamic systems may be a valid approach to develop new radical scavengers.

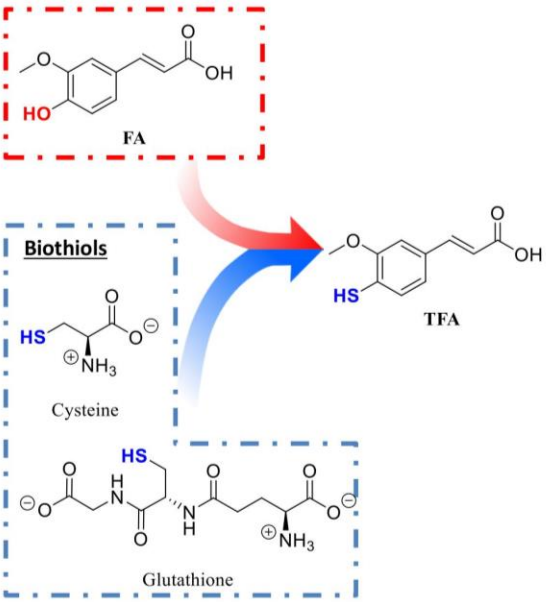


Fig. 1: The rationale of the development of thioferulic acid (TFA).

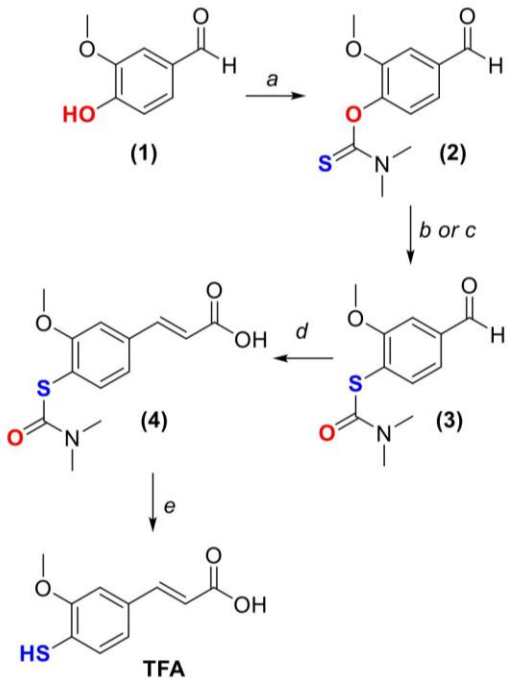
In this context, we developed 4-thioferulic acid (TFA, **Fig. 1**), a new sulphured analogue of FA. According to our knowledge, this is the first report on the synthesis of TFA. Since our goal was to boost the antioxidant activity of FA, we studied the effect of the OH to SH replacement on different parameters, namely radical scavenging activity, redox potential, acidity, cytotoxicity and neuroprotection against inducers of oxidative stress.

[a] *CIQUP/Department of Chemistry and Biochemistry, Faculty of Sciences, University of Porto, 4169-007 Porto, Portugal.*
Email: fborges@fc.up.pt
[b] *CNC - Center for Neuroscience and Cell Biology, University of Coimbra, UC Biotech, Biocant Park, Cantanhede, Portugal.*
[c] *Department of Chemical Engineering, School of Engineering (ISEP), Polytechnic of Porto, 4200-072 Porto, Portugal.*
[d] *UCIBIO-REQUIMTE, Laboratory of Toxicology, Department of Biological Sciences, Faculty of Pharmacy, University of Porto, Porto, Portugal.*
† These authors contributed equally to this work.
Electronic Supplementary Information (ESI) available: [details of any supplementary information available should be included here]. See DOI: 10.1039/x0xx00000x

Results and discussion

Synthesis

TFA was prepared by a four-step synthetic strategy (**Scheme 1**) using vanillin (compound **1**) as starting material. Compound **2** was easily obtained by the thiocarbamoylation of vanillin **1** with dimethylthiocarbamoyl chloride (DMTCl) in the presence of a strong base (diazabicyclo[2.2.2]octane, DABCO) (**Scheme 1**, step *a*). This reaction was followed by the Newman-Kwart rearrangement (**Scheme 1**, steps *b* and *c*).

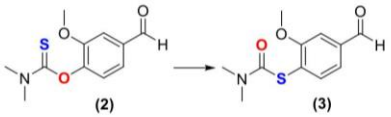


Scheme 1: Synthetic strategy followed for the preparation of TFA. (a) DMTCl, DABCO, THF, 70 °C, 3 h; (b) diphenyl ether, argon, 240 °C, 120 min; (c) diphenyl ether, argon, 220 ºC or 240 °C (μW), 10-30 min; (d) malonic acid, anhydrous pyridine, piperidine, 60 °C, 1 h; (e) MeOH, aqueous solution of NaOH 2 M, reflux, 1.5 h.

In this work we modified the procedure described by Garcia *et al.*[18] to adapt the Newman-Kwart rearrangement to microwave-assisted conditions, which significantly reduced the reaction time (**Table 1**). Then, a Knoevenagel-Doebner condensation between aldehyde **3** and malonic acid in pyridine and piperidine yielded cinnamic acid intermediate **4** (**Scheme 1**, step *d*). Finally, the *N*,*N*-dimethylcarbamoyl group of compound **4** was cleaved under hydrolytic alkaline conditions (**Scheme 1**, step *e*).

Prior to conducting *in vitro* radical scavenging and cytotoxicity assays, we studied the stability of TFA in solvents commonly used in biological assays (ethanol and dimethyl sulfoxide (DMSO)) at room temperature for 24 h by proton nuclear magnetic resonance (^{1}H NMR) spectroscopy. No significant chemical degradation of TFA in ethanol-d_6 was observed over a 24 h period (**Fig. S3**). However, TFA was less stable in DMSO-d_6 (**Fig. S4**). Additional peaks, with increasing intensity over the time, were observed in the experiment, with the concomitant decrease in the intensity of TFA ^{1}H NMR signals (**Fig. S4**). Based on these results, stock solutions of TFA were freshly prepared for conducting the assays described below.

Table 1. Optimization of the Newman-Kwart rearrangement to obtain synthetic intermediate **3**.



	t/min	T/ °C	η/%
Conventional heating	120	240	65
Microwave irradiation	10	220	52
	10	240	67
	20		72
	30		62

Evaluation of antioxidant profile in *in vitro* cell-free models

To study the antioxidant activity of TFA and compare it to FA, we evaluated the ability of both compounds to scavenge DPPH$^\bullet$, ABTS$^{\bullet+}$ and GO$^\bullet$ radicals. Trolox (TRX), a water-soluble analogue of vitamin E, was used as a standard antioxidant. The IC_{50} values of TFA were lower than FA in DPPH$^\bullet$ and GO$^\bullet$ assays and similar in ABTS$^{\bullet+}$ assay (**Table 2**). These results suggest that the replacement of the OH by an SH is well tolerated and may even enhance the antioxidant activity.

Table 2: Radical scavenging activity, redox potentials (E_{pa}) and pK_a values of FA and TFA

Entry	DPPH$^{\bullet}$[a]	ABTS$^{\bullet+}$[a]	GO$^{\bullet}$[a]	ORAC index	E_{pa}/mV	pK_a
FA	64.6±1.9	16.8±0.4	37.5±2.5	3.2±0.1	484	9.1
TFA	47.8±0.9	19.9±1.0	4.25±0.10	0.34±0.04	330	5.6
TRX	24.6±0.9	18.2±0.5	2.98±0.15	—	—	—

a The results are expressed as mean IC50 (μM) ± standard deviation (n = 3).

The kinetic curves obtained in obtained in DPPH$^\bullet$, ABTS$^{\bullet+}$ and GO$^\bullet$ assays showed marked differences between the reactivity of FA and TFA (**Fig. 2A-B** and **S5**). The hyperbolic kinetic curves obtained with FA during the experiment period indicated moderate radical scavenging activity with DPPH$^\bullet$, ABTS$^{\bullet+}$ and GO$^\bullet$ (**Fig. 2A** and **S5A-B**). On the other hand, TFA reacted almost instantaneously with the mentioned radicals. Increasing concentrations of TFA led to an abrupt decay on initial absorbance, reaching the steady state within the first minutes of reaction (**Fig. 2B** and **S5C-D**). Following the

This journal is © The Royal Society of Chemistry 20xx

categorization of antioxidants according to the shape of the reaction curves proposed by Xie *et al.*[19] and Tian *et al.*,[20] our results suggest that TFA and FA operate by dissimilar mechanisms.

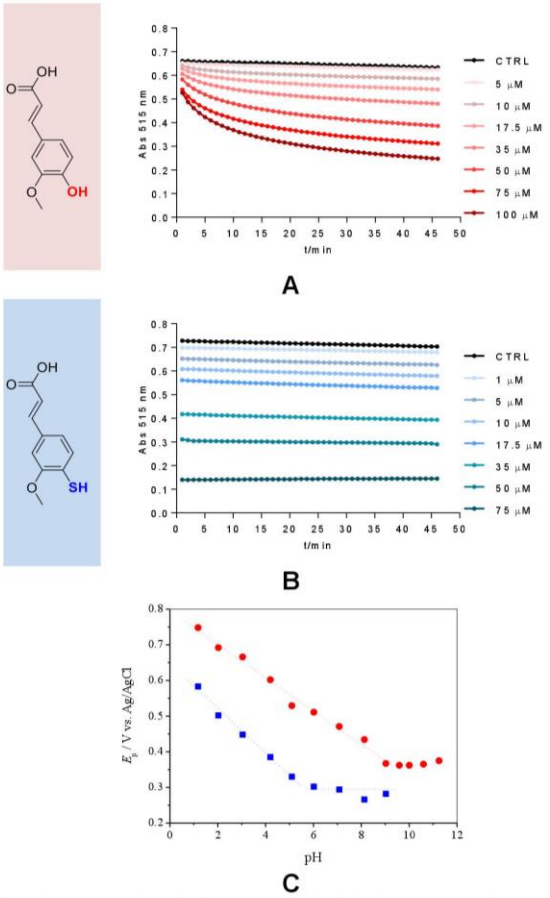


Fig. 2: Representative kinetic curves obtained in the presence of increasing concentrations of FA (**A**) and TFA (**B**) in DPPH$^{\bullet}$ assay. (**C**) Plots of E_{pa} vs. pH from differential pulse voltammograms of FA (●) and TFA (■) at 100 µM in different buffer electrolytes. Scan rate: 5 mV.s^{-1}.

We also evaluated the radical scavenging activity of TFA and FA against peroxyl radicals (ROO$^{\bullet}$) by the Oxygen Radical Absorbance Capacity (ORAC) assay. The ORAC index value of TFA was significantly lower than the one obtained for FA (**Table 1**), suggesting that TFA presents a lower ability to scavenge ROO$^{\bullet}$ radicals than FA.

In parallel, we studied the electrochemical behaviour of TFA and FA by cyclic voltammetry at physiological pH 7.4. The voltammograms obtained for FA and TFA showed one anodic peak at E_{pa} = + 0.484 V and E_{pa} = + 0.330 V, respectively, which were assigned to the oxidation of the OH and SH groups (**Table 2** and **Fig. 3**). The lower E_{pa} value obtained for TFA suggest that thiophenols are more prone to donate an electron than phenols, which is in accordance with the data obtained in DPPH$^{\bullet}$, ABTS$^{\bullet+}$ and GO$^{\bullet}$ assays (**Table 2**). The absence of reduction peaks on the reverse scan indicate that both oxidation processes were irreversible (**Fig. 3**).

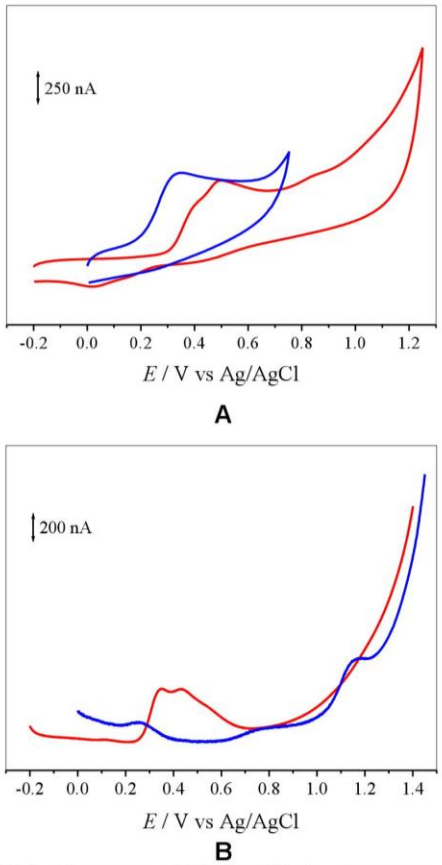


Fig. 3: (**A**) Cyclic voltammograms and (**B**) differential pulse voltammograms of 0.1 mM solutions of FA (—) and TFA (—) in a supporting electrolyte with the physiological pH of 7.3. The scan rates used in CV and DPV experiments were 50 mV.s^{-1} and 5 mV.s^{-1}, respectively.

To determine the pK_a values of the phenol and thiophenol groups of FA and TFA, we studied the electrochemical oxidation of FA and TFA by differential pulse voltammetry in aqueous buffer supporting electrolytes over a pH range from 1 to 12. The E_{pa}–pH plots showed different linear areas that reflect changes in the oxidation mechanism, as a result of the shifts in the balance of the protonation-deprotonation equilibrium during the oxidation process (**Fig. 2C**). The voltammetric pK_a values were estimated from the breaks in the E_{pa}–pH curves. The thiophenol function of TFA presented a pK_a value of 5.6 and the phenol group of FA displayed a pK_a value of 9.1. The data obtained are in good agreement with the literature for FA and also for similar thiophenolic systems.[15, 21, 22] Overall, the results

pointed out that TFA is mainly in the form of thiophenolate anion while in phenolic function of FA is predominantly in the protonated form at physiological pH.

The dissimilar kinetic radical scavenging observed for TFA and FA in DPPH$^{\bullet}$, ABTS$^{\bullet+}$ and GO$^{\bullet}$ assays can be influenced by the amount of thiophenolate/phenolate present in solution.[23] In solvents with high dielectric constants, i.e., with higher ability to solvate and thus stabilize anions (*e.g.* water, methanol, ethanol), sequential proton loss electron transfer (SPLET) is favoured for reactions of antioxidants having low pK_a's.[23] Thus, the higher acidity of TFA favours the thiophenol deprotonation and the electron transfer from the thiophenolate anion to a radical, causing an acceleration of the reaction rate, which was observed in our experiments (**Fig. 2A-B and S5**). Conversely, the phenol group of FA can operate by electron transfer followed by proton transfer (ETPT) mechanism.[24]

Evaluation of cytotoxicity in neuroblastoma cells

To evaluate the safety outline of TFA, we studied the cytotoxicity of TFA and FA on SH-SY5Y cells, a human-derived neuroblastoma cell line commonly used to study neuronal toxicity.[25] After differentiation into a dopaminergic phenotype, cells were treated with eight different concentrations of the test compounds ranging between 1.6-200 µM and incubated for 24 h. Cellular viability was assessed using the 3-(4,5-dimethylthiazol-2-yl)-2,5-diphenyltetrazolium (MTT) reduction assay and the neutral red (NR) uptake assay (**Fig. 4**).

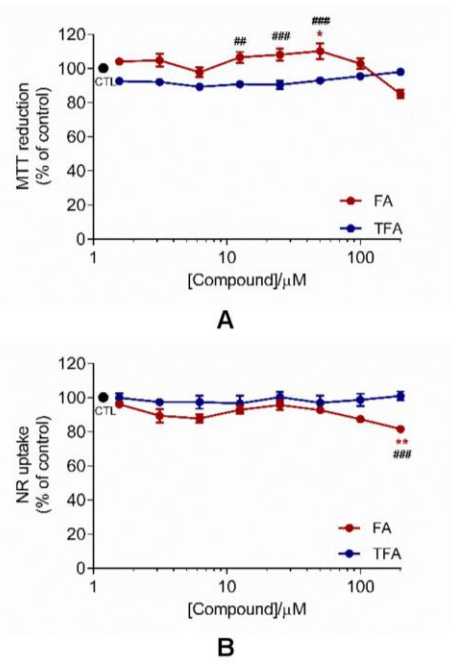


Fig. 4: Cellular viability of differentiated SH-SY5Y neuroblastoma cells after a 24 h treatment with FA (red) and TFA at eight different concentrations (1.6 µM – 200 µM). Cellular viability was evaluated using two methods: MTT reduction (**A**) and NR uptake (**B**). Results are expressed as the mean % of untreated controls ± SEM (n = 3). Statistical comparisons were carried out by two-way analysis of variance followed by Bonferroni's multiple-comparisons *post hoc* test. (* $p < 0.05$, ** $p < 0.01$, vs control; ## $p < 0.01$, #### $p < 0.0005$, FA vs TFA).

TFA presented a wide safety window, since the cell viability remained constant with increasing concentrations up to 200 µM (MTT reduction: 89.4±1.9–98.1±1.1 %; NR uptake: 96.7±4.1–101.0±2.6 %) (**Fig. 4A**). FA did not present toxic effects at concentrations up to 100 µM, which is in accordance with other reports.[26] However, we detected a slight decrease in mitochondrial (14.9 %) and lysosomal (18.1 %, $p < 0.001$) activities at 200 µM (**Fig. 4B**). Based on these results, we can conclude that the replacement of the OH by the highly reactive SH does not affect the cytotoxic profile of the cinnamic systems.

Finally, we studied the neuroprotective properties of TFA and FA against oxidative damage on the same cellular model (**Fig. 5**).

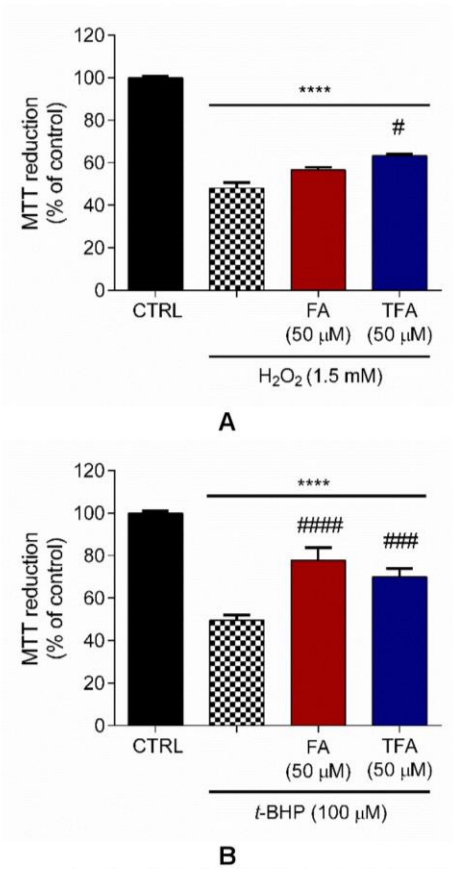


Fig. 5: Neuroprotective effects of FA (red) and TFA (blue) at 50 µM in SH-SY5Y cells using H_2O_2 (**A**) and *t*-BHP (**B**) as oxidative stress inducers. The data are expressed as the means of three independent experiments together with the standard error mean (Mean ± SEM). Statistical comparisons were made using one-way ANOVA followed by Dunnet's multiple comparison test or Kruskal-Wallis test in experiments (**A**) and (**B**), respectively. In all

This journal is © The Royal Society of Chemistry 20xx

cases, p values lower than 0.05 were considered significant ($^{****}p < 0.0001$ vs the control data; $^{\#}p < 0.05$, $^{\#\#\#}p < 0.001$, $^{\#\#\#\#}p < 0.0001$ vs oxidative inducer values).

After a pre-treatment with test compounds at 50 µM for 24 h, cells were treated with hydrogen peroxide (H_2O_2, 1.5 mM) or *tert*-butyl hydroperoxide (*t*-BHP, 100 µM) for additional 24 h. The oxidative stress induced by H_2O_2 and *t*-BHP result from dissimilar mechanisms.[27] The results presented in **Fig. 5** showed that both H_2O_2 and *t*-BHP decreased the cell viability to 48.1±2.5 % ($p < 0.0001$) and 49.5±2.5 % ($p < 0.0001$), respectively. TFA protected neuroblastoma cells against the damage inflicted by both H_2O_2 (MTT reduction: 63.2±0.9 %, $p < 0.05$, **Fig. 5A**) and *t*-BHP (MTT reduction: 70.0±4.0 %, $p < 0.001$, **Fig. 5B**). On the other hand, FA only displayed significant neuroprotective effects against *t*-BHP-mediated cytotoxicity (MTT reduction: 77.9±5.9 %, $p < 0.0001$, **Fig. 5A**), although a slight increase of metabolic activity was also observed in the pre-treatment with FA (**Fig. 5B**).

Conclusions

In summary, these studies demonstrate that the isosteric replacement of OH of FA with an SH enhanced the reactivity and changed the selectivity towards different radicals, reduced the oxidation potential and increased the acidity of the cinnamic systems. The higher reactivity of TFA did not increase the toxicity, at least in the cellular model used. The data collected in this work may contribute for the development of new multifunctional antioxidants with application in oxidative stress-related diseases.

Experimental Section

Reagents, materials and apparatus

Ferulic acid, vanillin, diazabicyclo[2.2.2]octane (DABCO), dimethylthiocarbamoyl chloride (DMTCl), malonic acid, piperidine, sodium hydroxide (NaOH), ammonium chloride (NH_4Cl), acetic acid, *N,N*-dimethylformamide (DMF), diphenyl ether, anhydrous pyridine, methanol and dichloromethane, were purchased from Sigma Aldrich (St. Louis, MO, USA), Alfa-Aesar (Haverhill, MA, USA) or TCI (Tokyo, Japan). Deionized water (conductivity < 0.1 $mS.cm^{-1}$) was used throughout all the experiments.

Microwave-assisted synthesis was performed in a Biotage® Initiator Microwave Synthesizer. The monitoring of reactions progress was performed by thin layer chromatography (TLC) on precoated silica gel 60 F254 acquired from Merck (Darmstad, Germany). TLC spots were visualized under UV detection (254 nm and 365 nm). Flash column chromatography was carried out on silica gel 60 Å acquired from Carlo-Erba Reactifs (SDS, France). The fractions with the desired compound were gathered and concentrated under reduced pressure. The solvents were evaporated using a Buchi Rotavapor.

^1H and ^{13}C NMR and DEPT135 data were acquired, at room temperature, on a Brüker AMX 300 spectrometer operating at 400.15 and 100.72 MHz, respectively. The solvents used in NMR experiments included $CDCl_3$-d_1, MeOD-d_4, EtOD-d_6 and DMSO-d_6. The chemical shifts are expressed in δ (ppm) values relative to tetramethylsilane (TMS) as internal reference and coupling constants (*J*) are given in Hz. Carbon signals present in DEPT135 spectra were underlined. Electron impact mass spectrometry (EI-MS) spectra were obtained on a Varian 320-MS apparatus. The data are reported as m/z (% of relative intensity of the most important fragments).

Synthetic procedures

Synthesis of O-(4-Formyl-2-methoxyphenyl) dimethylcarbamothioate (2).

Vanillin (compound **1**, 0.50 g, 3.31 mmol) was dissolved in DMF (5 mL). Then, DABCO (1.19 g, 10.6 mmol) and DMTCl (0.80 g, 6.48 mmol) were added. The mixture was heated at 70 ºC for 3 h. Upon completion, the mixture was poured onto water (15 mL), cooled on an ice bath and acidified with HCl 6 M. The product was collected by filtration under reduced pressure and washed with water. TLC analysis was performed in ethyl acetate/dichloromethane (3:7). The procedure was performed as reported by Nowakowska et al. [28]. η = 85 %. ^1H NMR ($CDCl_3$-d_1): δ (ppm) = 3.37 (s, 3H, NCH_3), 3.46 (s, 3H, NCH_3), 3.91 (s, 3H, OCH_3), 7.22 (d, J = 8.5 Hz, 1H, H5), 7.49 (m, 2H, H2, H6), 9.96 (s, 1H, CHO). ^{13}C NMR ($CDCl_3$-d_1): δ (ppm) = 38.9 (NCH_3), 43.4 (NCH_3), 56.2 (OCH_3), 111.1 (C2), 124.6 (C5), 124.7 (C6), 135.1 (C1), 147.8 (C4), 152.5 (C3), 186.9 (CSO), 191.1 (CHO). EI/MS m/z (%): 238.9 ($M^{\bullet+}$, 26), 111.0 (13), 88.0 (100), 72.0 (94).

Synthesis of S-(4-Formyl-2-methoxyphenyl)dimethylcarbamothioate (3).

Method A (conventional heating): Compound **2** (0.14 g, 0.58 mmol) was placed onto a 100 mL double neck round bottom flask with a condenser. The flask and the condenser were sealed with septa and the container was maintained under argon atmosphere for 30 min at room temperature. Then, diphenyl ether (5 mL) was added, and the mixture was heated at 250 ºC for 2 h. Purification by flash column chromatography (ethyl acetate/dichloromethane (3:7)) yielded compound 5. TLC analysis was performed in ethyl acetate/dichloromethane (3:7). The general procedure was adapted from Garcia et al.[18] with some modifications. The yield obtained is presented in Table S1.

Method B (microwave irradiation): Compound **2** was placed onto a 5 mL microwave glass vial. The vial was sealed with a septum and the content was maintained under argon atmosphere for 30 min at room temperature. After the addition of diphenyl ether, the vial was placed into the microwave cavity. The reaction took place under microwave irradiation. The reaction temperatures and the reaction times were described in **Table 1**. The compounds were isolated by flash column chromatography (ethyl acetate/dichloromethane (3:7)) and purified by recrystallization (dichloromethane/petroleum ether). TLC analysis was performed in ethyl acetate/dichloromethane (3:7). The general procedure developed by Garcia *et al.*[18] was adapted to microwave-assisted conditions. The yields obtained are presented in **Table 1**.

^1H NMR ($CDCl_3$-d_1): δ (ppm) = 3.02 (*bs*, 3H, $NC\underline{H}_3$), 3.15 (*bs*, 3H, $NC\underline{H}_3$), 3.95 (*s*, 3H, $OC\underline{H}_3$), 7.45 (*m*, 2H, H2, H6), 7.69 (*d*, J =

7.6 Hz, 1H, H5), 9.99 (*s*, 1H, CHO). ^{13}C NMR ($CDCl_3$-d_1): δ (ppm) = 37.1 (2×NCH_3), 56.4 (OCH_3), 109.6 (C2), 123.66 (C6), 125.1 (C4), 138.1 (C5), 138.5 (C1), 160.2 (C3), 164.9 (CSO), 191.6 (CHO). EI/MS m/z (%): 238.9 ($M^{\bullet+}$, 26), 111.0 (13), 88.0 (100), 72.0 (94).

Synthesis of (*E*)-3-(4-((Dimethylcarbamoyl)thio)-3-methoxyphenyl)acrylic acid (4).

Aldehyde **3** (0.61 g, 2.54 mmol) was dissolved in anhydrous pyridine (3 mL, 37.1 mmol). Then, malonic acid (0.41 g, 3.90 mmol) and piperidine (88 µL, 0.89 mmol) were added. The mixture was stirred at 60 ºC over 1 h. Once the reaction was complete, the mixture was poured onto water (15 mL), cooled on an ice bath and acidified with HCl 6 M. The product was collected by filtration under reduced pressure and washed with water. After suspension in methanol, the solid was centrifuged at 3000 *g* for 20 min. The supernatant was discarded, yielding the purified product. TLC analysis was performed in dichloromethane/methanol/formic acid (9:1:0.01). The general procedure was adapted from Teixeira et al.[29] with some modifications. η = 91 %. ^{1}H NMR (DMSO-d_6): δ (ppm) = 2.91 (bs, 3H, NCH_3), 3.05 (bs, 3H, NCH_3), 3.83 (s, 3H, OCH_3), 6.65 (d, *J* = 16.0 Hz, 1H, Hα), 7.26 (dd, J = 1.5 Hz, 8.0 Hz, 1H, H6), 7.41 (m, 2H, H2, H5), 7.60 (d, *J* = 16.0, 1H, Hβ), 12.46 (bs, 1H, COOH). ^{13}C NMR (DMSO-d_6): δ (ppm) = 37.0 (2×NCH_3), 56.6 (OCH_3), 111.4 (C2), 119.2 (C4), 121.1 (Cα), 121.2 (C6), 137.8 (C1), 138.2 (C5), 143.7 (Cβ), 160.3 (C3), 164.7 (COS), 167.9 (COOH). EI/MS m/z (%): 281.2 ($M^{\bullet+}$, 45), 192.1 (29), 72.1 (100).

Synthesis of (*E*)-3-(4-Sulfanyl-3-methoxyphenyl)acrylic acid (TFA).

To a solution of compound **5** (0.44 g, 1.57 mmol) in methanol (2 mL), aqueous solution of NaOH 2 M (4.0 mL, 8.00 mmol) was added dropwise. The reaction mixture was refluxed for 1.5 h. Upon completion, the mixture was allowed to cool at room temperature, then poured onto cooled aqueous saturated solution of NH_4Cl (15 mL) and acidified with aqueous solution of acetic acid 5 M. The solid was filtered under reduced pressure and washed with water. TLC analysis was performed in ethyl acetate/dichloromethane/formic acid (3:7:0.01). The procedure was adapted from Garcia et al. [18] with some modifications. η = 80 % (0.26 g; 1.25 mmol); white solid. ^{1}H NMR (MeOD-d_4): δ (ppm) = 3.92 (s, 3H, OCH_3), 6.44 (d, *J* = 15.9 Hz, 1H, Hα), 7.07 (dd, *J* = 1.5 Hz, 8.0 Hz, 1H, H6), 7.15 (d, *J* = 1.6 Hz, 1H, H2), 7.26 (d, *J* = 7.9 Hz, 1H, H5), 7.61 (d, *J* = 16.0 Hz, 1H, Hβ). ^{13}C NMR (MeOD-d_4): δ (ppm) = 55.1 (OCH_3), 109.2 (C2), 117.0 (Cα), 121.1 (C6), 124.9 (C4), 128.5 (C5), 135.6 (C1), 144.7 (Cβ), 155.0 (C3), 169.1 (COOH).EI/MS m/z (%): 210.0 ($M^{\bullet+}$, 100), 195.0 (19), 177.0 (9), 165.0 (23), 150.0 (13), 121.0 (22), 89.0 (14), 77.0 (17). 72.0 (19).

NMR stability studies

TFA solutions (0.7 M; 650 µL) were prepared in EtOD-d_6 or DMSO-d_6. ^{1}H NMR spectra were acquired at various timepoints for up to 24 h (15 min, 30 min, 1 h, 2 h, 4 h, 6 h and 24 h).

Radical scavenging activity

To measure the radical scavenging activity of FA and TFA, spectrophotometric methods (1,1-diphenyl-2-picrylhydrazyl radical, ($DPPH^{\bullet}$) 2,2′-azinobis-(3-ethylbenzothiazoline-6-sulfonic acid) radical cation ($ABTS^{\bullet+}$) and galvinoxyl ($GO^{\bullet}$) assays) and fluorometric methods (Oxygen radical absorbance capacity (ORAC) assay) were adopted.

Spectrophotometric assays

Sodium persulfate, $DPPH^{\bullet}$, 2,2′-azino-bis(3-ethylbenzothiazoline-6-sulfonic acid) diammonium salt (ABTS) and $GO^{\bullet}$ were acquired from Sigma Aldrich. In these methods, the scavenging of the colored radical by an antioxidant is followed by spectrophotometry. The absorbance decrease was monitored in a multiplate reader (BioTek Synergy HT from BioTek Instruments, Winooski, VT, USA). The results were expressed in IC_{50} as mean ± standard deviation (*n* = 3). Trolox (Sigma Aldrich), a water-soluble vitamin E derivative, was used as a standard reference. Kinetic curves were prepared using GraphPad PRISM version 6 for Windows (GraphPad Software®, San Diego, CA, USA).

$DPPH^{\bullet}$ radical assay

$DPPH^{\bullet}$ radical scavenging activity was performed as described by Teixeira *et al.*[29]. Briefly, solutions of the test compounds with increasing concentrations (ranging between 10 µM and 1 mM) were prepared in ethanol. A $DPPH^{\bullet}$ ethanolic solution (6.85 µM) was also prepared and then diluted to reach the absorbance of 0.72 ± 0.02 at 515 nm. After the addition of $DPPH^{\bullet}$ solution (180 µL) to the compound solution (20 µL) in triplicate, the absorbance at 515 nm was recorded every minute over 45 min. The percent inhibition of the radical was based on the comparison between the blank (20 µL of ethanol and 180 µL of $DPPH^{\bullet}$ solution), which corresponds to 100 % of the radical, and the test compound solutions. The dose–response curves allowed the determination of IC_{50} values.

$ABTS^{\bullet+}$ radical cation assay

$ABTS^{\bullet+}$ scavenging activity was evaluated as described by Teixeira *et al.*[29]. Briefly, ethanolic solutions of the test compounds with increasing concentrations (ranging between 50 µM and 500 µM) were prepared. $ABTS^{\bullet+}$ radical cation solution was obtained by the addition of aqueous solution of potassium persulfate (150 mM, 163 µL) to the aqueous solution of ABTS (7 mM, 10 mL) and the storage in the dark at room temperature for 16 h (2.45 mM final concentration). The solution was then diluted in ethanol to reach the absorbance of 0.72 ± 0.02 at 734 nm. After the addition of $ABTS^{\bullet+}$ solution (180 µL) to the compound solution (20 µL) in triplicate, the spectrophotometric measurement was carried out every minute over 15 min at 734 nm. The percent inhibition of the radical was based on the comparison between the blank (20 µL of ethanol and 180 µL of $ABTS^{\bullet+}$ solution), which corresponds to 100 % of radical, and the test compound solutions. The dose–response curves allowed the determination of IC_{50} values.

This journal is © The Royal Society of Chemistry 20xx

GO• radical assay

GO• radical scavenging protocol was adapted from the literature.[30-32] Solutions of test compounds with increasing concentrations (ranging between 5 µM to 1 mM) were prepared in ethanol. An ethanolic solution of GO• 5 mM was prepared and diluted to reach the absorbance of 1.00 ± 0.02 at 428 nm. After the addition in triplicate of compound solution (20 µL) to GO• solution (180 µL), the spectrophotometric measurement was performed at 428 nm over 30 min. The percent inhibition of radical was based on comparison between the blank (20 µL of ethanol and 180 µL of GO• solution), which corresponds to 100 % of response, and test compounds solutions. The dose-response curves allowed the determination of IC_{50} values.

Fluorometric methods (ORAC-FL assay)

The ORAC-FL analyses were performed on a multiplate reader (BioTek Synergy HT from BioTek Instruments, Winooski, VT, USA) using black polystyrene 96-well plates. Fluorescence was measured from the top, at an excitation wavelength of 485/20 nm and an emission at 528/20 nm. The plate reader was controlled by Gen5 software. 2,2'-Azobis-(amidinopropane) dihydrochloride (AAPH), (±)-6-hydroxy-2,5,7,8-tetramethylchromane-2-carboxylic acid (trolox) and fluorescein (FL) were purchased from Sigma-Aldrich. The general procedure was adapted from the literature [33, 34], with some modifications. The reaction was carried out in 75 mM of sodium phosphate buffer solution (pH = 7.4) at a final volume of 200 µL. Stock solutions of FL (5 mM) and antioxidants (5 mM) were prepared in ethanol due to their low solubility in buffer at high concentrations. Then, they were diluted in sodium phosphate buffer solution (pH = 7.4). The range of antioxidant concentrations was empirically selected to obtain a good separation between the fluorescence curves. The test compounds (final concentrations range of 0.1-2 µM) and fluorescein (40 nM, final concentration) were placed in each well and pre-incubated for 15 min at 37 ºC before the addition of AAPH (final concentration 18 mM). The microplate was immediately placed in the reader and automatically shaken prior to each reading. The fluorescence was measured minutely for 120 min. A control assay with fluorescein, AAPH and buffer (instead of the antioxidant solution) was performed for each assay. Trolox was also included in each assay as standard antioxidant in a final concentration range of 2-8 µM. All reaction mixtures were prepared in triplicate and at least three independent experiments were performed for each test compound. The fluorescence decay curves were normalized by the maximum value of fluorescence, and the areas under the curves (AUC) were determined according to the following **Equation 1**.

$$AUC = 1 + \sum_{i=1}^{i=120} \frac{f_i}{f_0} = 1 + \frac{f_1}{f_0} + \frac{f_2}{f_0} + \frac{f_3}{f_0} + \ldots + \frac{f_{120}}{f_0} \quad \textbf{(Equation 1)}$$

where f_0 = initial fluorescence reading at 0 min and f_i = fluorescence reading at time i. The net AUC is obtained by subtracting the AUC of the blank from that of a sample. The inhibition capacity, expressed as the relative Trolox equivalent ORAC values, was quantified employing the **Equation 2**.

$$\text{relative ORAC value} = \frac{AUC_{antioxidant} - AUC_{control}}{AUC_{trolox} - AUC_{control}} \times \frac{[Trolox]}{[antioxidant]} \quad \textbf{(Equation 2)}$$

where $AUC_{control}$ = area under the curve of control; $AUC_{antioxidant}$ = area under the curve of the test compound; AUC_{trolox} = area under the curve of Trolox (standard); [trolox] = Trolox concentration; and [antioxidant] = antioxidant concentration.

Electrochemical measurements

The voltammetric studies were carried out using an Autolab PGSTAT 12 potentiostat/galvanostat (Metrohm-Autolab, Netherlands) and one compartment glass electrochemical cell. The voltammetric data was acquired at room temperature using a three-electrode system: a glassy carbon working electrode (GCE) (d = 2 mm), a platinum wire counter electrode and an Ag/AgCl saturated KCl reference electrode (Metrohm, Switzerland). The working electrode was polished manually with an aqueous slurry of alumina powder (BDH Chemicals, VWR, USA) on a microcloth pad and rinsed with water before use. A Crison pH-meter with glass electrode was used for the pH measurements (Crison, Barcelona, Spain).

The voltammetric measurements were performed as described elsewhere.[11] The solutions for analysis were prepared directly in the electrochemical cell, by dilution of ethanolic solutions of the compounds under study (10 mM, 100 µL) in the supporting electrolyte (10 mL) to obtain a final concentration of 100 µM. The scan rates used in differential pulse voltammetry (DPV) and cyclic voltammetry (CV) were 5 $mV.s^{-1}$ and 50 $mV.s^{-1}$, respectively.

***In vitro* toxicology**

Materials.

All reagents used were of analytical grade or of the highest grade available. Neutral red (NR) solution, 3-(4,5-dimethylthiazol-2-yl)-2,5-diphenyltetrazolium (MTT) bromide, Dulbecco's Modified Eagle's Medium (DMEM) with 4,5 g/L glucose, retinoic acid and 12-O-tetradecanoylphorbol-13-acetate (TPA), tert-butyl hydroperoxide (t-BHP) and hydrogen peroxide (H2O2) were obtained from Sigma Aldrich. Reagents used in cell culture such as heat-inactivated fetal bovine serum (FBS), antibiotic (10,000 U/mL penicillin, 10,000 µg/mL streptomycin), MEM Non-Essential Amino Acids solution (100×) (MEM NEAA), Hanks' balanced salt solution without calcium and magnesium (HBSS(-/-)) and 0.25% trypsin/1 mM ethylenediamine tetraacetic acid (EDTA) were purchased from Gibco Laboratories (Lenexa, KS, USA). Dimethyl sulfoxide (DMSO), ethanol absolute and acetic acid were obtained from Merck (Darmstadt, Germany).

SH-SY5Y cell culture.

Human SH-SY5Y neuroblastoma cells were obtained from the American Type Culture Collection (ATCC, Manassas, VA,

USA). Cells were routinely cultured into 75 cm^3 flasks and maintained in DMEM with 4.5 g/L glucose, supplemented with 10 % heat-inactivated FBS (v/v), 1 % MEM NEAA (v/v) and 1 % penicillin/streptomycin (v/v). Cells were maintained at 37 °C in a humidified, 5 % CO2–95 % air atmosphere, and the cell culture medium was changed every 2-3 days. The cultures were passaged once a week by trypsinization (0.25 % trypsin/1 mM EDTA). To avoid phenotypic changes, the cells used for all experiments were used between 19th and 28th passages.

Cells were differentiated as described previously by Fernandes et al.[26]. Briefly, SH-SY5Y cells were seeded onto 96-well plates at a density of 25,000 cells/cm2 in cell culture medium with trans-retinoic acid (RA) (final concentration of 10 µM) and incubated for 3 days at 37 °C in a humidified, 5 % CO2–95 % air atmosphere. Then, the cell culture medium was removed and replaced with medium supplemented with 12-O-tetradecanoylphorbol-13-acetate (TPA) (final concentration 80 nM), and cells were incubated for an additional period of 3 days before being used in the assays. Stock solutions of RA (10 mM) and TPA (80 µM) were prepared in DMSO.

Cytotoxicity assays.

Stock solutions of the test compounds (100 mM) were freshly prepared in absolute ethanol. Final concentrations of the test compounds were obtained by diluting into cell culture medium immediately before use, giving a final maximum concentration of 0.2 % ethanol.

In cytotoxicity studies, differentiated SH-SY5Y cells were incubated with the test compounds (1.6 µM to 200 µM) for 24 h in a humidified, 5 % CO2–95 % air atmosphere. Controls were treated with culture media containing 0.2 % ethanol. Cell viability was estimated using the MTT reduction assay and the NR uptake assay.

Neuroprotection against oxidative stress.

In cytotoxicity studies, differentiated SH-SY5Y cells were incubated with the test compounds (50 µM) for 24 h in a humidified, 5 % CO2–95 % air atmosphere. Then, the cell culture medium was removed and replaced with medium containing H2O2 (1.5 mM) or t-BHP (100 µM), and cells were incubated for additional 24 h in a humidified, 5 % CO2–95 % air atmosphere. Cell viability was estimated using the MTT reduction assay.

Measurement of cell viability.

MTT reduction assay: In the MTT reduction assay, the water-soluble MTT tetrazolium salt is reduced inside viable cells with active metabolism. The resulting purple colored formazan product accumulates as an insoluble precipitate inside the cells. The amount of formazan formed, presumably directly proportional to the number of viable cells, can be quantified spectrophotometrically after solubilization in an organic solvent.[35, 36] Briefly, after the 24 h incubation periods with test compounds, the cell culture medium was removed and a solution of MTT 0.5 mg/mL in fresh cell culture medium was added. Cells were incubated at 37 °C in a humidified, 5 % CO_2–95 % air atmosphere for 1 h. Then, the cell culture medium was removed, and the formed formazan crystals were dissolved in 100 % DMSO. The absorbance was measured at 550 nm in a multiwell microplate reader (PowerWave XS from BioTek Instruments, Vermont, US). The percentage of MTT reduction relative to that of the control cells was used as the cytotoxicity measure [MTT reduction (% of control)].

NR uptake assay: The NR uptake assay is based on the ability of viable cells to incorporate the supravital dye neutral red and retain it inside the lysosomes.[37] Briefly, after the 24 h incubation periods with the test compounds, the cell culture medium was removed and a solution of NR 50 mg/mL in fresh cell culture medium was added. Cells were incubated at 37 °C in a humidified, 5 % CO2–95 % air atmosphere for 1 h. Then, the cell culture medium was removed and replaced by ethanol absolute/distilled water (1:1) with 5 % acetic acid to liberate the dye from the viable cells. The absorbance was measured at 540 nm in a multiwell microplate reader (PowerWave XS from BioTek Instruments, Vermont, USA). The percentage of NR uptake relative to that of the control cells was used as the cytotoxicity measure [NR uptake (% of control)].

Statistical analysis

The data obtained are expressed as mean ± standard error mean (SEM) of at least three independent experiments. All statistical analyses were performed using GraphPad PRISM version 6 for Windows (GraphPad Software®, San Diego, CA, USA). The normality of the data distribution was evaluated using three normality tests: KS normality test, D'Agostino and Pearson omnibus normality test, and Shapiro–Wilk normality test. In cytotoxicity studies, statistical comparisons between control and test groups were carried out by two-way analysis of variance (ANOVA) followed by Bonferroni's multiple-comparisons post hoc test. On the evaluation of the neuroprotection against oxidative stress, statistical comparisons of data with parametric distribution were carried out by one-way analysis of variance (ANOVA) followed by Dunnet's multiple comparison test. For data with a non-parametric distribution, statistical comparisons were estimated using the nonparametric method of Kruskal–Wallis [one-way ANOVA on ranks] followed by Dunn's post hoc test. In all cases, p values lower than 0.05 were considered significant.

Conflicts of interest

The authors declare that the research was conducted in the absence of any commercial or financial relationships that could be considered as a potential conflict of interest.

Acknowledgements

This project was supported by Foundation for Science and Technology (FCT) and FEDER/COMPETE research grants (UID/QUI/00081/2019, NORTE-01-0145-FEDER-000028, POCI-01-0145-FEDER-029164). D. Chavarria, C. Fernandes and T. Silva grants are supported by FCT, POPH and FEDER/COMPETE.

This journal is © The Royal Society of Chemistry 20xx

References

1. M. Srinivasan, A. R. Sudheer and V. P. Menon, *J. Clin. Biochem. Nutr.*, 2007, **40**, 92-100.
2. A. Bento-Silva, M. C. Vaz Patto and M. do Rosario Bronze, *Food Chem.*, 2018, **246**, 360-378.
3. P. Kylli, P. Nousiainen, P. Biely, J. Sipila, M. Tenkanen and M. Heinonen, *J. Agric. Food Chem.*, 2008, **56**, 4797-4805.
4. M. Leopoldini, N. Russo and M. Toscano, *Food Chem.*, 2011, **125**, 288-306.
5. A. T. Dinkova-Kostova and P. Talalay, *Mol. Nutr. Food Res.*, 2008, **52**, S128-S138.
6. S. Ghosh, S. Chowdhury, P. Sarkar and P. C. Sil, *Food Chem. Toxicol.*, 2018, **118**, 272-286.
7. A. Sgarbossa, D. Giacomazza and M. di Carlo, *Nutrients*, 2015, **7**, 5764-5782.
8. H. R. El-Seedi, A. M. El-Said, S. A. Khalifa, U. Goransson, L. Bohlin, A. K. Borg-Karlson and R. Verpoorte, *J. Agric. Food Chem.*, 2012, **60**, 10877-10895.
9. J. Kanski, M. Aksenova, A. Stoyanova and D. A. Butterfield, *J. Nutr. Biochem.*, 2002, **13**, 273-281.
10. S. Trombino, S. Serini, F. Di Nicuolo, L. Celleno, S. Ando, N. Picci, G. Calviello and P. Palozza, *J. Agric. Food Chem.*, 2004, **52**, 2411-2420.
11. J. Garrido, A. Gaspar, E. M. Garrido, R. Miri, M. Tavakkoli, S. Pourali, L. Saso, F. Borges and O. Firuzi, *Biochimie*, 2012, **94**, 961-967.
12. W. M. Wu, L. Lu, Y. Long, T. Wang, L. Liu, Q. Chen and R. Wang, *Food Chem.*, 2007, **105**, 107-115.
13. M. F. Andreasen, A. K. Landbo, L. P. Christensen, A. Hansen and A. S. Meyer, *J. Agric. Food Chem.*, 2001, **49**, 4090-4096.
14. J. C. Menezes, S. P. Kamat, J. A. Cavaleiro, A. Gaspar, J. Garrido and F. Borges, *Eur. J. Med. Chem.*, 2011, **46**, 773-777.
15. F. Borges, J. L. F. C. Lima, I. Pinto, S. Reis and C. Siquet, *Helv. Chim. Acta*, 2003, **86**, 3081-3087.
16. N. Güngör, M. Ozyürek, K. Güçlü, S. D. Cekiç and R. Apak, *Talanta*, 2011, **83**, 1650-1658.
17. C. K. Sen and L. Packer, *Am. J. Clin. Nutr.*, 2000, **72**, 653s-669s.
18. C. Garcia, C. Andraud and A. Collet, *Supramol. Chem.*, 1992, **1**, 31-45.
19. J. Xie and K. M. Schaich, *J. Agric. Food Chem.*, 2014, **62**, 4251-4260.
20. X. Tian and K. M. Schaich, *J. Agric. Food Chem.*, 2013, **61**, 5511-5519.
21. M. A. N. Manaia, V. C. Diculescu, E. D. S. Gil and A. M. Oliveira-Brett, *J. Electroanal. Chem.*, 2012, **682**, 83-89.
22. D. A. Armstrong, Q. Sun and R. H. Schuler, *J. Phys. Chem.*, 1996, **100**, 9892-9899.
23. M. Musialik, R. Kuzmicz, T. S. Pawlowski and G. Litwinienko, *J. Org. Chem.*, 2009, **74**, 2699-2709.
24. X. Y. Cao, J. Yang, F. Dai, D. J. Ding, Y. F. Kang, F. Wang, X. Z. Li, G. Y. Liu, S. S. Yu, X. L. Jin and B. Zhou, *Chemistry*, 2012, **18**, 5898-5905.
25. J. Kovalevich and D. Langford, *Methods Mol. Biol.*, 2013, **1078**, 9-21.
26. C. Fernandes, M. Pinto, C. Martins, M. J. Gomes, B. Sarmento, P. J. Oliveira, F. Remião and F. Borges, *Bioconjug. Chem.*, 2018, **29**, 1677-1689.
27. C. Fernandes, M. Pinto, C. Martins, M. J. Gomes, B. Sarmento, P. J. Oliveira, F. Remião and F. Borges, *Bioconj. Chem.*, 2018, **29**, 1677-1689.
28. Z. Nowakowska, *Phosphorus Sulfur*, 2006, **181**, 707-715.
29. J. Teixeira, T. Silva, S. Benfeito, A. Gaspar, E. M. Garrido, J. Garrido and F. Borges, *Eur. J. Med. Chem.*, 2013, **62**, 289-296.
30. A. Tai, T. Sawano and H. Ito, *Biosci. Biotechnol. Biochem.*, 2012, **76**, 314-318.
31. J. Y. Feng and Z. Q. Liu, *J. Agric. Food Chem.*, 2009, **57**, 11041-11046.
32. Y. Yang, Z. G. Song and Z. Q. Liu, *Free Radic. Res.*, 2011, **45**, 445-453.
33. B. Ou, M. Hampsch-Woodill and R. L. Prior, *J. Agric. Food Chem.*, 2001, **49**, 4619-4626.
34. F. Mura, T. Silva, C. Castro, F. Borges, M. C. Zuniga, J. Morales and C. Olea-Azar, *Free Radic. Res.*, 2014, **48**, 1473-1484.
35. L. Belyanskaya, P. Manser, P. Spohn, A. Bruinink and P. Wick, *Carbon*, 2007, **45**, 2643-2648.
36. J. C. Stockert, A. Blazquez-Castro, M. Canete, R. W. Horobin and A. Villanueva, *Acta Histochem.*, 2012, **114**, 785-796.
37. G. Repetto, A. del Peso and J. L. Zurita, *Nat. Protoc.*, 2008, **3**, 1125-1131.

Electronic Supplementary Information

Bioisosteric OH- to SH- replacement changes the antioxidant profile of ferulic acid

Daniel Chavarria,[a,b†] Carlos Fernandes,[a†] Tiago Silva,[a,b] Jorge Garrido,[c] Fernando Remião,[d] Paulo J. Oliveira[b] and Fernanda Borges[a*]

[a] CIQUP/Department of Chemistry and Biochemistry, Faculty of Sciences, University of Porto, 4169-007 Porto, Portugal

[b] CNC - Center for Neuroscience and Cell Biology, University of Coimbra, UC Biotech, Biocant Park, Cantanhede, Portugal.

[c] Department of Chemical Engineering, School of Engineering (ISEP), Polytechnic of Porto, 4200-072 Porto, Portugal

[d] UCIBIO-REQUIMTE, Laboratory of Toxicology, Department of Biological Sciences, Faculty of Pharmacy, University of Porto, Porto, Portugal

† These authors contributed equally to this work.

* Corresponding Author:
Fernanda Borges, CIQUP/Department of Chemistry and Biochemistry, Faculty of Sciences, University of Porto, Porto 4169-007, Portugal. E-mail: fborges@fc.up.pt

Additional figures

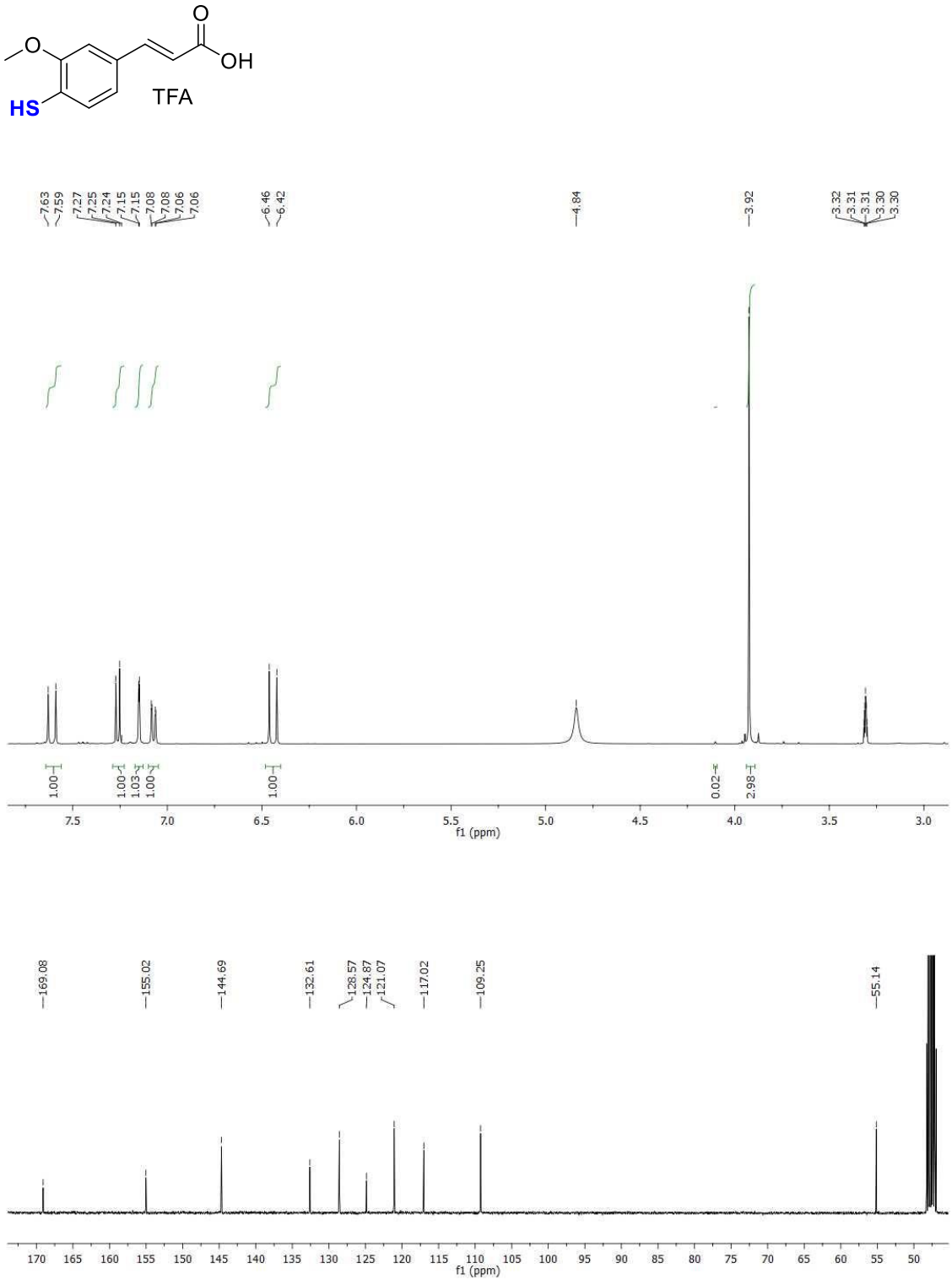


Figure S1. ^{1}H and ^{13}C NMR spectra of TFA (NMR spectra obtained in MeOD-d_4)

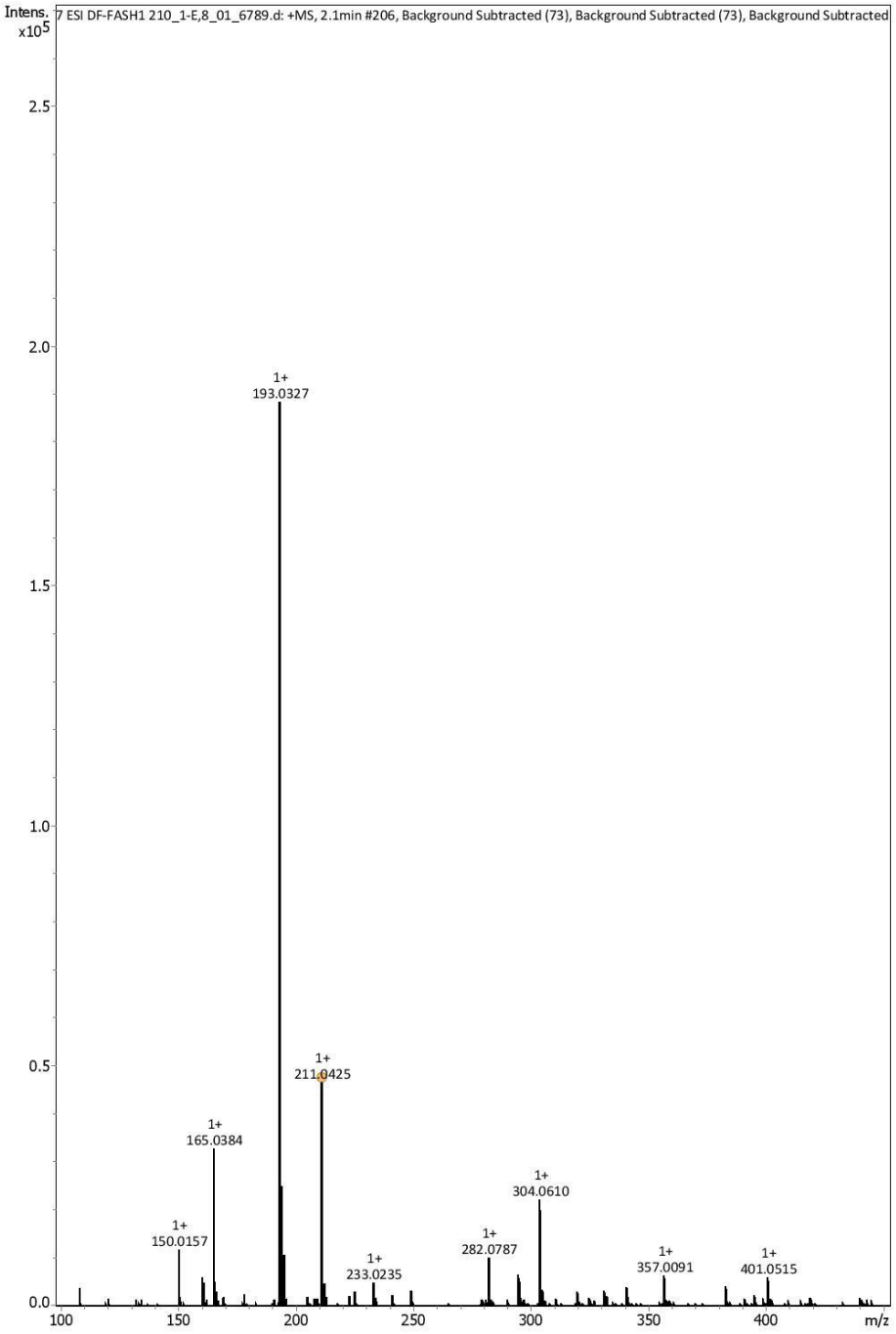


Figure S2. ESI-MS spectrum of TFA.

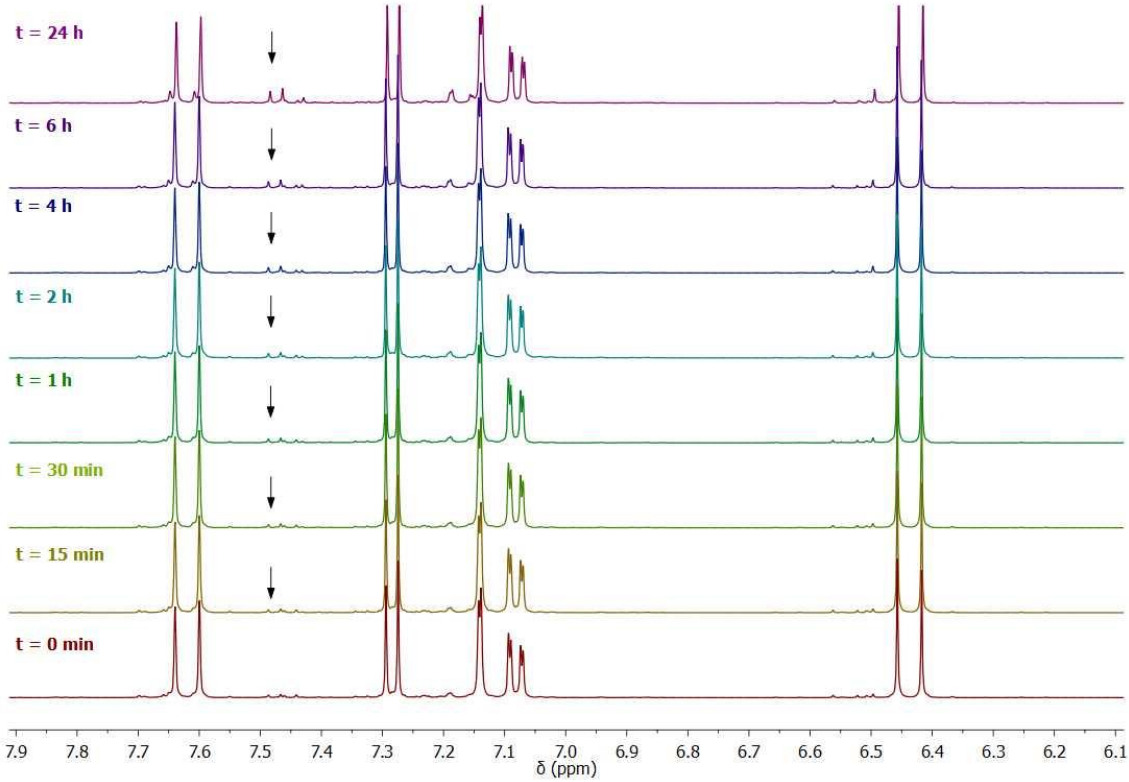


Figure S3: Expansion of the ^{1}H NMR spectra of TFA in ethanol-d_6 obtained at different timepoints (0 – 24 h).

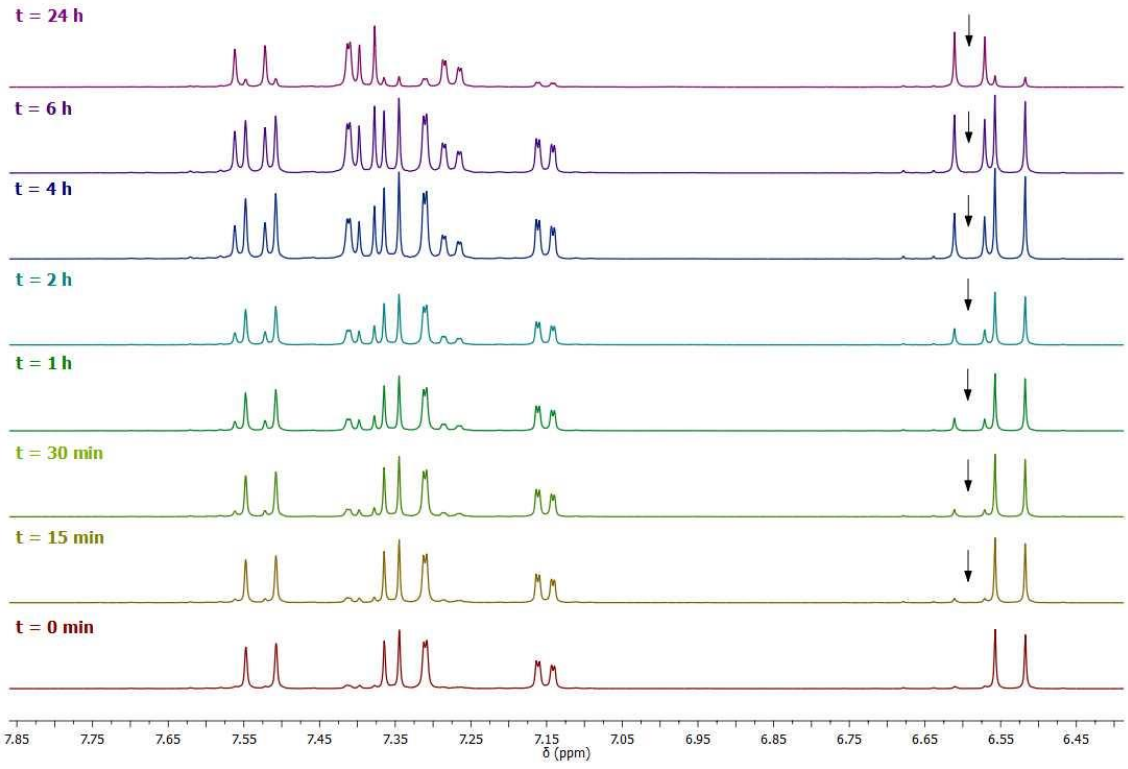


Figure S4. Expansion of the ^{1}H NMR spectra of TFA in DMSO-d_6 obtained at different timepoints (0 – 24 h).

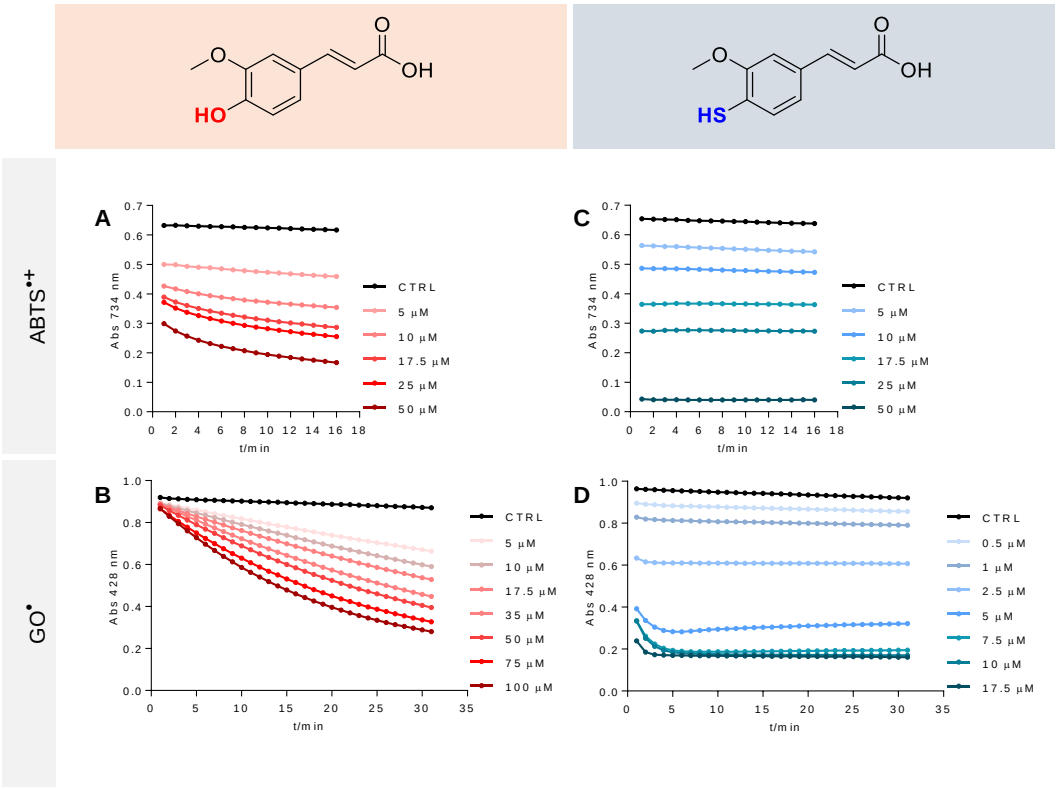


Figure S5: Kinetic curves obtained in the presence of increasing concentrations of FA (**A** and **B**) and TFA (**C** and **D**) in $ABTS^{\bullet+}$ and $GO^{\bullet}$ assays.

3.2. Manuscript III

Insights into the discovery of novel neuroprotective agents: a comparative study between sulfanylcinnamic acid derivatives and related phenolic analogues

Molecules, **2019**, 24(23): E4405.
DOI: 10.3390/molecules24234405

molecules

MDPI

Article

Insights into the discovery of novel neuroprotective agents: a comparative study between sulfanylcinnamic acid derivatives and related phenolic analogues

Daniel Chavarria [1,2,†], Carlos Fernandes [1,†], Brandon Aguiar [1], Tiago Silva [1,2], Jorge Garrido [3], Fernando Remião [4], Paulo J. Oliveira [2], Eugenio Uriarte[5] and Fernanda Borges [1,*]

[1] CIQUP/Department of Chemistry and Biochemistry, Faculty of Sciences, University of Porto, 4169-007 Porto, Portugal
[2] CNC - Center for Neuroscience and Cell Biology, University of Coimbra, UC Biotech, Biocant Park, Cantanhede, Portugal
[3] Department of Chemical Engineering, School of Engineering (ISEP), Polytechnic of Porto, 4200-072 Porto, Portugal
[4] UCIBIO-REQUIMTE, Laboratory of Toxicology, Department of Biological Sciences, Faculty of Pharmacy, University of Porto, Porto, Portugal
[5] Department of Organic Chemistry, Faculty of Pharmacy, University of Santiago de Compostela, 15782 Santiago de Compostela, Spain
† These authors contributed equally to this work
* Correspondence: Fernanda Borges, CIQUP/Department of Chemistry and Biochemistry, Faculty of Sciences, University of Porto, Porto 4169-007, Portugal. E-mail: fborges@fc.up.pt

Received: date; Accepted: date; Published: date

Abstract: Exogenous antioxidants may be beneficial therapeutic tools to tackle the oxidative damage in neurodegenerative diseases by regulation of the redox) state that is critical for cell viability and organ function. Inspired on natural plant polyphenols outline we developed cinnamic acid-based thiophenolic and phenolic compounds and studied their antioxidant and neuroprotective properties. In general, our results showed that the hydroxyl group (OH) to sulfhydryl group (SH) replacement increased the radical scavenging activity and enhanced the reaction rate with 1,1-diphenyl-2-picrylhydrazyl radical (DPPH$^{\bullet}$) and galvinoxyl radical (GO$^{\bullet}$) radicals. These results correlated well with the lower oxidation potential (E_P) values of thiophenols. However, for thiophenols a lower peroxyl radical (ROO$^{\bullet}$) scavenging activity was observed in oxygen radical absorbance capacity (ORAC-FL) assay. Furthermore, the introduction of 5-methoxy and 5-phenyl groups in the aromatic ring of TFA **2** and FA **1** did not significantly improve their antioxidant activity, despite the mild decreases of E_P observed for compounds **5**, **6** and **9**. For cinnamic acid amides the antioxidant profile was the same as their parent compounds. None of the compounds under study presented significant cytotoxic effects in human differentiated neuroblastoma cells. Thiophenolic amide **3** stands out as the most promising thiophenol-based antioxidant, showing cellular neuroprotective effects against oxidative-stress inducers (hydrogen peroxide and iron).

Keywords: cinnamic acid, 4-thioferulic acid derivatives, ferulic acid derivatives, antioxidant activity; Cytotoxicity; neuroprotection

1. Introduction

Oxidative stress is currently defined as the deregulation of the balance between the oxidants and antioxidants in favor of the former, with consequent disruption of the redox signaling and/or

molecular damage [1]. The harmful effects on human cells associated with the oxidative damage inflicted by reactive species (RS) may ultimately lead to programmed cell death [2]. Several lines of evidence implicate oxidative stress on the neurodegeneration process observed in Alzheimer's disease (AD) and Parkinson's disease (PD) patients [3]. Actually, markers of lipid peroxidation and protein oxidation were detected in individuals with AD and PD [4-8]. Both disorders were also associated with a decline on the pool of antioxidants and a decrease on the activity of antioxidant enzymes were reported [9-12].

Given the role of oxidative stress on the pathogenesis of neurodegenerative diseases, the use of exogenous antioxidants to assist the antioxidant defense system in upstream (prevention) or downstream (minimization) of the levels of reactive species (RS) may help to maintain neuronal integrity and delay the neurodegenerative processes [13,14].

Ferulic acid (3-(4-hydroxy-3-methoxyphenyl)-2-propenoic acid, FA, compound **1**, **Figure 1**) is a hydroxycinnamic acid (HCA) natural antioxidant able to act directly by scavenging hazardous oxidants, or indirectly by downregulation of pathways involved in cell-death and upregulation of the expression of antioxidant enzymes [15]. Neuroprotective properties in both *in vitro* and *in vivo* models, commonly assigned to its antioxidant and anti-inflammatory activity, have been ascribed to FA [16-18]. However, the therapeutic use of FA is hampered by its poor bioavailability, as a consequence of its low absorption and rapid metabolism and excretion [19,20].

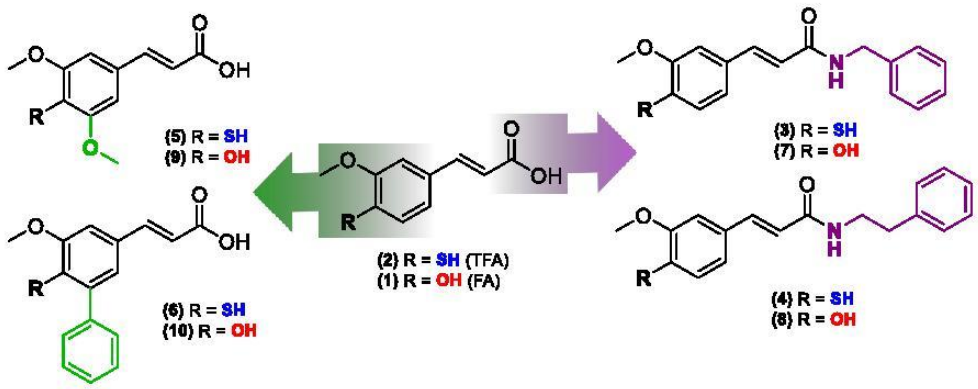


Figure 1. Rational design of new chemical entities based on FA (compound **1**) and TFA (compound **2**) scaffolds.

Ferulic acid has been used as a scaffold for the design and development of novel antioxidants with potential therapeutic interest [21-23]. Within this framework a new antioxidant 4-thioferulic acid (TFA, compound **2**, **Figure 1**), obtained by the isosteric replacement of the hydroxyl group (OH) by a sulfhydryl group (SH) in FA, was reported by our group [24].

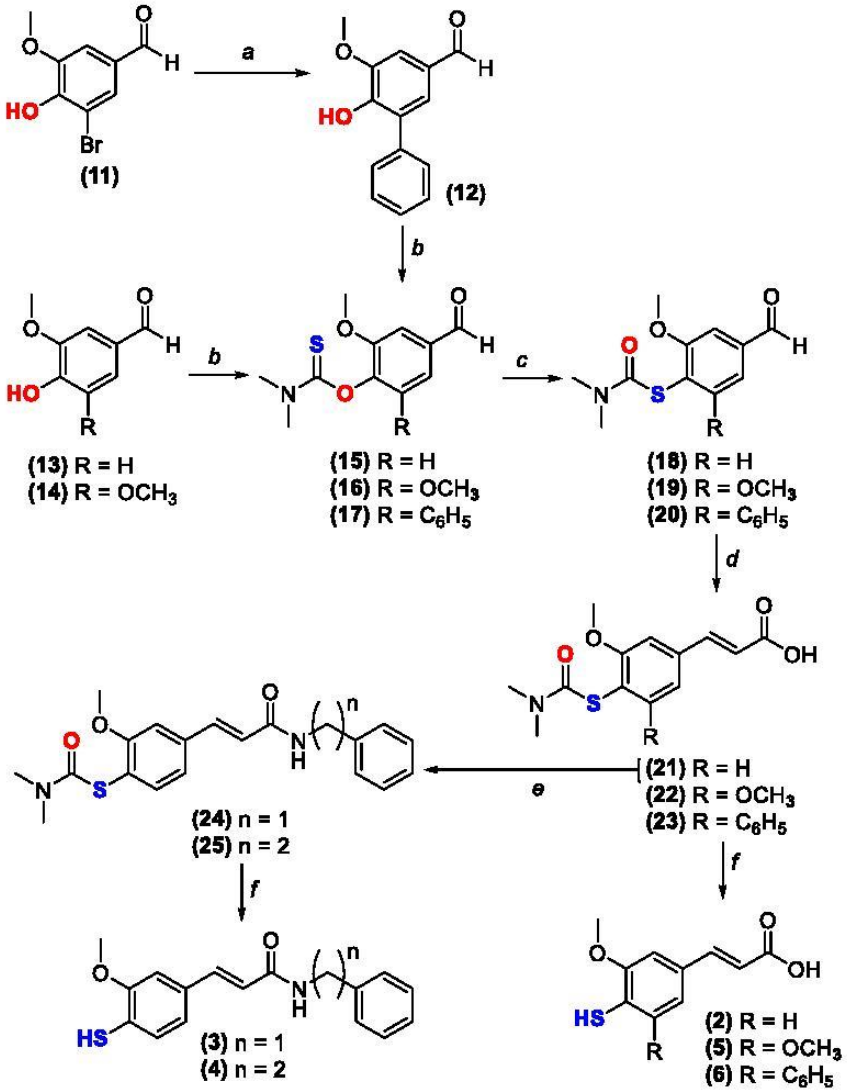
To gain insight on the advantages of thiophenol systems, herein we report the synthesis and the biological screening of novel TFA derivatives (compounds **3-6**, **Figure 1**). The corresponding hydroxycinnamic acid derivatives (compounds **7-10**, **Figure 1**) were synthesized to directly compare the effect of the OH to SH replacement. Following the studies of the antioxidant activity, we assessed the cytotoxicity of the new molecules in differentiated SH-SY5Y cells and their protective properties against oxidative stress insults (H_2O_2, iron) in the same cellular model.

2. Results and Discussion

2.1. Chemistry

The synthesis of TFA (compound **2**) [24] and derivatives thereof (compounds **3-6**) was performed following the strategy depicted in **Scheme 1**. First, the reaction between 5-bromovanillin (compound **11**) and phenylboronic acid in the presence of $Pd(OAc)_2$ and K_2CO_3 under microwave (MW) irradiation yielded 5-phenylvanillin (compound **12**) (**Scheme 1**, step *a*). Then, the

thiocarbamoylation of 4-hydroxybenzaldehyde derivatives **12-14** with dimethylthiocarbamoyl chloride (DMTCl) under alkaline conditions afforded compounds **15-17** (**Scheme 1**, step *b*). A MW-assisted Newman-Kwart rearrangement under inert atmosphere of compounds **15-17** yield compounds **18-20** (**Scheme 1**, step *c*). Cinnamic acid derivatives **21-23** were obtained via Knoevenagel-Doebner condensation between aldehydes **18-20** and malonic acid (**Scheme 1**, step *d*). The PyBOP-mediated amidation of compound **21** with benzylamine or phenethylamine led to the obtainment of the amides **24** and **25**, respectively (**Scheme 1**, step *e*). Finally, the alkaline hydrolysis of compounds **21-25** afforded the thiophenol derivatives **2-6** (**Scheme 1**, step *f*).



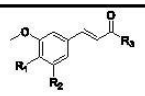
Scheme 1. Synthetic strategy used for the preparation of compounds **2-6**. (a) phenylboronic acid, K_2CO_3, $Pd(OAc)_2$, TBAB, DMF, 150 °C (microwave (MW) irradiation), 15 min; (b) DMTCl, DABCO, DMF, 70 °C, 3 h; (c) diphenyl ether, argon, 240 °C (MW irradiation), 20 min; (d) malonic acid, anhydrous pyridine, piperidine, 70 °C, 4-5 h; (e) 1. DMF, DIPEA, PyBOP, CH_2Cl_2, 0 °C, 30 min; 2. benzylamine or 2-phenylethylamine, rt, overnight; (f) MeOH, aqueous solution of NaOH 2 M, reflux, 1.5-16 h.

The corresponding hydroxycinnamic acid derivatives (compounds **7-10**, **Figure 1**) were synthesized according the procedures previously reported [21,25].

2.2. Evaluation of antioxidant activity

Following the synthesis of TFA and FA derivatives (compounds **1-10**), we evaluated their radical scavenging activity against three synthetic radicals: 1,1-diphenyl-2-picrylhydrazyl radical (DPPH$^{\bullet}$), 2,2′-azinobis-(3-ethylbenzothiazoline-6-sulfonic acid) radical cation (ABTS$^{\bullet+}$) and galvinoxyl (GO$^{\bullet}$). In these assays, after the generation of the synthetic colored radical, the radical scavenging activity is evaluated by spectrophotometry [26]. Trolox was used as a standard antioxidant. The results are presented as mean IC_{50} ± SD (n = 3) values (**Table 1**).

Table 1. Radical scavenging activities (DPPH$^{\bullet}$, ABTS$^{\bullet+}$, GO$^{\bullet}$ and ORAC-FL assays) and redox potentials (E_p) of thiophenols **2-6** and phenols **1**, **7-10**. The results obtained in DPPH$^{\bullet}$, ABTS$^{\bullet+}$, GO$^{\bullet}$ assays are expressed as mean IC_{50} ± standard deviation (n = 3).

Compound				IC_{50}/μM			ORAC-FL index	E_p/mV
	R_1	R_2	R_3	DPPH$^{\bullet}$	ABTS$^{\bullet+}$	GO$^{\bullet}$		
2 (TFA)	SH	H	OH	47.8±0.9[a]	19.9±1.0[a]	4.25±0.10[a]	0.34±0.04[a]	271
3	SH	H		49.8±0.7	20.6±0.7	4.50±0.08	0.12±0.02	198
4	SH	H		47.3±0.7	19.9±0.3	4.41±0.15	0.15±0.01	186
5	SH	O	OH	42.7±2.1	22.9±0.6	6.70±0.07	0.30±0.03	218
6	SH		OH	50.7±1.6	27.0±1.8	6.66±0.13	0.34±0.01	245
1(FA)	OH	H	OH	64.6±1.9[a]	16.8±0.4[a]	37.5±2.5[a]	3.2±0.1[a]	344[b]
7	OH	H		61.7±0.8	25.6±1.8	76.4±3.6	4.0±0.4	327
8	OH	H		61.2±0.7	26.0±1.7	70.7±2.5	3.7±0.3	338
9	OH	O	OH	43.9±1.6	16.6±0.3	3.90±0.1	3.2±0.3	291
10	OH		OH	69.7±3.8	19.8±0.8	31.2±3.9	2.7±0.1	351
Trolox	----	----	----	24.6±0.9	18.2±0.5	2.98±0.15	----	----

[a] Data from Chavarria *et al.* [24].

[b] Data from Garrido *et al.* [23].

In general, thiophenols **2-6** showed a higher scavenging of DPPH$^{\bullet}$ and GO$^{\bullet}$ radicals than phenols **1, 7-10**, while the scavenging of ABTS$^{\bullet+}$ radical was similar. The introduction of an additional 5-methoxy group (compound **5**) is not very productive as the TFA (compound **2**) antioxidant activity is only slightly changed (only noteworthy effects were observed on DPPH$^{\bullet}$ assay). Conversely, the presence of an additional aromatic ring (compound **6**) reduce TFA antioxidant activity. Although, an additional aromatic ring can increase the electron delocalization and stabilizes by resonance the generated thiophenoxyl radical, it may reduce the accessibility of the compound to the center of the radicals and thereby decrease the radical scavenging activity [27]. The same tendency was observed with the phenolic analogues (compounds **9** and **10**)

Considering that both 5-methoxy and 5-phenyl groups did not significantly increase the radical scavenging activity of TFA, we then evaluated the effect of the introduction of substituents on TFA carboxylic function. As shown in **Table 1**, benzyl and phenethyl amides of TFA (compound **3** and **4**, respectively) displayed similar IC_{50} values to the free carboxylic acid and thus the radical scavenging activity was maintained. The same tendency was observed for the phenolic analogues (compounds **7**

and **8**). Therefore, the carboxylic acid amidation with lipophilic substituents maintain TFA antioxidant activity.

The kinetic curves obtained in DPPH$^{\bullet}$, ABTS$^{\bullet+}$ and GO$^{\bullet}$ assays can provide information concerning the reactivity of the compounds under study (**Figures S1-S3**). As previously reported for TFA [24], thiophenols **3-6** reacted almost instantaneously with the radicals, leading to fast absorbance decays and reaching the steady state within the first minutes of reaction (**Figures S1A-E, S2A-E** and **S3A-E**). These results pointed out that the reaction rate was increased by the OH to SH replacement. Compared to TFA, the reactions of compounds **5** and **6** with the radicals occurred slower, requiring more time to reach the steady state (**Figures S1D** and **S1E**; **Figures S2D and S2E**; **Figures S3D and S3E**). Therefore, the presence of 5-methoxy and 5-phenyl groups in thiophenols delayed the reaction progress, possibly due to increased steric hindrance. On the other hand, compounds **3** and **4** displayed the same kinetic profile of TFA (**Figures S1B and S1C**; **Figures S2B and S2C**; **Figures S3B and S2C**), indicating that the reactivity of TFA was preserved with the functionalization of the carboxylic acid group with lipophilic groups. Like ferulic acid **1** [24], phenols **7-10** displayed hyperbolic kinetic curves indicating moderate reactivity towards DPPH$^{\bullet}$, ABTS$^{\bullet+}$ and GO$^{\bullet}$ (**Figures S1F-J, S2F-J** and **S3F-J**).

In addition, we also studied the antioxidant activity towards peroxyl radicals (ROO$^{\bullet}$) using the oxygen radical absorbance capacity (ORAC-FL) assay. In this assay, ROO$^{\bullet}$ radicals are scavenged by hydrogen atom transfer (HAT) or by radical addition processes [27]. Phenols (compounds **1**, **7-10**) showed ORAC-FL indexes ranging between 2.7-4.0 (**Table 1**) and displayed higher ORAC-FL indexes than thiophenols (compounds **2-6**). Thiophenols presented ORAC-FL indexes below 1 (**Table 1**). Therefore, contrary to what was observed in DPPH$^{\bullet}$, ABTS$^{\bullet+}$ and GO$^{\bullet}$assays, these results show that phenols are better ROO$^{\bullet}$ radical scavengers than thiophenols. The dissimilarities between the two sets of compounds may result from the differences on the acidity of the phenol and the thiophenol moieties. Since the thiophenol group of TFA **1** is significantly more acidic than the phenol group of FA ($pK_{a\ thiophenol}$ = 5.6; $pK_{a\ phenol}$ = 9.1) [24], there is a high amount of thiophenolate anions at pH 7.3 while the phenol group remains undissociated. Therefore, in opposition to phenols **1** and **7-10**, the deprotonated thiophenols **2-6** were unable to scavenge the ROO$^{\bullet}$ radicals.

2.3. Electrochemical studies

Voltammetric measurements are particularly useful to estimate the redox properties bioactive systems, thus enabling a prompt screening of its antioxidant capacity [28]. In this context, to obtain complementary information concerning the antioxidant activity of the compounds under study, differential pulse voltammetry (DPV) experiments were performed to study the electrochemical properties of compounds **2-6** and **7-10**. Experiments were carried out at physiological pH 7.4 using a glassy carbon-working electrode. The oxidation potential (E_P) values obtained are depicted in **Table 1**.

All compounds showed well-defined anodic waves at physiological pH, which may be attributed to the oxidation of the thiophenol or the phenol groups. Thiols and phenols can undergo one-electron oxidation processes with the formation of thiyl and phenoxyl radicals, respectively [29,30]. The E_P values of thiol-containing compounds **2-6** ranged between +186 mV and +271 mV, while phenols **1** and **7-10** displayed higher E_P values, ranging between +291 mV and +351 mV (**Table 1**). The results obtained showed that the replacement of the OH by an SH group shifted the peak potentials towards less positive values, suggesting that thiophenols are more prone to oxidation than phenols.

The introduction of a 5-methoxy (compounds **5** and **9**) or a 5-phenyl (compounds **6** and **10**) group did not significantly change the E_P values when compared to FA and TFA, although mild decreases were observed for compounds **5**, **6** and **9**. The lower potential values may result from the increased stabilization of the thiophenoxyl/phenoxyl radicals, which is associated with the electron-donating properties of the methoxy group [31] (compounds **5** and **9**) or the increased electron delocalization provided by the additional aromatic ring (compound **6**).

The voltammetric behavior of the cinnamic acid amides **3**, **4**, **7** and **8** was similar to that observed for the parent compounds (TFA and FA). The introduction of lipophilic groups at the side chain does not exert much influence in the redox active site of the molecules and therefore, as expected, no major changes in the redox potentials were observed.

2.4. Cellular studies

2.4.1. Evaluation of cytotoxicity profile

The cytotoxicity profile of thiophenols **3-6** and phenols **7-10** was assessed in human neuroblastoma SH-SY5Y cells differentiated into a dopaminergic phenotype [32]. After 24 h of exposure with the compounds at three different concentrations (1, 10 and 50 μM), the cell viability was evaluated using two approaches: the 3-(4,5-dimethylthiazol-2-yl)-2,5-diphenyltetrazolium (MTT) reduction assay, a method that relies on the reduction of MTT into the respective formazan by cells with active metabolism [33], and the neutral red (NR) uptake assay, which is based on the lysosomal uptake of the dye NR [34]. The results, expressed as mean MTT reduction (% of control) ± SEM and NR uptake (% of control) ± SEM (n = 3), are depicted in **Figure 3**.

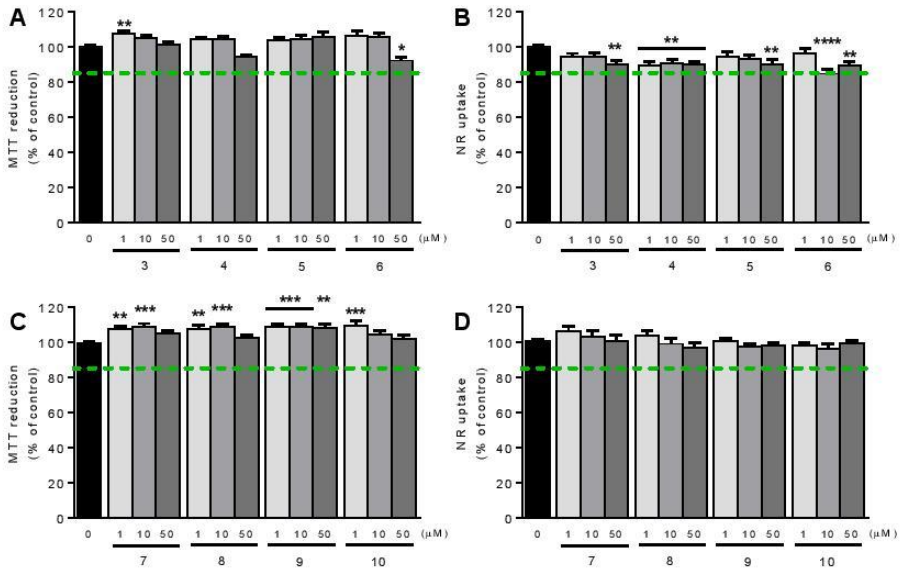


Figure 3. Cellular viability of differentiated SH-SY5Y cells after a 24 h treatment with thiophenols **3-6** and phenols **7-10** at three different concentrations (1, 10 and 50 μM). Cellular viability was evaluated using two methods: MTT reduction (**A**, **C**) and NR uptake (**B**, **D**) assays. Results are expressed as the mean % of untreated controls ± SEM (n = 3). Statistical comparisons were performed using the parametric method of one-way ANOVA, followed by the Dunnett's multiple comparisons test. In all cases, p values lower than 0.05 were considered significant (* $p < 0.05$, ** $p < 0.01$, *** $p < 0.001$, **** $p < 0.0001$ vs untreated cells).

Thiophenols **3-6** (**Figures 3A** and **3B**) and phenols **7-10** (**Figures 3C** and **3D**) did not cause marked decreases in MTT reduction and in NR uptake at concentrations up to 50 μM (MTT reduction and NR uptake were > 85 %), which is in accordance with the previous data obtained for FA **1** and TFA **2** [24]. Based on these results, we can conclude that the cytotoxicity profile within the tested concentration range was upheld with the OH to SH replacement, the introduction of 5-methoxy and

5-phenyl substituents, and the functionalization of the carboxylic acid group (benzyl or phenethyl amides).

2.4.2. Protection against H_2O_2- and ferric iron-oxidative damage

The protective properties of compounds **1-10** against oxidative stress in the same cell model were also examinated. Hydrogen peroxide (H_2O_2) and ferric nitrilotriacetate (FeNTA) were used as inducers of oxidative stress [32]. After the pre-treatment with the test compounds at 10 and 50 μM for 24 h, differentiated SH-SY5Y cells were exposed to H_2O_2 (1.5 mM) or FeNTA (4 mM) for 30 min and 24 h, respectively. The cellular viability was assessed using the MTT reduction assay. The results obtained are illustrated in **Figures 4** and **5**.

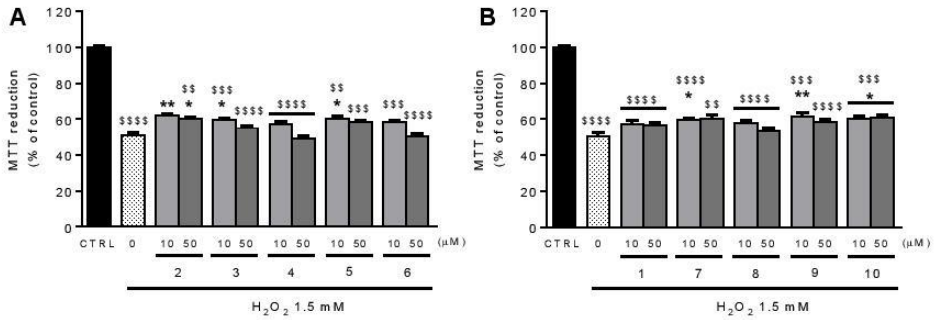


Figure 4. Protection against H_2O_2-induced damage in differentiated SH-SY5Y cells by thiophenols **2-6** and phenols **1**, **7-10**. After a pre-treatment with the compounds under study (10 and 50 μM) for 24 h, cells were exposed H_2O_2 1.5 mM for additional 30 min. Cellular viability was evaluated by the MTT reduction assay. Results are expressed as the mean % of untreated controls ± SEM (n = 3). Statistical comparisons were estimated using the nonparametric method of Kruskal–Wallis (one-way ANOVA on ranks), followed by Dunn's *post hoc* test (* $p < 0.05$, ** $p < 0.01$, ***, compared with cells treated only with H_2O_2; $^{\$\$}$ $p < 0.01$, $^{\$\$\$}$ $p < 0.001$; $^{\$\$\$\$}$ $p < 0.0001$ compared with CTRL).

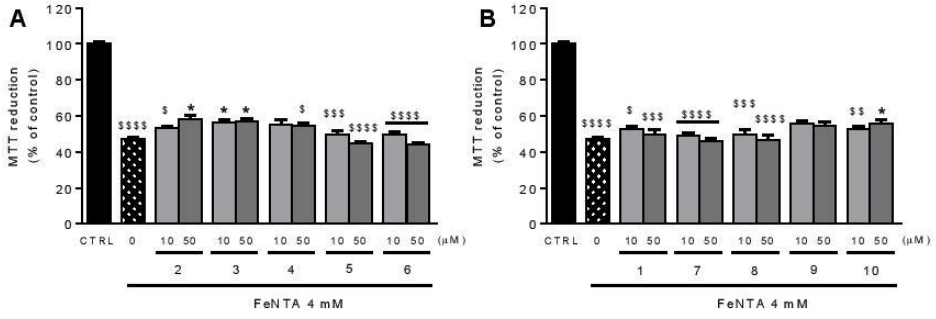


Figure 5. Protection against FeNTA-induced damage in differentiated SH-SY5Y cells by thiophenols **2-6** and phenols **1**, **7-10**. After a pre-treatment with the compounds under study (10 and 50 μM) for 24 h, cells were exposed FeNTA 4 mM for additional 24 h. Cellular viability was evaluated by the MTT reduction assay. Results are expressed as the mean % of untreated controls ± SEM (n = 3). Statistical comparisons were estimated using the nonparametric method of Kruskal–Wallis (one-way

ANOVA on ranks), followed by Dunn's post hoc test (* $p < 0.05$ compared with cells treated only with FeNTA; $^{\$}$ $p < 0.05$, $^{\$\$}$ $p < 0.01$, $^{\$\$\$}$ $p < 0.001$; $^{\$\$\$\$}$ $p < 0.0001$ compared with CTRL).

The incubation of differentiated SH-SY5Y cells with H_2O_2 (1.5 mM) decreased the MTT reduction to 50.7±1.9 % ($p < 0.0001$) in comparison to control cells (**Figure 4A** and **4B**). The damage inflicted by H_2O_2 was attenuated by thiophenols and phenols containing benzyl amide (compounds **3** and **7**, $p < 0.05$) and 5-methoxy groups (compound **5**, $p < 0.05$, and compound **9**, $p < 0.01$) at 10 μM (**Figure 4A** and **4B**). A mild protection against H_2O_2-induced cell death was also observed with pre-treatment of neuroblastoma cells with TFA (10 μM, $p < 0.01$; 50 μM, $p < 0.05$, **Figure 4A**) and compound **10** ($p < 0.05$, **Figure 4B**) at both tested concentrations. The data obtained for TFA **2** and FA **1** at 50 μM was previously reported by Chavarria et al. [24].

Transition metals like iron accumulate with age in specific brain areas, such as the *substantia nigra* and the hippocampus [35]. FeNTA was used to mimic iron overload conditions in SH-SY5Y cells. Treatment with FeNTA 4 mM decreased the MTT reduction to 47.2±1.2 % ($p < 0.0001$) in comparison to control cells (**Figure 5A and 5B**). Remarkably, TFA derivative **3** significantly protected neuroblastoma cells from the deleterious effects of FeNTA at both tested concentrations ($p < 0.05$, **Figure 5A**). The FeNTA-induced decrease in MTT reduction was also attenuated in neuroblastoma cells pre-treated with TFA **2** ($p < 0.05$, **Figure 5A**) and compound **10** ($p < 0.05$, **Figure 5B**) at 50 μM.

Taking these data together, we concluded that TFA **2**, TFA benzyl amide **3** and compound **10** significantly protected neuroblastoma cells against oxidative stress, both by the direct action of H_2O_2 and by high concentrations of iron. In addition, 5-methoxy derivatives (compounds **5** and **9**) and FA benzyl amide (compound **7**) were able to prevent the damage induced by H_2O_2, but were ineffective against the harmful effects caused by high concentrations of iron.

2.5. Estimation of drug-like properties

In early drug discovery, the balancing of key physicochemical properties within optimal ranges may improve the compounds' quality and thereby increase the likelihood of therapeutic success [36]. In this context, we calculated several physicochemical parameters of selected compounds TFA (compound **2**) and compounds **3** and **10** to predict their "drug-likeness". These compounds were considered the most promising cinnamic acid derivatives because they displayed significant neuroprotective activity against two oxidative stressors in neuroblastoma cells. The predicted physicochemical properties included topological polar surface area (TPSA in Å), number of hydrogen acceptors (HBA), number of hydrogen donors (HBD), number of rotatable bonds (RB) and logarithm of the ratio of the concentration of a drug in the brain and in the blood (logBB). The results obtained are presented in **Table 2**.

Table 2. Predicted physicochemical properties of TFA (compound **2**) and compounds **3** and **10**.

Compound	MW[a]	cLogP[b]	TPSA[a]	HBA[a]	HBD[a]	RB	LogBB
2	210.25	1.97	46.53	4	2	3	-0.9373
3	299.39	3.25	38.33	4	2	6	0.02948
10	270.28	2.76	66.76	4	2	4	-1.511
CNS^{+} drugs	< 500[37]	2 – 5[37]	< 90[37]	< 7[38]	< 3[38]	< 8[38]	<-1

[a] Properties predicted using the Stardrop software. MW: molecular weight; TPSA: topological polar surface area; HBA: number of H-bond acceptor atoms; HBD: number of H-bond donor atoms; RB: number of rotatable bonds; logBB: logarithm of the ratio of the concentration of a drug in the brain and in the blood.

[b] Properties predicted using the SwissADME (http://swissadme.ch/index.php); clogP: logarithm of the octanol/water partition coefficient.

The values obtained for compound **3** are within the optimal ranges of drugs able to act in the central nervous system (CNS). On the other hand, TFA and compound **10** presented cLogP and LogBB values below or close to the recommended limits. Therefore, TFA **2** and compound **10** are less likely to cross the blood-brain barrier by passive diffusion and thereby attain the CNS. The presence

of a free carboxylic acid may restrict the access to the brain, as observed previously for similar systems [21].

Overall, these results suggest that TFA benzyl amide (compound **3**) presents the most favourable drug-like properties among the selected candidates.

3. Materials and Methods

3.1. Chemistry

3.1.1. Synthesis

3.1.1.1. Synthesis of 6-Hydroxy-5-methoxy-[1,1'-biphenyl]-3-carbaldehyde (**12**). Synthesis and structural characterization are described in literature [21].

3.1.1.2. Thiocarbamoylation of phenols.

In a bottom flask with the phenol (1 mmol) dissolved in DMF, DABCO (4 mmol) and DMTCl (2 mmol) were added. The mixture was heated at 70 ºC for 3 h. Upon completion, the mixture was poured onto water (15 mL) cooled on an ice bath and acidified with HCl 6 M. The product was collected by filtration under reduced pressure and washed with water. The general procedure was adapted from Nowakowska *et al.* [39].

O-(4-Formyl-2-methoxyphenyl) dimethylcarbamothioate (**15**). Synthesis and structural analysis are described in literature [24,39].

O-(4-Formyl-2,6-dimethoxyphenyl) dimethylcarbamothioate (**16**). The reaction mixture was poured onto water (15 mL) cooled on an ice bath and acidified with HCl 6 M. The product was collected by filtration under reduced pressure and washed with water. η = 93 %. ^{1}H NMR ($CDCl_3$-*d*$_1$): δ (ppm) = 3.40 (*s*, 3H, NCH_3), 3.49 (*s*, 3H, NCH_3), 3.93 (*s*, 6H, 2×OCH_3), 7.19 (*s*, 2H, H2, H6), 9.94 (*s*, 1H, CHO). ^{13}C NMR ($CDCl_3$-*d*$_1$): δ (ppm) = 38.9 (NCH_3), 43.5 (NCH_3), 56.5 (2×OCH_3), 106.3 (C2, C6), 134.2 (C1), 136.9 (C4), 153.4 (C3, C5), 186.7 (CSO), 191.1 (CHO). EI/MS m/z (%): 269.0 ($M^{\bullet+}$, 69), 88.0 (99), 72.0 (100).

O-(5-Formyl-3-methoxy-[1,1'-biphenyl]-2-yl) dimethylcarbamothioate (**17**). The reaction mixture was poured onto water (15 mL) cooled on an ice bath and acidified with HCl 6 M. The product was collected by filtration under reduced pressure and washed with water. η = 75 %. ^{1}H NMR ($CDCl_3$-d$_1$): δ (ppm) = 3.17 (*s*, 3H, NCH_3), 3.34 (*s*, 3H, NCH_3), 3.94 (*s*, 3H, OCH_3), 7.39 (*m*, 3H, H3′, H4′, H5′), 7.52 (*m*, 4H, H2, H6, H2′, H6′), 9.98 (*s*, 1H, CHO). ^{13}C NMR ($CDCl_3$-*d*$_1$): δ (ppm) = 38.7 (NCH_3), 43.3 (NCH_3), 56.4 (OCH_3), 109.7 (C2), 126.6 (C6), 128.0 (C4′), 128.2 (C2′, C6′), 129.1 (C3′, C5′), 134.5 (C5), 136.4 (C1), 137.2 (C1′), 145.0 (C4), 153.1 (C3), 186.4 (CSO), 191.2 (CHO). EI/MS m/z (%): 315.1 ($M^{\bullet+}$, 38), 243.0 (29), 88.0 (100), 72.0 (89).

3.1.1.3. Microwave-assisted Newman-Kwart rearrangement.

O-phenyl-*N,N*-dimethylthiocarbamates **15-17** were placed onto a 5 mL microwave glass vial. The vial was sealed with a septum and the content was maintained under argon atmosphere for 30 min at room temperature. After the addition of diphenyl ether, the vial was placed into the microwave cavity. The reaction took place under microwave irradiation at 240 ºC for 20 min.

S-(4-Formyl-2-methoxyphenyl) dimethylcarbamothioate (**18**). Synthesis and structural analysis are described in literature [24].

S-(4-Formyl-2,6-dimethoxyphenyl) dimethylcarbamothioate (**19**). Compound **19** was isolated by flash column chromatography (ethyl acetate/dichloromethane (3:7)) and recrystallized in dichloromethane/petroleum ether. η = 91 %. ^{1}H NMR ($CDCl_3$-*d1*): δ (ppm) = 3.00 (*bs*, 3H, NCH_3), 3.18 (*bs*, 3H, NCH_3), 3.94 (*s*, 6H, 2×OCH_3), 7.16 (*s*, 2H, H2, H6), 9.97 (*s*, 1H, CHO). ^{13}C NMR ($CDCl_3$-*d1*): δ (ppm) = 37.1 (2×NCH_3), 56.7 (2×OCH_3), 105.0 (C2, C6), 112.7 (C4), 138.7 (C1), 161.8 (C3, C5), 164.5 (COS), 191.5 (CHO). EI/MS m/z (%): 269.0 ($M^{\bullet+}$, 48), 72.1 (100).

S-(5-Formyl-3-methoxy-[1,1'-biphenyl]-2-yl) dimethylcarbamothioate (**20**). Compound **20** was isolated by flash column chromatography (ethyl acetate/dichloromethane (3:7)) and recrystallized in dichloromethane/petroleum ether. η = 83 %. ^{1}H NMR (DMSO-*d6*): δ (ppm) = 2.96 (*bs*, 6H, 2×NCH_3), 3.98 (*s*, 3H, OCH_3), 7.38 (*m*, 5H, H2′, H3′, H4′, H5′, H6′), 7.46 (*d*, *J* = 1.6 Hz, 1H, H2), 7.48 (*d*, *J* = 1.6 Hz, 1H, H6), 10.01 (*s*, 1H, CHO). ^{13}C NMR (DMSO-*d6*): δ (ppm) = 37.2 (2×NCH_3), 56.8 (OCH_3), 108.2 (C2), 124.1 (C4), 125.8 (C6), 127.7 (C4′), 127.8 (C2′, C6′), 129.4 (C3′,), 137.8 (C5), 140.3 (C1), 149.6 (C1′), 161.0 (C3), 165.0 (COS), 191.7 (CHO). EI/MS m/z (%): 315.3 ($M^{\bullet+}$, 21), 243.2 (6), 200.1 (7), 171.1 (9), 84.0 (13), 72.1 (100).

3.1.1.4. Knoevenagel-Doebner condensation

In a round bottom flask with the aldehyde (1 mmol) dissolved in anhydrous pyridine (11.0 mmol), malonic acid (1.5 mmol) and piperidine (0.35 mmol) were added. The mixture was stirred at 70 ºC for 4-5 h. The general procedure was adapted from Teixeira *et al.* [40] with some modifications.

(*E*)-3-(4-((Dimethylcarbamoyl)thio)-3-methoxyphenyl)acrylic acid (**21**). Synthesis and structural analysis are described in literature [24].

(*E*)-3-(4-((Dimethylcarbamoyl)thio)-3,5-dimethoxyphenyl)acrylic acid (**22**). Once the reaction was complete, the reaction mixture was poured onto water (15 mL), cooled on an ice bath and acidified with HCl 6 M. The product was collected by filtration under reduced pressure and washed with water. After suspension in methanol, the solid was centrifuged at 3000 *g* for 20 min. The supernatant was discarded, yielding the purified product. η = 88 %. ^{1}H NMR (DMSO-*d6*): δ (ppm) = 2.88 (*bs*, 3H, NCH_3), 3.06 (*bs*, 3H, NCH_3), 3.80 (*s*, 6H, 2×OCH_3), 6.71 (d, *J* = 16.0 Hz, 1H, Hα), 7.05 (*s*, 2H, H2, H6), 7.59 (*d*, *J* = 16.0 Hz, 1H, Hβ), 12.46 (*bs*, 1H, COOH). ^{13}C NMR (DMSO-*d6*): δ (ppm) = 36.9 (2×NCH_3), 56.8 (2×OCH_3), 104.7 (C2, C6), 107.0 (C4), 121.3 (Cα), 138.0 (C1), 144.2 (Cβ), 161.6 (C3, C5), 164.6 (COS), 168.0 (COOH). EI/MS m/z (%): 311.1 ($M^{\bullet+}$, 40), 84.0 (9), 72.1 (100).

(*E*)-3-(6-((Dimethylcarbamoyl)thio)-5-methoxy-[1,1'-biphenyl]-3-yl)acrylic acid (**23**). Once the reaction was complete, the reaction mixture was poured onto water (15 mL), cooled on an ice bath and acidified with HCl 6 M. The product was collected by filtration under reduced pressure and washed with water. After suspension in methanol, the solid was centrifuged at 3000 *g* for 20 min. The supernatant was discarded, yielding the purified product. η = 59 %. ^{1}H NMR (DMSO-*d6*): δ (ppm) = 2.88 (*bs*, 6H, 2× NCH_3), 3.87 (*s*, 3H, OCH_3), 6.72 (*d*, *J* = 16.0 Hz, 1H, Hα), 7.24 (*d*, *J* = 1.5 Hz, 1H, H2), 7.28 (*m*, 2H, H2′, H6′), 7.39 (*m*, 3H, H3′, H4′, H5′), 7.45 (*d*, *J* = 1.6 Hz, 1H, H6), 7.63 (*d*, *J* = 16.0 Hz, 1H, Hβ), 12.46 (*bs*, 1H, COOH). ^{13}C NMR (DMSO-*d6*): δ (ppm) = 36.9 (2×NCH_3), 57.0 (OCH_3), 110.0 (C2), 118.3 (C4), 121.5 (Cα), 123.1 (C6), 127.9 (C4′), 128.2 (C2′, C6′), 129.0 (C3′, C5′), 137.2 (C5), 140.9 (C1), 143.6 (Cβ), 149.0 (C1′), 161.1 (C3), 165.0 (COS), 167.9 (COOH). EI/MS m/z (%): 357.3 ($M^{\bullet+}$, 46), 268.2 (28), 72.1 (100).

3.1.1.5. PyBOP-mediated cinnamic acid amidation.

In a round bottom flask, compound 21 (1 mmol) were dissolved in DMF and DIPEA (1.01 mmol). The mixture was cooled at 0 ºC on an ice bath, and a solution of PyBOP (1.01 mmol) in dichloromethane (2.25 mL) was added slowly. The mixture was stirred for 30 min, and the amine

(1.01 mmol) was added. The general procedure was adapted from Gaspar et al. [41] with some modifications.

(*E*)-*S*-(4-(3-(Benzylamino)-3-oxoprop-1-en-1-yl)-2-methoxyphenyl) dimethylcarbamothioate (**24**). Flash column chromatography was performed in ethyl acetate/dichloromethane (3:7). Recrystallization in dichloromethane/petroleum ether yielded a white solid. η = 95 %. ^{1}H NMR ($CDCl_3$-*d*1): δ (ppm) = 2.90 (*bs*, 3H, NCH_3), 3.10 *bs*, 3H, NCH_3), 3.86 (*s*, 3H, OCH_3), 4.53 (*d*, *J* = 5.7 Hz, 2H, $NHCH_2Ph$), 6.24 (*d*, *J* = 15.6 Hz, 1H, Hα), 6.44 (*t*, *J* = 5.5 Hz, 1H, CONH), 6.96 (*d*, *J* = 1.5 Hz, 1H, H2), 7.04 (*dd*, *J* = 1.5 Hz, 7.9 Hz, 1H, H6), 7.30 (m, 5H, H2′, H3′, H4′, H5′, H6′), 7.39 (*d*, *J* = 7.9 Hz, 1H, H5), 7.53 (*d*, *J* = 15.6 Hz, 1H, Hβ). ^{13}C NMR ($CDCl_3$-*d*1): δ (ppm) = 37.0 ($2\times NCH_3$), 43.9 ($NHCH_2Ph$), 56.1 (OCH_3), 110.9 (C2), 118.1 (C4), 120.2 (Cα), 122.0 (C6), 127.4 (C4′), 128.0 (C2′, C6′), 128.6 (C3′, C5′), 138.0 (C5) 138.3 (C1), 138.4 (C1′), 140.03 (Cβ), 160.1 (C3), 165.5 (COS), 166.3 (CONH). EI/MS m/z (%): 370.3 ($M^{\bullet+}$, 59), 281.2 (22), 91.1 (32), 72.1 (100).

(*E*)-*S*-(2-Methoxy-4-(3-oxo-3-(phenethylamino)prop-1-en-1-yl)phenyl) dimethylcarbamothioate (**25**). Flash column chromatography was performed in ethyl acetate/dichloromethane (3:7). Recrystallization in dichloromethane/petroleum ether yielded a white solid. η = 80 %. ^{1}H NMR ($CDCl_3$-*d*1): δ (ppm) = 2.87 (*t*, *J* = 7.0 Hz, 2H, $NHCH_2CH_2Ph$), 3.00 (*bs*, 3H, NCH_3), 3.13 (*bs*, 3H, NCH_3), 3.62 (*m*, 2H, $NHCH_2CH_2Ph$), 3.86 (*s*, 3H, OCH_3), 5.93 (*t*, *J* = 5.7 Hz, 1H, NH), 6.22 (*d*, *J* = 15.6 Hz, 1H, Hα), 6.98 (*d*, *J* = 1.5 Hz, 1H, H2), 7.06 (*dd*, *J* = 1.5 Hz, 7.9 Hz, 1H, H6), 7.28 (*m*, 5H, H2′, H3′, H4′, H5′, H6′), 7.42 (*d*, *J* = 7.9 Hz, 1H, H5), 7.52 (*d*, *J* = 15.6 Hz, 1H, Hβ). ^{13}C NMR ($CDCl_3$-*d*1): δ (ppm) = 35.0 ($NHCH_2CH_2Ph$), 37.0 ($2\times NCH_3$), 40.8 ($NHCH_2CH_2Ph$), 56.1 (OCH_3), 110.8 (C2), 118.3 (C4), 120.1 (Cα), 122.1 (C6), 126.5 (C4′), 128.7 (C2′, C6′), 128.8 (C3′, C5′), 138.1 (C5) 138.25 (C1), 139.0 (C1′), 140.0 (Cβ), 160.1 (C3), 165.6 (COS), 166.1 (CONH). EI/MS m/z (%): 384.3 ($M^{\bullet+}$, 47), 295.2 (13), 105.1 (16), 72.1 (100).

3.1.1.6. Alkaline hydrolysis

To a solution of the *S*-phenyl-*N*,*N*-dimethylthiocarbamate (1 mmol) in methanol (1.5 mL), aqueous solution of sodium hydroxide 2 M (5-17.5 mmol) was added dropwise. The reaction mixture was stirred at 90 °C until the TLC analysis showed maximal substrate consumption.

(*E*)-3-(4-Sulfanyl-3-methoxyphenyl)acrylic acid (**TFA**, **2**). Synthesis and structural analysis is described in literature [24].

(*E*)-*N*-Benzyl-3-(4-sulfanyl-3-methoxyphenyl)acrylamide (**3**). Compound **3** was obtained by an alkaline hydrolysis of compound **24** the following conditions: compound **24** (0.82 g, 2.20 mmol), methanol (4.5 mL) and aqueous solution of NaOH 2 M (5.50 mL, 11.0 mmol). The mixture was protected from the light and stirred at 90 °C for 1.5 h. Upon completion, the mixture was allowed to cool at room temperature, then poured onto cooled aqueous saturated solution of NH_4Cl (15 mL) and acidified with aqueous solution of acetic acid 5 M added dropwise. The solid was filtered under reduced pressure and washed with water. TLC analysis was performed in ethyl acetate/dichloromethane/formic acid (3:7:0.01). η = 53 %. ^{1}H NMR (MeOD-*d*4): δ (ppm) = 3.91 (*s*, 3H, OCH_3), 4.49 (*s*, 2H, $NHCH_2Ph$), 6.60 (*d*, *J* = 15.7 Hz, 1H, Hα), 7.05 (*dd*, *J* = 1.5 Hz, 8.0 Hz, 1H, H6), 7.10 (*d*, *J* = 1.3 Hz, 1H, H2), 7.24 (*m*, 2H, H5 H4′), 7.32 (*m*, 4H, H2′, H3′, H5′, H6′), 7.51 (*d*, *J* = 15.7 Hz, 1H, Hβ). ^{13}C NMR (MeOD-*d*4): δ (ppm) = 42.9 ($NHCH_2Ph$), 55.0 (OCH_3), 109.2 (C2), 119.4 (Cα), 120.5 (C6), 124.3 (C4), 126.9 (C4′), 127.2 (C2′, C6′), 128.2 (C3′, C5′), 128.7 (C5) 133.0 (C1), 138.5 (C1′), 140.4 (Cβ), 155.1 (C3), 167.2 (CONH). ESI/MS m/z (%): 300 (M^{+}+1, 100), 284 (55).

(*E*)-3-(4-Sulfanyl-3-methoxyphenyl)-*N*-phenethylacrylamide (**4**). Compound **4** was obtained by an alkaline hydrolysis of compound **25** the following conditions: compound **25** (0.42 g, 1.1 mmol), methanol (1.6 mL) and aqueous solution of NaOH 2 M (2.7 mL, 5.5 mmol). The mixture was protected from the light and stirred at 90 °C for 1.5 h. Upon completion, the mixture was allowed to cool at

room temperature, then poured onto cooled aqueous saturated solution of NH_4Cl (15 mL) and acidified with aqueous solution of acetic acid 5 M added dropwise. The solid was filtered under reduced pressure and washed with water. TLC analysis was performed in ethyl acetate/dichloromethane/formic acid (3:7:0.01). η = 45 %. ^{1}H NMR ($CDCl_3$-*d*$_1$): δ (ppm) = 2.89 (*t*, *J* = 7.0 Hz, 2H, $NHCH_2C\underline{H}_2Ph$), 3.66 (*m*, 2H, $NHC\underline{H}_2CH_2Ph$), 3.90 (*s*, 3H, $OC\underline{H}_3$), 5.66 (*m*, 1H, N<u>H</u>), 6.29 (*d*, *J* = 15.5 Hz, 1H, Hα), 6.92 (*d*, *J* = 1.5 Hz, 1H, H2), 6.99 (*dd*, *J* = 1.5 Hz, 8.0 Hz, 1H, H6), 7.23 (*m*, 4H, H5, H3′, H4′, H5′), 7.32 (*m*, H2′, H6′), 7.53 (*d*, *J* = 15.5 Hz, 1H, Hβ). ^{13}C NMR ($CDCl_3$-*d*$_1$): δ (ppm) = <u>35.7</u> ($NHCH_2\underline{C}H_2Ph$), <u>40.8</u> ($NH\underline{C}H_2CH_2Ph$), <u>55.9</u> ($O\underline{C}H_3$), <u>109.5</u> (C2), <u>119.9</u> (Cα), <u>120.8</u> (C6), 123.4 (C4), <u>126.6</u> (C4′), <u>128.7</u> (C2′, C6′), <u>128.8</u> (C3′, C5′), <u>129.1</u> (C5), 133.2 (C1), 138.9 (C1′), <u>140.7</u> (Cβ), 154.8 (C3), 165.9 (<u>C</u>ONH). ESI/MS m/z (%): 314 (M^{+}+1, 100).

(*E*)-3-(4-Sulfanyl-3,5-dimethoxyphenyl)acrylic acid (**5**). Compound **5** was obtained by an alkaline hydrolysis of compound **22** the following conditions: compound **22** (0.64 g, 2.05 mmol), methanol (2 mL) and aqueous solution of NaOH 2 M (12.5 mL, 2.5 mmol). The mixture was protected from the light and stirred at 90 °C for 9 h. Upon completion, the mixture was allowed to cool at room temperature, then poured onto cooled aqueous saturated solution of NH_4Cl (15 mL) and acidified with aqueous solution of acetic acid 5 M added dropwise. The solid was filtered under reduced pressure and washed with water. TLC analysis was performed in ethyl acetate/dichloromethane/formic acid (3:7:0.01). η = 79.6 %. ^{1}H NMR ($CDCl_3$-*d*$_1$): δ (ppm) = 3.94 (*s*, 6H, 2×$OC\underline{H}_3$), 4.19 (*s*, 1H, S<u>H</u>), 6.40 (d, *J* = 15.9 Hz, 1H, Hα), 6.74 (*s*, 2H, H2, H6), 7.72 (*d*, *J* = 16.0 Hz, 1H, Hβ). ^{13}C NMR ($CDCl_3$-*d*$_1$): δ (ppm) = <u>56.3</u> (2×$O\underline{C}H_3$), <u>103.8</u> (C2, C6), 114.2 (C4), <u>116.3</u> (Cα), 131.0 (C1), <u>147.1</u> (Cβ), 155.4 (C3, C5), 172.2 (<u>C</u>OOH). ESI/MS m/z (%): 241 (M^{+}+1, 100).

(*E*)-3-(6-Sulfanyl-5-methoxy-[1,1'-biphenyl]-3-yl)acrylic acid (**6**). Compound **6** was obtained by an alkaline hydrolysis of compound **23** the following conditions: compound **23** (0.36 g, 1.01 mmol), methanol (2 mL) and aqueous solution of NaOH 2 M (8.75 mL, 17.5 mmol). The mixture was protected from the light and stirred at 90 ºC for 16 h. Upon completion, the mixture was allowed to cool at room temperature, then poured onto cooled aqueous saturated solution of NH_4Cl (15 mL) and acidified with aqueous solution of acetic acid 5 M added dropwise. The solid was filtered under reduced pressure and washed with water. TLC analysis was performed in ethyl acetate/dichloromethane/formic acid (3:7:0.01). η = 73 %. ^{1}H NMR (MeOD-*d*$_4$): δ (ppm) = 3.99 (*s*, 3H, $OC\underline{H}_3$), 6.47 (*d*, *J* = 15.9 Hz, 1H, Hα), 7.03 (*d*, *J* = 1.4 Hz, 1H, H2), 7.20 (*d*, *J* = 1.7 Hz, 1H, H6), 7.40 (*m*, 5H, H2′ H3′, H4′, H5′, H6′), 7.63 (*d*, *J* = 15.9 Hz, 1H, Hβ). ^{13}C NMR (MeOD-*d*$_4$): δ (ppm) = <u>55.6</u> ($O\underline{C}H_3$), <u>107.7</u> (C2), <u>117.5</u> (Cα), <u>122.6</u> (C6), 124.3 (C4), <u>127.6</u> (C4′), <u>128.1</u> (C2′, C6′), <u>128.7</u> (C3′, C5′), 131.5 (C5), 140.2 (C1), 141.2 (C1′), <u>144.4</u> (Cβ), 154.5 (C3), 169.2 (<u>C</u>OOH). ESI/MS m/z (%): 287 (M^{+}+1, 100).

3.2. Radical scavenging activity

3.2.1. Spectrophotometric methods

3.2.1.1. DPPH$^{\bullet}$ radical assay

DPPH$^{\bullet}$ radical scavenging activity was performed as described by Teixeira *et al.* [40] (see supplementary information).

3.2.1.2. ABTS$^{\bullet+}$ radical cation assay

ABTS$^{\bullet+}$ scavenging activity was evaluated as described by Teixeira *et al.* [40] (see supplementary information).

3.2.1.3. GO$^{\bullet}$ radical assay

457 $GO^{\bullet}$ radical scavenging protocol was adapted from the literature [42-44] and described in
458 supplementary information.

459 3.2.2. Fluorometric methods (ORAC-FL assay)

460 The ORAC-FL analyses were performed using an experimental protocol adapted from the
461 literature [45,46] and described in supplementary information.

462 *3.3. Electrochemical measurements*

463 DPV experiments were performed as described elsewhere [23] (see supplementary information).

464 *3.4. In vitro toxicology*

465 3.4.1. SH-SY5Y cell culture

466 Human SH-SY5Y neuroblastoma cells were obtained from the American Type Culture
467 Collection (ATCC, Manassas, VA, USA). SH-SY5Y cell culture and differentiation were performed
468 as previously described by Fernandes *et al.* [32] and in supplementary information.

469 3.4.2. Cytotoxicity

470 Stock solutions of the test compounds (1, 10 and 50 mM) were freshly prepared in ethanol
471 absolute. Final test concentrations of the compounds under study were obtained by diluting into
472 culture medium immediately before use, giving a final maximum concentration of 0.1% ethanol.
473 In cytotoxicity experiments, differentiated SH-SY5Y cells were exposed to the test compounds
474 (1, 10 and 50 μM) for 24 h. Controls were treated with culture media containing 0.1 % ethanol. Cell
475 viability was estimated using the MTT reduction assay [32] and the NR uptake assay [47] (see
476 supplementary information).

477 3.4.3. Protection against oxidative stress inducers

478 To evaluate the ability of phenols and thiophenols to protect neuronal cells from oxidative stress,
479 hydrogen peroxide (H_2O_2) and ferric nitrilotriacetate (FeNTA) were used as inducers of oxidative
480 damage. Differentiated SH-SY5Y cells were pre-treated with the compounds under study for 24 h
481 and exposed to the oxidative stressors.

482 3.4.3.1. Cytoprotective properties against H_2O_2-induced damage

483 Differentiated SH-SY5Y cells were pretreated with the test compounds (10 and 50 μM) for 24 h.
484 Then, the culture medium was removed and replaced with medium containing H_2O_2 1.5 mM, and
485 cells were incubated for additional 30 min at 37 °C in a humidified, 5 % CO_2–95 % air atmosphere.
486 Cell viability was estimated by the MTT reduction assay [32].

487 3.4.3.2. Cytoprotective properties against FeNTA-induced damage

488 Nitrilotriacetic acid disodium salt solution (500 mM) and nitrilotriacetic acid trisodium salt
489 solution (500 mM) were mixed until pH 7 was achieved and diluted to obtain a concentration of 250
490 mM. This solution was added to the required amount of iron(III) chloride to obtain the NTA:iron(III)
491 molar ratio of 2.5:1 ([Fe(III) = 100 mM). Then, the ferric nitrilotriacetic acid (FeNTA) solution was
492 diluted in culture medium to obtain a final iron(III) solution with concentration of 4 mM.
493 Differentiated SH-SY5Y cells were pretreated with the test compounds (10 and 50 μM) for
494 24 h. Then, the culture medium was removed and replaced with medium containing FeNTA 4 mM.
495 Cells were incubated for additional 24 h at 37 °C in a humidified, 5 % CO_2–95 % air atmosphere. Cell
496 viability was estimated by the MTT reduction assay [32].

497 3.4.4. Statistical analysis

Data analysis for all the studies are specified in supplementary information.

3.5. Estimation of drug-like properties

The calculation of molecular weight (MW), topological polar surface area (TPSA), number of hydrogen bond donors (HBD) and acceptors (HBA), number of rotatable bonds (RB) and logarithm of the ratio of the concentration of a drug in the brain and in the blood (logBB) was performed using the Stardrop software. The calculation of octanol/water partition coefficient (clogP) was performed using the SwissADME (http://swissadme.ch/index.php).

4. Conclusion

In this work, we have successfully obtained a series of TFA and FA derivatives and evaluated their antioxidant activity, as well as their cytotoxicity and cytoprotective profiles. Structural diversity was attained by incorporating 5-methoxy or 5-phenyl groups at the aromatic ring, or benzyl and phenethyl amide groups at the carboxylic acid group.

Thiophenols displayed remarkable radical scavenging properties. Comparing with phenols, thiophenols reacted faster and more efficiently with $DPPH^{\bullet}$ and $GO^{\bullet}$ radicals and presented lower E_P values at physiological pH. However, unlike phenols, thiophenols were unable to scavenge $ROO^{\bullet}$ radicals in ORAC-FL assay. The presence of different substituents directly attached to the aromatic ring did not improve the antioxidant profile of the parent compounds (TFA and FA). Although a slight decrease of E_P values was observed, 5-methoxy and 5-phenyl derivatives showed similar or lower radical scavenging activity and slower reaction rates than the unsubstituted analogues. On the other hand, the carboxylic acid amidation was proven to be a beneficial structural modification of the cinnamic acid scaffold, since it preserved the antioxidant profile of the parent acids while improving the drug-like properties of the antioxidants. The cytotoxicity of FA and TFA derivatives in differentiated SH-SY5Y cells was similar to that of the parent compounds at concentrations up to 50 μM. Among the tested compounds, only TFA **2**, TFA benzyl amide **3** and 5-phenylferulic acid **10** attenuated the oxidative damage inflicted by H_2O_2 and iron overload. Compound **3** is highlighted as the best antioxidant of the series with favorable physicochemical properties.

Overall, the results obtained in this work emphasized the dissimilar biological outline of thiophenols and phenols) along with the effect of the structural modification of FA and TFA on their antioxidant properties. The data may be useful for the development of new drugs able to tackle the events that lead to the progression of neurodegenerative disorders.

Supplementary Materials: The following are available online at www.mdpi.com/xxx/s1, Experimental details, Statistics, **Figure S1:** $DPPH^{\bullet}$ kinetic curves of thiophenols **2-6** and phenols **1**, **7-10**; **Figure S2:** $ABTS^{\bullet+}$ kinetic curves of thiophenols **2-6** and phenols **1**, **7-10**; **Figure S3:** $GO^{\bullet}$ kinetic curves of thiophenols **2-6** and phenols **1**, **7-10**.

Author Contributions: Performing of experiments, data acquisition and analysis DC, CF, BA, TS and JG.; All authors contributed for writing and reviewing of manuscript.

B.**Funding:** This project was supported by Foundation for Science and Technology (FCT) and FEDER/COMPETE research grants (UID/QUI/00081, NORTE-01-0145-FEDER-000028, POCI-01-0145-FEDER-029164). D. Chavarria, C. Fernandes and T. Silva grants are supported by FCT, POPH and FEDER/COMPETE and NORTE-01-0145-FEDER-000028.This article is based upon work from COST Action CA15135.

Conflicts of Interest. The authors declare no conflict of interest.

References

1. Sies, H. Oxidative stress: a concept in redox biology and medicine. *Redox Biol.* **2015**, *4*, 180-183, doi:10.1016/j.redox.2015.01.002.

2. Uttara, B.; Singh, A.V.; Zamboni, P.; Mahajan, R.T. Oxidative stress and neurodegenerative diseases: a review of upstream and downstream antioxidant therapeutic options. *Curr. Neuropharmacol.* **2009**, *7*, 65-74, doi:10.2174/157015909787602823.
3. Bhat, A.H.; Dar, K.B.; Anees, S.; Zargar, M.A.; Masood, A.; Sofi, M.A.; Ganie, S.A. Oxidative stress, mitochondrial dysfunction and neurodegenerative diseases: a mechanistic insight. *Biomed. Pharmacother.* **2015**, *74*, 101-110, doi:10.1016/j.biopha.2015.07.025.
4. Lovell, M.A.; Xie, C.; Markesbery, W.R. Acrolein is increased in Alzheimer's disease brain and is toxic to primary hippocampal cultures. *Neurobiol. Aging* **2001**, *22*, 187-194, doi:10.1016/S0197-4580(00)00235-9.
5. Markesbery, W.R.; Lovell, M.A. Four-hydroxynonenal, a product of lipid peroxidation, is increased in the brain in Alzheimer's disease. *Neurobiol. Aging* **1998**, *19*, 33-36, doi:10.1016/S0197-4580(98)00009-8.
6. Dexter, D.T.; Carter, C.J.; Wells, F.R.; Javoy-Agid, F.; Agid, Y.; Lees, A.; Jenner, P.; Marsden, C.D. Basal lipid peroxidation in substantia nigra is increased in Parkinson's disease. *J. Neurochem.* **1989**, *52*, 381-389, doi:10.1111/j.1471-4159.1989.tb09133.x.
7. Good, P.F.; Werner, P.; Hsu, A.; Olanow, C.W.; Perl, D.P. Evidence of neuronal oxidative damage in Alzheimer's disease. *Am. J. Pathol.* **1996**, *149*, 21-28.
8. Good, P.F.; Hsu, A.; Werner, P.; Perl, D.P.; Olanow, C.W. Protein nitration in Parkinson's disease. *J. Neuropathol. Exp. Neurol.* **1998**, *57*, 338-342, doi:10.1097/00005072-199804000-00006.
9. Kim, T.S.; Pae, C.U.; Yoon, S.J.; Jang, W.Y.; Lee, N.J.; Kim, J.J.; Lee, S.J.; Lee, C.; Paik, I.H.; Lee, C.U. Decreased plasma antioxidants in patients with Alzheimer's disease. *Int. J. Geriatr. Psychiatry* **2006**, *21*, 344-348, doi:10.1002/gps.1469.
10. Marcus, D.L.; Thomas, C.; Rodriguez, C.; Simberkoff, K.; Tsai, J.S.; Strafaci, J.A.; Freedman, M.L. Increased peroxidation and reduced antioxidant enzyme activity in Alzheimer's disease. *Exp. Neurol.* **1998**, *150*, 40-44, doi:10.1006/exnr.1997.6750.
11. Venkateshappa, C.; Harish, G.; Mahadevan, A.; Srinivas Bharath, M.M.; Shankar, S.K. Elevated oxidative stress and decreased antioxidant function in the human hippocampus and frontal cortex with increasing age: implications for neurodegeneration in Alzheimer's disease. *Neurochem. Res.* **2012**, *37*, 1601-1614, doi:10.1007/s11064-012-0755-8.
12. Venkateshappa, C.; Harish, G.; Mythri, R.B.; Mahadevan, A.; Bharath, M.M.; Shankar, S.K. Increased oxidative damage and decreased antioxidant function in aging human *substantia nigra* compared to striatum: implications for Parkinson's disease. *Neurochem. Res.* **2012**, *37*, 358-369, doi:10.1007/s11064-011-0619-7.
13. Pocernich, C.B.; Lange, M.L.; Sultana, R.; Butterfield, D.A. Nutritional approaches to modulate oxidative stress in Alzheimer's disease. *Curr. Alzheimer Res.* **2011**, *8*, 452-469, doi:10.2174/156720511796391908.
14. Ramsay, R.R.; Majekova, M.; Medina, M.; Valoti, M. Key Targets for Multi-Target Ligands Designed to Combat Neurodegeneration. *Front. Neurosci.* **2016**, *10*, 1-24, doi:10.3389/fnins.2016.00375.
15. Mancuso, C.; Santangelo, R. Ferulic acid: pharmacological and toxicological aspects. *Food Chem. Toxicol.* **2014**, *65*, 185-195, doi:10.1016/j.fct.2013.12.024.
16. Ojha, S.; Javed, H.; Azimullah, S.; Abul Khair, S.B.; Haque, M.E. Neuroprotective potential of ferulic acid in the rotenone model of Parkinson's disease. *Drug Des. Devel. Ther.* **2015**, *9*, 5499-5510, doi:10.2147/dddt.S90616.

585 17. Nagarajan, S.; Chellappan, D.R.; Chinnaswamy, P.; Thulasingam, S. Ferulic acid pretreatment mitigates
586 MPTP-induced motor impairment and histopathological alterations in C57BL/6 mice. *Pharm. Biol.* **2015**,
587 *53*, 1591-1601, doi:10.3109/13880209.2014.993041.
588 18. Kanski, J.; Aksenova, M.; Stoyanova, A.; Butterfield, D.A. Ferulic acid antioxidant protection against
589 hydroxyl and peroxyl radical oxidation in synaptosomal and neuronal cell culture systems in vitro:
590 structure-activity studies. *J. Nutr. Biochem.* **2002**, *13*, 273-281, doi:10.1016/S0955-2863(01)00215-7.
591 19. Vashisth, P.; Kumar, N.; Sharma, M.; Pruthi, V. Biomedical applications of ferulic acid encapsulated
592 electrospun nanofibers. *Biotechnol. Rep. (Amst)* **2015**, *8*, 36-44, doi:10.1016/j.btre.2015.08.008.
593 20. Yakub, G.; Ignatova, M.; Manolova, N.; Rashkov, I.; Toshkova, R.; Georgieva, A.; Markova, N.
594 Chitosan/ferulic acid-coated poly(ε-caprolactone) electrospun materials with antioxidant, antibacterial
595 and antitumor properties. *Int. J. Biol. Macromol.* **2018**, *107*, 689-702, doi:10.1016/j.ijbiomac.2017.08.183.
596 21. Silva, T.; Bravo, J.; Summavielle, T.; Remião, F.; Pérez, C.; Gil, C.; Martínez, A.; Borges, F. Biology-
597 oriented development of novel lipophilic antioxidants with neuroprotective activity. *RSC Adv.* **2015**, *5*,
598 15800-15811, doi:10.1039/c4ra15164j.
599 22. Gaspar, A.; Garrido, E.M.; Esteves, M.; Quezada, E.; Milhazes, N.; Garrido, J.; Borges, F. New insights
600 into the antioxidant activity of hydroxycinnamic acids: Synthesis and physicochemical characterization
601 of novel halogenated derivatives. *Eur. J. Med. Chem.* **2009**, *44*, 2092-2099,
602 doi:10.1016/j.ejmech.2008.10.027.
603 23. Garrido, J.; Gaspar, A.; Garrido, E.M.; Miri, R.; Tavakkoli, M.; Pourali, S.; Saso, L.; Borges, F.; Firuzi, O.
604 Alkyl esters of hydroxycinnamic acids with improved antioxidant activity and lipophilicity protect
605 PC12 cells against oxidative stress. *Biochimie* **2012**, *94*, 961-967, doi:10.1016/j.biochi.2011.12.015.
606 24. Chavarria, D.; Fernandes, C.; Silva, T.; Garrido, J.; Remião, F.; Oliveira, P.J.; Borges, F. Bioisosteric OH-
607 to SH- replacement changes the antioxidant profile of ferulic acid. *Org. Biomol. Chem.* **2019,** Accepted
608 manuscript.
609 25. Chen, G.; Zhang, Y.; Liu, X.; Fang, Q.; Wang, Z.; Fu, L.; Liu, Z.; Wang, Y.; Zhao, Y.; Li, X., et al. Discovery
610 of a New Inhibitor of Myeloid Differentiation 2 from Cinnamamide Derivatives with Anti-
611 Inflammatory Activity in Sepsis and Acute Lung Injury. *J. Med. Chem.* **2016**, *59*, 2436-2451,
612 doi:10.1021/acs.jmedchem.5b01574.
613 26. Floegel, A.; Kim, D.O.; Chung, S.J.; Koo, S.I.; Chun, O.K. Comparison of ABTS/DPPH assays to measure
614 antioxidant capacity in popular antioxidant-rich US foods. *J. Food Compos. Anal.* **2011**, *24*, 1043-1048,
615 doi:10.1016/j.jfca.2011.01.008.
616 27. Schaich, K.M.; Tian, X.; Xie, J. Hurdles and pitfalls in measuring antioxidant efficacy: A critical
617 evaluation of ABTS, DPPH, and ORAC assays. *J. Funct. Foods* **2015**, *14*, 111-125,
618 doi:10.1016/j.jff.2015.01.043.
619 28. Pisoschi, A.M.; Cimpeanu, C.; Predoi, G. Electrochemical Methods for Total Antioxidant Capacity and
620 its Main Contributors Determination: A review. *Open Chem.* **2015**, *13*, 824-856, doi:10.1515/chem-2015-
621 0099.
622 29. Luc, R.; Vergely, C. Forgotten radicals in biology. *Int. J. Biomed. Sci.* **2008**, *4*, 255-259.
623 30. Teixeira, J.; Gaspar, A.; Garrido, E.M.; Garrido, J.; Borges, F. Hydroxycinnamic acid antioxidants: an
624 electrochemical overview. *Biomed. Res. Int.* **2013**, *2013*, 1-13, doi:10.1155/2013/251754.
625 31. Brand-Williams, W.; Cuvelier, M.E.; Berset, C. Use of a free radical method to evaluate antioxidant
626 activity. *LWT - Food Sci. Technol.* **1995**, *28*, 25-30, doi:10.1016/S0023-6438(95)80008-5.

627 32. Fernandes, C.; Pinto, M.; Martins, C.; Gomes, M.J.; Sarmento, B.; Oliveira, P.J.; Remião, F.; Borges, F.
628 Development of a PEGylated-Based Platform for Efficient Delivery of Dietary Antioxidants Across the
629 Blood-Brain Barrier. *Bioconjug. Chem.* **2018**, *29*, 1677-1689, doi:10.1021/acs.bioconjchem.8b00151.
630 33. Belyanskaya, L.; Manser, P.; Spohn, P.; Bruinink, A.; Wick, P. The reliability and limits of the MTT
631 reduction assay for carbon nanotubes-cell interaction. *Carbon* **2007**, *45*, 2643-2648,
632 doi:10.1016/j.carbon.2007.08.010.
633 34. Repetto, G.; del Peso, A.; Zurita, J.L. Neutral red uptake assay for the estimation of cell
634 viability/cytotoxicity. *Nat. Protoc.* **2008**, *3*, 1125-1131, doi:10.1038/nprot.2008.75.
635 35. Nunez, M.T.; Gallardo, V.; Munoz, P.; Tapia, V.; Esparza, A.; Salazar, J.; Speisky, H. Progressive iron
636 accumulation induces a biphasic change in the glutathione content of neuroblastoma cells. *Free Radic.*
637 *Biol. Med.* **2004**, *37*, 953-960, doi:10.1016/j.freeradbiomed.2004.06.005.
638 36. Arnott, J.A.; Planey, S.L. The influence of lipophilicity in drug discovery and design. *Expert Opin. Drug*
639 *Discov.* **2012**, *7*, 863-875, doi:10.1517/17460441.2012.714363.
640 37. Hitchcock, S.A.; Pennington, L.D. Structure-brain exposure relationships. *J. Med. Chem.* **2006**, *49*, 7559-
641 7583, doi:10.1021/jm060642i.
642 38. Pajouhesh, H.; Lenz, G.R. Medicinal Chemical Properties of Successful Central Nervous System Drugs.
643 *NeuroRx.* **2005**, *2*, 541-553, doi:10.1602/neurorx.2.4.541.
644 39. Nowakowska, Z. The conversion of stilbenols to stilbenethiols via *N,N*-dimethylthiocarbamates.
645 *Phosphorus Sulfur* **2006**, *181*, 707-715, doi:10.1080/10426500500270016.
646 40. Teixeira, J.; Silva, T.; Benfeito, S.; Gaspar, A.; Garrido, E.M.; Garrido, J.; Borges, F. Exploring nature
647 profits: development of novel and potent lipophilic antioxidants based on galloyl-cinnamic hybrids.
648 *Eur. J. Med. Chem.* **2013**, *62*, 289-296, doi:10.1016/j.ejmech.2012.12.049.
649 41. Gaspar, A.; Silva, T.; Yanez, M.; Vina, D.; Orallo, F.; Ortuso, F.; Uriarte, E.; Alcaro, S.; Borges, F.
650 Chromone, a privileged scaffold for the development of monoamine oxidase inhibitors. *J. Med. Chem.*
651 **2011**, *54*, 5165-5173, doi:10.1021/jm2004267.
652 42. Tai, A.; Sawano, T.; Ito, H. Antioxidative properties of vanillic acid esters in multiple antioxidant assays.
653 *Biosci. Biotechnol. Biochem.* **2012**, *76*, 314-318, doi:10.1271/bbb.110700.
654 43. Feng, J.Y.; Liu, Z.Q. Phenolic and enolic hydroxyl groups in curcumin: which plays the major role in
655 scavenging radicals? *J. Agric. Food Chem.* **2009**, *57*, 11041-11046, doi:10.1021/jf902244g.
656 44. Yang, Y.; Song, Z.G.; Liu, Z.Q. Synthesis and antioxidant capacities of hydroxyl derivatives of
657 cinnamoylphenethylamine in protecting DNA and scavenging radicals. *Free Radic. Res.* **2011**, *45*, 445-
658 453, doi:10.3109/10715762.2010.540576.
659 45. Ou, B.; Hampsch-Woodill, M.; Prior, R.L. Development and validation of an improved oxygen radical
660 absorbance capacity assay using fluorescein as the fluorescent probe. *J. Agric. Food Chem.* **2001**, *49*, 4619-
661 4626, doi:10.1021/jf010586o.
662 46. Mura, F.; Silva, T.; Castro, C.; Borges, F.; Zuniga, M.C.; Morales, J.; Olea-Azar, C. New insights into the
663 antioxidant activity of hydroxycinnamic and hydroxybenzoic systems: spectroscopic, electrochemistry,
664 and cellular studies. *Free Radic. Res.* **2014**, *48*, 1473-1484, doi:10.3109/10715762.2014.965702.
665 47. Fernandes, C.; Martins, C.; Fonseca, A.; Nunes, R.; Matos, M.J.; Silva, R.; Garrido, J.; Sarmento, B.;
666 Remiao, F.; Otero-Espinar, F.J., et al. PEGylated PLGA Nanoparticles As a Smart Carrier to Increase the
667 Cellular Uptake of a Coumarin-Based Monoamine Oxidase B Inhibitor. *ACS Appl. Mater. Interfaces* **2018**,
668 *10*, 39557-39569, doi:10.1021/acsami.8b17224.

669

Electronic Supplementary Information

Insights into the discovery of novel neuroprotective agents: a comparative study between sulfanylcinnamic acid derivatives and related phenolic analogues

Daniel Chavarria[1,2ǂ], Carlos Fernandes[1ǂ], Brandon Aguiar[1], Tiago Silva[1,2], Jorge Garrido[3], Fernando Remião[4], Paulo J. Oliveira[2], Fernanda Borges[1*]

[1] CIQUP/Department of Chemistry and Biochemistry, Faculty of Sciences, University of Porto, 4169-007 Porto, Portugal

[2] CNC - Center for Neuroscience and Cell Biology, University of Coimbra, UC Biotech, Biocant Park, Cantanhede, Portugal.

[3] Department of Chemical Engineering, School of Engineering (ISEP), Polytechnic of Porto, 4200-072 Porto, Portugal

[4] UCIBIO-REQUIMTE, Laboratory of Toxicology, Department of Biological Sciences, Faculty of Pharmacy, University of Porto, Porto, Portugal

ǂ These authors contributed equally to this work.

* Corresponding Authors:

Fernanda Borges, CIQUP/Department of Chemistry and Biochemistry, Faculty of Sciences, University of Porto, Porto 4169-007, Portugal. E-mail: fborges@fc.up.pt

Contents of Electronic Supplementary information:

1. Experimental section 144
1.1. Chemistry 144
1.1.1. Reagents 144
1.1.2. Materials and apparatus 144
1.2. Radical scavenging activity 144
1.2.1. Spectrophotometric methods 144
1.2.1.1. $DPPH^{\bullet}$ radical assay 145
1.2.1.2. $ABTS^{\bullet+}$ radical cation assay 145
1.2.1.3. $GO^{\bullet}$ radical assay 145
1.2.2. Fluorometric methods (ORAC-FL assay) 145
1.3. Electrochemical measurements 146
1.4. *In vitro* toxicology 147
1.4.1. Materials 147
1.4.2. SH-SY5Y cell culture 147
1.4.3. Cytotoxicity assays 147
1.4.3.1. MTT reduction assay 147
1.4.3.2. NR uptake assay 148
1.4.4. Statistical analysis 148
2. Additional figures 149
3. References 152

1. Experimental section

1.1. Chemistry

1.1.1. Reagents

Ferulic acid, vanillin, 5-bromovanillin, syringaldehyde, phenylboronic acid, potassium carbonate (K_2CO_3), tetrabutylammonium bromide (TBAB), diazabicyclo[2.2.2]octane (DABCO), dimethylthiocarbamoyl chloride (DMTCl), malonic acid, piperidine, sodium hydroxide, diisopropylethylamine (DIPEA), (Benzotriazol-1-yloxy)tripyrrolidinophosphonium hexafluorophosphate (PyBOP), benzylamine, phenethylamine, *N,N*-dimethylformamide (DMF), diphenyl ether, anhydrous pyridine, methanol and dichloromethane, were purchased from Sigma Aldrich, Alfa-Aesar or TCI. All solvents were *pro analysis* grade from Merck, Carlo Erba Reagents and Scharlab. Deionized water (conductivity < 0.1 $mS.cm^{-1}$) was used throughout all the experiments.

1.1.2. Materials and apparatus.

Microwave-assisted synthesis was performed in a Biotage® Initiator Microwave Synthesizer. The monitoring of reactions progress was performed by thin layer chromatography (TLC) on precoated silica gel 60 F254 acquired from Merck (Darmstad, Germany). TLC spots were visualized under UV detection (254 nm and 365 nm). After the extraction step, organic layers were washed with brine, dried over anhydrous sodium sulphate and concentrated under reduced pressure. Some crude products were purified by flash column chromatography. Flash column chromatography was carried out on silica gel 60 Å acquired from Carlo-Erba Reactifs (SDS, France). The fractions with the desired compound were gathered and concentrated *in vacuo*. The solvents were evaporated using a Buchi Rotavapor.

^{1}H and ^{13}C NMR and DEPT135 data were acquired, at room temperature, on a Brüker AMX 300 spectrometer operating at 400 and 100 MHz, respectively. The solvents used in NMR experiments included $CDCl_3$-d_1, MeOD-d_4, DMSO-d_6 and Acetone-d_6. The chemical shifts are expressed in δ (ppm) values relative to tetramethylsilane (TMS) as internal reference and coupling constants (*J*) are given in Hz. Carbon signals present in DEPT135 spectra were underlined. Electron impact mass spectrometry (EI-MS) spectra were obtained on a Varian 320-MS apparatus. Electrospray ionization mass spectrometry (ESI-MS) spectra were obtained on an LTQ Orbitrap™ XL hybrid mass spectrometer (Thermo Fischer Scientific, Bremen, Germany) controlled by *LTQ Tune Plus 2.5.5* and *Xcalibur 2.1.0*. The data are reported as m/z (% of relative intensity of the most important fragments).

1.2. Radical scavenging activity

1.2.1. Spectrophotometric methods

To measure the radical scavenging activity of the test compounds, $DPPH^{\bullet}$, $ABTS^{\bullet+}$ and $GO^{\bullet}$ assays were adopted. Sodium persulfate, $DPPH^{\bullet}$, 2,2′-azino-bis(3-ethylbenzothiazoline-6-sulfonic acid) diammonium salt (ABTS) and $GO^{\bullet}$ were acquired from Sigma Aldrich. In these methods, the scavenging of the colored radical by an antioxidant is recorded by spectrophotometry. The absorbance decrease was monitored in a multiplate reader (BioTek Synergy HT from BioTek Instruments, Winooski, VT, USA). The results were expressed in IC_{50} as mean ± standard deviation (n = 3). Trolox (Sigma Aldrich), a water-soluble vitamin E

derivative, was used as a standard reference. Kinetic curves were prepared using GraphPad PRISM version 6 for Windows (GraphPad Software®, San Diego, CA, USA).

1.2.1.1. DPPH$^{\bullet}$ radical assay

DPPH$^{\bullet}$ radical scavenging activity was performed as described by Teixeira *et al*.[1] Briefly, solutions of the test compounds with increasing concentrations (ranging between 10 µM and 1 mM) were prepared in ethanol. A DPPH$^{\bullet}$ ethanolic solution (6.85 µM) was also prepared and then diluted to reach the absorbance of 0.72 ± 0.02 at 515 nm. After the addition of DPPH$^{\bullet}$ solution (180 µL) to the compound solution (20 µL) in triplicate, the absorbance at 515 nm was recorded every minute over 45 min. The percent inhibition of the radical was based on the comparison between the blank (20 µL of ethanol and 180 µL of DPPH$^{\bullet}$ solution), which corresponds to 100% of the radical, and the test compound solutions. The dose–response curves allowed the determination of IC_{50} values.

1.2.1.2. ABTS$^{\bullet+}$ radical cation assay

ABTS$^{\bullet+}$ scavenging activity was evaluated as described by Teixeira *et al.* [1] Briefly, ethanolic solutions of the test compounds with increasing concentrations (ranging between 50 µM and 500 µM) were prepared. ABTS$^{\bullet+}$ radical cation solution was obtained by the addition of aqueous solution of potassium persulfate (150 mM, 163 µL) to the aqueous solution of ABTS (7 mM, 10 mL) and the storage in the dark at room temperature for 16 h (2.45 mM final concentration). The solution was then diluted in ethanol to reach the absorbance of 0.72 ± 0.02 at 734 nm. After the addition of ABTS$^{\bullet+}$ solution (180 µL) to the compound solution (20 µL) in triplicate, the spectrophotometric measurement was carried out every minute over 15 min at 734 nm. The percent inhibition of the radical was based on the comparison between the blank (20 µL of ethanol and 180 µL of ABTS$^{\bullet+}$ solution), which corresponds to 100% of radical, and the test compound solutions. The dose–response curves allowed the determination of IC_{50} values.

1.2.1.3. GO$^{\bullet}$ radical assay

GO$^{\bullet}$ radical scavenging protocol was adapted from the literature [2-4]. Solutions of test compounds with increasing concentrations (ranging between 5 µM to 1 mM) were prepared in ethanol. An ethanolic solution of GO$^{\bullet}$ 5 mM was prepared and diluted to reach the absorbance of 1.00 ± 0.02 at 428 nm. After the addition in triplicate of compound solution (20 µL) to GO$^{\bullet}$ solution (180 µL), the spectrophotometric measurement was performed at 428 nm over 30 min. The percent inhibition of radical was based on comparison between the blank (20 µL of ethanol and 180 µL of GO$^{\bullet}$ solution), which corresponds to 100 % of response, and test compounds solutions. The dose-response curves allowed the determination of IC_{50} values.

1.2.2. Fluorometric methods (ORAC-FL assay)

The ORAC-FL analyses were performed on a multiplate reader (BioTek Synergy HT from BioTek Instruments, Winooski, VT, USA) using black polystyrene 96-well plates. Fluorescence was measured from the top, at an excitation wavelength of 485/20 nm and an emission at 528/20 nm. The plate reader was

controlled by Gen5 software. 2,2'-Azobis-(amidinopropane) dihydrochloride (AAPH), (±)-6-hydroxy-2,5,7,8-tetramethylchromane-2-carboxylic acid (trolox) and fluorescein (FL) were purchased from Sigma-Aldrich. The general procedure was adapted from the literature [5, 6], with some modifications.

The reaction was carried out in 75 mM of sodium phosphate buffer solution (pH = 7.4) at a final volume of 200 µL. Stock solutions of FL (5 mM) and antioxidants (5 mM) were prepared in ethanol due to their low solubility in buffer at high concentrations. Then, they were diluted in sodium phosphate buffer solution (pH = 7.4). The range of antioxidant concentrations was empirically selected to obtain a good separation between the fluorescence curves. The test compounds (final concentrations range of 0.1-2 µM) and fluorescein (40 nM, final concentration) were placed in each well and pre-incubated for 15 min at 37 ºC before the addition of AAPH (final concentration 18 mM). The microplate was immediately placed in the reader and automatically shaken prior to each reading. The fluorescence was measured minutely for 120 min. A control assay with fluorescein, AAPH and buffer (instead of the antioxidant solution) was performed for each assay. Trolox was also included in each assay as standard antioxidant in a final concentration range of 2-8 µM. All reaction mixtures were prepared in triplicate and at least three independent experiments were performed for each test compound. The fluorescence decay curves were normalized by the maximum value of fluorescence, and the areas under the curves (AUC) were determined according to the following **Equation 1**.

$$AUC = 1 + \sum_{i=1}^{i=120} \frac{f_i}{f_0} = 1 + \frac{f_1}{f_0} + \frac{f_2}{f_0} + \frac{f_3}{f_0} + \ldots + \frac{f_{120}}{f_0} \quad \textbf{(Equation 1)}$$

where f_0 = initial fluorescence reading at 0 min and f_i = fluorescence reading at time i. The net AUC is obtained by subtracting the AUC of the blank from that of a sample. The inhibition capacity, expressed as the relative Trolox equivalent ORAC values, was quantified employing the **Equation 2**.

$$\text{relative ORAC value} = \frac{AUC_{antioxidant} - AUC_{control}}{AUC_{trolox} - AUC_{control}} \times \frac{[Trolox]}{[antioxidant]} \quad \textbf{(Equation 2)}$$

where $AUC_{control}$ = area under the curve of control; $AUC_{antioxidant}$ = area under the curve of the test compound; AUC_{trolox} = area under the curve of Trolox (standard); [trolox] = Trolox concentration; and [antioxidant] = antioxidant concentration.

1.3. Electrochemical measurements

Voltammetric studies were carried out using an Autolab PGSTAT 12 potentiostat/galvanostat (Metrohm-Autolab, Netherlands) and one compartment glass electrochemical cell. The voltammetric data was acquired at room temperature using a three-electrode system: a glassy carbon working electrode (GCE) (d = 2 mm), a platinum wire counter electrode and an Ag/AgCl saturated KCl reference electrode (Metrohm, Switzerland). The working electrode was polished manually with an aqueous slurry of alumina powder (BDH Chemicals, VWR, USA) on a microcloth pad and rinsed with water before use. A Crison pH-meter with glass electrode was used for the pH measurements (Crison, Barcelona, Spain).

Voltammetric measurements were performed as described elsewhere [7]. Test solutions were prepared directly in the electrochemical cell, by dilution of ethanolic solutions of the compounds under study (10 mM, 100 µL) in the supporting electrolyte (10 mL) to obtain a final concentration of 100 µM. The scan rates used in differential pulse voltammetry (DPV) was 5 $mV.s^{-1}$.

1.4. *In vitro* toxicology

1.4.1. Materials

All reagents used were of analytical grade or of the highest grade available. Neutral red (NR) solution, 3-(4,5-dimethylthiazol-2-yl)-2,5-diphenyltetrazolium (MTT) bromide, Dulbecco's Modified Eagle's Medium (DMEM) with 4.5 g/L glucose, retinoic acid, 12-*O*-tetradecanoylphorbol-13-acetate (TPA), ascorbic acid, hydrogen peroxide (H_2O_2) solution 30 % (w/w), iron(III) chloride and nitrilotriacetic acid disodium salt were obtained from Sigma Aldrich (St. Louis, MO, USA). Nitrilotriacetic acid trisodium salt was obtained from Alfa Aesar (Karlsruhe, Germany). Reagents used in cell culture such as heat-inactivated fetal bovine serum (FBS), antibiotic (10,000 U/mL penicillin, 10,000 µg/mL streptomycin), MEM Non-Essential Amino Acids solution (100×) (MEM NEAA), 0.25% trypsin/1 mM ethylenediamine tetraacetic acid (EDTA) and Hanks' balanced salt solution (HBSS) were purchased from Gibco Laboratories (Lenexa, KS, USA). Dimethylsulfoxide (DMSO), ethanol absolute, and acetic acid were obtained from Merck (Darmstadt, Germany).

1.4.2. SH-SY5Y cell culture

Human neuroblastoma SH-SY5Y cells were routinely cultured into 75 cm^3 flasks and maintained in DMEM with 4.5 g/L glucose supplemented with 10 % heat-inactivated FBS (v/v), 1 % MEM NEAA (v/v) and 1% penicillin/streptomycin (v/v). Cells were maintained at 37 °C, in a humidified 5% CO_2–95% air atmosphere, and the culture medium was changed every 2-3 days. The cultures were passaged once a week by trypsinization (0.25 % trypsin/1 mM EDTA). To avoid phenotypic changes, the cells used for all experiments were taken between 19th and 28th passages. Cells were differentiated as described previously by Fernandes *et al*. [8]. Briefly, SH-SY5Y cells were seeded onto 96-well plates at a density of 25,000 cells/cm^2 in cell culture medium with *trans*-retinoic acid (RA) (final concentration of 10 µM) and incubated for 3 days, at 37 °C, in a humidified 5% CO_2–95% air atmosphere. Then, the cell culture medium was removed and replaced with medium supplemented with 12-*O*-tetradecanoylphorbol-13-acetate (TPA) (final concentration 80 nM), and cells were incubated for an additional period of 3 days before being used in the assays. Stock solutions of RA (10 mM) and TPA (80 µM) were prepared in DMSO.

1.4.3. Cytotoxicity assays

1.4.3.1. MTT reduction assay

In the MTT reduction assay, the water-soluble MTT tetrazolium salt is reduced inside viable cells with active metabolism. The resulting purple colored formazan product accumulates as an insoluble precipitate inside the cells. The amount of formazan formed, presumably directly proportional to the number of viable cells, can be quantified spectrophotometrically after solubilization in an organic solvent [9, 10]. Briefly, after the incubation periods with test compounds or the oxidative stressors, the cell culture medium was removed and a solution of MTT 0.5 mg/mL in fresh culture medium was added. Cells were incubated at 37 °C in a humidified, 5% CO_2–95% air atmosphere for 1 h. Then, the cell culture medium was removed, and the formed formazan crystals were dissolved in 100 % DMSO. The absorbance was measured at 550 nm in a multiwell microplate reader (PowerWave XS from BioTek Instruments, Vermont, US). The results were expressed as the percentage of MTT reduction relative to that of the control [MTT reduction (% of control)] ± standard error mean (SEM) of at least three independent experiments.

1.4.3.2. NR uptake assay

The neutral red (NR) uptake assay is based on the ability of viable cells to incorporate the supravital dye NR and retain it inside the lysosomes [11]. NR uptake assay was performed as previously described by Fernandes *et al*. [12] Briefly, after the 24 h incubation periods with the test compounds, the cell culture medium was removed and a solution of NR (50 mg/mL) in fresh cell culture medium was added. Differentiated SH-SY5Y cells were incubated for 1 h at 37 °C in a humidified, 5% CO_2−95% air atmosphere. Then, the cell culture medium was removed and replaced by ethanol absolute/distilled water (1:1) with 5 % acetic acid to liberate the dye from the viable cells. The absorbance was measured at 540 nm in a multiwell microplate reader (PowerWave XS from BioTek Instruments). The results were expressed as the percentage of NR uptake relative to that of the control (non-treated) cells [NR uptake (% of control)] ± standard error mean (SEM) of at least three independent experiments.

1.4.4. Statistical analysis

The data obtained are expressed as mean ± standard error mean (SEM) of at least three independent experiments. All statistical analyses were performed using GraphPad PRISM version 6 for Windows (GraphPad Software®, San Diego, CA, USA). The normality of the data distribution was evaluated using three normality tests: KS normality test, D'Agostino and Pearson omnibus normality test, and Shapiro−Wilk normality test. For data with a parametric distribution, statistical comparisons were carried out by one-way analysis of variance (ANOVA) followed by Dunnet's multiple comparison test. For data with a non-parametric distribution, statistical comparisons were estimated using the nonparametric method of Kruskal–Wallis [one-way ANOVA on ranks] followed by Dunn's *post hoc* test. In all cases, *p* values lower than 0.05 were considered significant.

2. Additional figures

Figure S1: DPPH$^{\bullet}$ kinetic curves of thiophenols **2-6** and phenols **1**, **7-10**.

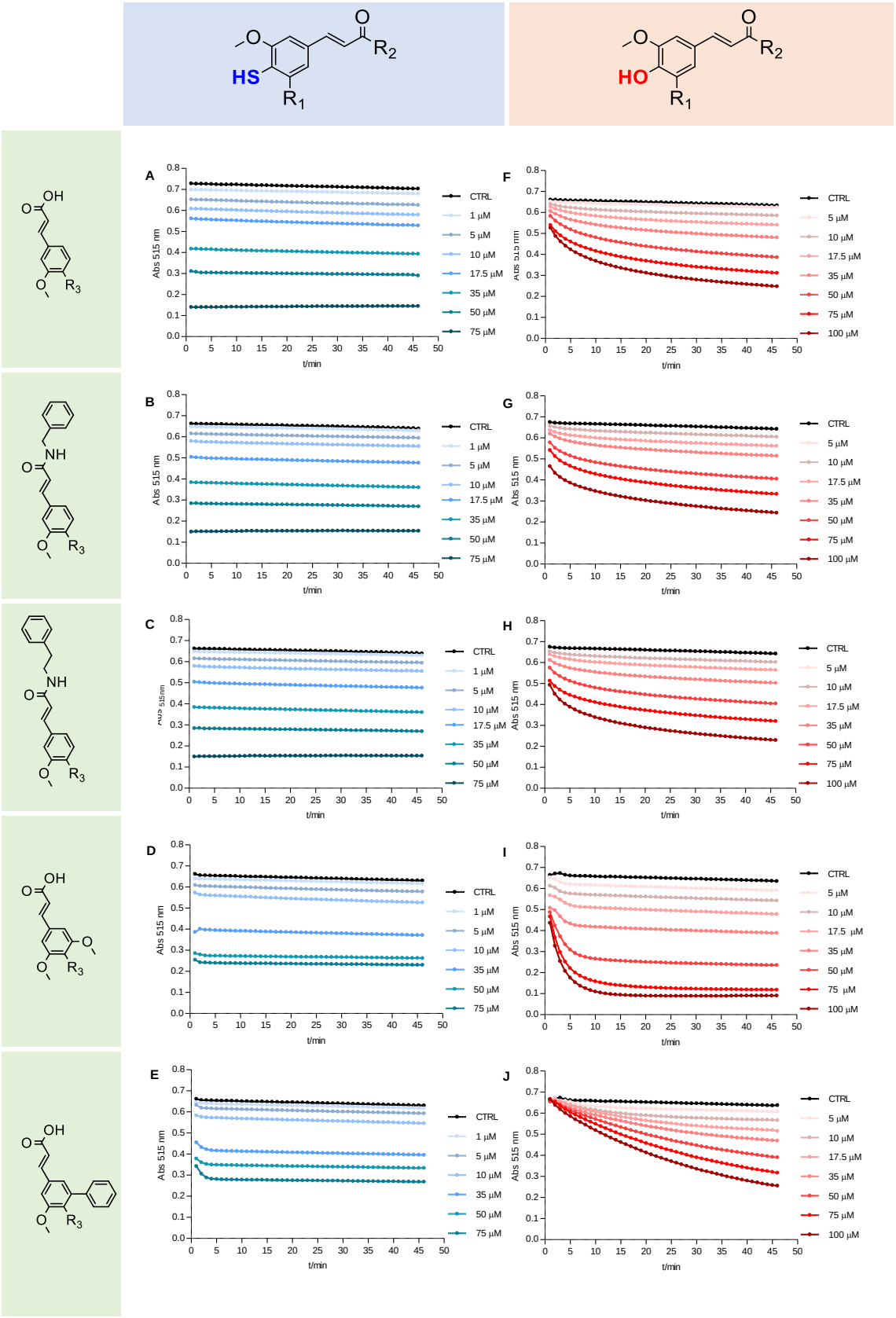


Figure S2: ABTS$^{\bullet+}$ kinetic curves of thiophenols **2-6** and phenols **1**, **7-10**.

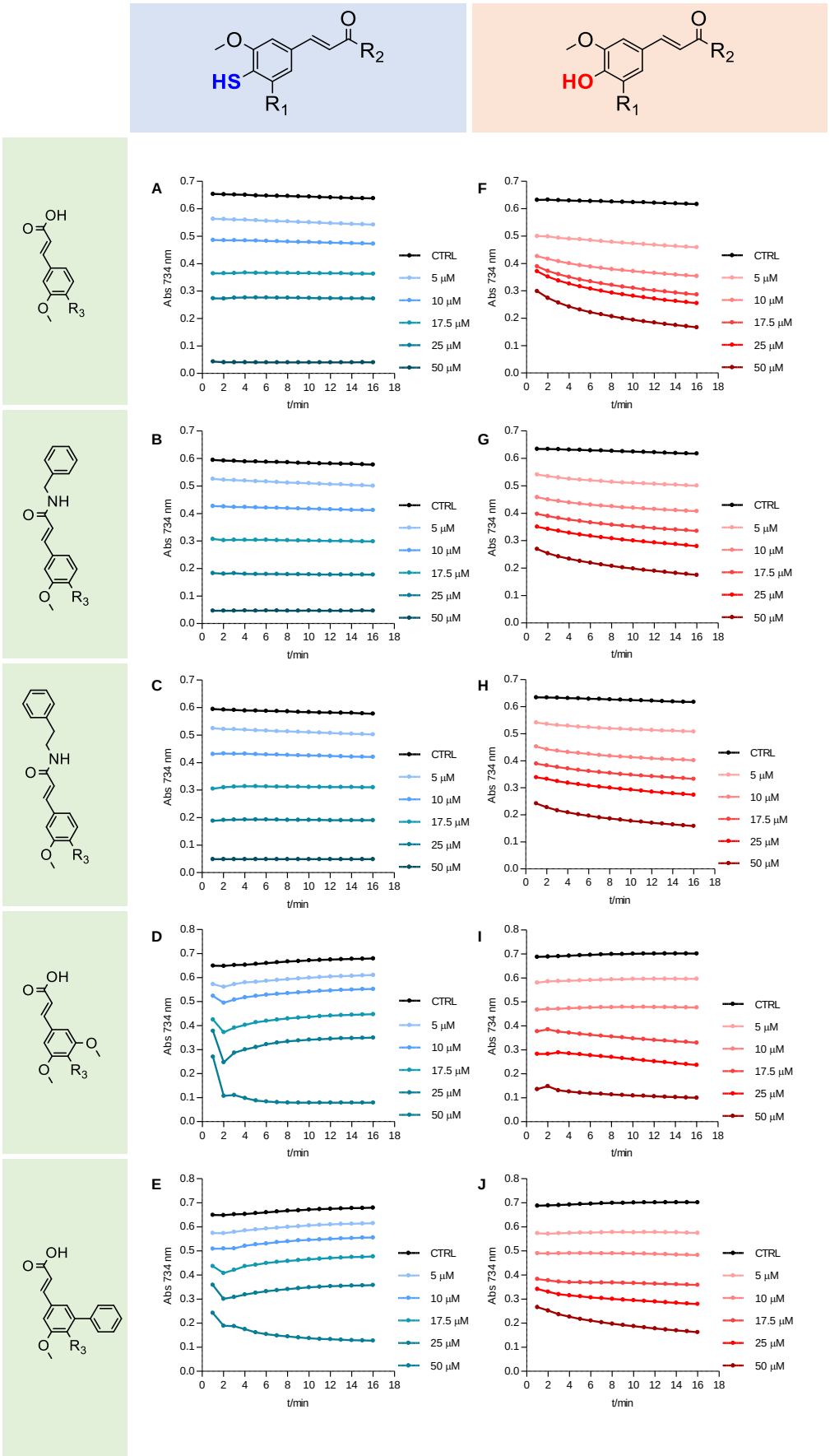
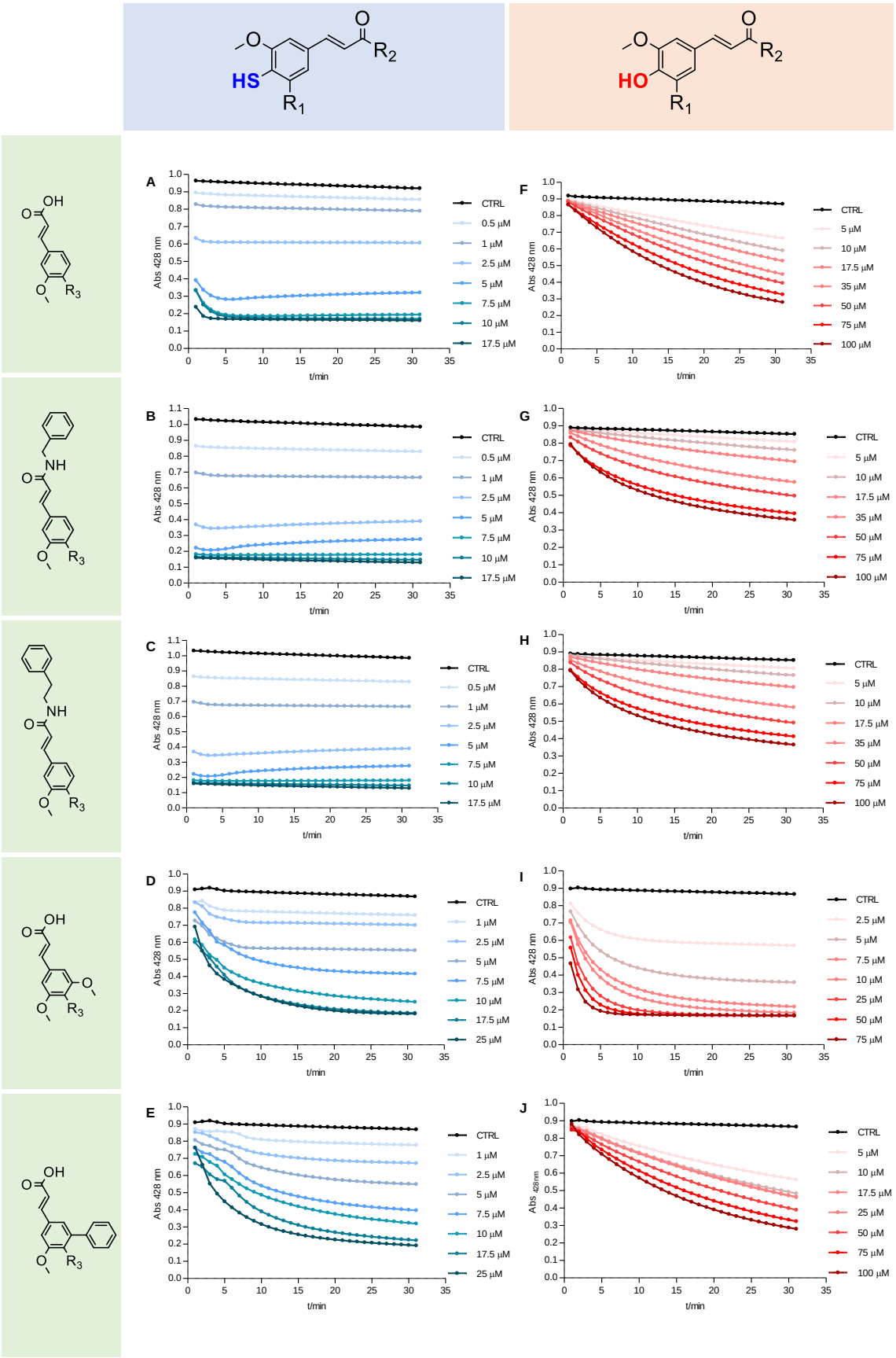


Figure S3: GO• kinetic curves of thiophenols **2-6** and phenols **1**, **7-10**.



3. References

[1] J. Teixeira, T. Silva, S. Benfeito, A. Gaspar, E.M. Garrido, J. Garrido, F. Borges, Exploring nature profits: development of novel and potent lipophilic antioxidants based on galloyl-cinnamic hybrids, Eur. J. Med. Chem., 62 (2013) 289-296. https://doi.org/10.1016/j.ejmech.2012.12.049

[2] A. Tai, T. Sawano, H. Ito, Antioxidative properties of vanillic acid esters in multiple antioxidant assays, Biosci. Biotechnol. Biochem., 76 (2012) 314-318. https://doi.org/10.1271/bbb.110700

[3] J.Y. Feng, Z.Q. Liu, Phenolic and enolic hydroxyl groups in curcumin: which plays the major role in scavenging radicals?, J. Agric. Food Chem., 57 (2009) 11041-11046. https://doi.org/10.1021/jf902244g

[4] Y. Yang, Z.G. Song, Z.Q. Liu, Synthesis and antioxidant capacities of hydroxyl derivatives of cinnamoylphenethylamine in protecting DNA and scavenging radicals, Free Radic. Res., 45 (2011) 445-453. https://doi.org/10.3109/10715762.2010.540576

[5] B. Ou, M. Hampsch-Woodill, R.L. Prior, Development and validation of an improved oxygen radical absorbance capacity assay using fluorescein as the fluorescent probe, J. Agric. Food Chem., 49 (2001) 4619-4626. https://doi.org/10.1021/jf010586o

[6] F. Mura, T. Silva, C. Castro, F. Borges, M.C. Zuniga, J. Morales, C. Olea-Azar, New insights into the antioxidant activity of hydroxycinnamic and hydroxybenzoic systems: spectroscopic, electrochemistry, and cellular studies, Free Radic. Res., 48 (2014) 1473-1484. https://doi.org/10.3109/10715762.2014.965702

[7] J. Garrido, A. Gaspar, E.M. Garrido, R. Miri, M. Tavakkoli, S. Pourali, L. Saso, F. Borges, O. Firuzi, Alkyl esters of hydroxycinnamic acids with improved antioxidant activity and lipophilicity protect PC12 cells against oxidative stress, Biochimie, 94 (2012) 961-967. https://doi.org/10.1016/j.biochi.2011.12.015

[8] C. Fernandes, M. Pinto, C. Martins, M.J. Gomes, B. Sarmento, P.J. Oliveira, F. Remião, F. Borges, Development of a PEGylated-Based Platform for Efficient Delivery of Dietary Antioxidants Across the Blood-Brain Barrier, Bioconjug. Chem., 29 (2018) 1677-1689. https://doi.org/10.1021/acs.bioconjchem.8b00151

[9] L. Belyanskaya, P. Manser, P. Spohn, A. Bruinink, P. Wick, The reliability and limits of the MTT reduction assay for carbon nanotubes-cell interaction, Carbon, 45 (2007) 2643-2648. https://doi.org/10.1016/j.carbon.2007.08.010

[10] J.C. Stockert, A. Blazquez-Castro, M. Canete, R.W. Horobin, A. Villanueva, MTT assay for cell viability: Intracellular localization of the formazan product is in lipid droplets, Acta Histochem., 114 (2012) 785-796. https://doi.org/10.1016/j.acthis.2012.01.006

[11] G. Repetto, A. del Peso, J.L. Zurita, Neutral red uptake assay for the estimation of cell viability/cytotoxicity, Nat. Protoc., 3 (2008) 1125-1131. https://doi.org/10.1038/nprot.2008.75

[12] C. Fernandes, C. Martins, A. Fonseca, R. Nunes, M.J. Matos, R. Silva, J. Garrido, B. Sarmento, F. Remiao, F.J. Otero-Espinar, E. Uriarte, F. Borges, PEGylated PLGA Nanoparticles As a Smart Carrier to Increase the Cellular Uptake of a Coumarin-Based Monoamine Oxidase B Inhibitor, ACS Appl. Mater. Interfaces, 10 (2018) 39557-39569. https://doi.org/10.1021/acsami.8b17224

3.3. Manuscript IV

Boosting caffeic acid performance as antioxidant and monoamine oxidase/catechol-O-methyltransferase inhibitor

To be submitted.

Boosting caffeic acid performance as antioxidant and monoamine oxidase/catechol-O-methyltransferase inhibitor

Daniel Chavarria‡[1,2], Sofia Benfeito‡[1], Tiago Silva[1,2], Cátia Silva[1], Pedro Soares[1], Jorge Garrido[3], Paula Serrão[4,5], Patrício Soares-da-Silva[4,5], Fernando Remião[6], Fernanda Borges[1*]

[1] CIQUP/Department of Chemistry and Biochemistry, Faculty of Sciences, University of Porto, 4169-007 Porto, Portugal

[2] CNC - Center for Neuroscience and Cell Biology, University of Coimbra, UC Biotech Building, Biocant Park, Cantanhede, Portugal.

[3] Department of Chemical Engineering, School of Engineering (ISEP), Polytechnic of Porto, 4200-072 Porto, Portugal.

[4] Department of Pharmacology and Therapeutics, Faculty of Medicine, University of Porto, 4200-319 Porto, Portugal

[5] MedInUP – Center for Drug Discovery and Innovative Medicines, University of Porto, 4200-319, Porto, Portugal

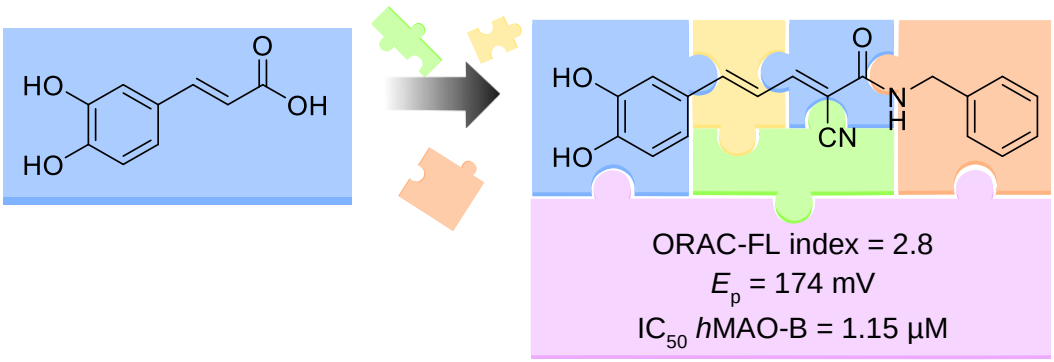
[6] UCIBIO-REQUIMTE, Laboratory of Toxicology, Department of Biological Sciences, Faculty of Pharmacy, University of Porto, Porto, Portugal

‡ These authors contributed equally to this work.

* Corresponding Authors:

Fernanda Borges, CIQUP/Department of Chemistry and Biochemistry, Faculty of Sciences, University of Porto, Porto 4169-007, Portugal. E-mail: fborges@fc.up.pt

Graphical abstract



4. Abstract

Increased oxidative stress and depletion of nigrostriatal dopamine (DA) are closely linked to the neurodegeneration observed in Parkinson's Disease (PD). Accordingly, we designed and developed ten caffeic acid (CA)-based antioxidants and screened the inhibitory activity towards DA-metabolizing enzymes (monoamine oxidases (MAOs) and catechol *O*-methyltransferase (COMT)). Our result show that the incorporation of an extra double bond enhanced the antioxidant properties of CA. α-CN derivatives displayed redox potentials (E_p) similar to CA and significant *h*MAO-B inhibitory activities (1.15-4.55 μM). Compounds **2**, **3**, and **7-11** presented safe cytotoxicity profiles in differentiated SH-SY5Y cells at concentrations up to 10 μM. The formation of reactive species (RS) induced by CA derivatives may be underlying the cytotoxic effects observed at higher concentrations. Compounds **10** and **11** at non-toxic concentrations protected SH-SY5Y cells against the oxidative damage inflicted by *tert*-butyl hydroperoxide (*t*-BHP). Compound **10** is highlighted as the best *h*MAO-B inhibitor with antioxidant activity towards lipophilic radicals and favorable physicochemical properties.

Keywords: Parkinson's disease, caffeic acid, antioxidants, catechol-O-methyltransferase, monoamine oxidase

5. Introduction

Parkinson's disease (PD) is a multifactorial, age-related neurodegenerative disorder characterized by the impairment in motor function [1]. The neuropathogenesis of PD includes the gradual depletion striatal dopamine (DA), associated with the selective and irreversible loss of dopaminergic neurons in the *substantia nigra* [1, 2]. Although the etiology of the disease is far from being completely elucidated, oxidative stress has been strongly correlated with the selective neurodegeneration observed in PD [3-5]. In fact, dopaminergic neurons are particularly prone to oxidative stress [6]. The main source of reactive species (RS) is mitochondria, but they can also be generated through DA autoxidation into DA quinone or DA enzymatic degradation by monoamine oxidases (MAOs, EC 1.4.3.4) [4, 7]. Dopamine (DA) quinone and the product of its intramolecular cyclization (aminochrome) form adducts with proteins such as α-synuclein, induce mitochondrial dysfunction and lead to glutathione depletion [8]. Dopaminergic neurons in *substantia nigra* also accumulate iron, which may act as a catalyst of harmful oxidative reactions [6]. The overproduction of RS together with the low pool of antioxidant defenses leads to oxidative damage in cellular lipids, proteins and nucleic acids (DNA and RNA), thereby inhibiting their normal function [5].

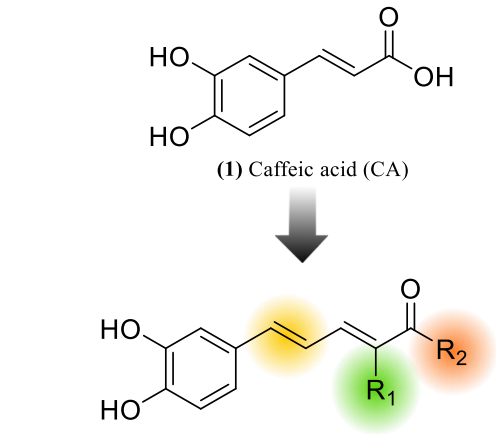
The available antiparkinsonian drugs are used in monotherapy or on combination therapy and offer valuable symptomatic relief, but they are unable to delay or stop the disease progression and lead to significant and severe side effects [9, 10] The management of PD symptoms include the use of drugs that inhibit monoamine oxidase B (MAO-B) and catechol-*O*-methyltransferase (COMT, EC 2.1.1.6), two enzymes involved in DA metabolism [11], as a mean to increase the synaptic levels and the half-life of DA [12].

Monoamine oxidase A (MAO-A) and MAO-B are two isozymes bound to the outer mitochondrial membrane that catalyze the oxidative deamination of DA [13]. Under normal conditions, DA levels are regulated by MAO-A present in pre-synaptic neurons [4, 14]. However, the activity MAO-B located in glial cells increases with age, possibly due to glial cell proliferation associated with neuronal loss [15]. Consequently, MAO-B becomes the main isoform involved in DA catabolism in PD [4]. Selective MAO-B inhibitors used in PD therapy include the irreversible propargylamine-based inhibitors selegiline and rasagiline and, more recently, the reversible inhibitor safinamide [16].

COMT is a magnesium-dependent enzyme that catalyzes the transfer of a methyl group from the cofactor *S*-adenosyl-*L*-methionine (SAM) to one of two hydroxyl groups of DA [17]. COMT inhibitors with clinical relevance (e.g.: tolcapone, entacapone and opicapone) are potent, selective and reversible inhibitors and contain a nitrocatechol pharmacophore [18, 19]. Although they present the same binding motif as the catechol substrates, the presence of the strong electron-withdrawing nitro group at the *ortho* position increases the acidity of the adjacent hydroxyl group, thus hindering the *O*-methylation of the resulting phenolate by delocalization of the negative charge [19, 20]. However, the use of nitrocatechol-based inhibitors in PD therapy is limited because they have been associated with severe hepatotoxicity (tolcapone) and gastrointestinal side effects (entacapone) [21, 22]. In addition, entacapone display a short half-life and thus require frequent administrations [18].

Following our line of research related with the development of multitarget agents based on natural scaffolds, our efforts were focused on the development of molecules based on caffeic acid (3-(3,4-dihydroxyphenyl)-2-propenoic acid, CA, compound **1**, **Figure 1**) with antioxidants and dual MAO-B/COMT inhibitory activities. Caffeic acid (CA) is a natural phenolic acid containing an *o*-diphenol and an α,β-

unsaturated carboxylic acid group, both of which are important for its potent antioxidant activity [23, 24]. In this context, the rationale behind the design of CA derivatives was based on the structural modification of the propenoic acid side chain (compounds **2-11**, **Figure 1**). We incorporated ethylenic and α-cyano groups to increase the electron delocalization throughout the molecule and the acidity of the phenol moiety, which may potentially lead to improved antioxidant and COMT inhibitory activities. In addition, lipophilic amide groups were added to improve the compounds' druglikeness (**Figure 1**). We then evaluated the biological profile of CA derivatives, namely radical scavenging activity, redox potential and inhibition of COMT and MAOs. Finally, the cytotoxicity, the induction of intracellular oxidative stress and the protection against *tert*-butyl hydroperoxide (*t*-BHP)-induced damage were assessed in differentiated SH-SY5Y cells.



(1) Caffeic acid (CA)

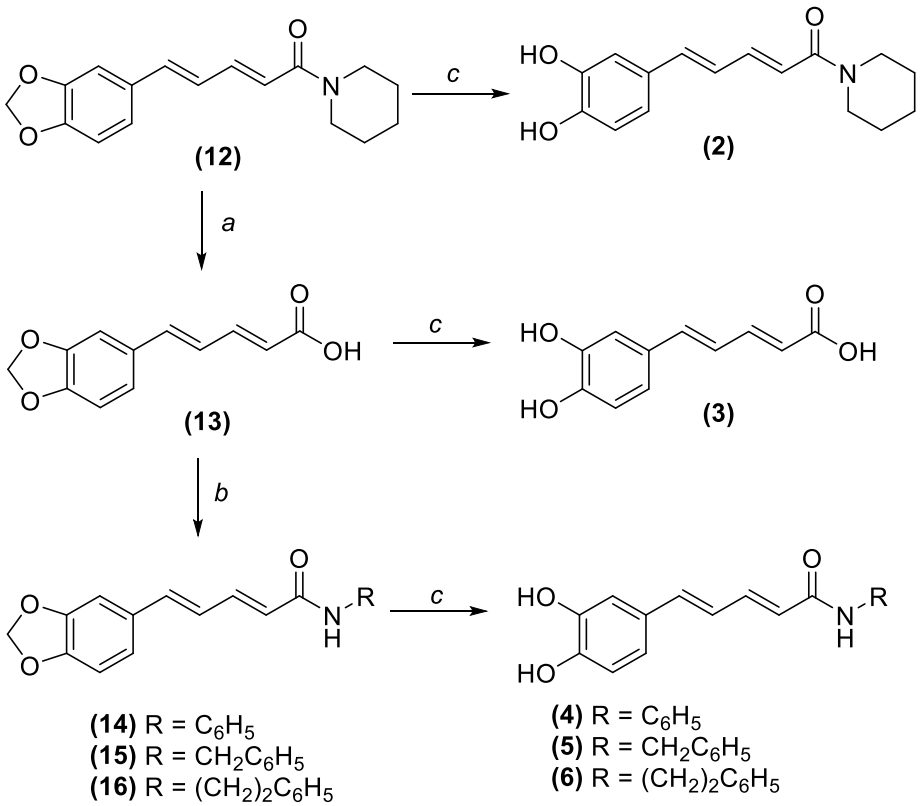
(2) R_1 = H; R_2 = OH
(3) R_1 = H; R_2 = piperidine
(4) R_1 = H; R_2 = NHPh
(5) R_1 = H; R_2 = $NHCH_2Ph$
(6) R_1 = H; R_2 = $NHCH_2CH_2Ph$
(7) R_1 = CN; R_2 = OH
(8) R_1 = CN; R_2 = piperidine
(9) R_1 = CN; R_2 = NHPh
(10) R_1 = CN; R_2 = $NHCH_2Ph$
(11) R_1 = CN; R_2 = $NHCH_2CH_2Ph$

Figure 1. Rational design of new chemical entities based on CA (compound **1**) scaffold.

6. Results and discussion

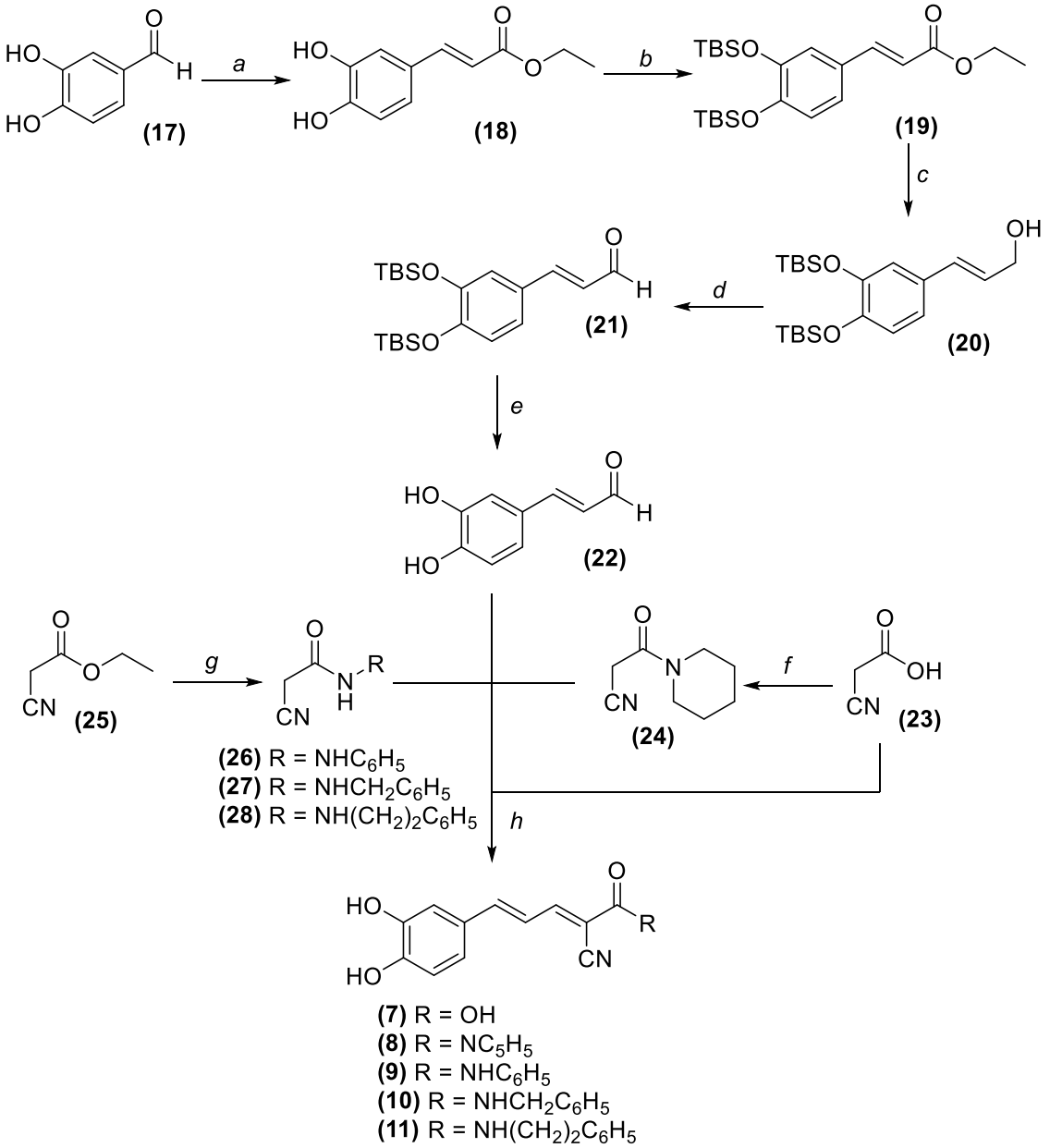
6.1. Chemistry

To obtain CA derivatives **2-6**, we first performed the alkaline hydrolysis of piperine (compound **12**) to obtain piperic acid (compound **13**) (**Scheme 1**, step *a*), which in turn was used in benzotriazol-1-yl-oxytripyrrolidinophosphonium hexafluorophosphate PyBOP-assisted amidation reactions under alkaline medium to yield piperic acid amides **14-16** (**Scheme 1**, step *b*). Then, the demethylenation of compounds **14-16** with BBr_3 afforded the catechols **2-6** (**Scheme 1**, step *c*).



Scheme 1. Synthetic strategy pursued to obtain CA derivatives **2-6**. (a) Methanolic solution of NaOH 2 M, reflux, 24 h; (b) 1. DMF, DIPEA, PyBOP, CH_2Cl_2, 0 ºC, 30 min; 2. Amine (aniline, benzylamine or 2-phenylethylamine), rt, overnight; (c) anhydrous CH_2Cl_2, BBr_3 1 M, -78 ºC to rt, overnight.

The preparation of α-cyano derivatives **7-11** involved a more complex synthetic pathway (**Scheme 2**). The synthesis started with a Knoevenagel-Doebner condensation between 3,4-dihydroxybenzaldehyde (compound **16**) and monoethyl malonate to obtain cinnamic ester **17 (Scheme 2,** step *a*)**.** Then, the catechol group of compound **17** was protected with *tert*-butyldimethylsilyl chloride (TBSCl) (compound **18**, **Scheme 2,** step *b*) before the reduction of the ester group into the corresponding primary alcohol (compound **19**, **Scheme 3,** step *c*) and subsequent oxidation into the aldehyde **20** (**Scheme 2,** step *d*). The protecting groups were then removed by a fluoride ion-catalyzed hydrolysis (**Scheme 2,** step *e*) to yield caffeic aldehyde (compound **21**). Cyanoacetic acid amides were prepared by a PyBOP-mediated amidation of cyanoacetic acid (compound **22**) with piperidine to yield compound **23** (**Scheme 2,** step *f*) or, alternatively, by heating ethyl cyanoacetate (compound **24**) with aniline, benzylamine or (2-bromoethyl)benzene to obtain compounds **25-27** (**Scheme 2,** step *g*). Finally, the Knoevenagel condensation between caffeic aldehyde and cyanoacetamides **22**, **23, 25-27** yielded compounds **7-11** (**Scheme 2,** step *h*).



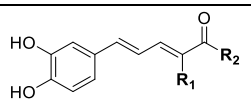
Scheme 2. Synthetic strategy pursued to obtain α-CN CA derivatives **7**-**11**. (a) mono-ethyl malonate, pyridine, piperidine, 70 ºC, 9 h; (b) TBSCl, imidazole, DMF, 50 ºC, 30 min; (c) 1. Argon atmosphere, -78 ºC, 30 min; 2. dry THF, $LiAlH_4$, -78 ºC to rt, 5 h; (d) MnO_2, CH_2Cl_2, rt, overnight; (e) TBAF, dry THF, 50 ºC, 30 min; (f) 1. DMF, DIPEA, PyBOP, CH_2Cl_2, 0 ºC, 30 min; 2. piperidine, rt, overnight; (g) ethyl cyanoacetate, amine (aniline, benzylamine or (2-bromoethyl)benzene), 100 ºC, 9 h; (h) activated methylene (compounds **23**, **24**, **29**-**31**) pyridine, piperidine, 60 ºC, 45 min.

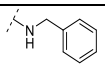
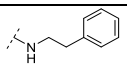
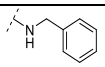
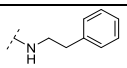
6.2. Monoamine oxidase inhibition studies

We screened the inhibitory activity of catechols **2-11** towards *h*MAOs by spectrophotometry using kynuramine as substrate and recombinant *h*MAO-A and -B isoforms [25, 26]. The *h*MAO-A and *h*MAO-B inhibitory potency (IC_{50}) and selectivity (SI) data of compounds **2-11** and standard inhibitors (clorgyline for *h*MAO-A and (*R*)-(−)-deprenyl, rasagiline, safinamide for *h*MAO-B) are presented in **Table 1**. Compound **3** and α-CN derivatives **8-11** presented modest *h*MAO-B inhibition properties, displaying IC_{50} values within the low micromolar range. These results indicate that the *h*MAO-B inhibition is enhanced with the presence of an

α-CN group. The α-CN benzyl amide derivative **10** stood out as the best *h*MAO-B inhibitor, showing the lowest IC_{50} value and the highest *h*MAO-B selectivity index (compound **10:** IC_{50} = 1.15 μM; SI = 9).

Table 2. Evaluation of *h*MAO and rat liver and brain COMT inhibitory activities of compounds **1-11** and reference inhibitors.



Compound	R_1	R_2	IC_{50}/μM		SI[b]	IC_{50}/μM	
			*h*MAO-A	*h*MAO-B		Rat liver COMT	Rat brain COMT
1	___	___	___[a]	___[a]	__	5.861[e]	0.0982[e]
2	H		___[a]	___[a]	__	___[d]	___[g]
3	H		___[a]	2.50±0.22	4[c]	___[d]	___[g]
4	H		___[a]	___[a]	__	___[d]	___[g]
5	H		___[a]	___[a]	__	___[d]	___[g]
6	H		___[a]	___[a]	__	___[d]	___[g]
7	CN		___[a]	___[a]	__	___[d]	___[g]
8	CN		___[a]	4.27±0.30	2[c]	___[d]	___[g]
9	CN		___[a]	4.55±0.31	2[c]	___[d]	___[g]
10	CN		___[a]	1.15±0.04	9[c]	___[d]	___[g]
11	CN		___[a]	4.38±0.51	2[c]	___[d]	___[g]
R-(-)-Deprenyl [25]			20.1±1.9	0.0386±0.0043	522	n.d.	n.d.
Rasagiline			3.65±0.31	147.3±249	24	n.d.	n.d.
Safinamide			___[a]	0.0231±0.0026	433[c]	n.d.	n.d.
Clorgyline [25]			0.00274±0.00047	2.21±0.26	0.00124	n.d.	n.d.
Tolcapone			n.d.	n.d.	n.d.	0.0306±0.008[f]	0.00091±0.00017[f]

[a] Inactive at 10 μM;
[b] SI (1): *h*MAO-B selectivity index = IC_{50}(*h*MAO-A)/IC_{50}(*h*MAO-B).
[c] Values obtained under the assumption that the corresponding IC_{50} against *h*MAO-A or *h*MAO-B is the highest concentration tested (10 μM).
[d] Inactive at 30 μM;
[e] Data from Silva *et al.* [27]
[f] in acquisition.
n.d.: not determined

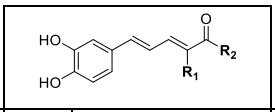
6.3. Catechol *O*-methyltransferase inhibition studies

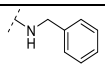
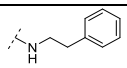
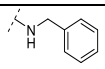
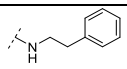
The inhibitory activity of compounds **1-11** towards COMT was also assessed in rat liver and brain homogenates. Preliminary results showed that CA derivatives **12-21** were potent brain COMT inhibitors. The data acquired so far is being confirmed by other assays and will be patented.

6.4. Antioxidant activity

We assessed the antioxidant activity of compounds **1-11** using the oxygen radical capacity (ORAC-FL) assay. This assay is based on the ability of an antioxidant to prevent the oxidation of fluorescein, a fluorescent probe, into a non-fluorescent product by peroxyl radicals ($ROO^{\bullet}$). The results, expressed as ORAC-FL indexes, are presented in **Table 2**. The ORAC-FL index of compound **2** was higher than that of CA indicating a higher $ROO^{\bullet}$ radical scavenging by the former. On the other hand, the introduction of an α-CN group in the conjugated dienone system (compound **7**) reduced the ORAC-FL indexes to a value close to CA. The results obtained with the free carboxylic acids (compounds **2** and **7**) and the corresponding amides (compounds **3-6** and **8-11**) showed that the ORAC-FL indexes also decreased with the increase of the number of carbons at the amide portion. Overall, we can conclude that the $ROO^{\bullet}$ radical scavenging was favored by the insertion of an ethylenic group, and impaired by the introduction of an α-cyano group and by the increased lipophilicity.

Table 3. Evaluation of ORAC-FL indexes and redox potentials of compounds **1-11.**



Compound	R_1	R_2	ORAC-FL index	E_p/mV
1	—	—	4.8±0.2	168[a]
2	H		5.5±0.1	129
3	H		4.3±0.3	113
4	H		4.1±0.2	114
5	H		4.0±0.2	129
6	H		3.3±0.3	124
7	CN		4.9±0.1	144
8	CN		3.5±0.2	154
9	CN		3.5±0.1	161
10	CN		2.8±0.2	174
11	CN		3.0±0.1	163

6.5. Electrochemical studies

The oxidative behavior of CA (compound **1**) and derivatives thereof **2-11** was then evaluated by differential pulse voltammetry (DPV) and cyclic voltammetry (CV). The electrochemical evaluation was conducted at physiological pH 7.4 using a glassy carbon working electrode. The results are depicted in **Table 2** and **Figure 2**.

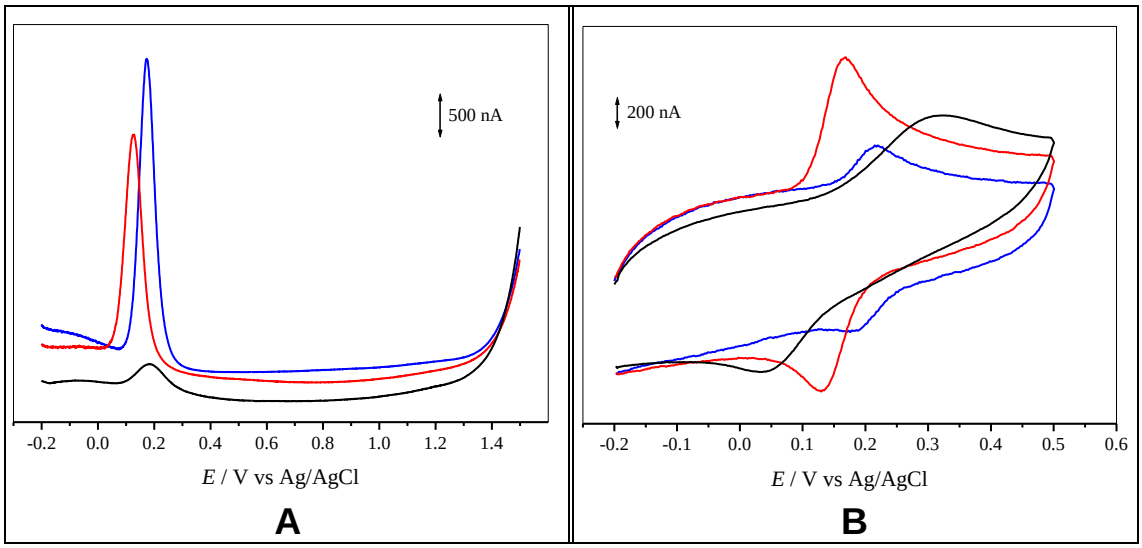


Figure 2: Representative voltammograms of CA and compounds **5** and **10**. (left) Differential pulse and (right) cyclic voltammograms for a 0.1 mM solutions of (—) CA, (—) compound **5** and (—) compound **10** in physiological pH 7.4 supporting electrolyte. Scan rate: 5 mV s^{-1} (DPV) and 50 mV s^{-1} (CV).

In DPV experiments, compounds **1-11** exhibited well-defined anodic waves at physiological pH, which may be assigned to the oxidation of the catechol moiety (**Figure 2A**). The oxidation potentials (E_p) of compounds **2-6** were lower than the obtained for CA and varied between 113 and 129 mV (**Table 2**). This decrease may arise from the higher stabilization of the radicals formed, as a result of the increased electron delocalization provided by the additional double bond [28]. On the other hand, α-CN derivatives **7-11** presented higher E_p values than compounds **2-6** and similar to CA, ranging between 144 and 174 mV (**Table 2**). These results indicate that the α-CN group decreased the compounds' reducing capacity, thus being in line with the tendency observed in ORAC-FL assay. Finally, amides **3-6** and **8-11** displayed similar E_p values to the parent carboxylic acids (compounds **2** and **7**, respectively), suggesting that the redox properties were maintained with the increased lipophilicity.

Linear correlations were found between the E_p values of CA derivatives with the ORAC-FL indexes, both obtained in phosphate buffer pH 7.4 (**Figure 3**). After gathering the compound into carboxylic acids and amides, it was observed a decrease of ORAC-FL indexes with the increase of E_p values. Indeed, compounds with low E_p values are more prone for electron donation and thus have higher antioxidant activity [29]. The tendency observed was also reported by Silva *et al.* [30].

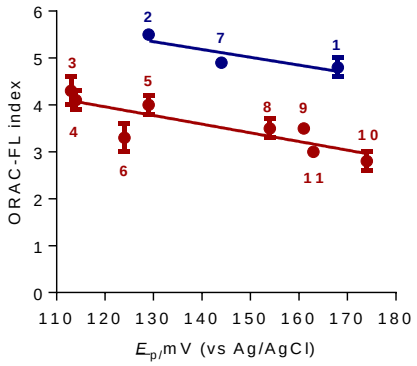


Figure 3. Correlation between ORAC-FL indexes and the oxidation potentials of compounds **1-11.**

Cyclic voltammograms of compounds **1-11** showed one anodic wave and one cathodic wave in the forward and in the reverse scans, respectively (**Figure 2B**), which are characteristic of reversible electrochemical reactions. Therefore, the modifications performed in the CA scaffold preserved its oxidative behavior. The results obtained were in line with the oxidative behavior of CA derivatives documented in previous reports [28, 31].

6.6. Cellular studies

6.6.1. Evaluation of cytotoxicity profile

The cytotoxicity of compounds **3** and **8-11** was assessed in differentiated human neuroblastoma (SH-SY5Y) cells after incubation with two concentrations (10 and 50 µM) for 24 h. These compounds were chosen due to their dual antioxidant and *h*MAO-B inhibitory activities (**Tables 1** and **2**). Despite the absence of *h*MAO-B inhibition, CA (compound **1**) and compounds **2** and **7** were also tested to study the effect of carboxylic acid in the cytotoxicity profile. Cellular viability was evaluated using the resazurin reduction assay and the neutral red (NR) uptake assay. The results, presented as mean resazurin fluorescence (% of control) ± SEM and NR uptake (% of control) ± SEM (n = 3), are depicted in **Figure 4**.

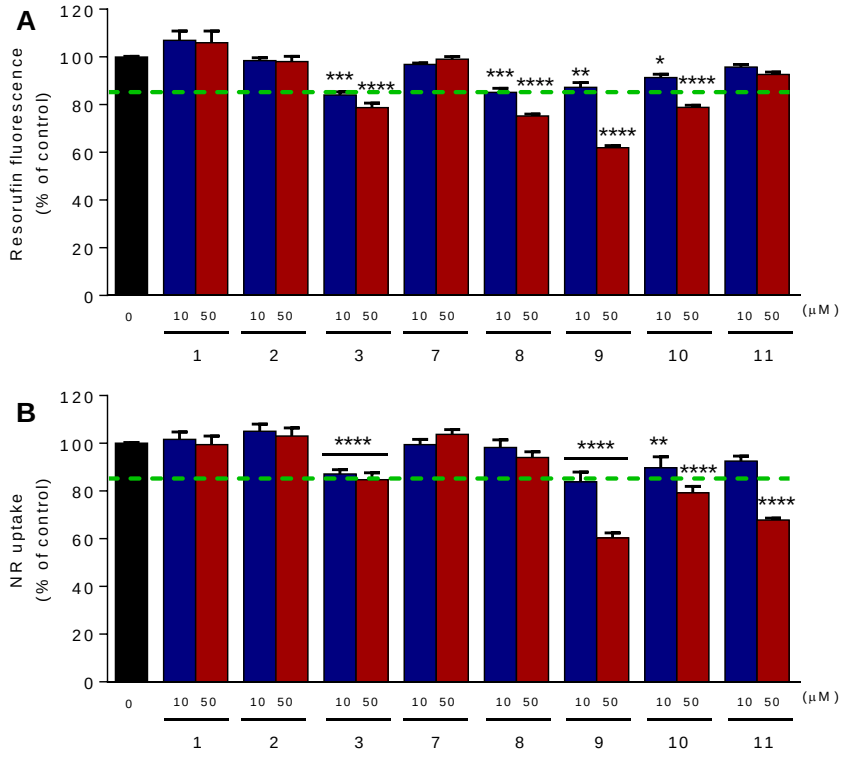


Figure 4. Cellular viability of differentiated SH-SY5Y cells after incubation with CA (compound **1**) and compounds **2**, **3**, **7-11** at two concentrations (10 and 50 µM) for 24 h. Cellular viability was evaluated by measuring metabolic (**A**) and lysosomal activities (**B**) using the resazurin reduction assay and the NR uptake assay, respectively. Statistical comparisons were made using one-way ANOVA followed by Kruskal-Wallis test or followed by Dunnet's multiple comparison test in experiments (A) and (B), respectively. In all cases, *p* values lower than 0.05 were considered significant (* $p < 0.05$, ** $p < 0.01$, *** $p < 0.001$; **** $p < 0.0001$).

Differentiated SH-SY5Y cells incubated with carboxylic acids **1**, **2** and **7** showed percentages of resorufin fluorescence similar to non-treated cells (**Figure 4A**). Treatment of neuroblastoma cells with compounds **3** (10 µM), **8-10 (**10 µM) and **11** (10 and 50 µM) did not markedly decrease the resazurin reduction (% resazurin reduction was > 85 %) (**Figure 4A**). However, significant decreases in resazurin reduction were observed after treatment with catechol amides **3**, **8-10** at 50 µM ($p < 0.0001$, **Figure 4A**).

The results obtained in NR assay (**Figure 4B**) showed that carboxylic acids **1, 2** and **7** and α-cyano piperidinyl amide **8** did not influence the internalization of NR dye by neuroblastoma cells. On the other hand, α-cyano phenyl amide **9** caused significant reductions in NR uptake at the tested concentrations ($p < 0.0001$, **Figure 4B**). Compounds **3**, **10** and **11** did not markedly decrease NR uptake at 10 µM but displayed moderate lysosomal toxicity at 50 µM ($p < 0.0001$, **Figure 4B**).

Taken these data together, the results indicate that CA and the carboxylic acids **2** and **7** present a safe cytotoxicity profile at concentrations up to 50 µM. Catechol amides **3**, **8-11** were well-tolerated at concentrations up to 10 µM, but they may present moderate cytotoxicity at higher concentrations.

6.6.2. Evaluation of intracellular oxidative stress

The reversible oxidation of compounds **1-11** observed in CV experiments suggested that these compounds can participate in redox cycling, a process where a molecule is continually reduced and oxidized. Catechols may be oxidized into the corresponding *ortho*-quinones, which in turn generate reactive species (RS) in the presence of oxygen and biological reducing agents [32, 33]. Quinones also lead to covalent modifications of biomolecules (proteins, DNA, glutathione) through Michael addition [32, 33]. Thus, we hypothesized whether the toxicity observed in differentiated SH-SY5Y cells at the highest concentrations resulted from the increased formation of RS. The 2',7'-dichlorofluorescein (DCF) fluorescence assay was used to measure the intracellular RS production after exposing differentiated neuroblastoma cells to the compounds under study at two different concentrations (10 and 50 μM) for 24 h. The results are expressed as DCF fluorescence (% of control)±SEM (n = 3) and are depicted in **Figure 5A**.

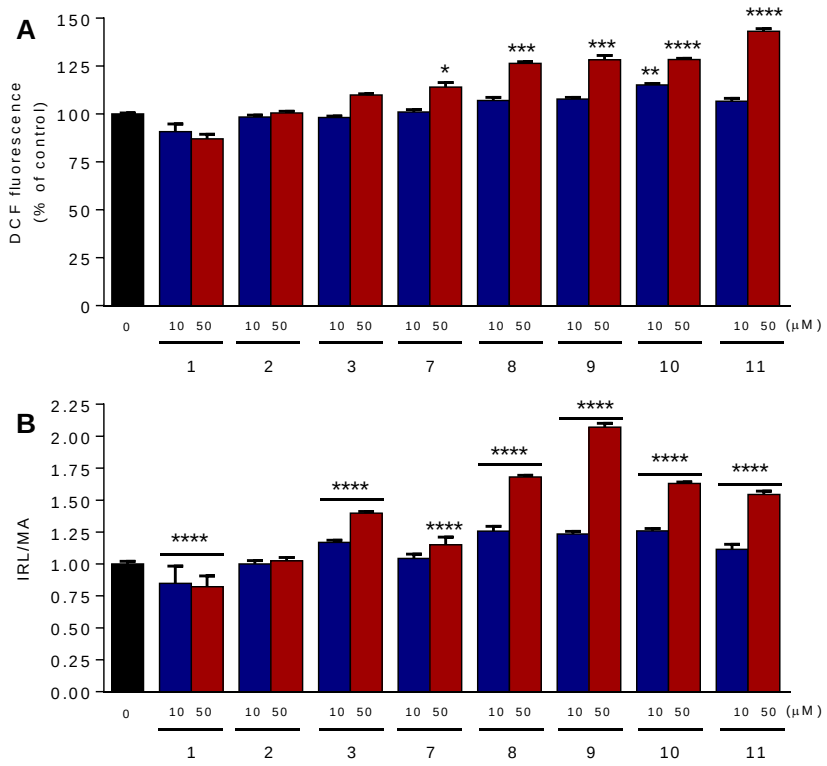


Figure 5. (**A**) Evaluation of intracellular oxidative stress levels in differentiated SH-SY5Y cells using the DCF fluorescence assay, after treatment with compounds 1-3 and 7-11 at 10 and 50 μM for 24 h. The results are expressed as DCF fluorescence (% of control) ± SEM (n = 3). Statistical comparisons were performed using the nonparametric method of Kruskal–Wallis (one-way ANOVA on ranks), followed by Dunn's *post hoc* test. (**B**) Ratio between intracellular RS levels and metabolic activity (IRL/MA) at 10 μM and 50 μM. Statistical comparisons were performed using the parametric method of one-way ANOVA, followed by the Dunnett's multiple comparisons test. In all cases, p values lower than 0.05 were considered significant (* $p < 0.05$, ** $p < 0.01$, *** $p < 0.001$, **** $p < 0.0001$ vs untreated cells).

In general, higher DCF fluorescence values were obtained after treatment of SH-SY5Y cells with α-CN derivatives (compound **7-11**) when compared with non-substituted compounds (compounds **1-3**) (Figure **5A**). In fact, compounds **7-11** (50 μM) showed significant increases in DCF fluorescence at 50 μM, ranging between 114 and 143 % (**Figure 5A**).

The ratio between intracellular RS levels and metabolic activity (IRL/MA) was also calculated to normalize the intracellular RS levels with the number of viable cells (**Figure 5B**). With the exception of CA and compound **2**, all compounds at 50 µM displayed IRL/MA ratios significantly higher than non-treated cells. Compound **3**, **8**, **9** and **10** at 50 µM displayed IRL/MA ratios ranging between 1.4 and 2.1 ($p < 0.0001$, **Figure 5B**), because a reduced number of living cells treated with these derivatives produced a higher amount of RS than non-treated cells. Therefore, the mechanism underlying the toxic effects observed at 50 µM may involve the formation of *ortho*-quinones and the intracellular formation of RS in redox cycling processes.

On the other hand, treatments with compounds **9** and **10** (10 µM) and compound **11** (10 and 50 µM) showed significant increases in IRL/MA ratios ($p < 0.0001$, **Figure 5B**), although the resazurin reduction was preserved in comparison to non-treated cells (**Figure 4A**). This apparent contradictory data may be associated with a hormetic-like effect already reported for catecholic systems, in which the mild increase in RS levels leads to the activation of cytoprotective pathways in detriment of an oxidative status [34].

6.6.3. Protection against *t*-BHP-induced oxidative stress

Considering the results obtained in the antioxidant, *h*MAO inhibition and cytotoxicity studies, we selected compounds **10** and **11** as the most promising CA derivatives. Indeed, α-CN benzyl amide **10** was the most potent *h*MAO-B inhibitor and did not display cytotoxic effects at 10 µM; compound **11** presented the safest cytotoxicity profile among the tested amides and showed moderate *h*MAO-B inhibitory activity.

Therefore, we decided to evaluate the antioxidant profile of CA derivatives **10** and **11** in differentiated SH-SY5Y cells. The corresponding α-CN carboxylic acid (compound **7**) was also included to assess whether the carboxylic acid amidation influences the antioxidant efficiency of catechols. In this study, *t*-BHP was used as an inducer of oxidative stress. *Tert*-butyl hydroperoxide (*t*-BHP), a membrane-permeable organic hydroperoxide, accelerates lipid peroxidation and decreases intracellular glutathione levels after its decomposition into *tert*-butoxyl radicals [35, 36]. Following the cell exposure of neuroblastoma cells to the test compounds at a non-toxic concentration (10 µM) for 30 min, *t*-BHP (200 µM) was added and cells were incubated for additional 24 h. Cellular viability was estimated using the resazurin reduction assay.

As shown in **Figure 6**, *t*-BHP at 200 µM decreased resazurin reduction to 41.8 ± 6.2 % ($p < 0.0001$). Carboxylic acid **7** was unable to prevent the *t*-BHP-mediated decrease of resorufin fluorescence (**Figure 6**). Indeed, the ionization of the carboxylic acid may decrease the compounds' ability to cross the cell membranes by passive diffusion, which may explain the absence of cytotoxic effects and radical scavenging activity in differentiated SH-SY5Y cells. On the other hand, cells pre-treated with α-CN catechol amides **10** and **11** displayed resorufin fluorescence values significantly higher than that of the *t*-BHP treatment alone ($p < 0.0001$, **Figure 6**) and similar to that of non-treated cells. Overall, the results obtained pointed out that compounds **10** and **11** display remarkable antioxidant properties, protecting neuroblastoma cells against oxidative damage.

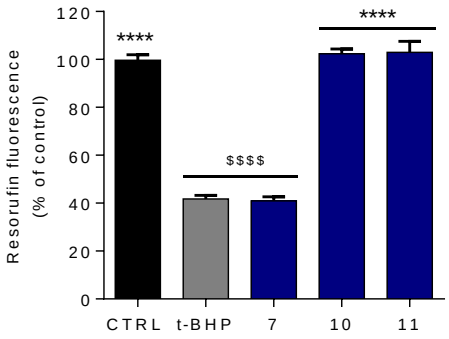


Figure 6. Neuroprotection against *t*-BHP-induced damage in differentiated SH-SY5Y cells by α-CN derivatives **7**, **10** and **11**. After a pre-treatment with the test compounds (10 μM) for 30 min, cells were exposed to *t*-BHP 200 μM for additional 24 h. Cellular viability was evaluated by the resazurin reduction assay. Results are expressed as the mean % of untreated controls ± SEM ($n = 3$). Statistical comparisons were performed using the one-way ANOVA followed by Dunnet's multiple comparison test. In all cases, p values lower than 0.05 were considered significant (**** $p < 0.0001$, compared with *t*-BHP; $^{\$\$\$\$}$ $p < 0.0001$, compared with non-treated cells).

6.7. Estimation of drug-like properties

To characterize the drug-like properties of the most promising CA derivatives (compounds **10** and **11**), we first determined the chromatographic hydrophobicity index (CHI) based on the retention times observed in a fast gradient reverse-phase HPLC (**Table 3**). Chromatographic hydrophobicity index (CHI) values of neutral molecules are directly correlated with the compounds' lipophilicity [37]. To evaluate the effect of the different structural modifications (presence of ethylenic and α-CN groups, carboxylic acid amidation) in the compounds' lipophilicity, CA **(**compound **1**) and compounds **2** and **7** were also tested. The determination of CHI values was carried out using acidic conditions (pH 2.3) to prevent the ionization of the catechol group.

The results presented in **Table 3** showed that the CHI values at pH 2.3 varied between 30.4 and 63.8. Caffeic acid (CA, compound **1**) displayed the lowest CHI value at pH 2.3, followed by compounds **2**, **7**, **10** and **11**. These results suggest that the compounds lipophilicity was increased with the incorporation of ethylenic (CA vs compound **2**) and α-CN groups (compound **2** vs compound **7**) and with the functionalization of the carboxylic acid with amide groups (compound **7** vs compounds **10** and **11**).

Table 4. Retention times (t_R) obtained by LC/UV at pH 2.3 and calculated CHI parameters of CA (compound **1**) and compounds **2**, **7**, **10** and **11**.

Compound	t_R/min	CHI pH 2.3
1	7.84	30.4
2	8.25	37.1
7	8.43	40.0
10	9.68	60.3
11	9.89	63.8

We also calculated several physicochemical properties including topological polar surface area (TPSA in Å), number of hydrogen acceptors (HBA), number of hydrogen donors (HBD) and number of rotatable bonds (RB) (**Table 4**). The predicted parameters of compounds **7** and **10** were in accordance or close to the suggested limits for drugs active in the central nervous system (CNS) (**Table 4**). The permeability across the blood-brain barrier (BBB) can be described by the logarithm of the ratio of the concentration of the compound in the brain and in the blood (logBB). Compound with logBB < -1 are poorly distributed in the brain [38]. The predicted values of logBB of CA derivatives **10** and **11** were higher than -1 (**Table 4**), suggesting that these compounds may have access to the CNS.

Table 5. Predicted drug-like properties of CA (compound **1**) and compounds **2, 7, 10** and **11.**

Compound	MW[a]	TPSA[a]	HBA[a]	HBD[a]	RB[a]	logBB[a]
1	180.2	77.76	4	3	3	-0.9155
2	206.2	77.76	4	3	3	-0.7507
7	231.2	101.55	5	3	3	-1.091
10	320.4	93.35	5	3	6	-0.8517
11	334.38	93.35	5	3	8	-0.8520
CNS^+ drugs	< 500[39]	< 90[39]	< 7[40]	< 3[40]	< 8[40]	≥ -1 [41]

[a] Properties predicted using the Stardrop software. MW: molecular weight; TPSA: topological polar surface area; HBA: number of H-bond acceptor atoms; HBD: number of H-bond donor atoms; RB: number of rotatable bonds; logBB: logarithm of the ratio of the concentration of a drug in the brain and in the blood.

7. Conclusion

In this work, we explored several modifications of the propenoic acid group of CA and evaluated their effect on the antioxidant activity and on the inhibition of *h*MAOs and COMT. In ORAC-FL assays and in cellular assays with *t*-BHP, CA derivatives clearly showed remarkable radical scavenging activity against lipophilic radicals, suggesting that they may prevent the propagation of lipid peroxidation cascades. The ORAC-FL indexes and the E_p values obtained by DPV indicated that the elongation of the diene tether enhanced the antioxidant properties of CA. α-CN derivatives presented lower antioxidant activity than the non-substituted analogues but displayed significant *h*MAO-B inhibitory properties. Cytotoxicity studies in differentiated SH-SY5Y cells pointed out that CA derivatives **2**, **3, 7-11** were well-tolerated at concentrations up to 10 µM. The moderate toxicity observed at higher concentrations may result from the formation of RS in redox cycles, associated to the reversible oxidation of catechols into *ortho*-quinones. However, despite the toxicity observed at 50 µM, it is important to highlight that both antioxidant and *h*MAO-B inhibitory activities were observed at non-toxic concentrations. Compounds **10** and **11** were predicted to have suitable physicochemical properties to attain the CNS. Compound **10** stands out as the best *h*MAO-B inhibitor with remarkable radical scavenging activity and favorable physicochemical properties. Overall, these findings represent an advance toward the development of new antiparkinsonian agents targeting oxidative stress and DA metabolism.

8. Experimental section

8.1. Synthesis of caffeic acid derivatives

8.1.1. Synthesis of (*2E,4E*)-5-(benzo[*d*][1,3]dioxol-5-yl)penta-2,4-dienoic acid (13). Synthesis and structural analysis described in literature [25].

8.1.2. General procedures for the synthesis of amides

8.1.2.1. Method A (PyBOP-mediated amidation). In a 100 mL round bottom flask, piperic acid **13** or cyanoacetic acid **23** (1 mmol) were dissolved in DMF and DIPEA (1.01 mmol). The mixture was cooled at 0 ºC on an ice bath, and a solution of PyBOP (1.01 mmol) in dichloromethane was slowly added. The mixture was stirred for 30 minutes, and the appropriate amine (aniline, benzylamine, (2-bromoethyl)benzene or piperidine, 1.01 mmol) was added. The mixture was stirred overnight at room temperature. Purification conditions are described in literature [25, 42].

(*2E,4E*)-5-(benzo[*d*][1,3]dioxol-5-yl)-N-phenylpenta-2,4-dienamide (14). Synthesis and structural analysis described in literature [25].

(*2E,4E*)-5-(benzo[*d*][1,3]dioxol-5-yl)-N-benzylpenta-2,4-dienamide (15). Synthesis and structural analysis described in literature [25].

(*2E,4E*)-5-(benzo[*d*][1,3]dioxol-5-yl)-N-phenethylpenta-2,4-dienamide (16). η = 82 %. ^{1}H NMR (400 MHz, $CDCl_3$-d_1)*:* δ (ppm) = 2.87 (*t, J* = 6.9 Hz, 2H, $NHCH_2C\underline{H}_2Ph$), 3.62 (*m*, 2H, $NHC\underline{H}_2CH_2Ph$), 5.54 (*t, J* = 5.4 Hz, 1H, N<u>H</u>), 5.84 (*d, J* = 14.9 Hz, 1H, Hα), 5.97 (*s*, 2H, $OC\underline{H}_2O$), 6.65 (*dd, J* = 11.0 Hz, 15.2 Hz, 1H, Hγ), 6.76 (*m, 2*H, H5, Hδ), 6.88 (*dd, J* = 1.6 Hz, 8.1 Hz, 1H, H6), 6.90 (*d, J* = 1.6 Hz, 1H, H2), 7.23 (*m*, 3H, H3', H4', H5'), 7.33 (*m*, 3H, H2', H6', Hβ). ^{13}C NMR (100 MHz, $CDCl_3$-d_1)*:* δ (ppm) = <u>37.7</u> ($NHCH_2\underline{C}H_2Ph$), <u>40.7</u> ($NH\underline{C}H_2CH_2Ph$), <u>101.3</u> ($O\underline{C}H_2O$), <u>105.7</u> (C2), <u>108.5</u> (C5), <u>122.6</u> (Cα), <u>123.0</u> (C6), <u>124.6</u> (Cγ), <u>126.5</u> (C4'), <u>128.7</u> (C2', C6'), <u>128.8</u> (C3', C5'), 130.9 (C1), <u>139.0</u> (Cδ, C1'), <u>141.1</u> (Cβ), 148.2 (C3), 148.3 (C4), 166.0 (<u>C</u>ONH). EI/MS m/z (%): 321.2 ($M^{\bullet+}$, 48), 201.1 (100), 143.1 (19), 115.1 (73), 96.1 (26).

3-oxo-3-(piperidin-1-yl)propanenitrile (24). η = 25 %. ^{1}H NMR (400 MHz, $CDCl_3$-d_1)*:* δ (ppm) = 1.63 (*m*, 6H, 2×$NCH_2C\underline{H}_2CH_2$, $NCH_2CH_2C\underline{H}_2$), 3.40 (*m*, 2H, $NC\underline{H}_2CH_2CH_2$), 3.47 (*s*, 2H, $CNC\underline{H}_2$), 3.56 (*m*, 2H, $NC\underline{H}_2CH_2CH_2$). ^{13}C NMR (100 MHz, $CDCl_3$-d_1)*:* δ (ppm) = <u>24.1</u> ($NCH_2\underline{C}H_2CH_2$), <u>25.0</u> ($NCH_2\underline{C}H_2CH_2$), <u>25.2</u> ($NCH_2CH_2\underline{C}H_2$), <u>26.1</u> ($CN\underline{C}H_2$), <u>43.6</u> ($N\underline{C}H_2CH_2CH_2$), 47.6 ($N\underline{C}H_2CH_2CH_2$), 114.1 (<u>C</u>N), 159.7 (<u>C</u>ON). EI/MS m/z (%): 152.2 ($M^{\bullet+}$, 100), 112.1 (24), 84.2 (20), 69.2 (22), 56.1 (26).

8.1.2.2. Method B. Ethyl cyanoacetate (1 mmol) and the appropriate amine (1.5 mmol) were mixed and heated at 100 or 150 ºC for 9 to 15 h. Cooling gave a solid which was purified by flash column chromatography (silica gel) and/or recrystallization. The procedure was adapted from Roifman *et al*. 2006 [43] with some modifications.

2-cyano-*N*-phenylacetamide (26). The reaction mixture was heated at 150 ºC for 15 h. TLC analysis and flash column chromatography were performed in dichloromethane/methanol (9:1). The solid was recrystallized from dichloromethane. η = 27 %. ^{1}H NMR (400 MHz, DMSO-d_6): δ (ppm) = 3.89 (*s*, 2H, CNC$\underline{H}_2$), 7.09 (*m*, 1H, H4), 7.33 (*m*, 2H, H3, H5), 7.54 (*m*, 2H, H2, H6), 10.28 (*m*, 1H, N$\underline{H}$). ^{13}C NMR (100 MHz, DMSO-d_6): δ (ppm) = $\underline{27.2}$ (CN$\underline{C}H_2$), 116.4 ($\underline{C}$N), $\underline{119.7}$ (C2, C6), $\underline{124.4}$ (C4), $\underline{129.4}$ (C3, C5), 138.8 (C1), 161.5 ($\underline{C}$ONH). EI/MS m/z (%): 160.1 ($M^{\bullet+}$, 55), 120.0 (27), 93.1 (100), 77.1 (38), 65.1 (46), 51.0 (21).

***N*-benzyl-2-cyanoacetamide (27).** The reaction mixture was heated at 100 ºC for 9 h. TLC analysis was performed in dichloromethane/methanol (9:1). Recrystallization in dichloromethane/diethyl ether and in dichloromethane/petroleum ether yielded the product. η = 24 %. ^{1}H NMR (400 MHz, DMSO-d_6): δ (ppm) = 3.69 (*s*, 2H, CNC$\underline{H}_2$), 4.29 (*d*, *J* = 5.8 Hz, 2H, NHC$\underline{H}_2$Ph), 7.25 (*m*, 3H, H2, H4, H6), 7.34 (*m*, 2H, H3, H5), 8.71 (*m*, 1H, N$\underline{H}$). ^{13}C NMR (100 MHz, DMSO-d_6): δ (ppm) = $\underline{25.8}$ (CN$\underline{C}H_2$), $\underline{43.1}$ (NH$\underline{C}H_2$Ph), 116.7 ($\underline{C}$N), $\underline{126.5}$ (C4), $\underline{127.9}$ (C2, C6), $\underline{128.8}$ (C3, C5), 139.0 (C1), 162.6 ($\underline{C}$ONH). EI/MS m/z (%): 174.1 ($M^{\bullet+}$, 64), 106.0 (22), 91.1 (100), 77.2 (29), 65.2 (29), 51.1 (34).

2-cyano-*N*-phenethylacetamide (28). The reaction mixture was heated at 100 ºC for 9 h. TLC analysis was performed in dichloromethane/methanol (9:1). Recrystallization in dichloromethane/diethyl ether and in dichloromethane/petroleum ether yielded the product. η = 42 %. ^{1}H NMR (400 MHz, $CDCl_3$-d_1): δ (ppm) = 2.85 (*t*, *J* = 7.0 Hz, 2H, NHCH$_2$C$\underline{H}_2$Ph), 3.31 (*s*, 2H, CNC$\underline{H}_2$), 3.56 (*dd*, *J* = 7.0 Hz, 12.9 Hz, 2H, NHC$\underline{H}_2$CH$_2$Ph), 6.14 (*bs*, 1H, N$\underline{H}$), 7.20 (*m*, 2H, H2, H6), 7.25 (*m*, 1H, H4), 7.33 (*m*, 2H, H3, H5). ^{13}C NMR (100 MHz, $CDCl_3$-d_1): δ (ppm) = $\underline{25.8}$ (CN$\underline{C}H_2$), $\underline{35.3}$ (NHCH$_2$$\underline{C}H_2$Ph), $\underline{41.5}$ (NH$\underline{C}$H$_2$CH$_2$Ph), 114.6 ($\underline{C}$N), $\underline{126.9}$ (C4), $\underline{128.7}$ (C2, C6), $\underline{128.9}$ (C3, C5), 130.0 (C1), 160.8 ($\underline{C}$ONH). EI/MS m/z (%): 188.2 ($M^{\bullet+}$, 5), 104.1 (100), 91.1 (48), 65.2 (19).

8.1.3. Demethylenation reaction. Compounds **12-16** derivatives (1 mmol) were maintained under argon atmosphere at -78 ºC. Then, the compound was dissolved in anhydrous dichloromethane and BBr_3 1 M (1.3 mmol) was added. The mixture was stirred under inert atmosphere, protected from the light, and allowed to reach room temperature for 12 hours.

(*2E*,*4E*)-5-(3,4-dihydroxyphenyl)penta-2,4-dienoic acid (2). The reaction mixture was quenched with water (5 mL). The resulting solid was isolated by filtration under reduced pressure, then suspended in dichloromethane/methanol (95:5) and centrifuged at 3000 g for 20 min. The supernatant was discarded, yielding the purified product. η = 5 %. ^{1}H NMR (400 MHz, DMSO-d_6): δ (ppm) = 5.91 (*d*, *J* = 15.2 Hz, 1H, Hα), 6.82 (*m*, 5H, Hγ, Hδ, H2, H5, H6), 7.30 (*dd*, *J* = 10.7 Hz, 15.1 Hz, 1H, Hβ), 9.03 (*bs*, 1H, O$\underline{H}$),9.34 (*bs*, 1H, O$\underline{H}$), 12.07 (*bs*, 1H, COO$\underline{H}$). ^{13}C NMR (100 MHz, DMSO-d_6): δ (ppm) = $\underline{114.4}$ (C2), $\underline{116.2}$ (C5), $\underline{120.3}$ (Cα), $\underline{120.5}$ (C6), $\underline{123.7}$ (Cγ), 128.1 (C1), $\underline{141.2}$ (Cδ), $\underline{145.5}$ (Cβ), 146.0 (C3), 147.5 (C4), 168.2 ($\underline{C}$OOH). EI/MS m/z (%): 206.1 ($M^{\bullet+}$, 32), 161.1 (64), 143.1 (28), 131.1 (23), 115.1 (100), 103.1 (23), 63.0 (24), 50.9 (33).

(*2E,4E*)-5-(3,4-dihydroxyphenyl)-1-(piperidin-1-yl)penta-2,4-dien-1-one (3). The reaction mixture was quenched with water (5 mL). The resulting solid was dissolved in dichloromethane/methanol (9:1) and extracted with water (3×10 mL). The product was purified by flash column chromatography (cellulose, dichloromethane/methanol (98:2)) and recrystallized in dichloromethane. η = 50 %. ^{1}H NMR (400 MHz, DMSO-*d*$_6$)*:* δ (ppm) = 1.47 (*s*, 4H, 2×NCH$_2$C<u>H$_2$</u>CH$_2$), 1.60 (*m*, 2H, NCH$_2$CH$_2$C<u>H$_2$</u>), 3.51 (*s*, 4H, 2×NC<u>H$_2$</u>CH$_2$CH$_2$), 6.66 (*d, J* = 14.5 Hz, 1H, Hα), 6.72 (*d, J* = 8.1 Hz, 1H, H5), 6.80 (*m*, 3H, H6, Hγ, Hδ), 6.92 (*d, J* = 2.0 Hz, 1H, H2), 7.20 (*m*, 1H, Hβ), 9.14 (*bs*, 2H, 2×O<u>H</u>). ^{13}C NMR (100 MHz, DMSO-*d*$_6$)*:* δ (ppm) = <u>24.6</u> (NCH$_2$CH$_2$<u>C</u>H$_2$), <u>25.9</u> (NCH$_2$<u>C</u>H$_2$CH$_2$), <u>27.0</u> (NCH$_2$<u>C</u>H$_2$CH$_2$), <u>43.0</u> (N<u>C</u>H$_2$CH$_2$CH$_2$), 46.5 (N<u>C</u>H$_2$CH$_2$CH$_2$), <u>114.0</u> (C2), <u>116.2</u> (C5), <u>119.8</u> (Cα), <u>120.2</u> (C6), <u>124.5</u> (Cγ), 128.4 (C1), <u>139.0</u> (Cδ), <u>142.7</u> (Cβ), 146.0 (C3), 147.0 (C4), 164.9 (<u>C</u>ON). EI/MS m/z (%): 273.2 ($M^{\bullet+}$, 68), 245.1 (64), 217.2 (100), 189.2 (33), 161.1 (32), 131.0 (22), 115.1 (72), 84.1 (99), 69.2 (26), 55.2 (25).

(*2E,4E*)-5-(3,4-dihydroxyphenyl)-*N*-phenylpenta-2,4-dienamide (4). The reaction mixture was quenched with water (5 mL). The resulting solid was dissolved in dichloromethane/methanol (9:1) and extracted with water (3×15 mL). The product was purified by column chromatography (cellulose, dichloromethane and dichloromethane/methanol 99.5:0.5) and recrystallized in dichloromethane. η = 12 %. ^{1}H NMR (400 MHz, MeOD-*d*$_4$)*:* δ (ppm) = 6.23 (*d, J* = 14.9 Hz, 1H, Hα), 6.80 (*m*, 3H, H5, Hγ, Hδ), 6.89 (*dd, J* = 1.8 Hz, 8.2 Hz, 1H, H6), 7.00 (*d, J* = 2.0 Hz, 1H, H2), 7.11 (*t, J* = 7.4 Hz, 1H, H4'), 7.33 (*t, J* = 7.9 Hz, 2H, H3', H5'), 7.43 (*m*, 1H, Hβ), 7.64 (d, J = 7.9 Hz, 2H, H2', H6'). ^{13}C NMR (100 MHz, MeOD-*d*$_4$)*:* δ (ppm) = <u>113.1</u> (C2), <u>115.1</u> (C5), 119.8 (C3', C5'), <u>119.9</u> (Cα), <u>122.0</u> (C6), <u>123.2</u> (Cγ), <u>123.8</u> (C4'), <u>128.4</u> (C2', C6'), 128.6 (C1), 138.7 (C1'), <u>140.3</u> (Cδ), <u>142.4</u> (Cβ), 145.3 (C3), 146.6 (C4), 165.9 (<u>C</u>ONH). ESI/MS m/z (%): 282 (M^{+}+1, 100). ESI/HRMS calcd. for $C_{17}H_{16}NO_3$ (M^{+}+H): 282.1130, found 282.1127.

(*2E,4E*)-*N*-benzyl-5-(3,4-dihydroxyphenyl)penta-2,4-dienamide (5). The reaction mixture was quenched with water (10 mL). The resulting solid was dissolved in dichloromethane/methanol (9:1) and extracted with water (3×15 mL). The product was purified by column chromatography (cellulose, dichloromethane and dichloromethane/methanol 99.5:0.5) and recrystallized in dichloromethane. η = 17 %. ^{1}H NMR (400 MHz, MeOD-*d*$_4$)*:* δ (ppm) = 4.47 (*s*, 2H, NHC<u>H$_2$</u>Ph), 6.10 (*d, J* = 15.0 Hz, 1H, Hα), 6.76 (*m*, 3H, H5, Hγ, Hδ), 6.87 (*dd, J* = 1.7 Hz, 8.2 Hz, 1H, H6), 6.98 (*d, J* = 1.8 Hz, 1H, H2), 7.31 (*m*, 6H, Hβ, H2', H3', H4', H5', H6'). ^{13}C NMR (100 MHz, MeOD-*d*$_4$)*:* δ (ppm) = <u>43.7</u> (NH<u>C</u>H$_2$Ph), <u>113.9</u> (C2), <u>116.0</u> (C5), <u>120.7</u> (Cα), <u>122.5</u> (C6), <u>124.2</u> (Cγ), <u>127.7</u> (C4'), <u>128.1</u> (C2', C6'), <u>129.0</u> (C3', C5'), 129.5 (C1), 139.5 (C1'), <u>140.7</u> (Cδ), <u>142.5</u> (Cβ), 146.1 (C3), 147.4 (C4), 168.6 (<u>C</u>ONH). ESI/MS m/z (%): 296 (M^{+}+1, 100). ESI/HRMS calcd. for $C_{18}H_{18}NO_3$ (M^{+}+H): 296.1287, found 296.1288.

(*2E,4E*)-5-(3,4-dihydroxyphenyl)-*N*-phenethylpenta-2,4-dienamide (6). The reaction mixture was quenched with water (10 mL). The resulting solid was dissolved in dichloromethane/methanol (9:1) and extracted with water (3×10 mL). The product was purified by column chromatography (cellulose, dichloromethane and dichloromethane/methanol 99.5:0.5) and recrystallized in dichloromethane. η = 20 %. ^{1}H NMR (400 MHz, MeOD-*d*$_4$)*:* δ (ppm) = 2.85 (*t, J* = 7.4 Hz, 2H, NHCH$_2$C<u>H$_2$</u>Ph), 3.51 (*m*, 2H, NHC<u>H$_2$</u>CH$_2$Ph), 6.01 (*d, J* = 15.0 Hz, 1H, Hα), 6.76 (*m*, 3H, H5, Hγ, Hδ), 6.86 (*dd, J* = 2.0 Hz, 8.2 Hz, 1H, H6), 6.97 (*d, J* = 2.0 Hz, 1H, H2), 7.24 (*m*, 6H, Hβ, H2', H3', H4', H5', H6'). ^{13}C NMR (100 MHz, MeOD-*d*$_4$)*:* δ (ppm) = <u>35.2</u> (NHCH$_2$<u>C</u>H$_2$Ph), <u>40.8</u> (NH<u>C</u>H$_2$CH$_2$Ph), <u>113.0</u> (C2), <u>115.1</u> (C5), <u>119.8</u> (Cα), <u>121.7</u> (C6), <u>123.3</u> (Cγ), <u>126.0</u> (C4'), <u>128.1</u> (C2', C6'), <u>128.4</u> (C3', C5'), 128.6 (C1), 139.2 (C1'), <u>139.7</u> (Cδ), <u>141.2</u> (Cβ), 145.2 (C3), 146.4 (C4), 167.8 (<u>C</u>ONH). ESI/MS m/z (%): 301 (M^++1, 100). ESI/HRMS calcd. for $C_{19}H_{20}NO_3$ (M^++H): 310.1443, found 310.1444.

8.1.4. Knoevenagel-Doebner condensation. In a round bottom flask with the aldehydes **17** or **22** (1 mmol) dissolved in anhydrous pyridine, the appropriate activated methylene (mono-ethyl malonate, cyanoacetic acid, cyanoacetic acid amides **26-28**, 1.3-1.5 mmol) and piperidine (0.35 mmol) were added. The mixture was heated until the maximum aldehyde consumption was observed. The procedure was adapted from Teixeira *et al.* [28] with some modifications.

Ethyl (E)-3-(3,4-dihydroxyphenyl)acrylate (18). The reaction mixture was heated at 70 ºC for 9 h. The product was purified by column chromatography (dichloromethane/methanol 95:5). TLC analysis was performed in dichloromethane/methanol (95:5). η = 54 %. ^{1}H NMR (400 MHz, DMSO-*d*$_6$)*:* δ (ppm) = 1.24 (*t, J* = 7.1 Hz, 3H, OCH$_2$C<u>H$_3$</u>), 4.15 (*q, J* = 7.0 Hz, 2H, OC<u>H$_2$</u>CH$_3$), 6.15 (*d, J* = 15.9 Hz, 1H, Hα), 6.76 (*dd, J* = 1.0 Hz, 8.1 Hz, 1H, H6), 7.00 (*d, J* = 8.2 Hz, 1H, H5), 7.04 (*d, J* = 1.0 Hz, 1H, H2), 7.47 (*d, J* = 15.9 Hz, 1H, Hβ), 9.43 (*bs*, 2H, 2×OH). ^{13}C NMR (100 MHz, DMSO-*d*$_6$)*:* δ (ppm) = <u>14.8</u> (OCH$_2$<u>C</u>H$_3$), <u>60.1</u> (O<u>C</u>H$_2$CH$_3$), <u>114.5</u> (C2), <u>115.3</u> (C5), <u>116.2</u> (Cα), <u>121.8</u> (C6), 126.0 (C1), <u>145.4</u> (Cβ), 146.0 (C3), 148.8 (C4), 167.0 (<u>C</u>OO). EI/MS m/z (%): 208.2 ($M^{\bullet+}$, 78), 180.1 (21), 163.1 (100), 136.1 (60), 117.1 (32), 89.1 (56), 77.1 (28), 63.1 (28), 51.0 (24).

(*2E,4E*)-2-cyano-5-(3,4-dihydroxyphenyl)penta-2,4-dienoic acid (7). The reaction mixture was heated at 60 ºC for 45 min. Upon completion, the mixture was poured onto water (20 mL) and acidified with HCl 6 M. The product was collected by filtration under reduced pressure and washed with water. TLC analysis was performed in dichloromethane/methanol/formic acid (9:1:0.01). η = 67 %. ^{1}H NMR (400 MHz, MeOD-*d*$_4$)*:* δ (ppm) = 6.81 (*d, J* = 8.2 Hz, 1H, H5), 7.04 (*m*, 2H, Hγ, H6), 7.12 (*d, J* = 2.0 Hz, 1H, H2), 7.32 (*d, J* = 15.1 Hz, 1H, Hδ), 8.03 (*d, J* = 11.6 Hz, 1H, Hβ). ^{13}C NMR (100 MHz, MeOD-*d*$_4$)*:* δ (ppm) = 101.6 (Cα), <u>113.8</u> (C2), 114.8 (<u>C</u>N), <u>115.4</u> (C5), <u>119.5</u> (C6), <u>122.7</u> (Cγ), 127.2 (C1), 145.7 (C3), 149.3 (C4), <u>150.0</u> (Cδ), <u>156.2</u> (Cβ), 164.1 (<u>C</u>OOH). EI/MS m/z (%): 231.2 ($M^{\bullet+}$, 97) 186.1 (100), 175.2 (19), 140.1 (57).

(*2E,4E*)-2-cyano-5-(3,4-dihydroxyphenyl)-*N*-piperidinylpenta-2,4-dienamide (8). The reaction mixture was heated at 60 ºC for 45 min. The solid was washed with dichloromethane and recrystallized from ethyl acetate/petroleum ether to yield a yellow solid. TLC analysis was performed in dichloromethane/methanol (9:1). η = 55 %. ^{1}H NMR (400 MHz, MeOD-*d*$_4$)*:* δ (ppm) = 1.65 (*m*, 4H, $NCH_2C\underline{H}_2CH_2$), 1.72 (*m*, 2H, $NCH_2CH_2C\underline{H}_2$), 3.60 (*m*, 4H, $NC\underline{H}_2CH_2CH_2$), 6.79 (*d, J* = 8.2 Hz, 1H, H5), 6.97 (*dd, J* = 2.0 Hz, 8.3 Hz, 1H, H6), 7.02 (*dd, J* = 11.3 Hz, 15.2 Hz, 1H, Hγ), 7.08 (*d, J* = 2.1 Hz, 1H, H2), 7.17 (*d, J* = 15.2 Hz, 1H, Hδ), 7.54 (*d, J* = 11.3 Hz, 1H, Hβ). ^{13}C NMR (100 MHz, MeOD-*d*$_4$)*:* δ (ppm) = 23.9 ($NCH_2CH_2\underline{C}H_2$), 25.5 ($N\underline{C}H_2CH_2CH_2$, $NCH_2\underline{C}H_2CH_2$), 103.8 (Cα), 113.5 (C2), 115.1 (CN), 115.3 (C5), 119.6 (C6), 121.9 (Cγ), 127.4 (C1), 145.6 (C3), 147.1 (Cδ), 148.6 (C4), 152.9 (Cβ), 163.4 (CON). EI/MS m/z (%): 298.3 ($M^{\bullet+}$, 87), 189.1 (21), 147.0 (33), 140.0 (35), 112.1 (29), 84.2 (100), 69.2 (27), 56.2 (24).

(*2E,4E*)-2-cyano-5-(3,4-dihydroxyphenyl)-*N*-phenylpenta-2,4-dienamide (9). The reaction mixture was heated at 60 ºC for 45 min. The solid was washed with dichloromethane and recrystallized from ethyl acetate/petroleum ether to yield a brown solid. TLC analysis was performed in dichloromethane/methanol (9:1). η = 46 %. ^{1}H NMR (400 MHz, MeOD-*d*$_4$)*:* δ (ppm) = 6.81 (*d, J* = 8.2 Hz, 1H, H5), 7.02 (*dd, J* = 2.0 Hz, 8.3 Hz, 1H, H6), 7.13 (*m*, 3H, Hγ, H2, H4'), 7.29 (*d, J* = 15.2 Hz, 1H, Hδ), 7.34 (*m*, 2H, Hγ, H3', H5'), 7.60 (*m*, 2H, Hγ, H2', H6'), 8.03 (*d, J* = 11.2 Hz, 1H, Hβ). ^{13}C NMR (100 MHz, MeOD-*d*$_4$)*:* δ (ppm) = 104.6 (Cα), 113.7 (C2), 115.0 (CN), 115.4 (C5), 119.8 (C6), 121.1 (C2', C6'), 122.4 (Cγ), 124.6 (C4'), 127.3 (C1), 128.4 (C3', C5'), 137.8 (C1'), 145.7 (C3), 148.9 (Cδ), 149.1 (C4), 153.2 (Cβ), 161.1 (CONH). EI/MS m/z (%): 306.2 ($M^{\bullet+}$, 58), 214.2 (42), 147.0 (36), 140.0 (30), 93.1 (100), 65.1 (24).

(*2E,4E*)-2-cyano-5-(3,4-dihydroxyphenyl)-*N*-benzylpenta-2,4-dienamide (10). The reaction mixture was heated at 60 ºC for 45 min. The solid was washed with dichloromethane and recrystallized from ethyl acetate/petroleum ether to yield a yellow solid. TLC analysis was performed in dichloromethane/methanol (9:1). η = 54 %. ^{1}H NMR (400 MHz, DMSO-*d*$_6$)*:* δ (ppm) = 4.38 (*d, J* = 5.7 Hz, 1H, 23.92 $NHC\underline{H}_2Ph$), 6.80 (*d, J* = 8.2 Hz, 1H, H5), 6.90 (*dd, J* = 11.5 Hz, 15.1 Hz, 1H, Hγ), 6.99 (*dd, J* = 2.0 Hz, 8.3 Hz, 1H, H6), 7.29 (*m*, 6H, Hδ, H2', H3', H4', H5', H6'), 7.97 (*d, J* = 11.5 Hz, 1H, Hβ), 8.81 (*d, J* = 5.8 Hz, 1H, N<u>H</u>). ^{13}C NMR (100 MHz, DMSO-*d*$_6$)*:* δ (ppm) = 43.4 ($NH\underline{C}H_2Ph$), 104.8 (Cα), 114.6 (C2), 116.3 (CN), 116.5 (C5), 119.9 (C6), 122.6 (Cγ), 127.0 (C1), 127.4 (C4'), 127.8 (C2', C6'), 128.8 (C3', C5'), 139.5 (C1'), 146.3 (C3), 148.6 (Cδ), 149.6 (C4), 152.6 (Cβ), 161.7 (CONH). EI/MS m/z (%): 320.2 ($M^{\bullet+}$, 36), 106.1 (32), 91.1 (100).

(*2E,4E*)-2-cyano-5-(3,4-dihydroxyphenyl)-*N*-phenethylpenta-2,4-dienamide (11). The reaction mixture was heated at 60 ºC for 45 min. The solid was washed with dichloromethane and recrystallized from ethyl acetate/petroleum ether to yield a yellow solid. TLC analysis was performed in dichloromethane/methanol (9:1). η = 66 %. ^{1}H NMR (400 MHz, MeOD-*d*$_4$)*:* δ (ppm) = 2.86 (*m*, 2H, NHCH$_2$C<u>H$_2$</u>Ph), 3.52 (*m*, 2H, NHC<u>H$_2$</u>CH$_2$Ph), 6.80 (*d, J* = 8.2 Hz, 1H, H5), 7.01 (*m*, 2H, Hγ, H6), 7.10 (*d, J* = 2.0 Hz, 1H, H2), 7.23 (*m*, 6H, H2', H3', H4', H5', H6', Hδ), 7.88 (*d, J* = 11.5 Hz, 1H, Hβ). ^{13}C NMR (100 MHz, MeOD-*d*$_4$)*:* δ (ppm) = <u>36.5</u> (NHCH$_2$<u>C</u>H$_2$Ph), <u>42.9</u> (NH<u>C</u>H$_2$CH$_2$Ph), 105.2 (Cα), <u>115.1</u> (C2), <u>116.4</u> (C5), 116.8 (<u>C</u>N), <u>121.3</u> (C6), <u>123.6</u> (Cγ), <u>127.5</u> (C4'), 128.8 (C1), <u>129.6</u> (C2', C6'), <u>129.9</u> (C3', C5'), 140.4 (C1'), 147.1 (C3), <u>150.0</u> (Cδ), 150.4 (C4), <u>154.2</u> (Cβ), 163.7 (<u>C</u>ONH). EI/MS m/z (%): 334.2 ($M^{\bullet+}$, 40), 270.1 (74), 214.1 (100), 147.1 (37), 140.1 (27), 91.1 (37).

8.1.5. Synthesis of ethyl (*E*)-3-(3,4-bis((tert-butyldimethylsilyl)oxy)phenyl)acrylate (19). In a round bottom flask with caffeic acid ethyl ester **18** (1 mmol) dissolved in DMF (4 mL), TBSCl (2.5 mmol) and imidazole (5 mmol) were added. The mixture was heated at 50 ºC for 1 h. Once the reaction was complete, water was added, and the mixture was extracted with dichloromethane (3×10 mL). The organic layer was washed with brine, dried over Na_2SO_4, filtered and concentrated. Purification by flash column chromatography (silica gel, dichloromethane) yielded a white solid. TLC analysis was performed in ethyl acetate/dichloromethane (3:7). The procedure was adapted from Roifman *et al.* 2006 [43] with some modifications. η = 83 %. ^{1}H NMR (400 MHz, $CDCl_3$-*d*$_1$)*:* δ (ppm) = 0.21 (*s*, 6H, Si(C<u>H$_3$</u>)$_2$), 0.22 (*s*, 6H, Si(C<u>H$_3$</u>)$_2$), 0.98 (*s*, 9H, SiC(C<u>H$_3$</u>)$_3$), 0.99 (*s*, 9H, SiC(C<u>H$_3$</u>)$_3$), 1.33 (*t, J* = 7.1 Hz, 3H, OCH$_2$C<u>H$_3$</u>), 4.25 (*q, J* = 7.1 Hz, 2H, OC<u>H$_2$</u>CH$_3$), 6.23 (*d, J* = 15.9 Hz, 1H, Hα), 6.81 (*d, J* = 8.9 Hz, 1H, H5), 7.01 (*m*, 2H, H2, H6), 7.56 (*d, J* = 15.9 Hz, 1H, Hβ). ^{13}C NMR (100 MHz, $CDCl_3$-*d*$_1$)*:* δ (ppm) = <u>-4.1</u> ((Si<u>C</u>H$_3$)$_2$), <u>-4.0</u> ((Si<u>C</u>H$_3$)$_2$), <u>14.4</u> (OCH$_2$<u>C</u>H$_3$), 18.5 (2×Si<u>C</u>(CH$_3$)$_3$), <u>25.9</u> (2×SiC(<u>C</u>H$_3$)$_3$), <u>60.4</u> (O<u>C</u>H$_2$CH$_3$), <u>115.9</u> (C2), <u>120.4</u> (C5), <u>121.4</u> (Cα), <u>122.2</u> (C6), 128.1 (C1), <u>144.6</u> (Cβ), 147.2 (C3), 149.4 (C4), 167.4 (<u>C</u>OO). ESI/MS m/z (%): 437 (M^++1, 100).

8.1.6. Synthesis of (*E*)-3-(3,4-bis((tert-butyldimethylsilyl)oxy)phenyl)prop-2-en-1-ol (20). Cinnamic ester **19** (1 mmol) was dissolved under argon atmosphere in dry THF (6 mL) and cooled to −78 °C. Lithium aluminum hydride (1.6 mmol) was added, and the mixture was stirred for 5 h. Once the reaction was complete, the unreacted $LiAlH_4$ was quenched with methanol until gas evolution stopped, and water was added. The mixture was neutralized with HCl 6 M, then extracted with dichloromethane (3×30 mL). The combined organic layers were washed with brine, dried over anhydrous sodium sulfate, filtered and concentrated. Purification by flash column chromatography (silica gel, dichloromethane) yielded the cinnamyl alcohol **20**. The procedure was adapted from Jirásek *et al.* 2014 [44] with some modifications. η = 73 %. ^{1}H NMR (400 MHz, $CDCl_3$-*d*$_1$)*:* δ (ppm) = -0.01 (*s*, 6H, Si(C$\underline{H}_3$)$_2$), 0.00 (*s*, 6H, Si(C$\underline{H}_3$)$_2$), 0.78 (*s*, 9H, SiC(C$\underline{H}_3$)$_3$), 0.79 (*s*, 9H, SiC(C$\underline{H}_3$)$_3$), 4.05 (*d, J* = 5.5 Hz, 2H, CH=CHC$\underline{H}_2$OH) 5.96 (*dt*, *J* = 5.9 Hz, 15.8 Hz,1H, CH=C$\underline{H}$CH$_2$OH), 6.26 (*d, J* = 15.8 Hz, 1H, C$\underline{H}$=CHCH$_2$OH), 6.56 (*d, J* = 8.2 Hz, 1H, H5), 6.63 (*dd, J* = 2.1 Hz, 8.2 Hz, 1H, H6), 6.68 (*d, J* = 2.1 Hz, 1H, H2). ^{13}C NMR (100 MHz, $CDCl_3$-*d*$_1$): δ (ppm) = $\underline{-4.1}$ (2×(Si$\underline{C}$H$_3$)$_2$), 18.5 (2×Si$\underline{C}$(CH$_3$)$_3$), $\underline{26.0}$ (2×SiC(C$\underline{H}_3$)$_3$), $\underline{63.8}$ (CH=CH$\underline{C}$H$_2$OH), $\underline{119.0}$ (C2), $\underline{120.0}$ (C5), $\underline{121.1}$ (C6), $\underline{126.4}$ (Cα), $\underline{128.09}$ (CH=$\underline{C}$HCH$_2$OH), $\underline{130.4}$ ($\underline{C}$H=CHCH$_2$OH), 131.1 (C1), 146.9 (C3, C4). EI/MS m/z (%): 394.3 ($M^{\bullet+}$, 18), 205.2 (75), 83.0 (42), 73.2 (100).

8.1.7. Synthesis of (*E*)-3-(3,4-bis((tert-butyldimethylsilyl)oxy)phenyl)acrylaldehyde (21). Cinnamyl alcohol **20** (1 mmol) was dissolved in dichloromethane (30 mL). Then, MnO_2 (8 mmol) was added, and the mixture was stirred overnight at room temperature. Then, the mixture was filtered through Celite to remove the MnO_2 and washed with dichloromethane. The filtrate was concentrated and purified by flash column chromatography (silica gel, dichloromethane). TLC analysis was performed in dichloromethane. The procedure was adapted from Jirásek *et al.* 2014[44] with some modifications. η = 54 %. ^{1}H NMR (400 MHz, $CDCl_3$-*d*$_1$): δ (ppm) = 0.22 (*s*, 6H, Si(C$\underline{H}_3$)$_2$), 0.23 (*s*, 6H, Si(C$\underline{H}_3$)$_2$), 0.99 (*s*, 9H, SiC(C$\underline{H}_3$)$_3$), 1.00 (*s*, 9H, SiC(C$\underline{H}_3$)$_3$), 6.54 (*dd, J* = 7.8 Hz, 15.9 Hz, 1H, Hα), 6.86 (*d, J* = 8.8 Hz, 1H, H5), 7.05 (*m*, 2H, H2, H6), 7.35 (*d, J* = 15.8 Hz, 1H, Hβ), 9.64 (*d, J* = 7.8 Hz, 1H, C$\underline{H}$O). ^{13}C NMR (100 MHz, $CDCl_3$-*d*$_1$): δ (ppm) = $\underline{-4.1}$ ((Si$\underline{C}$H$_3$)$_2$), $\underline{-4.0}$ ((Si$\underline{C}$H$_3$)$_2$), 18.5 (2×Si$\underline{C}$(CH$_3$)$_3$), $\underline{25.9}$ (2×SiC(C$\underline{H}_3$)$_3$), $\underline{120.5}$ (C2), $\underline{121.3}$ (C5), $\underline{123.2}$ (Cα), $\underline{126.7}$ (C6), 127.8 (C1), 147.5 (C3), 150.5 (C4), $\underline{153.0}$ (Cβ), $\underline{193.7}$ ($\underline{C}$HO). ESI/MS m/z (%): 393 (M^++1, 100).

8.1.8. Synthesis of (E)-3-(3,4-dihydroxyphenyl)acrylaldehyde (22). Silly ether 21 (0.38 g, 0.97 mmol) was dissolved in dry THF (3 mL). Then, TBAF (1 mmol) was added, and the mixture was heated at 50 ºC for 1 h. Upon completion, water was added, and the mixture was acidified at 0 ºC with HCl 6 M. Then, the mixture was extracted with ethyl acetate. The combined organic layers were washed with brine (10 mL), dried over anhydrous sodium sulfate, filtered and concentrated. The solid was washed with ethyl acetate to yield caffeic aldehyde **22**. TLC analysis was performed in dichloromethane/methanol (9:1). The procedure was adapted from Roifman *et al.* 2006 [43]. η = 76 %. ^{1}H NMR (400 MHz, MeOD-d_4): δ (ppm) = 6.54 (*dd, J* = 7.8 Hz, 15.7 Hz, 1H, Hα), 6.82 (*d, J* = 8.2 Hz, 1H, H5), 7.04 (*dd, J* = 1.9 Hz, 8.2 Hz, 1H, H6), 7.11 (*d, J* = 1.9 Hz, 1H, H2), 7.52 (*d, J* = 15.7 Hz, 1H, Hβ), 9.55 (*d, J* = 7.9 Hz, 1H, C<u>H</u>O). ^{13}C NMR (100 MHz, MeOD-d_4): δ (ppm) = <u>114.2</u> (C2), <u>115.2</u> (C5), <u>122.6</u> (Cα), <u>125.0</u> (C6), 126.0 (C1), 145.6 (C3), 149.3 (C4), <u>155.0</u> (Cβ), <u>194.8</u> (<u>C</u>HO). EI/MS m/z (%): 164.0 ($M^{\bullet+}$, 100), 147.0 (56), 136.0 (35), 118.1 (39), 110.1 (62), 107.1 (22), 89.1 (70), 77.2 (49), 63.1 (50), 51.0 (47).

8.2. Evaluation of human monoamine oxidase (*h*MAO) inhibitory activity

The inhibitory activity of CA derivatives on *h*MAO-A and *h*MAO-B was studied using an experimental protocol described elsewhere [25, 26] (see supplementary information).

8.3. Evaluation of catechol *O*-methyltransferase inhibitory activity

COMT inhibitory activities of CA derivatives was assessed using an experimental protocol described elsewhere [27, 45] (see supplementary information).

8.4. Oxygen radical absorbance capacity (ORAC-FL) assay

The ORAC-FL analyses were performed using an experimental protocol adapted from the literature [30, 46] and described in supplementary information.

8.5. Electrochemical measurements

DPV and CV experiments were performed as described elsewhere [31] (see supplementary information).

8.6. *In vitro* toxicology

8.6.1. Cell lines and culture conditions

Human neuroblastoma (SH-SY5Y) cells were obtained from the American Type Culture Collection (ATCC, Manassas, VA, USA). Cell cultures and SH-SY5Y cell differentiation were performed as previously described by Fernandes *et al*. [47] and in supplementary information.

8.6.2. Evaluation of cytotoxicity profile

Stock solutions of the test compounds (100 mM) were freshly prepared in DMSO. Final concentrations of the test compounds were obtained by diluting into culture medium immediately before use, giving a final maximum concentration of 0.1 % DMSO.

In cytotoxicity studies, differentiated SH-SY5Y cells were exposed to the test compounds (10 µM and 50 µM) for 24 h. Controls were treated with culture media containing 0.1 % DMSO. Cell viability was estimated using two different methods: resazurin reduction and NR uptake assays.

8.6.3. Evaluation of intracellular oxidative stress levels

The formation of intracellular RS was evaluated using the 2',7'-dichlorofluorescein (DCF) fluorescence assay as previously described by da Fernandes *et al*. [47] and in (supplementary information).

8.6.4. Protection against *tert*-butyl hydroperoxide (*t*-BHP-induced) oxidative stress

The evaluation of the neuroprotective properties against oxidative stress-induced damage was performed as previously described by Fernandes *et al*. [47], with some modifications. Differentiated SH-SY5Y cells were pre-treated with the test compounds (10 µM) for 30 min. Then, culture medium containing *t*-BHP (200 µM) was added, and cells were incubated for additional 24 h. A negative control (cells treated with culture medium containing vehicle) and a positive control (cells treated with culture medium containing vehicle followed by treatment with *t*-BHP) were also included. Cell viability was estimated using the resazurin reduction assay.

8.6.5. Statistical analysis

Data analysis for all the studies are specified in supplementary information.

8.7. Evaluation of the chromatographic hydrophobicity index at pH 2.3

Chromatographic hydrophobicity index (CHI) values at pH 2.3 were determined were determined using an experimental protocol described elsewhere [48, 49] and in supplementary information.

8.8. Estimation of drug-like properties

The calculation of molecular weight (MW), topological polar surface area (TPSA), number of hydrogen bond donors (HBD) and acceptors (HBA), number of rotatable bonds (RB) and logarithm of the ratio of the concentration of a drug in the brain and in the blood (logBB) was performed using the StarDrop software.

9. References

[1] B. Das, S. Vedachalam, D. Luo, T. Antonio, M.E. Reith, A.K. Dutta, Development of a Highly Potent D_2/D_3 Agonist and a Partial Agonist from Structure-Activity Relationship Study of N^6-(2-(4-(1H-Indol-5-yl)piperazin-1-yl)ethyl)-N^6-propyl-4,5,6,7-tetrahydrobenzo[*d*]thiazole-2,6-diamine Analogues: Implication in the Treatment of Parkinson's Disease, J. Med. Chem., 58 (2015) 9179-9195. https://doi.org/10.1021/acs.jmedchem.5b01031

[2] W. Oertel, J.B. Schulz, Current and experimental treatments of Parkinson disease: A guide for neuroscientists, J. Neurochem., 139 Suppl 1 (2016) 325-337. https://doi.org/10.1111/jnc.13750

[3] J.D. Guo, X. Zhao, Y. Li, G.R. Li, X.L. Liu, Damage to dopaminergic neurons by oxidative stress in Parkinson's disease (Review), Int. J. Mol. Med., 41 (2018) 1817-1825. https://doi.org/10.3892/ijmm.2018.3406

[4] V. Dias, E. Junn, M.M. Mouradian, The role of oxidative stress in Parkinson's disease, J Parkinsons Dis, 3 (2013) 461-491. https://doi.org/10.3233/JPD-130230
[5] A.H. Bhat, K.B. Dar, S. Anees, M.A. Zargar, A. Masood, M.A. Sofi, S.A. Ganie, Oxidative stress, mitochondrial dysfunction and neurodegenerative diseases: a mechanistic insight, Biomed. Pharmacother., 74 (2015) 101-110. https://doi.org/10.1016/j.biopha.2015.07.025
[6] O. Hwang, Role of oxidative stress in Parkinson's disease, Exp. Neurobiol., 22 (2013) 11-17. https://doi.org/10.5607/en.2013.22.1.11
[7] S. Gandhi, A.Y. Abramov, Mechanism of oxidative stress in neurodegeneration, Oxid. Med. Cell Longev., (2012) 428010. https://doi.org/10.1155/2012/428010
[8] F.A. Zucca, J. Segura-Aguilar, E. Ferrari, P. Munoz, I. Paris, D. Sulzer, T. Sarna, L. Casella, L. Zecca, Interactions of iron, dopamine and neuromelanin pathways in brain aging and Parkinson's disease, Prog. Neurobiol., 155 (2017) 96-119. https://doi.org/10.1016/j.pneurobio.2015.09.012
[9] A. Elmabruk, B. Das, D. Yedlapudi, L. Xu, T. Antonio, M.E.A. Reith, A.K. Dutta, Design, Synthesis, and Pharmacological Characterization of Carbazole Based Dopamine Agonists as Potential Symptomatic and Neuroprotective Therapeutic Agents for Parkinson's Disease, ACS Chem. Neurosci., 10 (2019) 396-411. https://doi.org/10.1021/acschemneuro.8b00291
[10] E. Zanforlin, G. Zagotto, G. Ribaudo, The Medicinal Chemistry of Natural and Semisynthetic Compounds against Parkinson's and Huntington's Diseases, ACS Chem. Neurosci., 8 (2017) 2356-2368. https://doi.org/10.1021/acschemneuro.7b00283
[11] P.B. Huleatt, M.L. Khoo, Y.Y. Chua, T.W. Tan, R.S. Liew, B. Balogh, R. Deme, F. Goloncser, K. Magyar, D.P. Sheela, H.K. Ho, B. Sperlagh, P. Matyus, C.L. Chai, Novel arylalkenylpropargylamines as neuroprotective, potent, and selective monoamine oxidase B inhibitors for the treatment of Parkinson's disease, J. Med. Chem., 58 (2015) 1400-1419. https://doi.org/10.1021/jm501722s
[12] A.H. Schapira, Monoamine oxidase B inhibitors for the treatment of Parkinson's disease: a review of symptomatic and potential disease-modifying effects, CNS Drugs, 25 (2011) 1061-1171. https://doi.org/10.2165/11596310-000000000-00000
[13] C. Binda, J. Wang, L. Pisani, C. Caccia, A. Carotti, P. Salvati, D.E. Edmondson, A. Mattevi, Structures of human monoamine oxidase B complexes with selective noncovalent inhibitors: safinamide and coumarin analogs, J. Med. Chem., 50 (2007) 5848-5852. https://doi.org/10.1021/jm070677y
[14] J.P.M. Finberg, Inhibitors of MAO-B and COMT: their effects on brain dopamine levels and uses in Parkinson's disease, J. Neural. Transm. (Vienna), 126 (2018) 433-448. https://doi.org/10.1007/s00702-018-1952-7
[15] R.K.P. Tripathi, S.R. Ayyannan, Monoamine oxidase-B inhibitors as potential neurotherapeutic agents: An overview and update, Med. Res. Rev., (2019) 1-104. https://doi.org/10.1002/med.21561
[16] A. Stößel, M. Schlenk, S. Hinz, P. Küppers, J. Heer, M. Gütschow, C.E. Müller, Dual targeting of adenosine A_{2A} receptors and monoamine oxidase B by 4*H*-3,1-benzothiazin-4-ones, J. Med. Chem., 56 (2013) 4580-4596. https://doi.org/10.1021/jm400336x
[17] C. Lerner, R. Jakob-Roetne, B. Buettelmann, A. Ehler, M. Rudolph, R.M. Rodriguez Sarmiento, Design of Potent and Druglike Nonphenolic Inhibitors for Catechol O-Methyltransferase Derived from a Fragment

Screening Approach Targeting the S-Adenosyl-l-methionine Pocket, J. Med. Chem., 59 (2016) 10163-10175. https://doi.org/10.1021/acs.jmedchem.6b00927

[18] P. Solla, A. Cannas, F. Marrosu, M.G. Marrosu, Therapeutic interventions and adjustments in the management of Parkinson disease: role of combined carbidopa/levodopa/entacapone (Stalevo), Neuropsychiatr Dis Treat, 6 (2010) 483-490. https://doi.org/10.2147/ndt.s5190

[19] P.N. Palma, M.J. Bonifacio, A.I. Loureiro, L.C. Wright, D.A. Learmonth, P. Soares-da-Silva, Molecular modeling and metabolic studies of the interaction of catechol-*O*-methyltransferase and a new nitrocatechol inhibitor, Drug Metab. Dispos., 31 (2003) 250-258. https://doi.org/10.1124/dmd.31.3.250

[20] L.E. Kiss, P. Soares-da-Silva, Medicinal chemistry of catechol O-methyltransferase (COMT) inhibitors and their therapeutic utility, J. Med. Chem., 57 (2014) 8692-8717. https://doi.org/10.1021/jm500572b

[21] R.G. Robinson, S.M. Smith, S.E. Wolkenberg, M. Kandebo, L. Yao, C.R. Gibson, S.T. Harrison, S. Polsky-Fisher, J.C. Barrow, P.J. Manley, J.J. Mulhearn, K.K. Nanda, J.W. Schubert, B.W. Trotter, Z. Zhao, J.M. Sanders, R.F. Smith, D. McLoughlin, S. Sharma, D.L. Hall, T.L. Walker, J.L. Kershner, N. Bhandari, P.H. Hutson, N.A. Sachs, Characterization of non-nitrocatechol pan and isoform specific catechol-*O*-methyltransferase inhibitors and substrates, ACS Chem. Neurosci., 3 (2011) 129-140. https://doi.org/10.1021/cn200109w

[22] S.D. Pinheiro, M.P. Serrao, T. Silva, F. Borges, P. Soares-da-Silva, Pharmacodynamic evaluation of novel Catechol-*O*-methyltransferase inhibitors, Eur. J. Pharmacol., 847 (2019) 53-60. https://doi.org/10.1016/j.ejphar.2019.01.027

[23] J.K. Yang, E. Lee, I.J. Hwang, D. Yim, J. Han, Y.S. Lee, J.H. Kim, β-Lactoglobulin Peptide Fragments Conjugated with Caffeic Acid Displaying Dual Activities for Tyrosinase Inhibition and Antioxidant Effect, Bioconjug. Chem., 29 (2018) 1000-1005. https://doi.org/10.1021/acs.bioconjchem.8b00050

[24] T. Masuda, K. Yamada, J. Akiyama, T. Someya, Y. Odaka, Y. Takeda, M. Tori, K. Nakashima, T. Maekawa, Y. Sone, Antioxidation mechanism studies of caffeic acid: identification of antioxidation products of methyl caffeate from lipid oxidation, J. Agric. Food Chem., 56 (2008) 5947-5952. https://doi.org/10.1021/jf800781b

[25] D. Chavarria, F. Cagide, M. Pinto, L.R. Gomes, J.N. Low, F. Borges, Development of piperic acid-based monoamine oxidase inhibitors: Synthesis, structural characterization and biological evaluation, J. Mol. Struct., 1182 (2019) 298-307. https://doi.org/10.1016/j.molstruc.2019.01.060

[26] S. Hagenow, A. Stasiak, R.R. Ramsay, H. Stark, Ciproxifan, a histamine H_3 receptor antagonist, reversibly inhibits monoamine oxidase A and B, Sci. Rep., 7 (2017) 1-6. https://doi.org/10.1038/srep40541

[27] T. Silva, T. Mohamed, A. Shakeri, P.P. Rao, L. Martinez-Gonzalez, D.I. Perez, A. Martinez, M.J. Valente, J. Garrido, E. Uriarte, P. Serrao, P. Soares-da-Silva, F. Remiao, F. Borges, Development of Blood-Brain Barrier Permeable Nitrocatechol-Based Catechol O-Methyltransferase Inhibitors with Reduced Potential for Hepatotoxicity, J. Med. Chem., 59 (2016) 7584-7597. https://doi.org/10.1021/acs.jmedchem.6b00666

[28] J. Teixeira, T. Silva, S. Benfeito, A. Gaspar, E.M. Garrido, J. Garrido, F. Borges, Exploring nature profits: development of novel and potent lipophilic antioxidants based on galloyl-cinnamic hybrids, Eur. J. Med. Chem., 62 (2013) 289-296. https://doi.org/10.1016/j.ejmech.2012.12.049

[29] A. Gaspar, E.M. Garrido, M. Esteves, E. Quezada, N. Milhazes, J. Garrido, F. Borges, New insights into the antioxidant activity of hydroxycinnamic acids: Synthesis and physicochemical characterization of novel halogenated derivatives, Eur. J. Med. Chem., 44 (2009) 2092-2099. https://doi.org/10.1016/j.ejmech.2008.10.027

[30] F. Mura, T. Silva, C. Castro, F. Borges, M.C. Zuniga, J. Morales, C. Olea-Azar, New insights into the antioxidant activity of hydroxycinnamic and hydroxybenzoic systems: spectroscopic, electrochemistry, and cellular studies, Free Radic. Res., 48 (2014) 1473-1484. https://doi.org/10.3109/10715762.2014.965702

[31] J. Garrido, A. Gaspar, E.M. Garrido, R. Miri, M. Tavakkoli, S. Pourali, L. Saso, F. Borges, O. Firuzi, Alkyl esters of hydroxycinnamic acids with improved antioxidant activity and lipophilicity protect PC12 cells against oxidative stress, Biochimie, 94 (2012) 961-967. https://doi.org/10.1016/j.biochi.2011.12.015

[32] C.E. Rodriguez, M. Shinyashiki, J. Froines, R.C. Yu, J.M. Fukuto, A.K. Cho, An examination of quinone toxicity using the yeast *Saccharomyces cerevisiae* model system, Toxicology, 201 (2004) 185-196. https://doi.org/10.1016/j.tox.2004.04.016

[33] A.G. Siraki, T.S. Chan, P.J. O'Brien, Application of quantitative structure-toxicity relationships for the comparison of the cytotoxicity of 14 *p*-benzoquinone congeners in primary cultured rat hepatocytes versus PC12 cells, Toxicol. Sci., 81 (2004) 148-159. https://doi.org/10.1093/toxsci/kfh182

[34] S. Benfeito, C. Oliveira, C. Fernandes, F. Cagide, J. Teixeira, R. Amorim, J. Garrido, C. Martins, B. Sarmento, R. Silva, F. Remiao, E. Uriarte, P.J. Oliveira, F. Borges, Fine-tuning the neuroprotective and blood-brain barrier permeability profile of multi-target agents designed to prevent progressive mitochondrial dysfunction, Eur. J. Med. Chem., 167 (2019) 525-545. https://doi.org/10.1016/j.ejmech.2019.01.055

[35] K. Zhao, G. Luo, S. Giannelli, H.H. Szeto, Mitochondria-targeted peptide prevents mitochondrial depolarization and apoptosis induced by tert-butyl hydroperoxide in neuronal cell lines, Biochem. Pharmacol., 70 (2005) 1796-1806. https://doi.org/10.1016/j.bcp.2005.08.022

[36] Kanupriya, D. Prasad, M. Sai Ram, R. Kumar, R.C. Sawhney, S.K. Sharma, G. Ilavazhagan, D. Kumar, P.K. Banerjee, Cytoprotective and antioxidant activity of Rhodiola imbricata against tert-butyl hydroperoxide induced oxidative injury in U-937 human macrophages, Mol. Cell. Biochem., 275 (2005) 1-6.

[37] K. Valko, C. Bevan, D. Reynolds, Chromatographic Hydrophobicity Index by Fast-Gradient RP-HPLC: A High-Throughput Alternative to log P/log D, Anal. Chem., 69 (1997) 2022-2029. https://doi.org/10.1021/ac961242d

[38] S. Vilar, M. Chakrabarti, S. Costanzi, Prediction of passive blood-brain partitioning: straightforward and effective classification models based on in silico derived physicochemical descriptors, J. Mol. Graph. Model., 28 (2010) 899-903. https://doi.org/10.1016/j.jmgm.2010.03.010

[39] S.A. Hitchcock, L.D. Pennington, Structure-brain exposure relationships, J. Med. Chem., 49 (2006) 7559-7583. https://doi.org/10.1021/jm060642i

[40] H. Pajouhesh, G.R. Lenz, Medicinal Chemical Properties of Successful Central Nervous System Drugs, NeuroRx., 2 (2005) 541-553. https://doi.org/10.1602/neurorx.2.4.541

[41] D.E. Clark, Rapid calculation of polar molecular surface area and its application to the prediction of transport phenomena. 2. Prediction of blood-brain barrier penetration, J. Pharm. Sci., 88 (1999) 815-821. https://doi.org/10.1021/js980402t

[42] A. Gaspar, T. Silva, M. Yanez, D. Vina, F. Orallo, F. Ortuso, E. Uriarte, S. Alcaro, F. Borges, Chromone, a privileged scaffold for the development of monoamine oxidase inhibitors, J. Med. Chem., 54 (2011) 5165-5173. https://doi.org/10.1021/jm2004267

[43] C.M. Roifman, P. Demin, A. Freywald, T. Grunberger, O. Rounova, N. Sharfe, HSC Research and Development Limited Partnership, Novel compounds for modulating cell proliferation, WO 2001/079158, 2006.

[44] P. Jirasek, S. Amslinger, J. Heilmann, Synthesis of natural and non-natural curcuminoids and their neuroprotective activity against glutamate-induced oxidative stress in HT-22 cells, J. Nat. Prod., 77 (2014) 2206-2217. https://doi.org/10.1021/np500396y

[45] M.A. Vieira-Coelho, P. Soares-da-Silva, Effects of tolcapone upon soluble and membrane-bound brain and liver catechol-O-methyltransferase, Brain Res., 821 (1999) 69-78. https://doi.org/10.1016/s0006-8993(99)01063-x

[46] B. Ou, M. Hampsch-Woodill, R.L. Prior, Development and validation of an improved oxygen radical absorbance capacity assay using fluorescein as the fluorescent probe, J. Agric. Food Chem., 49 (2001) 4619-4626. https://doi.org/10.1021/jf010586o

[47] C. Fernandes, M. Pinto, C. Martins, M.J. Gomes, B. Sarmento, P.J. Oliveira, F. Remião, F. Borges, Development of a PEGylated-Based Platform for Efficient Delivery of Dietary Antioxidants Across the Blood-Brain Barrier, Bioconjug. Chem., 29 (2018) 1677-1689. https://doi.org/10.1021/acs.bioconjchem.8b00151

[48] G. Camurri, A. Zaramella, High-throughput liquid chromatography/mass spectrometry method for the determination of the chromatographic hydrophobicity index, Anal. Chem., 73 (2001) 3716-3722. https://doi.org/10.1021/ac001388j

[49] K. Valko, S. Nunhuck, C. Bevan, M.H. Abraham, D.P. Reynolds, Fast gradient HPLC method to determine compounds binding to human serum albumin. Relationships with octanol/water and immobilized artificial membrane lipophilicity, J. Pharm. Sci., 92 (2003) 2236-2248. https://doi.org/10.1002/jps.10494

Electronic Supplementary Information

Boosting caffeic acid performance as antioxidant and monoamine oxidase/catechol-O-methyltransferase inhibitor

Daniel Chavarria‡[1,2], Sofia Benfeito‡[1], Tiago Silva[1,2], Cátia Silva[1], Pedro Soares[1], Jorge Garrido[3], Paula Serrão[4,5], Patrício Soares-da-Silva[4,5], Fernando Remião[6], Fernanda Borges[1*]

[1] CIQ/Department of Chemistry and Biochemistry, Faculty of Sciences, University of Porto, 4169-007 Porto, Portugal

[2] CNC - Center for Neuroscience and Cell Biology, University of Coimbra, UC Biotech Building, Biocant Park, Cantanhede, Portugal.

[3] Department of Chemical Engineering, School of Engineering (ISEP), Polytechnic of Porto, 4200-072 Porto, Portugal.

[4] Department of Pharmacology and Therapeutics, Faculty of Medicine, University of Porto, 4200-319 Porto, Portugal

[5] MedInUP – Center for Drug Discovery and Innovative Medicines, University of Porto, 4200-319, Porto, Portugal

[6] UCIBIO-REQUIMTE, Laboratory of Toxicology, Department of Biological Sciences, Faculty of Pharmacy, University of Porto, Porto, Portugal

‡ These authors contributed equally to this work.

* Corresponding Authors:

Fernanda Borges, CIQUP/Department of Chemistry and Biochemistry, Faculty of Sciences, University of Porto, Porto 4169-007, Portugal. E-mail: fborges@fc.up.pt

Contents of electronic supplementary information:

1. Experimental section 186
1.1. Chemistry 186
1.1.1. Reagents 186
1.1.2. Materials and apparatus 186
1.2. Oxygen radical absorbance capacity (ORAC-FL) assay 186
1.3. Electrochemical measurements 187
1.4. Enzymatic assays 187
1.4.1. Evaluation of human monoamine oxidase (*h*MAO) inhibitory activity 187
1.4.2. Evaluation of catechol *O*-methyltransferase inhibitory activity 188
1.4.2.1. Animals 188
1.4.2.2. Homogenate Preparation 188
1.4.2.3. Determination of catechol *O*-methyltransferase activity 188
1.5. *In vitro* toxicology 189
1.5.1. Materials 189
1.5.2. Cell culture 189
1.5.3. Cytotoxicity assays 190
1.5.3.1. Resazurin reduction assay 190
1.5.3.2. Neutral red (NR) uptake assay 190
1.5.4. Evaluation of intracellular oxidative stress levels 302
1.5.5. Statistical analysis 304
1.6. Evaluation of the chromatographic hydrophobicity index at pH 2.3 191
2. References 8

1. Experimental section

1.1. Chemistry

1.1.1. Reagents

Piperine, sodium hydroxide (NaOH), diisopropylethylamine (DIPEA), (Benzotriazol-1-yloxy)tripyrrolidinophosphonium hexafluorophosphate (PyBOP), aniline, benzylamine, (2-bromoethyl)benzene, 1 M solution of boron tribromide (BBr_3) in dichloromethane, ethyl cyanoacetate, cyanoacetic acid, mono-ethyl malonate, pyridine, piperidine, tert-butyldimethylsilyl chloride (TBSCl), imidazole, lithium aluminum hydride ($LiAlH_4$), manganese dioxide (MnO_2), tetra-*n*-butylammonium fluoride (TBAF) were purchased from Sigma Aldrich (St. Louis, MO, USA), Alfa-Aesar (Haverhill, MA, USA) or TCI (Tokyo, Japan). All other reagents and solvents were *pro analysis* grade and were acquired from Carlo Erba Reagents (SDS, France) and Scharlab (Barcelona, Spain) and were used without additional purification.

1.1.2. Materials and apparatus.

The monitoring of reactions progress was performed by thin layer chromatography (TLC) on precoated silica gel 60 F254 acquired from Merck (Darmstad, Germany). TLC spots were visualized under UV detection (254 nm and 365 nm). Some crude products were purified by flash column chromatography. Flash column chromatography was carried out on silica gel 60A acquired from Carlo-Erba Reactifs or on cellulose powder MN 2100 (Macherey Nagel GmbH & Co.KG, Germany). The fractions with the desired compound were gathered and concentrated under reduce pressure. The solvents were evaporated using a Buchi Rotavapor.

^{1}H and ^{13}C NMR and DEPT135 data were acquired, at room temperature, on a Brüker AMX 300 spectrometer operating at 400 and 100 MHz, respectively. The solvents used in NMR experiments included $CDCl_3$-d_1, MeOD-d_4 and DMSO-d_6. The chemical shifts are expressed in δ (ppm) values relative to tetramethylsilane (TMS) as internal reference and coupling constants (*J*) are given in Hz. Electron impact mass spectrometry (EI-MS) spectra were obtained on a Varian 320-MS apparatus. Electrospray ionization mass spectra (ESI-MS) were obtained on an LTQ Orbitrap™ XL hybrid mass spectrometer (Thermo Fischer Scientific, Bremen, Germany) controlled by *LTQ Tune Plus 2.5.5* and *Xcalibur 2.1.0*. The data are reported as m/z (% of relative intensity of the most important fragments).

1.2. Oxygen radical absorbance capacity (ORAC-FL) assay

The ORAC-FL analyses were performed on a multiplate reader (BioTek Synergy HT from BioTek Instruments, Winooski, VT, USA) using black polystyrene 96-well plates. Fluorescence was measured from the top, at an excitation wavelength of 485/20 nm and an emission at 528/20 nm. The plate reader was controlled by Gen5 software. 2,2'-Azobis-(amidinopropane) dihydrochloride (AAPH), (±)-6-hydroxy-2,5,7,8-tetramethylchromane-2-carboxylic acid (trolox) and fluorescein (FL) were purchased from Sigma-Aldrich. The general procedure was adapted from the literature [1, 2], with some modifications.

The reaction was carried out in 75 mM of sodium phosphate buffer solution (pH = 7.4) at a final volume of 200 µL. Stock solutions of FL (5 mM) and antioxidants (5 mM) were prepared in ethanol due to their low solubility in buffer at high concentrations. Then, they were diluted in sodium phosphate buffer solution (pH = 7.4). The range of antioxidant concentrations was empirically selected to obtain a good separation between the fluorescence curves. The test compounds (final concentrations range of 0.1-2 µM) and

fluorescein (40 nM, final concentration) were placed in each well and pre-incubated for 15 min at 37 ºC before the addition of AAPH (final concentration 18 mM). The microplate was immediately placed in the reader and automatically shaken prior to each reading. The fluorescence was measured minutely for 120 min. A control assay with fluorescein, AAPH and buffer (instead of the antioxidant solution) was performed for each assay. Trolox was also included in each assay as standard antioxidant in a final concentration range of 2-8 μM. All reaction mixtures were prepared in triplicate and at least three independent experiments were performed for each test compound. The fluorescence decay curves were normalized by the maximum value of fluorescence, and the areas under the curves (AUC) were determined according to the following **Equation 1**.

$$AUC = 1 + \sum_{i=1}^{i=120} \frac{f_i}{f_0} = 1 + \frac{f_1}{f_0} + \frac{f_2}{f_0} + \frac{f_3}{f_0} + \ldots + \frac{f_{120}}{f_0} \quad \textbf{(Equation 1)}$$

where f_0 = initial fluorescence reading at 0 min and f_i = fluorescence reading at time i. The net AUC is obtained by subtracting the AUC of the blank from that of a sample. The inhibition capacity, expressed as the relative Trolox equivalent ORAC values, was quantified employing the **Equation 2**.

$$\text{relative ORAC value} = \frac{AUC_{antioxidant} - AUC_{control}}{AUC_{trolox} - AUC_{control}} \times \frac{[Trolox]}{[antioxidant]} \quad \textbf{(Equation 2)}$$

where $AUC_{control}$ = area under the curve of control; $AUC_{antioxidant}$ = area under the curve of the test compound; AUC_{trolox} = area under the curve of Trolox (standard); [trolox] = Trolox concentration; and [antioxidant] = antioxidant concentration.

1.3. Electrochemical measurements

Voltammetric studies were carried out using an Autolab PGSTAT 12 potentiostat/galvanostat (Metrohm-Autolab, Netherlands) and one compartment glass electrochemical cell. The voltammetric data was acquired at room temperature using a three-electrode system: a glassy carbon working electrode (GCE) (d = 2 mm), a platinum wire counter electrode and an Ag/AgCl saturated KCl reference electrode (Metrohm, Switzerland). The working electrode was polished manually with an aqueous slurry of alumina powder (BDH Chemicals, VWR, USA) on a microcloth pad and rinsed with water before use. A Crison pH-meter with glass electrode was used for the pH measurements (Crison, Barcelona, Spain).

Voltammetric measurements were performed as described elsewhere [3]. Test solutions were prepared directly in the electrochemical cell, by dilution of ethanolic solutions of the compounds under study (10 mM, 100 μL) in the supporting electrolyte (10 mL) to obtain a final concentration of 100 μM. The scan rates used in differential pulse voltammetry (DPV) and cyclic voltammetry (CV) were 5 $mV.s^{-1}$ and 50 $mV.s^{-1}$, respectively.

1.4. Enzymatic assays

1.4.1. Evaluation of human monoamine oxidase (*h*MAO) inhibitory activity

The human monoamine oxidase (*h*MAO) inhibitory outline was assessed in microsomal MAO isoforms prepared from insect cells (BTI-TN-5B1-4) infected with recombinant baculovirus containing cDNA inserts for *h*MAO-A or *h*MAO-B and by measuring the enzymatic conversion rates of kynuramine into 4-hydroxyquinoline. The appropriate amounts of *h*MAO-A and *h*MAO-B were adjusted to obtain, in our experimental conditions, the same maximum velocity (V_{max} = 50 $pmol.min^{-1}$) for both isoforms (*h*MAO-A: 3

ng.μL^{-1}; *h*MAO-B: 12 ng.μL^{-1}). All assays were performed in sodium phosphate buffer solution 50 mM pH 7.4.

The compounds under study and reference inhibitors were pre-incubated at 37 ºC for 10 min in the presence of kynuramine (K_m *h*MAO-A = 20 μM; K_m *h*MAO-B = 20 μM; final concentration: 2×K_m) in 96-well microplates (BRANDplates, pureGrade™, BRAND GMBH, Wertheim, Germany). Then, the reaction was started with the addition of *h*MAO-A or *h*MAO-B. Initial velocities were determined spectrophotometrically in a microplate reader (BioTek Synergy HT from BioTek Instruments, Winooski, VT, USA) at 37 °C by measuring the formation of 4-hydroxyquinoline at 316 nm, over a period of at least 30 minutes (interval of 1 minute). Data were analysed using GraphPad PRISM version 6 for Windows (GraphPad Software®, San Diego, CA, USA). The initial velocities, obtained from the linear phase of product formation, were normalized and plotted against the respective inhibitor concentration. IC_{50} values were obtained from dose-response curves and were expressed as mean ± standard deviation. IC_{50} values were determined from at least three independent experiments, each performed in triplicate.

1.4.2. Evaluation of catechol *O*-methyltransferase inhibitory activity

1.4.2.1. Animals

Male Wistar rats obtained from Harlan (Barcelona, Spain) were kept 8 per cage, under controlled environmental conditions (12 h light/dark cycle and room temperature of 22 ±1 °C) with food and tap water allowed *ad libitum*. Twenty minutes before sacrifice, animals were anesthetized with sodium pentobarbital (60 mg/kg) administered intraperitoneally. After sample collection, anaesthetized animals were euthanized by decapitation. All experiments were approved by the local Ethics Committee for the welfare of experimental animals and performed in accordance with national legislation.

1.4.2.2. Homogenate Preparation

Tissues were thawed at room temperature and homogenized using a Diax homogenizer (Heidolph, 2 cycles of 20 s in position 5, on ice). Total protein content in homogenates was measured by the Bio-Rad standard protein assay using a standard curve of bovine serum albumin (50-250 μg/mL). Then, samples were diluted to obtain a concentration of 4 mg/mL.

1.4.2.3. Determination of catechol *O*-methyltransferase activity

COMT inhibitory activities was assessed in rat liver and brain homogenates by measuring the *O*-methylation of adrenaline into metanephrine [4, 5]. Aliquots of liver or brain homogenates (100 μL, 2 mg/mL protein) were preincubated for 20 min with 80 μL of test compounds in phosphate buffer 5 mM containing pargyline (100 μM), $MgCl_2$ (100 μM), ethylene glycol tetracetic acid (EGTA, 1 mM) and saturating concentrations of SAM (500 μM and 100 μM for liver and and brain homogenates, respectively). For experiments with liver homogenates, adrenaline (1000 μM) was added, and the mixture was incubated for additional 5 min. For experiments with brain homogenates, adrenaline (5 μM) was added, and the mixture was incubated for additional 15 min. The pre-incubation and incubation were performed at 37 °C, in conditions of light protection, with continuous shaking and without oxygenation. After the incubation period, the reaction was stopped with the addition of perchloric acid 2 M (50 μL) and the tubes were transferred to ice. The samples were then centrifuged (200 g, 4 min, 4 °C), and aliquots of the supernatant (250 μL) were filtered on 0.22 μm

pore size Spin-X filter tubes Costar. Aliquots of the filtered supernatant (50 µL) were injected into the chromatograph. The chromatography system consisted of a pump Gilson model 302 (Gilson Medical Electronics, Villiers le Bel, France) connected to a manometric module (Gilson model 802 C) and a stainless steel 5 mm ODS column (Biophase; Boanalytical Systems, West Lafayette, IN) of 25 cm length; samples were injected by means of an automatic sample injector (Gilson model 234). The mobile phase was a degassed solution of citric acid (0.1 mM), sodium octylsulfate (0.5 mM), sodium acetate (0.1 M), EDTA (0.17 mM), dibutylamine (1 mM), and methanol 6% (v/v), adjusted to pH 3.5 with perchloric acid 2 M and pumped at a rate of 1.0 mL/min. The detection was carried out electrochemically with a glassy carbon electrode, an Ag/AgCl reference electrode, and an amperometric detector Gilson (model 141); the detector cell was operated at 0.75 V. The current produced was monitored using the Gilson 712 HPLC software. The lower limits for detection of metanephrine ranged from 350 to 500 fmol. To determine the IC_{50} values, the parameters of the equation for one site inhibition were fitted to the experimental data.

1.5. *In vitro* toxicology

1.5.1. Materials

All reagents used were of analytical grade or of the highest grade available. Neutral red (NR) solution, resazurin, Dulbecco's Modified Eagle's Medium (DMEM) with 4.5 g/L glucose, retinoic acid, 12-*O*-tetradecanoylphorbol-13-acetate (TPA), 2',7'-dichorofluorescein diacetate (DCFH-DA) and *tert*-butyl hydroperoxide (*t*-BHP) were obtained from Sigma Aldrich (St. Louis, MO, USA). Reagents used in cell culture such as heat-inactivated fetal bovine serum (FBS), antibiotic (10,000 U/mL penicillin, 10,000 µg/mL streptomycin), MEM Non-Essential Amino Acids solution (100×) (MEM NEAA), 0.25% trypsin/1 mM ethylenediamine tetraacetic acid (EDTA) and Hanks' balanced salt solution (HBSS) were purchased from Gibco Laboratories (Lenexa, KS, USA). Dimethylsulfoxide (DMSO), absolute ethanol, and acetic acid were obtained from Merck (Darmstadt, Germany).

1.5.2. Cell culture

Human neuroblastoma SH-SY5Y cells were routinely cultured into 75 cm^3 flasks and maintained in DMEM with 4.5 g/L glucose, supplemented with 10 % heat-inactivated FBS (v/v), 1 % MEM NEAA (v/v) and 1% penicillin/streptomycin (v/v). Cells were maintained at 37 °C in a humidified, 5% CO_2−95% air atmosphere, and the culture medium was changed every 2-3 days. The cultures were passaged once a week by trypsinization (0.25 % trypsin/1 mM EDTA). To avoid phenotypic changes, the cells used for all experiments were taken between 19th and 28th passages. Cells were differentiated as described previously by Fernandes *et al*. [6]. Briefly, SH-SY5Y cells were seeded onto 96-well plates at a density of 25,000 cells/cm^2 in cell culture medium with *trans*-retinoic acid (RA) (final concentration of 10 µM) and incubated for 3 days at 37 °C in a humidified, 5% CO_2−95% air atmosphere. Then, the cell culture medium was removed and replaced with medium supplemented with 12-*O*-tetradecanoylphorbol-13-acetate (TPA) (final concentration 80 nM), and cells were incubated for 3 days. Stock solutions of RA (10 mM) and TPA (80 µM) were prepared in DMSO.

1.5.3. Cytotoxicity assays

1.5.3.1. Resazurin reduction assay

Resazurin is a non-fluorescent, non-toxic water-soluble dye able to permeate through cell membranes [7]. Inside the cells, resazurin is enzymatically reduced into the pink-colored and highly fluorescent resorufin [8, 9]. Since the conversion of resazurin into resorufin occurs mostly in mitochondria, the amount of resorufin produced can be used as indicator of metabolic activity [10]. The quantity of resorufin production is proportional to the number of viable cells in culture and can be quantified fluorometrically or colorimetrically [8].

Resazurin reduction assay was performed as previously described by Fernandes *et al.* [6]. Briefly, after the 24 h incubation periods with the test compounds, the cell culture medium was removed and replaced with fresh culture medium with resazurin (10 μg/mL) prepared in cell culture medium. Differentiated SH-SY5Y cells were incubated for 2 h at 37 °C in a humidified 5% CO_2–95% air atmosphere. Then, the fluorescence was read in a multiwell microplate reader (PowerWave XS from BioTek Instruments, Vermont, US), using an excitation wavelength of 540 nm and an emission wavelength of 590 nm. The results were expressed as the percentage of resazurin reduction relative to that of the control (non-treated) cells [resazurin reduction (% of control)] ± standard error mean (SEM) of at least three independent experiments.

1.5.3.2. Neutral red (NR) uptake assay

The neutral red (NR) uptake assay is based on the ability of viable cells to incorporate the supravital dye NR and retain it inside the lysosomes [11]. NR uptake assay was performed as previously described by Fernandes *et al*. [12] Briefly, after the 24 h incubation periods with the test compounds, the cell culture medium was removed and a solution of NR (50 mg/mL) in fresh cell culture medium was added. Differentiated SH-SY5Y cells were incubated for 2 h at 37 °C in a humidified, 5% CO_2–95% air atmosphere. Then, the cell culture medium was removed and replaced by ethanol absolute/distilled water (1:1) with 5 % acetic acid to liberate the dye from the viable cells. The absorbance was measured at 540 nm in a multiwell microplate reader (PowerWave XS from BioTek Instruments). The results were expressed as the percentage of NR uptake relative to that of the control (non-treated) cells [NR uptake (% of control)] ± standard error mean (SEM) of at least three independent experiments.

1.5.4. Evaluation of intracellular oxidative stress levels

The evaluation of intracellular oxidative stress using 2',7'-dichorofluorescein diacetate (DCFH-DA), a non-fluorescent probe able to cross the cell membrane. Inside the cells, DCFH-DA is hydrolyzed by esterases to the polar non-fluorescent reduced derivative 2',7'-dichlorofluorescein (DCFH), which, due to its polarity, is trapped within the cells. The subsequent oxidation of DCFH by reactive species (RS) yields the green fluorescent 2',7'-dichlorofluorescein (DCF) [13, 14].

DCF fluorescence assay was performed as previously described by Fernandes *et al.* [6]. SH-SY5Y cells were seeded and differentiated onto 96-well black plates (Greiner CELLSTARW, Sigma Aldrich). Cells were pre-incubated with DCFH-DA 4 μM in culture medium on the day of the experiment for 1.5 h, at 37 ºC, in the dark. Then, cells were incubated with the test compound (10 and 50 μM) in culture medium for 24 h. A blank (vehicle and culture medium without cells) and a negative control (cells treated with culture medium

containing vehicle) were also included in the plate to measure the background fluorescence and the basal RS production, respectively. Fluorescence was recorded at the selected timepoint on a fluorescence microplate reader (BioTek Instruments, Vermont, USA) set to 485 nm excitation and 530 nm emission.

1.5.5. Statistical analysis

The data obtained are expressed as mean ± standard error mean (SEM) of at least three independent experiments (n = 3). All statistical analyses were performed using GraphPad PRISM version 6 for Windows. The normality of the data distribution was evaluated using three normality tests: KS normality test, D'Agostino and Pearson omnibus normality test, and Shapiro−Wilk normality test. For data with a parametric distribution, statistical comparisons between groups were estimated using the parametric method one-way analysis of variance (ANOVA) followed by Dunnett's multiple comparison test. For data with a non-parametric distribution, statistical comparisons were estimated using the nonparametric method of Kruskal–Wallis [one-way ANOVA on ranks] followed by Dunn's *post hoc* test. In all cases, p values lower than 0.05 were considered significant.

1.6. Evaluation of the chromatographic hydrophobicity index at pH 2.3

Chromatographic hydrophobicity index (CHI) values at pH 2.3 were determined using the retention times of samples and a mixture of standard compounds measured on a Shimadzu high-performance liquid chromatograph SPD-M20A system (Shimadzu, Kyoto, Japan) with a Luna C18 (2) column (Phenomenex, CA, USA) 150×4.6 mm, 5 µm. Mobile phase A was aqueous solution of acetic acid 1 % (v/v) (pH 2.3), and mobile phase B was acetonitrile. The following gradient program was applied: 1 mL/min flow, rt, injection volume 20 µL, gradient 0−6 min 0-100 % B, 6−14 min 100% B, 14−16 min 100-0 % B.

A calibration curve was obtained using a mixture of the following compounds: paracetamol, theophylline, caffeine, benzimidazole, colchicine, carbamazepine, indole, propiophenone, butyrophenone, valerophenone, and heptanophenone. Stock solutions of the test compounds (10 µM) were prepared in DMSO and diluted in acetonitrile/water (1:1) to obtain a final concentration of 250 µM. Chromatographic hydrophobicity index (CHI) were calculated as previously described [15, 16].

2. References

[1] B. Ou, M. Hampsch-Woodill, R.L. Prior, Development and validation of an improved oxygen radical absorbance capacity assay using fluorescein as the fluorescent probe, J. Agric. Food Chem., 49 (2001) 4619-4626. https://doi.org/10.1021/jf010586o

[2] F. Mura, T. Silva, C. Castro, F. Borges, M.C. Zuniga, J. Morales, C. Olea-Azar, New insights into the antioxidant activity of hydroxycinnamic and hydroxybenzoic systems: spectroscopic, electrochemistry, and cellular studies, Free Radic. Res., 48 (2014) 1473-1484. https://doi.org/10.3109/10715762.2014.965702

[3] J. Garrido, A. Gaspar, E.M. Garrido, R. Miri, M. Tavakkoli, S. Pourali, L. Saso, F. Borges, O. Firuzi, Alkyl esters of hydroxycinnamic acids with improved antioxidant activity and lipophilicity protect PC12 cells against oxidative stress, Biochimie, 94 (2012) 961-967. https://doi.org/10.1016/j.biochi.2011.12.015

[4] M.A. Vieira-Coelho, P. Soares-da-Silva, Effects of tolcapone upon soluble and membrane-bound brain and liver catechol-O-methyltransferase, Brain Res., 821 (1999) 69-78. https://doi.org/10.1016/s0006-8993(99)01063-x

[5] T. Silva, T. Mohamed, A. Shakeri, P.P. Rao, L. Martinez-Gonzalez, D.I. Perez, A. Martinez, M.J. Valente, J. Garrido, E. Uriarte, P. Serrao, P. Soares-da-Silva, F. Remiao, F. Borges, Development of Blood-Brain Barrier Permeable Nitrocatechol-Based Catechol O-Methyltransferase Inhibitors with Reduced Potential for Hepatotoxicity, J. Med. Chem., 59 (2016) 7584-7597. https://doi.org/10.1021/acs.jmedchem.6b00666

[6] C. Fernandes, M. Pinto, C. Martins, M.J. Gomes, B. Sarmento, P.J. Oliveira, F. Remião, F. Borges, Development of a PEGylated-Based Platform for Efficient Delivery of Dietary Antioxidants Across the Blood-Brain Barrier, Bioconjug. Chem., 29 (2018) 1677-1689. https://doi.org/10.1021/acs.bioconjchem.8b00151

[7] S.N. Rampersad, Multiple applications of Alamar Blue as an indicator of metabolic function and cellular health in cell viability bioassays, Sensors (Basel), 12 (2012) 12347-12360. https://doi.org/10.3390/s120912347

[8] J. O'Brien, I. Wilson, T. Orton, F. Pognan, Investigation of the Alamar Blue (resazurin) fluorescent dye for the assessment of mammalian cell cytotoxicity, Eur. J. Biochem., 267 (2000) 5421-5426. https://doi.org/10.1046/j.1432-1327.2000.01606.x

[9] E.M. Czekanska, Assessment of cell proliferation with resazurin-based fluorescent dye, Methods Mol. Biol., 740 (2011) 27-32. https://doi.org/10.1007/978-1-61779-108-6_5

[10] A. van Tonder, A.M. Joubert, A.D. Cromarty, Limitations of the 3-(4,5-dimethylthiazol-2-yl)-2,5-diphenyl-2H-tetrazolium bromide (MTT) assay when compared to three commonly used cell enumeration assays, BMC Res. Notes, 8 (2015) 47. https://doi.org/10.1186/s13104-015-1000-8

[11] G. Repetto, A. del Peso, J.L. Zurita, Neutral red uptake assay for the estimation of cell viability/cytotoxicity, Nat. Protoc., 3 (2008) 1125-1131. https://doi.org/10.1038/nprot.2008.75

[12] C. Fernandes, C. Martins, A. Fonseca, R. Nunes, M.J. Matos, R. Silva, J. Garrido, B. Sarmento, F. Remiao, F.J. Otero-Espinar, E. Uriarte, F. Borges, PEGylated PLGA Nanoparticles As a Smart Carrier to Increase the Cellular Uptake of a Coumarin-Based Monoamine Oxidase B Inhibitor, ACS Appl. Mater. Interfaces, 10 (2018) 39557-39569. https://doi.org/10.1021/acsami.8b17224

[13] S. Aula, S. Lakkireddy, K. Jamil, A. Kapley, A.V.N. Swamy, H.R. Lakkireddy, Biophysical, biopharmaceutical and toxicological significance of biomedical nanoparticles, RSC Adv., 5 (2015) 47830-47859. https://doi.org/10.1039/c5ra05889a

[14] K.A. Kang, H.C. Lee, J.J. Lee, M.N. Hong, M.J. Park, Y.S. Lee, H.D. Choi, N. Kim, Y.G. Ko, J.S. Lee, Effects of combined radiofrequency radiation exposure on levels of reactive oxygen species in neuronal cells, J. Radiat. Res., 55 (2014) 265-276. https://doi.org/10.1093/jrr/rrt116

[15] G. Camurri, A. Zaramella, High-throughput liquid chromatography/mass spectrometry method for the determination of the chromatographic hydrophobicity index, Anal. Chem., 73 (2001) 3716-3722. https://doi.org/10.1021/ac001388j

[16] K. Valko, S. Nunhuck, C. Bevan, M.H. Abraham, D.P. Reynolds, Fast gradient HPLC method to determine compounds binding to human serum albumin. Relationships with octanol/water and immobilized artificial membrane lipophilicity, J. Pharm. Sci., 92 (2003) 2236-2248. https://doi.org/10.1002/jps.10494

3.4. Manuscript V

Development of piperic acid-based monoamine oxidase inhibitors: synthesis, structural characterization and biological evaluation

Journal of Molecular Structure, **2019**, 1182: 298-307.
DOI: 10.1016/j.molstruc.2019.01.060

Journal of Molecular Structure 1182 (2019) 298–307

Contents lists available at ScienceDirect

Journal of Molecular Structure

journal homepage: http://www.elsevier.com/locate/molstruc

Development of piperic acid-based monoamine oxidase inhibitors: Synthesis, structural characterization and biological evaluation

Daniel Chavarria [a], Fernando Cagide [a], Miguel Pinto [a], Lígia R. Gomes [b, c], John N. Low [d], Fernanda Borges [a, *]

[a] *CIQUP, Department of Chemistry and Biochemistry, Faculty of Sciences, University of Porto, Porto, Portugal*
[b] *FP-ENAS, Faculty of Health Sciences, University of Fernando Pessoa, Porto, Portugal*
[c] *REQUIMTE /LAQV, Department of Chemistry and Biochemistry, Faculty of Sciences, University of Porto, Porto, Portugal*
[d] *Department of Chemistry, University of Aberdeen, Meston Walk, Scotland, UK*

ARTICLE INFO

Article history:
Received 1 December 2018
Received in revised form
18 January 2019
Accepted 18 January 2019
Available online 22 January 2019

Keywords:
Piperine derivatives
1D NMR
2D NMR
X-ray crystallography
MAO inhibitors

ABSTRACT

A series of piperic acid esters and amides were synthesized using a two-step strategy. Mass spectrometry and unidimensional (^{1}H NMR, ^{13}C NMR, DEPT) and bidimensional (COSY, HSQC, HMBC) NMR methodologies were used to study the molecular structure of the final compounds, resulting in the assignment of all detected signals.

Preliminary biological data of piperine and the derivatives thereof showed that piperic acid **2** and amides **3** and **4** did not display significant inhibitory activity at 10 μM against both *h*MAO-A and *h*MAO-B. In contrast, the esters **5** and **6** displayed relevant *h*MAO inhibitory activities, with IC_{50} values for *h*MAO-B lower than piperine and within the nanomolar range (compound **1**: $IC_{50} = 1.05$ μM; compound **6**: $IC_{50} = 169$ nM; compound **5**: $IC_{50} = 156$ nM). Moreover, X-ray crystallographic analyses showed relevant differences between amides **3** and **4** and esters **5** and **6** constituting a valuable information to understand the ligand-target interactions.

Additional studies are warranted for a systematic lead optimization process that can lead in the future to a more potent and selective *h*MAO-B inhibitor based on piperine scaffold.

© 2019 Elsevier B.V. All rights reserved.

1. Introduction

Piperine (*trans*, *trans* isomer of 1-[5-[1,3-benzodioxol-5-yl]-1-oxo-2,4-penta-dienyl]piperidine, Fig. 1) is the major pungent alkaloid extracted from the fruits of black and long pepper plants (*Piper nigrum* Linn and *Piper longum* Linn, respectively) [1].

Black and long peppers have been used in traditional medicine in Asia and Pacific Islands to treat several disorders [1,2], the effects of which have been mainly assigned to piperine [1,3]. In fact, piperine has been ascribed to diverse biological properties (*e.g.*: bioavailability enhancement, anti-inflammatory, antioxidant, antitumoral, antidepressant) [3,4], and therefore used as inspiration for the development of new pharmacologically relevant compounds with application in numerous human diseases [3].

Piperine is considered a privileged scaffold for drug discovery programs. Structurally, piperine can be divided into three regions that are considered to be connected with its versatile pharmacological profile: (A) an aromatic ring with a methylenedioxy bridge, (B) a conjugated dienone system and (C) the piperidine ring, which is attached to the side chain through a carbonylamide linkage (Fig. 1) [5,6]. Accordingly, the structural modification of each region and the establishment of structure-activity relationships have been performed to obtain piperine-like derivatives with enhanced therapeutic potential [3,7].

Monoamine oxidases (MAOs, EC 1.4.3.4) are mitochondrial flavoenzymes that catalyze the oxidative deamination of endogenous and exogenous amines including, among others, neurotransmitters, hormones and dietary amines [8,9]. Two subtypes have been identified in mammals – MAO-A and MAO-B – that have different clinical importance due to the substrate specificity, sensitivity to inhibitors and distribution in tissues and brain regions [10]. In particular, inhibitors of MAO-B are used on the therapy of Parkinson's disease [10], a disease that is pathologically characterized by the loss of dopaminergic neurons in the *substantia nigra pars compacta* [11]. Although dopamine is a substrate for both isoforms,

* Corresponding author. Department of Chemistry and Biochemistry, Faculty of Sciences, University of Porto, Rua do Campo Alegre 687, 4169-007, Porto, Portugal.
E-mail address: fborges@fc.up.pt (F. Borges).

https://doi.org/10.1016/j.molstruc.2019.01.060
0022-2860/© 2019 Elsevier B.V. All rights reserved.

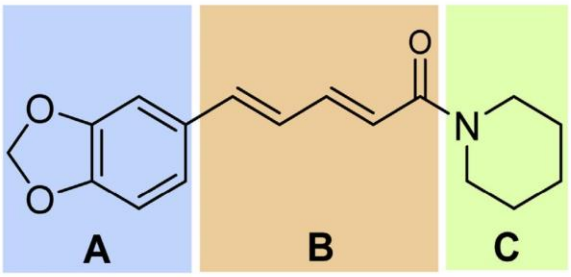


Fig. 1. Chemical structure of piperine (**1**).

it is mainly degraded by MAO-B in the *substantia nigra* [8]. Remarkably, the expression and the activity of MAO-B in neuronal tissue enhance 4-fold with aging. As a result, dopamine metabolism is increased, leading to dopamine deficiency and to a higher production of hydrogen peroxide and other reactive species during the substrate degradation, processes that ultimately lead to neuronal degeneration [8,12].

Along the last years our R&D project has been focused on the discovery of new chemical entities (NCEs) for MAO inhibition. The MAO-inhibitory properties of piperine have been described in previous studies [13,14]. Accordingly, based on a bioinspired strategy, a small piperine-based library was developed by our group aimed to find out a new MAO-B inhibitor for Parkinson's disease therapy. The main modifications of the piperine scaffold included the replacement of the piperidine ring by phenyl or benzyl groups linked to piperic acid by ester or amide functions. Within this framework, a complete structural elucidation of piperine-like compounds was found to be relevant. Herein, we report the synthesis and complete structural characterization, using unidimensional and bidimensional nuclear magnetic resonance (NMR) techniques, electrospray ionization mass spectrometry (ESI-MS) and single X-ray crystallography, of some piperine derivatives. Moreover, the compounds were screened toward human MAOs isoforms (*h*MAO-A and *h*MAO-B) to evaluate their potency/selectivity ratio.

2. Experimental section

2.1. Materials

Piperine, sodium hydroxide (NaOH), diisopropylethylamine (DIPEA), (Benzotriazol-1-yloxy)tripyrrolidinophosphonium hexafluorophosphate (PyBOP), aniline, benzylamine, *N*-(3-dimethylaminopropyl)-*N*′-ethylcarbodiimide hydrochloride (EDC.HCl), 4-(dimethylamino)pyridine (DMAP), phenol, potassium carbonate (K_2CO_3) and benzyl bromide were purchased from Sigma Aldrich, Alfa-Aesar or TCI. All other reagents and solvents were pro analysis grade, and used without additional purification, and acquired from Carlo Erba Reagents and Scharlab.

The monitoring of reactions progress was performed by thin layer chromatography (TLC) on precoated silica gel 60 F254 acquired from Merck (Darmstad, Germany). TLC spots were visualized under UV detection (254 nm and 365 nm). After the extraction step, organic layers were washed with brine, dried over anhydrous sodium sulphate and concentrated under reduced pressure. Generally, crude products were purified by flash column chromatography carried out on silica gel 60 Å acquired from Carlo-Erba Reactifs (SDS, France). The fractions with the desired compound were gathered and concentrated. The solvents were evaporated using a Buchi Rotavapor.

2.2. NMR spectroscopy

^{1}H and ^{13}C NMR data were acquired on a Bruker Advance III 400 NMR spectrometer operating at 400.15 and 100.62 MHz, respectively. In ^{1}H NMR experiments, the relaxation delay was 90° pulse, spectral width of 8012 Hz and 65 K data points. In the case of the ^{13}C NMR experiments, the corresponding parameters were 30° pulse, 24038 Hz and 65 K, respectively, and 2.0-s relaxation delay. For the Distortionless Enhancement by Polarization Transfer (DEPT) sequence, the width of the 90° pulse for ^{13}C was 7.7 μs, and the 90° pulse for ^{1}H was 9.8 μs; the delay 2JC, H was set to 2.0 ms. For correlation spectroscopy (COSY) and heteronuclear single quantum coherence (HSQC), the data points were set to 2K × 256 (t2 × t1) with a relaxation delay D_1 of 1.5 s. The heteronuclear multiple bond connectivity (HMBC) was acquired with data points set to 4 K × 256 (t2 × t1) and relaxation delay D_1 of 1 s. Furthermore, the long-range coupling time for HMBC was set to 71 ms. The data were processed using quadratic sine-bell weighting functions in both dimensions. ^{1}H and ^{13}C spectra of the samples were recorded at room temperature in 5 mm outer diameter tubes. Samples were prepared in deuterated chloroform ($CDCl_3$-d_1) or deuterated dimethylsulfoxide (DMSO-d_6). Tetramethylsilane was used as internal reference; chemical shifts (δ) were expressed in parts per million (ppm) and coupling constants (J) were given in Hertz (Hz).

2.3. Mass spectrometry

Electrospray ionization mass spectra (ESI-MS) were obtained on a LTQ Orbitrap™ XL hybrid mass spectrometer (Thermo Fischer Scientific, Bremen, Germany) controlled by *LTQ Tune Plus 2.5.5* and *Xcalibur 2.1.0*. The data were reported as *m/z* (% of relative intensity).

2.4. Chemistry

2.4.1. Synthesis of (2E,4E)-5-(benzo[d][1,3]dioxol-5-yl)penta-2,4-dienoic acid (piperic acid, **2**)

In a double neck round bottom flask a methanolic solution of NaOH 2 M (26.4 mL, 52.8 mmol) was added to piperine (compound **1**) (3.01 g, 10.6 mmol). The mixture was protected from the light and refluxed for 24 h. Once the reaction was complete, water (30 mL) was added and the mixture was acidified with HCl 6 M at 0 °C. The solid was isolated by filtration under reduced pressure and washed with methanol and dichloromethane. TLC analysis was performed in dichloromethane/methanol/formic acid (9:1:0.001). The procedure was adapted from Venkatasamy et al. [15] with slight modifications.

Yield (%): 83.3; **ESI/MS m/z (%)**: 219 (M^++1, 100).

2.4.2. Synthesis of amides based on piperic acid

Piperic acid (**2**) (1 mmol) was dissolved in DMF and DIPEA (1.01 mmol). Then, the mixture was cooled at 0 °C, and a solution of PyBOP (1.01 mmol) in dichloromethane (2.25 mL) was added slowly. After stirring for 30 min aniline or benzylamine (1.01 mmol) was added and the reaction stirred overnight at room temperature. Upon completion, the mixture was dissolved in dichloromethane (30 mL) and extracted with HCl 1 M (3 × 10 mL), saturated aqueous solution of $NaHCO_3$ (3 × 10 mL) and water (3 × 15 mL). The product was purified by flash column chromatography (ethyl acetate/dichloromethane (3:7)) and recrystallized from dichloromethane/petroleum ether. TLC analysis was performed in ethyl acetate/dichloromethane (3:7). The procedure was adapted from Gaspar

et al. [16].

*2.4.2.1. (2E,4E)-5-(benzo[d][1,3]dioxol-5-yl)-N-phenylpenta-2,4-dienamide (**3**).*

Yield (%): 44.5; **ESI/MS m/z (%)**: 294 (M^++1, 100).

*2.4.2.2. (2E,4E)-5-(benzo[d][1,3]dioxol-5-yl)-N-benzylpenta-2,4-dienamide (**4**).*

Yield (%): 82.7; **ESI/MS m/z (%)**: 308 (M^++1, 100).

2.4.3. Synthesis of esters based on piperic acid

*2.4.3.1. Synthesis of phenyl (2E,4E)-5-(benzo[d][1,3]dioxol-5-yl) penta-2,4-dienoate (**5**).* To a stirred solution of piperic acid (0.25 g, 1.15 mmol) in dichloromethane (5 mL), EDC.HCl (0.27 g, 1.41 mmol) and DMAP (0.0178 g, 0.15 mmol) were added. The reaction was stirred at room temperature for 30 min. Then, phenol (0.17 g, 1.81 mmol) was added and the resulting mixture was stirred overnight, protected from the light. Upon completion, dichloromethane (30 mL) was added and the mixture was extracted with saturated aqueous solution of $NaHCO_3$ (3 × 15 mL), HCl 1 M (3 × 15 mL) and water (3 × 15 mL). The crude product was chromatographed on silica gel (dichloromethane) and recrystallized in dichloromethane/petroleum ether. The procedure was adapted from Soda et al. [17] with some modifications.

Yield (%): 67.9; **ESI/MS m/z (%)**: 295 (M^++1, 100).

*2.4.3.2. Synthesis of benzyl (2E,4E)-5-(benzo[d][1,3]dioxol-5-yl) penta-2,4-dienoate (**6**).* Piperic acid (0.26 g, 1.17 mmol) was dissolved in DMF (3 mL) and K_2CO_3 (0.19 g, 1.39 mmol) was added. The mixture was stirred at room temperature for 30 min. Then, benzyl bromide (200 μL, 1.68 mmol) was added and the mixture was stirred at 80 °C for 8 h, protected from the light. Upon completion, the reaction was quenched with water (25 mL) and extracted with dichloromethane (3 × 10 mL). The crude product was purified by flash column chromatography (silica, dichloromethane) and recrystallized in dichloromethane/petroleum ether. TLC analysis was performed in dichloromethane. The procedure was adapted from Shi et al. [18] with minor modifications.

Yield (%): 84.5; **ESI/MS m/z (%)**: 309 (M^++1, 100).

2.5. X-ray diffraction

Crystals of compounds **3**–**6** used for X-ray crystallographic analysis were prepared by recrystallization from CH_2Cl_2/*n*-hexane (1:1). Information about crystal data, experimental data collection conditions, and refinement as well as the structural geometric parameters are available as an Electronic Supplementary Publication from the Cambridge Crystallographic Data Centre, (CCDC1811725, 1811726, 1811723 and 1811722 for compounds **3**–**6** respectively) at https://www.ccdc.cam.ac.uk/structures in CIF format. The structure of (piperic acid, (2*E*,4*E*)-5-(3,4-methylenedioxyphenyl)-2,4-pentadienoic acid) was published by the authors as the CSD Communication (HENPOI, CCDC 1811724).

2.6. Evaluation of human monoamine oxidase (hMAO) inhibitory activity

The inhibitory activity of piperine and derivatives thereof on *h*MAO-A and *h*MAO-B was studied using an experimental protocol described elsewhere [19], with some modifications. The *h*MAO inhibitory outline was assessed in microsomal MAO isoforms prepared from insect cells (BTI-TN-5B1-4) infected with recombinant baculovirus containing cDNA inserts for *h*MAO-A or *h*MAO-B (Sigma-Aldrich Quimica S.A.) and by measuring the enzymatic conversion rates of kynuramine into 4-hydroxyquinoline. The appropriate amounts of *h*MAO-A and *h*MAO-B were adjusted to obtain, in our experimental conditions, the same maximum velocity (V_{max} = 50 pmol.min^{-1}) for both isoforms (*h*MAO-A: 3 ng μL^{-1}; *h*MAO-B: 12 ng μL^{-1}). All assays were performed under sodium phosphate buffered conditions (50 mM, pH = 7.4).

The compounds under study and reference inhibitors were pre-incubated at 37 °C for 10 min in the presence of kynuramine (K_m *h*MAO-A = 20 μM; K_m *h*MAO-B = 20 μM; final concentration: 2 × K_m) in 96-well microplates (BRANDplates, pureGradeTM, BRAND GMBH, Wertheim, Germany). Then, the reaction was started with the addition of *h*MAO-A or *h*MAO-B. Initial velocities were determined spectrophotometrically in a microplate reader (Biotek Synergy HT) at 37 °C by measuring the formation of 4-hydroxyquinoline at 316 nm, over a period of at least 30 min (interval of 1 min). Data were analysed using GraphPad PRISM version 6 for Windows (GraphPad Software®, San Diego, CA, USA). The initial velocities, obtained from the linear phase of product formation, were normalized and plotted against the respective inhibitor concentration. IC_{50} values were obtained from dose-response curves and were expressed as mean ± standard deviation. IC_{50} values were determined from at least three independent experiments, each performed in triplicate.

3. Results and discussion

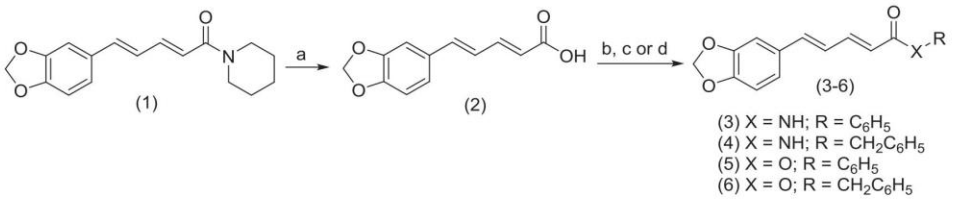
3.1. Chemistry

Piperic acid derivatives **3**–**6** were obtained following the synthetic strategy depicted in Scheme 1. First, piperic acid (compound **2**) was obtained by an alkaline hydrolysis of piperine (Scheme 1, step *a*). Then, a PyBOP-mediated amidation of piperic acid with aniline or benzylamine, under alkaline conditions, yielded the piperic acid amides **3** and **4** (Scheme 1, step *b*). The piperic acid esters (compounds **5** and **6**) were synthesized following two different strategies: piperic acid phenyl ester (compound **5**) was prepared by a Steglich esterification between piperic acid and phenol, assisted by EDC and DMAP (Scheme 1, step *c*) and piperic acid benzyl ester (compound **6**) was synthesized from piperic acid by a bimolecular nucleophilic substitution reaction with benzyl bromide (Scheme 1, step *d*).

3.2. Nuclear magnetic resonance spectroscopic analysis

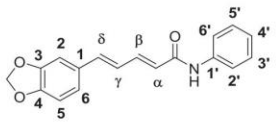
The structural characterization of piperic acid amides **3**–**4** and esters **5**–**6** was performed by ESI-MS, and unidimensional (^{1}H NMR, ^{13}C NMR, DEPT135) and bidimensional (COSY, HSQC and HMBC) NMR techniques. The ^{1}H and ^{13}C chemical shifts (δ) and the HMBC ^{13}C-^{1}H correlations are described in Tables 1 and 2.

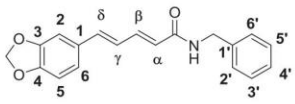
Regarding the piperonyl moiety, the protons of the methylenedioxyphenyl (MDP) ring (H2, H5, H6 and CH_2) and the diene tether (Hα, Hβ, Hγ and Hδ) were unequivocally assigned according to their chemical shifts, signal multiplicities (Tables 1 and 2) and COSY (Fig. 2A) correlations. Slight variations of the δ values were recorded for compound **3**, which were ascribed to the different



Scheme 1. Synthetic strategy pursued to obtain piperine derivatives (**3**–**6**). Reagents and conditions: (*a*) NaOH 2 M in methanol, reflux, 24 h; (*b*) 1. DMF, DIPEA, PyBOP, CH_2Cl_2, 0 °C, 30 min; 2. Benzylamine, rt, overnight; (*c*) 1. EDC.HCl, DMAP, CH_2Cl_2, rt, 30 min; 2. phenol, rt, overnight; (*d*) 1. K_2CO_3, DMF, rt, 30 min; 2. benzylbromide, 80 °C, 8 h.

Table 1
^{1}H and ^{13}C chemical shifts and HMBC correlations for compounds **3** (DMSO-d_6) and **4** ($CDCl_3$-d_1).





	Compound **3**			Compound **4**		
	^{1}H NMR[a]	^{13}C NMR	HMBC[b]	^{1}H NMR	^{13}C NMR	HMBC
OCH_2O	6.06 (s)	101.8	C3, C4	5.97 (s)	101.3	C3, C4
1	—	131.2	—	—	130.8	—
2	7.32 (m)	106.2	C3, C4, C5, C6, Cδ	6.90 (d, 1.6)	105.8	C3, C4, C5, C6, Cδ
3	—	148.4	—	—	148.2	—
4	—	148.4	—	—	148.3	—
5	6.93 (d, 8.0)	108.9	C1, C2, C3, C4, C6, Cγ	6.76 (m)	108.5	—[c]
6	7.04 (m)	123.4	C2, C3, C4, Cδ	6.88 (dd, 1.6, 8.1)	122.7	C2, C3, C4, Cγ, Cδ
α	6.30 (d, 14.9)	124.8	Cβ, Cγ, Cδ, CO	5.93 (d, 14.9)	122.7	Cβ, Cγ, Cδ, CO
β	7.32 (m)	141.5	Cα, Cγ, Cδ, CO	7.40 (dd, 10.8, 15.2)	141.6	Cα, Cγ, Cδ, CO
γ	6.99 (m)	125.6	—[c]	6.66 (dd, 11.0, 15.2)	124.6	C1, Cα, Cβ, Cδ,
δ	6.99 (m)	139.4	—[c]	6.76 (m)	139.2	—[c]
CO	—	164.3	—	—	166.0	—
NH	10.09 (s)	—	Cα, CO, C1′, C2′, C6′	5.86 (m)	—	—
CH_2	—	—	—	4.54 (d, 5.7)	43.8	CO, C1′, C2′, C6′
1′	—	139.9	—	—	138.3	—
2′	7.68 (m)	119.6	C1′, C4′, C6′	7.32 (m)	127.9	—[c]
3′	7.32 (m)	129.2	C1′, C2′, C4′, C5′, C6′	7.32 (m)	128.8	—[c]
4′	7.04 (m)	123.6	C1′, C2′, C3′, C5′, C6′	7.32 (m)	127.6	—[c]
5′	7.32 (m)	129.2	C1′, C2′, C3′, C4′, C6′	7.32 (m)	128.8	—[c]
6′	7.68 (m)	119.6	C1′, C2′, C4′	7.32 (m)	127.9	—[c]

[a] Chemical shifts δ in ppm (multiplicity, *J* in Hz).
[b] Carbons coupled to the corresponding H atom.
[c] The peaks in HMBC could not be determined due to signal overlap.

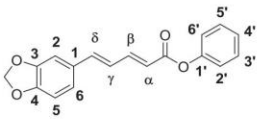
deuterated solvent used in the NMR experiments.

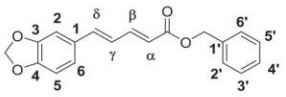
In the MDP ring, the H2 protons were observed as a duplet at $\delta = 6.90–7.32$ ppm with a *meta* coupling constant of 1.6–1.7 Hz; H5 as a duplet at 6.76–6.93 ppm with an *ortho* coupling constant of 8.0 Hz; H6 as a double duplet at $\delta = 6.88–7.04$ ppm with *ortho* and *meta* coupling constants of 8.1 Hz and 1.6 Hz, respectively; and $C\underline{H}_2$ as a singlet integrated for two protons at $\delta = 5.97–6.06$ ppm (Tables 1 and 2). The signals of the carbons directly linked to H2, H5, H6 and $C\underline{H}_2$ were attributed by the correlations observed in HSQC experiments (Fig. 2B): C2 ($\delta = 105.8–106.2$ ppm), C5 ($\delta = 108.5–108.9$), C6 ($\delta = 122.7–123.4$ ppm) and CH_2 ($\delta = 101.3–101.8$ ppm). The quaternary carbons of the MDP ring were assigned by HMBC correlation (Fig. 3): C1 carbons are located at 130.4–131.2 ppm and are correlated with H5 (compounds **3**, **5** and **6**), Hγ (compounds **5** and **6**) and Hδ (compounds **4**, **5** and **6**). C3 was assigned at 148.2–148.4 ppm, showing cross peaks with $OC\underline{H}_2O$ (compounds **3**, **4**, **5** and **6**), H2 (compounds **3**, **4**, **5** and **6**), H5 (compounds **3**, **4**, **5** and **6**) and H6 (compounds **3** and **4**). Finally, C4 carbons are located at 148.3–148.8 ppm and are correlated with $OC\underline{H}_2O$ (compounds **3**, **4**, **5** and **6**), H2 (compounds **3**, **4**, **5** and **6**), H5 (compounds **3**, **4**, **5** and **6**) and H6 (compounds **3**, **4**, **5** and **6**).

In the conjugated system, Hα protons were recorded as duplets at $\delta = 5.93–6.30$ ppm with a *trans* coupling constant of 14.9–15.2 Hz; Hβ as double duplets $\delta = 7.32–7.59$ ppm with *trans* coupling constants of 10.8 Hz and 15.2 Hz; Hγ as double duplets at $\delta = 6.66–6.99$ ppm with *trans* coupling constants of 10.8–12.0 Hz and 15.2–15.5 Hz; and Hδ as duplets at $\delta = 6.76–6.99$ Hz with a *trans* coupling constant of 15.5 Hz (Tables 1 and 2). The corresponding carbon signals are as follows: Cα ($\delta = 119.3–124.8$ ppm), Cβ ($\delta = 141.5–146.7$ ppm), Cγ ($\delta = 124.3–125.6$ ppm) and Cδ ($\delta = 139.2–141.3$ ppm) (Tables 1 and 2). The ^{1}H and ^{13}C NMR signals occurred according to the following order: $\delta(\alpha) < \delta(\gamma) < \delta(\delta) < \delta(\beta)$, a ranking order that is related with the deprotection of the protons and carbons at positions β and, to a lesser extent, at position δ by mesomeric effects. The carbonyl group ($\delta = 164.34–166.93$ ppm) was assigned by chemical displacement (Tables 1 and 2) and by HMBC correlations with Hα (compounds **3**, **4**, **5** and **6**), Hβ (compounds **3**, **4**, **5** and **6**), NH (compound **3**) and $C\underline{H}_2$Ph (compounds **4** and **6**).

Regarding the side chain linked by amide or ester moieties to the conjugated system, some differences in the chemical shifts of the

Table 2
^{1}H and ^{13}C chemical shifts and HMBC correlations for compounds **5** ($CDCl_3$-d_1) and **6** ($CDCl_3$-d_1).





	Compound **5**			Compound **6**		
	^{1}H NMR[a]	^{13}C NMR	HMBC[b]	^{1}H NMR	^{13}C NMR	HMBC
OCH_2O	5.99 (s)	101.5	C3, C4	5.98 (s)	101.4	C3, C4
1	—	130.4	—	—	130.6	—
2	7.02 (d, 1.7)	106.0	C3, C4, C5, C6, Cδ	6.98 (d, 1.7)	105.9	C3, C4, C5, C6, Cδ
3	—	148.4	—	—	148.3	—
4	—	148.8	—	—	148.6	—
5	6.78 (m)	108.6	C1, C2, C3, C4, C6, Cδ	6.80 (m)	108.6	C1, C2, C3, C4, C6
6	6.94 (dd, 1.6, 8.1)	123.2	C2, C4, Cδ	6.90 (dd, 1.6, 8.1)	123.0	C2, C4, Cγ, Cδ
α	6.13 (d, 15.2)	119.3	Cβ, Cγ, Cδ, CO	5.99 (d, 15.2)	120.0	Cγ, CO
β	7.59 (dd, 10.8, 15.2)	146.7	Cα, Cγ, Cδ, CO	7.45 (dd, 10.8, 15.2)	145.3	Cα, Cγ, Cδ, CO
γ	6.78 (m)	124.3	C1, C6, Cα, Cβ, Cδ,	6.69 (ddd, 0.6, 10.8, 15.5)	124.5	C1, C6, Cα, Cβ, Cδ
δ	6.89 (d, 15.5)	141.3	C1, C2, C6, Cα, Cβ, Cγ	6.80 (m)	140.4	C1, C2, C6, Cα, Cβ, Cγ
CO	—	165.5	—	—	166.9	—
OCH_2	—	—	—	5.21 (s)	66.1	CO, C1′, C2′, C3', C5', C6′
1'	—	150.9	—	—	136.2	—
2'	7.14 (m)	121.7	C1′, C3′, C4′, C5′, C6′	7.35 (m)	128.2	—[c]
3'	7.32 (m)	129.4	C1′, C2′, C4′, C5′, C6′	7.35 (m)	128.6	—[c]
4'	7.23 (m)	125.6	C2′, C3′, C5′, C6′	7.35 (m)	128.2	—[c]
5'	7.32 (m)	129.4	C1′, C2′, C3′, C4′, C6′	7.35 (m)	128.6	—[c]
6'	7.14 (m)	121.7	C1′, C2′, C3′,C4′, C5′	7.35 (m)	128.2	—[c]

[a] Chemical shifts δ in ppm (multiplicity, *J* in Hz).
[b] Carbons coupled to the corresponding H atom.
[c] The signals in HMBC could not be determined due to signal overlap.

protons and carbons of the aromatic ring were detected, depending whether the ring is directly attached to the oxygen or nitrogen atom (compounds **3** and **5**) or by a methylene spacer (compounds **4** and **6**) (Tables 1 and 2). The spectroscopic results were also upheld by COSY, HSQC and HMBC correlations.

For compound **5**, H2′ and H6′ were assigned as a multiplet at $\delta = 7.14$ ppm, H3′ and H5′ as a multiplet at $\delta = 7.32$ ppm, integrating for two protons each and H4′ as a multiplet at $\delta = 7.23$ ppm (Table 2). For compound **3**, H2′ and H6′ signals appeared at higher chemical shift than H3′ and H5′ (H2′ and H6′at $\delta = 7.68$ ppm; H3′ and H5′at $\delta = 7.32$ ppm) and H4′ was assigned a multiplet at $\delta = 7.04$ ppm (Table 2). As for the benzyl amide **4** and benzyl ester **6**, the abovementioned signals appeared overlapped as multiplets at $\delta = 7.32$ ppm and 7.35 ppm, respectively (Tables 1 and 2). ^{13}C NMR signals in compounds **3** and **5** appeared as follows: C1′ at $\delta = 139.9$ ppm and 150.9 ppm, respectively, C2′and C6′ at $\delta = 119.6$ ppm and 121.7 ppm, respectively; C3′and C5′ at $\delta = 129.2$ ppm and 129.4 ppm, respectively, C4′ at $\delta = 123.6$ ppm and 125.6 ppm, respectively (Tables 1 and 2). Similarly, for compounds **4** and **6**, C1′ appeared at $\delta = 138.3$ ppm and 136.2 ppm, respectively, C2′ and C6′ at $\delta = 127.9$ ppm and 128.2 ppm, respectively; C3′ and C5′ at $\delta = 128.8$ ppm and 128.6 ppm, respectively; and C4′ at $\delta = 127.6$ ppm and 128.2 ppm, respectively (Tables 1 and 2). The ^{1}H NMR signal corresponding to the hydrogen of the N-H bond in the amide **3** was identified by the HMBC correlation with the carbonyl group, while in compound **4** it was identified by the COSY correlation with the CH_2 group (Table 1). For compound **3**, the N-H signal appeared as a singlet at $\delta = 10.1$ ppm, while for compound **4** the signal was identified as a multiplet at $\delta = 5.9$ ppm. Regarding the CH_2 group in benzylamide **4** and benzylester **6**, the ^{1}H and ^{13}C NMR signals were assigned based on the HMBC correlation with the carbons CO, C1′, C2′ and C6′ (Tables 1 and 2). For compound **4**, CH_2 group appeared as a duplet at $\delta = 4.54$ ppm with a coupling constant of 5.7 Hz, while for compound **6** it appeared as a singlet at $\delta = 5.21$ ppm. The corresponding carbon signals appeared at $\delta = 43.8$ ppm for compounds **4** and at $\delta = 66.1$ ppm for compound **6** (Tables 1 and 2).

3.3. X-ray diffraction analysis

Thermal-Ellipsoid diagrams produced by the program Mercury [7] for compounds **3**–**6**, and X-Ray structure numbering, are shown in Fig. 4. Compound **3** crystallized with two molecules with distinct conformations in the asymmetric unit (mol#1 with atomic labels prefixed with 1 and mol#2 prefixed with 2). Compounds **3** and **4** are (*2E,4E*) -5-phenyl-2,4-pentadienamides while compounds **5** and **6** are (*2E,4E*)-5-phenyl-2,4-pentadienoates. All compounds contain a benzo[*d*][1,3]dioxole ring whose conformation will be first discussed. The ring may be virtually planar or slightly bent at the dioxole fragment (-OCH_2O-) as the dioxole moiety confer an "envelope"-like or a "twisted"-like conformation at the end of the fragment. Mol#2 of compound **3** and compounds **5** and **6** had tended toward the first conformation, while mol#1 of compounds **3** and **4** had tended toward the second conformation (Fig. 4). The degree of the bend may be assessed by measuring the linear distance of the carbon atom of the dioxole fragment from the best mean plane formed by the remaining atoms of the heterocyclic ring and by pseudo-rotation parameters *P* and τ(m), calculated as described by Rao and co-workers [20]. Mol#1 of compound **3** displayed an envelope conformation with the pseudo-rotation parameters *P* and τ(m) of 122.0(9)° and 12.2(3)°, respectively. The deviation of carbon atom C12 from the best square plane formed by the remaining atoms of the heterocyclic ring was 0.2498(54) Å. This conformation contrasted with the one shown by the second molecule (mol #2) where the ring was practically planar. In this case, C12 presented a deviation of 0.0161(51) Å from the mentioned plane. In compound **4**, the benzodioxole ring also displayed an envelope conformation at C2 with $P = 301.2(7)°$ and $\tau(m) = 9.6(1)°$.

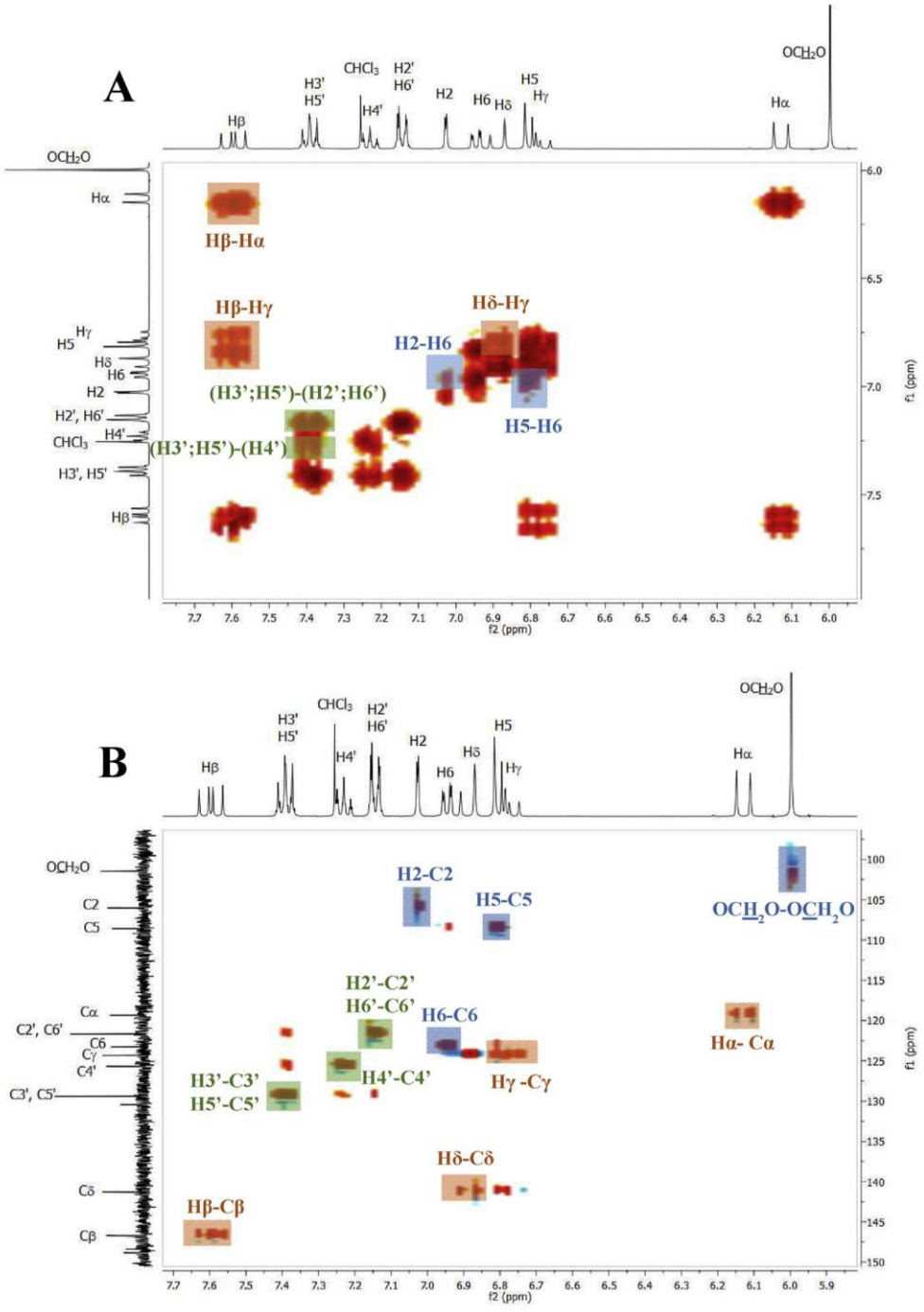


Fig. 2. Representative (A) COSY and (B) HSQC spectra of compound **5**.

The deviation of C2 from the best plane was −0.1317(22) Å. Compound **6** presented a twisted conformation on C2-O3 with $P = 317.0(9)^{o}$ and $\tau(m) = 7.6(1)^{o}$. The deviation of C2 from the best plane formed by the remaining atoms of the heterocyclic ring was 0.0842(22) Å. In compound **5**, the ring did not present puckering and the deviation of C2 from the main plane was 0.0760(14) Å.

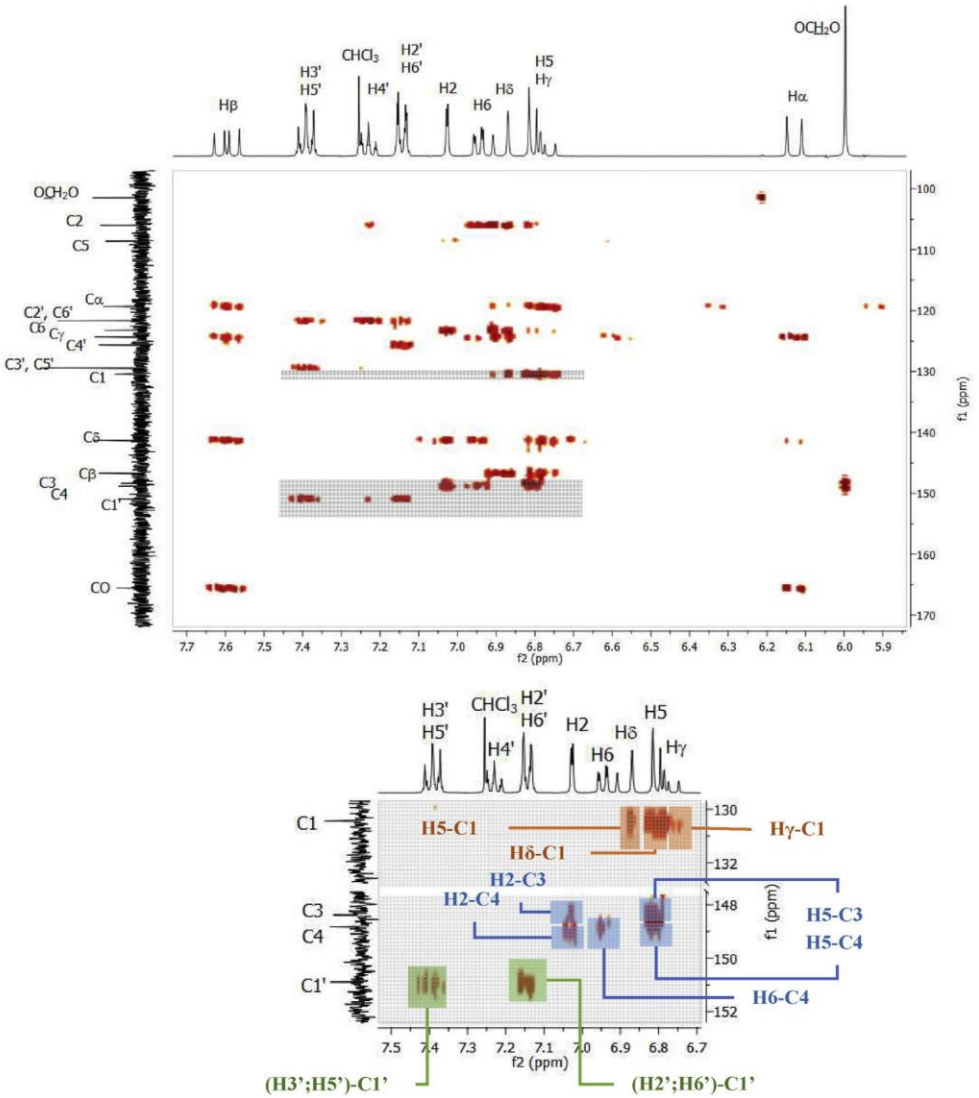


Fig. 3. Representative HMBC spectrum of compound **5**.

The aliphatic chain had a zig-zag shape as expected for the conjugated double bonds (Fig. 4).

With regard to the type of functional groups that link the side chain to the conjugated system relevant data for subsequent biological studies was attained. Due the presence of an amide function compounds **3** and **4** presented a C–N rotamer that displayed an anti-configuration (Fig. 4). The distances and the angles of the amide portion were typical of this functional group, showing a partial Csp_2–N character (for C–N, the distances between the atoms were 1.356(4) Å in mol#1 and 1.356(4) Å in mol#2 in compound **3** and 1.335(2) Å in compound **4**). The benzene ring of the phenyl substituent in compound **3** had a torsion of −47.0(5)° in mol#1 and −37.6(5)° in mol#2 from the position of the amide moiety (C=N-C_{ar}-C_{ar}), while the benzene ring of the benzyl substituent in compound **4** presented a N56-C57-C571-C576 torsion angle of −52.3(2)° (Fig. 4).

Since the amide group had a partial Csp_2-N character, a higher rotational degree of freedom around the C55-C54 bond is enabled in amides **3** and **4** when compared with the esters **5** and **6** (distances between C55-C54 in compound **3**: 1.4717(5) Å (mol#1) and 1.475(5) Å (mol#2); compound **4**: 1.479(2) Å; compound **5**: 1.4617(1) Å; and compound **6**: 1.460(2) Å) (Fig. 4). The rotational degree may be assessed by measuring the torsion of the C53-C54-C55-N56/O56 angle. The following angles were obtained: compound **3** = 159.7(3)° for mol#1 and 158.3(3)° for mol#2; compound **4** = 158.34(16)°, compound **5** = 172.93(10)°, and compound **6** = 2.6(2)°. The value obtained for compound **6** contrasted with the other compounds as the ester group showed a different conformation regarding the relative positions of the oxygen atoms.

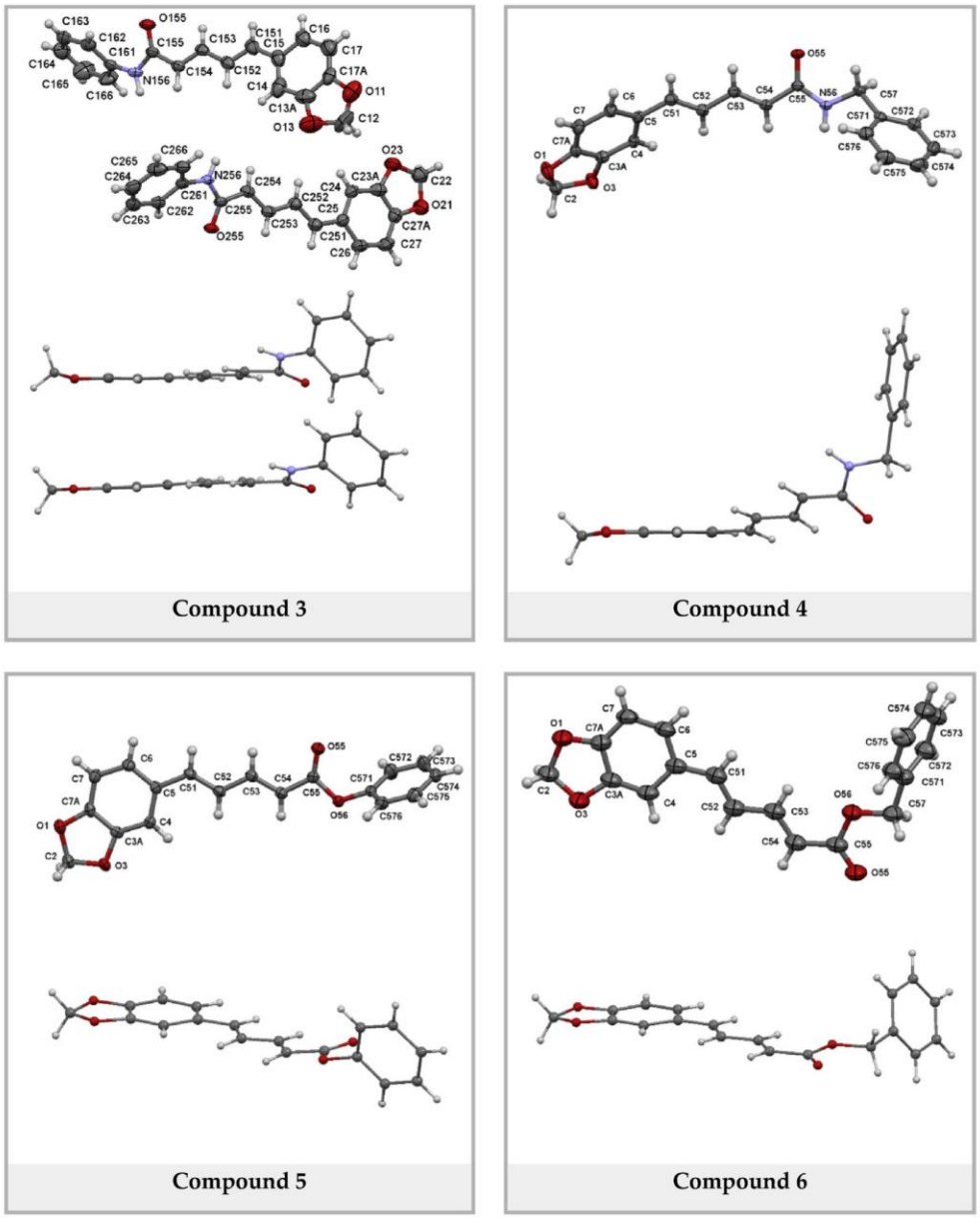


Fig. 4. Atom arrangements and side-on views of the molecular conformations of compounds **3**–**6**. Ellipsoids were drawn at the 70% probability level.

3.4. Evaluation of human monoamine oxidase (hMAO) inhibitory activity

The assessment of *h*MAO inhibitory activity by piperic acid and derivatives thereof **1**–**6**, and reference inhibitors used in therapy, was performed by a spectrophotometric assay by measuring the formation of 4-hydroxyquinoline, a product formed from the deamination of kynuramine (a common substrate for both *h*MAO-A and *h*MAO-B) [21]. The results of the *in vitro* inhibitory potency (IC_{50} values) and the selectivity towards *h*MAO-B (SI = [IC_{50}(MAO-A)]/[IC_{50}(MAO-B)]) of the compounds under study and reference inhibitors (clorgyline towards MAO-A and (R)-(−)-deprenyl for MAO-B) are depicted in Table 3.

The natural compound piperine was shown to inhibit *h*MAO-B (compound **1**: IC_{50} = 1.05 μM), while no inhibitory activity was recorded for *h*MAO-A at 10 μM. This result is in accordance with previous reports [22]. Piperic acid (compound **2**) and piperic acid amides **3** and **4** did not display significant inhibitory activity against both *h*MAO-A and *h*MAO-B at 10 μM. On the other hand, piperic acid ester **6** inhibited both isoforms with higher potency towards

Table 3
MAO inhibitory activities of piperic acid amides **3**–**4** and esters **5**–**6** and reference inhibitors.

Compound	IC_{50}/μM		SI[c]
	*h*MAO-A	*h*MAO-B	
1	___[a]	1.05±0.08	10[d]
2	___[a]	___[a]	___
3	___[a]	___[a]	___
4	___[a]	___[a]	___
5	___[b]	0.156±0.008	64[d]
6	4.24±0.56	0.169±0.012	25
Clorgyline	0.00274±0.00047	2.21±0.26	0.00124
(*R*)-(−)-Deprenyl	20.1±1.9	0.0386±0.0043	522

[a] Inactive at 10 μM.
[b] Not soluble in phosphate buffer at concentrations higher than 10 μM.
[c] SI: *h*MAO-B selectivity index = IC_{50}(*h*MAO-A)/IC_{50}(*h*MAO-B).
[d] Value obtained under the assumption that the corresponding IC_{50} against *h*MAO-A is the highest concentration tested (10 μM).

*h*MAO-B (compound **6**: SI = 25), displaying *h*MAO-B IC_{50} values within the nanomolar range (compound **6**: IC_{50} = 169 nM) and micromolar range for *h*MAO-A (compound **6**: IC_{50} = 4.24 μM). Compound **5** also presented inhibitory properties towards *h*MAO-B similar to compound **6** (compound **5**: IC_{50} = 156 nM). However, solubility issues at concentrations higher than 10 μM precluded the determination of *h*MAO-A inhibitory activity.

Overall, the results obtained point out that the replacement of the piperidinyl amide moiety of piperine by a carboxylic acid or a primary amide abolish the ability to inhibit *h*MAO-B. On the other hand, piperic acid esters were shown to be better *h*MAO-B inhibitors than the natural alkaloid.

4. Conclusion

Piperic acid amides and esters were successfully synthesized in moderate to high yields. Their complete structural elucidation by mass and unidimensional and bidimensional NMR spectroscopy and X-ray crystallography was accomplished. The data obtained constitute a useful database for the unambiguous characterization of homologous compounds of drug discovery programs based on piperine scaffold.

Preliminary data on the biological profile of the piperine and derivatives thereof suggest that structural modifications of the carbonylamide group affect not only the ability to inhibit *h*MAOs at physiologically relevant concentrations, but also the potency of the obtained compounds. Piperine showed inhibitory activity towards *h*MAO-B with an IC_{50} value in the low micromolar range. Piperic acid **2** and piperic acid amides **3** and **4** did not present significant inhibitory activity at 10 μM against both *h*MAO-A and *h*MAO-B. Remarkably, piperic acid esters **5** and **6** displayed *h*MAO inhibitory activities with IC_{50} values within the nanomolar range for *h*MAO-B.

Overall, the data obtained so far allow the identification of important structural features (the presence hydrogen donor groups like COOH and CONH groups seem be not tolerated) for further lead optimization process and fine-tuning of the solubility drawbacks, enabling the development of more potent and selective *h*MAO-B inhibitors based on a natural scaffold. In addition, the acquired X-ray data, which show a higher rotational degree of freedom around the C55-C54 bond for amides **3** and **4** when compared with the esters **5** and **6**, constitute a valuable information to understand the ligand-target interactions.

Conflict of interest statement

The authors declare that the research was conducted in the absence of any commercial or financial relationships that could be considered as a potential conflict of interest.

Acknowledgements

This work was funded by FEDER funds through the Operational Programme Competitiveness Factors – COMPETE and national funds by FCT – Foundation for Science and Technology under research grants (UID/QUI/00081, NORTE-01-0145-FEDER-000028, POCI-01-0145-FEDER-029164 and POCI-01-0145-FEDER-028397). D. Chavarria (SFRH/BD/108119/2015) and F. Cagide (NORTE-01-0145-FEDER-000028) grants are supported by FCT, POPH and FEDER/COMPETE. Crystallographic data were collected at the Engineering and Physical Sciences Research Council (EPSRC) X-ray crystallography service UK. Thanks are due to the staff at the National Crystallographic Service, University of Southampton for the data collection, help and advice.

Appendix A. Supplementary data

Supplementary data to this article can be found online at https://doi.org/10.1016/j.molstruc.2019.01.060.

References

[1] P.B. Yaffe, M.R. Power Coombs, C.D. Doucette, M. Walsh, D.W. Hoskin, Piperine, an alkaloid from black pepper, inhibits growth of human colon cancer cells via G1 arrest and apoptosis triggered by endoplasmic reticulum stress, Mol. Carcinog. 54 (10) (2015) 1070–1085. https://doi.org/10.1002/mc.22176.
[2] R.A. Gupta, M.N. Motiwala, N.G. Dumore, K.R. Danao, A.B. Ganjare, Effect of piperine on inhibition of FFA induced TLR4 mediated inflammation and amelioration of acetic acid induced ulcerative colitis in mice, J. Ethnopharmacol. 164 (2015) 239–246. https://doi.org/10.1016/j.jep.2015.01.039.
[3] I.P. Singh, A. Choudhary, Piperine and derivatives: Trends in structure-activity relationships, Curr. Top. Med. Chem. 15 (17) (2015) 1722–1734. https://doi.org/10.2174/1568026615666150427123213.
[4] Ajazuddin, A. Alexander, A. Qureshi, L. Kumari, P. Vaishnav, M. Sharma, S. Saraf, S. Saraf, Role of herbal bioactives as a potential bioavailability enhancer for Active Pharmaceutical Ingredients, Fitoterapia 97 (2014) 1–14. https://doi.org/10.1016/j.fitote.2014.05.005.
[5] A.S. Hammad, S. Ravindran, A. Khalil, S. Munusamy, Structure-activity relationship of piperine and its synthetic amide analogs for therapeutic potential to prevent experimentally induced ER stress in vitro, Cell Stress Chaperones 22 (3) (2017) 417–428. https://doi.org/10.1007/s12192-017-0786-9.
[6] S. Chithra, B. Jasim, P. Sachidanandan, M. Jyothis, E.K. Radhakrishnan, Piperine production by endophytic fungus Colletotrichum gloeosporioides isolated from Piper nigrum, Phytomedicine 21 (4) (2014) 534–540. https://doi.org/10.1016/j.phymed.2013.10.020.
[7] D. Chavarria, T. Silva, D. Magalhaes e Silva, F. Remiao, F. Borges, Lessons from black pepper: piperine and derivatives thereof, Expert Opin. Ther. Pat. 26 (2) (2016) 245–264. https://doi.org/10.1517/13543776.2016.1118057.
[8] N.T. Tzvetkov, H.G. Stammler, B. Neumann, S. Hristova, L. Antonov, M. Gastreich, Crystal structures, binding interactions, and ADME evaluation of brain penetrant *N*-substituted indazole-5-carboxamides as subnanomolar, selective monoamine oxidase B and dual MAO-A/B inhibitors, Eur. J. Med. Chem. 127 (2017) 470–492. https://doi.org/10.1016/j.ejmech.2017.01.011.
[9] M. Naoi, W. Maruyama, K. Inaba-Hasegawa, Type A and B monoamine oxidase in age-related neurodegenerative disorders: their distinct roles in neuronal death and survival, Curr. Top. Med. Chem. 12 (20) (2012) 2177–2188. https://doi.org/10.2174/1568026611212200006.
[10] J. Tong, J.H. Meyer, Y. Furukawa, I. Boileau, L.J. Chang, A.A. Wilson, S. Houle, S.J. Kish, Distribution of monoamine oxidase proteins in human brain: implications for brain imaging studies, J. Cerebr. Blood Flow Metabol. 33 (6) (2013) 863–871. https://doi.org/10.1038/jcbfm.2013.19.
[11] P. Rane, D. Sarmah, S. Bhute, H. Kaur, A. Goswami, K. Kalia, A. Borah, K.R. Dave, N. Sharma, P. Bhattacharya, Novel targets for Parkinson's disease: Addressing different therapeutic paradigms and conundrums, ACS Chem. Neurosci. (2018). https://doi.org/10.1021/acschemneuro.8b00180.
[12] A. Nicotra, F. Pierucci, H. Parvez, O. Senatori, Monoamine oxidase expression during development and aging, Neurotoxicology 25 (1–2) (2004) 155–165. https://doi.org/10.1016/s0161-813x(03)00095-0.
[13] S.A. Lee, S.S. Hong, X.H. Han, J.S. Hwang, G.J. Oh, K.S. Lee, M.K. Lee, B.Y. Hwang, J.S. Ro, Piperine from the fruits of Piper longum with inhibitory effect on monoamine oxidase and antidepressant-like activity, Chem. Pharm. Bull. (Tokyo) 53 (7) (2005) 832–835.

[14] L.D. Kong, C.H. Cheng, R.X. Tan, Inhibition of MAO A and B by some plant-derived alkaloids, phenols and anthraquinones, J. Ethnopharmacol. 91 (2–3) (2004) 351–355. https://doi.org/10.1016/j.jep.2004.01.013.
[15] R. Venkatasamy, L. Faas, A.R. Young, A. Raman, R.C. Hider, Effects of piperine analogues on stimulation of melanocyte proliferation and melanocyte differentiation, Bioorg. Med. Chem. 12 (8) (2004) 1905–1920. https://doi.org/10.1016/j.bmc.2004.01.036.
[16] A. Gaspar, T. Silva, M. Yanez, D. Vina, F. Orallo, F. Ortuso, E. Uriarte, S. Alcaro, F. Borges, Chromone, a privileged scaffold for the development of monoamine oxidase inhibitors, J. Med. Chem. 54 (14) (2011) 5165–5173. https://doi.org/10.1021/jm2004267.
[17] M. Soda, D. Hu, S. Endo, M. Takemura, J. Li, R. Wada, S. Ifuku, H.T. Zhao, O. El-Kabbani, S. Ohta, K. Yamamura, N. Toyooka, A. Hara, T. Matsunaga, Design, synthesis and evaluation of caffeic acid phenethyl ester-based inhibitors targeting a selectivity pocket in the active site of human aldo-keto reductase 1B10, Eur. J. Med. Chem. 48 (2012) 321–329. https://doi.org/10.1016/j.ejmech.2011.12.034.
[18] H. Shi, D. Xie, R. Yang, Y. Cheng, Synthesis of caffeic acid phenethyl ester derivatives, and their cytoprotective and neuritogenic activities in PC12 cells, J. Agric. Food Chem. 62 (22) (2014) 5046–5053. https://doi.org/10.1021/jf500464k.
[19] S. Hagenow, A. Stasiak, R.R. Ramsay, H. Stark, Ciproxifan, a histamine H_3 receptor antagonist, reversibly inhibits monoamine oxidase A and B, Sci. Rep. 7 (40541) (2017) 1–6. https://doi.org/10.1038/srep40541.
[20] S.T. Rao, E. Westhof, M. Sundaralingam, Exact method for the calculation of pseudorotation parameters P, τm and their errors. A comparison of the Altona–Sundaralingam and Cremer–Pople treatment of puckering of five-membered rings, Acta Crystallogr. A 37 (3) (1981) 421–425. https://doi.org/10.1107/S0567739481000892.
[21] Z. Yan, G.W. Caldwell, B. Zhao, A.B. Reitz, A high-throughput monoamine oxidase inhibition assay using liquid chromatography with tandem mass spectrometry, Rapid Commun. Mass Spectrom. 18 (8) (2004) 834–840. https://doi.org/10.1002/rcm.1415.
[22] O.B. Al-Baghdadi, N.I. Prater, C.J. Van der Schyf, W.J. Geldenhuys, Inhibition of monoamine oxidase by derivatives of piperine, an alkaloid from the pepper plant *Piper nigrum*, for possible use in Parkinson's disease, Bioorg. Med. Chem. Lett 22 (23) (2012) 7183–7188. https://doi.org/10.1016/j.bmcl.2012.09.056.

Development of piperic acid-based monoamine oxidase inhibitors: Synthesis, structural characterization and biological evaluation

Daniel Chavarria[1], Fernando Cagide[1], Miguel Pinto[1], Lígia R. Gomes[2,3], John N. Low[4], Fernanda Borges[1*]

[1] CIQUP, Department of Chemistry and Biochemistry, Faculty of Sciences, University of Porto, Porto, Portugal

[2] FP-ENAS, Faculty of Health Sciences, University of Fernando Pessoa, Porto, Portugal

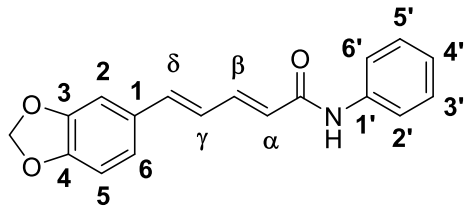
[3] REQUIMTE /LAQV, Department of Chemistry and Biochemistry, Faculty of Sciences, University of Porto, Porto, Portugal

[4] Department of Chemistry, University of Aberdeen, Meston Walk, Scotland

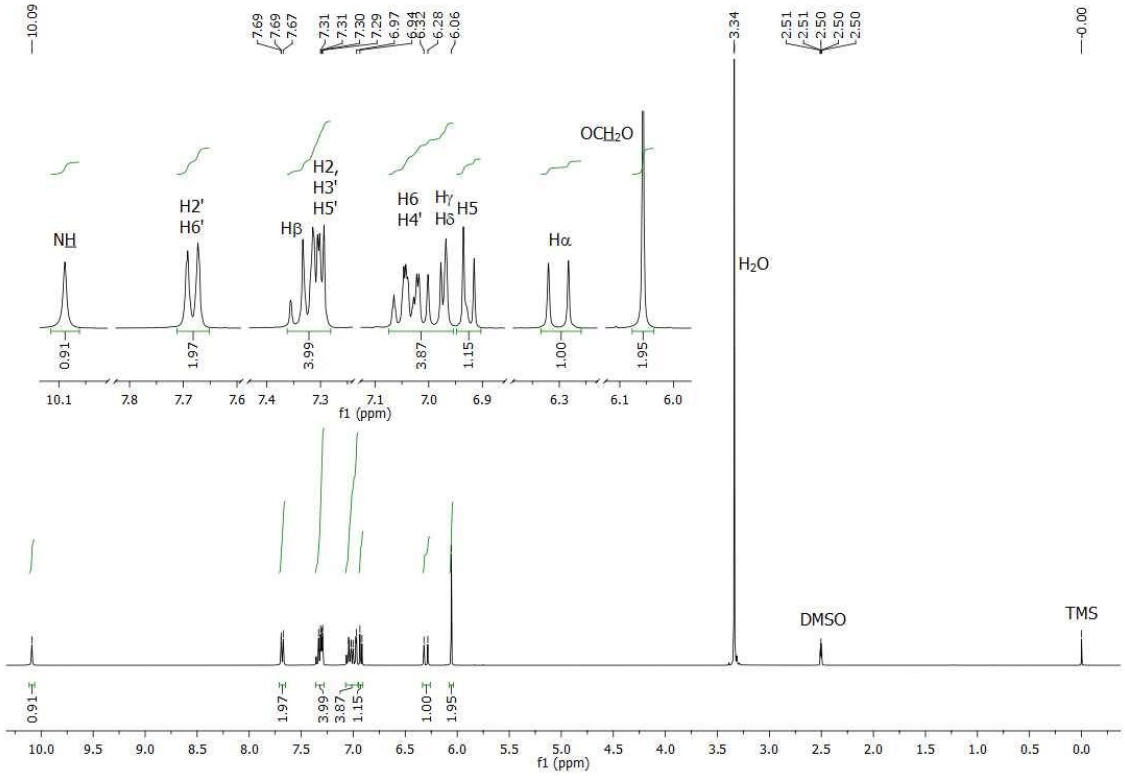
Contents of Supporting information:

S1. Structural data – Compound 3 208
S2. Structural data – Compound 4 210
S3. Structural data – Compound 5 212
S4. Structural data – Compound 6 214

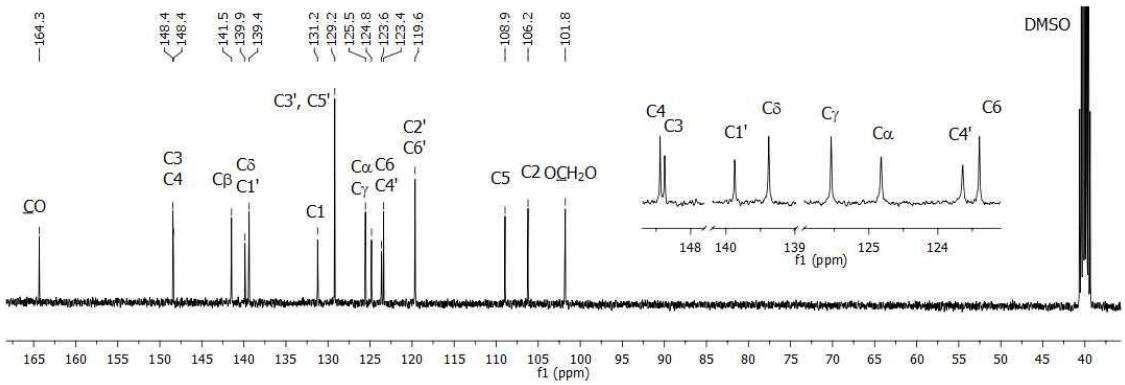
S1. Structural data – Compound 3



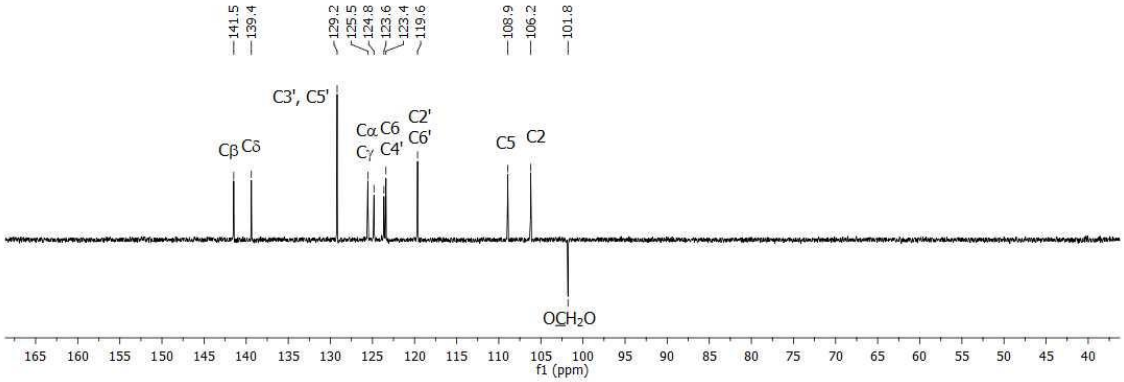
^{1}H NMR



^{13}C NMR

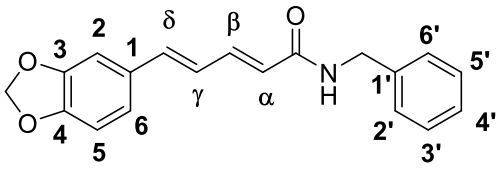


DEPT135

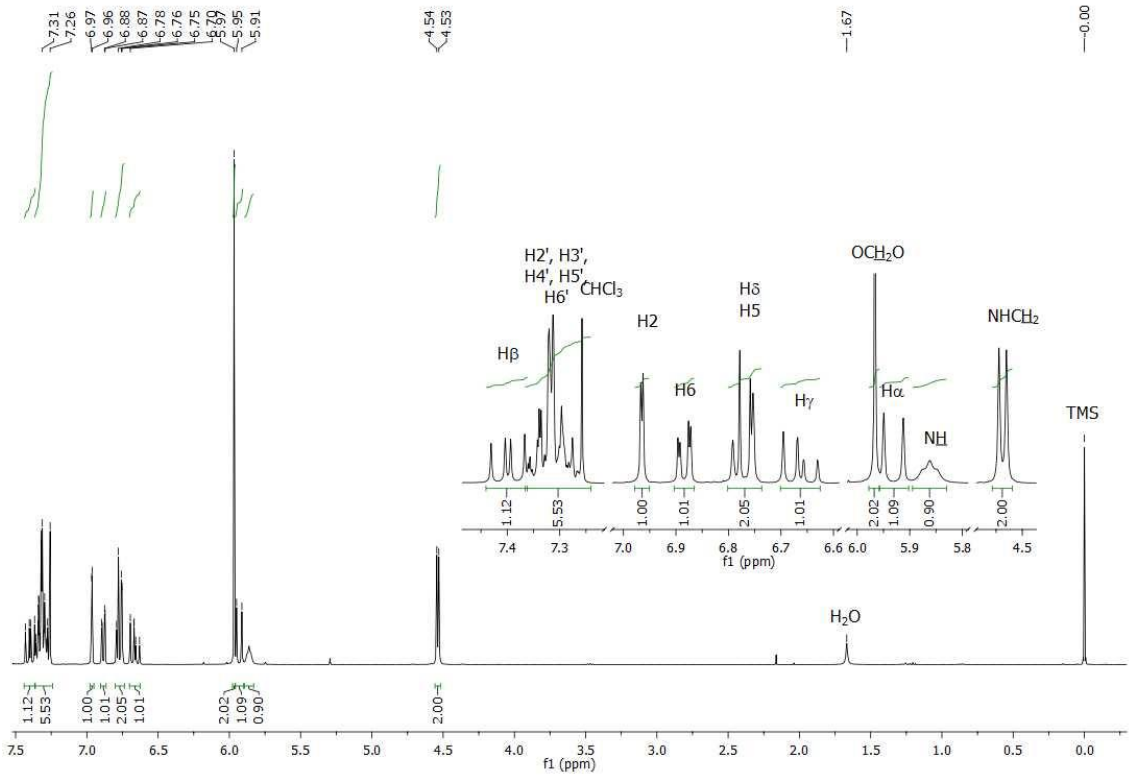

141.5
139.4
129.2
125.5
124.8
123.6
123.4
119.6
108.9
106.2
101.8
C3', C5'
Cβ Cδ
Cα C6 C2'
Cγ C4' C6'
C5 C2
OCH2O
165 160 155 150 145 140 135 130 125 120 115 110 105 100 95 90 85 80 75 70 65 60 55 50 45 40
f1 (ppm)

S2. Structural data – Compound 4

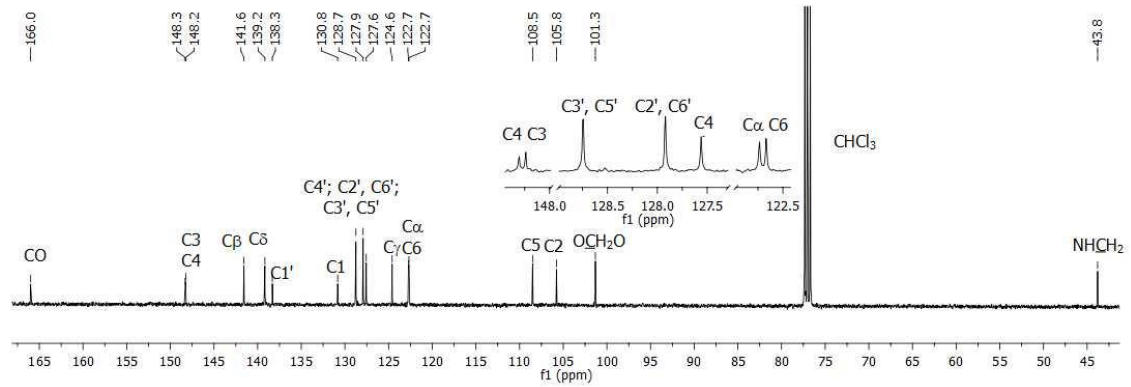
Compound 4



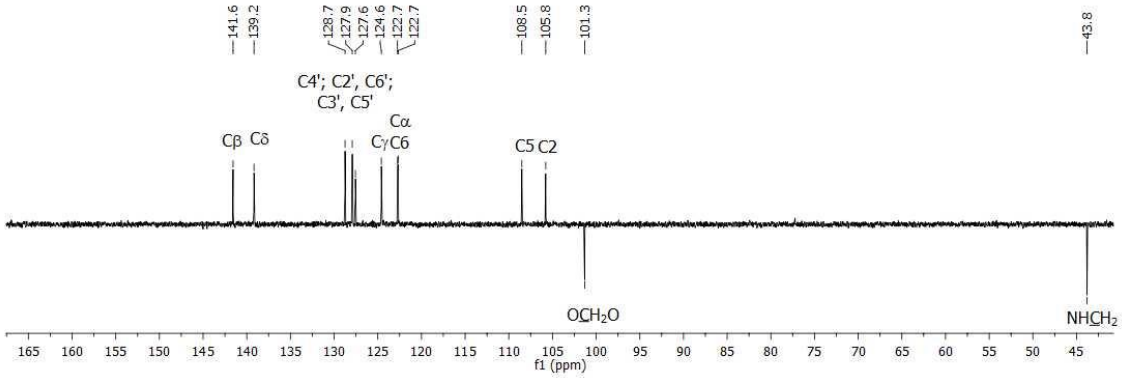
^{1}H NMR



^{13}C NMR

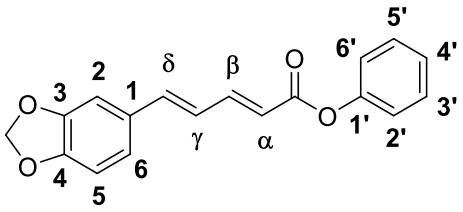


DEPT135

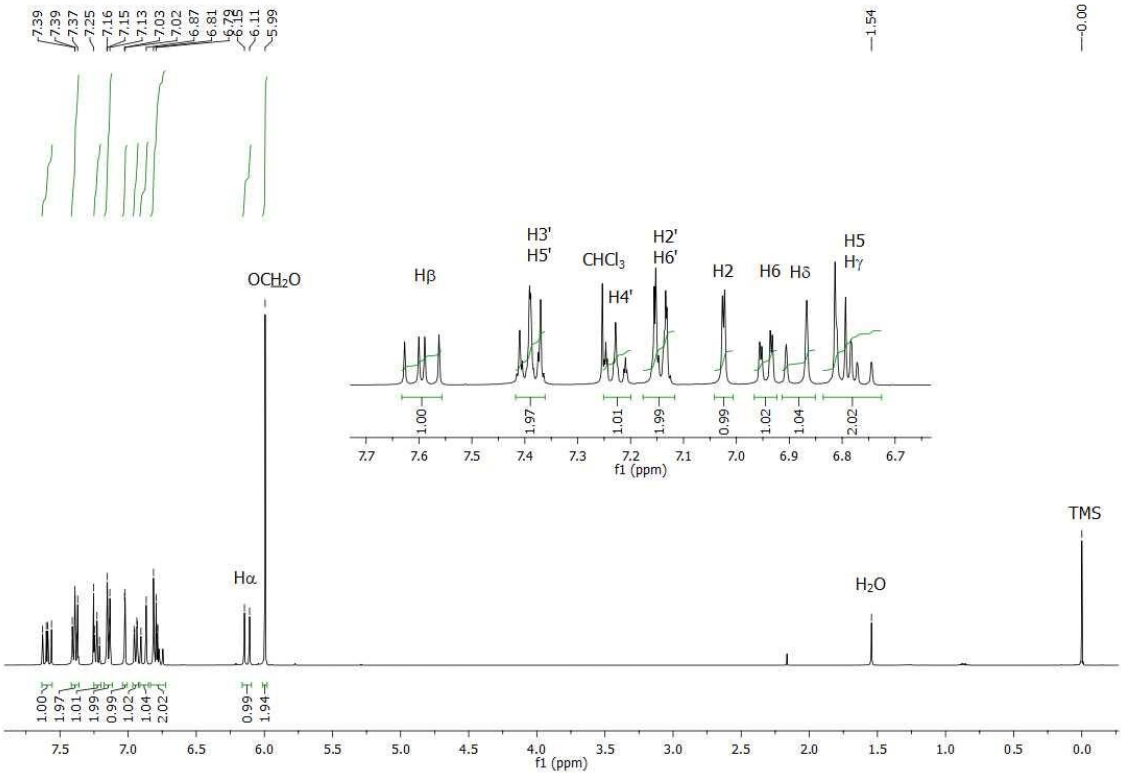

141.6
139.2
128.7
127.9
127.6
124.6
122.7
122.7
108.5
105.8
101.3
43.8
C4'; C2', C6';
C3', C5'
Cβ Cδ
Cα
CγC6
C5 C2
OCH2O
NHCH2
165 160 155 150 145 140 135 130 125 120 115 110 105 100 95 90 85 80 75 70 65 60 55 50 45
f1 (ppm)

S3. Structural data – Compound 5

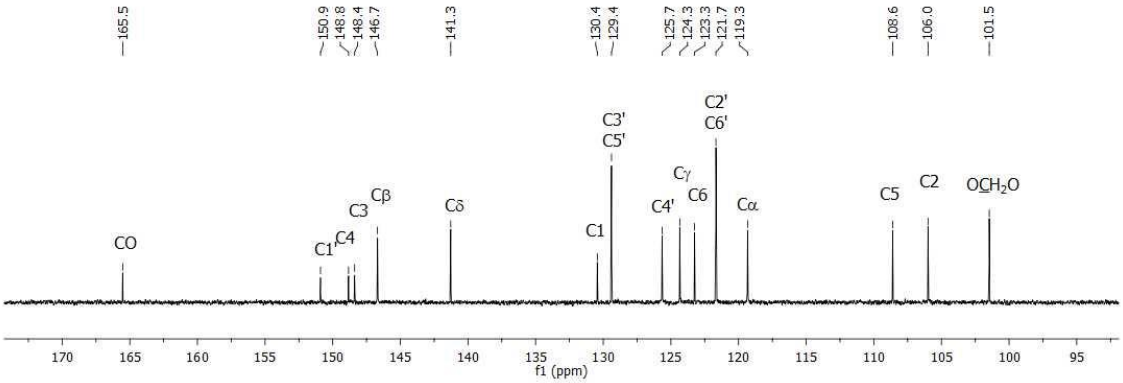
Compound 5



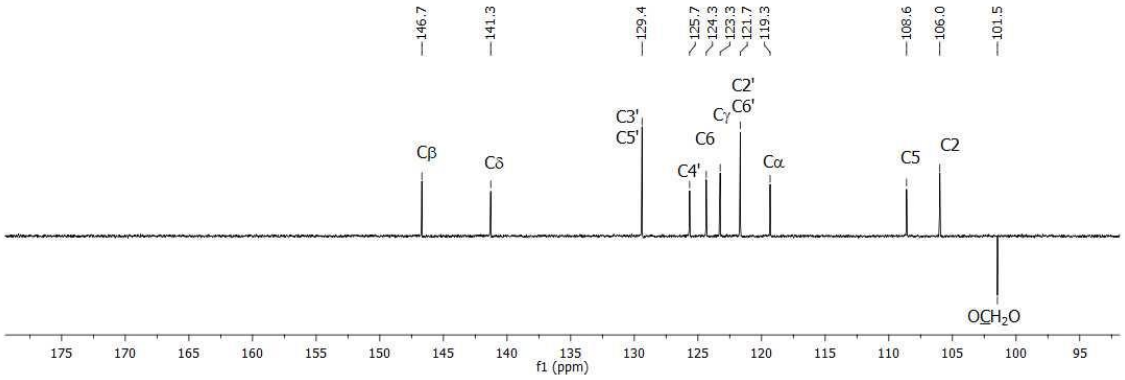
^{1}H NMR



^{13}C NMR

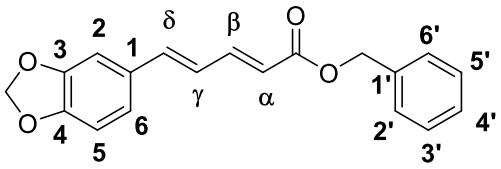


DEPT135

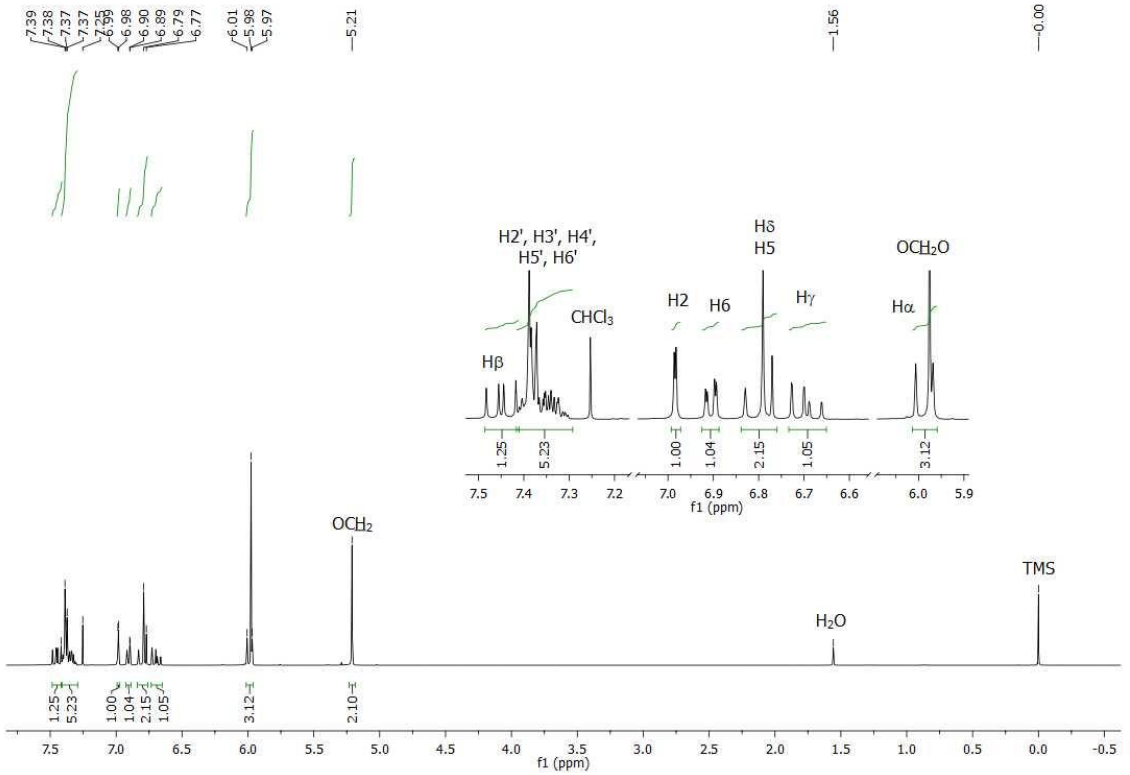

146.7
141.3
129.4
125.7
124.3
123.3
121.7
119.3
108.6
106.0
101.5
Cβ
Cδ
C3'
C5'
C4'
C6
Cγ
C2'
C6'
Cα
C5
C2
OCH2O
175
170
165
160
155
150
145
140
135
130
125
120
115
110
105
100
95
f1 (ppm)

S4. Structural data – Compound 6

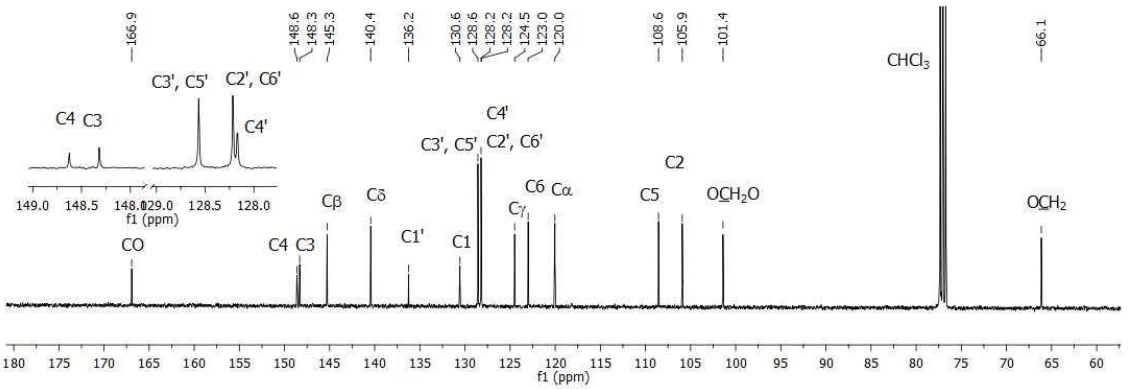
Compound 6



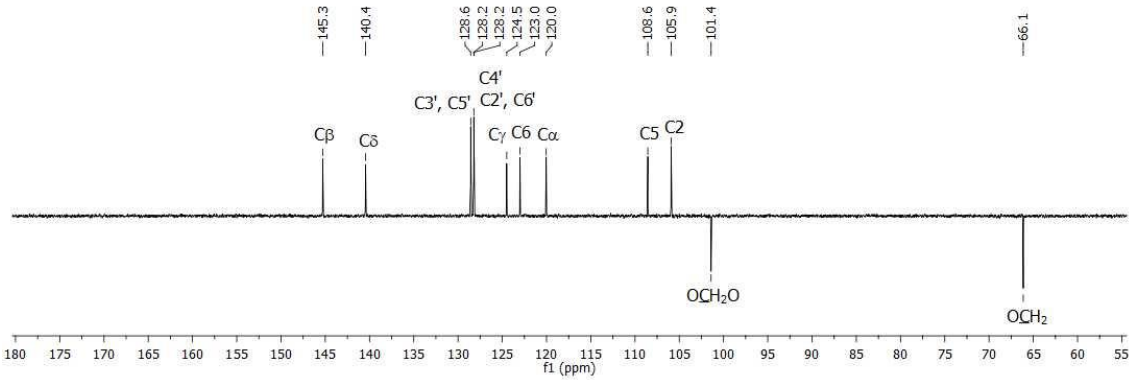
^{1}H NMR



^{13}C NMR



DEPT135


145.3
140.4
128.6
128.2
128.2
124.5
123.0
120.0
108.6
105.9
101.4
66.1
C4'
C3', C5'
C2', C6'
Cβ
Cδ
Cγ
C6
Cα
C5
C2
OCH2O
OCH2
180 175 170 165 160 155 150 145 140 135 130 125 120 115 110 105 100 95 90 85 80 75 70 65 60 55
f1 (ppm)

3.5. Manuscript VI

Design of novel monoamine oxidase-B inhibitors based on piperine scaffold: structure-activity-toxicity, drug-likeness and efflux transport studies

European Journal of Medicinal Chemistry, **2020**, 185:111770.
DOI: 10.1016/j.ejmech.2019.111770.

Design of novel monoamine oxidase-B inhibitors based on piperine scaffold: structure-activity-toxicity, drug-likeness and efflux transport studies

Daniel Chavarria‡[1,2], Carlos Fernandes‡[1], Vera Silva[1,3], Cátia Silva[1], Eva Gil-Martins[1,3], Pedro Soares[1], Tiago Silva[1,2], Renata Silva[3], Fernando Remião[3], Paulo J. Oliveira[2], Fernanda Borges[1*]

[1] CIQUP/Department of Chemistry and Biochemistry, Faculty of Sciences, University of Porto, Porto, Portugal

[2] CNC - Center for Neuroscience and Cell Biology, University of Coimbra, UC Biotech, Biocant Park, Cantanhede, Portugal.

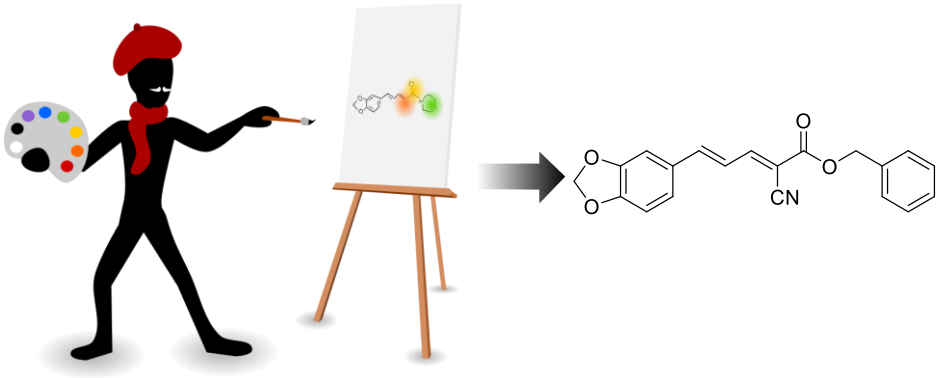
[3] UCIBIO-REQUIMTE, Laboratory of Toxicology, Department of Biological Sciences, Faculty of Pharmacy, University of Porto, Porto, Portugal

‡ These authors contributed equally.

* Corresponding Authors:

Fernanda Borges, CIQUP/Department of Chemistry and Biochemistry, Faculty of Sciences, University of Porto, Porto 4169-007, Portugal. E-mail: fborges@fc.up.pt

Graphical abstract



Highlights

- A series of piperine derivatives was synthesized, eight of which acted as *h*MAO-B inhibitors.
- α-Cyano and benzyl ester substituents increased both potency and selectivity towards *h*MAO-B.
- Compounds **15** and **16** displayed slight P-gp inhibitory activity in Caco-2 cells.
- Compound **15** is highlighted as a potent, selective and competitive *h*MAO-B inhibitor.
- Compound **15** displayed favourable drug-like properties and a safe cytotoxic profile.

Abstract

Piperine has been associated with neuroprotective effects and monoamine oxidase (MAO) inhibition, thus being an attractive scaffold to develop new antiparkinsonian agents. Accordingly, we prepared a small library of piperine derivatives and screened the inhibitory activities towards human MAO isoforms (*h*MAO-A and *h*MAO-B). Structure-activity relationship (SAR) studies pointed out that the combination of α-cyano and benzyl ester groups increased both potency and selectivity towards *h*MAO-B. Kinetic experiments with compounds **7**, **10** and **15** indicated a competitive *h*MAO-B inhibition mechanism. Compounds **15** and **16**, at 10 μM, caused a small but significant decrease in P-gp efflux activity in Caco-2 cells. Compound **15** stands out as the most potent piperine-based *h*MAO-B inhibitor (IC_{50} = 47.4 nM), displaying favourable drug-like properties and a broad safety window. Compound **15** is thus a suitable candidate for lead optimization and the development of multitarget-directed ligands.

Keywords: Parkinson's disease, Piperine, Monoamine oxidase, Cholinesterase, Structure-activity relationship.

Abbreviations: BBB: Blood-brain barrier; CHI: Chromatographic Hydrophobic Index; CNS: Central nervous system; DMAP: 4-(dimethylamino)pyridine; DCF: 2',7'-dichlorofluorescein; DCFH-DA: 2',7'-dichlorofluorescein diacetate; EDC: *N*-(3-dimethylaminopropyl)-*N'*-ethylcarbodiimide; HBA: hydrogen bond atom acceptor; HBD: hydrogen bond atom donor; K_m: Michaelis constant; K_i: inhibition constant; MAO: monoamine oxidase; MW: molecular weight; NR: Neutral Red; PD: Parkinson's disease; P-gp: P-glycoprotein; PyBOP: benzotriazol-1-yl-oxytripyrrolidinophosphonium hexafluorophosphate; RB: rotatable bonds; RHO 123: Rhodamine 123; RS: reactive species; SAR: Structure-Activity Relationship; V_{max}: maximum velocity.

1. Introduction

Parkinson's disease (PD) is the second most common neurodegenerative disorder after Alzheimer's disease [1]. PD is characterized by the progressive and selective loss of dopaminergic neurons in the *substantia nigra* and by the presence of Lewy bodies [2], which decreases interstitial dopamine levels and leads to motor dysfunction [3, 4]. PD is also associated with non-motor symptoms such as cognitive decline, depression and sleep disorders, with some of them preceding the development of the classical motor symptoms [5, 6]. Current drug treatment of PD almost exclusively focuses on restoring the dopaminergic function and reducing the severity of motor handicap [7]. The main pharmacological approaches include dopamine replacement therapy with L-DOPA, inhibition of dopamine metabolism and reuptake, or the use of direct agonists of post-synaptic dopamine receptors [7, 8].

Monoamine oxidases (MAOs, EC 1.4.3.4) are flavin-dependent enzymes bound to the outer mitochondrial membrane [9]. Two MAO isoforms (MAO-A and MAO-B) may participate in the regulation of dopamine levels in neuronal tissue [10]. However, MAO-B is the main MAO isozyme involved in dopamine metabolism in parkinsonian brains, because MAO-B activity and expression are increased in most brain areas while MAO-A activity remains unchanged [11]. Selective irreversible MAO-B inhibitors, like selegiline and rasagiline, are used in PD monotherapy or in combination with dopamine precursor L-DOPA to reduce dopamine catabolism and thereby increase its half-life [12, 13]. More recently, safinamide, a reversible MAO-B inhibitor, was approved in the European Union to treat patients with mid- to late-stage PD [14].

Considering that the prevalence of PD is drastically increasing and no disease-modifying treatment emerged over the last few decades [15], great interest remains in the development of new antiparkinsonian drugs. Piperine (1-[5-(1,3-benzodioxol-5-yl)-1-oxo-2,4-pentadienyl]piperidine), compound **1**, **Figure 1**), the pungent component of several piper species [16], presents several biological properties with potential therapeutic interest for PD. Piperine displayed antioxidant, anti-inflammatory and antiapoptotic activities in cultured neuronal cells [17] and in PD animal models [18-20]. Moreover, piperine was reported as a competitive, reversible and non-selective rMAO inhibitor [21]. Within this framework, we explored the piperine scaffold in a preliminary study, wherein the unequivocal structural elucidation of five piperine bioisosteres along with their *h*MAO inhibitory activities were assessed [22]. The data acquired put forward the significance of piperidinyl amide group to modulate the interaction of piperine derivatives with *h*MAOs [22].

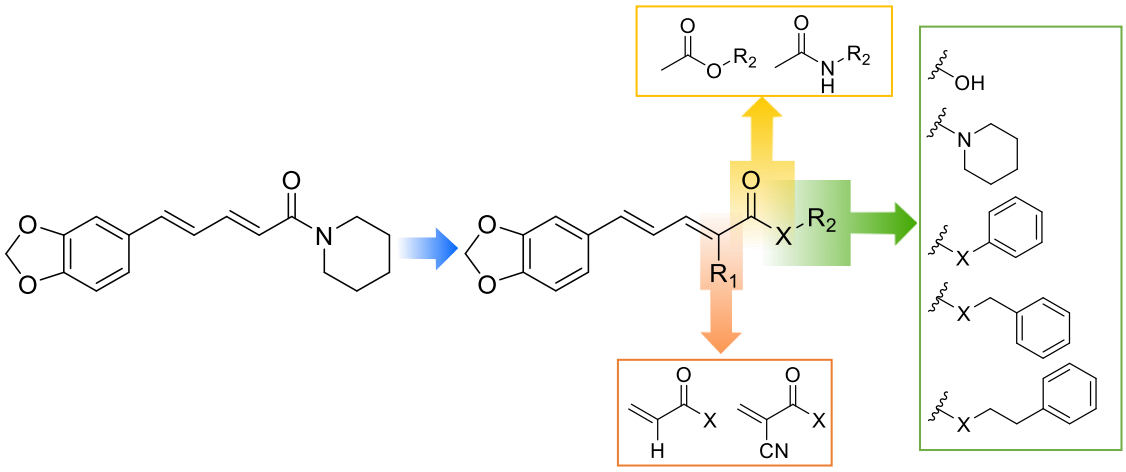


Figure 1. Rational design of the library based on piperine (compound **1**) scaffold.

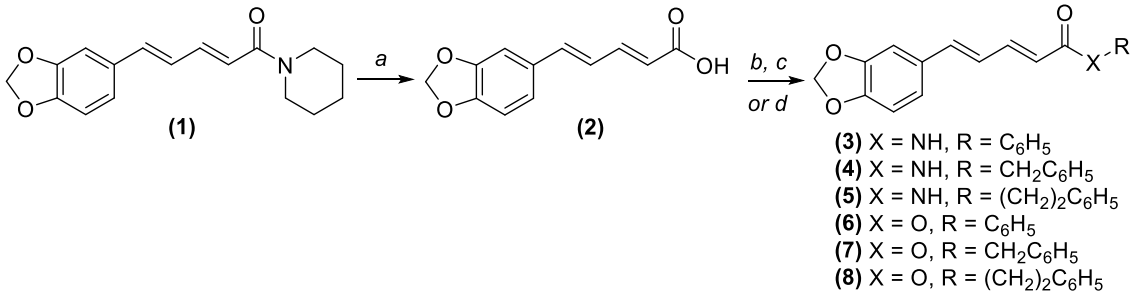
The promising results encouraged a second project aiming to identify the most favourable chemical modifications on the piperine scaffold required for the development of novel ligands with potential application in PD. Herein, we report the synthesis of a new library of piperine derivatives (**Figure 1**) and the establishment of new structure-activity-relationships (SAR). Following *h*MAO-B enzymatic and mechanistic studies, we investigated the cytotoxicity of the best inhibitors in two different human-derived cell lines (neuroblastoma cells (SH-SY5Y) and colon adenocarcinoma cells (Caco-2)). The compounds' ability to induce intracellular oxidative stress in SH-SY5Y cells and to modulate the P-glycoprotein (P-gp) activity by piperine derivatives in Caco-2 cells was also evaluated. Finally, we studied the drug-like properties of the best compounds. The compound´s lipophilicity was evaluated by chromatographic hydrophobicity index (CHI).

2. Results and discussion

2.1. Chemistry

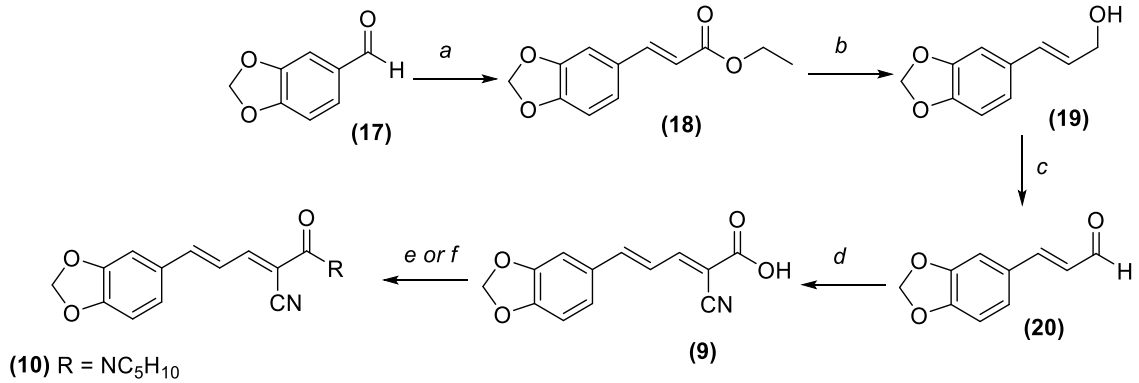
Piperine-based compounds **2-16** were synthesized following the strategies represented in **Schemes 1** and **2**. Several modifications were performed at the diene tether and at the piperidinyl amide group to attain structural diversity (**Figure 1**). Piperidinyl moiety was removed to obtain free carboxylic acids or replaced by lipophilic groups (phenyl, benzyl or phenethyl) linked through ester or amide bonds. In addition, an α-cyano group was incorporated in the diene tether.

The hydrolysis of piperine in alkaline medium (**Scheme 1,** step *a*) yielded piperic acid (compound **2**, **Scheme 1**), which in turn reacted with the appropriate amines or alcohols to afford the corresponding amides **3-5** and esters **6-8**, respectively. Accordingly, amides **3-5** were synthesized via benzotriazol-1-yl-oxytripyrrolidinophosphonium hexafluorophosphate (PyBOP)-mediated amidation reaction, under alkaline conditions, between piperic acid and aniline, benzylamine or phenylethylamine (**Scheme 1,** step *b*). Piperic acid ester **6** was obtained by a Steglich esterification reaction, assisted by *N*-(3-dimethylaminopropyl)-*N'*-ethylcarbodiimide (EDC) and 4-(dimethylamino)pyridine (DMAP), between piperic acid **2** and phenol (**Scheme 1,** step *c*). Esters **7** and **8** were synthesized from piperic acid **2** by bimolecular nucleophilic substitution with benzyl bromide and (2-bromoethyl)benzene, respectively (**Scheme 1,** step *d*).



Scheme 1. Synthetic strategy pursued to obtain piperine derivatives **2**-**8**. (a) Methanolic solution of NaOH 2 M, reflux, 24 h; (b) 1. DMF, DIPEA, PyBOP, CH_2Cl_2, 0 ºC, 30 min; 2. Amine (aniline, benzylamine or phenylethylamine), rt, overnight; (c) 1. EDC•HCl, DMAP, CH_2Cl_2, rt, 30 min; 2. phenol, rt, overnight; (d) 1. K_2CO_3, DMF, rt, 30 min; 2. benzylbromide or (2-bromoethyl)benzene, 80 ºC, 8 h.

The synthetic route used to obtain α-cyanopiperic acid (compound **9**) and derivatives **10**-**16** is shown in **Scheme 2**. The cinnamic derivative (compound **18)** used as starting material was prepared by a Knoevenagel-Doebner condensation between piperonal (compound **17**) and mono-ethyl malonate in pyridine and catalytic amounts of piperidine (**Scheme 2,** step *a*). The reduction of compound **18** with lithium aluminium hydride ($LiAlH_4$) afford the 3,4-methylenedioxycinnamyl alcohol (compound **19**) (**Scheme 2,** step *b*) that was subsequently oxidized to the 3,4-methylenedioxycinnamic aldehyde (compound **20**) with manganese dioxide (MnO_2) (**Scheme 2,** step *c*). α-Cyanopiperic acid (compound **9**) was obtained by a Knoevenagel condensation between compound **20** and cyanoacetic acid (**Scheme 2,** step *d*). Subsequent amidation (**Scheme 2,** step *e*) or Steglich esterification (**Scheme 2,** step *f*) reactions afforded compounds **10**-**16**.



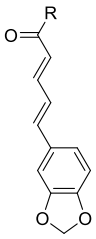
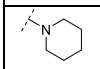
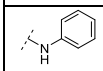
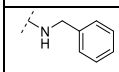
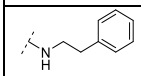
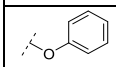
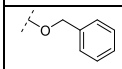
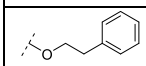
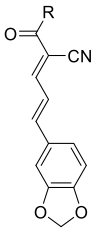
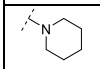
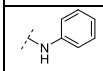
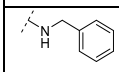
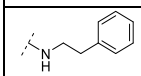
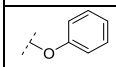
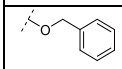
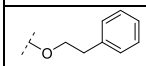
Scheme 2. Synthetic strategy pursued to obtain α-CN derivatives **9**-**16**. (a) mono-ethyl malonate, pyridine, piperidine, 70 ºC, 9 h; (b) 1. Argon atmosphere, dry THF, -78 ºC, 30 min; 2. $LiAlH_4$, -78 ºC to rt, 5 h; (c) MnO_2, CH_2Cl_2, rt, overnight; (d) cyanoacetic acid, pyridine, piperidine, 60 ºC, 30 min; (e) 1. DMF, DIPEA, PyBOP, CH_2Cl_2, 0 ºC, 30 min; 2. Amine (piperidine, aniline, benzylamine or phenylethylamine), rt, overnight; (f) 1. EDC•HCl, DMAP, CH_2Cl_2, rt, 30 min; 2. Phenol, benzyl alcohol or 2-phenylethanol, rt, overnight.

2.2. Monoamine oxidase inhibition studies

The potential effects of piperine and its analogues (compounds **1**-**16**) on *h*MAOs activity were studied by spectrophotometry, using kynuramine as substrate and recombinant *h*MAO-A and -B isoforms [22, 23] . The *h*MAO-A and *h*MAO-B inhibitory potency (IC_{50}) and selectivity (SI) data obtained with the compounds

under study and standard inhibitors (clorgyline for *h*MAO-A and (*R*)-(−)-deprenyl, rasagiline, safinamide for *h*MAO-B) are reported in **Table 1**.

Table 1. *h*MAO inhibitory activities of compounds **1-16** and standard inhibitors.

	R	Compound	IC_{50} (μM)		SI[b]
			*h*MAO-A	*h*MAO-B	
		**2**[e]	___[a]	___[a]	__
		**1**[e]	___[a]	1.05±0.08	10[d]
		**3**[e]	___[a]	___[a]	__
		**4**[e]	___[a]	___[a]	__
		**5**	___[a]	___[a]	__
		**6**[e]	___[c]	0.156±0.008	> 64[d]
		**7**[e]	4.24±0.56	0.167±0.011	25
		**8**	___[a]	0.448±0.043	> 22[d]
		**9**	___[a]	___[a]	__
		**10**	___[a]	0.143±0.080	> 70[d]
		**11**	___[a]	___[a]	__
		**12**	___[a]	0.471±0.008	> 21[d]
		**13**	___[a]	___[a]	__
		**14**	___[a]	0.215±0.038	>47[d]
		**15**	___[a]	0.0474±0.0042	> 211[d]
		**16**	___[a]	0.0992±0.0082	> 101[d]
(*R*)-(−)-Deprenyl[e]		__	20.1±1.9	0.0386±0.0043	522
Rasagiline		__	3.65±0.31	147.3±249	24
Safinamide		__	___[a]	0.0231±0.0026	> 433[d]
Clorgyline[e]		__	0.00274±0.00047	2.21±0.26	0.00124

[a] Inactive at 10 μM taking into account an MAO-B inhibitory activity threshold of 50 %.

[b] SI: *h*MAO-B selectivity index = IC_{50}(*h*MAO-A)/IC_{50}(*h*MAO-B).

[c] Not soluble in phosphate buffer at concentrations higher than 10 μM.

[d] Values obtained under the assumption that the corresponding IC_{50} value against *h*MAO-A or *h*MAO-B is the highest concentration tested (10 μM).

[e] Data from Chavarria *et al.* [22].

2.2.1. Structure-activity relationship studies

The results obtained show that the compounds that presented *h*MAOs inhibitory activity were more selective towards the isoform B. As previously reported, piperine displayed moderate and selective inhibition towards *h*MAO-B (compound **1**, IC_{50} = 1.05 µM, SI = 10) in our experimental conditions [22]. Interestingly, the introduction of an α-CN group at the diene tether improved the *h*MAO-B inhibitory activity (compound **10**: IC_{50} = 143 nM).

Compounds containing a piperidinyl amide moiety were active towards *h*MAO-B (compounds **1** and **10**). The replacement of the piperidinyl group by a carboxylic acid (compounds **2** and **9**) completely abolished *h*MAO inhibition. Primary amides were also unable to inhibit both *h*MAO isoforms (compounds **3-5**, **11** and **13**) or have modest inhibitory activity towards *h*MAO-B (compounds **12**). On the other hand, except for compound **14**, esters **6-8**, **15** and **16** were more potent and selective *h*MAO-B inhibitors than piperidinyl derivatives **1** and **10**.

Concerning ester and primary amide substituents, benzyl derivatives displayed the most promising results. Piperic acid benzyl ester presented an IC_{50} value similar to that of the phenyl derivative and lower than the phenethyl analogue (compound **7**: IC_{50} = 167 nM; compound **6**: IC_{50} = 156 nM; compound **8**: IC_{50} = 448 nM). All α-cyanobenzyl derivatives acted as *h*MAO-B inhibitors. Compound **12** was the only primary amide of α-cyanopiperic acid acting as *h*MAO-B inhibitor (compound **12**: IC_{50} = 471 nM). Benzyl ester **15** was more active than phenethyl ester **16**, which in turn was more potent than phenyl ester **14** (compound **15**: IC_{50} = 47.4 nM; compound **16**: IC_{50} = 99.2 nM; compound **14**: IC_{50} = 215 nM). Therefore, we concluded that the combination of the benzyl group with a cyano group enhanced the *h*MAO-B inhibitory properties.

In fact, with the exception of compound **14**, compounds containing an α-CN presented lower IC_{50} values towards *h*MAO-B than their unsubstituted counterparts, without showing significant *h*MAO-A inhibitory activity at 10 µM. This chemical modification also influenced the selectivity of the compounds. The SI of compounds **10**, **15** and **16** were 5 to 8.4-fold higher than that of piperine and compounds **7** and **8** (compound **1** [SI = 10] *vs* compound **10** [SI = 70]; compound **7** [SI = 25] *vs* compound **15** [SI = 211]; compound **8** [SI = 22] *vs* compound **16** [SI = 101]. Compound **15** showed the lowest IC_{50} value towards *h*MAO-B and the highest *h*MAO-B SI (compound **15:** IC_{50} = 47.4 nM; SI = 211).

2.2.2. Evaluation of human monoamine oxidase-B inhibition mechanism

To further investigate the *h*MAO-B inhibition mechanism of the best *h*MAO-B inhibitor (compound **15**), kinetic experiments were performed. The study was extended to compounds **7** and **10** to evaluate the influence of the α-CN or piperidinyl amide groups in the enzyme inhibition mechanisms. We measured the initial rates of the *h*MAO-catalyzed deamination of six different concentrations of kynuramine in the absence or presence of three different concentrations of the inhibitors. The results obtained are depicted in **Figure 2**. Kinetic parameters of Michaelis-Menten reaction (Michaelis constant, K_m, and maximum velocity, V_{max}) were determined by the graphical analysis of the double reciprocal Lineweaver-Burk plots. The presence of increasing concentrations of compounds **7**, **10** and **15** resulted in an increase of K_m values and a maintenance of V_{max}. The Lineweaver-Burk plots (**Figures 2A-C**) of these compounds remained linear and intersected at the y-axis. These observations indicate that the piperine derivatives **7**, **10** and **15** act as competitive inhibitors.

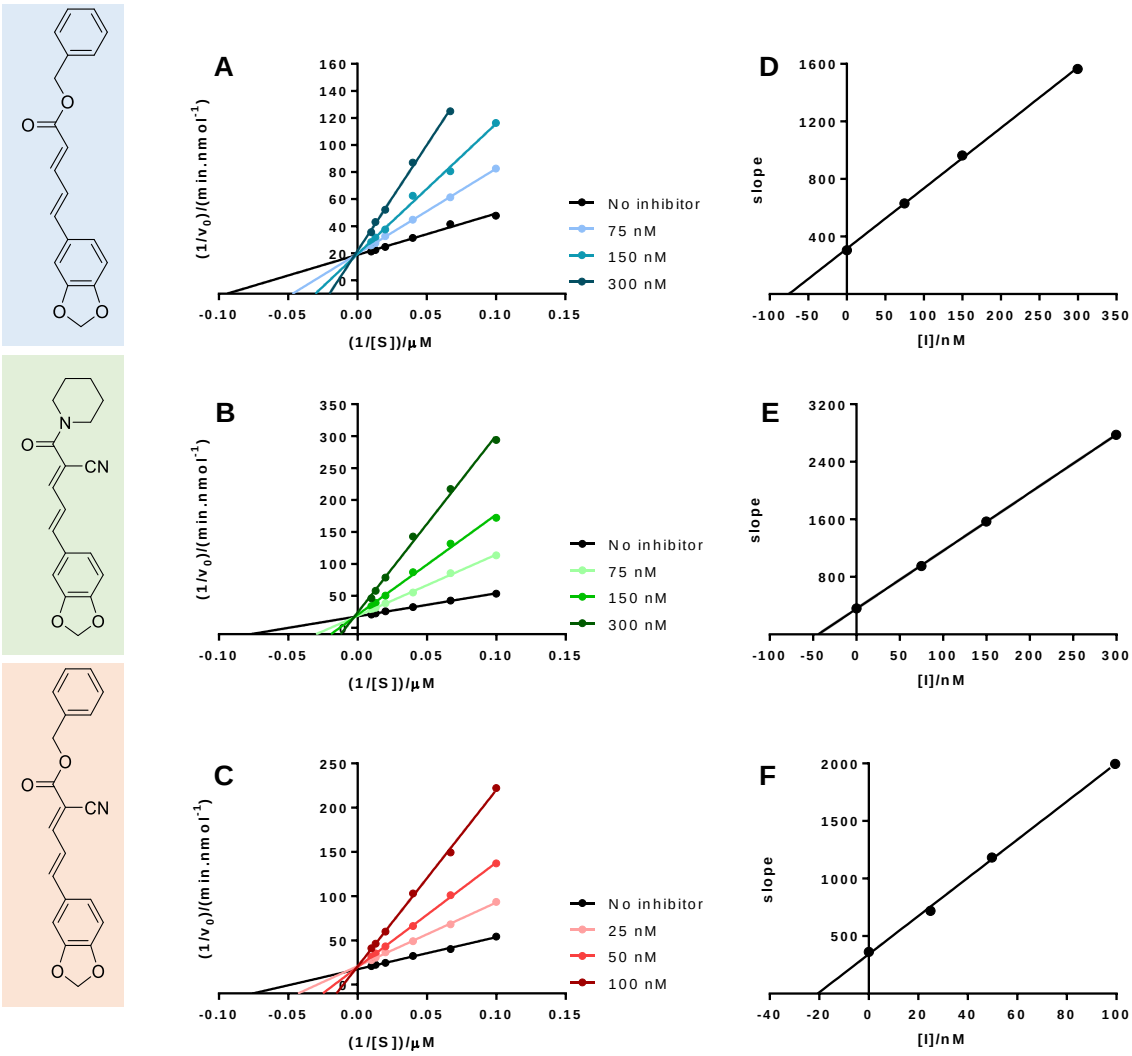


Figure 2. Kinetic studies on the mechanism of *h*MAO-B inhibition by compounds **7 (A** and **D)**, **10** (**B** and **E**) and **15** (**C** and **F**). (**A-C**) Double reciprocal plots of the initial velocity of *h*MAO-B at increasing substrate concentrations (10-100 µM) in the absence or the presence of the inhibitor. (**D-F**) Secondary plots of the slope of each Lineweaver-Burk (K_m/V_{max}) versus the inhibitor concentration.

The data obtained from the Lineweaver-Burk were then replotted as the slope against the inhibitor concentrations to obtain the inhibition constants (K_i) of the mentioned compounds. The x-axis intercept is - K_i (**Figures 2D-F**). Compounds **7**, **10** and **15** displayed K_i values of 75.0 nM, 20.6 nM and 44.1 nM, respectively. The estimated K_i values were well correlated with the inhibition mechanism established from the kinetic experiments.

Moreover, the type of binding between *h*MAO-B and compound **15** was assessed by time-dependent inhibition studies [24]. The binding behavior of rasagiline (irreversible inhibitor) and safinamide (reversible inhibitor) was also evaluated under the same experimental conditions (**Figure 3**).

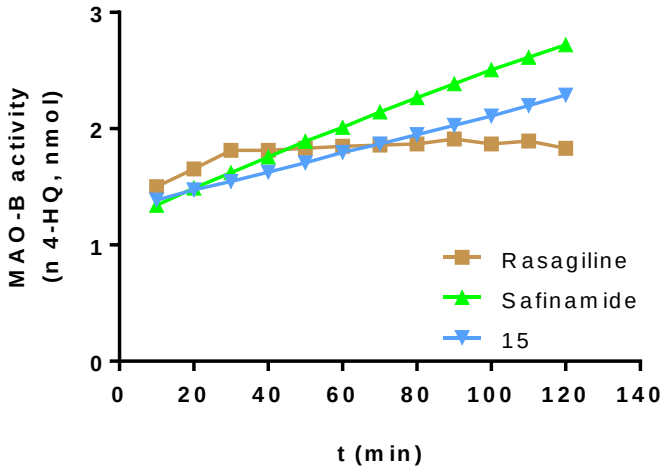


Figure 3. Time-dependent inhibition of recombinant *h*MAO-B by reference drugs rasagiline and safinamide, and compound **15**. The MAO-B activity is expressed in amount of 4-hidroxyquinoline (nmol).

The studies of reversibility showed that the enzyme residual activity decayed continuously after the first 30 minutes of incubation with rasagiline, which is consistent with irreversible enzymatic inhibition. Contrarily, for safinamide and compound **15**, the enzymatic activity increases constantly along the analysis times showing that compound **15** behaves as a reversible MAO-B inhibitor [24].

2.3. Cellular studies

2.3.1. Evaluation of cytotoxicity profile

To study the cytotoxicity profile of the most promising piperine-based compounds (*h*MAO-B IC_{50} < 200 nM), we performed cellular cytotoxicity assays in differentiated neuroblastoma (SH-SY5Y) cells and in colon adenocarcinoma (Caco-2) cells. SH-SY5Y and Caco-2 cells are commonly used to evaluate the safety of drug candidates [25, 26]. In this study, SH-SY5Y cells were treated with a differentiation-inducing agent to obtain cells morphologically similar to mature dopaminergic neurons [27]. Considering that PD mainly affects dopaminergic neurons [28], differentiated SH-SY5Y cells are a suitable *in vitro* model to study the neurotoxicity of drug candidates with potential application in PD [29].

Differentiated SH-SY5Y cells and Caco-2 cells were incubated with two different concentrations (10 and 50 µM) of compounds **6**, **7**, **10**, **15** and **16** for 24 h. Piperine (compound **1**) was also tested to study the effect of the structural modification of piperine scaffold on the cytotoxicity profile of compounds. Cellular cytotoxicity was evaluated using the resazurin reduction assay, which estimates the metabolic activity of viable cells [30], and the neutral red (NR) uptake assay, which relies on the lysosomal accumulation of the dye NR in living cells [31]. The results are presented in **Figure 3** and expressed as mean (% of control) ± SEM of three independent experiments (n = 3).

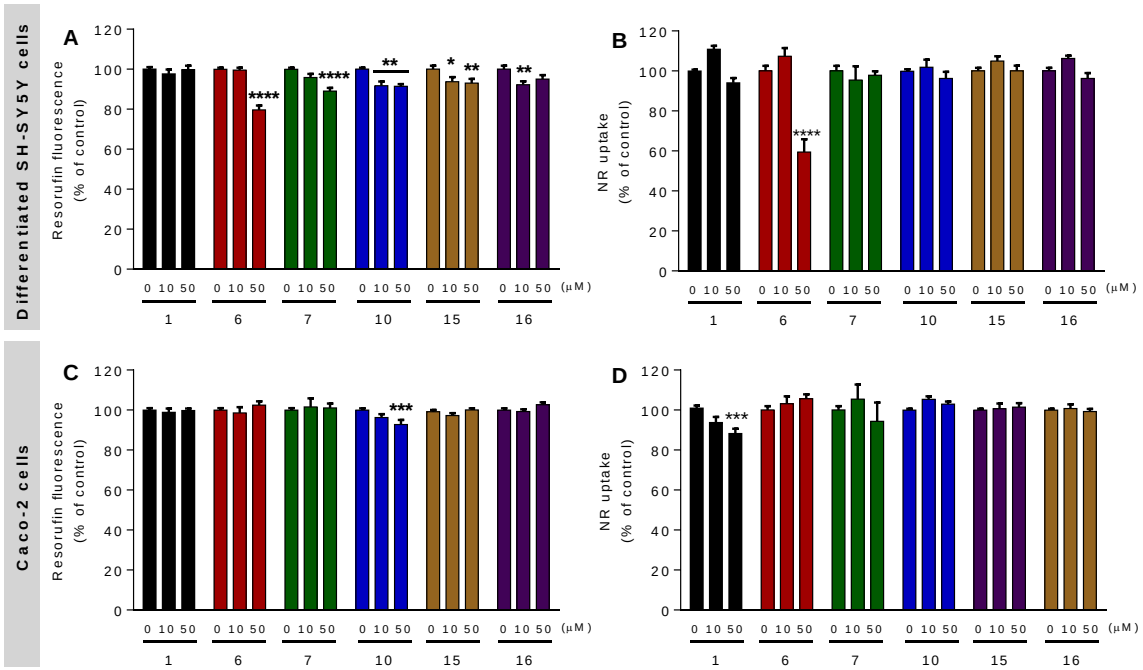


Figure 3. Cellular viability of differentiated SH-SY5Y cells (**A**-**B**) and Caco-2 cells (**C**-**D**) after incubation with piperine (**1**) and compounds **6**, **7**, **10**, **15** and **16** at two different concentrations (10 μM and 50 μM) for 24 h. Cellular viability was evaluated by measuring metabolic (**A** and **C**) and lysosomal activities (**B** and **D**) using the resazurin reduction assay and the neutral red uptake assay, respectively. Statistical comparisons were performed using the parametric method of two-way ANOVA, followed by the Dunnett's multiple comparisons test. In all cases, *p* values lower than 0.05 were considered significant (* $p < 0.05$, ** $p < 0.01$, *** $p < 0.001$, **** $p < 0.0001$ vs untreated cells). Positive control with H_2O_2 (1.5 mM) was performed under the same conditions described above. The results are depicted in supplementary information (**Figure S1A-B**).

The results obtained show that the treatment of differentiated SH-SY5Y cells with compounds **1**, **7**, **10**, **15** and **16** did not markedly decrease the resazurin reduction or the NR uptake when compared to control cells (% resazurin reduction and NR uptake were always > 85 %) (**Figure 3A** and **3B**). However, treatment with compound **6** at the highest tested concentration (50 μM) led to significant reductions in both resorufin fluorescence (79.7 ± 2.1 %, $p < 0.0001$, **Figure 3A**) and in NR uptake (59.4 ± 6.5 %, $p < 0.0001$, **Figure 3B**). In addition, both cellular metabolic and lysosomal activities in Caco-2 cells (**Figures 3C** and **3D**, respectively) were not markedly affected by the treatment with any of the tested piperine derivatives.

Overall, the acquired data suggest that piperine derivatives **7**, **10**, **15** and **16** present a safe cytotoxicity profile in both human-derived neuroblastoma and adenocarcinoma cells (% resazurin reduction and NR uptake were always > 85 %).

2.3.2. Evaluation of intracellular oxidative stress

The toxicity of numerous xenobiotics may be linked to the increased levels of oxidative stress, which are largely related with the unbalance between endogenous antioxidant systems and the levels of reactive species (RS) [32]. Structurally, the compounds under study contain a diene group that can react with glutathione via Michael addition [33]. As an example, the stability assay with compound **15** in the presence of glutathione performed by ^{1}H NMR analysis [34] showed no structural modification in this compound (see supplementary

information, **Figure S2**), suggesting that no interaction occurred between the diene group of compound **15** and the thiol group of glutathione.

It has been reported that several cytochrome P450 isoenzymes are expressed in SH-SY5Y cells [35]. Compounds containing a benzodioxole ring are usually substrates of cytochrome P450 isoenzymes, which can oxidize the methylene carbon of the benzodioxole group into a catechol [36]. The subsequent oxidation of the catechol group generates *o*-quinones that may participate in the formation of RS in redox-cycling processes [37]. Therefore, we evaluated the intracellular oxidative stress levels in differentiated SH-SY5Y cells. After exposing the cells to piperine (compound **1**) and compounds **6**, **7**, **10**, **15** and **16** at two different concentrations (10 and 50 μM) for 24 h, the intracellular RS levels were measured using the 2',7'-dichlorofluorescein diacetate (DCFH-DA) method. The results are expressed as 2',7'-dichlorofluorescein (DCF) fluorescence (% of control) ± SEM (n = 3) and are depicted in **Figure 4**.

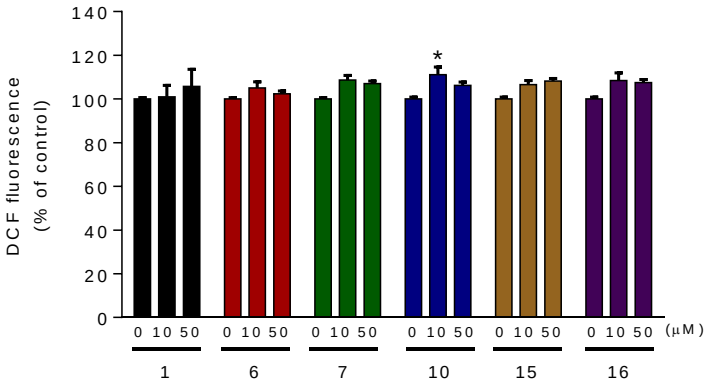


Figure 4. Evaluation of intracellular oxidative stress levels in differentiated SH-SY5Y cells using the DCF fluorescence assay, after treatment with piperine (compound **1**) and compounds **6**, **7**, **10** and **15** and **16** at two different concentrations (10 μM and 50 μM) for 24 h. Results are expressed as DCF fluorescence (% of control) ± SEM (n = 3). Statistical comparisons were performed using the parametric method of two-way ANOVA, followed by the Dunnett's multiple comparisons test. Positive control with H_2O_2 (1.5 mM) was performed under the same conditions described above. The result is depicted in supplementary information (**Figure S1C**).

Among the tested piperine derivatives, only compound **10** led to a slight but significant increase in DCF fluorescence (111.1 ± 3.5 %, $p < 0.5$) when compared to non-treated cells (**Figure 4**). Given that compound **10** did not exhibit cytotoxicity at the tested concentrations (**Figures 3A and 3B**), the results obtained suggest that the slightly increased RS levels did not inflict oxidative damage in SH-SY5Y cells. Cells treated with compound **6** showed similar DCF fluorescence values to non-treated cells (**Figure 4**), despite the significant decrease in resazurin reduction (79.7 ± 2.1 %, $p < 0.0001$, **Figure 3A)**. Therefore, a reduced number of living cells treated with compound **6** produced a higher amount of RS than non-treated cells. These results suggest that compound **6** induced an overproduction of RS in neuroblastoma cells [37].

2.3.3. Evaluation of P-glycoprotein (P-gp) transport activity

The delivery of therapeutic agents into the brain is strongly hampered by the blood-brain barrier (BBB) [38]. In fact, more than 98 % of all small drugs are unable to cross the BBB [39]. An important

gatekeeper of the BBB is P-gp, an ATP-driven efflux pump localized in the luminal membrane of brain capillary endothelial cells [40]. P-glycoprotein restricts the access of a large number of prescribed drugs to the central nervous system (CNS) and contributes to the poor success rates of CNS drug candidates [40].

Considering that P-gp is highly expressed in Caco-2 cells, this cellular model is widely used not only to screen the P-gp-mediated transport of drugs [41], but also to evaluate the influence of new drug candidates in P-gp expression and/or activity [42, 43].

We evaluated the P-gp modulatory activity of piperine (compound **1**) and compounds **7**, **10**, **15** and **16** in Caco-2 cells, using Rhodamine 123 (RHO 123) as a P-gp substrate and zosuquidar (Zos) as a specific third-generation P-gp inhibitor [24]. Increased P-gp activity enhances RHO 123 efflux, leading to a decrease in the intracellular fluorescence intensity under normal conditions (FI_{NA}). Therefore, the RHO 123 accumulation ratio (FI_{IA}/FI_{NA}) will be higher than the control experiments (see supplementary information, **Equation S3**). On the other hand, lower P-gp activity is associated with higher FI_{NA}, as a result of the decreased RHO 123 efflux and consequent increase of RHO 123 intracellular accumulation. Thus, the FI_{IA}/FI_{NA} ratio will be lower than the control experiments (see supplementary information, **Equation S3**). To demonstrate the Zos ability for P-gp inhibition, the RHO 123 intracellular fluorescence of control cells (0 μM) in the presence and absence of Zos are depicted in supplementary information (**Figure S1D**), demonstrating an increased accumulation of the fluorescent substrate under P-gp inibition.

The results presented in **Figure 5** show that compounds **10**, **15** and **16**, at 10 μM, significantly affected the intracellular accumulation of RHO 123, resulting in significant differences in P-gp transport activity. On the other hand, piperine (compound **1**) and compound **7** did not significantly change P-gp-mediated RHO 123 efflux.

Compound **10** significantly increased P-gp activity in a short-incubation period, resulting in a decreased RHO123 accumulation and, consequently, in a higher FI_{IA}/FI_{NA} ratio. Therefore, compound **10** demonstrated potential for P-gp activation. Given the short incubation period with both the P-gp substrate and the test compounds, the effect observed with compound **10** did not reflect the potential contribution of an increased protein expression. (**Figure 5**).

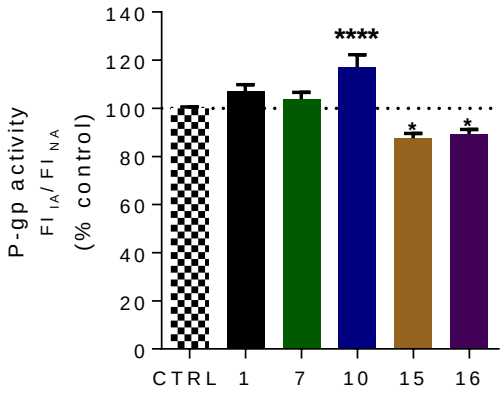


Figure 5. Evaluation of P-gp activity by fluorescence spectroscopy in Caco-2 cells exposed to compounds **1**, **7**, **10, 15** and **16** (10 μM) only during the incubation period with the fluorescent substrate (RHO 123, 5 μM). Results are presented as mean ± SEM from at least three independent experiments, performed in triplicate. Statistical comparisons were made using

the parametric method of one-way ANOVA, followed by the Dunnett's multiple comparisons test (****$p < 0.0001$ vs. control cells).

Piperine derivatives **15** and **16,** at 10 μM, significantly reduced RHO 123 efflux, resulting in a decreased FI_{IA}/FI_{NA} ratio that indicates mild P-gp inhibition. Together with the data obtained in *h*MAO inhibition studies, these findings show that compounds **15** and **16** are potent *h*MAO-B inhibitors with mild P-gp inhibitory activity.

Mild P-gp inhibition can be advantageous in combination therapy of PD. Since several antiparkinsonian agents such as L-DOPA are P-gp substrates [44], mild P-gp inhibition may decrease the drug efflux at the BBB, improve the drug delivery into the CNS and provide a longer symptomatic relief [45].

2.4. Evaluation of drug-like properties

We studied drug-like properties of piperine and the most promising *h*MAO-B inhibitors (compounds **7**, **15** and **16**) to predict their ability to attain the CNS. Compound **10** was excluded because it presented a positive modulatory effect on P-gp (**Figure 5**).

First, we determined the chromatographic hydrophobic index logD at pH 7.4 (CHI $logD_{7.4}$), a parameter used to assess the compounds' hydrophobicity [46, 47]. Overall, the tested compounds presented CHI $logD_{7.4}$ values between 2.4 and 3.8 (**Table 2**). Compounds **7**, **15** and **16** displayed higher CHI values than piperine. These results indicate an increase in lipophilicity with the replacement of the piperidinyl ring by benzyl or phenethyl ester groups.

Table 2. Retention times (t_R) obtained by LC/UV at pH 7.4 and calculated CHI and CHI $logD_{7.4}$ parameters of compounds **1**, **7**, **15** and **16**

Compound	t_R (min)	CHI[a]	CHI $LogD_{7.4}$[b]
1	10.61	73.45	2.39
7	12.46	102.14	3.90
15	12.11	96.73	3.61
16	12.37	100.75	3.82

[a] CHI values were calculated using the equation obtained in the linear correlation (see supplementary information, **Figure S3)**.

[b] CHI $logD_{7.4}$ were back-calculated using the equation CHI $logD_{7.4} = (0.0525 \times CHI)-1.467$.

Other physicochemical properties were also estimated. These included molecular weight (MW), topological polar surface area (TPSA in Å), number of hydrogen acceptors (HBA), number of hydrogen donors (HBD) and number of rotatable bonds (RB). The values obtained were in line with the reported limits of CNS-active drugs (**Table 3**). Another parameter used to assess the ability of a molecule to cross the BBB by passive diffusion is the logarithm of the ratio of the concentration of the compound in the brain and in the blood (logBB) [48]. Compounds with logBB < −1 have low distribution into the brain and thus are unlikely to act as CNS drugs [49]. Piperine and compounds **7**, **15** and **16** showed estimated logBB values above −1 suggesting that they may be able to cross the BBB and reach the CNS (**Table 3**). These data are of particular relevance since

piperine and compounds **15** and **16** presented values of logBB similar to the value reported for ibuprofen (-0.18), a BBB permeable compound [48].

Table 3. Predicted drug-like properties of piperine and compounds **7**, **10**, **15** and **16**.

Compound	MW[a]	TPSA[a]	HBA[a]	HBD[a]	RB[a]	logBB[a]
1	285.3	38.77	3	0	4	-0.185
7	308.3	44.76	4	0	6	0.059
15	333.3	68.55	5	0	6	-0.194
16	347.4	68.55	5	0	7	-0.175
CNS^+ drugs	< 500[50]	< 90[50]	< 7[51]	< 3[51]	< 8[51]	≥ -1[49]

[a] Properties predicted using the Stardrop software. MW: molecular weight; TPSA: topological polar surface area; HBA: number of H-bond acceptor atoms; HBD: number of H-bond donor atoms; RB: number of rotatable bonds; logBB: logarithm of the ratio of the concentration of a drug in the brain and in the blood.

3. Conclusion

We successfully obtained a small library of piperine derivatives and explored their inhibitory activities towards *h*MAO-A and hMAO-B. Piperine and derivatives thereof displayed selective *h*MAO-B inhibition. SAR studies indicated that the presence of an α-cyano group increase *h*MAO-B inhibitory properties and that ester derivatives were considerably more active towards *h*MAO-B than amides and carboxylic acids. Concerning the lipophilic group bound to the ester/amide function, benzyl derivatives were the most potent *h*MAO-B inhibitors, followed by phenethyl and phenyl derivatives. Remarkably, the combination of an α-cyano group with ester groups enhanced *h*MAO-B inhibition potency and selectivity, leading to an up to 22-fold decrease of *h*MAO-B IC_{50} values in comparison to piperine (**1**). Compounds **6**, **7**, **10**, **15** and **16** were the most potent *h*MAO-B inhibitors, with IC_{50} values within the nanomolar range. Kinetic studies indicated that the piperine derivatives operated via a competitive inhibition mechanism. In general, piperine and compounds **7**, **10**, **15** and **16** presented safe cytotoxicity profiles in human-derived neuroblastoma and colon adenocarcinoma cells. Small decreases of FI_{IA}/FI_{NA} ratios associated with increased intracellular RHO 123 accumulation in Caco-2 cells were also observed for compounds **15** and **16** at 10 μM, indicating a slight P-gp inhibition.

Compound **15** stands out as a non-cytotoxic, potent and selective *h*MAO-B inhibitor (IC_{50} = 47.4 nM, SI = 211) with small P-gp inhibitory activity and suitable physicochemical properties for BBB permeation. Therefore, compound **15** is a valid candidate for lead optimization. In this context, the modification of the benzyl ester group or the benzodioxole ring can be looked as a valid strategy to obtain new molecules with improved efficacy and potency. Considering that PD and other neurodegenerative diseases result from the interplay between multiple pathological mechanisms, compound **15** can also be fused or merged with other neuroprotective agents to obtain drug candidates with a polypharmacological profile.

4. Experimental section

4.1. Synthesis of piperine derivatives

4.1.1. Synthesis of (2*E*,4*E*)-5-(benzo[*d*][1,3]dioxol-5-yl)penta-2,4-dienoic acid (2). Synthesis and structural analysis were previously reported [22].

4.1.2. General procedure for the synthesis of amides. Piperic acid **2** or cyanopiperic acid **9** (1.0 mmol) were dissolved in DMF and DIPEA (1.0 mmol). The mixture was cooled at 0 ºC on an ice bath, and a solution of PyBOP (1.0 mmol) in dichloromethane was slowly added. The mixture was stirred for 30 min, and the appropriate amine (phenyl amine, benzyl amine or phenethyl amine) (1.0 mmol) was added. The mixture was stirred overnight at room temperature. Purification conditions are described in literature [22, 52]. In the cases that different conditions were used they were reported.

(2*E*,4*E*)-5-(benzo[*d*][1,3]dioxol-5-yl)-*N*-phenylpenta-2,4-dienamide (3). Synthesis and structural analysis were previously reported [22].

(2*E*,4*E*)-5-(benzo[*d*][1,3]dioxol-5-yl)-*N*-benzylpenta-2,4-dienamide (4). Synthesis and structural analysis were previously reported [22].

(2*E*,4*E*)-5-(benzo[*d*][1,3]dioxol-5-yl)-*N*-phenethylpenta-2,4-dienamide (5). η = 82 %. ^{1}H NMR ($CDCl_3$-d_1): δ (ppm) = 2.87 (*t*, *J* = 6.9 Hz, 2H, $NHCH_2C\underline{H}_2Ph$), 3.62 (*q*, *J* = 8.0 Hz, 2H, $NHC\underline{H}_2CH_2Ph$), 5.54 (*bs*, 1H, N<u>H</u>), 5.84 (*d*, *J* = 14.9 Hz, 1H, Hα), 5.97 (*s*, 2H, $OC\underline{H}_2O$), 6.65 (*dd*, *J* = 11.0 Hz, 15.2 Hz, 1H, Hγ), 6.74-6.78 (*m*, 2H, H5, Hδ), 6.88 (*dd*, *J* = 1.6 Hz, 8.1 Hz, 1H, H6), 6.96 (*d*, *J* = 1.6 Hz, 1H, H2), 7.20-7.25 (*m*, 3H, H3', H4', H5'), 7.30-738 (*m*, 3H, H2', H6', Hβ). ^{13}C NMR ($CDCl_3$-d_1): δ (ppm) = <u>35.9</u> ($NHCH_2\underline{C}H_2Ph$), <u>40.9</u> ($NH\underline{C}H_2CH_2Ph$), <u>101.4</u> ($O\underline{C}H_2O$), <u>106.9</u> (C2), <u>108.6</u> (C5), <u>122.7</u> (Cα), <u>123.1</u> (C6), <u>124.8</u> (Cγ), <u>126.7</u> (C4'), <u>128.8</u> (C2', C6'), <u>128.9</u> (C3', C5'), 131.0 (C1), <u>139.1</u> (Cδ, C1'), <u>141.3</u>(Cβ), 148.3 (C3), 148.4 (C4), 166.2 (<u>C</u>ONH). EI/MS m/z (%): 321.2 ($M^{\bullet+}$, 48), 201.1 (100), 143.1 (19), 115.1 (73), 96.1 (26).

(2*E*,4*E*)-5-(benzo[*d*][1,3]dioxol-5-yl)-2-(piperidine-1-carbonyl)penta-2,4-dienenitrile (10). η = 70 %. ^{1}H NMR (DMSO-d_6)*:* δ (ppm) = 1.54-1.62 (*m*, 6H, $NCH_2C\underline{H}_2C\underline{H}_2$), 3.48-3.51 (*m*, 4H, $NC\underline{H}_2CH_2CH_2$), 6.10 (*s*, 2H, $OC\underline{H}_2O$), 6.98 (*d*, *J* = 8.2 Hz, 1H, H5), 7.03 (*dd*, *J* = 11.4 Hz, 15.2 Hz, 1H, Hγ), 7.13 (*dd*, *J* = 1.5 Hz, 8.1 Hz, 1H, H6), 7.31-7.35 (*m*, 2H, H2, Hδ), 7.55 (*d*, *J* = 11.4 Hz, 1H, Hβ). ^{13}C NMR (DMSO-d_6)*:* δ (ppm) = <u>23.8</u> ($NCH_2CH_2\underline{C}H_2$), <u>25.4</u> ($N\underline{C}H_2CH_2CH_2$, $NCH_2\underline{C}H_2CH_2$), <u>101.7</u> ($O\underline{C}H_2O$), 105.3 (Cα), <u>106.4</u> (C2), <u>108.7</u> (C5), 115.5 (<u>C</u>N), <u>121.2</u> (C6), <u>124.7</u> (Cγ), 129.5 (C1), <u>145.7</u> (Cδ), 148.2 (C3), 149.4 (C4), <u>151.5</u> (Cβ), 161.8 (<u>C</u>ON). EI/MS m/z (%): 310.1 ($M^{\bullet+}$, 88), 225.0 (81), 197.0 (65), 159.0 (40), 140.0 (100), 113.0 (30), 84 (32).

(2*E*,4*E*)-5-(benzo[*d*][1,3]dioxol-5-yl)-2-cyano-*N*-phenylpenta-2,4-dienamide (11). The crude product was purified by flash column chromatography (silica gel, dichloromethane). η = 44 %. ^{1}H NMR (DMSO-d_6)*:* δ (ppm) = 6.12 (*s,* 2H, OC<u>H</u>$_2$O), 7.01 (*d, J* = 8.1 Hz, 1H, H5), 7.07-7.14 (*m,* 2H, Hγ, Hδ), 7.22 (*dd, J* = 1.6 Hz, 8.2 Hz, 1H, H6), 7.33-7.37 (*m,* 2H, H2, H4'), 7.42-7.46 (*m*, 2H, H3', H5'), 7.66 (*dd, J* = 4.0 Hz, 8.0 Hz, 2H, H2', H6'), 8.05 (*d, J* = 8.1 Hz, 1H, Hβ), 10.17 (*s,* 1H, N<u>H</u>). ^{13}C NMR (DMSO-d_6)*:* δ (ppm) = <u>101.8</u> (O<u>C</u>H$_2$O), 106.6 (Cα), <u>106.7</u> (C2), <u>108.8</u> (C5), 115.3 (<u>C</u>N), <u>120.5</u> (C2', C6'), <u>121.2</u> (C6), <u>124.2</u> (C4'), <u>125.3</u> (Cγ), <u>128.7</u> (C3', C5'), 129.4 (C1), 138.3 (C1'), <u>147.6</u> (Cδ), 148.2 (C3), 149.8 (C4), <u>152.1</u> (Cβ), 160.3 (<u>C</u>ONH). EI/MS m/z (%): 318.1 ($M^{\bullet+}$, 55), 226.1 (100), 196.0 (30), 159.0 (42), 140.0 (54).

(2*E*,4*E*)-5-(benzo[*d*][1,3]dioxol-5-yl)-*N*-benzyl-2-cyanopenta-2,4-dienamide (12). The crude product was purified by flash column chromatography (silica gel, dichloromethane). η = 64 %. ^{1}H NMR (DMSO-d_6)*:* δ (ppm) = 4.39 (*d, J* = 5.9 Hz, 2H, NHC<u>H</u>$_2$Ph), 6.10 (*s,* 2H, OC<u>H</u>$_2$O), 6.99 (*d, J* = 8.1 Hz, 1H, H5), 7.06 (*dd, J* = 11.5 Hz, 15.2 Hz, 1H, Hγ), 7.18 (*dd, J* = 1.6 Hz, 8.2 Hz, 1H, H6), 7.25-7.41 (*m,* 7H, Hδ, H2, H2', H3', H4', H5', H6'), 7.96 (*d, J* = 12.0 Hz, 1H, Hβ). 8.86 (*t, J* = 5.9 Hz, 1H, N<u>H</u>). ^{13}C NMR (DMSO-d_6)*:* δ (ppm) = <u>43.0</u> (NH<u>C</u>H$_2$Ph), <u>101.8</u> (O<u>C</u>H$_2$O), 105.7 (Cα), <u>106.6</u> (C2), <u>108.8</u> (C5), 115.5 (<u>C</u>N), <u>121.1</u> (C6), <u>125.2</u> (Cγ), <u>126.7</u> (C4'), <u>127.4</u> (C2', C6'), <u>128.3</u> (C3', C5'), 129.4 (C1), 139.0 (C1'), <u>147.3</u> (Cδ), 148.2 (C3), 149.7 (C4), <u>151.8</u> (Cβ), 161.0 (<u>C</u>ONH). EI/MS m/z (%): 332.1 ($M^{\bullet+}$, 100), 241.1 (65), 227.1 (54), 198.1 (32), 140.0 (61), 113.1 (19), 91.0 (98), 65.1 (20).

(2*E*,4*E*)-5-(benzo[*d*][1,3]dioxol-5-yl)-2-cyano-*N*-phenethylpenta-2,4-dienamide (13). The crude product was purified by flash column chromatography (silica gel, dichloromethane). η = 87 %. ^{1}H NMR (DMSO-d_6): δ (ppm) = 2.81 (*t, J* = 8.0 Hz, 2H, NHCH$_2$C<u>H</u>$_2$Ph), 3.42 (*dt, J* = 6.1 Hz, 7.6 Hz, 2H, NHC<u>H</u>$_2$CH$_2$Ph), 6.10 (*s,* 2H, OC<u>H</u>$_2$O), 7.00 (*d, J* = 8.1 Hz, 1H, H5), 7.04 (*dd, J* = 11.5 Hz, 15.2 Hz, 1H, Hγ), 7.18 (*dd, J* = 1.6 Hz, 8.3 Hz, 1H, H6), 7.21-7.23 (*m*, 3H, H2, H4', Hδ), 7.28-7.32 (*m*, 2H, H2', H6'), 7.36-7.39 (*m*, 2H, H3', H5'), 7.88 (*d, J* = 11.5 Hz, 1H, Hβ), 8.36 (*t, J* = 5.6 Hz, 1H, N<u>H</u>). ^{13}C NMR (DMSO-d_6): δ (ppm) = <u>34.9</u> (NHCH$_2$<u>C</u>H$_2$Ph), <u>41.1</u> (NH<u>C</u>H$_2$CH$_2$Ph), <u>101.8</u> (O<u>C</u>H$_2$O), 105.8 (Cα), <u>106.6</u> (C2), <u>108.7</u> (C5), 115.5 (CN), <u>121.1</u> (C6), <u>125.1</u> (Cγ), <u>126.1</u> (C4'), <u>128.4</u> (C2', C6'), <u>128.6</u> (C3', C5'), 129.4 (C1), 139.2 (C1'), <u>147.1</u> (Cβ), 148.2 (C3), 149.6 (C4), <u>151.6</u> (Cδ), 160.8 (<u>C</u>ONH). EI/MS m/z (%): 346.1 ($M^{\bullet+}$, 100), 241.1 (24), 226.1 (100), 196.0 (21), 159.0 (27), 140.0 (35).

4.1.3. General procedures for the synthesis of esters

4.1.3.1. ***Method A (Steglich esterification).*** To a stirred solution of piperic acid **2** (1.0 mmol) in dichloromethane, EDC.HCl (1.2 mmol) and DMAP (0.1 mmol) were added. The mixture was stirred at room temperature for 30 min. Then, the phenol (1.2 mmol) was added and the resulting mixture was stirred, protected from the light, overnight. Purification conditions are described in literature [22, 53].

Phenyl (2*E*,4*E*)-5-(benzo[*d*][1,3]dioxol-5-yl)penta-2,4-dienoate (6). Synthesis and structural analysis were previously reported [22].

Phenyl (2*E*,4*E*)-5-(benzo[*d*][1,3]dioxol-5-yl)-2-cyanopenta-2,4-dienoate (14). η = 66 %. ^{1}H NMR ($CDCl_3$-d_1)*:* δ (ppm) = 6.06 (*s*, 2H, OC<u>H</u>$_2$O), 6.86 (*d*, *J* = 8.0 Hz, 1H, H5), 7.10 (*dd*, *J* = 1.6 Hz, 8.2 Hz, 1H, H6), 7.15 (*d*, *J* = 1.6 Hz, 1H, H2), 7.18-7.26 (*m*, 4H, Hγ, Hδ, H2', H6'), 7.26-7.30 (*m*, 1H, H4') 7.40-7.44 (*m*, 2H, H3',H5'), 8.11 (*d*, *J* = 11.0 Hz, 1H, Hβ). ^{13}C NMR ($CDCl_3$-d_1)*:* δ (ppm) = <u>102.1</u> (O<u>C</u>H$_2$O), 102.3 (Cα), <u>107.0</u> (C2), <u>109.0</u> (C5), 114.7 (<u>C</u>N), <u>121.4</u> (C6), <u>121.5</u> (C2', C6'), <u>126.1</u> (Cγ), <u>126.5</u> (C4'), 129.4 (C1), <u>129.7</u> (C3', C5'), 148.9 (C1'), <u>150.0</u> (Cδ), 150.5 (C3), 151.1 (C4), <u>157.3</u> (Cβ), 161.4 (<u>C</u>OO). EI/MS m/z (%): 319.0 ($M^{\bullet+}$, 16), 226.0 (100), 196.0 (25), 159.0 (38), 140.0 (39).

Benzyl (2*E*,4*E*)-5-(benzo[*d*][1,3]dioxol-5-yl)-2-cyanopenta-2,4-dienoate (15). η = 50 %. ^{1}H NMR ($CDCl_3$-d_1)*:* δ (ppm) = 5.31 (*s*, 2H, OC<u>H</u>$_2$Ph), 6.04 (*s*, 2H, OC<u>H</u>$_2$O), 6.84 (*d*, *J* = 8.1 Hz, 1H, H5), 7.06 (*dd*, *J* = 1.6 Hz, 8.2 Hz, 1H, H6), 7.09-7.16 (*m*, 3H, Hγ, Hδ, H2), 7.35-7.44 (*m*, 5H, H2', H3', H4', H5', H6'), 7.97 (*d*, *J* = 10.9 Hz, 1H, Hβ). ^{13}C NMR ($CDCl_3$-d_1)*:* δ (ppm) = <u>67.8</u> (O<u>C</u>H$_2$Ph), <u>102.0</u> (O<u>C</u>H$_2$O), 103.0 (Cα), <u>106.9</u> (C2), <u>109.0</u> (C5), 114.8 (<u>C</u>N), <u>121.4</u> (C6), <u>125.8</u> (Cγ), <u>128.4</u> (C2', C6'), <u>128.6</u> (C4'), <u>128.8</u> (C3', C5'), 129.4 (C1), 135.3 (C1'), 148.9 (C3), <u>149.1</u> (Cδ), 150.8 (C4), <u>156.1</u> (Cβ), 162.6 (<u>C</u>OO). EI/MS m/z (%): 333.1 ($M^{\bullet+}$, 19), 242.0 (29), 175.0 (25), 91.0 (100).

Phenethyl (2*E*,4*E*)-5-(benzo[*d*][1,3]dioxol-5-yl)-2-cyanopenta-2,4-dienoate (16). η = 51 %. ^{1}H NMR ($CDCl_3$-d_1)*:* δ (ppm) = 3.04 (*t*, *J* = 7.0 Hz, 2H, OCH$_2$C<u>H</u>$_2$Ph), 4.46 (*t*, *J* = 7.1 Hz, 2H, OC<u>H</u>$_2$CH$_2$Ph), 6.04 (*s*, 2H, OC<u>H</u>$_2$O), 6.84 (*d*, *J* = 8.0 Hz, 1H, H5), 7.06-7.18 (*m*, 4H, H6, H2, Hδ, Hγ), 7.25-7.28 (*m*, 3H, H2', H4', H6'), 7.31-7.35 (*m*, 2H, H3', H5'), 7.92 (*d*, *J* = 10.9 Hz, 1H, Hβ). ^{13}C NMR ($CDCl_3$-d_1)*:* δ (ppm) = <u>35.2</u> (OCH$_2$<u>C</u>H$_2$Ph), <u>66.8</u> (O<u>C</u>H$_2$CH$_2$Ph), <u>102.0</u> (O<u>C</u>H$_2$O), 103.1 (Cα), <u>106.9</u> (C2), <u>109.0</u> (C5), 114.8 (<u>C</u>N), <u>121.4</u> (C6), <u>125.7</u> (Cγ), <u>126.9</u> (C4'), <u>128.7</u> (C2', C6'), <u>129.2</u> (C3', C5'), 129.4 (C1), 137.4 (C1'), 148.9 (C3), <u>148.9</u> (Cδ), 150.8 (C4), <u>155.9</u> (Cβ), 162.6 (<u>C</u>OO). EI/MS m/z (%): 347.1 ($M^{\bullet+}$, 34), 243.1 (21), 198.1 (31), 140.0 (37), 105.1 (100).

4.1.3.2. ***Method B*** **(bimolecular nucleophilic substitution).** Piperic acid **2** (1.0 mmol) was dissolved in DMF and K_2CO_3 (1.2 mmol) was added. The mixture was stirred at room temperature for 30 min. Then, the appropriate alkyl bromide (benzyl bromide or (2-bromoethyl)benzene) (1.2 mmol) was added and the mixture was stirred, protected from the light, at 80 ºC for 8 h. Purification conditions are described in literature [22, 54].

Benzyl (2*E*,4*E*)-5-(benzo[*d*][1,3]dioxol-5-yl)penta-2,4-dienoate (7). Synthesis and structural analysis were previously reported [22].

Phenethyl (2*E*,4*E*)-5-(benzo[d][1,3]dioxol-5-yl)penta-2,4-dienoate (8). η = 84 %. ^{1}H NMR ($CDCl_3$-*d_1*)*:* δ (ppm) = 3.00 (*t, J* = 7.1 Hz, 2H, $OCH_2C\underline{H}_2Ph$), 4.39 (*t, J* = 7.1 Hz, 2H, $OC\underline{H}_2CH_2Ph$), 5.94 (*d, J* = 15.3 Hz, 1H, Hα), 5.99 (*s*, 2H, $OC\underline{H}_2O$), 6.70 (*dd, J* = 10.8 Hz, 15.5 Hz, 1H, Hγ), 6.78-6.83 (*m, 2*H, H5, Hδ), 6.91 (*dd, J* = 1.6 Hz, 8.2 Hz, 1H, H6), 6.99 (*d, J* = 1.6 Hz, 1H, H2), 7.22-7.26 (*m*, 3H, H2', H4', H6'), 7.30-7.34 (*m*, 2H, H3', H5'), 7.40 (*dd, J* = 10.7 Hz, 15.2 Hz, 1H, Hβ). ^{13}C NMR ($CDCl_3$-*d_1*)*:* δ (ppm) = $\underline{35.4}$ ($OCH_2\underline{C}H_2Ph$), $\underline{65.0}$ ($O\underline{C}H_2CH_2Ph$), $\underline{101.5}$ ($O\underline{C}H_2O$), $\underline{106.0}$ (C2), $\underline{108.7}$ (C5), $\underline{120.4}$ (Cα), $\underline{123.1}$ (C6), $\underline{124.7}$ (Cγ), $\underline{126.7}$ (C4'), $\underline{128.6}$ (C2', C6'), $\underline{129.1}$ (C3', C5'), 130.7 (C1), 138.1 (C1'), $\underline{140.4}$ (Cδ), $\underline{145.1}$ (Cβ), 148.4 (C3), 148.7 (C4), 167.2 ($\underline{C}OO$). EI/MS m/z (%): 322.1 ($M^{\bullet+}$, 65), 218.2 (17), 173.1 (100), 143.1 (38), 115.1 (94), 91.2 (20), 77.2 (19), 65.2 (18).

4.1.4. Synthesis of (*E*)-3-(benzo[*d*][1,3]dioxol-5-yl)acrylate (18). Aldehyde **17** (1.0 mmol) dissolved in anhydrous pyridine. Then, mono-ethyl malonate (1.5 mmol) and piperidine (0.35 mmol) were added. The mixture was heated until the maximum aldehyde consumption was observed by TLC. Once the reaction was complete, the product was purified by column chromatography (silica gel, dichloromethane). The procedure was adapted from Teixeira *et al.* [55] with some modifications. η = 91 %. ^{1}H NMR ($CDCl_3$-*d_1*)*:* δ (ppm) = 1.33 (*t, J* = 7.1 Hz, 3H, $OCH_2C\underline{H}_3$), 4.25 (*q, J* = 7.1 Hz, 2H, $OC\underline{H}_2CH_3$), 6.00 (*s*, 2H, $OC\underline{H}_2O$), 6.26 (*d, J* = 15.9 Hz, 1H, Hα), 6.81 (*d, J* = 8.0 Hz, 1H, H5), 7.00 (*dd, J* = 1.5 Hz, 8.1 Hz, 1H, H6), 7.03 (*d, J* = 1.7 Hz, 1H, H2), 7.59 (*d, J* = 15.9 Hz, 1H, Hβ). ^{13}C NMR ($CDCl_3$-*d_1*)*:* δ (ppm) = $\underline{14.4}$ ($OCH_2\underline{C}H_3$), $\underline{60.4}$ ($O\underline{C}H_2CH_3$), $\underline{101.5}$ ($O\underline{C}H_2O$), $\underline{106.5}$ (C2), $\underline{108.5}$ (C5), $\underline{116.3}$ (Cα), $\underline{124.4}$ (C6), 128.9 (C1), $\underline{144.3}$ (Cβ), 148.3 (C3), 149.6 (C4), 167.2 ($\underline{C}OO$). EI/MS m/z (%): 220.2 ($M^{\bullet+}$, 100), 175.1 (58), 117.0 (31), 89.0 (64), 63.1 (41).

4.1.5. Synthesis of (*E*)-3-(benzo[*d*][1,3]dioxol-5-yl)prop-2-en-1-ol (19). Cinnamic ester **18** (1.0 mmol) was dissolved in dry THF under argon atmosphere and cooled to −78 °C. Then, $LiAlH_4$ (1.5 mmol) was added, and the mixture was stirred for 5 h. Once the reaction was complete, the unreacted $LiAlH_4$ was quenched with methanol until gas evolution stopped, and water (60 mL) was added. The mixture was neutralized with HCl 6 M, then extracted with dichloromethane (3×30 mL). The combined organic layer was washed with brine (20 mL), dried over anhydrous sodium sulfate, filtered and concentrated. Purification by flash column chromatography (silica gel, dichloromethane) yielded the cinnamyl alcohols **19**. The procedure was adapted from Jirásek *et al.* [56] with some modifications. η = 43 %. ^{1}H NMR ($CDCl_3$-*d_1*)*:* δ (ppm) = 4.29 (*dd, J* = 0.9 Hz, 5.8 Hz, 2H, $C\underline{H}_2OH$), 5.95 (*s*, 2H, $OC\underline{H}_2O$), 6.19 (*d, J* = 5.9 Hz, 15.8 Hz, 1H, Hα), 6.52 (*d, J* = 15.8 Hz, 1H, Hβ), 6.75 (*d, J* = 8.0 Hz, 1H, H5), 6.81 (*dd, J* = 1.6 Hz, 8.1 Hz, 1H, H6), 6.93 (*d, J* = 1.7 Hz, 1H, H2). ^{13}C NMR ($CDCl_3$-*d_1*)*:* δ (ppm) = $\underline{63.8}$ ($\underline{C}H_2OH$), $\underline{101.1}$ ($O\underline{C}H_2O$), $\underline{105.8}$ (C2), $\underline{108.3}$ (C5), $\underline{121.2}$ (C6), $\underline{126.7}$ (Cα), $\underline{131.0}$ (Cβ), 131.2 (C1), 147.3 (C3), 148.0 (C4). EI/MS m/z (%): 178.2 ($M^{\bullet+}$, 80). 135.1 (100), 122.1 (42), 91.1 (24).

4.1.6. Synthesis of (*E*)-3-(benzo[*d*][1,3]dioxol-5-yl)acrylaldehyde (20). Cinnamyl alcohol **19** (1.0 mmol) was dissolved in dichloromethane, and MnO_2 (9.0 mmol) was added. The mixture was stirred overnight at room temperature. Then, the mixture was filtered through celite to remove the MnO_2 and washed with dichloromethane. The filtrate was concentrated and purified by flash column chromatography (silica gel, dichloromethane). The procedure was adapted from Jirásek *et al.* [56] with some modifications. η = 62 %. ^{1}H NMR ($CDCl_3$-d_1): δ (ppm) = 6.04 (*s*, 2H, OC<u>H</u>$_2$O), 6.56 (*dd, J* = 7.7 Hz, 15.8 Hz, 1H, Hα), 6.86 (*d, J* = 8.5 Hz, 1H, H5), 7.07 (*m*, 2H, H2, H6), 7.38 (*d, J* = 15.8 Hz, 1H, Hβ), 9.05 (*d, J* = 7.7 Hz, 1H, C<u>H</u>O). ^{13}C NMR ($CDCl_3$-d_1): δ (ppm) =<u>101.8</u> (O<u>C</u>H$_2$O), <u>106.8</u> (C2), <u>108.8</u> (C5), <u>125.3</u> (Cα), <u>126.9</u> (C6), 128.5 (C1), 148.6 (C3), 150.5 (C4), <u>152.5</u> (Cβ), <u>193.5</u> (<u>C</u>HO). EI/MS m/z (%): 176.1 ($M^{\bullet+}$, 100), 147.1 (67), 118.1 (48), 89.2 (88), 63.1 (74), 51.1 (20).

4.1.7. Synthesis of (2*E*,4*E*)-5-(benzo[*d*][1,3]dioxol-5-yl)-2-cyanopenta-2,4-dienoic acid (9). Aldehyde **20** (1.0 mmol) was dissolved in anhydrous pyridine. Then, cyanoacetic acid (1.5 mmol) and piperidine (0.35 mmol) were added. The mixture was heated until the maximum aldehyde consumption was observed by TLC. Upon completion, the reaction mixture was acidified with HCl 6 M and the solid formed was isolated by filtration under reduced pressure. The procedure was adapted from Teixeira *et al.* [55] with some modifications. η = 87 %. ^{1}H NMR (DMSO-d_6): δ (ppm) = 6.11 (*s*, 2H, OC<u>H</u>$_2$O), 7.00 (*d, J* = 8.0 Hz, 1H, H5), 7.07 (*dd, J* = 11.7 Hz, 15.0 Hz, 1H, Hγ), 7.19 (*dd, J* = 1.4 Hz, 8.1 Hz, 1H, H6), 7.40 (*d, J* = 1.6 Hz, 1H, H2), 7.54 (*d, J* = 15.1 Hz, 1H, Hδ), 8.02 (*d, J* = 11.6 Hz, 1H, Hβ). ^{13}C NMR (DMSO-d_6): δ (ppm) = <u>101.9</u> (O<u>C</u>H$_2$O), 102.9 (Cα), <u>106.1</u>7(C2), <u>108.8</u> (C5), 115.2 (CN), <u>120.9</u> (C6), <u>125.8</u> (Cγ), 129.3 (C1), 148.3 (C3), <u>149.4</u> (Cβ), 150.0 (C4), <u>155.6</u> (Cδ), 163.5 (<u>C</u>OOH). EI/MS m/z (%): 243.2 ($M^{\bullet+}$, 27), 198.2 (34), 140.1 (100), 113.1 (24).

4.2. Enzymatic assays

4.2.1. Evaluation of human monoamine oxidase (hMAO) inhibitory activity

The inhibitory activity of piperine and the derivatives thereof on *h*MAO-A and *h*MAO-B was studied using an experimental protocol described elsewhere [22, 23] (see supplementary information).

4.2.2. Evaluation of human monoamine oxidases kinetics and human monoamine oxidase-B-inhibitor kinetics

To determine the steady-state kinetic parameters (K_m, Michaelis constant, and V_{max}, maximum velocity) of *h*MAO-A and *h*MAO-B, the enzymatic activity of both isoforms was studied in the presence six different concentrations of kynuramine (see supplementary information). To evaluate the mechanism of *h*MAO-B inhibition of compounds **7**, **10** and **15**, substrate-dependent kinetic experiments were also performed (see supplementary information).

4.2.3. Determination of the type of binding affinity between inhibitor and *h*MAO-B

The type of *h*MAO-B binding of compound **15** and reference inhibitors (rasagiline, safinamide) was evaluated by a time-dependent inhibition assay [24]. The *h*MAO-B was incubated for a 90 minutes period with the compound **15** as well as with the inhibitors, at their IC_{80} values. The final well concentrations were: compound **15** (213 nM), safinamide (40 nM), rasagiline (200 nM) and MAO-B (12 ng.μL^{-1}). The enzymatic

activity was evaluated as described in supplementary information. The MAO-B activity was presented based on the amount of 4-hydroxiquinoline (nmol) and plotted against the incubation time to determine time-dependent enzyme-inhibition.

4.3. *In vitro* toxicology

4.3.1. Cell lines and culture conditions

Human SH-SY5Y neuroblastoma cells and human epithelial colorectal adenocarcinoma (Caco-2) cells were obtained from the American Type Culture Collection (ATCC, Manassas, VA, USA). Cell cultures and SH-SY5Y cell differentiation were performed as previously described by Fernandes *et al.* [57] and in supplementary information.

4.3.2. Evaluation of cytotoxicity profile

Stock solutions of the test compounds (100 mM) were freshly prepared in DMSO. Final concentrations of the test compounds were obtained by diluting into culture medium immediately before use, giving a final maximum concentration of 0.1 % DMSO.

In cytotoxicity studies, differentiated SH-SY5Y cells were exposed to the test compounds (10 µM and 50 µM) for 24 h. Controls were treated with culture media containing 0.1 % DMSO. Cell viability was estimated using two different methods: resazurin reduction assay and NR uptake assay. The cytotoxicity end-points were performed as described in literature [24, 57] and in supplementary information.

4.3.3. Evaluation of intracellular oxidative stress levels

The formation of intracellular RS was evaluated using the 2',7'-dichlorofluorescein (DCF) fluorescence assay as previously described by da Fernandes *et al.* [57] and in supplementary information.

4.3.4. Evaluation of P-glycoprotein (P-gp) transport activity

The effects of the tested compounds on P-gp transport activity was evaluated using rhodamine 123 (RHO 123) as a P-gp fluorescent substrate in Caco-2 cells as previously described by Fernandes *et al.* [24] and in supplementary information.

4.4. Statistical analysis

Data analysis for all the studies are specified in supplementary information.

4.5. Evaluation of the chromatographic hydrophobicity index

Chromatographic hydrophobicity index logD at pH 7.4 (CHI $logD_{7.4}$) values were determined using an experimental protocol described elsewhere [46, 58]**.** Chromatographic hydrophobicity index logD at pH 7.4 (CHI $logD_{7.4}$) values were determined using the retention times of samples and a mixture of standard compounds. The data was acquired on a Shimadzu high-performance liquid chromatograph SPD-M20A system (Shimadzu, Kyoto, Japan) with a Luna C18 (2) column (Phenomenex, CA, USA) 150×4.6 mm, 5 µm. The mobile phase A was 10 mM ammonium acetate solution (pH 7.4), and mobile phase B was acetonitrile.

The following gradient program was applied: 1 mL/min flow, rt, injection volume 20 µL, gradient 0−6 min 0-100 % B, 6−14 min 100% B, 14−16 min 100-0 % B.

A calibration plot was obtained using a mixture of the following compounds: paracetamol, theophylline, caffeine, benzimidazole, colchicine, carbamazepine, indole, propiophenone, butyrophenone, valerophenone, and heptanophenone (see supplementary information, **Figure S1** and **Table S1**). Stock solutions of the test compounds (10 µM) were prepared in DMSO and diluted in acetonitrile/water (1:1) to obtain a final concentration of 250 µM. CHI $logD_{7.4}$ values were calculated as previously described [46, 58].

4.6. Estimation of drug-like properties

The calculation of molecular weight (MW), topological polar surface area (TPSA), number of hydrogen bond donors (HBD) and acceptors (HBA), number of rotatable bonds (RB) and logarithm of the ratio of the concentration of a drug in the brain and in the blood (logBB) was performed using the StarDrop software.

5. Acknowledgements

This project was supported by Foundation for Science and Technology (FCT) and FEDER/COMPETE research grants (UID/QUI/00081, NORTE-01-0145-FEDER-000028, POCI-01-0145-FEDER-029164). D. Chavarria, C. Fernandes, E. Martins, V. Silva, C. Silva, P. Soares and T. Silva grants are supported by FCT, POPH and FEDER/COMPETE and NORTE-01-0145-FEDER-000028.This article is based upon work from COST Action CA15135.

6. References

[1] M. Goedert, Alzheimer's and Parkinson's diseases: The prion concept in relation to assembled Aβ, tau, and α-synuclein, Science, 349 (2015) 1255555. https://doi.org/10.1126/science.1255555

[2] Y. He, Z. Yu, S. Chen, Alpha-Synuclein Nitration and Its Implications in Parkinson's Disease, ACS Chem. Neurosci., 10 (2019) 777-782. https://doi.org/10.1021/acschemneuro.8b00288

[3] G. Foffani, J.A. Obeso, A Cortical Pathogenic Theory of Parkinson’s Disease, Neuron, 99 (2018) 1116-1128. https://doi.org/10.1016/j.neuron.2018.07.028

[4] S. Hisahara, S. Shimohama, Dopamine receptors and Parkinson's disease, Int J Med Chem., 2011 (2011) 403039-403039. https://doi.org/10.1155/2011/403039

[5] L.V. Kalia, A.E. Lang, Parkinson's disease, Lancet, 386 (2015) 896-912. https://doi.org/10.1016/s0140-6736(14)61393-3

[6] S.F. Graham, N.L. Rey, A. Yilmaz, P. Kumar, Z. Madaj, M. Maddens, R.O. Bahado-Singh, K. Becker, E. Schulz, L.K. Meyerdirk, J.A. Steiner, J. Ma, P. Brundin, Biochemical Profiling of the Brain and Blood Metabolome in a Mouse Model of Prodromal Parkinson's Disease Reveals Distinct Metabolic Profiles, J. Proteome Res., 17 (2018) 2460-2469. https://doi.org/10.1021/acs.jproteome.8b00224

[7] J. Zheng, X. Zhang, X. Zhen, Development of Adenosine A_{2A} Receptor Antagonists for the Treatment of Parkinson's Disease: A Recent Update and Challenge, ACS Chem. Neurosci., 10 (2019) 783-791. https://doi.org/10.1021/acschemneuro.8b00313

[8] Y.D. Wang, X.Q. Bao, S. Xu, W.W. Yu, S.N. Cao, J.P. Hu, Y. Li, X.L. Wang, D. Zhang, S.S. Yu, A Novel Parkinson's Disease Drug Candidate with Potent Anti-neuroinflammatory Effects through the Src Signaling Pathway, J. Med. Chem., 59 (2016) 9062-9079. https://doi.org/10.1021/acs.jmedchem.6b00976

[9] C. Binda, P. Newton-Vinson, F. Hubalek, D.E. Edmondson, A. Mattevi, Structure of human monoamine oxidase B, a drug target for the treatment of neurological disorders, Nat. Struct. Biol., 9 (2002) 22-26. https://doi.org/10.1038/nsb732

[10] P. Riederer, G. Laux, MAO-inhibitors in Parkinson's Disease, Exp Neurobiol, 20 (2011) 1-17. https://doi.org/10.5607/en.2011.20.1.1

[11] H.P. Booysen, C. Moraal, G. Terre'Blanche, A. Petzer, J.J. Bergh, J.P. Petzer, Thio- and aminocaffeine analogues as inhibitors of human monoamine oxidase, Bioorg. Med. Chem., 19 (2011) 7507-7518. https://doi.org/10.1016/j.bmc.2011.10.036

[12] N.M. Malek, D.G. Grosset, Investigational agents in the treatment of Parkinson's disease: focus on safinamide, J. Exp. Pharmacol., 4 (2012) 85-90. https://doi.org/10.2147/JEP.S34343

[13] A. Stößel, M. Schlenk, S. Hinz, P. Küppers, J. Heer, M. Gütschow, C.E. Müller, Dual targeting of adenosine A_{2A} receptors and monoamine oxidase B by 4*H*-3,1-benzothiazin-4-ones, J. Med. Chem., 56 (2013) 4580-4596. https://doi.org/10.1021/jm400336x

[14] H.A. Blair, S. Dhillon, Safinamide: A Review in Parkinson's Disease, CNS Drugs, 31 (2017) 169-176. https://doi.org/10.1007/s40263-017-0408-1

[15] D. Robakis, S. Fahn, Defining the Role of the Monoamine Oxidase-B Inhibitors for Parkinson's Disease, CNS Drugs, 29 (2015) 433-441. https://doi.org/10.1007/s40263-015-0249-8

[16] J. Wattanathorn, P. Chonpathompikunlert, S. Muchimapura, A. Priprem, O. Tankamnerdthai, Piperine, the potential functional food for mood and cognitive disorders, Food and Chemical Toxicology : an international journal published for the British Industrial Biological Research Association, 46 (2008) 3106-3110. https://doi.org/10.1016/j.fct.2008.06.014

[17] Q.Q. Mao, Z. Huang, S.P. Ip, Y.F. Xian, C.T. Che, Protective effects of piperine against corticosterone-induced neurotoxicity in PC12 cells, Cell. Mol. Neurobiol., 32 (2012) 531-537. https://doi.org/10.1007/s10571-011-9786-y

[18] W. Yang, Y.H. Chen, H. Liu, H.D. Qu, Neuroprotective effects of piperine on the 1-methyl-4-phenyl-1,2,3,6-tetrahydropyridine-induced Parkinson's disease mouse model, Int. J. Mol. Med., 36 (2015) 1369-1376. https://doi.org/10.3892/ijmm.2015.2356

[19] P. Shrivastava, K. Vaibhav, R. Tabassum, A. Khan, T. Ishrat, M.M. Khan, A. Ahmad, F. Islam, M.M. Safhi, F. Islam, Anti-apoptotic and Anti-inflammatory effect of Piperine on 6-OHDA induced Parkinson's Rat model, J. Nutr. Biochem., 24 (2013) 680-687. https://doi.org/10.1016/j.jnutbio.2012.03.018

[20] Y. Bi, P.C. Qu, Q.S. Wang, L. Zheng, H.L. Liu, R. Luo, X.Q. Chen, Y.Y. Ba, X. Wu, H. Yang, Neuroprotective effects of alkaloids from Piper longum in a MPTP-induced mouse model of Parkinson's disease, Pharm. Biol., 53 (2015) 1516-1524. https://doi.org/10.3109/13880209.2014.991835

[21] S.A. Lee, S.S. Hong, X.H. Han, J.S. Hwang, G.J. Oh, K.S. Lee, M.K. Lee, B.Y. Hwang, J.S. Ro, Piperine from the fruits of Piper longum with inhibitory effect on monoamine oxidase and antidepressant-like activity, Chem. Pharm. Bull. (Tokyo), 53 (2005) 832-835. https://doi.org/10.1248/cpb.53.832

[22] D. Chavarria, F. Cagide, M. Pinto, L.R. Gomes, J.N. Low, F. Borges, Development of piperic acid-based monoamine oxidase inhibitors: Synthesis, structural characterization and biological evaluation, J. Mol. Struct., 1182 (2019) 298-307. https://doi.org/10.1016/j.molstruc.2019.01.060

[23] S. Hagenow, A. Stasiak, R.R. Ramsay, H. Stark, Ciproxifan, a histamine H_3 receptor antagonist, reversibly inhibits monoamine oxidase A and B, Sci. Rep., 7 (2017) 1-6. https://doi.org/10.1038/srep40541

[24] C. Fernandes, C. Martins, A. Fonseca, R. Nunes, M.J. Matos, R. Silva, J. Garrido, B. Sarmento, F. Remiao, F.J. Otero-Espinar, E. Uriarte, F. Borges, PEGylated PLGA Nanoparticles As a Smart Carrier to Increase the Cellular Uptake of a Coumarin-Based Monoamine Oxidase B Inhibitor, ACS Appl. Mater. Interfaces, 10 (2018) 39557-39569. https://doi.org/10.1021/acsami.8b17224

[25] Y.T. Cheung, W.K. Lau, M.S. Yu, C.S. Lai, S.C. Yeung, K.F. So, R.C. Chang, Effects of all-*trans*-retinoic acid on human SH-SY5Y neuroblastoma as in vitro model in neurotoxicity research, Neurotoxicology, 30 (2009) 127-135. https://doi.org/10.1016/j.neuro.2008.11.001

[26] Z. Ujhelyi, F. Fenyvesi, J. Varadi, P. Feher, T. Kiss, S. Veszelka, M. Deli, M. Vecsernyes, I. Bacskay, Evaluation of cytotoxicity of surfactants used in self-micro emulsifying drug delivery systems and their effects on paracellular transport in Caco-2 cell monolayer, Eur. J. Pharm. Sci., 47 (2012) 564-573. https://doi.org/10.1016/j.ejps.2012.07.005

[27] J. Kovalevich, D. Langford, Considerations for the Use of SH-SY5Y Neuroblastoma Cells in Neurobiology, Methods Mol. Biol., 1078 (2013) 9-21. https://doi.org/10.1007/978-1-62703-640-5_2

[28] F.M. Lopes, R. Schroder, M.L. da Frota, Jr., A. Zanotto-Filho, C.B. Muller, A.S. Pires, R.T. Meurer, G.D. Colpo, D.P. Gelain, F. Kapczinski, J.C. Moreira, C. Fernandes Mda, F. Klamt, Comparison between proliferative and neuron-like SH-SY5Y cells as an in vitro model for Parkinson disease studies, Brain Res., 1337 (2010) 85-94. https://doi.org/10.1016/j.brainres.2010.03.102

[29] F.M. Lopes, G.F. Londero, L.M. de Medeiros, L.L. da Motta, G.A. Behr, V.A. de Oliveira, M. Ibrahim, J.C. Moreira, L.O. Porciuncula, J.B. da Rocha, F. Klamt, Evaluation of the neurotoxic/neuroprotective role of organoselenides using differentiated human neuroblastoma SH-SY5Y cell line challenged with 6-hydroxydopamine, Neurotox. Res., 22 (2012) 138-149. https://doi.org/10.1007/s12640-012-9311-1

[30] F.S. Silva, I.G. Starostina, V.V. Ivanova, A.A. Rizvanov, P.J. Oliveira, S.P. Pereira, Determination of Metabolic Viability and Cell Mass Using a Tandem Resazurin/Sulforhodamine B Assay, Curr. Protoc. Toxicol., 68 (2016) 2.24.21-22.24.15. https://doi.org/10.1002/cptx.1

[31] G. Repetto, A. del Peso, J.L. Zurita, Neutral red uptake assay for the estimation of cell viability/cytotoxicity, Nat. Protoc., 3 (2008) 1125-1131. https://doi.org/10.1038/nprot.2008.75

[32] J.P. Kehrer, L.O. Klotz, Free radicals and related reactive species as mediators of tissue injury and disease: implications for Health, Crit. Rev. Toxicol., 45 (2015) 765-798. https://doi.org/10.3109/10408444.2015.1074159

[33] E. Arsovska, J. Trontelj, N. Zidar, T. Tomasic, L.P. Masic, D. Kikelj, J. Plavec, A. Zega, Evaluation of Michael-type acceptor reactivity of 5-benzylidenebarbiturates, 5-benzylidenerhodanines, and related heterocycles using NMR, Acta chimica Slovenica, 61 (2014) 637-644.

[34] A. Gandini, M. Bartolini, D. Tedesco, L. Martinez-Gonzalez, C. Roca, N.E. Campillo, J. Zaldivar-Diez, C. Perez, G. Zuccheri, A. Miti, A. Feoli, S. Castellano, S. Petralla, B. Monti, M. Rossi, F. Moda, G. Legname, A. Martinez, M.L. Bolognesi, Tau-Centric Multitarget Approach for Alzheimer's Disease: Development of

First-in-Class Dual Glycogen Synthase Kinase 3beta and Tau-Aggregation Inhibitors, J Med Chem, 61 (2018) 7640-7656. https://doi.org/10.1021/acs.jmedchem.8b00610

[35] A. Mann, R.F. Tyndale, Cytochrome P450 2D6 enzyme neuroprotects against 1-methyl-4-phenylpyridinium toxicity in SH-SY5Y neuronal cells, Eur. J. Neurosci., 31 (2010) 1185-1193. https://doi.org/10.1111/j.1460-9568.2010.07142.x

[36] S.K. Amit, G. Iain, R.S. Obach, L.S. Christopher, C. Ernesto, R.H. Kirk, E.M. Abdul, K.D. Deepak, S.L. Jae, N. Yasuhiro, P.O.D. John, B. Jason, P.H. Shawn, A Comprehensive Listing of Bioactivation Pathways of Organic Functional Groups, Curr. Drug Metab., 6 (2005) 161-225. https://doi.org/http://dx.doi.org/10.2174/1389200054021799

[37] S. Benfeito, C. Oliveira, C. Fernandes, F. Cagide, J. Teixeira, R. Amorim, J. Garrido, C. Martins, B. Sarmento, R. Silva, F. Remião, E. Uriarte, P.J. Oliveira, F. Borges, Fine-tuning the neuroprotective and blood-brain barrier permeability profile of multi-target agents designed to prevent progressive mitochondrial dysfunction, Eur. J. Med. Chem., 167 (2019) 525-545. https://doi.org/https://doi.org/10.1016/j.ejmech.2019.01.055

[38] Q. Liu, J. Hou, X. Chen, G. Liu, D. Zhang, H. Sun, J. Zhang, P-glycoprotein mediated efflux limits the transport of the novel anti-Parkinson's disease candidate drug FLZ across the physiological and PD pathological in vitro BBB models, PLoS One, 9 (2014) e102442. https://doi.org/10.1371/journal.pone.0102442

[39] L. Partridge, Intervening in ageing to prevent the diseases of ageing, Trends Endocrinol. Metab., 25 (2014) 555-557. https://doi.org/10.1016/j.tem.2014.08.003

[40] D.S. Miller, B. Bauer, A.M.S. Hartz, Modulation of P-glycoprotein at the blood-brain barrier: opportunities to improve central nervous system pharmacotherapy, Pharmacol. Rev., 60 (2008) 196-209. https://doi.org/10.1124/pr.107.07109

[41] F. Faassen, G. Vogel, H. Spanings, H. Vromans, Caco-2 permeability, P-glycoprotein transport ratios and brain penetration of heterocyclic drugs, Int. J. Pharm., 263 (2003) 113-122. https://doi.org/10.1016/S0378-5173(03)00372-7

[42] R. Silva, H. Carmo, R. Dinis-Oliveira, A. Cordeiro-da-Silva, S.C. Lima, F. Carvalho, L. Bastos Mde, F. Remiao, *In vitro* study of P-glycoprotein induction as an antidotal pathway to prevent cytotoxicity in Caco-2 cells, Arch. Toxicol., 85 (2011) 315-326. https://doi.org/10.1007/s00204-010-0587-8

[43] M. Gameiro, R. Silva, C. Rocha-Pereira, H. Carmo, F. Carvalho, M.L. Bastos, F. Remiao, Cellular Models and *In Vitro* Assays for the Screening of modulators of P-gp, MRP1 and BCRP, Molecules: a journal of synthetic chemistry and natural product chemistry., 22 (2017) 1-48. https://doi.org/10.3390/molecules22040600

[44] A.L. Bartels, Blood-brain barrier P-glycoprotein function in neurodegenerative disease, Curr. Pharm. Des., 17 (2011) 2771-2777. https://doi.org/10.2174/138161211797440122

[45] T. Müller, ABCB1: is there a role in the drug treatment of Parkinson's disease?, Expert Opin. Drug Metab. Toxicol., 14 (2018) 127-129. https://doi.org/10.1080/17425255.2018.1416096

[46] G. Camurri, A. Zaramella, High-throughput liquid chromatography/mass spectrometry method for the determination of the chromatographic hydrophobicity index, Anal. Chem., 73 (2001) 3716-3722. https://doi.org/10.1021/ac001388j

[47] K. Valko, C. Bevan, D. Reynolds, Chromatographic Hydrophobicity Index by Fast-Gradient RP-HPLC: A High-Throughput Alternative to log P/log D, Anal. Chem., 69 (1997) 2022-2029. https://doi.org/10.1021/ac961242d

[48] T.S. Carpenter, D.A. Kirshner, E.Y. Lau, S.E. Wong, J.P. Nilmeier, F.C. Lightstone, A method to predict blood-brain barrier permeability of drug-like compounds using molecular dynamics simulations, Biophys J, 107 (2014) 630-641. https://doi.org/10.1016/j.bpj.2014.06.024

[49] D.E. Clark, Rapid calculation of polar molecular surface area and its application to the prediction of transport phenomena. 2. Prediction of blood-brain barrier penetration, J. Pharm. Sci., 88 (1999) 815-821. https://doi.org/10.1021/js980402t

[50] S.A. Hitchcock, L.D. Pennington, Structure-brain exposure relationships, J. Med. Chem., 49 (2006) 7559-7583. https://doi.org/10.1021/jm060642i

[51] H. Pajouhesh, G.R. Lenz, Medicinal Chemical Properties of Successful Central Nervous System Drugs, NeuroRx., 2 (2005) 541-553. https://doi.org/10.1602/neurorx.2.4.541

[52] A. Gaspar, T. Silva, M. Yanez, D. Vina, F. Orallo, F. Ortuso, E. Uriarte, S. Alcaro, F. Borges, Chromone, a privileged scaffold for the development of monoamine oxidase inhibitors, J. Med. Chem., 54 (2011) 5165-5173. https://doi.org/10.1021/jm2004267

[53] M. Soda, D. Hu, S. Endo, M. Takemura, J. Li, R. Wada, S. Ifuku, H.T. Zhao, O. El-Kabbani, S. Ohta, K. Yamamura, N. Toyooka, A. Hara, T. Matsunaga, Design, synthesis and evaluation of caffeic acid phenethyl ester-based inhibitors targeting a selectivity pocket in the active site of human aldo-keto reductase 1B10, Eur. J. Med. Chem., 48 (2012) 321-329. https://doi.org/10.1016/j.ejmech.2011.12.034

[54] H. Shi, D. Xie, R. Yang, Y. Cheng, Synthesis of caffeic acid phenethyl ester derivatives, and their cytoprotective and neuritogenic activities in PC12 cells, J. Agric. Food Chem., 62 (2014) 5046-5053. https://doi.org/10.1021/jf500464k

[55] J. Teixeira, T. Silva, S. Benfeito, A. Gaspar, E.M. Garrido, J. Garrido, F. Borges, Exploring nature profits: development of novel and potent lipophilic antioxidants based on galloyl-cinnamic hybrids, Eur. J. Med. Chem., 62 (2013) 289-296. https://doi.org/10.1016/j.ejmech.2012.12.049

[56] P. Jirasek, S. Amslinger, J. Heilmann, Synthesis of natural and non-natural curcuminoids and their neuroprotective activity against glutamate-induced oxidative stress in HT-22 cells, J. Nat. Prod., 77 (2014) 2206-2217. https://doi.org/10.1021/np500396y

[57] C. Fernandes, M. Pinto, C. Martins, M.J. Gomes, B. Sarmento, P.J. Oliveira, F. Remião, F. Borges, Development of a PEGylated-Based Platform for Efficient Delivery of Dietary Antioxidants Across the Blood-Brain Barrier, Bioconjug. Chem., 29 (2018) 1677-1689. https://doi.org/10.1021/acs.bioconjchem.8b00151

[58] K. Valko, S. Nunhuck, C. Bevan, M.H. Abraham, D.P. Reynolds, Fast gradient HPLC method to determine compounds binding to human serum albumin. Relationships with octanol/water and immobilized artificial membrane lipophilicity, J. Pharm. Sci., 92 (2003) 2236-2248. https://doi.org/10.1002/jps.10494

Electronic Supplementary Information

Design of novel monoamine oxidase-B inhibitors based on piperine scaffold: structure-activity-toxicity, drug-likeness and efflux transport studies

Daniel Chavarria‡[1,2], Carlos Fernandes‡[1], Vera Silva[1,3], Cátia Silva[1], Eva Gil-Martins[1,3], Pedro Soares[1], Tiago Silva[1,2], Renata Silva[3], Fernando Remião[3], Paulo J. Oliveira[2], Fernanda Borges[1*]

[1] CIQUP/Department of Chemistry and Biochemistry, Faculty of Sciences, University of Porto, Porto, Portugal

[2] CNC - Center for Neuroscience and Cell Biology, University of Coimbra, UC Biotech, Biocant Park, Cantanhede, Portugal.

[3] UCIBIO-REQUIMTE, Laboratory of Toxicology, Department of Biological Sciences, Faculty of Pharmacy, University of Porto, Porto, Portugal

‡ These authors contributed equally.

* Corresponding Author:

Fernanda Borges, CIQUP/Department of Chemistry and Biochemistry, Faculty of Sciences, University of Porto, Porto 4169-007, Portugal. E-mail: fborges@fc.up.pt

Contents of electronic supporting information:

1. Experimental section 186
1.1. Chemistry 186
1.1.1. Reagents 186
1.1.2. Materials and apparatus. 186
1.2. Oxygen radical absorbance capacity (ORAC-FL) assay 186
1.3. Electrochemical measurements 187
1.4. Enzymatic assays 187
1.4.1. Evaluation of human monoamine oxidase (*h*MAO) inhibitory activity 187
1.4.2. Evaluation of catechol *O*-methyltransferase inhibitory activity 188
1.4.2.1. Animals 188
1.4.2.2. Homogenate Preparation 188
1.4.2.3. Determination of catechol *O*-methyltransferase activity 188
1.5. *In vitro* toxicology 189
1.5.1. Materials 189
1.5.2. Cell culture 189
1.5.3. Cytotoxicity assays 190
1.5.3.1. Resazurin reduction assay 190
1.5.3.2. Neutral red (NR) uptake assay 190
1.5.4. Evaluation of intracellular oxidative stress levels 302
1.5.5. Statistical analysis 304
1.6. Evaluation of the chromatographic hydrophobicity index at pH 2.3 191
2. References 191

7. Experimental section

7.1. Chemistry

7.1.1. Reagents

Piperine, sodium hydroxide (NaOH), diisopropylethylamine (DIPEA), (benzotriazol-1-yloxy)tripyrrolidinophosphonium hexafluorophosphate (PyBOP), aniline, benzylamine, (2-bromoethyl)benzene, *N*-(3-dimethylaminopropyl)-*N'*-ethylcarbodiimide hydrochloride (EDC.HCl), 4-(dimethylamino)pyridine (DMAP), phenol, potassium carbonate (K_2CO_3), benzyl bromide, (2-bromoethyl)benzene, cyanoacetic acid, mono-ethyl malonate, pyridine, piperidine, lithium aluminum hydride ($LiAlH_4$) and manganese dioxide (MnO_2) were purchased from Sigma Aldrich (St. Louis, MO, USA), Alfa-Aesar (Haverhill, MA, USA) or TCI (Tokyo, Japan). All other reagents and solvents were pro analysis grade and were acquired from Carlo Erba Reagents (SDS, France) and Scharlab (Barcelona, Spain) and were used without additional purification.

7.1.2. Materials and apparatus

The monitoring of reactions progress was performed by thin layer chromatography (TLC) on precoated silica gel 60 F254 acquired from Merck (Darmstad, Germany). TLC spots were visualized under UV detection (254 nm and 365 nm). Some crude products were purified by flash column chromatography that was carried out on silica gel 60A acquired from Carlo-Erba Reagents (Val-de-Reuil, France). The fractions with the desired compound were gathered and concentrated under reduced pressure. The solvents were evaporated using a Buchi Rotavapor.

^{1}H and ^{13}C NMR and DEPT135 data were acquired, at room temperature, on a Brüker AMX 300 spectrometer operating at 400 and 100 MHz, respectively. The solvents used in NMR experiments included $CDCl_3$-d_1 and DMSO-d_6. The chemical shifts are expressed in δ (ppm) values relative to tetramethylsilane (TMS) as internal reference and coupling constants (*J*) are given in Hz. Electron impact mass spectrometry (EI-MS) spectra were obtained on a Varian 320-MS apparatus. The data are reported as m/z (% of relative intensity of the most important fragments).

7.2. Enzymatic assays

7.2.1. Materials

Microsomal MAO isoforms prepared from insect cells (BTI-TN-5B1-4) infected with recombinant baculovirus containing cDNA inserts for *h*MAO-A or *h*MAO-B, kynuramine, (*R*)-(−)-deprenyl, rasagiline, safinamide and clorgyline were purchased from Sigma Aldrich.

7.2.2. Evaluation of human monoamine oxidase (*h*MAO) inhibitory activity

The human monoamine oxidase (*h*MAO) inhibitory outline was assessed in microsomal MAO isoforms prepared from insect cells (BTI-TN-5B1-4) infected with recombinant baculovirus containing cDNA inserts for *h*MAO-A or *h*MAO-B and by measuring the enzymatic conversion rates of kynuramine into 4-hydroxyquinoline. The appropriate amounts of *h*MAO-A and *h*MAO-B were adjusted to obtain, in our experimental conditions, the same maximum velocity (V_{max} = 50 *p*mol.min^{-1}) for both isoforms (*h*MAO-A: 3

ng.μL^{-1}; *h*MAO-B: 12 ng.μL^{-1}). All assays were performed in sodium phosphate buffer solution 50 mM pH 7.4.

The compounds under study and reference inhibitors were pre-incubated at 37 ºC for 10 min in the presence of kynuramine (K_m *h*MAO-A = 20 μM; K_m *h*MAO-B = 20 μM; final concentration: 2×K_m) in 96-well microplates (BRANDplates, pureGrade™, BRAND GMBH, Wertheim, Germany). Then, the reaction was started with the addition of *h*MAO-A or *h*MAO-B. Initial velocities were determined spectrophotometrically in a microplate reader (BioTek Synergy HT from BioTek Instruments, Winooski, VT, USA) at 37 °C by measuring the formation of 4-hydroxyquinoline at 316 nm, over a period of at least 30 min (interval of 1 min). Data were analysed using GraphPad PRISM version 6 for Windows (GraphPad Software®, San Diego, CA, USA). The initial velocities, obtained from the linear phase of product formation, were normalized and plotted against the respective inhibitor concentration. IC_{50} values were obtained from dose-response curves and were expressed as mean ± standard deviation. IC_{50} values were determined from at least three independent experiments, each performed in triplicate.

7.2.3. Evaluation of human monoamine oxidases kinetics

To determine the steady-state kinetic parameters (K_m, Michaelis constant, and V_{max}, maximum velocity) of human monoamine oxidases (*h*MAO-A and *h*MAO-B), the enzymatic activity of both isoforms was studied, under the experimental conditions described above, in the presence of six different concentrations of kynuramine (10-100 μM). Accordingly, *h*MAO-A showed a K_m of 19.7 ± 0.5 μM and a V_{max} of 52.3 ± 0.5 pmol.min^{-1}, whereas *h*MAO-B displayed a K_m of 20.8 ± 1.8 μM and a V_{max} of 51.4 ± 2.4 pmol.min^{-1}.

7.2.4. Evaluation of human monoamine oxidase-B-inhibitor kinetics

To evaluate the mechanism of *h*MAO-B inhibition of compounds **7**, **10** and **15**, substrate-dependent kinetic experiments were performed under the conditions described above (n = 3). The catalytic rates of *h*MAO-B were measured at six different concentrations of kynuramine (10-100 μM), in the absence or the presence of three different concentrations of the selected inhibitors. The results are depicted as double reciprocal Lineweaver-Burk plots (1/V vs 1/[S]). The kinetic data (K_m and V_{max}) were estimated by employing the Michaelis-Menten equation. The results are presented as double reciprocal Lineweaver-Burk plots (**Equation S1**).

$$\frac{1}{v} = \frac{K_m}{V_{max}}\left(\frac{1}{[S]}\right)\left(1 + \frac{[I]}{K_i}\right) + \frac{1}{V_{max}} \quad \textbf{(Equation S1)}$$

Equation S1: Lineweaver-Burk equation used to describe a competitive inhibition.

The inhibition constants (Ki) were determined by constructing secondary plots from the slope of each Lineweaver-Burk plot versus the inhibitor concentration.

$$\text{slope} = \frac{K_m[I]}{V_{max}K_i} + \frac{K_m}{V_{max}} \quad \textbf{(Equation S2)}$$

Equation S2: equation describing the replot of data from the Lineweaver-Burk for determination of K_i values of competitive inhibitors.

In **Equations S1** and **S2**, K_i represents the dissociation constants of the enzyme-inhibitor.

The enzymatic reactions and measurements were performed using the same experimental conditions described above (n = 3). Linear regression analysis was performed using GraphPad PRISM version 6 for Windows (GraphPad Software®, San Diego, CA, USA).

7.2.5. Thiol trapping assay

The stability assay of compound **15** with glutathione was performed as described previously by Gandini et al. [1]. Briefly, compound **15** (2.5 mg, 0.0075 mmol) and glutathione (2.3 mg, 0.0075 equiv.) were solubilized in a mixture of DMSO-d_6 and D_2O (7:3). The ^{1}H NMR spectra of the sample was then acquired in a Brüker AMX 300 spectrometer operating at 400 MHz, 30 minutes and 1h after preparation of the sample. The ^{1}H NMR of a sample containing only compound **15** was also acquired and used as a representation of the initial state of the system.

7.3. *In vitro* toxicology

7.3.1. Materials

All reagents used were of analytical grade or of the highest grade available. Neutral red (NR) solution, resazurin, Dulbecco's Modified Eagle's Medium (DMEM) with 4.5 g/L glucose, retinoic acid, 12-*O*-tetradecanoylphorbol-13-acetate (TPA), 2',7'-dichorofluorescein diacetate (DCFH-DA), Rhodamine 123 (RHO 123) and zosuquidar (ZOS) were obtained from Sigma Aldrich. Reagents used in cell culture such as heat-inactivated fetal bovine serum (FBS), antibiotic (10,000 U/mL penicillin, 10,000 µg/mL streptomycin), MEM Non-Essential Amino Acids solution (100×) (MEM NEAA), Hanks' balanced salt solution (HBSS) with or without calcium and magnesium (HBSS (+/+) or HBSS (-/-), respectively) and 0.25% trypsin/1 mM ethylenediamine tetraacetic acid (EDTA) were purchased from Gibco Laboratories (Lenexa, KS, USA). Dimethylsulfoxide (DMSO), absolute ethanol, sodium bicarbonate and acetic acid were obtained from Merck (Darmstadt, Germany). Triton™ X-100 detergent solution was acquired from Thermo Fisher Scientific (Waltham, MA, USA).

7.3.2. Cell culture

Human neuroblastoma SH-SY5Y cells were routinely cultured into 75 cm^3 flasks and maintained in DMEM with 4.5 g/L glucose supplemented with 10 % heat-inactivated FBS (v/v), 1 % MEM NEAA (v/v) and 1% penicillin/streptomycin (v/v). Cells were maintained at 37 °C, in a humidified 5% CO_2–95% air atmosphere, and the culture medium was changed every 2-3 days. The cultures were passaged once a week by trypsinization (0.25 % trypsin/1 mM EDTA). To avoid phenotypic changes, the cells used for all experiments were taken between 19th and 28th passages. Cells were differentiated as described previously by Fernandes *et al*. [2]. Briefly, SH-SY5Y cells were seeded onto 96-well plates at a density of 25,000 cells/cm^2 in cell culture medium with *trans*-retinoic acid (RA) (final concentration of 10 µM) and incubated for 3 days, at 37 °C, in a humidified 5% CO_2–95% air atmosphere. Then, the medium was removed and replaced with medium supplemented with 12-*O*-tetradecanoylphorbol-13-acetate (TPA) (final concentration 80 nM), and cells were incubated for an additional period of 3 days before being used in the assays. Stock solutions of RA (10 mM) and TPA (80 µM) were prepared in DMSO.

Human epithelial colorectal adenocarcinoma (Caco-2) cells (ATCC; Manassas, VA, USA) were cultured as previously reported by Fernandes *et al.* [2]. Briefly, cells were routinely cultured into 75 cm^3 flasks and maintained in DMEM medium, supplemented with 10 % heat-inactivated FBS, 1 % MEM NEAA (v/v) and 1 % penicillin/streptomycin (v/v). Cells were maintained in a 37 °C, in a humidified 5% CO_2–95% air atmosphere, and the cell culture medium was changed every 2-3 days. The cultures were passaged weekly by trypsinization (0.25 % trypsin/1 mM EDTA). The cells used for all experiments were taken between 56^{th} and 62^{nd} passages. Caco-2 cells were seeded onto 96-well or 24-well plates for cytotoxicity assays and for the evaluation of P-gp transport activity, respectively, at a density of 60,000 cells/cm^2, and used 4 days after seeding, when confluent monolayers were obtained.

7.3.3. Cytotoxicity assays

7.3.3.1. Resazurin reduction assay

Resazurin is a non-fluorescent, non-toxic water-soluble dye able to permeate through cell membranes [3]. Inside the cells, resazurin is enzymatically reduced into the pink-colored and highly fluorescent resorufin [4, 5]. Since the conversion of resazurin into resorufin occurs mostly in mitochondria, the amount of resorufin produced can be used as indicator of metabolic activity [6]. The quantity of resorufin production is proportional to the number of viable cells in culture and can be quantified fluorometrically or colorimetrically [4].

Resazurin reduction assay was performed as previously described by Fernandes *et al.* [2]. Briefly, after the 24 h incubation periods with the test compounds, the cell culture medium was removed and replaced with fresh culture medium with resazurin (10 μg/mL) prepared in cell culture medium. Differentiated SH-SY5Y cells and Caco-2 cells were incubated for 2 h and 1 h, respectively, at 37 °C in a humidified 5% CO_2–95% air atmosphere. Then, the fluorescence was read in a multiwell microplate reader (PowerWave XS from BioTek Instruments, Vermont, US), using an excitation wavelength of 540 nm and an emission wavelength of 590 nm. The results were expressed as the percentage of resazurin reduction relative to that of the control (non-treated) cells [resazurin reduction (% of control)] ± standard error mean (SEM) of at least three independent experiments.

7.3.3.2. Neutral red uptake assay

The neutral red (NR) uptake assay is based on the ability of viable cells to incorporate the supravital dye NR and retain it inside the lysosomes [7]. NR uptake assay was performed as previously described by Fernandes *et al*. [8] Briefly, after the 24 h incubation periods with the test compounds, the cell culture medium was removed and a solution of NR (50 mg/mL) in fresh cell culture medium was added. Differentiated SH-SY5Y cells and Caco-2 cells were incubated for 2 h and 1 h, respectively, at 37 °C in a humidified, 5% CO_2–95% air atmosphere. Then, the cell culture medium was removed and replaced by ethanol absolute/distilled water (1:1) with 5 % acetic acid to liberate the dye from the viable cells. The absorbance was measured at 540 nm in a multiwell microplate reader (PowerWave XS from BioTek Instruments). The results were expressed as the percentage of NR uptake relative to that of the control (non-treated) cells [NR uptake (% of control)] ± standard error mean (SEM) of at least three independent experiments.

7.3.4. Evaluation of intracellular oxidative stress levels

The evaluation of intracellular oxidative stress was monitored using DCFH-DA, a non-fluorescent probe able to cross the cell membrane. Inside the cells, DCFH-DA is hydrolyzed by esterases to the polar non-fluorescent reduced derivative 2',7'-dichlorofluorescein (DCFH), which, due to its polarity, is trapped within the cells. The subsequent oxidation of DCFH by reactive species (RS) yields the green fluorescent 2',7'-dichlorofluorescein (DCF) [9, 10].

The assay was performed as previously described by Fernandes *et al.* [2]. SH-SY5Y cells were seeded and differentiated onto 96-well black plates (Greiner CELLSTARW, Sigma Aldrich). Cells were pre-incubated with DCFH-DA (10 µM) in culture medium on the day of the experiment for 1.5 h, at 37 ºC, in the dark. Then, cells were incubated with the test compound (10 and 50 µM) in cell culture medium for 24 h. A blank (vehicle and culture medium without cells) and a negative control (cells treated with cell culture medium containing vehicle) were also included in the plate to measure the background fluorescence and the basal RS production, respectively. Fluorescence was recorded at the selected timepoint on a fluorescence microplate reader (PowerWave XS from BioTek Instruments) set to 485 nm excitation and 530 nm emission. The results were expressed as the percentage of DCF fluorescence relative to that of the control (non-treated) cells [DCF fluorescence (% of control)] ± standard error mean (SEM) of at least three independent experiments.

7.3.5. Evaluation of P-glycoprotein transport activity

The effects of the tested compounds on P-glycoprotein (P-gp) transport activity was evaluated by the rhodamine 123 (RHO 123) accumulation assay, in which RHO 123 was used as a P-gp fluorescent substrate [8]. Briefly, Caco-2 cells were seeded in 24 well plates at a density of 60,000 cells/cm^2 and used 4 days after seeding. On the day of the experiment, the cell culture medium was removed, and cells were pre-exposed to the test compounds (10 µM) for 30 minutes in the presence or the absence of zosuquidar (Zos, 5 µM), a potent third-generation P-gp inhibitor. Then, RHO 123 (10 µM) was added, and cells were incubated for 90 minutes at 37 ºC, in a humidified 5% CO_2 - 95% O_2 air atmosphere. Control cells were only exposed to the P-gp fluorescent substrate, in the presence or the absence of Zos. After incubation with the P-gp substrate, the medium containing RHO 123 was removed. Then, the cells were washed twice with HBSS (-/-) and lysed with 1% Triton™ X100 (30 min, in the dark, and at room temperature) to release the RHO 123 accumulated inside cells. RHO 123 intracellular fluorescence was then measured at excitation/emission wavelengths of 485/528 nm, respectively, in a multi-well plate reader (PowerWave-X, BioTek Instruments) and expressed as fluorescence intensity (FI). The ratio between the FI of Zos-inhibited RHO 123 accumulation (IA – inhibited accumulation) and the FI of non-inhibited RHO 123 accumulation (NA – normal accumulation) was the parameter used for comparison. The results were expressed as percentage of control cells (**Equation S3**) of at least three independent experiments performed in triplicate.

$$\text{RHO 123 Accumulation ratio} = \frac{\text{FI of RHO 123 accumulation under P-gp inhibition (IA)}}{\text{FI of RHO 123 accumulation under normal conditions (NA)}} \qquad (\textbf{Equation S3})$$

Equation S3. P-gp activity assessed by the ratio between the fluorescence intensity of RHO 123 accumulated in the presence of the inhibitor (5 µM Zos) and the fluorescence intensity of RHO 123accumulated in the absence of P-gp inhibition. FI (fluorescence intensity).

7.3.6. Statistical analysis

The data obtained are expressed as mean ± standard error mean (SEM) of at least three independent experiments (n = 3). All statistical analyses were performed using GraphPad PRISM version 6 for Windows. The normality of the data distribution was evaluated using three normality tests: KS normality test, D'Agostino and Pearson omnibus normality test, and Shapiro−Wilk normality test. For data with a parametric distribution, statistical comparisons between groups were estimated using the parametric method one-way or two-way analysis of variance (ANOVA) followed by Dunnett's multiple comparison test. For data with a non-parametric distribution, statistical comparisons were estimated using the nonparametric method of Kruskal–Wallis [two-way ANOVA on ranks] followed by Dunn's post hoc test. In all cases, p values lower than 0.05 were considered significant.

8. Additional tables

Table S1. Retention times (t_R) of the standard mixture obtained by LC/UV at pH 7.4. CHI_0 values at pH 7.4 were taken from Camurri *et al.* [11].

Compounds	t_R(min)	CHI_0
Theophylline	7.31	18.19
Paracetamol	7.45	20.59
Caffeine	7.56	24.12
Benzimidazole	8.00	30.71
Colchicine	8.35	44.32
Carbamazepine	9.30	58.45
Indole	10.27	69.15
Propiophenone	10.63	78.41
Butyrophenone	11.32	88.49
Valerophenone	12.04	97.67
Heptanophenone	13.67	111.8

9. Additional figures

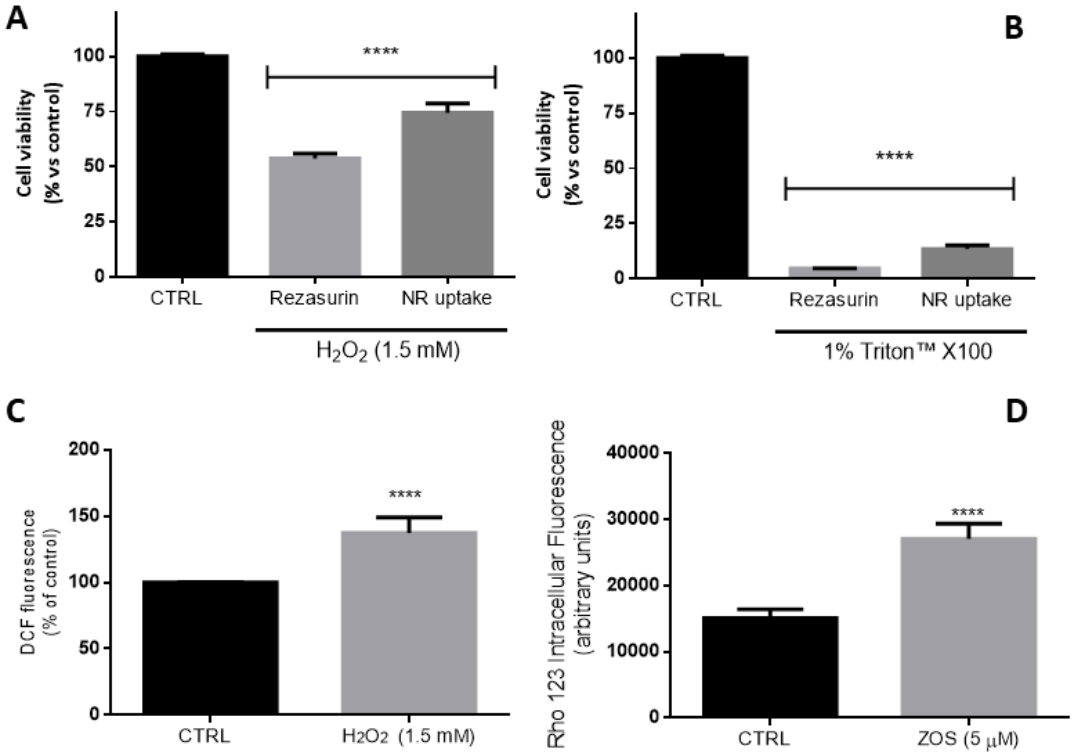


Figure S1. (A) Cellular viability of differentiated SH-SY5Y after treatment with H_2O_2 (1.5 mM) for 24 h. (B) Cellular viability of Caco-2 cells after treatment with 1 % Triton for 24 h. (C) Intracellular oxidative stress levels after treatment of differentiated SH-SY5Y with H_2O_2 (1.5 mM) for 24 h. (D) Accumulation of RHO 123 (5 μM) in Caco-2 cells after treatment with the P-gp reference inhibitor Zos at 5 μM. In all cases, statistical comparisons were made using the unpaired *t* test (****$p < 0.0001$ vs. control cells).

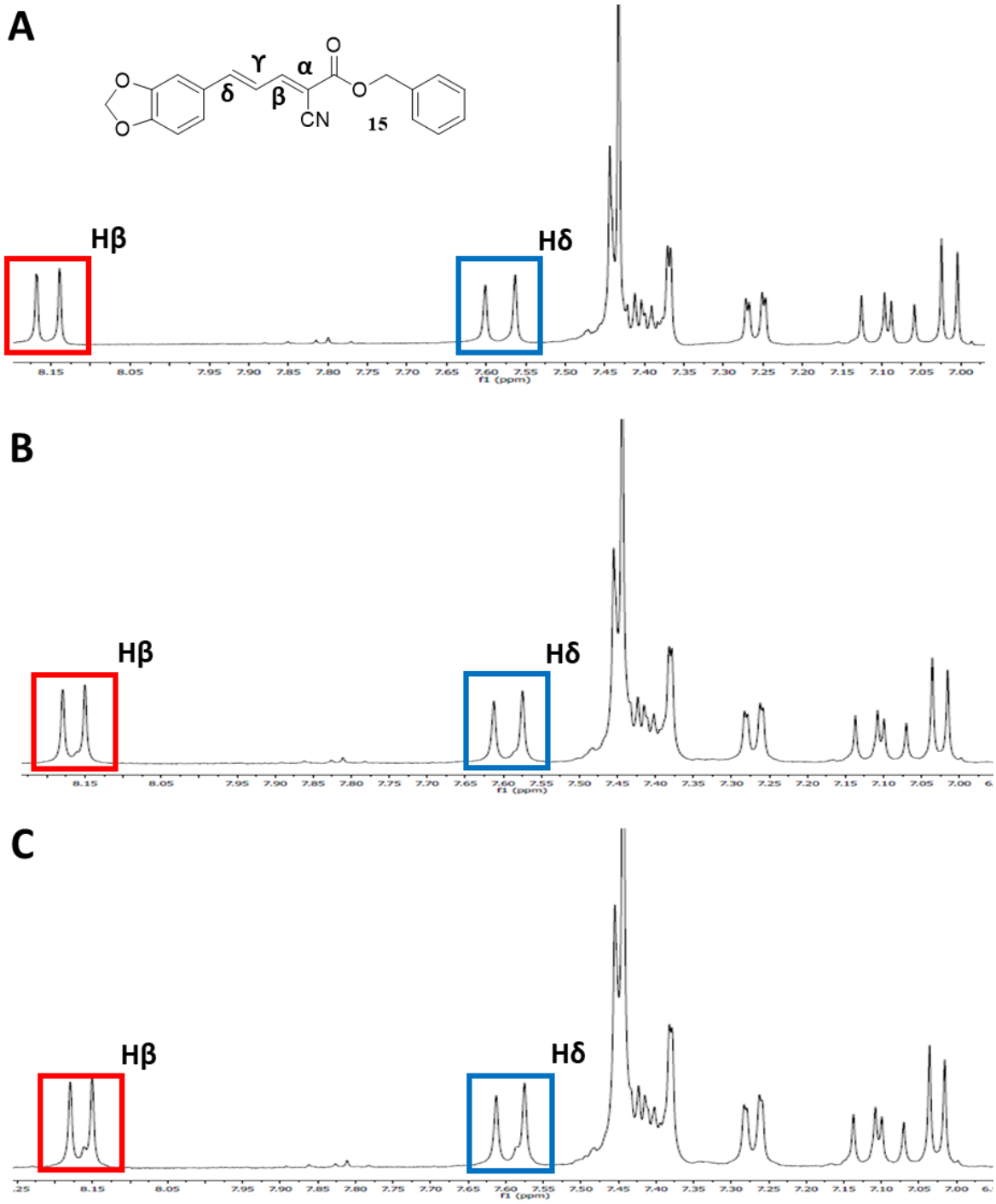


Figure S2. Thiol trapping assay. ^{1}H NMR spectrum of **15** in DMSO-d_6 and D_2O (7:3) in absence of glutathione (A) and in the presence of glutathione (1:1) (B and C). The signals of Hβ and Hδ are highlighted with a red and blue square, respectively. No reaction is observed after 30 minutes (B) or after 1 h (C).

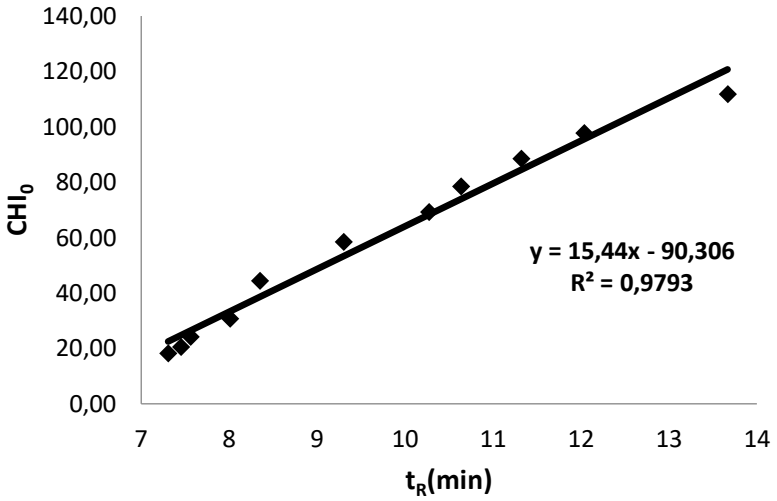
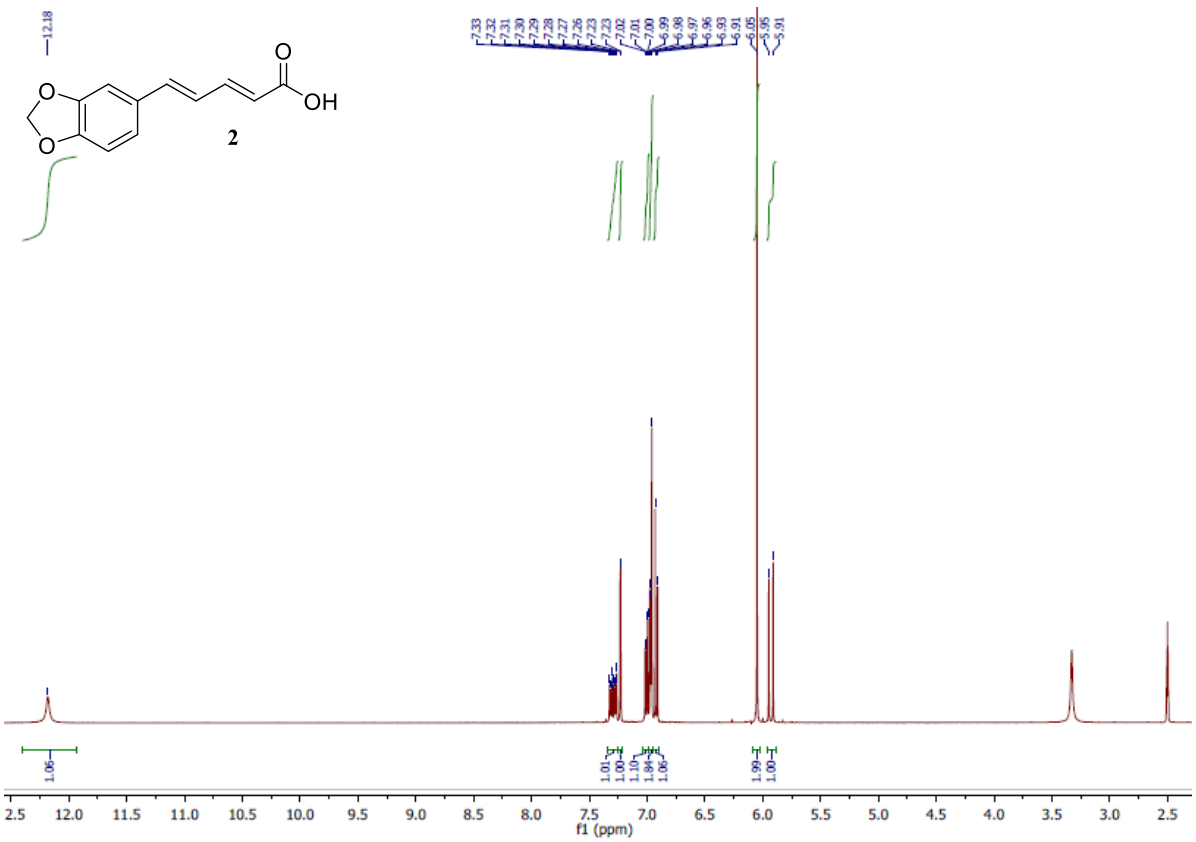


Figure S3. Linear correlation obtained by plotting the retention times (t_R) of each of the individual standard mixture compounds against the CHI values at pH 7.4 (CHI_0) reported by Camurri et al. [11].



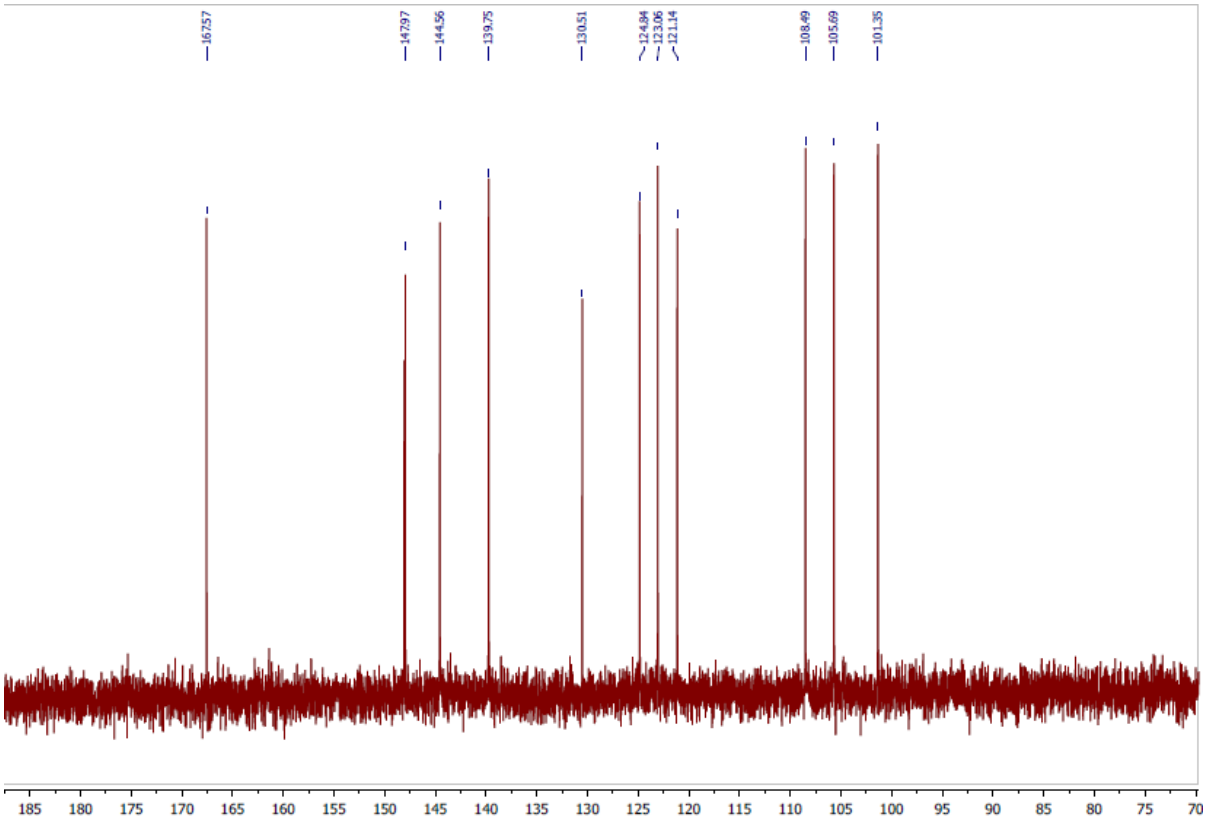


Figure S4. ^{1}H and ^{13}C NMR spectra of final compound **2** (NMR spectrum obtained in DMSO-d_6)

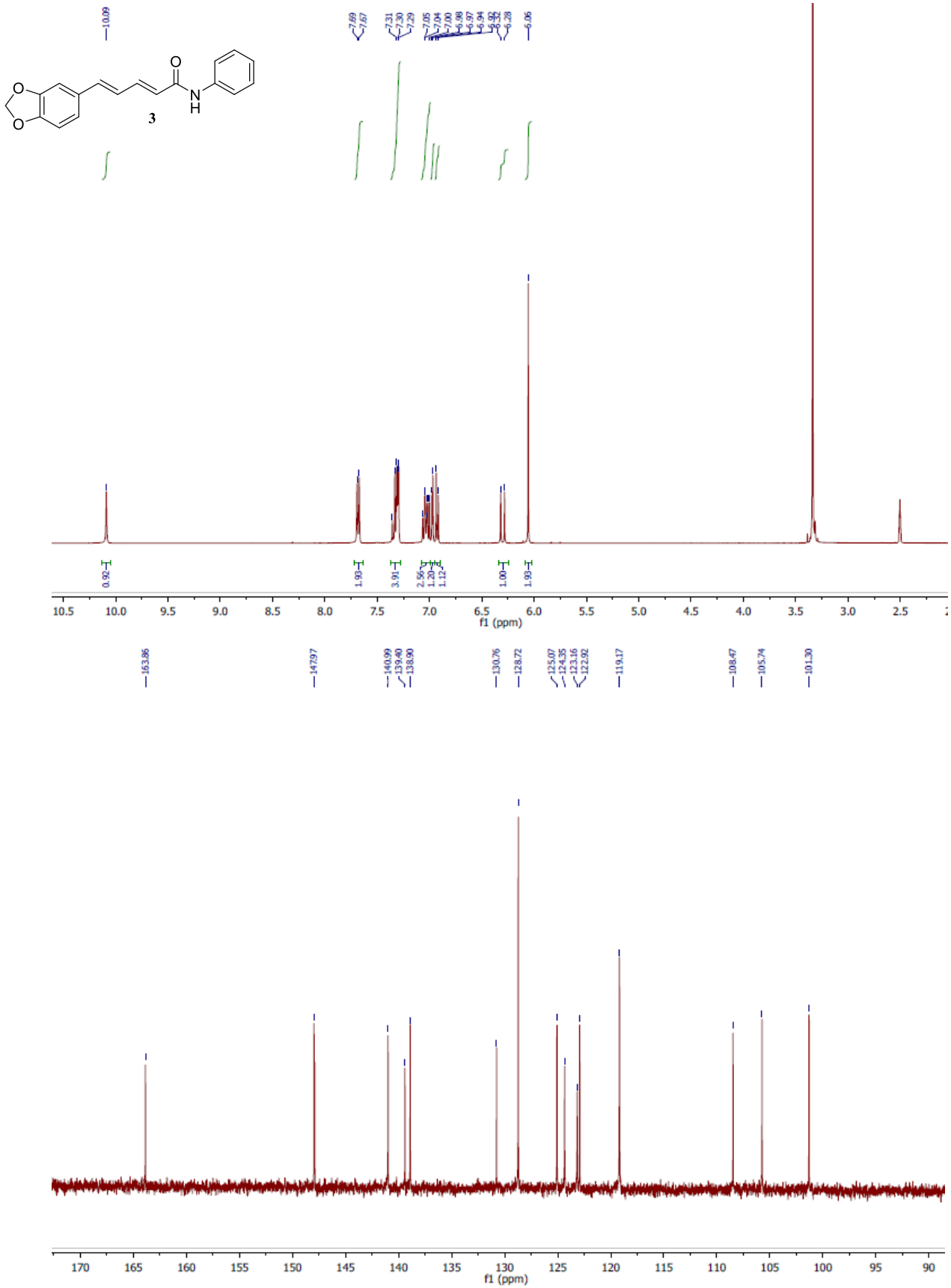


Figure S5. ^{1}H and ^{13}C NMR spectra of final compound **3** (NMR spectrum obtained in DMSO-d_6)

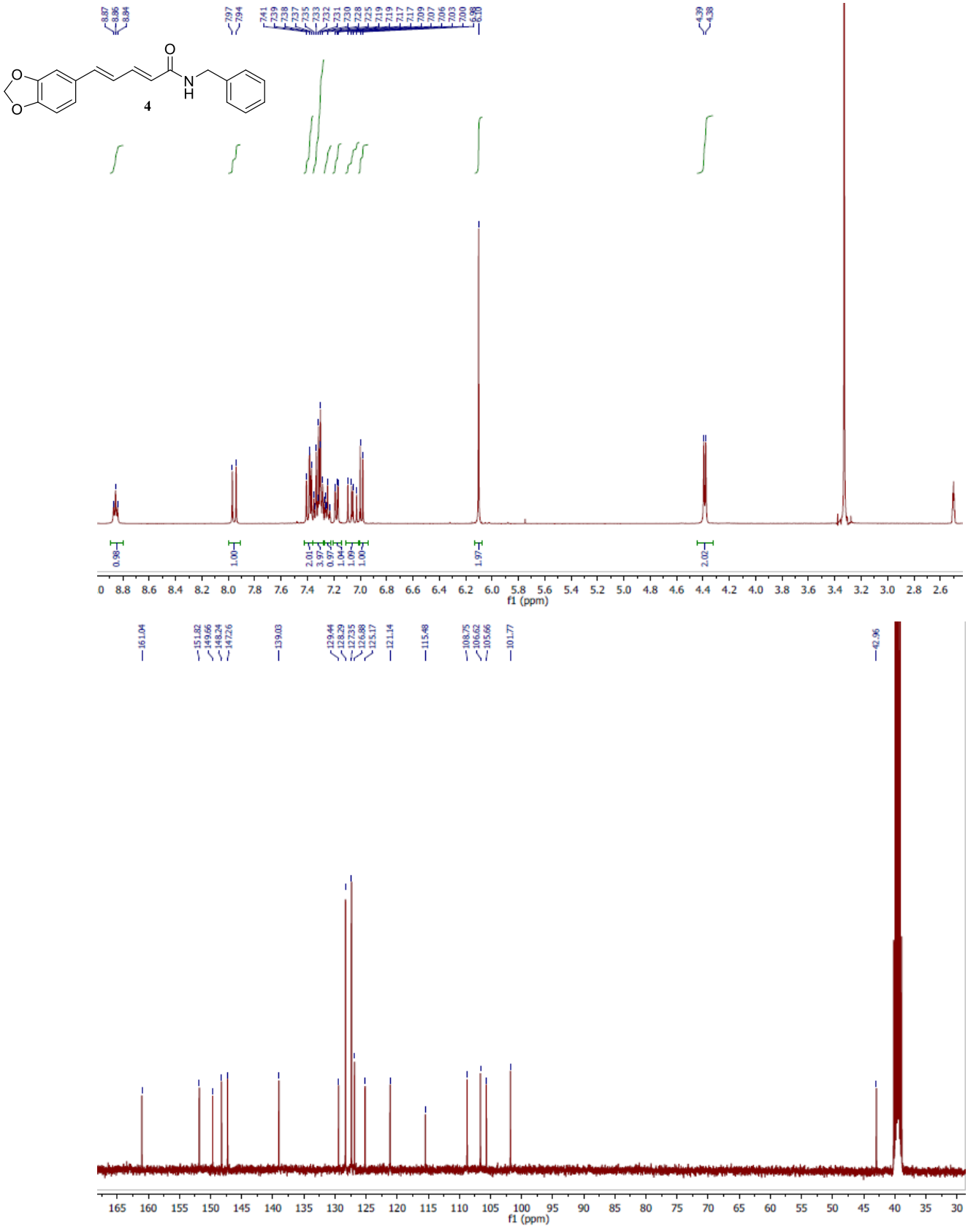


Figure S6. ^{1}H and ^{13}C NMR spectra of final compound **4** (NMR spectrum obtained in DMSO-d_6)

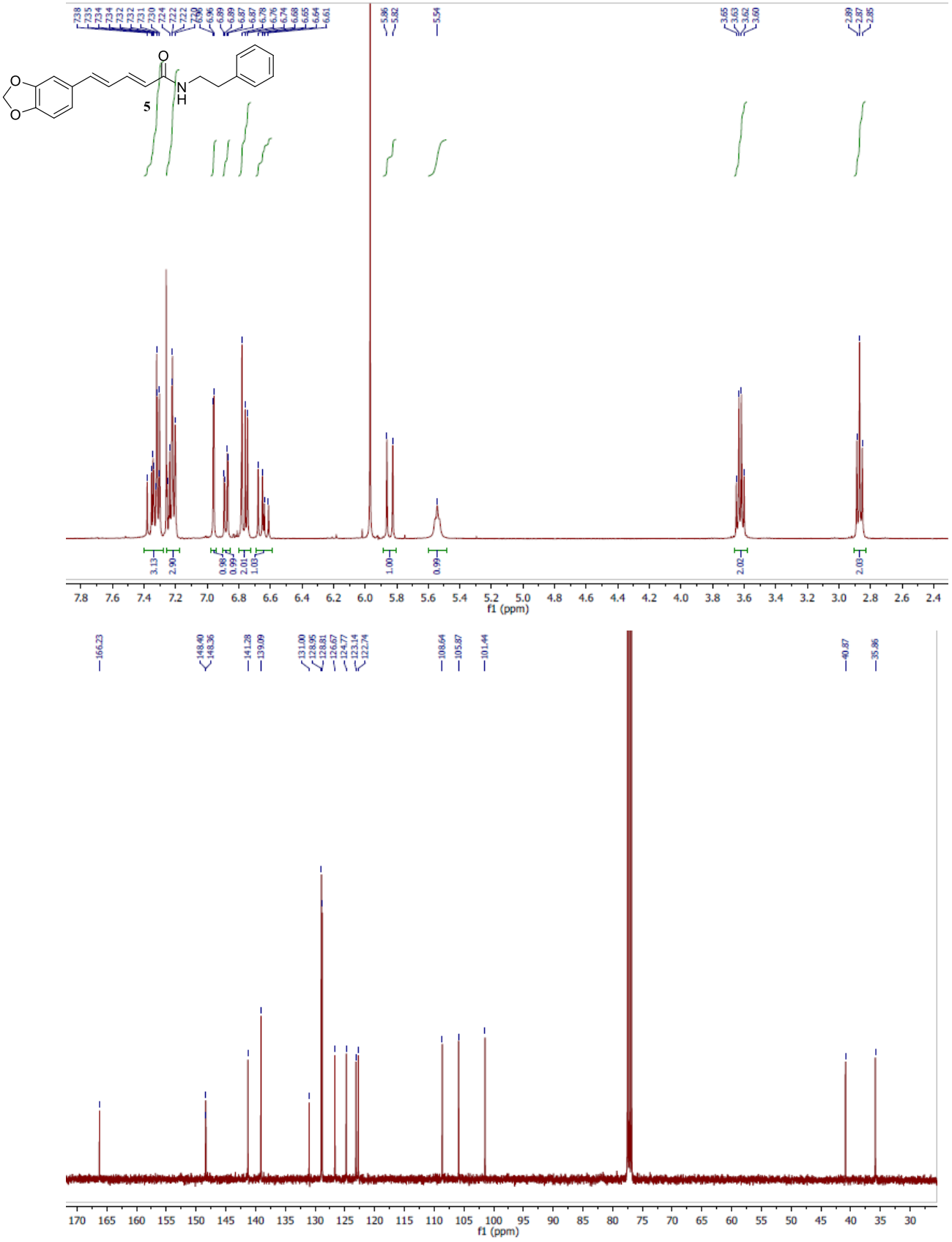


Figure S7. ^{1}H and ^{13}C NMR spectra of final compound **5** (NMR spectrum obtained in $CDCl_3$)

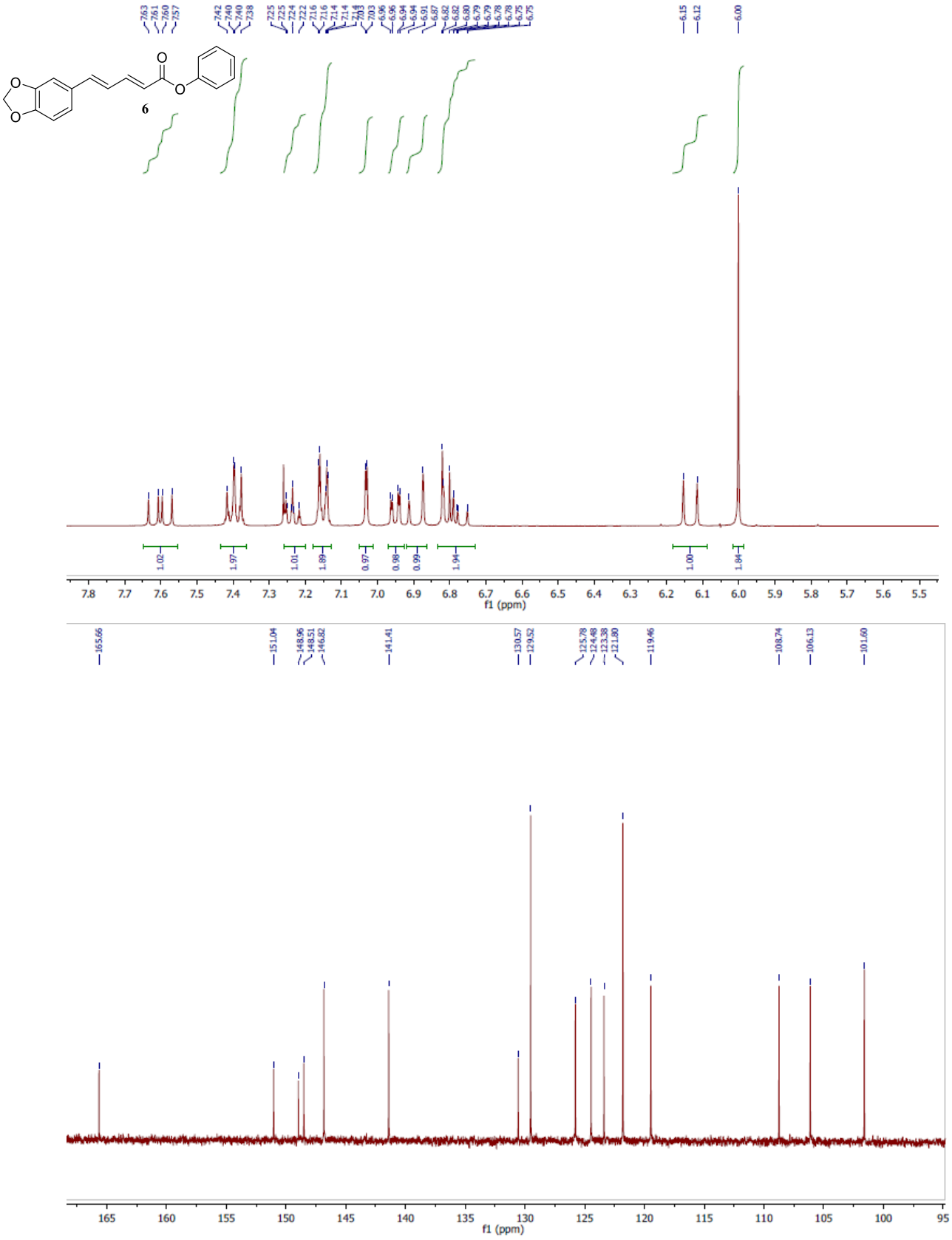


Figure S8. ^{1}H and ^{13}C NMR spectra of final compound **6** (NMR spectrum obtained in $CDCl_3$)

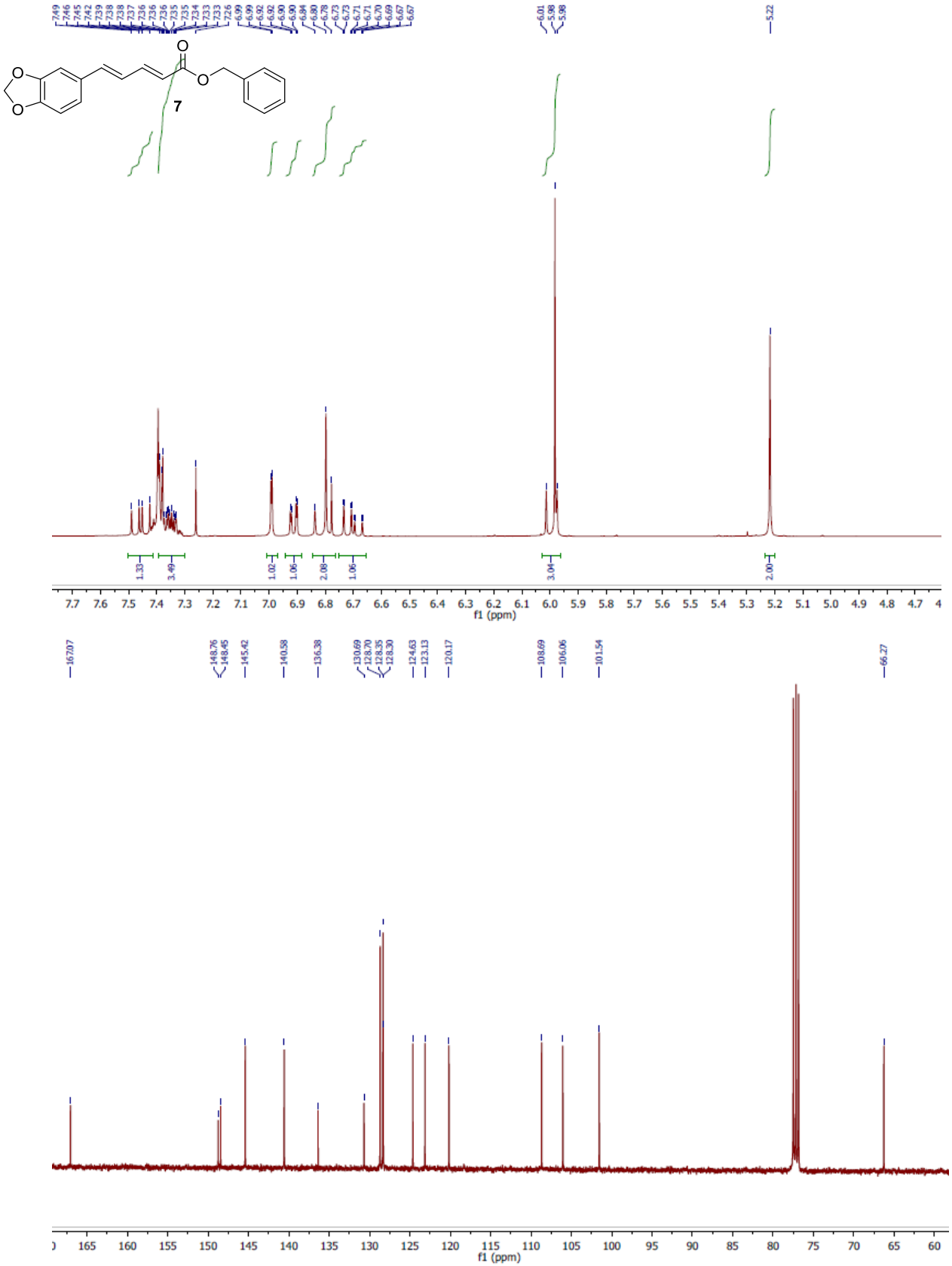


Figure S9. ^{1}H and ^{13}C NMR spectra of final compound **7** (NMR spectrum obtained in $CDCl_3$)

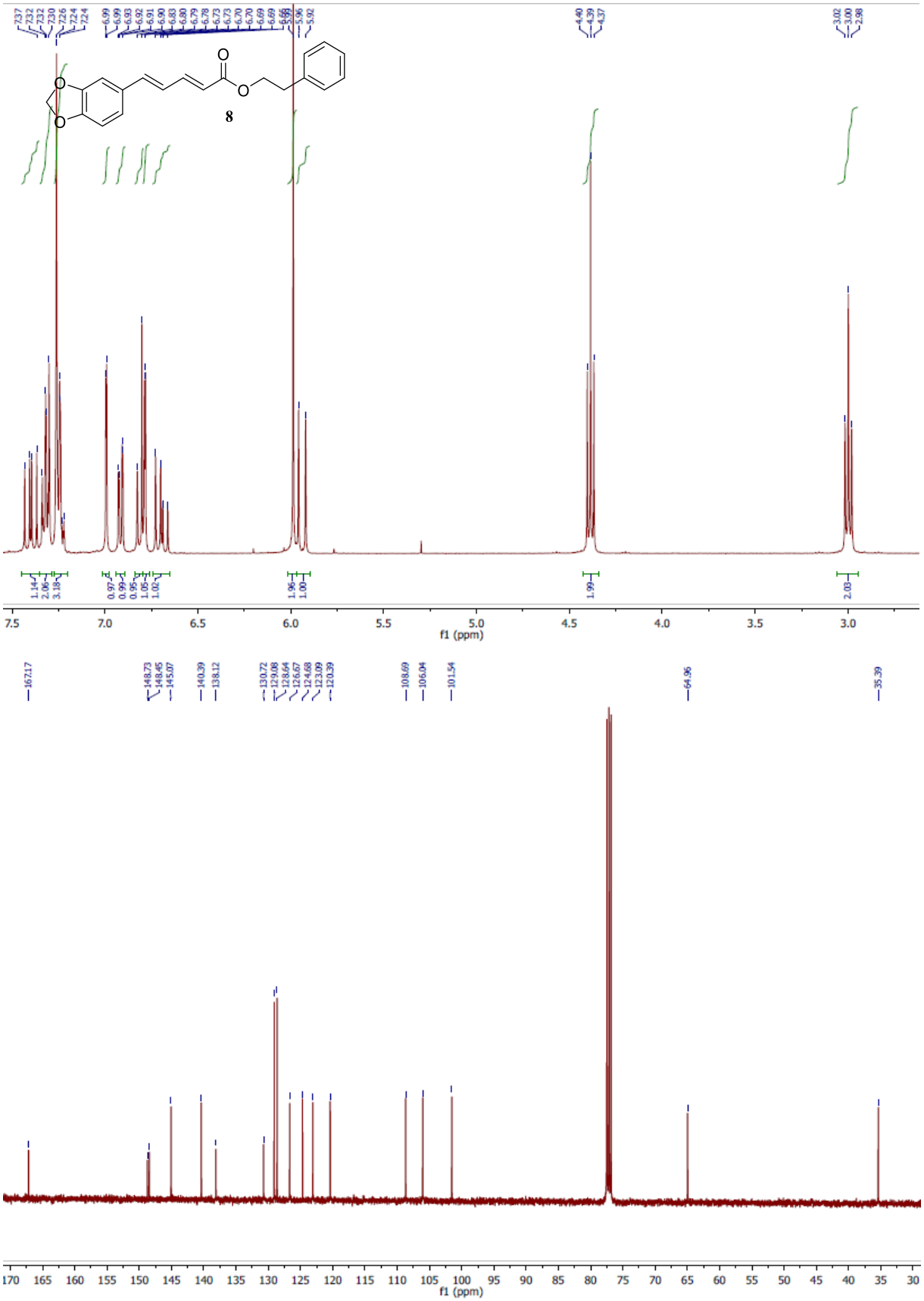


Figure S10. ^{1}H and ^{13}C NMR spectra of final compound **8** (NMR spectrum obtained in $CDCl_3$)

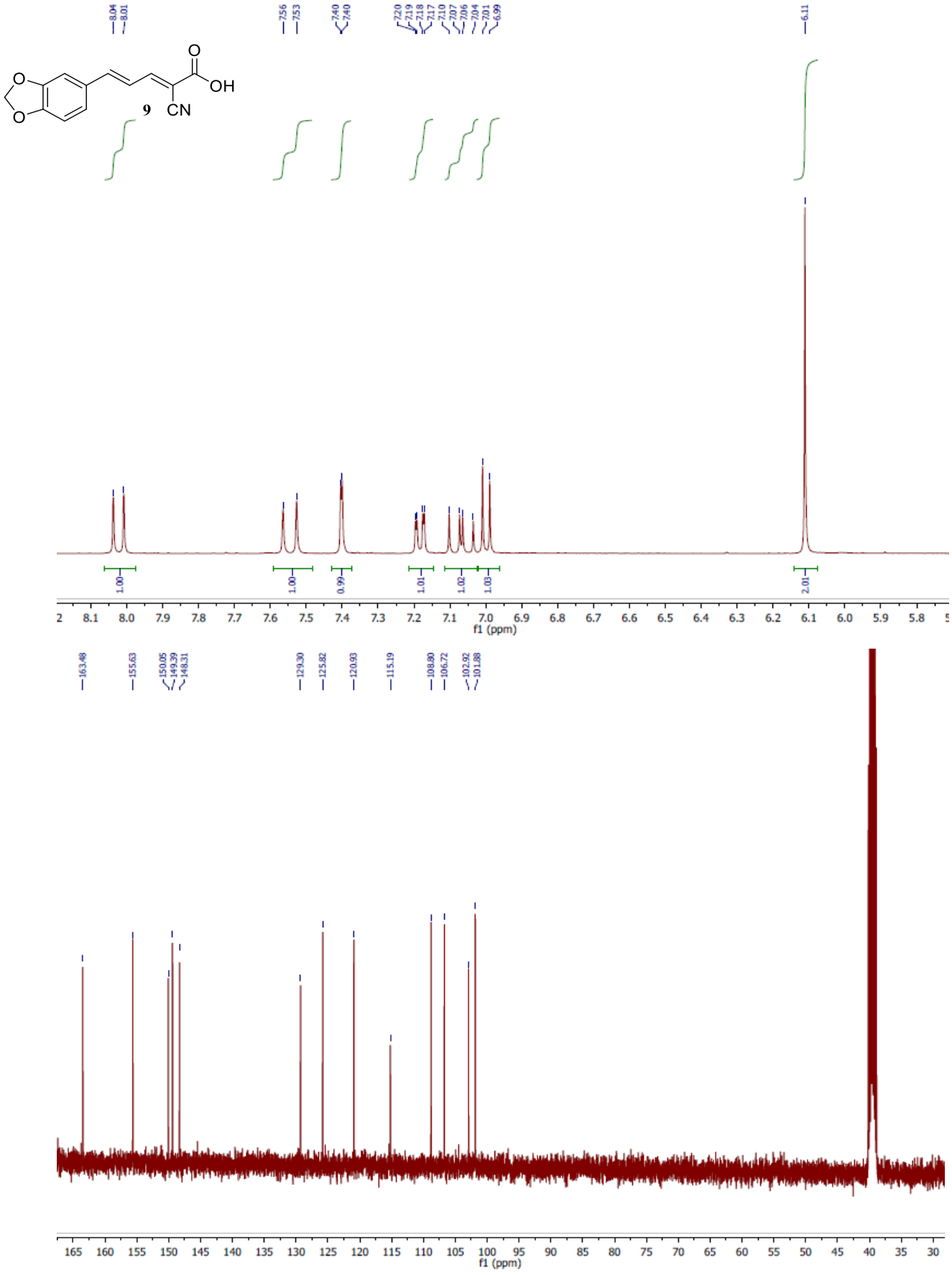


Figure S11. ^{1}H and ^{13}C NMR spectra of final compound **9** (NMR spectrum obtained in DMSO-d_6)

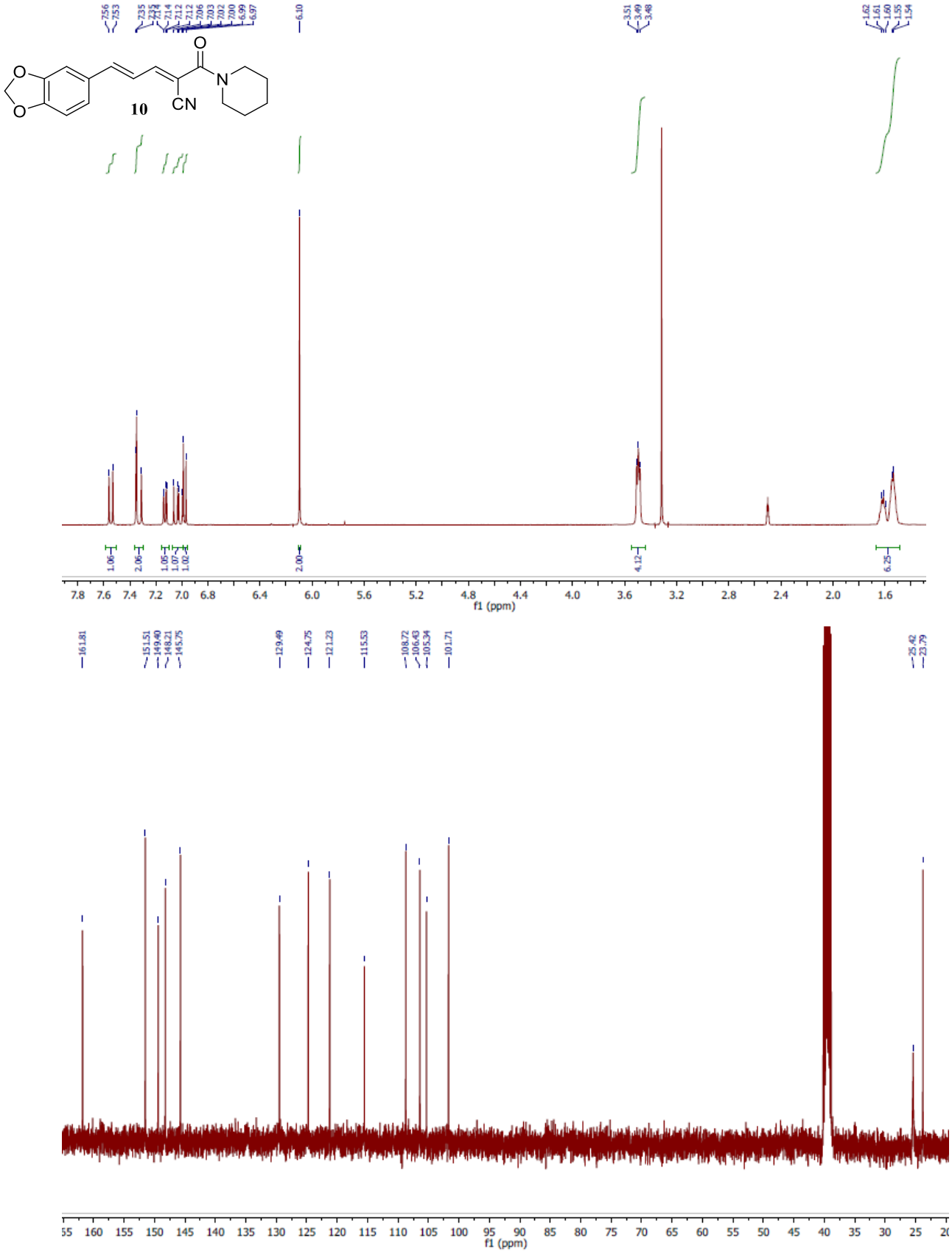


Figure S12. ^{1}H and ^{13}C NMR spectra of final compound **10** (NMR spectrum obtained in DMSO-d_6)

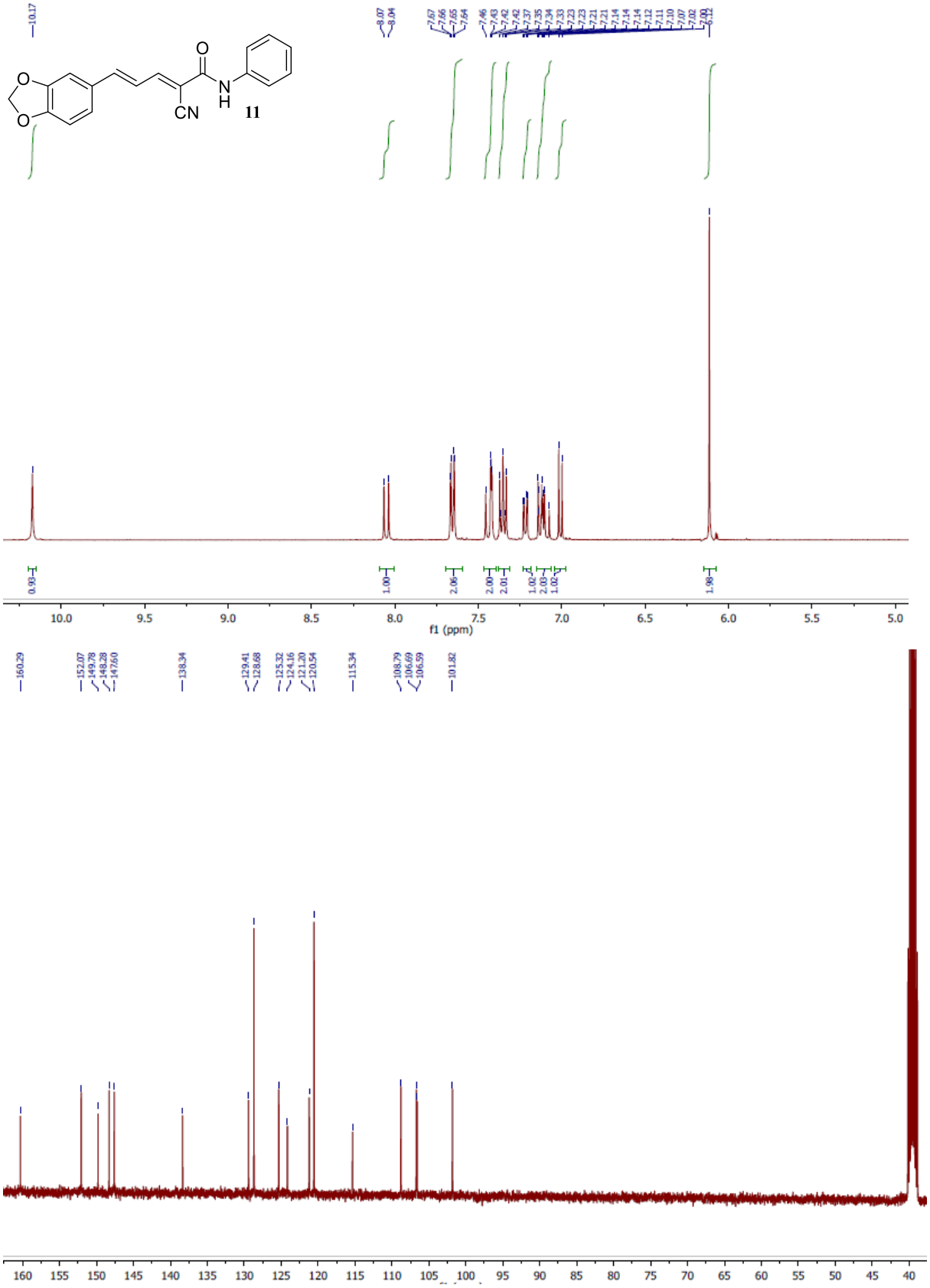


Figure S13. ^{1}H and ^{13}C NMR spectra of final compound **11** (NMR spectrum obtained in DMSO-d_6)

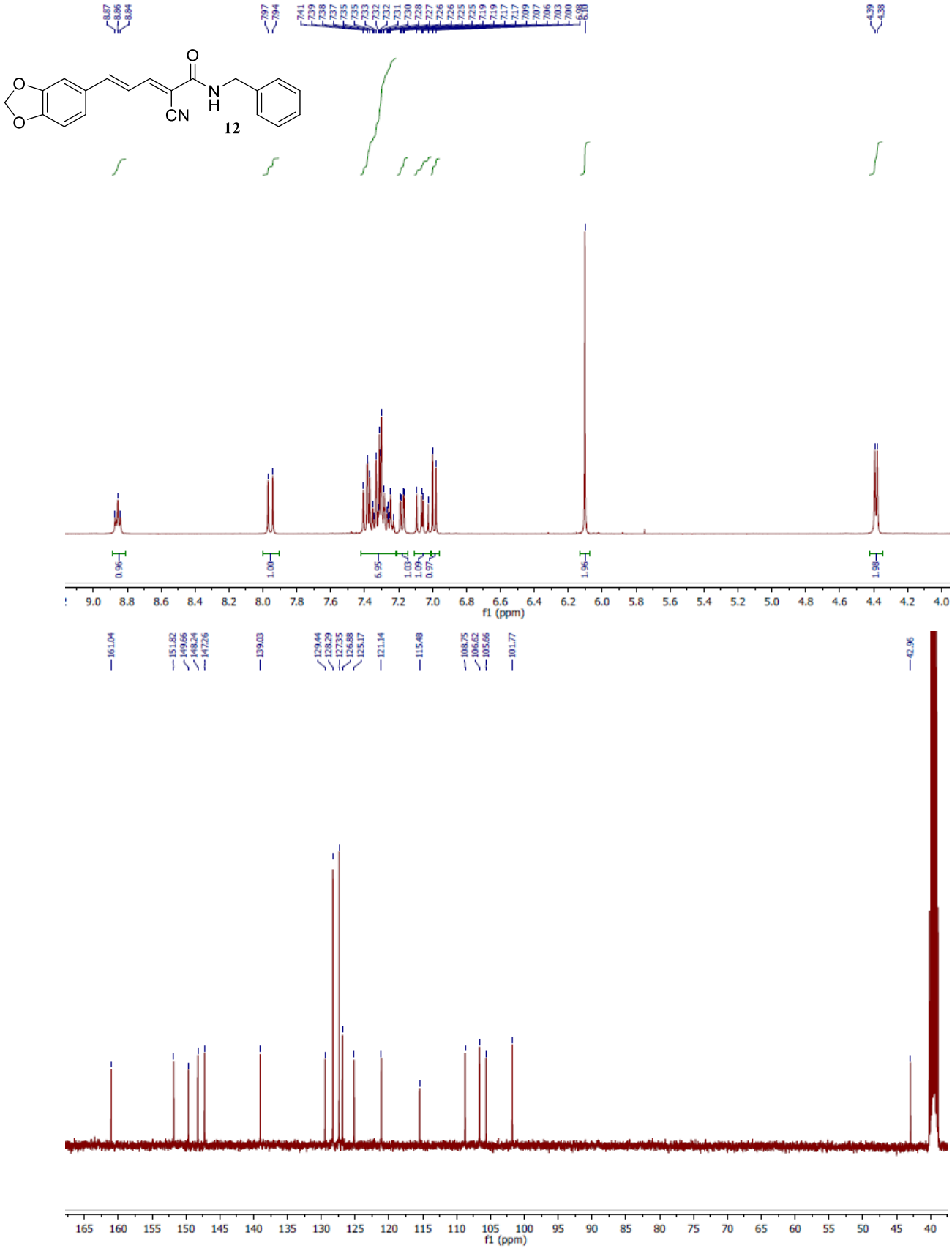


Figure S14. ^{1}H and ^{13}C NMR spectra of final compound **12** (NMR spectrum obtained in DMSO-d_6)

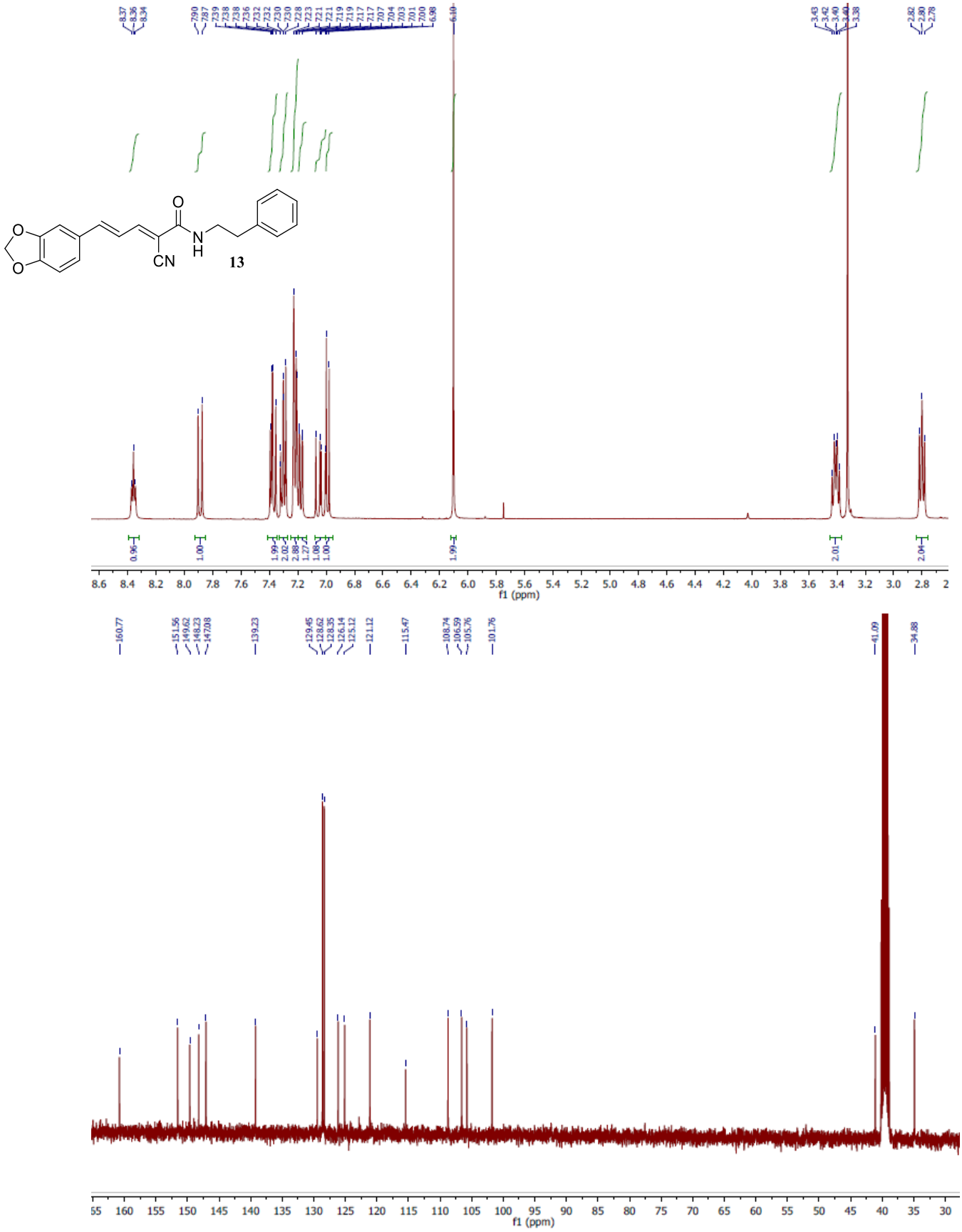


Figure S15. ^{1}H and ^{13}C NMR spectra of final compound **13** (NMR spectrum obtained in DMSO-d_6)

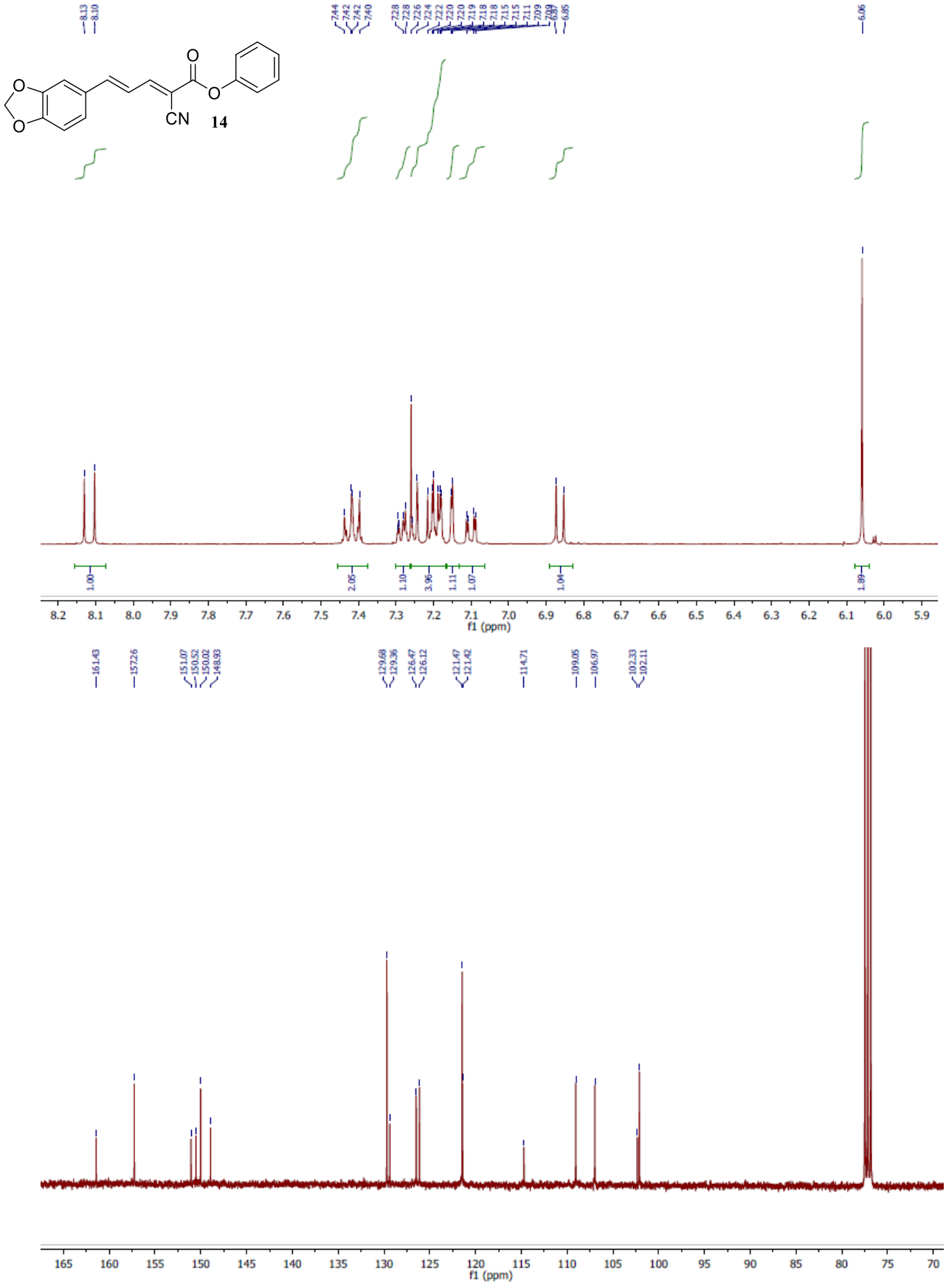


Figure S16. ^{1}H and ^{13}C NMR spectra of final compound **14** (NMR spectrum obtained in $CDCl_3$)

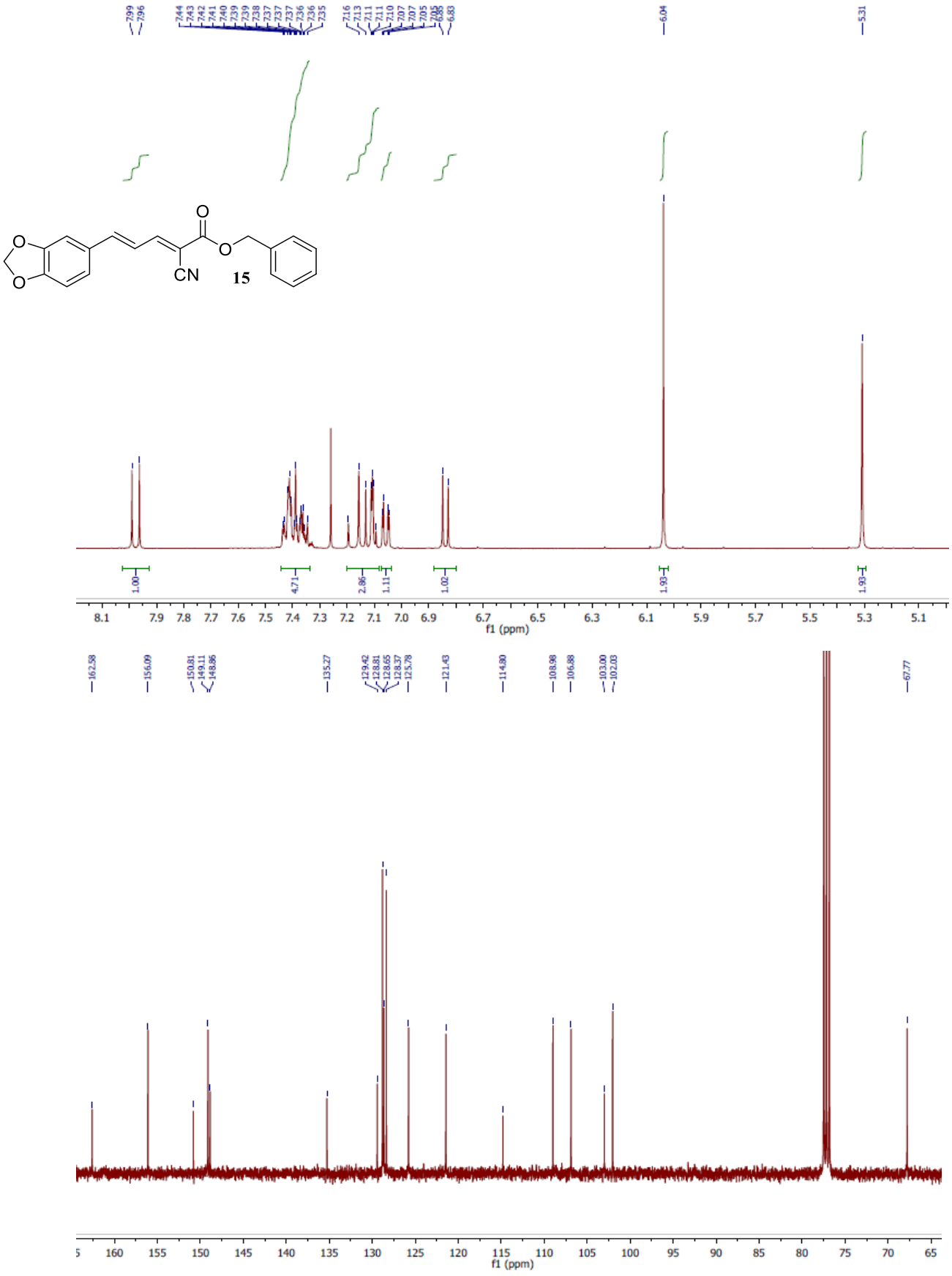


Figure S17. ^{1}H and ^{13}C NMR spectra of final compound **15** (NMR spectrum obtained in $CDCl_3$)

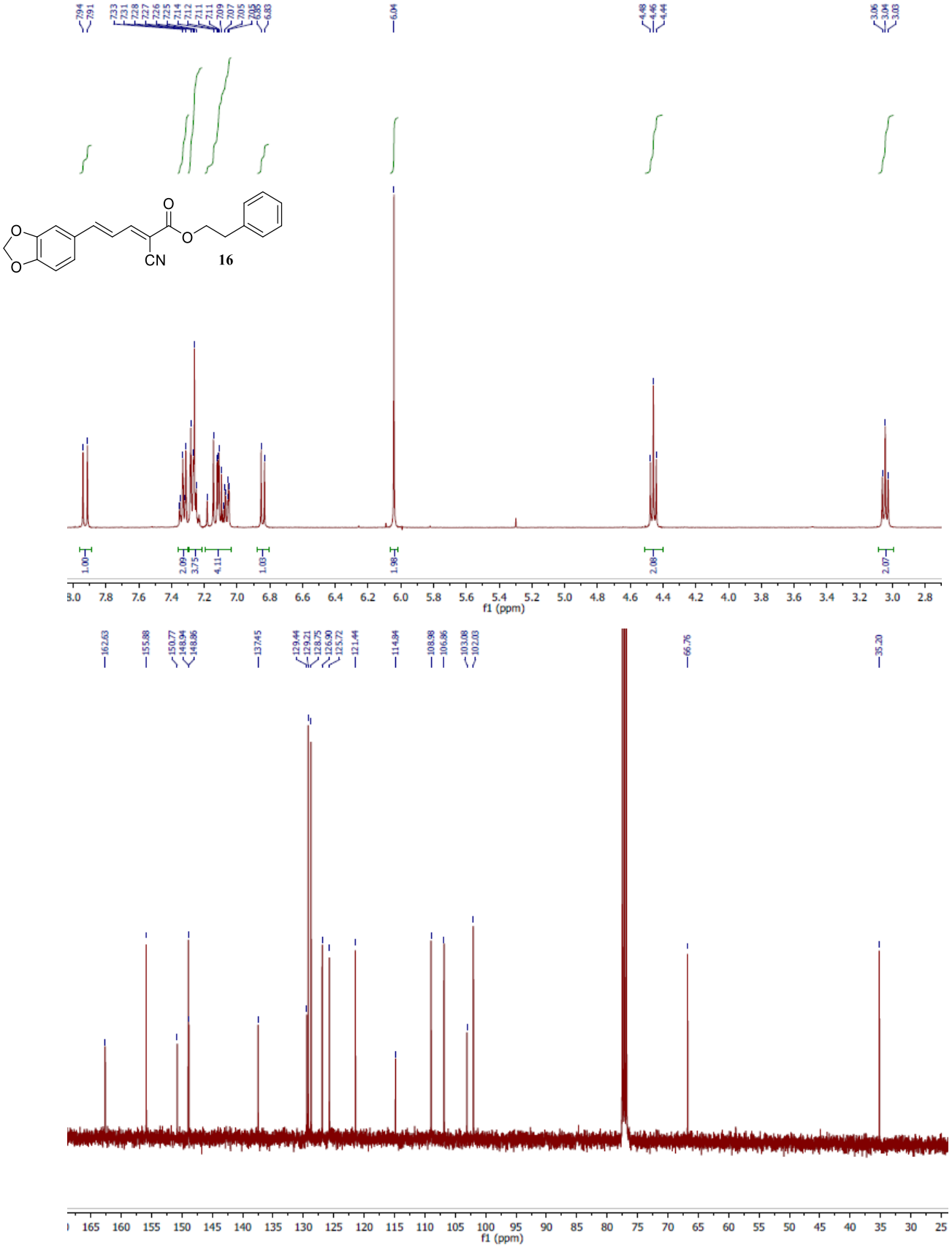


Figure S18. ^{1}H and ^{13}C NMR spectra of final compound **16** (NMR spectrum obtained in $CDCl_3$)

10. References

[1] A. Gandini, M. Bartolini, D. Tedesco, L. Martinez-Gonzalez, C. Roca, N.E. Campillo, J. Zaldivar-Diez, C. Perez, G. Zuccheri, A. Miti, A. Feoli, S. Castellano, S. Petralla, B. Monti, M. Rossi, F. Moda, G. Legname, A. Martinez, M.L. Bolognesi, Tau-Centric Multitarget Approach for Alzheimer's Disease: Development of First-in-Class Dual Glycogen Synthase Kinase 3beta and Tau-Aggregation Inhibitors, J Med Chem, 61 (2018) 7640-7656. https://doi.org/10.1021/acs.jmedchem.8b00610

[2] C. Fernandes, M. Pinto, C. Martins, M.J. Gomes, B. Sarmento, P.J. Oliveira, F. Remião, F. Borges, Development of a PEGylated-Based Platform for Efficient Delivery of Dietary Antioxidants Across the Blood-Brain Barrier, Bioconjug. Chem., 29 (2018) 1677-1689. https://doi.org/10.1021/acs.bioconjchem.8b00151

[3] S.N. Rampersad, Multiple applications of Alamar Blue as an indicator of metabolic function and cellular health in cell viability bioassays, Sensors (Basel), 12 (2012) 12347-12360. https://doi.org/10.3390/s120912347

[4] J. O'Brien, I. Wilson, T. Orton, F. Pognan, Investigation of the Alamar Blue (resazurin) fluorescent dye for the assessment of mammalian cell cytotoxicity, Eur. J. Biochem., 267 (2000) 5421-5426. https://doi.org/10.1046/j.1432-1327.2000.01606.x

[5] E.M. Czekanska, Assessment of cell proliferation with resazurin-based fluorescent dye, Methods Mol. Biol., 740 (2011) 27-32. https://doi.org/10.1007/978-1-61779-108-6_5

[6] A. van Tonder, A.M. Joubert, A.D. Cromarty, Limitations of the 3-(4,5-dimethylthiazol-2-yl)-2,5-diphenyl-2H-tetrazolium bromide (MTT) assay when compared to three commonly used cell enumeration assays, BMC Res. Notes, 8 (2015) 47. https://doi.org/10.1186/s13104-015-1000-8

[7] G. Repetto, A. del Peso, J.L. Zurita, Neutral red uptake assay for the estimation of cell viability/cytotoxicity, Nat. Protoc., 3 (2008) 1125-1131. https://doi.org/10.1038/nprot.2008.75

[8] C. Fernandes, C. Martins, A. Fonseca, R. Nunes, M.J. Matos, R. Silva, J. Garrido, B. Sarmento, F. Remiao, F.J. Otero-Espinar, E. Uriarte, F. Borges, PEGylated PLGA Nanoparticles As a Smart Carrier to Increase the Cellular Uptake of a Coumarin-Based Monoamine Oxidase B Inhibitor, ACS Appl. Mater. Interfaces, 10 (2018) 39557-39569. https://doi.org/10.1021/acsami.8b17224

[9] S. Aula, S. Lakkireddy, K. Jamil, A. Kapley, A.V.N. Swamy, H.R. Lakkireddy, Biophysical, biopharmaceutical and toxicological significance of biomedical nanoparticles, RSC Adv., 5 (2015) 47830-47859. https://doi.org/10.1039/c5ra05889a

[10] K.A. Kang, H.C. Lee, J.J. Lee, M.N. Hong, M.J. Park, Y.S. Lee, H.D. Choi, N. Kim, Y.G. Ko, J.S. Lee, Effects of combined radiofrequency radiation exposure on levels of reactive oxygen species in neuronal cells, J. Radiat. Res., 55 (2014) 265-276. https://doi.org/10.1093/jrr/rrt116

[11] G. Camurri, A. Zaramella, High-throughput liquid chromatography/mass spectrometry method for the determination of the chromatographic hydrophobicity index, Anal. Chem., 73 (2001) 3716-3722. https://doi.org/10.1021/ac001388j

3.6. Manuscript VII

Development of piperine-based mitochondria-targeted agents as antioxidants and monoamine oxidase/cholinesterase inhibitors

To be submitted

Development of piperine-based mitochondria-targeted agents as antioxidants and monoamine oxidase/cholinesterase inhibitors

Daniel Chavarria‡[1,2], Sofia Benfeito‡[1], José Teixeira[2], Jorge Garrido[3], Fernando Cagide[1], Fernando Remião[4], Paulo Jorge Oliveira[2], Fernanda Borges[1*]

[1] CIQUP/Department of Chemistry and Biochemistry, Faculty of Sciences, University of Porto, 4169-007 Porto, Portugal

[2] CNC - Center for Neuroscience and Cell Biology, University of Coimbra, UC Biotech, Biocant Park, Cantanhede, Portugal.

[3] Department of Chemical Engineering, School of Engineering (ISEP), Polytechnic of Porto, 4200-072 Porto, Portugal.

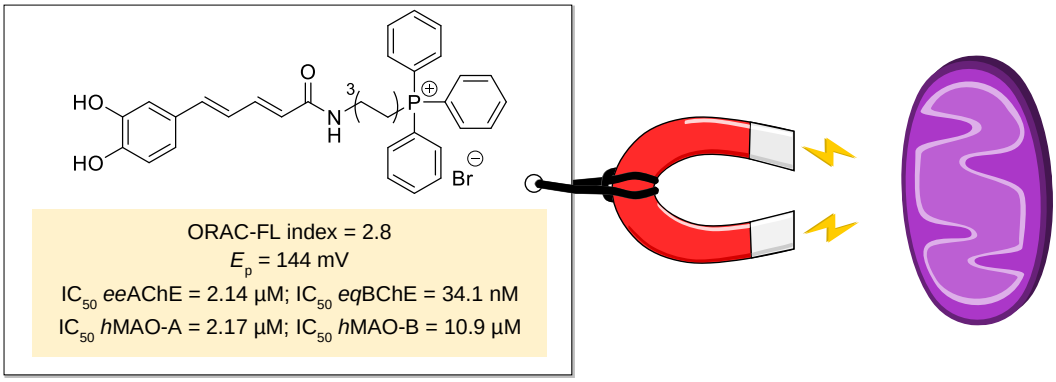
[4] UCIBIO-REQUIMTE, Laboratory of Toxicology, Department of Biological Sciences, Faculty of Pharmacy, University of Porto, Porto, Portugal

‡ These authors contributed equally.

* Corresponding Authors:

Fernanda Borges, CIQUP/Department of Chemistry and Biochemistry, Faculty of Sciences, University of Porto, Porto 4169-007, Portugal. E-mail: fborges@fc.up.pt

1. Graphical abstract



2. Abstract

In neurodegenerative diseases, neurotransmitter depletion and mitochondrial dysfunction are among the multiple pathological events that lead to neurodegeneration. In this context, we synthesized four piperine-based lipophilic triphenylphosphonium (TPP) conjugates. Then, we evaluated their antioxidant and mitochondriotropic activities, as well as their effect on neurotransmitter-metabolizing enzymes and in mitochondrial bioenergetics. Cholinesterase inhibition studies showed that compounds **2-5** are potent and selective equine butyrylcholinesterase (*eq*BChE) inhibitors, presenting a mixed-type inhibition profile. They also displayed moderate human monoamine oxidase (*h*MAO) inhibitory activity. The antioxidant properties of catechol derivatives **4** and **5** were demonstrated using fluorometric and voltammetric assays. Compounds **2-5** were well-tolerated by differentiated SH-SY5Y cells at concentrations up to 12.5 µM. The increased formation of reactive species (RS) induced by these compounds may be underlying the metabolic toxicity at higher concentrations. Piperine derivatives **2-5** accumulated within the matrix of energized mouse liver mitochondria (MLM) and, depending on the presence of benzodioxole or catechol groups, they may affect mitochondrial bioenergetics at non-toxic concentrations. Compound **5** is highlighted as a mitochondria-targeted antioxidant with dual ChE/MAO inhibitory activity. Compound **5** also presented suitable drug-like properties and cytotoxicity profile, thus being a promising candidate for the treatment of neurodegenerative disease.

Keywords: Neurodegenerative diseases, piperine, triphenylphosphonium, monoamine oxidase, cholinesterases, antioxidant activity, mitochondria-targeted agents

3. Introduction

Neurodegeneration is a complex process that result from multiple mechanisms acting concurrently [1]. The main neuropathological hallmarks of Alzheimer's disease (AD) and Parkinson's Disease (PD) are the neuronal loss with consequent decrease of neurotransmitter levels, and the formation of protein aggregates [2, 3]. Based on these observations, enzymes involved in neurotransmitter breakdown (cholinesterases (ChEs); monoamine oxidases (MAOs); catechol *O*-methyltransferase) are among the primary biological targets for potential therapeutics [1].

Mitochondria is also a central player involved in the pathogenesis of AD and PD [4], since they are both the main source and one of the critical targets of reactive species (RS) [5]. Mitochondria play important roles in the ATP synthesis, homeostasis of intracellular second messengers (calcium; RS), and apoptosis [6, 7]. In the central nervous system (CNS), the high energy demand required for neuronal survival and excitability is particularly dependent on mitochondrial ATP generation [8]. Improper function of mitochondria may increase the susceptibility of neurons to oxidative stress [9] and compromise neuronal survival [6]. Indeed, mitochondrial dysfunction is associated with increased RS production, intracellular calcium dyshomeostasis and decreased ATP generation [4, 10].

Considering the pivotal role of mitochondria in fundamental cellular processes [11], drugs that act on or accumulate in mitochondria emerged as an important class of pharmaceuticals with potential therapeutic interest [12]. Compounds that are poorly taken up by mitochondria but able to act on mitochondrial targets often need to be directed towards these organelles [13]. One of the most commonly used strategies to deliver bioactive molecules to mitochondria is the conjugation with lipophilic cations such as triphenylphosphonium (TPP) [13, 14]. The selective accumulation of lipophilic cations into the mitochondrial matrix occurs against the concentration gradient [15] and is driven by the plasma and mitochondrial membrane potentials [16]. Our research group recently developed lipophilic TPP cations conjugated with phenolic acids [17-21]. In addition to the remarkable antioxidant properties [17-21], these mitochondria-targeted derivatives displayed potent ChE inhibitory activities [17].

To continue our project related with the development of effective neuroprotective agents based on natural scaffolds, we focused our efforts on the development lipophilic TPP conjugates based on piperine (1-[5-(1,3-benzodioxol-5-yl)-1-oxo-2,4-pentadienyl]piperidine), compound **1**, **Figure 1**). Piperine is the main alkaloid found in numerous piper species [22]. Recent pharmacological studies in AD and PD animal models showed that piperine improves cognitive function [23, 24], attenuates rotenone-induced motor function and mitigates neuronal loss in *substantia nigra* [25] and in hippocampus [24]. Piperine also protected neurons against rotenone-induced mitochondrial damage [25] and oxidative stress [24, 26], and presented MAO inhibition properties [27].

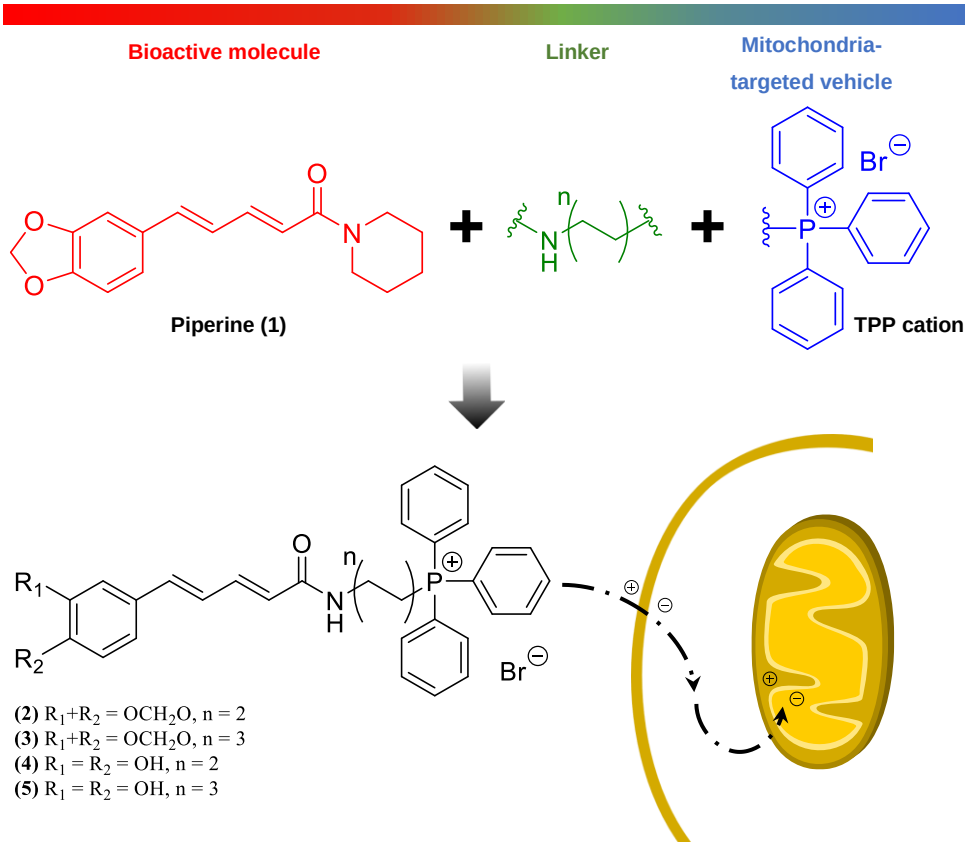


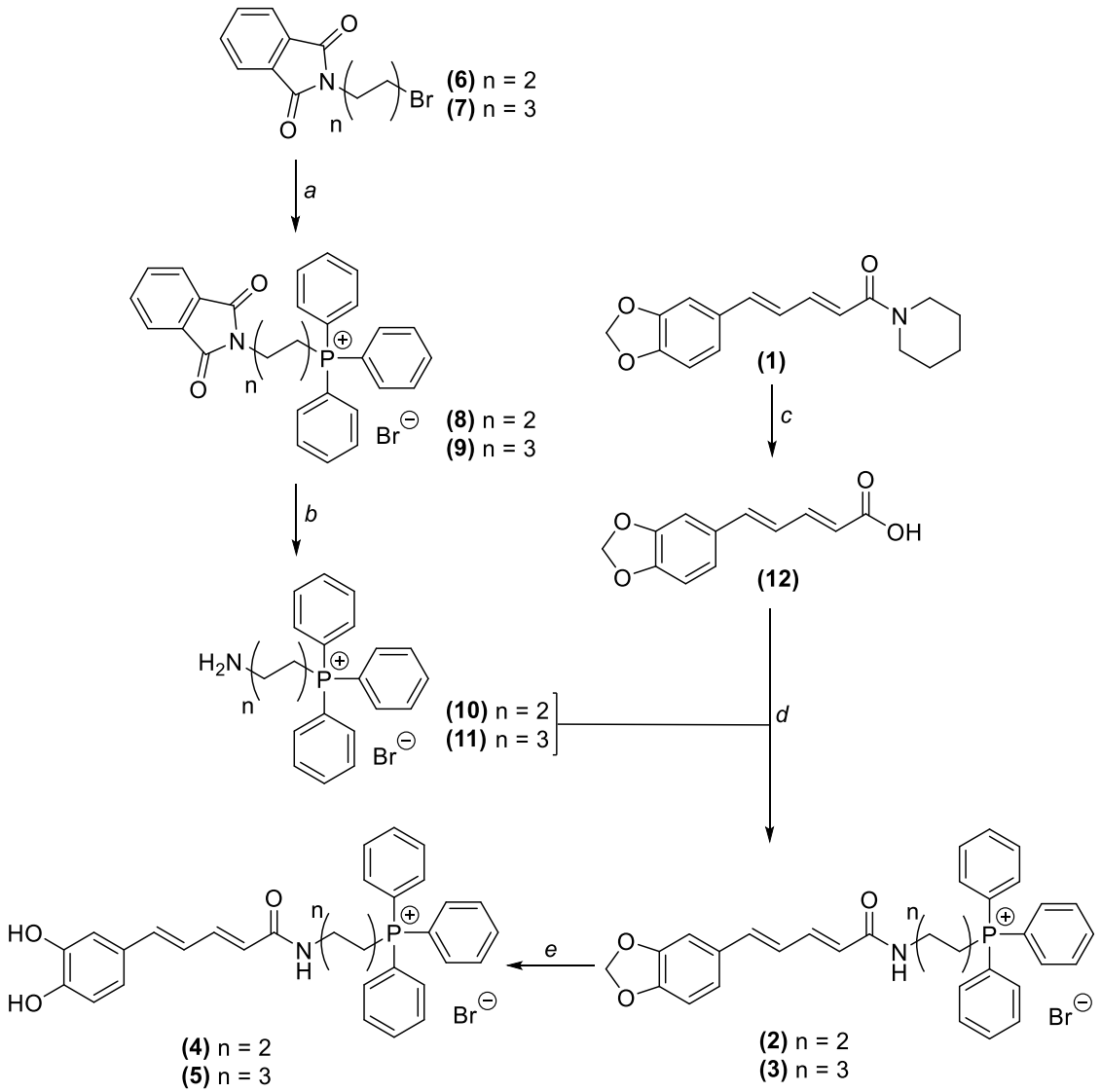
Figure 7. Rational design of mitochondria-targeted compounds 2-5 based on piperine (compound **1**) scaffold.

Herein, we report the synthesis of four piperine derivatives linked to a TPP cation by four- or six-carbon spacers (compounds **2-5**, **Figure 1**). We then evaluated their inhibition profile towards cholinesterases (acetylcholinesterase (AChE, EC 3.1.1.7) and butyrylcholinesterase (BChE, EC 3.1.1.8)) and MAOs (MAO-A and MAO-B), as well as their antioxidant and redox properties. Following the preliminary biological evaluation, we studied the mitochondrial accumulation, cytotoxicity in SH-SY5Y cells, induction of intracellular RS and the compounds' effect on glycolytic and mitochondrial oxidative phosphorylation fluxes.

4. Results and discussion

4.1. Chemistry

The synthetic route used to obtain the piperine-based TPP conjugates **2-5** is depicted in **Scheme 1**. Aminoalkyltriphenylphosphonium salts **10** and **11** were prepared in 2 steps**.** The appropriate bromoalkylphthalymides (compounds **6** and **7**) were heated with triphenylphosphine to obtain compounds **8** and **9** (**Scheme 1**, step *a*), which in turn were refluxed with butylamine in ethanol to induce the phthalymidyl ring cleavage, yielding compounds **10** and **11 (Scheme 1,** step *b***)**. The alkaline hydrolysis of piperine (compound **1**) afforded piperic acid (compound **12**) (**Scheme 1**, step *c*). Piperic acid was then acylated with ethyl chloroformate in alkaline media and reacted with the amines **10** and **11** to afford compounds **2** and **3**, respectively (**Scheme 1**, step *d*). Catechol derivatives **4** and **5** were prepared by the demethylenation of compounds **2** and **3**, respectively, using boron tribromide (**Scheme 1**, step *e*).



Scheme 3. General procedure pursued to obtain the mitochondria-targeted compounds **2**-**5**. (a) TPP, argon atmosphere, 130 ºC, 1.5-4 h; (b) $BuNH_2$, ethanol, reflux, 1.5-10 h; (c) Methanolic solution of NaOH 2 M, reflux, 24 h; (d) 1. CH_2Cl_2, Et_3N, ethyl chloroformate, rt, 2 h; 2. Compounds **10** and **11**, rt, overnight; (e) $BBr_3.S(CH_3)_2$, dichloromethane, argon atmosphere, reflux, 6 h.

4.2. Cholinesterase inhibition studies

The *ee*AChE and *eq*BChE inhibitory activities of piperine and derivatives thereof were then studied using the Ellman's method [28, 29]. Donepezil, a reversible and selective AChE inhibitor widely prescribed for AD [30, 31], was used as standard. The results are expressed as IC_{50} values and are displayed in **Table 1**.

Table 6. Evaluation of ChE (*ee*AChE and *eq*BChE) inhibitory activity of piperine (compound **1**), compounds **2-5** and reference inhibitors.

Compound	IC_{50}/μM		SI (1)[b]
	*ee*AChE	*eq*BChE	
1	___[a]	___[a]	___
2	6.39±0.28	0.0282±0.0014	226
3	5.74±0.32	0.0179±0.0009	314
4	2.23±0.12	0.0619±0.0042	36
5	2.14±0.06	0.0341±0.0029	62
Donepezil	0.0129±0.0008	2.50±0.07	0.0052

[a] Inactive at 10 μM;
[b] SI (1): *eq*BChE selectivity index = IC_{50}(*ee*AChE)/IC_{50}(*eq*BChE).

While piperine did not display significant *ee*AChE and *eq*BChE inhibitory activities at 10 μM, compounds **2-5** inhibited both *ee*AChE and *eq*BChE in our experimental conditions. Concerning *ee*AChE inhibition, the IC_{50} values were within the micromolar range. Catechol derivatives **4** and **5** showed lower IC_{50} values than the counterparts containing the benzodioxole ring (compounds **2** and **3**, respectively). The spacer length did not significantly influence *ee*AChE inhibition.

Interestingly, compounds **2-5** displayed higher potency towards *eq*BChE, presenting IC_{50} values within the nanomolar range. Compounds bearing a six-carbon chain were better *eq*BChE inhibitors than the four-carbon chain analogues. In contrast to the results obtained with *ee*AChE, benzodioxole derivatives **2** and **3** showed lower IC_{50} values than catechols **4** and **5**, respectively.

The *eq*BChE selectivity index, determined from the ratio of the IC_{50} values of *ee*AChE and *eq*BChE, showed that benzodioxole derivatives **2** and **3** were more selective towards *eq*BChE (226-fold and 314-fold, respectively) than catechols **4** and **5** (36-fold and 62-fold, respectively).

4.2.1. Evaluation of equine butyrylcholinesterase inhibition mechanism

Kinetic studies were then carried out to evaluate the *eq*BChE inhibition mechanism of piperine-based TPP conjugates. Six-carbon chain derivatives **3** and **5** were selected to assess the influence of benzodioxole and catechol groups in the inhibition mechanism, respectively. We conducted enzymatic inhibition kinetics using seven different substrate concentrations in the absence and the presence of three inhibitor concentrations. Graphical analyses of the double reciprocal Lineweaver-Burk plots enabled the determination of Michaelis−Menten reaction kinetic parameters (Michaelis constant, K_m, and maximum velocity, V_{max}). In the absence of inhibitor, the enzymatic parameters of *eq*BChE were: K_m = 217±21 μM and V_{max} = 0.1427±0.0021 $\Delta Abs.min^{-1}$.

The Lineweaver-Burk plots remained linear with increasing concentrations of compound **3** and intersected to the same point above the x-axis and on the left of the y-axis (**Figure 2A**). The results obtained indicate that the apparent K_m values increased, while the apparent V_{max} values decreased with crescent inhibitor concentrations. Therefore, compound **3** acted as a mixed-type inhibitor, binding both free enzyme and the enzyme-substrate binding complex at a site other than the active site. To obtain the inhibition constants K_i and K_i', the data from the Lineweaver-Burk were replotted as the slope (**Figure 2B**) or the y-axis intercept against the concentrations of compound **3** (**Figure 2C**), respectively. The x-axis intercept for the former is $-K_i$, while

the x-axis intercept for the latter is -K_i'. A slight upward curvature of the secondary plots was observed (**Figures 2B** and **2C**), which may indicate that compound **3** binds to more than one site of *eq*BChE [32]. The inhibition constants K_i and K_i' were estimated by the linearization of the lowest three inhibitor concentrations. For compound **3**, K_i = 14.7 nM and K_i' = 62.1 nM. Since K_i value was lower than K_i', compound **3** preferably binds to the free enzyme over the enzyme-substrate binding complex.

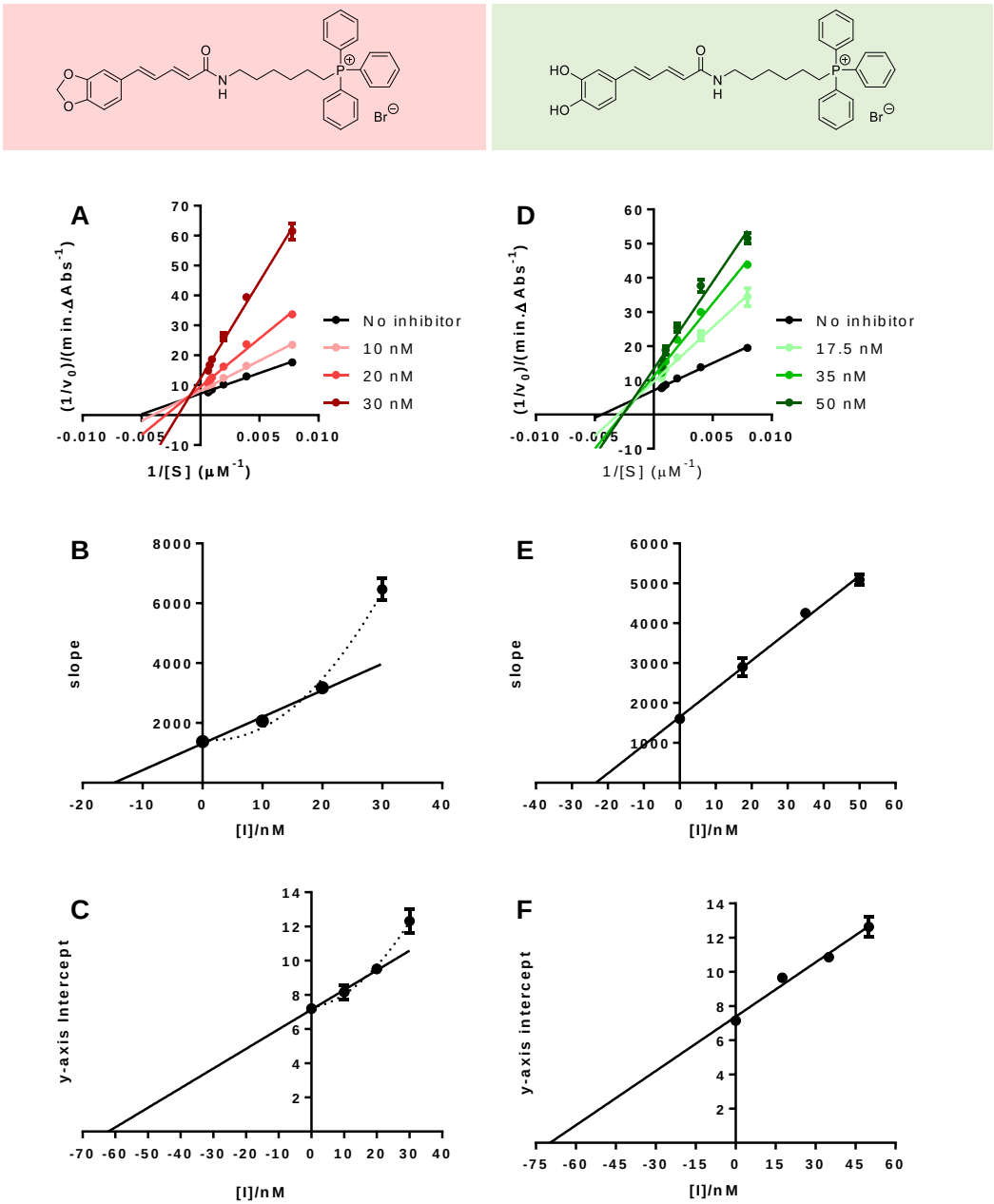


Figure 8. Kinetic studies on the mechanism of *eq*BChE inhibition by compounds **3** (**A-C**) and compound **5** (**D-F**). (A, D) Double reciprocal plots of the initial velocity of *eq*BChE at increasing substrate concentrations (0.063 – 1.3 mM), in the absence or the presence of the inhibitor. (**B, E**) Secondary plot of slope of each Lineweaver-Burk (K_m/V_{max}) versus the inhibitor concentration. (**C, F**) Secondary plot constructed from the slope of the y-axis intercepts of each Lineweaver-Burk ($1/V_{max}$) versus the inhibitor concentration.

The results obtained for compound **5** also showed variations in both the apparent V_{max} and the apparent K_m values in line with a mixed-type inhibition (**Figure 2D**). Contrary to the benzodioxole analogue, the secondary replots constructed from the Lineweaver-Burk plots of the catechol **5** were linearly fitted (**Figure 2E** and **2F**), indicating that compound **5** has a single binding site. The inhibition constants K_i and K_i' obtained for compound **5** were 23.3 nM and 69.7 nM, respectively.

4.3. Monoamine oxidase inhibition studies

We evaluated the *h*MAO inhibition properties of piperine (compound **1**) and piperine-based TPP cations **2-5,** using kynuramine as substrate and recombinant *h*MAO-A and -B isoforms [33, 34]. The *h*MAO-A and *h*MAO-B inhibitory potency (IC_{50}) and selectivity (SI) data of the compounds under study and reference inhibitors (clorgyline for *h*MAO-A and (R)-(−)-deprenyl, rasagiline, safinamide for *h*MAO-B) are reported in **Table 2.**

Table 7. Evaluation of *h*MAOs (*h*MAO-A and *h*MAO-B) inhibitory activity of piperine (compound **1**), compounds **2-5** and reference inhibitors**.**

Compound	IC_{50}/μM		SI[b]
	*h*MAO-A	*h*MAO-B	
1	___[a,d]	1.05±0.08[e]	10[c, e]
2	0.888±0.022	12.4±1.9	0.07
3	1.23±0.13	4.64±0.29	0.26
4	5.17±0.54	13.5±1.1	0.38
5	2.17±0.28	10.9±0.7	0.20
R-(-)-Deprenyl	20.1±1.9[d]	0.0386±0.0043[d]	522[d]
Rasagiline	3.65±0.31	147.3±249	24
Safinamide	___[a]	0.0231±0.0026	433[c]
Clorgyline	0.00274±0.00047[d]	2.21±0.26[d]	0.00124[d]

[a] Inactive at 10 μM;
[b] SI: *h*MAO-B selectivity index = IC_{50} (*h*MAO-A)/IC_{50} (*h*MAO-B).
[c] Values obtained under the assumption that the corresponding IC_{50} against *h*MAO-A or *h*MAO-B is the highest concentration tested (10 μM).
[d] Data from Chavarria *et al.* [33].

In previous reports, piperine showed moderate and selective *h*MAO-B inhibitory activity (compound **1**, IC_{50} = 1.05 μM, SI = 10) [33]. In contrast, compounds **2-5** inhibited both *h*MAO isoforms with slightly higher selectivity towards *h*MAO-A, presenting IC_{50} values within the micromolar or high nanomolar range. Compounds **2** and **3** displayed similar or lower IC_{50} values towards *h*MAOs than compounds **4** and **5**, respectively. Therefore, the benzodioxole ring opening decreases the ability to inhibit both *h*MAO isoforms. Concerning the spacer length, compounds containing a six-carbon chain (compounds **3** and **5**) were more effective *h*MAO-B inhibitors than compounds with a four-carbon chain (compounds **2** and **4**). However, no correlation was found between *h*MAO-A inhibition and the spacer length.

4.4. Antioxidant activity

To evaluate the radical scavenging activity of piperine (compound **1**) and compounds **2-5**, we employed the oxygen radical absorbance capacity (ORAC) assay. This method measures the antioxidant activity against peroxyl radical ($ROO^{\bullet}$)-induced oxidation of fluorescein, a fluorescent probe, into a non-fluorescent product [35]. While piperine (compound **1**) and compounds **2** and **3** were unable to scavenge $ROO^{\bullet}$ radicals, catechols **4** and **5** were effective on protecting fluorescein from oxidation (**Table 3**). Compounds **4** and **5** showed lower ORAC-FL indexes than the parent carboxylic acid (ORAC-FL index = 5.5±0.1), indicating an inverse correlation between the ORAC-FL indexes and increased lipophilicity (**Manuscript IV**). This tendency was also observed in previous reports (**Manuscript IV**). Overall, the data obtained point out that the compounds **4** and **5** act as chain-breaking antioxidants against peroxyl radicals.

Table 8. ORAC-FL indexes and redox potentials (E_p) of compounds **2-5**.

Compound	ORAC-FL index	E_p/mV
1	___	n.d.
2	___	942; 1070
3	___	931; 1083
4	3.3±0.1	125
5	2.8±0.1	144

4.5. Electrochemical studies

The redox behavior of compounds **2-5** was studied by differential pulse voltammetry (DPV) and cyclic voltammetry (CV) at physiological pH 7.4, using a glassy carbon-working electrode. Benzodioxole derivatives **2** and **3** presented two overlapped anodic peaks at physiological pH. The high positive redox potential (E_p) values obtained with these compounds is not consistent with molecules with high antioxidant activity. Indeed, compounds **2** and **3** do not present functional groups with recognized reducing power, such as aromatic hydroxyl groups [36]. In contrast, catechols **4** and **5** displayed well-defined anodic peaks associated with the oxidation of the catechol groups (**Figure 3A**). The redox potential (E_p) values obtained for compounds **4** and **5** were 125 mV and 144 mV (**Table 3**), respectively. These values were consistent with those obtained with catechols having a similar conjugated dienone system (E_p values of 113-129 mV) (**Manuscript IV**). Moreover, E_p values of compounds **4** and **5** were lower than those obtained with protocatechuic acid-based TPP cations (E_p = 210-216 mV [17, 18]) and, to a lesser extent, with caffeic acid derivatives (164-174 mV [19, 20]). Therefore, the progressively higher electron delocalization between the aromatic ring and the carbonyl group shifted the peak potentials towards less positive values, thus enhancing the reducing power of catechols.

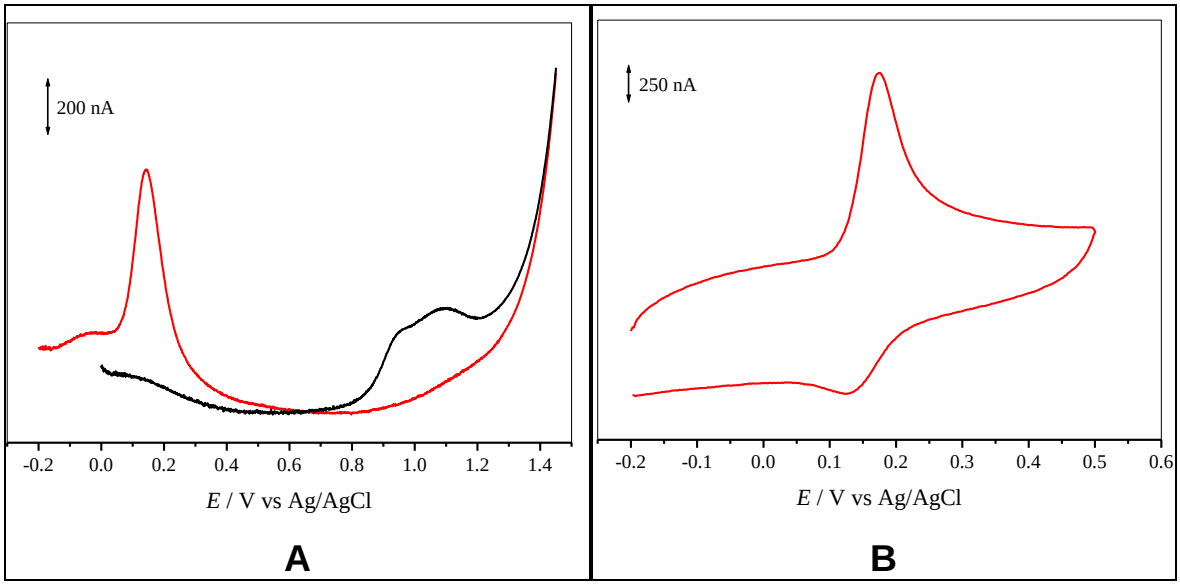
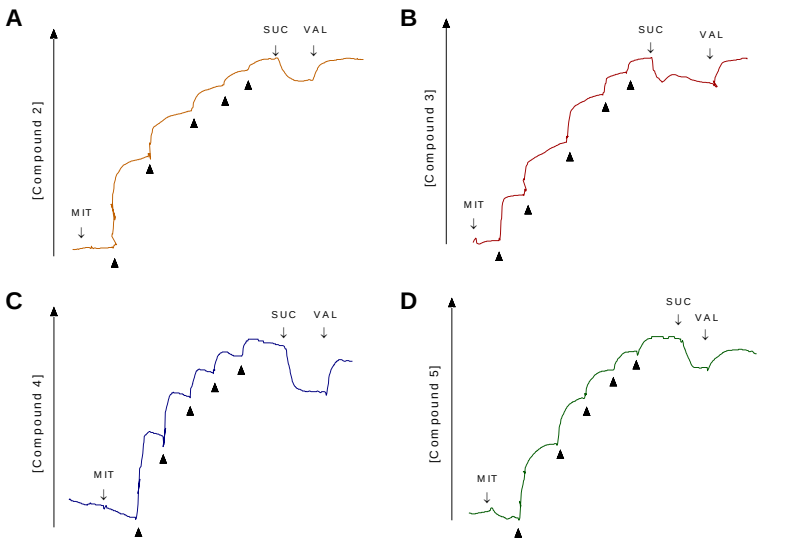


Figure 9. Representative voltammograms of mitochondria-targeted agents **3** and **5**. (**A**) Differential pulse voltammogram and (**B**) cyclic voltammograms for a 0.1 mM solutions of (**—**) compound **3** and (**—**) compound **5** in physiological pH 7.4 supporting electrolyte. Scan rates: 5 mV s^{-1} (DPV) and 50 mV s^{-1} (CV).

In cyclic voltammograms obtained for compounds **4** and **5**, we observed one anodic wave and one cathodic wave in the forward and in the reverse scans, respectively (**Figure 3B**). This behavior is characteristic of a reversible electrochemical reaction, which is in accordance with the results obtained with other catechols [18, 19].

4.6. Mitochondrial uptake

Isolated mouse liver mitochondria (MLM) were used to evaluate whether piperine-based TPP cations **2-5** are taken up by mitochondria. Accordingly, the complex II substrate succinate (SUC) was used to generate a transmembrane electric potential (ΔΨ), leading to a decrease of the extramitochondrial concentration of the compound. Valinomycin (VAL), a K^+-selective ionophore, was then used to induce a depolarization of ΔΨ and thereby release the accumulated TPP cation from the mitochondrial matrix (**Figure 4A-D**).



E

Compound	Accumulation ratio
2	1457
3	1130
4	1457
5	1970

Figure 10. Measurement of mitochondrial uptake of compound **2** (**A**), compound **3** (**B**), compound **4** (**C**) and compound **5** (**D**) in MLM. (**E**) Accumulation ratios of compounds **2-5** in MLM.

The results presented in **Figure 4** clearly show that piperine-based TPP cations **2-5** accumulate into the matrix of energized mitochondria, presenting accumulation ratio values ranging between 1130 and 1970. The highest mitochondrial uptake was observed with compound **5**, the catechol derivative with a six-carbon linker (**Figures 4D and 4E)**. This compound was followed by compounds **2** and **4**, the derivatives containing a four-carbon lipophilic spacer, which displayed the same accumulation ratio (**Figures 4A, 4C** and **4E)**. Finally, the TPP derivative with a benzodioxole ring and a six-carbon linker (compound **3**) presented the lowest mitochondrial accumulation ratio (**Figure 4B** and **4E)**.

4.7. Cellular studies

4.7.1. Evaluation of cytotoxicity profile

To evaluate the cytotoxicity of lipophilic TPP cations **2-5**, differentiated SH-SY5Y cells were incubated with increasing concentrations of the test compounds (0.20-100 µM) for a 24 h period. Cellular cytotoxicity was assessed using the resazurin reduction assay, which estimates metabolic activity of viable cells [37], and the neutral red (NR) uptake assay, which relies on the lysosomal incorporation of the dye NR in living cells [38]. The results, presented as mean resorufin fluorescence (% of control)±SEM and NR uptake (% of control) ± SEM (n = 3), are depicted in **Figure 5**.

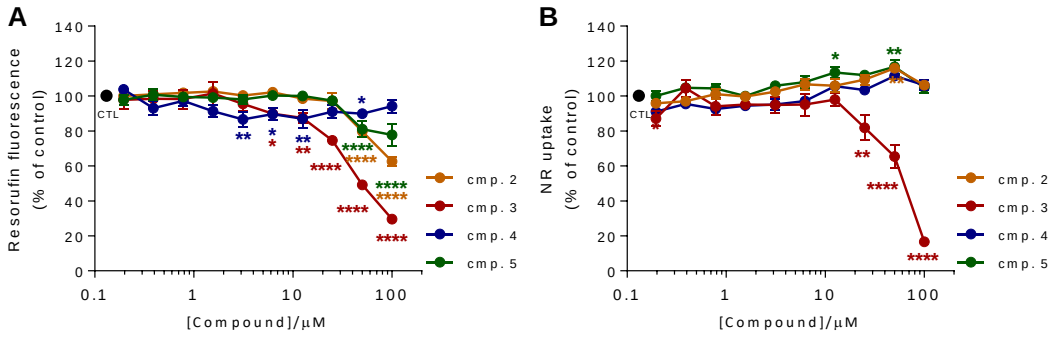


Figure 11. Cellular viability of differentiated SH-SY5Y neuroblastoma cells after a 24 h treatment with increasing concentrations of compounds **2-5** (0.20-100 µM). Cellular viability was evaluated using the resazurin reduction assay (**A**) and the NR uptake assay (**B**). Results are expressed as the mean % of untreated controls ± SEM (n = 3). Statistical comparisons were made using two-way ANOVA followed by Dunnet's multiple comparison test. In all cases, p values lower than 0.05 were considered significant (* $p < 0.05$, ** $p < 0.01$, *** $p < 0.001$, **** $p < 0.0001$ vs untreated cells).

Significant concentration-dependent drops in resorufin fluorescence were observed with compounds **2**, **3** and **5** (**Figure 5A**). Compound **3** presented the most prominent decay, showing significant decreases in resazurin reduction (resorufin fluorescence < 85 %) at concentrations above 12.5 µM (**Figure 5A**). This tendency was also observed with compounds **2** and **5** at concentrations above 25 µM (**Figure 5A**). On the other hand, resorufin fluorescence was virtually maintained after incubation of neuroblastoma cells with increasing concentrations of compound **4** (**Figure 5A**).

Resazurin reduction was influenced by the substitution pattern of the aromatic ring and by the length of the lipophilic spacer. The effects of the structural components of lipophilic TPP cations **2-5** were particularly noticeable at the highest tested concentration (100 µM). In fact, compounds containing a catechol group (compounds **4** and **5**) presented higher resorufin fluorescence values than the compounds with a benzodioxole ring (compounds **2** and **3**) (**Figure 5A**). Moreover, compounds with a four-carbon alkyl chain (compounds **2** and **4**) displayed lower metabolic toxicity than the six-carbon alkyl chain analogues (compounds **3** and **5**, respectively) (**Figure 5A**).

Interestingly, the same conclusions were not drawn up with the NR uptake assay (**Figure 5B**). Neutral red (NR) uptake remained constant with increasing concentrations of compounds **2**, **4** and **5** (**Figure 5B**), even at concentrations in which the resazurin reduction was significantly reduced (**Figure 5A**, compounds **2** and **5**, ≥ 50 µM). Only compound **3** displayed the same tendency observed with the resazurin reduction assay, showing significant lysosomal toxicity at concentrations above 12.5 µM.

Overall, these results indicate that compounds **2-5** are well tolerated at concentrations up to 12.5 µM but they may affect cellular metabolism at higher concentrations.

4.7.2. Evaluation of intracellular oxidative stress

To assess whether the compounds **2-5** induce the formation of the intracellular reactive species (RS), differentiated SH-SY5Y were incubated for 24 h with two different concentrations of each compound (10 and 50 µM). Intracellular RS levels were detected using the 2',7'-dichorofluorescein (DCF) fluorescence assay. The results, expressed as DCF fluorescence (% of control)±SEM (n = 3), are shown in **Figure 6A**. Then, the

intracellular RS levels were normalized with the number of viable cells (data taken from resazurin reduction assay) to calculate the ration between the intracellular RS levels and metabolic activity (IRL/MA) (**Figure 6B**).

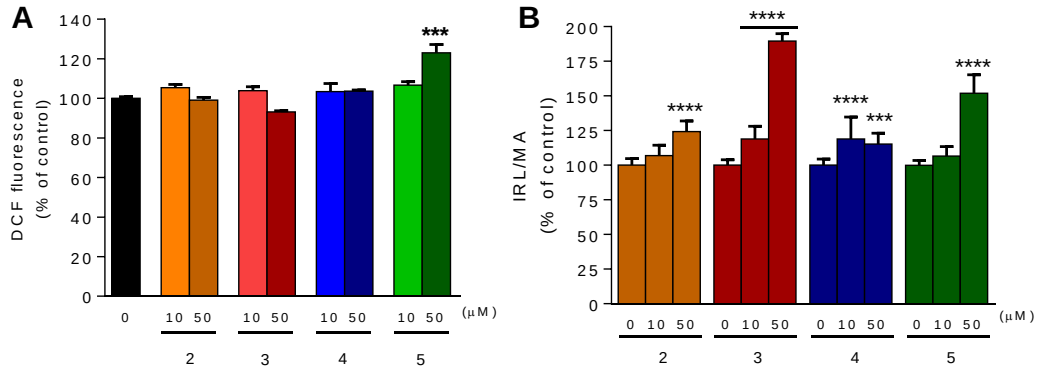


Figure 12. (**A**) Evaluation of intracellular oxidative stress levels in differentiated SH-SY5Y cells using the DCF fluorescence assay, after incubation for 24 h with compounds **2-5** at 10 and 50 μM. Results are expressed as DCF fluorescence (% of control) ± SEM (n = 3). Statistical comparisons were performed using the nonparametric method of Kruskal–Wallis (one-way ANOVA on ranks), followed by Dunn's *post hoc* test (**B**) Ratio between intracellular RS levels and metabolic activity (IRL/MA) at 10 and 50 μM. Statistical comparisons were performed using the parametric method of two-way ANOVA, followed by the Dunnett's multiple comparisons test. In all cases, p values lower than 0.05 were considered significant (* $p < 0.05$, ** $p < 0.01$, *** $p < 0.001$, **** $p < 0.0001$ vs untreated cells).

A significant increase of DCF fluorescence was observed for compound **5** at 50 μM ($p < 0.001$, **Figure 6A**). However, all piperine-based TPP conjugates at 50 μM presented IRL/MA ratios significantly higher than non-treated cells, resulting from a higher production of intracellular RS by a reduced number of living cells (**Figure 6B**). The highest IRL/MA ratios at 50 μM were obtained with compounds **3** (189.5± 5.4, $p < 0.0001$, **Figure 6B**), followed by compound **5** (151.9± 13.3, $p < 0.0001$, **Figure 6B**), compound **2** (124.3±7.6, $p < 0.001$, **Figure 6B**) and compound **3** (115.3±7.8, $p < 0.0001$, **Figure 6B**).

Taken these data together, the results indicate that piperine-based TPP cations **2-5** increase the intracellular oxidative stress levels in neuroblastoma cells, which may be underlying the metabolic toxicity obtained at high concentrations. The increased oxidative stress is particularly noticeable with six-carbon chain derivatives (compounds **3** and **5**), highlighting the potential negative impact of more hydrophobic alkyl linkers.

4.7.3. Evaluation of glycolytic and mitochondrial oxidative phosphorylation fluxes

The effect of piperine (compound **1**) and piperine-based TPP cations (compounds **2-5**) on glycolytic and mitochondrial oxidative phosphorylation fluxes in differentiated SH-SY5Y cells were investigated. To this end, cells were treated with non-toxic concentrations of compounds **1-5** for 24 h. Then, oxygen consumption rates (OCR) and extracellular acidification rates (ECAR) were measured under basal conditions. Moreover, OCR was measured after consecutive additions of oligomycin (OLIG, adenosine triphosphate (ATP) synthase inhibitor), carbonyl cyanide *p*-triflouromethoxyphenylhydrazone (FCCP, mitochondrial uncoupler), and rotenone and antimycin A (ROT/AA, inhibitors of complexes I and III, respectively) [39]. Oxygen consumption rate (OCR) and ECAR values were normalized to the cell mass, which was determined using the

sulphorhodamine B (SRB) assay. Multiple parameters were determined from the OCR measurements, namely basal respiration, proton leak, maximal respiration, spare respiratory capacity and ATP production-linked respiration. The results obtained are illustrated in **Figure 7**.

Piperine (compound **1**, 50 µM) and catechol derivatives (compound **4**, 100 µM; compound **5**, 25 µM) did not significantly affect both glycolytic and mitochondrial oxidative phosphorylation fluxes in differentiated neuroblastoma cells. In contrast, a significant reduction in maximal respiration was observed with compound **3** (12.5 µM , $p < 0.05$, **Figure 7D**). Moreover, treatment of neuroblastoma cells with benzodioxole derivatives **2** (25 µM) and **3** (12.5 µM) significantly decreased the spare respiratory capacity ($p < 0.05$, **Figure 7E**). This parameter describes the ability of cells to produce ATP in response to cellular stress (e.g.: oxidative stress) [40] or increased work (e.g.: cell division, cell proliferation and cell migration) [41], and is important for long-term cellular survival and function [42]. Thus, benzodioxole derivatives **2** (25 µM) and **3** (12.5 µM) may reduce the ability of differentiated SH-SY5Y cells to survive under oxidative stress conditions.

Overall, these results indicate that glycolytic and mitochondrial oxidative phosphorylation fluxes of neuroblastoma cells were maintained in the presence catechol derivatives (compounds **4** and **5**), while benzodioxole derivates (compounds **2** and **3**) may negatively affect mitochondrial bioenergetics.

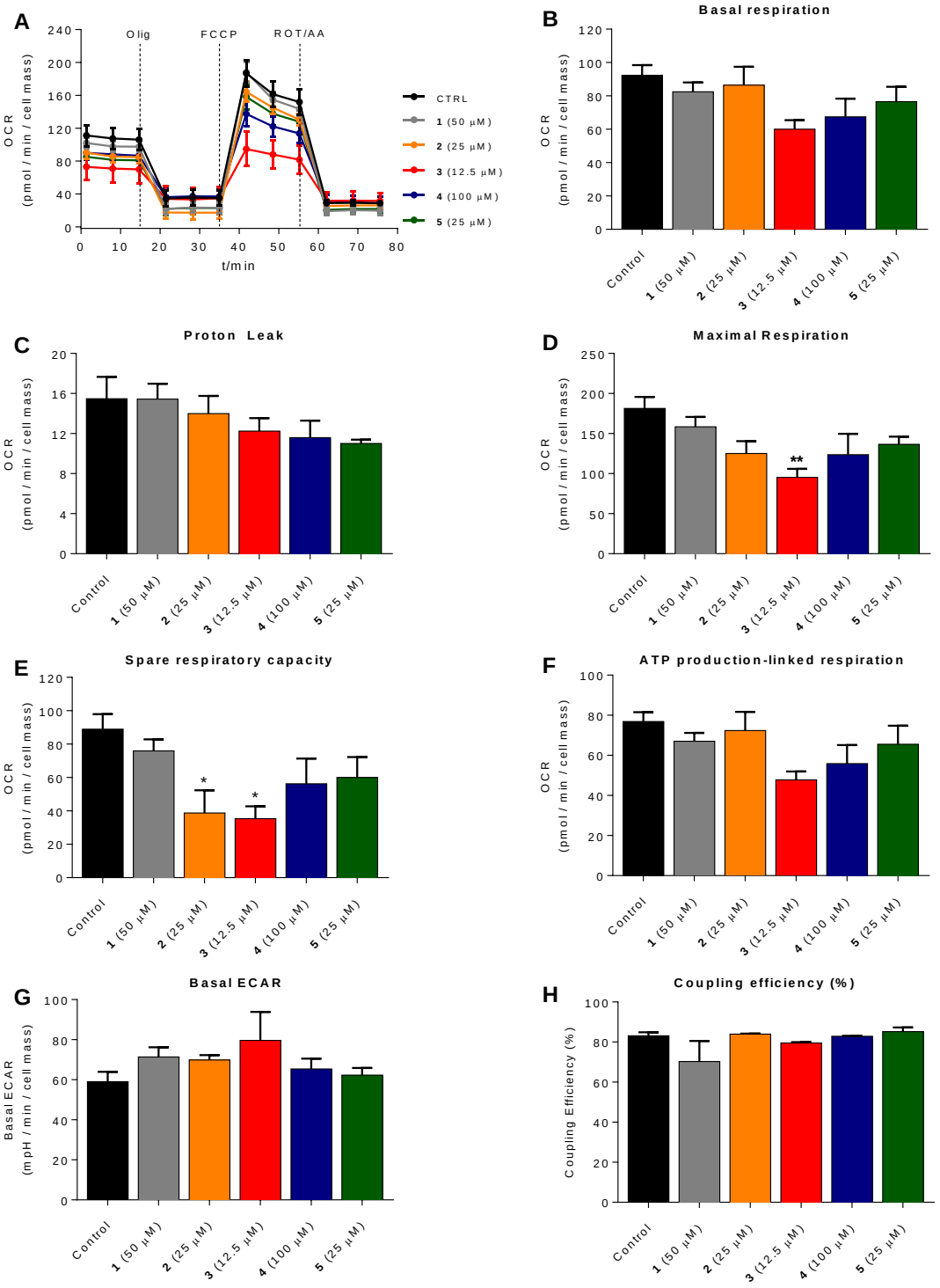


Figure 13. Effect of compounds **1-5** on mitochondrial oxygen consumption. (**A**) Representative image of OCR measurements in differentiated SH-SY5Y cells treated with vehicle (Control) and non-toxic concentrations of compounds 1-5 for 24 h using the Seahorse XF96 Extracellular Flux Analyzer. Several respiratory parameters were evaluated, namely (**B**) basal cellular respiration, (**C**) proton leak, (**D**) maximal respiration, (**E**) spare respiratory capacity, (**F**) ATP production-linked respiration, (**G**) basal ECAR and (**H**) coupling efficiency. Data are expressed as pmol O_2/min/cell mass (measured using the SRB assay) for OCR (**B-F**) and mpH/min/cell mass for ECAR (**G**). Results are presented as mean ± SEM (n = 4). Statistical comparisons were performed using the parametric method of one-way ANOVA, followed by the Dunnett's multiple comparisons test. In all cases, p values lower than 0.05 were considered significant (* $p < 0.05$, ** $p < 0.01$ vs untreated cells).

4.8. Estimation of drug-like properties

To study the drug-likeness of lipophilic cations **2-5**, we first determined the chromatographic hydrophobic index (CHI). Chromatographic hydrophobicity index (CHI) values of neutral molecules are directly correlated with the compounds' lipophilicity [43]. Thus, the determination of CHI of compounds **4** and **5** was carried out under acidic conditions (pH 2.3) to prevent the ionization of the catechol moiety. The experiments performed with piperine (compound **1**) and compounds **2** and **3** were conducted both at pH 2.3 and at physiological pH (7.4). The results obtained are presented in **Table 4**.

Table 9. Retention times (t_R) obtained by LC/UV at pH 2.3 and 7.4 and calculated CHI parameters of piperine (compound **1**) and lipophilic TPP cations **2-5**.

	pH 2.3		pH 7.4	
Compound	t_R/min	CHI	t_R/min	CHI
1	10.59	73.4	10.62	74.2
2	8.72	42.8	9.97	63.9
3	8.90	45.8	10.25	68.3
4	8.20	34.4	n.d.	n.d.
5	8.38	37.2	n.d.	n.d.

Chromatographic hydrophobicity index (CHI) values at pH 2.3 of compounds **2-5** were considerably lower than the obtained with piperine (**Table 4**). Therefore, despite the presence of bulky groups with high lipophilicity, the positive charge of TPP cations may decrease the affinity towards the hydrophobic stationary phase. Moreover, CHI values at pH 2.3 increased with the presence of a benzodioxole ring (compounds **2** and **3** vs compounds **4** and **5**, respectively) and longer alkyl linkers (compounds **2** and **4** vs compounds **3** and **5**, respectively) (**Table 4**), which is associated with higher hydrophobicity.

Interestingly, while piperine presented similar CHI values under both tested pH, different CHI values were obtained for compounds **2** and **3**. Indeed, the retention times (t_R) of compounds **2** and **3** at pH 7.4 were higher than the obtained at pH 2.3. Since compounds **2** and **3** do not contain ionizable groups, the variations observed may result from differences in the ionic strength of the eluents used in CHI determinations.

The lipophilicity of TPP cations **2-5** may influence their mitochondrial uptake and their metabolic toxicity. After replotting the CHI values at pH 2.3 against the mitochondrial accumulation ratio, a biphasic behavior was observed (**Figure 8**). Mitochondrial uptake increased until an optimal lipophilicity was attained, and then decreased with increasing lipophilicity. Moreover, the resazurin reduction of neuroblastoma cells after treatment with compounds **2-5** at 100 µM was inversely correlated with the CHI values at pH 2.3 (**Figure 8**). In fact, more lipophilic TPP cations may have a negative effect on respiratory chain activity and on mitochondrial membrane potential [44], thus being associated with higher toxicity. These trends demonstrate the interest of modulating the lipophilicity of TPP conjugates to obtain optimal mitochondrial accumulation and minimal cytotoxic effects.

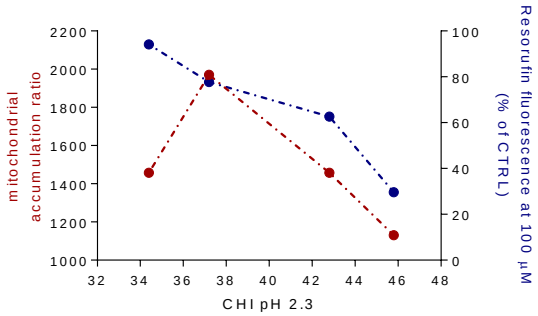


Figure 14. Plots constructed from the CHI values at pH 2.3 against mitochondrial accumulation ratio (red) and resazurin fluorescence (blue).

We also calculated several physicochemical properties to predict the ability of the compounds **2-5** to attain the central nervous system (CNS). These include molecular weight (MW), topological polar surface area (TPSA in Å), number of hydrogen acceptors (HBA), number of hydrogen donors (HBD) and number of rotatable bonds (RB) (**Table 5**). Among the estimated parameters, MW and RB values of compounds **2-5** exceeded the limits suggested for CNS-active drugs (MW < 500 $g.mol^{-1}$; RB < 8). Nonetheless, despite the high volume, several lipophilic TPP cations were taken up by mitochondria within several tissues (brain, heart, liver) following long-term oral administration [45]. The other predicted physicochemical properties (TPSA, HBA, HBD) fell within the proposed limits.

Table 10. Predicted drug-like properties of mitochondria-targeted compounds **2-5**.

Compound	MW[a] /($g.mol^{-1}$)	TPSA[a]	HBA[a]	HBD[a]	RB[a]	LogBB[a]
1	285.3	38.77	3	0	4	-0.185
2	614.5	47.56	4	1	12	-0.314
3	642.6	47.56	4	1	14	-0.293
4	602.5	69.56	4	3	12	-0.784
5	630.6	69.56	4	3	14	-0.771
CNS^+ drugs	< 500[46]	< 90[46]	< 7[47]	< 3[47]	< 8[47]	≥ -1 [48]

[a] Properties predicted using the Stardrop software. MW: molecular weight; TPSA: topological polar surface area; HBA: number of H-bond acceptor atoms; HBD: number of H-bond donor atoms; RB: number of rotatable bonds; logBB: logarithm of the ratio of the concentration of a drug in the brain and in the blood.

Another parameter used to predict the blood-brain barrier permeability is the logarithm of the ratio of the concentration of the compound in the brain and in the blood (LogBB). Molecules with LogBB < -1 are poorly distributed in the brain and are unlikely to act as CNS drugs [48]. Compounds **2-5** displayed calculated logBB values above -1, suggesting that these compounds may attain the CNS.

5. Conclusion

In this work, we successfully synthesized four piperine-based mitochondria-targeted agents that differ in the length of the alkyl spacer and the substitution pattern of the aromatic ring. Then, we explored their antioxidant activity and their effect on enzymes involved in acetylcholine (*ee*AChE and *eq*BChE) and dopamine (*h*MAO-A and *h*MAO-B) breakdown. Compounds **2-5** displayed remarkable *eq*BChE inhibitory activity, presenting IC_{50} values within the nanomolar range. The results obtained in kinetic experiments were consistent with a mixed-type inhibition mechanism. These compounds also acted as moderate *ee*AChE and *h*MAOs inhibitors. Catechol derivatives **4** and **5** were able to scavenge peroxyl radicals. Moreover, they presented lower E_p values than other catechol-based lipophilic TPP conjugates, while preserving the reversible oxidative behavior. Compounds **2-5** were well-tolerated by differentiated SH-SY5Y cells at concentrations up to 12.5 µM. The metabolic toxicity observed at higher concentrations may result from the induction of intracellular oxidative stress, which was particularly noticeable with compounds containing longer alkyl linkers. All piperine-based lipophilic TPP cations accumulated within the matrix of energized MLM. Benzodioxole derivatives (compounds **2** and **3**) significantly decreased the mitochondrial spare respiratory capacity in neuroblastoma cells, which is associated with a reduced ability of cells to survive under oxidative stress conditions. On the other hand, catechol derivatives (compounds **4** and **5**) did not significantly affect mitochondrial parameters.

Compound **5** stands out as the best mitochondria-targeted agent of the series. In addition to the dual ChE/MAO inhibition profile, compound **5** is endowed with antioxidant activity and presented the highest mitochondrial accumulation ratio in isolated LM. Therefore, compound **5** may prevent the formation of RS in mitochondria and restore decreased dopamine and acetylcholine levels. Compound **5** also present a safe cytotoxicity profile in neuroblastoma cells (< 25 µM) and favorable drug-like properties.

Overall, the data obtained represent an advance towards the development of neuroprotective agents able to tackle neurotransmitter depletion and mitochondria-associated oxidative stress.

6. Experimental section

6.1. Chemistry. General methods and apparatus.

Piperine, sodium hydroxide (NaOH), *N*-(4-bromobutyl)phthalimide, *N*-(6-bromohexyl)phthalimide, triphenylphosphine (TPP), butylamine, piperine, sodium hydroxide (NaOH), triethylamine (Et_3N), ethyl chloroformate, and boron tribromide dimethyl sulfide complex ($BBr_3.S(CH_3)_2$) were purchased from Sigma Aldrich, Alfa-Aesar or TCI. All other reagents and solvents were pro analysis grade and were acquired from Carlo Erba Reagents and Scharlab and were used without additional purification.

The monitoring of reactions progress was performed by thin layer chromatography (TLC) on precoated silica gel 60 F254 acquired from Merck (Darmstad, Germany). TLC spots were visualized under UV detection (254 nm and 365 nm). Some crude products were purified by flash column chromatography. Flash column chromatography was carried out on silica gel 60 Å acquired from Carlo-Erba Reactifs (SDS, France). The fractions with the desired compound were gathered and concentrated *in vacuo*. The solvents were evaporated using a Buchi Rotavapor.

^1H and ^{13}C NMR and DEPT135 data were acquired, at room temperature, on a Brüker AMX 300 spectrometer operating at 400 and 100 MHz, respectively. The solvents used in NMR experiments included

$CDCl_3$-d_1, MeOD-d_4 and DMSO-d_6. The chemical shifts are expressed in δ (ppm) values relative to tetramethylsilane (TMS) as internal reference and coupling constants (*J*) are given in Hz. Electrospray ionization mass spectra (ESI-MS) were carried out on a Bruker Microtof apparatus or on a LTQ Orbitrap™ XL hybrid mass spectrometer (Thermo Fischer Scientific, Bremen, Germany) controlled by *LTQ Tune Plus 2.5.5* and *Xcalibur 2.1.0*. The data are reported as m/z (% of relative intensity of the most important fragments).

6.1.1. Synthesis of piperine-based mitochondria-targeted agents

6.1.1.1. General procedure for the obtention of phtalimidylalkylltriphenylphosphonium salts. A mixture containing the appropriate *N*-(bromoalkyl)phthalimide (1 mmol) and triphenylphosphine (1.2 mmol) was thoroughly mixed under argon atmosphere and heated at 130 ºC, protected from the light. The solid obtained was recrystallized from dichloromethane/diethyl ether. The procedure was adapted from Cheng *et al.* 2016 [49] with some modifications.

(4-(1,3-dioxoisoindolin-2-yl)butyl)triphenylphosphonium bromide (8). Compound **8** was obtained in the following conditions: compound **6** (1.00 g, 3.56 mmol), triphenylphosphine (1.06 g, 4.03 mmol). The mixture was heated at 130 ºC for 10 h, protected from the light. η = 97 %. ^{1}H NMR ($CDCl_3$-d_1): δ (ppm) = 1.62 (*m*, 2H, $N(CH_2)_2C\underline{H}_2CH_2$), 2.15 (*m*, 2H, $NCH_2C\underline{H}_2(CH_2)_2$), 3.77 (*t*, *J* = 6.3 Hz, 2H, $N(CH_2)_3C\underline{H}_2$), 4.01 (*m*, 2H, $NC\underline{H}_2(CH_2)_3$), 7.71 (*m*, 13 H, PPh_3, H5, H6, H7, H8), 7.85 (*m*, 6H, PPh_3). ^{13}C NMR ($CDCl_3$-d_1): δ (ppm) = 19.5 (*d*, *J* = 3.9 Hz, $NCH_2\underline{C}H_2(CH_2)_2$), 21.7 (*d*, *J* = 50.4 Hz, $N(CH_2)_3\underline{C}H_2$), 28.6 (*d*, *J* = 16.8 Hz, $N(CH_2)_2\underline{C}H_2CH_2$), 36.4 ($N\underline{C}H_2(CH_2)_3$), 118.3 (*d*, *J* = 86.0 Hz, C1'), 123.2 (C5, C8), 130.4 (*d*, *J* = 12.5 Hz, C3', C5'), 131.9 (C4, C9), 133.8 (*d*, *J* = 9.9 Hz, C2', C6'), 134.1 (C6, C7), 135.0 (*d*, *J* = 2.9 Hz, C4'), 168.4 (C1, C3). ESI/MS m/z (%): 464 (M^+-Br, 100).

(6-(1,3-dioxoisoindolin-2-yl)hexyl)triphenylphosphonium bromide (9). Compound **9** was obtained in the following conditions: compound **7** (0.50 g, 1.61 mmol), triphenylphosphine (0.63 g, 2.42 mmol). The mixture was heated at 130 ºC for 1.5 h, protected from the light. η = 87 %. ^{1}H NMR ($CDCl_3$-d_1): δ (ppm) = 1.32 (*m*, 2H, $NCH_2C\underline{H}_2(CH_2)_4$), 1.61 (*m*, 4H, $N(CH_2)_2C\underline{H}_2(CH_2)_3$, $N(CH_2)_3C\underline{H}_2(CH_2)_2$), 1.72 (*m*, 2H, $N(CH_2)_4C\underline{H}_2CH_2$)), 3.62 (*t*, *J* = 7.0 Hz, 2H, $NC\underline{H}_2(CH_2)_5$), 3.87 (*m*, 2H, $N(CH_2)_5C\underline{H}_2$), 7.77 (*m*, 19H, PPh_3, H5, H6, H7, H8). ^{13}C NMR ($CDCl_3$-d_1): δ (ppm) = 22.1 (*d*, *J* = 4.9 Hz, $N(CH_2)_3\underline{C}H_2(CH_2)_2$), 22.8 (*d*, *J* = 49.1 Hz, $N(CH_2)_5\underline{C}H_2$), 26.5 ($N(CH_2)_2\underline{C}H_2(CH_2)_3$), 28.2 ($NCH_2\underline{C}H_2(CH_2)_4$), 29.8 (*d*, *J* = 15.7 Hz, $N(CH_2)_4\underline{C}H_2CH_2$), 37.8 ($NH\underline{C}H_2(CH_2)_5$), 118.5 (*d*, *J* = 85.8 Hz, C1'), 123.2 (C5, C8), 130.5 (*d*, *J* = 12.5 Hz, C3', C5'), 132.2 (C4, C9), 133.8 (*d*, *J* = 10.1 Hz, C2', C6'), 133.9 (C6, C7), 134.9 (*d*, *J* = 2.9 Hz, C4'), 168.4 (C1, C3). ESI/MS m/z (%): 492 (M^+-Br, 100).

6.1.1.2. General procedure for the obtention of aminoalkylltriphenylphosphonium salts. In a round bottom flask with compounds **8** and **9** (1 mmol) dissolved in ethanol, butylamine (10-24 mmol) was added. The mixture was refluxed until the reaction was complete. Then, the solvent was partially concentrated, and water was added. The solid obtained was filtered off and the filtrate was extracted with dichloromethane. Then, the aqueous phase was concentrated. The material was used without further purification in the next step. The procedure was adapted from Cheng *et al.*[49] 2016 with some modifications.

(4-aminobutyl)triphenylphosphonium bromide (10). Compound **10** was obtained in the following conditions: compound **8** (0.93 g, 1.71 mmol), ethanol (10 mL), butylamine (2.2 mL, 40.6 mmol). The mixture was refluxed for 10 h. η = 86 %. ^{1}H NMR (MeOD-*d*$_4$): δ (ppm) = 1.74 (*m*, 4H, $NH_2CH_2C\underline{H}_2(CH_2)_2$, $NH_2(CH_2)_2C\underline{H}_2CH_2$), 2.73 (*t, J* = 6.8 Hz, 2H, $NH_2C\underline{H}_2(CH_2)_3$), 3.44 (*m*, 2H, $NH_2(CH_2)_3C\underline{H}_2$), 7.77 (*m*, 15H, PPh_3). ^{13}C NMR (MeOD-*d*$_4$): δ (ppm) = <u>19.7</u> (*d, J* = 4.2 Hz, $NH_2CH_2\underline{C}H_2(CH_2)_2$), <u>21.3</u> (*d, J* = 51.5 Hz, $NH_2(CH_2)_3\underline{C}H_2$), <u>31.8</u> (*d, J* = 16.8 Hz, $NH_2(CH_2)_2\underline{C}H_2CH_2$), <u>39.8</u> ($NH_2\underline{C}H_2(CH_2)_3$), 118.5 (*d, J* = 86.6 Hz, C1'), <u>130.2</u> (*d, J* = 12.6 Hz, C3', C5'), <u>133.5</u> (*d, J* = 10.1 Hz, C2', C6'), <u>134.9</u> (*d, J* = 3.1 Hz, C4'). ESI/MS m/z (%): 334 (M^+-Br, 100).

(6-aminohexyl)triphenylphosphonium bromide (11). Compound **11** was obtained in the following conditions: compound **9** (2.00 g, 3.49 mmol), ethanol (24 mL), butylamine (3.5 mL, 34.9 mmol). The mixture was refluxed for 1.5 h. η = 80 %. ^{1}H NMR (MeOD-*d*$_4$): δ (ppm) = 1.44 (*m*, 2H, $NHCH_2C\underline{H}_2(CH_2)_4$), 1.68 (*m*, 6H, $NH_2(CH_2)_2C\underline{H}_2(CH_2)_3$, $NH_2(CH_2)_3C\underline{H}_2(CH_2)_2$, $NH_2(CH_2)_4C\underline{H}_2CH_2$)), 2.92 (*t, J* = 6.8 Hz, 2H, $NH_2C\underline{H}_2(CH_2)_5$), 3.42 (*m*, 2H, $NH_2(CH_2)_5C\underline{H}_2$), 7.84 (*m*, 15H, PPh_3). ^{13}C NMR (MeOD-*d*$_4$): δ (ppm) = <u>21.3</u> (*d, J* = 51.4 Hz, $NH_2(CH_2)_5\underline{C}H_2$), <u>22.0</u> (*d, J* = 4.3 Hz, $NH_2(CH_2)_3\underline{C}H_2(CH_2)_2$), <u>25.3</u> ($NH_2(CH_2)_2\underline{C}H_2(CH_2)_3$), <u>26.9</u> ($NH_2CH_2\underline{C}H_2(CH_2)_4$), <u>29.6</u> (*d, J* = 16.6 Hz, $NH(CH_2)_4\underline{C}H_2CH_2$), <u>39.1</u> ($NH\underline{C}H_2(CH_2)_5$), 118.5 (*d, J* = 86.4 Hz, C1'), <u>130.2</u> (*d, J* = 12.6 Hz, C3', C5'), <u>133.4</u> (*d, J* = 9.9 Hz, C2', C6'), <u>134.9</u> (*d, J* = 3.0 Hz, C4'). ESI/MS m/z (%): 362 (M^+-Br, 100).

6.1.1.3. Synthesis of (*2E,4E*)-5-(benzo[d][1,3]dioxol-5-yl)penta-2,4-dienoic acid (13). Synthesis and structural analysis described in literature [33].

6.1.1.4. Piperic acid amidation. Piperic acid (compound 2, 1 mmol) was dissolved in dichloromethane (2.5 mL) and Et_3N (2 mmol). To the stirred solution kept in an ice bath, ethyl chloroformate (2 mmol) was added dropwise. After stirring for 2 h at room temperature, the mixture was cooled again in an ice bath and the appropriate amine (2 mmol) was slowly added. The reaction was stirred overnight at room temperature. Upon completion, dichloromethane (30 mL) was added. The mixture was extracted with HBr 1 M (3 x 10 mL) and washed with water. The combined organic phases were dried over anhydrous Na_2SO_4, filtered and concentrated. The residue was purified by flash column chromatography (silica, dichloromethane/methanol (9:1)) and recrystallized from methanol/water. The procedure was adapted from Teixeira *et al.[20]* with some modifications.

(4-((*2E,4E*)-5-(benzo[*d*][1,3]dioxol-5-yl)penta-2,4-dienamido)butyl)triphenylphosphonium bromide (2). Compound **2** was obtained in the following conditions: compound **12** (0.42 g, 1.93 mmol), dichloromethane (8 mL), Et_3N (700 µL, 3.65 mmol), ethyl chloroformate (362 µL, 4.18 mmol), compound **10** (1.09 g, 2.46 mmol). η = 44 %. ^{1}H NMR ($CDCl_3$-d_1): δ (ppm) = 1.76 (*m*, 2H, $NHCH_2C\underline{H}_2(CH_2)_2$), 1.98 (*m*, 2H, $NH(CH_2)_2C\underline{H}_2CH_2$), 3.47 (*dd*, *J* = 11.7 Hz, 5.8 Hz, 2H, $NHC\underline{H}_2(CH_2)_3$), 3.65 (*m*, 2H, $NH(CH_2)_3C\underline{H}_2$), 5.98 (*s*, 2H, $OC\underline{H}_2O$), 6.43 (*d*, *J* = 15.0 Hz, 1H, Hα), 6.77 (*m*, 3H, H5, Hγ, Hδ), 6.90 (*dd*, *J* = 1.6 Hz, 8.2 Hz, 1H, H6), 6.99 (*d*, *J* = 1.6 Hz, 1H, H2), 7.31 (*dd*, *J* = 10.4 Hz, 15.0 Hz, 1H, Hβ), 7.74 (*m*, 15 H, PPh_3), 8.55 (*t*, *J* = 5.6 Hz, 1H, $CON\underline{H}$). ^{13}C NMR ($CDCl_3$-d_1): δ (ppm) = 19.5 (*d*, *J* = 4.0 Hz, $NHCH_2\underline{C}H_2(CH_2)_2$), 22.4 (*d*, *J* = 50.4 Hz, $NH(CH_2)_3\underline{C}H_2$), 28.7 (*d*, *J* = 16.6 Hz, $NH(CH_2)_2\underline{C}H_2CH_2$), 37.4 ($NH\underline{C}H_2(CH_2)_3$), 101.2 ($O\underline{C}H_2O$), 105.9 (C2), 108.4 (C5), 118.2 (*d*, *J* = 86.0 Hz, C1'), 122.2 (Cα), 125.0 (C6), 125.7 (Cγ), 130.5 (*d*, *J* = 12.5 Hz, C3', C5'), 131.3 (C1), 133.7 (*d*, *J* = 10.0 Hz, C2', C6'), 135.1 (*d*, *J* = 2.9 Hz, C4'), 137.5 (Cδ), 139.5 (Cβ), 147.9 (C3), 148.2 (C4), 167.3 (CONH). ESI/MS m/z (%): 534 (M^+-Br, 100).

(6-((*2E,4E*)-5-(benzo[*d*][1,3]dioxol-5-yl)penta-2,4-dienamido)hexyl)triphenylphosphonium bromide (3). Compound **3** was obtained in the following conditions: compound **12** (0.76 g, 3.48 mmol), dichloromethane (20 mL), Et_3N (1 mL, 7.12 mmol), ethyl chloroformate (665 µL, 6.96 mmol), compound **11** (2.0023 g, 4.52 mmol). η = 46 %. ^{1}H NMR ($CDCl_3$-d_1): δ (ppm) = 1.60 (*m*, 8H, $NHCH_2C\underline{H}_2(CH_2)_4$, $NH(CH_2)_2C\underline{H}_2(CH_2)_3$, $NH(CH_2)_3C\underline{H}_2(CH_2)_2$, $NH(CH_2)_4C\underline{H}_2CH_2$), 3.37 (*m*, 2H, $NHC\underline{H}_2(CH_2)_5$), 3.68 (*m*, 2H, $NH(CH_2)_5C\underline{H}_2$), 5.97 (*s*, 2H, $OC\underline{H}_2O$), 6.61 (*d*, *J* = 15.0 Hz, 1H, Hα), 6.67 (*d*, *J* = 15.6 Hz, 1H, Hδ), 6.76 (*m*, 2H, H5, Hγ), 6.86 (*dd*, *J* = 1.6 Hz, 8.2 Hz, 1H, H6), 6.95 (*d*, *J* = 1.6 Hz, 1H, H2), 7.34 (*dd*, *J* = 11.6 Hz, 15.0 Hz, 1H, Hβ), 7.71 (*m*, 6H, PPh_3), 7.82 (*m*, 9H, PPh_3), 8.24 (*t*, *J* = 4.9 Hz, 1H, $CON\underline{H}$). ^{13}C NMR ($CDCl_3$-d_1): δ (ppm) = 22.1 (*d*, *J* = 4.4 Hz, $NH(CH_2)_3\underline{C}H_2(CH_2)_2$), 22.3 (*d*, *J* = 50.2 Hz, $NH(CH_2)_5\underline{C}H_2$), 25.5 ($NH(CH_2)_2\underline{C}H_2(CH_2)_3$), 28.4 ($NHCH_2\underline{C}H_2(CH_2)_4$), 29.2 (*d*, *J* = 16.2 Hz, $NH(CH_2)_4\underline{C}H_2CH_2$), 38.7 ($NH\underline{C}H_2(CH_2)_5$), 101.2 ($O\underline{C}H_2O$), 105.8 (C2), 108.4 (C5), 118.3 (*d*, *J* = 85.8 Hz, C1'), 122.2 (Cα), 125.2 (C6), 126.0 (Cγ), 130.5 (*d*, *J* = 12.5 Hz, C3', C5'), 131.4 (C1), 133.6 (*d*, *J* = 10.0 Hz, C2', C6'), 135.1 (*d*, *J* = 2.9 Hz, C4'), 137.3 (Cδ), 139.6 (Cβ), 147.8 (C3), 148.1 (C4), 167.1 (CONH). ESI/MS m/z (%): 562 (M^+-Br, 100).

6.1.1.5. Demethylenation reaction. In a round bottom flask, compounds **2** and **3** (1 mmol) were maintained under argon atmosphere. Then, the compounds were dissolved in anhydrous dichloromethane and $BBr_3.S(CH_3)_2$ (4 mmol) was added. The mixture was protected from the light and refluxed for 6 h. Upon completion, water was added to destroy BBr_3 and separated from the solid formed. The crude product was purified by flash column chromatography (silica, dichloromethane/methanol (95:5)). The procedure was adapted from Williard *et al.*[50] 1980 with some modifications.

(4-((*2E,4E*)-5-(3,4-dihydroxyphenyl)penta-2,4-dienamido)butyl)triphenylphosphonium bromide (4). Compound **4** was obtained in the following conditions: compound **2** (1.28 g, 2.10 mmol), dichloromethane (35 mL), $BBr_3.S(CH_3)_2$ (2.85 g, 9.1 mmol). η = 29 %. ^{1}H NMR (DMSO-d_6): 1.55 (*m*, 2H, $NH(CH_2)_2C\underline{H}_2CH_2$), 1.64 (*m*, 2H, $NHCH_2C\underline{H}_2(CH_2)_2$), 3.77 (*dd*, *J* = 3.7 Hz, 7.8 Hz, 2H, $NH(CH_2)_3C\underline{H}_2$), 4.01 (*m*, 2H, $NHC\underline{H}_2(CH_2)_3$), 5.98 (*d*, *J* = 15.0 Hz, 1H, Hα), 6.74 (*m*, 3H, Hδ, H5, Hγ), 6.85 (*dd*, *J* = 2.0 Hz, 8.2 Hz, 1H, H6), 6.95 (*d*, *J* = 1.9 Hz, 1H, H2), 7.12 (*dd*, *J* = 10.2 Hz, 15.0 Hz, 1H, Hβ), 7.78 (*m*, 12H, PPh_3), 7.89 (*m*, 3H, PPh_3), 8.00 (*t*, *J* = 5.4 Hz, 1H, CON<u>H</u>), 9.11 (*s*, 2H, 2×O<u>H</u>). ^{13}C NMR (DMSO-d_6): δ (ppm) = <u>19.1</u> (*d*, *J* = 3.9 Hz, $NHCH_2\underline{C}H_2(CH_2)_2$), <u>19.8</u> (*d*, *J* = 50.1 Hz, $NH(CH_2)_3\underline{C}H_2$), <u>29.8</u> (*d*, *J* = 16.9 Hz, $NH(CH_2)_2\underline{C}H_2CH_2$), <u>37.1</u> ($N\underline{C}H_2(CH_2)_3$), <u>113.7</u> (C2), <u>115.6</u> (C5), 118.4 (*d*, *J* = 85.7 Hz, C1'), <u>119.3</u> (Cα), <u>123.2</u> (C6), <u>123.4</u> (Cγ), 127.8 (C1), <u>130.2</u> (*d*, *J* = 12.4 Hz, C3', C5'), <u>133.5</u> (*d*, *J* = 10.1 Hz, C2', C6'), <u>134.8</u> (*d*, *J* = 2.5 Hz, C4'), <u>138.7</u> (Cδ), <u>139.6</u> (Cβ), 145.4 (C3), 146.5 (C4), 165.4 (<u>C</u>ONH). ESI/MS m/z (%): 522 (M^+-Br, 100).

(6-((*2E,4E*)-5-(3,4-dihydroxyphenyl)penta-2,4-dienamido)hexyl)triphenylphosphonium bromide (5). Compound **5** was obtained in the following conditions: compound **3** (1.11 g, 1.72 mmol), dichloromethane (30 mL), $BBr_3.S(CH_3)_2$ (2.35 g, 7.52 mmol). η = 44 %. ^{1}H NMR (DMSO-d_6): δ (ppm) = 1.28 (*m*, 2H, $NH(CH_2)_2C\underline{H}_2(CH_2)_3$), 1.38 (*m*, 2H, $NH(CH_2)_3C\underline{H}_2(CH_2)_2$), 1.49 (*m*, 4H, $NHCH_2C\underline{H}_2(CH_2)_4$, $NH(CH_2)_4C\underline{H}_2CH_2$), 3.11 (*m*, 2H, $NHC\underline{H}_2(CH_2)_5$), 3.58 (*m*, 2H, $NH(CH_2)_5C\underline{H}_2$), 6.03 (*d*, *J* = 15.0 Hz, 1H, Hα), 6.71 (*m*, 3H, Hδ, H5, Hγ), 6.83 (*dd*, *J* = 2.0 Hz, 8.3 Hz, 1H, H6), 6.94 (*d*, *J* = 2.0 Hz, 1H, H2), 7.11 (*dd*, *J* = 9.8 Hz, 15.1 Hz, 1H, Hβ), 7.79 (*m*, 12H, PPh_3), 7.90 (*m*, 3H, PPh_3), 7.94 (*t*, *J* = 5.6 Hz, 1H, CON<u>H</u>), 8.98 (*s*, 1H, O<u>H</u>), 9.27 (*s*, 1H, O<u>H</u>). ^{13}C NMR (DMSO-d_6): δ (ppm) = <u>20.1</u> (*d*, *J* = 49.9 Hz, $NH(CH_2)_5\underline{C}H_2$), <u>21.6</u> (*d*, *J* = 4.3 Hz, $NH(CH_2)_3\underline{C}H_2(CH_2)_2$), <u>25.5</u> ($NH(CH_2)_2\underline{C}H_2(CH_2)_3$), <u>28.8</u> ($NHCH_2\underline{C}H_2(CH_2)_4$), <u>29.4</u> (*d*, *J* = 16.7 Hz, $NH(CH_2)_4\underline{C}H_2CH_2$), <u>38.3</u> ($NH\underline{C}H_2(CH_2)_5$), <u>113.6</u> (C2), <u>115.6</u> (C5), 118.5 (*d*, *J* = 85.6 Hz, C1'), <u>119.2</u> (Cα), <u>123.5</u> (C6), <u>123.5</u> (Cγ), 127.8 (C1), <u>130.1</u> (*d*, *J* = 12.4 Hz, C3', C5'), <u>133.5</u> (*d*, *J* = 10.1 Hz, C2', C6'), <u>134.8</u> (*d*, *J* = 2.8 Hz, C4'), <u>138.4</u> (Cδ), <u>139.3</u> (Cβ), 145.4 (C3), 146.4 (C4), 165.1 (<u>C</u>ONH). ESI/MS m/z (%): 550 (M^+-Br, 100).

6.2. Enzymatic assays

6.2.1. Acetylcholinesterase and butyrylcholinesterase

6.2.1.1. Evaluation of cholinesterases inhibitory activity

The AChE and BChE inhibitory activities of the compounds under study were studied following the Ellman's method.[28, 29] Eel acetylcholinesterase (*ee*AChE, E.C. 3.1.1.7, from *Electrophorus electricus*), equine butyrylcholinesterase (*eq*BuChE, E.C. 3.1.1.8, from equine serum), DTNB, acetylthiocholine iodide (ATCI), and butylthiocholine iodide (BTCI) were purchased from Sigma Aldrich. Enzyme and DTNB solutions were prepared in sodium phosphate buffered conditions (50 mM, pH = 7.4). Substrate solutions (ATCI or BCTI) were prepared in deionized water (conductivity < 0.1 $\mu S.cm^{-1}$).

Briefly, a mixture containing sodium phosphate buffer, enzyme (final concentration: *ee*AChE 0.05 U/mL and *ee*BChE 0.05 U/mL), DTNB (final concentration: 400 µM) and the test compounds/reference inhibitors were preincubated for 5 minutes at 30 ºC in a 96-well microplate (BRANDplates, pureGradeTM, BRAND GMBH, Wertheim, Germany). In control experiments, sodium phosphate buffer was used instead of the compound solution. Then, the substrate solution (final concentration: ATCI 150 µM; BTCI 400 µM) was

added, and the absorbance values at 412 nm were recorded minutely for 5 minutes at 30 ºC in a microplate reader (BioTek Synergy HT from BioTek Instruments, Winooski, VT, USA). The rates of the substrate enzymatic hydrolysis were determined, normalized and plotted against the respective inhibitor concentration. IC_{50} values were obtained from de dose-response curves and were expressed as mean ± standard deviation. IC_{50} values were determined in at least three independent experiments, each performed at least in triplicates.

6.2.1.2. Evaluation of equine butyrylcholinesterase kinetics.

To determine the steady-state kinetic parameters (K_m, Michaelis-Menten constant, and V_{max}, maximum reaction rate), the enzymatic activity of *eq*BChE was evaluated, under the experimental conditions described above, in the presence of different substrate concentrations (0.063 – 1.3 mM). In our experimental conditions, *eq*BChE displayed a K_m = 217±21 µM and V_{max} = 0.143±0.002 ΔAbs.min^{-1} (n = 3).

6.2.1.3. Evaluation of equine butyrylcholinesterase-inhibitor kinetics.

To study the mechanisms of BChE inhibition of donepezil and compounds **3** and **5**, substrate-dependent kinetic experiments were performed. The catalytic rates of BChE were measured at seven different concentrations of BTCI (0.063 – 1.3 mM) in the absence or the presence of the three concentrations of the selected inhibitors. The results are presented as double reciprocal Lineweaver-Burk plots (1/V vs 1/[S]). The kinetic data (K_m and V_{max}) were estimated employing the Michaelis-Menten equation. To describe a mixed-type inhibition, the Lineweaver-Burk equation can be written as:

$$\frac{1}{v} = \frac{K_m}{V_{max}}\left(\frac{1}{[S]}\right)\left(1+\frac{[I]}{K_i}\right)+\frac{1}{V_{max}}\left(1+\frac{[I]}{K_i'}\right) \quad \textbf{(Equation 1)}$$

The inhibition constants were determined by constructing secondary plots from the slope and the y-axis intercepts of each Lineweaver-Burk plot versus the inhibitor concentration.

$$\text{slope} = \frac{K_m}{V_{max}}+\frac{K_m[I]}{V_{max}K_i} \quad \textbf{(Equation 2)}$$

$$\text{y-axis intercept} = \frac{1}{V_{max}}+\frac{[I]}{V_{max}K_i'} \quad \textbf{(Equation 3)}$$

In equations (2) and (3), K_i and K_i' represent the dissociation constants of the enzyme-inhibitor and the enzyme-inhibitor-substrate complexes, respectively.

The enzymatic reactions and measurements were performed using the same experimental conditions described above (n = 3). Linear regression analysis was performed using GraphPad PRISM version 6 for Windows (GraphPad Software®, San Diego, CA, USA).

6.2.2. Evaluation of human monoamine oxidase inhibitory activity

The inhibitory activity of TPP cations on *h*MAO-A and *h*MAO-B was studied using an experimental protocol described elsewhere [33, 34]. The *h*MAO inhibitory outline was assessed in microsomal MAO isoforms prepared from insect cells (BTI-TN-5B1-4) infected with recombinant baculovirus containing cDNA inserts for *h*MAO-A or *h*MAO-B (Sigma Aldrich) by measuring the enzymatic conversion rates of kynuramine into 4-hydroxyquinoline. The appropriate amounts of *h*MAO-A and *h*MAO-B were adjusted to obtain, in our

experimental conditions, the same maximum velocity (V_{max} = 50 pmol.min^{-1}) for both isoforms (*h*MAO-A: 3 ng.µL^{-1}; *h*MAO-B: 12 ng.µL^{-1}). All assays were performed under sodium phosphate buffered conditions (50 mM, pH = 7.4).

The compounds under study and reference inhibitors were pre-incubated at 37 ºC for 10 min in the presence of kynuramine (K_m *h*MAO-A = 20 µM; K_m *h*MAO-B = 20 µM; final concentration: 2×K_m) in 96-well microplates (BRANDplates, pureGrade™, BRAND GMBH, Wertheim, Germany). Then, the reaction was started with the addition of *h*MAO-A or *h*MAO-B. Initial velocities were determined spectrophotometrically in a microplate reader (BioTek Synergy HT from BioTek Instruments, Winooski, VT, USA) at 37 °C by measuring the formation of 4-hydroxyquinoline at 316 nm, over a period of at least 30 minutes (interval of 1 minute). Data were analysed using GraphPad PRISM version 6 for Windows (GraphPad Software®, San Diego, CA, USA). The initial velocities, obtained from the linear phase of product formation, were normalized and plotted against the respective inhibitor concentration. IC_{50} values were obtained from dose-response curves and were expressed as mean ± standard deviation. IC_{50} values were determined from at least three independent experiments, each performed in triplicate.

6.3. Oxygen radical absorbance capacity (ORAC-FL) assay

The ORAC-FL analyses were performed on a multiplate reader (BioTek Synergy HT from BioTek Instruments, Winooski, VT, USA) using black polystyrene 96-well plates. Fluorescence was measured from the top, at an excitation wavelength of 485/20 nm and an emission at 528/20 nm. The plate reader was controlled by Gen5 software. 2,2'-Azobis-(amidinopropane) dihydrochloride (AAPH), (±)-6-hydroxy-2,5,7,8-tetramethylchromane-2-carboxylic acid (trolox) and fluorescein (FL) were purchased from Sigma-Aldrich. The general procedure was adapted from the literature [51, 52], with some modifications.

The reaction was carried out in 75 mM of sodium phosphate buffer solution (pH = 7.4) at a final volume of 200 µL. Stock solutions of FL (5 mM) and antioxidants (5 mM) were prepared in ethanol due to their low solubility in buffer at high concentrations. Then, they were diluted in sodium phosphate buffer solution (pH = 7.4). The range of antioxidant concentrations was empirically selected to obtain a good separation between the fluorescence curves. The test compounds (final concentrations range of 0.1-2 µM) and fluorescein (40 nM, final concentration) were placed in each well and pre-incubated for 15 min at 37 ºC before the addition of AAPH (final concentration 18 mM). The microplate was immediately placed in the reader and automatically shaken prior to each reading. The fluorescence was measured minutely for 120 min. A control assay with fluorescein, AAPH and buffer (instead of the antioxidant solution) was performed for each assay. Trolox was also included in each assay as standard antioxidant in a final concentration range of 2-8 µM. All reaction mixtures were prepared in triplicate and at least three independent experiments were performed for each test compound. The fluorescence decay curves were normalized by the maximum value of fluorescence, and the areas under the curves (AUC) were determined according to the following **Equation 1**.

$$AUC = 1 + \sum_{i=1}^{i=120} \frac{f_i}{f_0} = 1 + \frac{f_1}{f_0} + \frac{f_2}{f_0} + \frac{f_3}{f_0} + \ldots + \frac{f_{120}}{f_0} \quad \textbf{(Equation 1)}$$

where f_0 = initial fluorescence reading at 0 min and f_i = fluorescence reading at time i. The net AUC is obtained by subtracting the AUC of the blank from that of a sample. The inhibition capacity, expressed as the relative Trolox equivalent ORAC values, was quantified employing the **Equation 2**.

$$\text{relative ORAC value} = \frac{AUC_{antioxidant}\text{-}AUC_{control}}{AUC_{trolox}\text{-}AUC_{control}} \times \frac{[Trolox]}{[antioxidant]} \quad \textbf{(Equation 2)}$$

where $AUC_{control}$ = area under the curve of control; $AUC_{antioxidant}$ = area under the curve of the test compound; AUC_{trolox} = area under the curve of Trolox (standard); [trolox] = Trolox concentration; and [antioxidant] = antioxidant concentration.

6.4. Electrochemical measurements

Voltammetric studies were carried out using an Autolab PGSTAT 12 potentiostat/galvanostat (Metrohm-Autolab, Netherlands) and one compartment glass electrochemical cell. The voltammetric data was acquired at room temperature using a three-electrode system: a glassy carbon working electrode (GCE) (d = 2 mm), a platinum wire counter electrode and an Ag/AgCl saturated KCl reference electrode (Metrohm, Switzerland). The working electrode was polished manually with an aqueous slurry of alumina powder (BDH Chemicals, VWR, USA) on a microcloth pad and rinsed with water before use. A Crison pH-meter with glass electrode was used for the pH measurements (Crison, Barcelona, Spain).

Voltammetric measurements were performed as described elsewhere [53]. Test solutions were prepared directly in the electrochemical cell, by dilution of ethanolic solutions of the compounds under study (10 mM, 100 μL) in the supporting electrolyte (10 mL) to obtain a final concentration of 100 μM. The scan rates used in differential pulse voltammetry (DPV) and cyclic voltammetry (CV) were 5 $mV.s^{-1}$ and 50 $mV.s^{-1}$, respectively.

6.5. Measurement of mitochondrial accumulation

6.5.1. Animals

Male C57BL/6J mouse (22 weeks old) were housed in our accredited animal colony (Biotech Research Center, Center for Neuroscience and Cell Biology, University of Coimbra (CNC-UC Biotech)). Animals were group-housed in type III-H cages (Tecniplast, Italy) and maintained in specific environmental requirements (22 °C, 45–65% humidity, 15–20 changes/h ventilation, 12 h artificial light/dark cycle, noise level<55 dB) and with free access to standard rodent food (4RF21 GLP certificate, Mucedola, Italy) and acidified water (at pH 2.6 with HCl to avoid bacterial contamination). All experiments involving animals were performed in accordance with the European convention for the protection of vertebrate animal used for experimental and other scientific purposes (CETS no. 123 of 18 March 1986 and 2005 revision) and the Commission Recommendation of 18 June 2007 on guidelines for the accommodation and care of animals used for experimental and other scientific purposes (C (2007) 2525). Animal experiments were approved by the animal welfare commission of the Center for Neuroscience and Cell Biology, University of Coimbra, Portugal. Further approval was obtained from the National Agency for Veterinary and Agriculture (DGAV), reference 0421/000/000/2016.

6.5.2. Isolation of mouse liver mitochondria

The isolation of mouse liver mitochondria (MLM) and the evaluation of the mitochondrial uptake were carried out as previously described by Teixeira *et al*. [19] with some modifications. Briefly, MLM were prepared by tissue homogenization and subsequent differential centrifugations in ice-cold buffer containing 225 mM mannitol, 75 mM sucrose, 50 mM Tris-HCl, 0.1 mM EGTA, pH 7.4 and 0.5% fat-free bovine serum

albumin (BSA). After obtaining a crude mitochondrial preparation, pellets were washed twice and resuspended in washing buffer (225 mM mannitol, 75 mM sucrose, 50 mM Tris-HCl, pH 7.4). The determination of the protein content was performed by the Pierce™ BCA Protein Assay Kit using bovine serum albumin (BSA) as a standard.

6.5.3. Measurement of mitochondrial uptake in mouse liver mitochondria

To evaluate the uptake by energized MLM, a tetraphenylphosphonium-selective electrode was used to measure the distribution of the test compounds as previously described in literature [54]. An Ag/AgCl electrode was also used as reference. MLM were first incubated with constant stirring at 37 °C in 1 mL of KCl medium (120 mM KCl, 10 mM HEPES pH 7.2, and 1 mM EGTA), in the presence of rotenone (1.5 µM) to prevent the formation of a transmembrane electric potential (ΔΨ). Five sequential additions of the test compounds (5×1 µM) were performed to calibrate the electrode response. Then, succinate (SUC, 10 mM) was added to generate a ΔΨ, and valinomycin (VAL, 0.2 $\mu g.mL^{-1}$) was added at the end of the assay to dissipate the ΔΨ. The mitochondrial accumulation ratio was calculated by the disappearance of the test compound from extra- to intramitochondrial medium, considering an intramitochondrial volume of ∼0.5 $\mu L.mg^{-1}$ protein and a binding correction expected for the mitochondrial uptake of TPP compounds.

6.6. *In vitro* toxicology

6.6.1. Materials

All reagents used were of analytical grade or of the highest grade available. Neutral red (NR) solution, resazurin, Dulbecco's Modified Eagle's Medium (DMEM) with 4.5 g/L glucose, retinoic acid, 12-*O*-tetradecanoylphorbol-13-acetate (TPA), 2',7'-dichorofluorescein diacetate (DCFH-DA) and sulforhodamine B (SRB) were obtained from Sigma Aldrich. Reagents used in cell culture such as heat-inactivated fetal bovine serum (FBS), antibiotic (10,000 U/mL penicillin, 10,000 µg/mL streptomycin), MEM Non-Essential Amino Acids solution (100×) (MEM NEAA), 0.25% trypsin/1 mM ethylenediamine tetraacetic acid (EDTA) and Hanks' balanced salt solution (HBSS) were purchased from Gibco Laboratories (Lenexa, KS, USA). Dimethylsulfoxide (DMSO), absolute ethanol, and acetic acid were obtained from Merck (Darmstadt, Germany).

6.7.2. Cell lines and culture conditions

Human neuroblastoma SH-SY5Y cells were routinely cultured into 75 cm^3 flasks and maintained in DMEM with 4.5 g/L glucose, supplemented with 10 % heat-inactivated FBS (v/v), 1 % MEM NEAA (v/v) and 1% penicillin/streptomycin (v/v). Cells were maintained at 37 °C in a humidified, 5% CO_2–95% air atmosphere, and the cell culture medium was changed every 2-3 days. The cultures were passaged once a week by trypsinization (0.25 % trypsin/1 mM EDTA). To avoid phenotypic changes, the cells used for all experiments were taken between 19th and 28th passages. Cells were differentiated as described previously by Fernandes *et al*. [55]. Briefly, SH-SY5Y cells were seeded onto 96-well plates at a density of 25,000 cells/cm^2 in cell culture medium with *trans*-retinoic acid (RA) (final concentration of 10 µM) and incubated for 3 days at 37 °C in a humidified, 5% CO_2–95% air atmosphere. Then, the cell culture medium was removed and replaced with medium supplemented with 12-*O*-tetradecanoylphorbol-13-acetate (TPA) (final concentration

80 nM), and cells were incubated for 3 days. Stock solutions of RA (10 mM) and TPA (80 µM) were prepared in DMSO.

6.7.3. Cytotoxicity

Stock solutions of the test compounds (100 mM) were freshly prepared in DMSO. Final concentrations of the test compounds were obtained by diluting into cell culture medium immediately before use, giving a final maximum concentration of 0.1 % DMSO.

In cytotoxicity studies, differentiated SH-SY5Y cells were exposed to increasing concentrations of the test compounds (0.20-100 µM) for 24 h. Controls were treated with culture media containing 0.1 % DMSO. Cell viability was estimated using two different methods: resazurin reduction assay and NR uptake assay.

6.6.2. Evaluation of intracellular oxidative stress levels

The evaluation of intracellular oxidative stress using 2',7'-dichorofluorescein diacetate (DCFH-DA), a non-fluorescent probe able to cross the cell membrane. Inside the cells, DCFH-DA is hydrolyzed by esterases to the polar non-fluorescent reduced derivative 2',7'-dichlorofluorescein (DCFH), which, due to its polarity, is trapped within the cells. The subsequent oxidation of DCFH by reactive species (RS) yields the green fluorescent 2',7'-dichlorofluorescein (DCF) [56, 57].

DCF fluorescence assay was performed as previously described by Fernandes *et al.* [55]. SH-SY5Y cells were seeded and differentiated onto 96-well black plates (Greiner CELLSTARW, Sigma Aldrich). Cells were pre-incubated with DCFH-DA 4 µM in culture medium on the day of the experiment for 1.5 h, at 37 ºC, in the dark. Then, cells were incubated with the test compound (10 and 50 µM) in culture medium for 24 h. A blank (vehicle and culture medium without cells) and a negative control (cells treated with culture medium containing vehicle) were also included in the plate to measure the background fluorescence and the basal RS production, respectively. Fluorescence was recorded at the selected timepoint on a fluorescence microplate reader (BioTek Instruments, Vermont, USA) set to 485 nm excitation and 530 nm emission.

6.7.4. Measurement of oxygen consumption rates and extracellular acidification rates

The measurement of oxygen consumption rates (OCR) and extracellular acidification rates (ECARs) was performed using the experimental conditions described in the literature [58, 59]. Briefly, SH-SY5Y cells were seeded in 96-well plates at a density of 5,000 cells/100µL/well and differentiated into the dopaminergic phenotype. Then, cells were treated with non-toxic concentrations of the test compounds for 24 h. Following the incubation period, the oxygen consumption was measured at 37 °C in a Seahorse XF96 Extracellular Flux Analyzer (Seahorse Bioscience, Billerica, MA).

On the day prior to the assay, an XFe96 sensor cartridge for each cell plate was placed in a 96-well calibration plate containing 200 µL/well calibration buffer and left to hydrate overnight at 37 ºC. On the day of the experiment, the cell culture medium from the plates was removed and replaced with 175 µL/well of pre-warmed low-buffered serum-free minimal DMEM (102353, Bioscience) medium with the pH adjusted to 7.4. Then, cells were incubated at 37 ºC for 1 h to allow the temperature and pH of the medium to reach equilibrium before the first measurement. Oligomycin, FCCP, rotenone and antimycin A were prepared in DMSO.

To measure OCRs, oligomycin (2 µM), injected into reagent delivery port A, FCPP (1 µM), injected into port B, and rotenone (1 µM) and antimycin A (1µM), injected into reagent delivery port C, were diluted

in low-buffered serum-free DMEM medium and the pH adjusted to 7.4 with NaOH (1 M). Twenty-five µL of oligomycin, FCPP and rotenone/antimycin A were then pre-loaded into the ports of each well in the XFe96 sensor cartridge. The sensor cartridge and the calibration plate were loaded into the XFe96 Extracellular Flux Analyzer for calibration. Once the calibration was complete, the calibration plate was replaced with the cell culture microplate. Three baseline rate measurements of OCRs and ECARs of differentiated SH-SY5Y cells were made using a 3 min mix, 5 min measure cycle. Oligomycin, FCPP and rotenone/antimycin A were then pneumatically injected by the XFe 96 Analyzer into each well. The OCRs were measured using a 3 min mix, 5 min measure cycle. Results were analysed by using the Software Version Wave Desktop 2.6.

6.7.5. Measurement of cellular viability

6.7.5.1. Resazurin reduction assay

Resazurin is a non-fluorescent, non-toxic water-soluble dye able to permeate through cell membranes [60]. Inside the cells, resazurin is enzymatically reduced into the pink-colored and highly fluorescent resorufin [61, 62]. Since the conversion of resazurin into resorufin occurs mostly in mitochondria, the amount of resorufin produced can be used as indicator of metabolic activity [63]. The quantity of resorufin production is proportional to the number of viable cells in culture and can be quantified fluorometrically or colorimetrically [61].

Resazurin reduction assay was performed as previously described by Fernandes *et al.* [55]. Briefly, after the 24 h incubation periods with the test compounds, the cell culture medium was removed and replaced with fresh culture medium with resazurin (10 µg/mL) prepared in cell culture medium. Differentiated SH-SY5Y cells were incubated for 2 h at 37 °C in a humidified 5% CO_2–95% air atmosphere. Then, the fluorescence was read in a multiwell microplate reader (PowerWave XS from BioTek Instruments, Vermont, US), using an excitation wavelength of 540 nm and an emission wavelength of 590 nm. The results were expressed as the percentage of resazurin reduction relative to that of the control (non-treated) cells [resazurin reduction (% of control)] ± standard error mean (SEM) of at least three independent experiments.

6.7.5.2. Neutral red (NR) uptake assay

The neutral red (NR) uptake assay is based on the ability of viable cells to incorporate the supravital dye NR and retain it inside the lysosomes [38]. Neutral red (NR) uptake assay was performed as previously described by Fernandes *et al*. [64] Briefly, after the 24 h incubation periods with the test compounds, the cell culture medium was removed and a solution of NR (50 mg/mL) in fresh cell culture medium was added. Differentiated SH-SY5Y cells were incubated for 2 h at 37 °C in a humidified, 5% CO_2–95% air atmosphere. Then, the cell culture medium was removed and replaced by ethanol absolute/distilled water (1:1) with 5 % acetic acid to liberate the dye from the viable cells. The absorbance was measured at 540 nm in a multiwell microplate reader (PowerWave XS from BioTek Instruments). The results were expressed as the percentage of NR uptake relative to that of the control (non-treated) cells [NR uptake (% of control)] ± standard error mean (SEM) of at least three independent experiments.

6.7.5.3. Sulphorhodamine B (SRB) uptake assay

The sulphorhodamine B assay relies on the ability of SRB, a bright-pink aminoxanthene dye with two sulfonic groups, to bind electrostatically and pH-dependent to protein components of acid-fixed cells [65]. The dye binds to protein basic amino-acid residues under mild acidic conditions. Under basic conditions, SRB dissociates and can be quantified by spectrophotometry [65]. Since the binding of SRB to cell proteins is stoichometric, the amount of dye extracted from stained cells is indirectly proportional to total cell mass, which in turn correlates with cell number [37, 66].

Sulphorhodamine B (SRB) assay was performed as previously described by Fernandes *et al.* [58]. Following the measurements of OCRs, the cell culture medium was removed, and cells were washed with PBS (1X), fixed with methanolic solution of acetic acid (1 % (v/v)) and frozen at -20 °C for at least 2 h. Then, the fixation solution was discarded, and the plates were dried in an oven at 37 °C. An SRB solution (0.05 % (w/v)) in MilliQ purified water with acetic acid (1 % (v/v)) was added, and cells were incubated for 1 h at 37 ºC in a humidified 5% CO_2−95% air atmosphere. The SRB solution was then removed and cells were washed with MilliQ purified water with acetic acid (1 % (v/v)). Tris(hydroxymethyl)aminomethane (TRIS) solution (10 mM, pH 10) was added, the plate was stirred until all dye was dissolved, and the absorbance was measured at 540 nm in a multiwell microplate reader (Biotek Cytation 3 from BioTek Instruments, Vermont, US). The percentage of SRB absorbance relative to that of the control cells was used as the cytotoxicity measure [SRB absorbance (% of control)].

6.6.3. Statistical analysis

The data obtained are expressed as mean ± standard error mean (SEM) of at least three independent experiments (n = 3). All statistical analyses were performed using GraphPad PRISM version 6 for Windows. The normality of the data distribution was evaluated using three normality tests: KS normality test, D'Agostino and Pearson omnibus normality test, and Shapiro−Wilk normality test. For data with a parametric distribution, statistical comparisons between groups were estimated using the parametric method one-way analysis of variance (ANOVA) followed by Dunnett's multiple comparison test. For data with a non-parametric distribution, statistical comparisons were estimated using the nonparametric method of Kruskal–Wallis [one-way ANOVA on ranks] followed by Dunn's *post hoc* test. In all cases, p values lower than 0.05 were considered significant.

6.7. Evaluation of the chromatographic hydrophobicity index

Chromatographic hydrophobicity indexes (CHIs) at pH 2.3 and pH 7.4 were determined using an experimental protocol described elsewhere [67, 68]**.** Chromatographic hydrophobicity indexes (CHIs) values were determined using the retention times of samples and a mixture of standard compounds. The data was acquired on a Shimadzu high-performance liquid chromatograph SPD-M20A system (Shimadzu, Kyoto, Japan) with a Luna C18 (2) column (Phenomenex, CA, USA) 150×4.6 mm, 5 µm. In CHI determinations at pH 2.3, mobile phase A was aqueous solution of acetic acid 1 % (v/v) (pH 2.3), and mobile phase B was acetonitrile. The following gradient program was applied: 1 mL/min flow, rt, injection volume 20 µL, gradient 0−6 min 0-100 % B, 6−14 min 100% B, 14−16 min 100-0 % B. In CHI determinations at pH 7.4, the mobile phase A was 10 mM ammonium acetate solution (pH 7.4), and mobile phase B was acetonitrile. The following

gradient program was applied: 1 mL/min flow, rt, injection volume 20 µL, gradient 0−6 min 0-100 % B, 6−14 min 100% B, 14−16 min 100-0 % B.

Calibration plots were obtained using a mixture of the following compounds: paracetamol, theophylline, caffeine, benzimidazole, colchicine, carbamazepine, indole, propiophenone, butyrophenone, valerophenone, and heptanophenone. Stock solutions of the test compounds (10 µM) were prepared in DMSO and diluted in acetonitrile/water (1:1) to obtain a final concentration of 250 µM. Chromatographic hydrophobicity index (CHI) values were calculated as previously described [67, 68].

6.8. Estimation of drug-like properties

The calculation of molecular weight (MW), topological polar surface area (TPSA), number of hydrogen bond donors (HBD) and acceptors (HBA), number of rotatable bonds (RB) and logarithm of the ratio of the concentration of a drug in the brain and in the blood (logBB) was performed using the StarDrop software.

7. References:

[1] R.R. Ramsay, M. Majekova, M. Medina, M. Valoti, Key Targets for Multi-Target Ligands Designed to Combat Neurodegeneration, Front. Neurosci., 10 (2016) 1-24. https://doi.org/10.3389/fnins.2016.00375

[2] N. Guzior, A. Wieckowska, D. Panek, B. Malawska, Recent development of multifunctional agents as potential drug candidates for the treatment of Alzheimer's disease, Curr. Med. Chem., 22 (2015) 373-404. https://doi.org/10.2174/0929867321666141106122628

[3] A. Elmabruk, B. Das, D. Yedlapudi, L. Xu, T. Antonio, M.E.A. Reith, A.K. Dutta, Design, Synthesis, and Pharmacological Characterization of Carbazole Based Dopamine Agonists as Potential Symptomatic and Neuroprotective Therapeutic Agents for Parkinson's Disease, ACS Chem. Neurosci., 10 (2019) 396-411. https://doi.org/10.1021/acschemneuro.8b00291

[4] M. Rosini, E. Simoni, A. Milelli, A. Minarini, C. Melchiorre, Oxidative stress in Alzheimer's disease: are we connecting the dots?, J. Med. Chem., 57 (2014) 2821-2831. https://doi.org/10.1021/jm400970m

[5] E.K. Fetisova, A.V. Avetisyan, D.S. Izyumov, M.V. Korotetskaya, B.V. Chernyak, V.P. Skulachev, Mitochondria-targeted antioxidant SkQR1 selectively protects MDR (Pgp 170)-negative cells against oxidative stress, FEBS Lett., 584 (2010) 562-566. https://doi.org/10.1016/j.febslet.2009.12.002

[6] A. Johri, M.F. Beal, Mitochondrial dysfunction in neurodegenerative diseases, J. Pharmacol. Exp. Ther., 342 (2012) 619-630. https://doi.org/10.1124/jpet.112.192138

[7] E. Lezi, R.H. Swerdlow, Mitochondria in neurodegeneration, Adv. Exp. Med. Biol., 942 (2012) 269-286. https://doi.org/10.1007/978-94-007-2869-1_12

[8] M. Golpich, E. Amini, Z. Mohamed, R. Azman Ali, N. Mohamed Ibrahim, A. Ahmadiani, Mitochondrial Dysfunction and Biogenesis in Neurodegenerative diseases: Pathogenesis and Treatment, CNS Neurosci. Ther., 23 (2017) 5-22. https://doi.org/10.1111/cns.12655

[9] K. Facecchia, L.A. Fochesato, S.D. Ray, S.J. Stohs, S. Pandey, Oxidative toxicity in neurodegenerative diseases: role of mitochondrial dysfunction and therapeutic strategies, J. Toxicol., 2011 (2011) 683728. https://doi.org/10.1155/2011/683728

[10] K.A. Jellinger, Basic mechanisms of neurodegeneration: a critical update, J. Cell. Mol. Med., 14 (2010) 457-487. https://doi.org/10.1111/j.1582-4934.2010.01010.x

[11] L. Biasutto, A. Mattarei, M. La Spina, M. Azzolini, S. Parrasia, I. Szabò, M. Zoratti, Strategies to target bioactive molecules to subcellular compartments. Focus on natural compounds, Eur. J. Med. Chem., 181 (2019). https://doi.org/10.1016/j.ejmech.2019.07.060

[12] L. Milane, M. Trivedi, A. Singh, M. Talekar, M. Amiji, Mitochondrial biology, targets, and drug delivery, J. Control. Release, 207 (2015) 40-58. https://doi.org/10.1016/j.jconrel.2015.03.036

[13] D. Guzman-Villanueva, V. Weissig, Mitochondria-Targeted Agents: Mitochondriotropics, Mitochondriotoxics, and Mitocans, Handb. Exp. Pharmacol., 240 (2017) 423-438. https://doi.org/10.1007/164_2016_37
[14] H. He, D.W. Li, L.Y. Yang, L. Fu, X.J. Zhu, W.K. Wong, F.L. Jiang, Y. Liu, A novel bifunctional mitochondria-targeted anticancer agent with high selectivity for cancer cells, Sci. Rep., 5 (2015) 13543. https://doi.org/10.1038/srep13543
[15] J. Zielonka, J. Joseph, A. Sikora, M. Hardy, O. Ouari, J. Vasquez-Vivar, G. Cheng, M. Lopez, B. Kalyanaraman, Mitochondria-Targeted Triphenylphosphonium-Based Compounds: Syntheses, Mechanisms of Action, and Therapeutic and Diagnostic Applications, Chem. Rev., 117 (2017) 10043-10120. https://doi.org/10.1021/acs.chemrev.7b00042
[16] C.M. Porteous, A. Logan, C. Evans, E.C. Ledgerwood, D.K. Menon, F. Aigbirhio, R.A. Smith, M.P. Murphy, Rapid uptake of lipophilic triphenylphosphonium cations by mitochondria in vivo following intravenous injection: implications for mitochondria-specific therapies and probes, Biochim. Biophys. Acta., 1800 (2010) 1009-1017. https://doi.org/10.1016/j.bbagen.2010.06.001
[17] C. Oliveira, F. Cagide, J. Teixeira, R. Amorim, L. Sequeira, F. Mesiti, T. Silva, J. Garrido, F. Remiao, S. Vilar, E. Uriarte, P.J. Oliveira, F. Borges, Hydroxybenzoic Acid Derivatives as Dual-Target Ligands: Mitochondriotropic Antioxidants and Cholinesterase Inhibitors, Front. Chem., 6 (2018) 126. https://doi.org/10.3389/fchem.2018.00126
[18] J. Teixeira, C. Oliveira, R. Amorim, F. Cagide, J. Garrido, J.A. Ribeiro, C.M. Pereira, A.F. Silva, P.B. Andrade, P.J. Oliveira, F. Borges, Development of hydroxybenzoic-based platforms as a solution to deliver dietary antioxidants to mitochondria, Sci. Rep., 7 (2017) 6842. https://doi.org/10.1038/s41598-017-07272-y
[19] J. Teixeira, F. Cagide, S. Benfeito, P. Soares, J. Garrido, I. Baldeiras, J.A. Ribeiro, C.M. Pereira, A.F. Silva, P.B. Andrade, P.J. Oliveira, F. Borges, Development of a Mitochondriotropic Antioxidant Based on Caffeic Acid: Proof of Concept on Cellular and Mitochondrial Oxidative Stress Models, J. Med. Chem., 60 (2017) 7084-7098. https://doi.org/10.1021/acs.jmedchem.7b00741
[20] J. Teixeira, P. Soares, S. Benfeito, A. Gaspar, J. Garrido, M.P. Murphy, F. Borges, Rational discovery and development of a mitochondria-targeted antioxidant based on cinnamic acid scaffold, Free Radic. Res., 46 (2012) 600-611. https://doi.org/10.3109/10715762.2012.662593
[21] S. Benfeito, C. Oliveira, C. Fernandes, F. Cagide, J. Teixeira, R. Amorim, J. Garrido, C. Martins, B. Sarmento, R. Silva, F. Remiao, E. Uriarte, P.J. Oliveira, F. Borges, Fine-tuning the neuroprotective and blood-brain barrier permeability profile of multi-target agents designed to prevent progressive mitochondrial dysfunction, Eur. J. Med. Chem., 167 (2019) 525-545. https://doi.org/10.1016/j.ejmech.2019.01.055
[22] W. Yang, Y.H. Chen, H. Liu, H.D. Qu, Neuroprotective effects of piperine on the 1-methyl-4-phenyl-1,2,3,6-tetrahydropyridine-induced Parkinson's disease mouse model, Int. J. Mol. Med., 36 (2015) 1369-1376. https://doi.org/10.3892/ijmm.2015.2356
[23] J. Wattanathorn, P. Chonpathompikunlert, S. Muchimapura, A. Priprem, O. Tankamnerdthai, Piperine, the potential functional food for mood and cognitive disorders, Food and Chemical Toxicology : an international journal published for the British Industrial Biological Research Association, 46 (2008) 3106-3110. https://doi.org/10.1016/j.fct.2008.06.014
[24] P. Chonpathompikunlert, J. Wattanathorn, S. Muchimapura, Piperine, the main alkaloid of Thai black pepper, protects against neurodegeneration and cognitive impairment in animal model of cognitive deficit like condition of Alzheimer's disease, Food Chem. Toxicol., 48 (2010) 798-802. https://doi.org/10.1016/j.fct.2009.12.009
[25] J. Liu, M. Chen, X. Wang, Y. Wang, C. Duan, G. Gao, L. Lu, X. Wu, X. Wang, H. Yang, Piperine induces autophagy by enhancing protein phosphotase 2A activity in a rotenone-induced Parkinson's disease model, Oncotarget, 7 (2016) 60823-60843. https://doi.org/10.18632/oncotarget.11661
[26] Q.Q. Mao, Z. Huang, S.P. Ip, Y.F. Xian, C.T. Che, Protective effects of piperine against corticosterone-induced neurotoxicity in PC12 cells, Cell. Mol. Neurobiol., 32 (2012) 531-537. https://doi.org/10.1007/s10571-011-9786-y

[27] S.A. Lee, S.S. Hong, X.H. Han, J.S. Hwang, G.J. Oh, K.S. Lee, M.K. Lee, B.Y. Hwang, J.S. Ro, Piperine from the fruits of Piper longum with inhibitory effect on monoamine oxidase and antidepressant-like activity, Chem. Pharm. Bull. (Tokyo), 53 (2005) 832-835. https://doi.org/10.1248/cpb.53.832
[28] G.L. Ellman, K.D. Courtney, V. Andres, Jr., R.M. Feather-Stone, A new and rapid colorimetric determination of acetylcholinesterase activity, Biochem. Pharmacol., 7 (1961) 88-95. https://doi.org/10.1016/0006-2952(61)90145-9
[29] S. Di Giovanni, A. Borloz, A. Urbain, A. Marston, K. Hostettmann, P.A. Carrupt, M. Reist, *In vitro* screening assays to identify natural or synthetic acetylcholinesterase inhibitors: thin layer chromatography versus microplate methods, Eur. J. Pharm. Sci., 33 (2008) 109-119. https://doi.org/10.1016/j.ejps.2007.10.004
[30] P. Anand, B. Singh, A review on cholinesterase inhibitors for Alzheimer's disease, Arch Pharm Res, 36 (2013) 375-399. https://doi.org/10.1007/s12272-013-0036-3
[31] B. Seltzer, Donepezil: a review, Expert Opin Drug Metab Toxicol, 1 (2005) 527-536. https://doi.org/10.1517/17425255.1.3.527
[32] H. Mu, S.-M. Zhou, Y. Xia, H. Zou, F. Meng, Y.-B. Yan, Inactivation and unfolding of the hyperthermophilic inorganic pyrophosphatase from *Thermus thermophilus* by sodium dodecyl sulfate, Int. J. Mol. Sci., 10 (2009) 2849-2859. https://doi.org/10.3390/ijms10062849
[33] D. Chavarria, F. Cagide, M. Pinto, L.R. Gomes, J.N. Low, F. Borges, Development of piperic acid-based monoamine oxidase inhibitors: Synthesis, structural characterization and biological evaluation, J. Mol. Struct., 1182 (2019) 298-307. https://doi.org/10.1016/j.molstruc.2019.01.060
[34] S. Hagenow, A. Stasiak, R.R. Ramsay, H. Stark, Ciproxifan, a histamine H_3 receptor antagonist, reversibly inhibits monoamine oxidase A and B, Sci. Rep., 7 (2017) 1-6. https://doi.org/10.1038/srep40541
[35] H. Li, Z. Deng, T. Wu, R. Liu, S. Loewen, R. Tsao, Microwave-assisted extraction of phenolics with maximal antioxidant activities in tomatoes, Food Chem., 130 (2012) 928-936. https://doi.org/10.1016/j.foodchem.2011.08.019
[36] D.H.S. Silva, F.C. Pereira, M.V.B. Zanoni, M. Yoshida, Lipophyllic antioxidants from Iryanthera juruensis fruits, Phytochemistry, 57 (2001) 437-442. https://doi.org/10.1016/S0031-9422(00)00477-5
[37] F.S. Silva, I.G. Starostina, V.V. Ivanova, A.A. Rizvanov, P.J. Oliveira, S.P. Pereira, Determination of Metabolic Viability and Cell Mass Using a Tandem Resazurin/Sulforhodamine B Assay, Curr. Protoc. Toxicol., 68 (2016) 2.24.21-22.24.15. https://doi.org/10.1002/cptx.1
[38] G. Repetto, A. del Peso, J.L. Zurita, Neutral red uptake assay for the estimation of cell viability/cytotoxicity, Nat. Protoc., 3 (2008) 1125-1131. https://doi.org/10.1038/nprot.2008.75
[39] B. Kalyanaraman, G. Cheng, M. Hardy, O. Ouari, M. Lopez, J. Joseph, J. Zielonka, M.B. Dwinell, A review of the basics of mitochondrial bioenergetics, metabolism, and related signaling pathways in cancer cells: Therapeutic targeting of tumor mitochondria with lipophilic cationic compounds, Redox Biol., 14 (2018) 316-327. https://doi.org/10.1016/j.redox.2017.09.020
[40] K.P. Nickens, J.D. Wikstrom, O.S. Shirihai, S.R. Patierno, S. Ceryak, A bioenergetic profile of non-transformed fibroblasts uncovers a link between death-resistance and enhanced spare respiratory capacity, Mitochondrion, 13 (2013) 662-667. https://doi.org/10.1016/j.mito.2013.09.005
[41] J.T. Teh, W.L. Zhu, C.B. Newgard, P.J. Casey, M. Wang, Respiratory Capacity and Reserve Predict Cell Sensitivity to Mitochondria Inhibitors: Mechanism-Based Markers to Identify Metformin-Responsive Cancers, Mol. Cancer Ther., 18 (2019) 693-705. https://doi.org/10.1158/1535-7163.Mct-18-0766
[42] G.J.W. van der Windt, C.-H. Chang, E.L. Pearce, Measuring Bioenergetics in T Cells Using a Seahorse Extracellular Flux Analyzer, Curr Protoc Immunol, 113 (2016) 3.16B.11-13.16B.14. https://doi.org/10.1002/0471142735.im0316bs113
[43] K. Valko, C. Bevan, D. Reynolds, Chromatographic Hydrophobicity Index by Fast-Gradient RP-HPLC: A High-Throughput Alternative to log P/log D, Anal. Chem., 69 (1997) 2022-2029. https://doi.org/10.1021/ac961242d

[44] J. Trnka, M. Elkalaf, M. Anděl, Lipophilic triphenylphosphonium cations inhibit mitochondrial electron transport chain and induce mitochondrial proton leak, PLoS One, 10 (2015) e0121837. https://doi.org/10.1371/journal.pone.0121837
[45] R.A.J. Smith, C.M. Porteous, A.M. Gane, M.P. Murphy, Delivery of bioactive molecules to mitochondria *in vivo*, Proc. Natl. Acad. Sci. U.S.A., 100 (2003) 5407-5412. https://doi.org/10.1073/pnas.0931245100
[46] S.A. Hitchcock, L.D. Pennington, Structure-brain exposure relationships, J. Med. Chem., 49 (2006) 7559-7583. https://doi.org/10.1021/jm060642i
[47] H. Pajouhesh, G.R. Lenz, Medicinal Chemical Properties of Successful Central Nervous System Drugs, NeuroRx., 2 (2005) 541-553. https://doi.org/10.1602/neurorx.2.4.541
[48] D.E. Clark, Rapid calculation of polar molecular surface area and its application to the prediction of transport phenomena. 2. Prediction of blood-brain barrier penetration, J. Pharm. Sci., 88 (1999) 815-821. https://doi.org/10.1021/js980402t
[49] G. Cheng, J. Zielonka, O. Ouari, M. Lopez, D. McAllister, K. Boyle, C.S. Barrios, J.J. Weber, B.D. Johnson, M. Hardy, M.B. Dwinell, B. Kalyanaraman, Mitochondria-Targeted Analogues of Metformin Exhibit Enhanced Antiproliferative and Radiosensitizing Effects in Pancreatic Cancer Cells, Cancer Res, 76 (2016) 3904-3915. https://doi.org/10.1158/0008-5472.can-15-2534
[50] P.G. Williard, C.B. Fryhle, Boron trihalide-methyl sulfide complexes as convenient reagents for dealkylation of aryl ethers, Tetrahedron Lett., 21 (1980) 3731-3734. https://doi.org/10.1016/0040-4039(80)80164-X
[51] B. Ou, M. Hampsch-Woodill, R.L. Prior, Development and validation of an improved oxygen radical absorbance capacity assay using fluorescein as the fluorescent probe, J. Agric. Food Chem., 49 (2001) 4619-4626. https://doi.org/10.1021/jf010586o
[52] F. Mura, T. Silva, C. Castro, F. Borges, M.C. Zuniga, J. Morales, C. Olea-Azar, New insights into the antioxidant activity of hydroxycinnamic and hydroxybenzoic systems: spectroscopic, electrochemistry, and cellular studies, Free Radic. Res., 48 (2014) 1473-1484. https://doi.org/10.3109/10715762.2014.965702
[53] J. Garrido, A. Gaspar, E.M. Garrido, R. Miri, M. Tavakkoli, S. Pourali, L. Saso, F. Borges, O. Firuzi, Alkyl esters of hydroxycinnamic acids with improved antioxidant activity and lipophilicity protect PC12 cells against oxidative stress, Biochimie, 94 (2012) 961-967. https://doi.org/10.1016/j.biochi.2011.12.015
[54] N. Kamo, M. Muratsugu, R. Hongoh, Y. Kobatake, Membrane potential of mitochondria measured with an electrode sensitive to tetraphenyl phosphonium and relationship between proton electrochemical potential and phosphorylation potential in steady state, J. Membr. Biol., 49 (1979) 105-121. https://doi.org/10.1007/BF01868720
[55] C. Fernandes, M. Pinto, C. Martins, M.J. Gomes, B. Sarmento, P.J. Oliveira, F. Remião, F. Borges, Development of a PEGylated-Based Platform for Efficient Delivery of Dietary Antioxidants Across the Blood-Brain Barrier, Bioconjug. Chem., 29 (2018) 1677-1689. https://doi.org/10.1021/acs.bioconjchem.8b00151
[56] S. Aula, S. Lakkireddy, K. Jamil, A. Kapley, A.V.N. Swamy, H.R. Lakkireddy, Biophysical, biopharmaceutical and toxicological significance of biomedical nanoparticles, RSC Adv., 5 (2015) 47830-47859. https://doi.org/10.1039/c5ra05889a
[57] K.A. Kang, H.C. Lee, J.J. Lee, M.N. Hong, M.J. Park, Y.S. Lee, H.D. Choi, N. Kim, Y.G. Ko, J.S. Lee, Effects of combined radiofrequency radiation exposure on levels of reactive oxygen species in neuronal cells, J. Radiat. Res., 55 (2014) 265-276. https://doi.org/10.1093/jrr/rrt116
[58] C. Fernandes, S. Benfeito, R. Amorim, J. Teixeira, P.J. Oliveira, F. Remiao, F. Borges, Desrisking the Cytotoxicity of a Mitochondriotropic Antioxidant Based on Caffeic Acid by a PEGylated Strategy, Bioconjug. Chem., 29 (2018) 2723-2733. https://doi.org/10.1021/acs.bioconjchem.8b00383
[59] C.M. Deus, C. Zehowski, K. Nordgren, K.B. Wallace, A. Skildum, P.J. Oliveira, Stimulating basal mitochondrial respiration decreases doxorubicin apoptotic signaling in H9c2 cardiomyoblasts, Toxicology, 334 (2015) 1-11. https://doi.org/10.1016/j.tox.2015.05.001

[60] S.N. Rampersad, Multiple applications of Alamar Blue as an indicator of metabolic function and cellular health in cell viability bioassays, Sensors (Basel), 12 (2012) 12347-12360. https://doi.org/10.3390/s120912347
[61] J. O'Brien, I. Wilson, T. Orton, F. Pognan, Investigation of the Alamar Blue (resazurin) fluorescent dye for the assessment of mammalian cell cytotoxicity, Eur. J. Biochem., 267 (2000) 5421-5426. https://doi.org/10.1046/j.1432-1327.2000.01606.x
[62] E.M. Czekanska, Assessment of cell proliferation with resazurin-based fluorescent dye, Methods Mol. Biol., 740 (2011) 27-32. https://doi.org/10.1007/978-1-61779-108-6_5
[63] A. van Tonder, A.M. Joubert, A.D. Cromarty, Limitations of the 3-(4,5-dimethylthiazol-2-yl)-2,5-diphenyl-2H-tetrazolium bromide (MTT) assay when compared to three commonly used cell enumeration assays, BMC Res. Notes, 8 (2015) 47. https://doi.org/10.1186/s13104-015-1000-8
[64] C. Fernandes, C. Martins, A. Fonseca, R. Nunes, M.J. Matos, R. Silva, J. Garrido, B. Sarmento, F. Remiao, F.J. Otero-Espinar, E. Uriarte, F. Borges, PEGylated PLGA Nanoparticles As a Smart Carrier to Increase the Cellular Uptake of a Coumarin-Based Monoamine Oxidase B Inhibitor, ACS Appl. Mater. Interfaces, 10 (2018) 39557-39569. https://doi.org/10.1021/acsami.8b17224
[65] W. Voigt, Sulforhodamine B assay and chemosensitivity, Methods Mol. Med., 110 (2005) 39-48. https://doi.org/10.1385/1-59259-869-2:039
[66] V. Vichai, K. Kirtikara, Sulforhodamine B colorimetric assay for cytotoxicity screening, Nat. Protoc., 1 (2006) 1112-1116. https://doi.org/10.1038/nprot.2006.179
[67] G. Camurri, A. Zaramella, High-throughput liquid chromatography/mass spectrometry method for the determination of the chromatographic hydrophobicity index, Anal. Chem., 73 (2001) 3716-3722. https://doi.org/10.1021/ac001388j
[68] K. Valko, S. Nunhuck, C. Bevan, M.H. Abraham, D.P. Reynolds, Fast gradient HPLC method to determine compounds binding to human serum albumin. Relationships with octanol/water and immobilized artificial membrane lipophilicity, J. Pharm. Sci., 92 (2003) 2236-2248. https://doi.org/10.1002/jps.10494

CHAPTER IV

Integrated discussion, conclusions and future perspectives

The work presented in this Thesis envisaged the discovery and validation of new neuroprotective agents able to restore dopaminergic and cholinergic neurotransmissions and/or redox homeostasis. With this in mind, small libraries of compounds were developed using the chemical structures of FA, CA and piperine as starting scaffolds (**Figure 4.1**). The libraries developed in this work were refined following the assessment of their biological effects, cytotoxicity and cytoprotective profiles, and drug-like properties. Accordingly, the derivatives obtained were screened for antioxidant activity and inhibition of neurotransmitter-metabolizing enzymes (MAOs, COMT, ChEs). Then, the cytotoxicity and cytoprotective profiles of compounds with relevant biological activity were evaluated in two cell lines commonly used to assess the safety of drug candidates (SH-SY5Y cells and Caco-2 cells). Finally, the physicochemical properties of the most promising compounds were evaluated and/or estimated to predict their drug-likeness. At the end, the results obtained provided valid candidates for lead optimization.

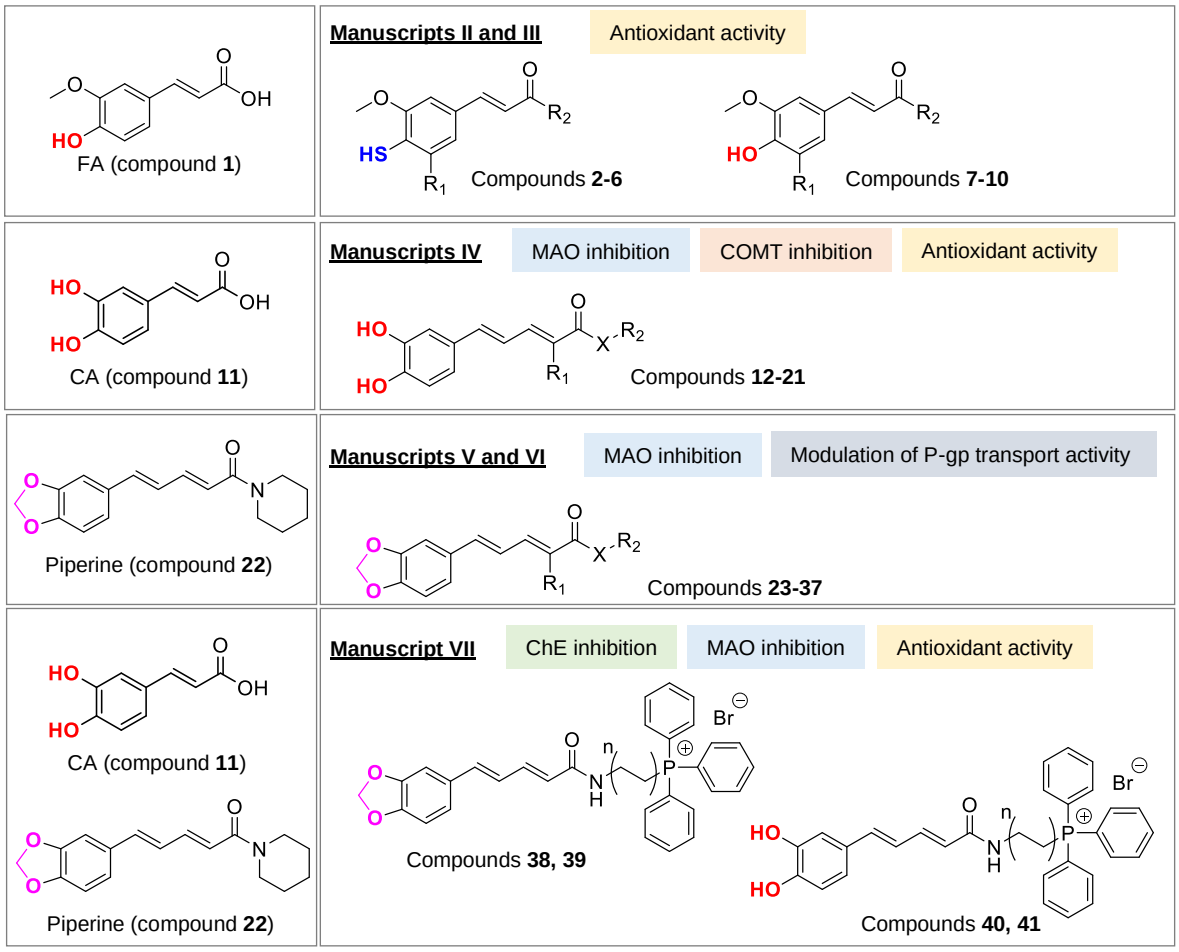


Figure 4.1: compound libraries developed in this Thesis based on the chemical scaffolds of ferulic acid (FA), caffeic acid (CA) and piperine.

4.1. Design and development of new chemical entities based on natural scaffolds

The compounds developed in the present Thesis were designed to achieve specific goals. In particular, the bioisosteric replacement of the phenol group by a thiophenol in the FA scaffold was performed to boost its antioxidant activity (**Manuscript II**) (**Figure 4.1**). To improve the antioxidant profile and the drug-like properties of the resulting thiophenol, other structural modifications were then introduced at the aromatic ring and the carboxylic acid group (**Manuscript III**). In **Manuscripts IV-VI**, several chemical modifications were introduced to the piperine and CA scaffolds to improve their biological activity and drug-likeness and to establish structure-activity relationships. Finally, piperine and CA derivatives were conjugated with TPP cations with the aim of directing the bioactive compounds towards mitochondria (**Manuscript VII**).

Overall, cost-effective starting materials were used in the synthetic strategies presented in this work, namely FA, benzaldehydes with the appropriate substitution pattern, and piperine (**Figure 4.2**). Whenever possible, reactions with simple, safe and straightforward purification steps and work ups were chosen envisaging the putative scale up of the synthetic processes. Some reactions were adapted to microwave-assisted conditions to considerably reduce reaction time, increase reaction yields and improve the purity of the product when compared to conventional heating (390). Structural characterization of all compounds was performed using NMR (^{1}H NMR, ^{13}C NMR, DEPT 135, COSY, HSQC, HMBC) and mass spectrometry (EI-MS or ESI) techniques.

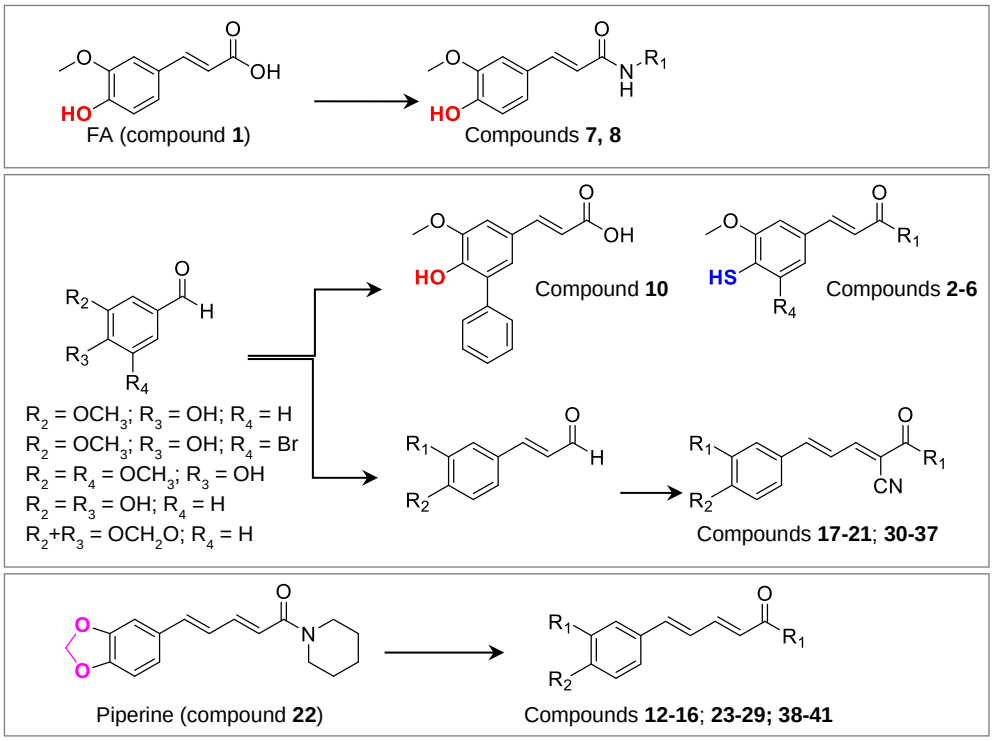


Figure 4.2: general overview of the starting materials and the resulting final compounds.

A general overview of the synthetic strategies employed to obtain the compound libraries will be presented in the following subsections.

4.1.1. Synthesis of ferulic acid-based thiophenols

Ferulic acid-based thiophenols **2-6** were synthesized according to the synthetic strategy depicted in **Figure 4.3 (Manuscripts II** and **III)**. First, 5-phenylvanillin (compound **43**) was obtained by a Suzuki cross-coupling reaction between 5-bromovanillin (compound **42**) and phenylboronic acid, in the presence of palladium (II) acetate ($Pd(OAc)_2$) and potassium carbonate (K_2CO_3), and under microwave irradiation (**Figure 4.3**, step *a*). Then, 4-hydroxybenzaldehyde derivatives **43-45** were reacted with dimethylthiocarbamoyl chloride (DMTCl) in the presence of a strong base (1,4-diazabicyclo[2.2.2]octane (DABCO)), yielding compounds **46-48** (**Figure 4.3**, step *b*).This reaction was followed by a Newman-Kwart rearrangement under inert atmosphere, in which an *O*- to *S*-aryl migration occurs at high reaction temperatures (**Figure 4.3**, step *c*). The Newman-Kwart rearrangement was adapted to microwave-assisted conditions. Compared to conventional heating, microwave irradiation considerably decreased the reaction time and improved the reaction yield (**Manuscript II**). A Knoevenagel-Doebner reaction between intermediates **49-51** and malonic acid in pyridine and catalytic amounts of piperidine afforded the cinnamic

acid derivatives **52-54** (**Figure 4.3**, step *d*). An amidation reaction of compound **52** with benzylamine or 2-phenylethylamine was also performed under alkaline conditions, using benzotriazol-1-yloxy)tripyrrolidinophosphonium hexafluorophosphate (PyBOP) as a coupling agent (**Figure 4.3**, step *e*). Finally, compounds **52-56** were refluxed in the presence of NaOH to yield thiophenols **2-6** (**Figure 4.3**, step *f*). The removal of *N,N*-dimethylcarbamoyl groups from compounds **5** and **6** required longer reaction periods and higher amounts of NaOH in comparison to compounds **2-4**, suggesting that the presence of substituents at the position 5 of the aromatic ring may hinder the alkaline hydrolysis. Overall, all compounds were obtained in moderate to high yields (**Table 4.1**).

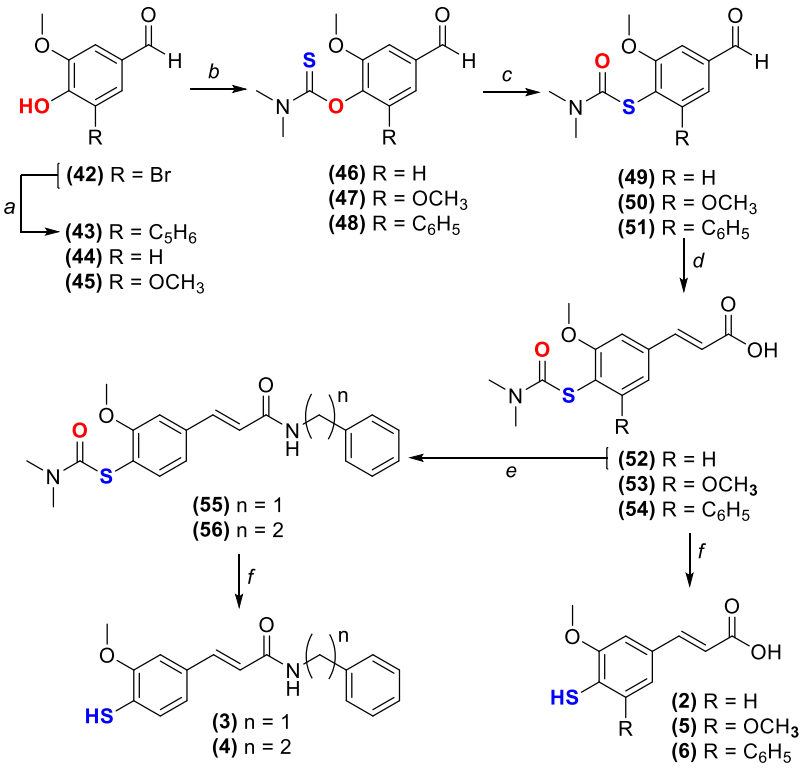
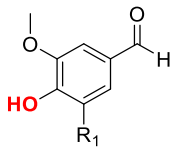
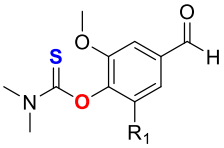
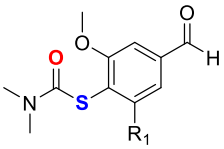
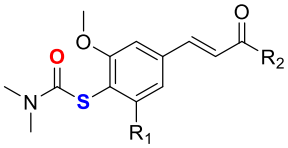
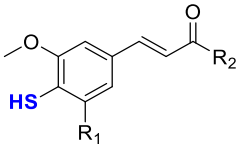


Figure 4.3: Synthetic strategy pursued to obtain ferulic acid-based thiophenols **2-6**. (a) phenylboronic acid, K_2CO_3, $Pd(OAc)_2$, TBAB, DMF, 150 ºC (microwave irradiation), 15 min; (b) DMTCl, DABCO, DMF, 70 ºC, 3 h; (c) diphenyl ether, argon, 240 ºC (microwave irradiation), 20 min; (d) malonic acid, anhydrous pyridine, piperidine, 70 ºC, 4-5 h; (e) 1. DMF, DIPEA, PyBOP, CH_2Cl_2, 0 ºC, 30 min; 2. benzylamine or 2-phenylethylamine, rt, overnight; (f) MeOH, aqueous solution of NaOH 2 M, reflux, 1.5-16 h.

Table 4.1: chemical structures and reaction yields of ferulic acid-based thiophenols **2-6** and related intermediates.

	React.	Comp.	R_1	R_2	η/%	Manuscr.
	*a*	**43**	-C_6H_5	___	52	**III**
	*b*	**46**	-H	___	85	**II, III**
		47	-OCH_3	___	93	**III**
		48	-C_6H_5	___	75	**III**
	*c*	**49**	-H	___	91	**II, III**
		50	-OCH_3	___	91	**III**
		51	-C_6H_5	___	83	**III**
	*d*	**52**	-H	-OH	91	**II, III**
		53	-OCH_3	-OH	88	**III**
		54	-C_6H_5	-OH	59	**III**
	e	**55**	-H	-$NHCH_2C_6H_5$	95	**III**
		56	-H	-$NH(CH_2)_2C_6H_5$	80	**III**
	*f*	**2**	-H	-OH	80	**II, III**
		3	-H	-$NHCH_2C_6H_5$	53	**III**
		4	-H	-$NH(CH_2)_2C_6H_5$	45	**III**
		5	-OCH_3	-OH	80	**III**
		6	-C_6H_5	-OH	73	**III**

4.1.2. Synthesis of ferulic acid derivatives

The synthesis and structural characterization of compounds **7**, **8** and **10** (**Figure 4.4**; **Table 4.2**) was already described in previous publications (280, 391). However, these compounds were synthesized *de novo* in the present work to compare their antioxidant properties with the corresponding thiophenols (**Manuscript III**).

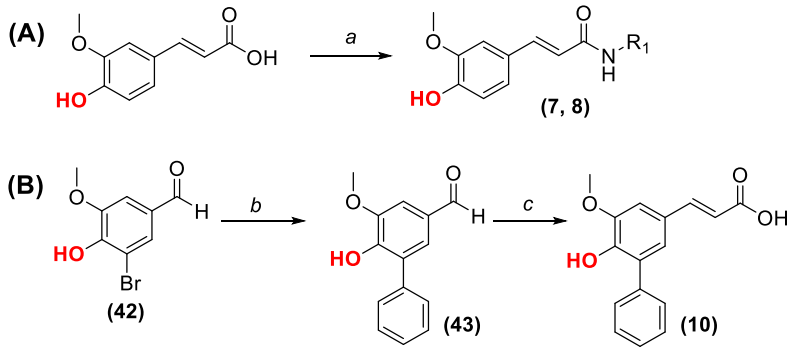
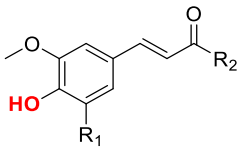


Figure 4.4: Synthetic strategy pursued to obtain compounds **7**, **8** and **10**. (a) 1. DMF, DIPEA, PyBOP, CH_2Cl_2, 0 ºC, 30 min; 2. benzylamine or 2-phenylethylamine, rt, overnight; (b) phenylboronic acid, K_2CO_3, $Pd(OAc)_2$, TBAB, DMF, 150 ºC (microwave irradiation), 15 min; (c) malonic acid, anhydrous pyridine, piperidine, 70 ºC, 5 h.

Table 4.2: chemical structures and reaction yields of compounds **7**, **8** and **10**.

	React.	Comp.	R_1	R_2	η/%	Manuscr.
	*a* (A)	**7**	H	$-NHCH_2C_6H_5$	61	**III**
		8	H	$-NH(CH_2)_2C_6H_5$	54	**III**
	c (B)	**10**	C_6H_5	-OH	39	**III**

Ferulic acid amides (compounds **7** and **8**) (**Table 4.2**) were obtained by a PyBOP-mediated amidation performed with commercially available FA, benzylamine and 2-phenylethylamine (**Figure 4.4A**).

Following the synthesis of compound **43** (**Figure 4.3,** *step a;* **Figure 4.4 B,** *step b*), a Knoevenagel-Doebner condensation between compound **43** and malonic acid yielded 5-phenylferulic acid (compound **10**, **Figure 4.4B**).

Compounds **7**, **8** and **10** were obtained in moderate yields (**Table 4.2**).

4.1.3. Synthesis of piperine and caffeic acid derivatives

To obtain piperine and CA derivatives **12-16** and **23-29** (**Figure 4.5**, **Table 4.3**)., piperine (compound **22**) was used as starting material. The synthetic route started with the synthesis of piperic acid (compound **23**) by refluxing piperine under alkaline conditions (**Figure 4.5**, step *a*) (**Manuscripts IV**, **V**, **VI** and **VII**). Then, a PyBOP-mediated amidation of piperic acid with aniline, benzylamine or 2-phenylethylamine afforded piperic acid amides **24-26** (**Figure 4.5**, step *b*). Two synthetic methodologies were used to obtain piperic acid esters **27-29**. While compound **27** was synthesized by a Steglich esterification between piperic acid and phenol (**Figure 4.5**, step *c*), compounds **25** and **26** were obtained from a bimolecular nucleophilic substitution reaction with benzyl bromide and (2-

bromoethyl)benzene, respectively, under alkaline conditions (**Figure 4.5**, step *d*) (**Manuscripts IV**, **V** and **VI**). Finally, *O*-demethylenation reactions of compounds **22-26** using a solution of boron tribromide (BBr_3) afforded catechols **12-16** (**Figure 4.5**, step *e*) (**Manuscript IV**). In reactions *a-d*, all compounds were obtained on moderate to high yields (**Table 4.3**). On the other hand, catechols **12-16** were obtained in low yields, which is mostly due to the formation of undesirable by-products and to the difficulties in isolating the final compounds.

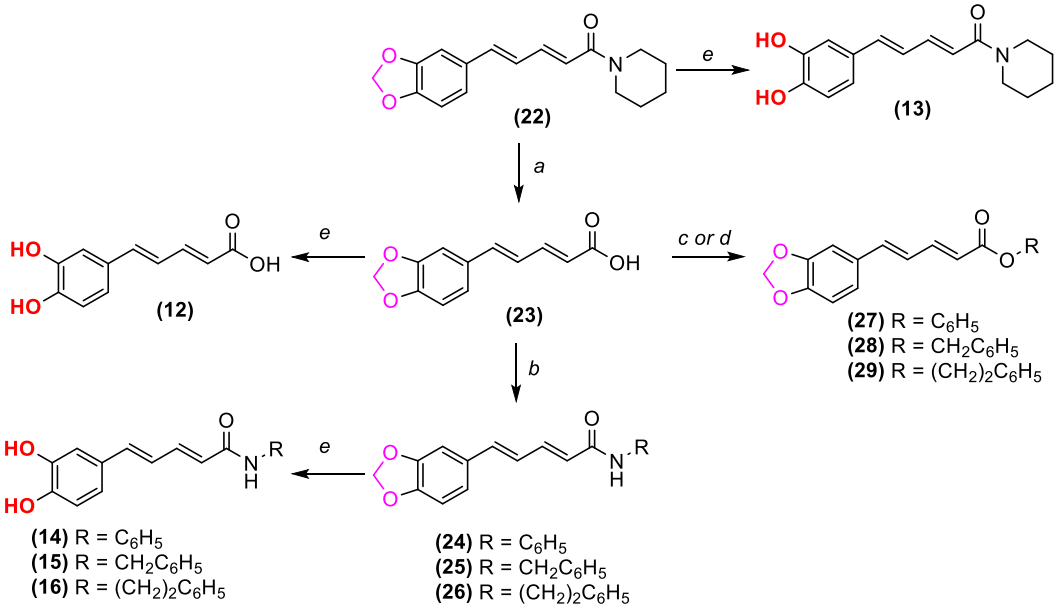
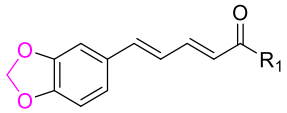
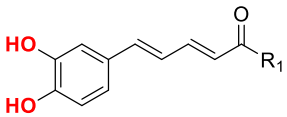


Figure 4.5: Synthetic strategy pursued to obtain compounds **12-16** and **23-29**. (a) Methanolic solution of NaOH 2 M, reflux, 24 h; (b) 1. DMF, DIPEA, PyBOP, CH_2Cl_2, 0 ºC, 30 min; 2. Amine (aniline, benzylamine or 2-phenylethylamine), rt, overnight; (c) 1. EDC.HCl, DMAP, CH_2Cl_2, rt, 30 min; 2. phenol, rt, overnight; (d) 1. K_2CO_3, DMF, rt, 30 min; 2. benzylbromide or (2-bromoethyl)benzene, 80 ºC, 8 h; (e) anhydrous CH_2Cl_2, BBr_3 1 M, -78 ºC to rt, overnight.

Table 4.3: chemical structures and reaction yields of compounds **12-16** and **30-37**.

	React.	Comp.	R_1	η/%	Manuscr.
	*a*	**23**	-OH	83	**IV, V, VI, VII**
	b	**24**	$-NHC_5H_6$	44	**IV, V, VI**
		25	$-NHCH_2C_6H_5$	83	**IV, V, VI**
		26	$-NH(CH_2)_2C_6H_5$	82	**IV, VI**
	c	**27**	$-OC_5H_6$	68	**V, VI**
	d	**28**	$-OCH_2C_6H_5$	84	**V, VI**
		29	$-O(CH_2)_2C_6H_5$	84	**VI**
	e	**12**	-OH	5	**IV**
		13	$-NC_5H_{10}$	50	**IV**
		14	$-NHC_5H_6$	12	**IV**
		15	$-NHCH_2C_6H_5$	17	**IV**
		16	$-NH(CH_2)_2C_6H_5$	20	**IV**

In **Manuscript V**, a complete structural characterization of compounds **24**, **25**, **27** and **28** was performed, using both unidimensional and bidimensional RMN techniques (^{1}H NMR, ^{13}C NMR, DEPT135, COSY, HSQC and HMBC), electrospray ionization mass spectrometry (ESI-MS) and single X-ray crystallography.

4.1.4. Synthesis of α-cyano compounds based on piperine and caffeic acid

Contrary to the compounds described in the previous subsection, the synthesis of α-cyano derivatives **17-21** and **30-37** (**Figure 4.6, Table 4.4**) required the construction of the (*2E*,*4E*)-5-phenylpenta-2,4-dienoyl moiety. To obtain compounds **17-21** and **30-37**, cinnamaldehydes with the desired substitution pattern were synthesized from the parent benzaldehydes (**Figure 4.6A**). These intermediates were then used in Knoevenagel condensations and amidation reactions to afford the final compounds (**Figure 4.6B** and **4.5C**) (**Manuscripts IV** and **VI**).

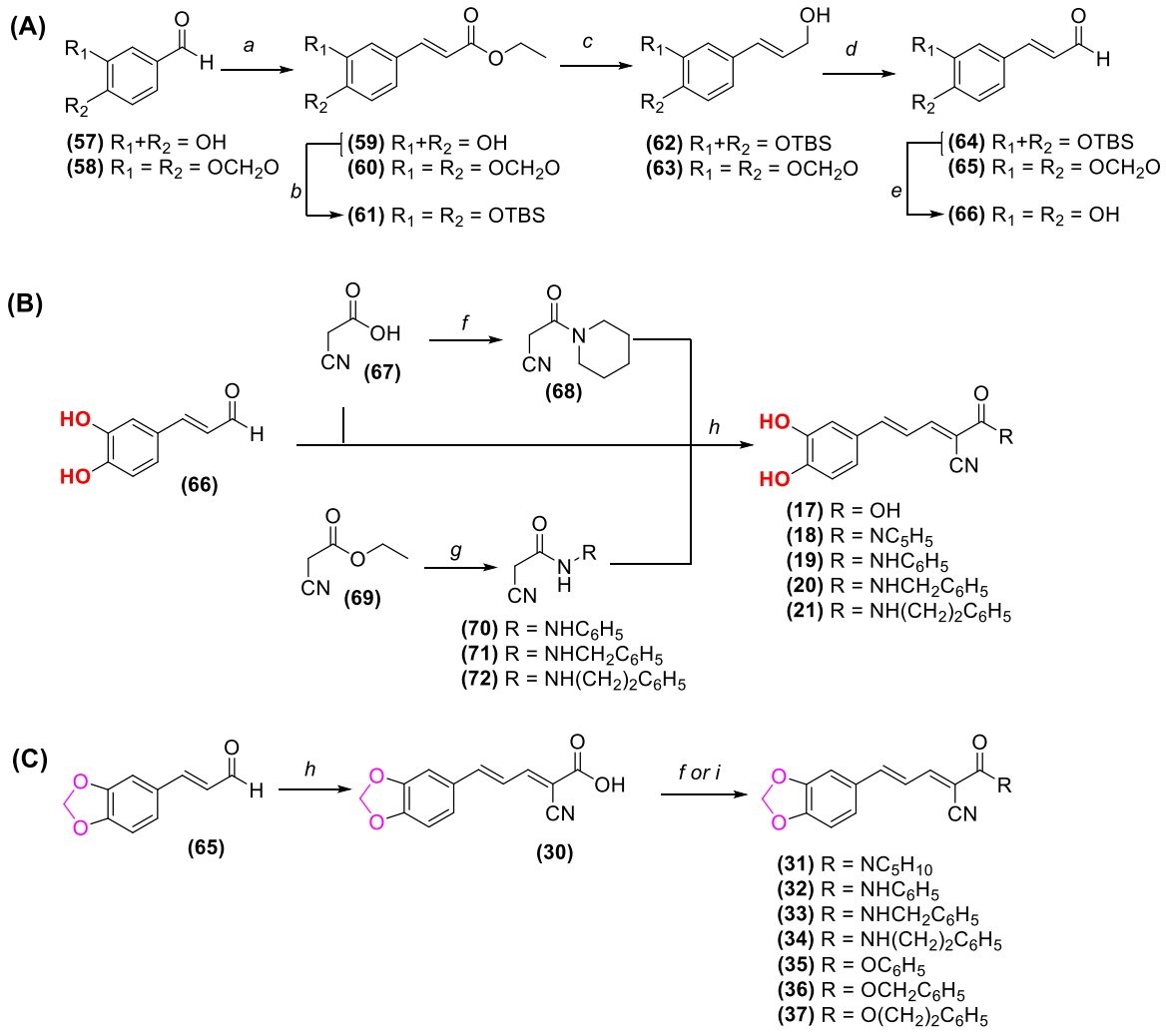
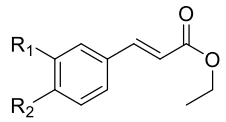
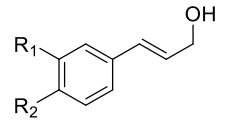
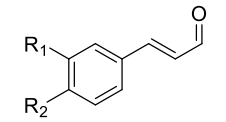
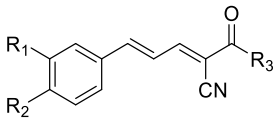


Figure 4.6: Synthetic strategy pursued to obtain α-CN derivatives **17-21** and **30-37**. (a) mono-ethyl malonate, pyridine, piperidine, 70 ºC, 9 h; (b) TBSCl, imidazole, DMF, 50 ºC, 30 min; (c) 1. Argon atmosphere, -78 ºC, 30

min; 2. dry THF, $LiAlH_4$, -78 ºC to rt, 5 h; (d) MnO_2, CH_2Cl_2, rt, overnight; (e) TBAF, dry THF, 50 ºC, 30 min; (f) 1. DMF, DIPEA, PyBOP, CH_2Cl_2, 0 ºC, 30 min; 2. Amine (piperidine, aniline, benzylamine or 2-phenylethylamine), rt, overnight; (g) ethyl cyanoacetate, amine (aniline, benzylamine or 2-phenylethylamine), 100 ºC, 9 h; (h) activated methylene (compounds **67, 68, 70-72**), pyridine, piperidine, 60 ºC, 45 min; (i) 1. EDC.HCl, DMAP, CH_2Cl_2, rt, 30 min; 2. phenol, benzyl alcohol or 2-phenylethanol, rt, overnight.

Table 4.4: chemical structures and reaction yields of α-CN derivatives **17-21** and **30-37** and related intermediates.

	React.	Comp.	R_1	R_2	R_3	η/%	Manuscr.
	*a* (A)	**59**	-OH	-OH	___	54	**IV**
		60	-OCH_2O-		___	91	**VI**
	b (A)	**61**	-OTBS	-OTBS	___	83	**IV**
	*c* (A)	**62**	-OTBS	-OTBS	___	73	**IV**
		63	-OCH_2O-		___	43	**VI**
	*d* (A)	**64**	-OTBS	-OTBS	___	54	**IV**
		65	-OCH_2O-		___	62	**VI**
	e (A)	**66**	-OH	-OH	___	76	**IV**
	*f* (B)	**68**	___		-NC_5H_{10}	25	**IV**
	g (B)	**70**	___		-NHC_5H_6	27	**IV**
		71	___		-$NHCH_2C_6H_5$	24	**IV**
		72	___		-$NH(CH_2)_2C_6H_5$	42	**IV**
	*h* (B)	**17**	-OH	-OH	-OH	67	**IV**
		18	-OH	-OH	-NC_5H_{10}	55	**IV**
		19	-OH	-OH	-NHC_5H_6	46	**IV**
		20	-OH	-OH	-$NHCH_2C_6H_5$	54	**IV**
		21	-OH	-OH	-$NH(CH_2)_2C_6H_5$	66	**IV**
	h (C)	**30**	OCH_2O		-OH	87	**VI**
	f (C)	**31**	OCH_2O		-NC_5H_{10}	70	**VI**
		32	OCH_2O		-NHC_5H_6	44	**VI**
		33	OCH_2O		-$NHCH_2C_6H_5$	64	**VI**
		34	OCH_2O		-$NH(CH_2)_2C_6H_5$	87	**VI**
	i (C)	**35**	OCH_2O		-OC_5H_6	66	**VI**
		36	OCH_2O		-$OCH_2C_6H_5$	50	**VI**
		37	OCH_2O		-$O(CH_2)_2C_6H_5$	51	**VI**

Accordingly, cinnamic acid ethyl esters **59** and **60** were obtained from a Knoevenagel-Doebner reaction between benzaldehydes **57** and **58**, respectively, and mono-ethyl malonate (**Figure 4.6A**, step *a*). To avoid the potential formation of by-products associated to the high reactivity of phenols, the hydroxyl groups of compound **59** were protected with *tert*-butyldimethylsilyl chloride (TBSCl) using imidazole as a silylating agent (**Figure 4.6A**, step *b*). The ester groups of compounds **60** and **61** were then reduced to the corresponding primary alcohols with lithium aluminium hydride ($LiAlH_4$) (compounds **62** and

63, **Figure 4.6A**, step *c*), which in turn were oxidized into aldehydes with manganese dioxide (MnO_2) (compounds **64** and **65**, **Figure 4.6A**, step *d*). The protecting groups of compound **64** were removed with tetra-*n*-butylammonium fluoride (TBAF) yielding caffeic aldehyde (compound **66**, **Figure 4.6A**, step *e*).

To synthesize catecholic α-cyano derivatives **17-21**, cyanoacetamides **68**, **70-72** were prepared prior to the Knoevenagel condensation with caffeic aldehyde. Two methodologies were employed to obtain compounds **68**, **70-72**. A PyBOP-mediated amidation between cyanoacetic acid and piperidine yielded compound **68** (**Figure 4.6B**, step *f*). Alternatively, ethyl cyanoacetate was refluxed with the appropriate amine to afford compounds **70-72** (**Figure 4.6B**, step *g*). Final compounds were obtained after a Knoevenagel condensation between caffeic aldehyde (compound **66**) and compounds **67**, **68**, **70-72** (**Figure 4.6B**, step *h*) (**Manuscript IV**).

On the other hand, the synthesis of α-cyanopiperic acid and derivatives thereof (compounds **30-37**) involved a Knoevenagel condensation followed by amidation or esterification reactions. Aldehyde **65** was used to synthesize α-cyanopiperic acid (compound **30**) by a Knoevenagel condensation with cyanoacetic acid (**Figure 4.6C**, step *h*). Subsequent PyBOP-mediated amidation afforded compounds **31-34** (**Figure 4.6C**, step *f*). Compounds **35-37** were obtained by a Steglich esterification reaction, assisted by *N*-(3-dimethylaminopropyl)-*N'*-ethylcarbodiimide (EDC) and 4-(dimethylamino)pyridine (DMAP), between compound **30** and the appropriate alcohol (**Figure 4.6B**, step *i*) (**Manuscript VI**).

Overall, final compounds and related intermediates were obtained in moderate to high yields (**Table 4.4**).

4.1.5. Synthesis of piperine-based triphenylphosphonium conjugates

To obtain piperine-based TPP conjugates **38-41** (**Figure 4.7, Table 4.5**), aminoalkyl TPP salts **77** and **78** were synthesized in a two-step sequence prior to piperic acid amidation. First, bromoalkylphthalymides **73** and **74** were heated with triphenylphosphine yielding the parent phthalimidylalkylltriphenylphosphonium salts (**Figure 4.7**, step *a*). Then, compounds **75** and **76** were refluxed with butylamine ($BuNH_2$) to induce the phthalymidyl ring cleavage affording amines **77** and **78**, respectively (**Figure 4.7**, step *b*). Following the alkaline hydrolysis of piperine (**Figure 4.7**, step *c*), the resulting piperic acid was acylated with ethyl chloroformate under alkaline conditions and reacted with amines **77** and **78**, yielding compounds **38** and **39**, respectively (**Figure 4.7**, step *d*). Finally, *O*-demethylenation reactions were performed by refluxing compounds **38** and **39** with boron tribromide dimethyl sulfide complex ($BBr_3.S(CH_3)_2$), leading to the corresponding catechols (**Figure 4.7**, step *e*) (**Manuscript VII**).

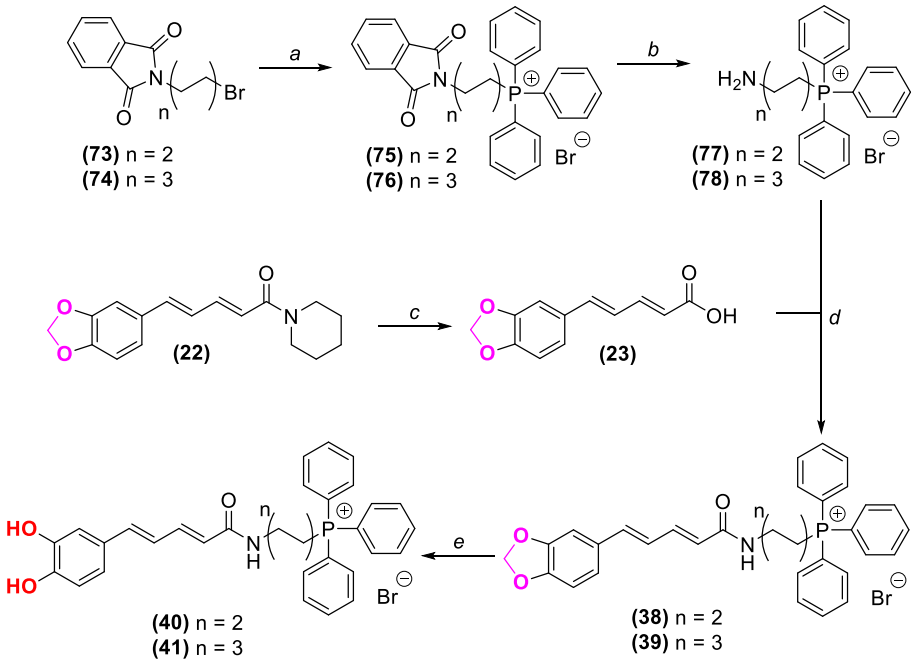
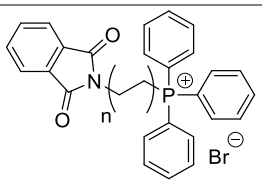
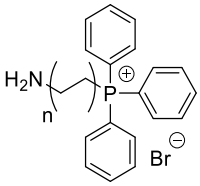
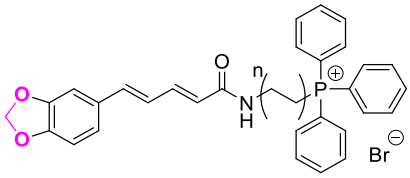
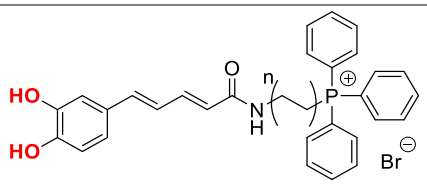


Figure 4.7: Synthetic strategy pursued to obtain mitochondria-targeted agents **38-41**. (a) triphenylphosphine, argon atmosphere, 130 ºC, 1.5-4 h; (b) $BuNH_2$, ethanol, reflux, 1.5-10 h; (c) Methanolic solution of NaOH 2 M, reflux, 24 h; (d) 1. CH_2Cl_2, Et_3N, ethyl chloroformate, rt, 2 h; 2. Compounds **77** and **78**, rt, overnight; (e) $BBr_3.S(CH_3)_2$, CH_2Cl_2, argon atmosphere, reflux, 6 h.

Table 4.5: chemical structures and reaction yields of alkyl triphenylphosphonium conjugates **38-41** and related intermediates.

	React.	Comp.	n	η/%	Manuscr.
	*a*	**75**	2	97	**VII**
		76	3	87	**VII**
	*b*	**77**	2	86	**VII**
		78	3	80	**VII**
	*d*	**38**	2	44	**VII**
		39	3	46	**VII**

	*e*	**40**	2	29	**VII**
		41	3	44	**VII**

4.2. Biological and toxicological profiles of compound libraries

4.2.1. Boosting the antioxidant activity of ferulic acid

Produced as a secondary metabolite in most plant families (359), FA is a HCA associated with numerous health benefits (392). One of the best documented biological activities of FA is its antioxidant activity, which arises from its ability to scavenge free radicals and activate cell stress responses (393). The antioxidant activity of FA could be beneficial in preventing or treating oxidative stress-related disorders (394), but its use in therapy is hampered by its physicochemical properties. Indeed, FA and other HCAs present marked hydrophilicity, which significantly hinders their distribution throughout the body and difficult to their biological targets (278, 279).

The antioxidant activity of FA is also outperformed by other HCAs such as CA and sinapic acid (279, 395-397). In this context, an innovative strategy was adopted to boost the antioxidant activity of FA. Based on the negative standard reduction potentials of biothiols (217), and inspired by their physiological role in redox-regulated and redox-mediated processes (215), our research group developed 4-thioferulic acid (compound **2**), a new sulphured analogue of FA (**Figure 4.8**; **Manuscript II**). Then, several methods were used to study the differences between FA and compound **2** concerning rate and mechanism of radical scavenging activity, electrochemical behaviour, acidity of phenol and thiophenol groups, cytotoxicity in differentiated neuroblastoma (SH-SY5Y cells) and protection against oxidative stress-induced damage (**Manuscript II**).

To complement the studies with thiophenol-based molecules, other thiophenols (compounds **3-6**) were developed in **Manuscript III** (**Figure 4.8**). Accordingly, methoxy and phenyl groups were directly attached to the aromatic ring to increase the antioxidant activity of thiophenols. These substituents were expected to provide additional stabilization of thiophenoxyl radicals formed following radical scavenging, either by acting as an electron-donating group (5-methoxy) (369, 370) or by increasing the electron delocalization throughout the molecule (5-phenyl). Lipophilic substituents were also introduced at the carboxylic acid group to provide a higher mobility across lipid membranes, thereby modulating the antioxidant activity of thiophenols in biological systems (222, 398). The

antioxidant properties of thiophenols **3-6** were compared with the parent phenols (compounds **7**-**10**) (**Manuscript III**).

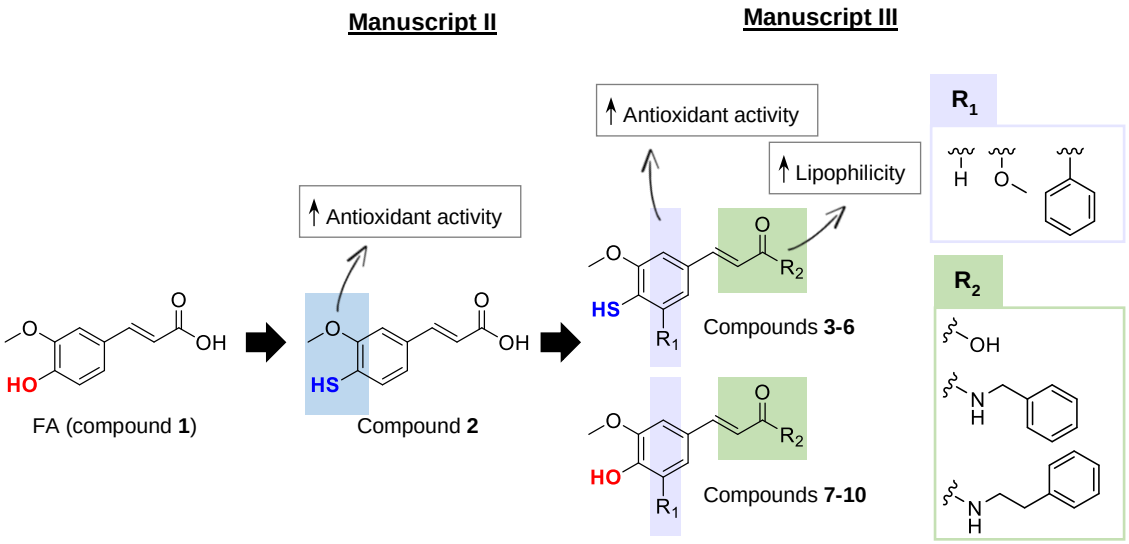


Figure 4.8: Drug design strategy used to improve the antioxidant activity of FA.

4.2.1.1. Antioxidant profile in cell-free systems

The antioxidant activity of thiophenols **2-6** and phenols **1**, **7-10** was first evaluated by measuring their ability to scavenge $DPPH^{\bullet}$, $ABTS^{\bullet+}$ and $GO^{\bullet}$ radicals. The isosteric replacement of the hydroxyl group (OH) with a sulfhydryl group (SH) maintained or even enhanced the antioxidant activity of cinnamic acid derivatives (**Figure 4.9**; **Manuscripts II** and **III**). In addition, marked differences were observed in the kinetic curves obtained for phenols and thiophenols indicating dissimilar reactivity. Thiophenols **2-6** reacted almost instantaneously with $DPPH^{\bullet}$, $ABTS^{\bullet+}$ and $GO^{\bullet}$ radicals, causing abrupt decays on the initial absorbances with increasing concentrations (**Figure 4.9**; **Manuscripts II** and **III**). On the other hand, the hyperbolic kinetic curves obtained with phenols **1**, **7-10** suggest that the radical scavenging occurred slower, requiring more time to reach the steady state (**Manuscripts II** and **III**). The tendencies observed were corroborated by the data obtained in voltammetric studies. The OH to SH replacement shifted the oxidation potentials (E_p) towards lower values, suggesting that thiophenols **2-6** are more prone to donate electrons than phenols **1**, **7-10** (**Figure 4.9**; **Manuscripts II** and **III**). In cyclic voltammetry (CV) experiments, the absence of reduction peaks on the reverse scan indicated that the oxidation processes of FA and compound **2** were irreversible.

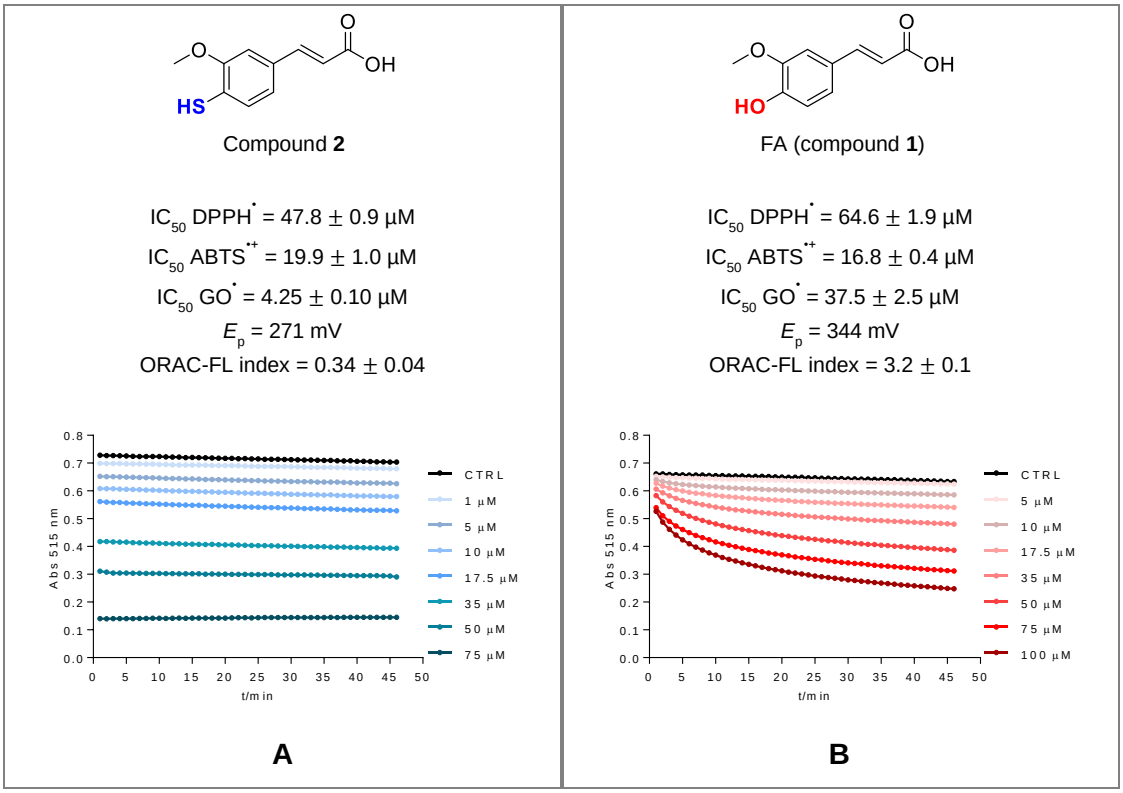


Figure 4.9: Representative results obtained with FA **1** and compound **2** (radical scavenging activity, redox potentials (E_p) and kinetic curves obtained in DPPH• assay).

The antioxidant activity of compounds **1-10** was also studied towards peroxyl radicals (ROO•) using the oxygen radical absorbance capacity (ORAC-FL) assay. Contrary to the tendency observed in DPPH•, ABTS•+ and GO• assays, phenols **1**, **7-10** scavenged ROO• radicals more efficiently than thiophenols **2-6** (**Manuscripts II** and **III**). The differences observed may result from the marked differences in the acidity of phenol and thiophenol groups. In differential pulse voltammetry (DPV) experiments with FA and compound **2** performed over a pH range of 1-12, the thiophenol group of compound **2** was considerably more acidic than the phenol group of FA ($pK_{a\ thiophenol}$ = 5.6; $pK_{a\ phenol}$ = 9.1) (**Manuscript II**). As a result, while phenols are predominantly in the neutral form at physiological pH 7.4, thiophenols are mainly in the form of thiophenolate anions. Since the scavenging of ROO• radicals occurs via hydrogen atom transfer (HAT) or by radical addition (399), the deprotonated thiophenols are less able to scavenge ROO• radicals by HAT than the protonated phenols at physiological pH 7.4 (**Manuscripts II** and **III**).

The incorporation of 5-methoxy and 5-phenyl groups did not improve the antioxidant profile of the parent compounds (FA and compound **2**). Despite the modest decrease of E_p values, 5-methoxy and 5-phenyl derivatives exhibited similar or lower radical scavenging activity and slower reaction rates than the unsubstituted analogues. On the other hand,

carboxylic acid amidation with lipophilic groups maintained the antioxidant properties of the parent compounds while improving their drug-like properties (**Manuscript III**).

4.2.1.2. Cytotoxicity and antioxidant activity in differentiated SH-SY5Y cells

Following the assessment of the antioxidant activity in cell-free systems, the cytotoxicity of compounds **1-10** was studied in differentiated SH-SY5Y cells. Both thiophenols **2-6** and phenols **1**, **7-10** were well-tolerated by neuroblastoma cells at concentrations up to 50 µM (**Figure 4.10**; **Manuscripts II** and **III**).

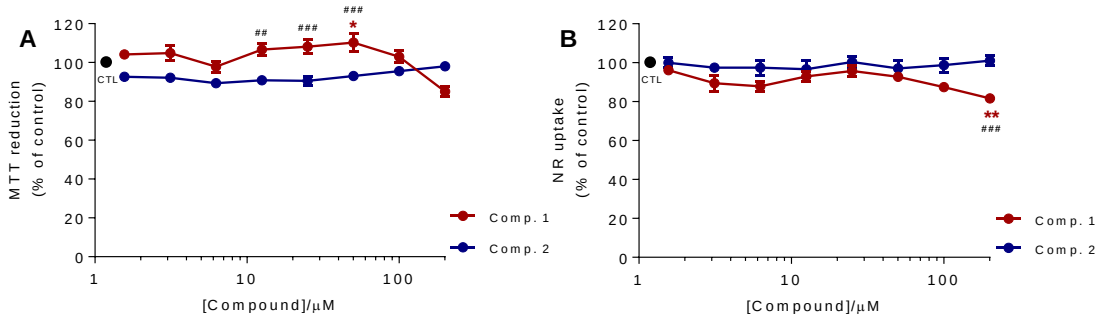


Figure 4.10: Cellular viability of differentiated SH-SY5Y neuroblastoma cells after a 24 h treatment with FA (compound **1**, red) and compound **2** at eight different concentrations (1.6 µM – 200 µM). Cellular viability was evaluated using two methods: MTT reduction (**A**) and NR uptake (**B**) assays. Results are expressed as the mean % of untreated controls ± SEM (n = 3). Statistical comparisons were carried out by two-way ANOVA followed by Bonferroni's multiple-comparisons *post hoc* test. (* $p < 0.05$, ** $p < 0.01$, vs control; ## $p < 0.01$, ### $p < 0.0005$, compound **1** vs compound **2**).

Then, their cytoprotective properties were evaluated against three inducers of oxidative stress (*tert*-butyl hydroperoxide, *t*-BHP; H_2O_2; and ferric nitrilotriacetate, FeNTA) in the same cellular model, after a pre-treatment of cells with the test compounds at 10 and 50 µM for 24 h. Thiophenols **2** and **3** and phenol **10** displayed the most promising cytoprotective profiles among the two sets of compounds. Compounds **2**, **3** and **10** significantly attenuated the oxidative stress induced by H_2O_2 (MTT reduction of 60-62 %, **Figure 4.11**) and FeNTA (MTT reduction of 56-58 %, **Figure 4.12**). Compound **2** at 50 µM also protected differentiated SH-SY5Y cells against the harmful effects of *t*-BHP (MTT reduction of 70 %) (**Manuscript II**).

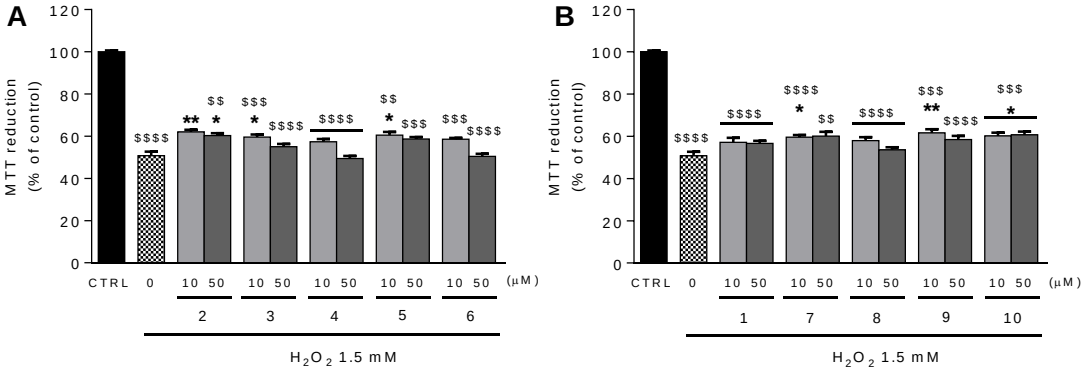


Figure 4.11: Protection against H_2O_2-induced damage in differentiated SH-SY5Y neuroblastoma cells by thiophenols **2-6** and phenols **1**, **7-10**. After a pre-treatment with the compounds under study (10 μM and 50 μM) for 24 h, cells were exposed H_2O_2 1.5 mM for additional 30 min. Cellular viability was evaluated by the MTT reduction assay. Results are expressed as the mean % of untreated controls ± SEM (*n* = 3). Statistical comparisons were estimated using the nonparametric method of Kruskal–Wallis (one-way ANOVA on ranks), followed by Dunn's *post hoc* test (* $p < 0.05$, ** $p < 0.01$, *** $p < 0.0005$, ****$p < 0.0001$, compared with H_2O_2 1.5 mM; $^{\$\$}$ $p < 0.01$, $^{\$\$\$}$ $p < 0.001$; $^{\$\$\$\$}$ $p < 0.0001$ compared with CTRL).

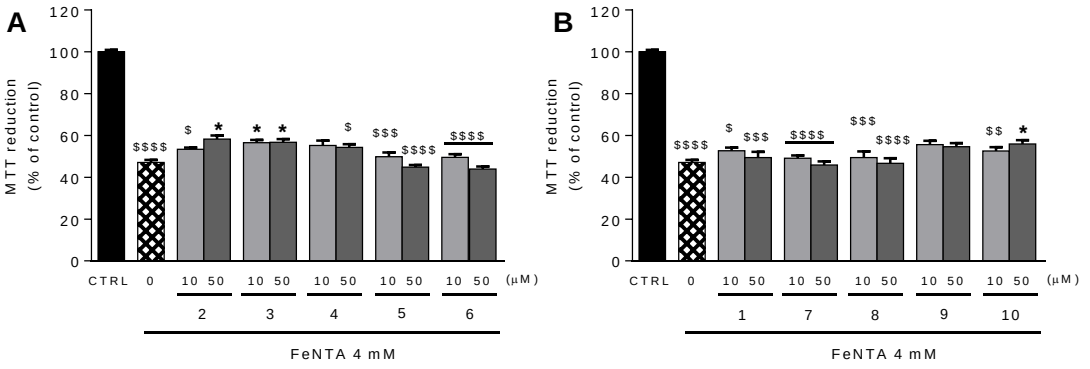


Figure 4.12: Protection against FeNTA-induced damage in differentiated SH-SY5Y neuroblastoma cells by thiophenols **2-6** and phenols **1**, **7-10**. After a pre-treatment with the compounds under study (10 μM and 50 μM) for 24 h, cells were exposed FeNTA 4 mM for additional 24 h. Cellular viability was evaluated by the MTT reduction assay. Results are expressed as the mean % of untreated controls ± SEM (*n* = 3). Statistical comparisons were estimated using the nonparametric method of Kruskal–Wallis (one-way ANOVA on ranks), followed by Dunn's post hoc test (* $p < 0.05$, ** $p < 0.01$, *** $p < 0.0005$, ****$p < 0.0001$, compared with FeNTA 4 mM; $^{\$}$ $p < 0.05$, $^{\$\$}$ $p < 0.01$, $^{\$\$\$}$ $p < 0.001$; $^{\$\$\$\$}$ $p < 0.0001$ compared with CTRL).

Overall, these results provide valuable data concerning the differences in the reactivity, antioxidant activity and cytotoxicity of phenolic and thiophenolic compounds. Despite the higher reactivity of thiophenols, the OH to SH replacement preserved the cytotoxicity profile of cinnamic acid derivatives while improving their antioxidant activity.

4.2.2. Fine-tuning the pharmacological profile of caffeic acid and piperine

Motor symptoms of PD are associated with the decrease of nigrostriatal dopamine levels, as a result of the loss of dopaminergic neurons in the *substantia nigra pars compacta* (131). In this sense, inhibitors of MAO-B and COMT, two enzymes involved in DA decomposition, are currently used in PD to boost the DA tone in the brain (130).

Although the etiology of PD is not fully understood, the selective neurodegeneration observed in this disease has been linked to oxidative stress (250). In fact, dopaminergic neurons are particularly sensitive to oxidative stress (263) because the enzymatic and non-enzymatic oxidation of DA generates RS (236, 239). Furthermore, nigrostriatal dopaminergic neurons accumulate iron, which may catalyse the formation of RS through Fenton reaction (263).

The biological effects of piperine and CA are of particular relevance within the scope of PD. Piperine is well-known for its P-gp inhibitory activity (400), but several lines of evidence indicate that piperine is a competitive and reversible MAO inhibitor (389, 401). A set of chemical modifications were performed on the piperine scaffold at the diene tether and the piperidinyl amide group in **Manuscripts V** and **VI** (**Figure 4.13**). The resulting piperine derivatives were screened towards *h*MAOs and new structure-activity relationships were established.

.

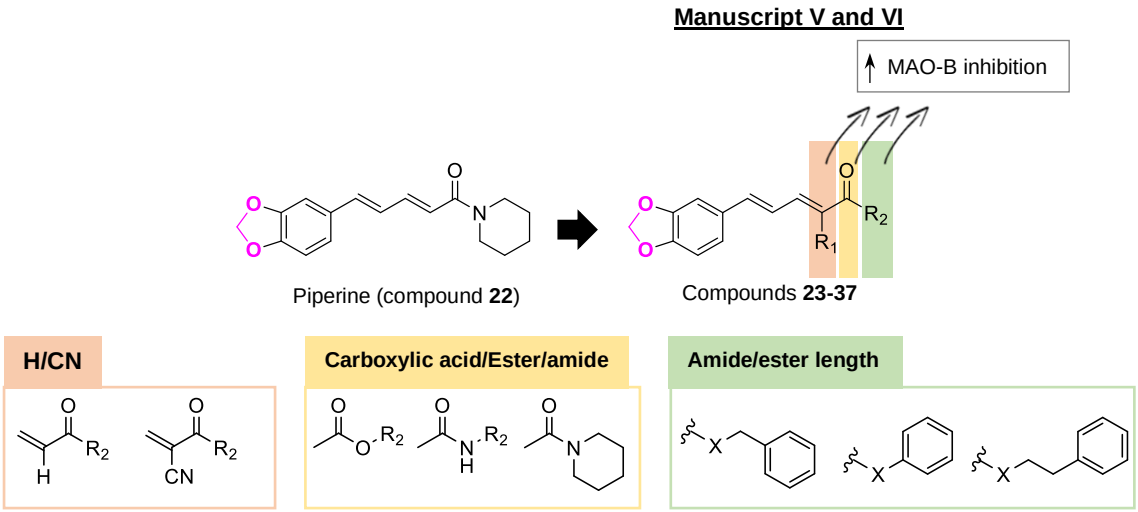


Figure 4.13: Drug design strategy used to obtain piperine-based MAO-B inhibitors.

Caffeic acid is widely described as a potent antioxidant (377). In addition, synthetic derivatives of CA were reported as potent COMT inhibitors (170, 402). Ethylenic and α-CN groups were incorporated in the chemical scaffold of CA in **Manuscript IV** (**Figure 4.14**). These chemical modifications were explored as an alternative to the nitrocatechol

pharmacophore found in COMT inhibitors such as tolcapone and entacapone. Accordingly, ethylenic and α-CN groups were introduced to mimic the effect of 5-nitro group in decreasing the pK_a of the phenol, thus reducing the extent of *O*-methylation of the resulting phenolate. The additional double bond was also incorporated to enhance the antioxidant activity of catechols by increasing the electron delocalization throughout the molecule. To improve the drug-like properties of CA derivatives, the carboxylic acid moiety was functionalized with lipophilic groups. Since CA derivatives contain similar chemical structures to piperine, they were also screened towards *h*MAOs.

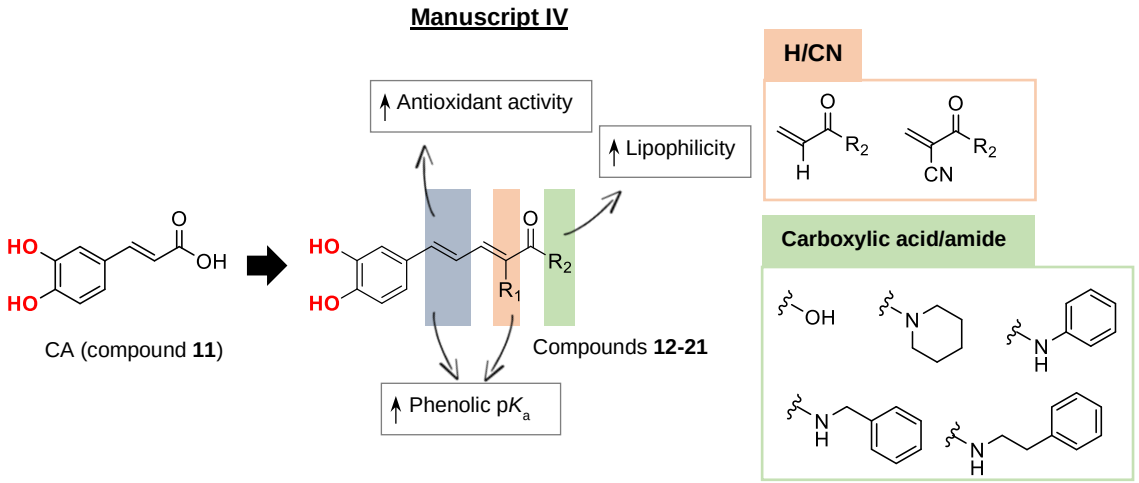


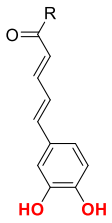
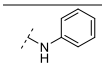
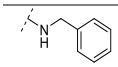
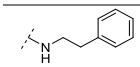
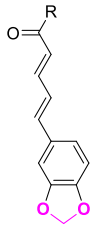
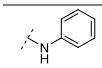
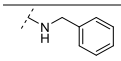
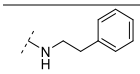
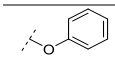
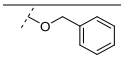
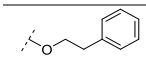
Figure 4.14: Drug design strategy used to obtain CA-based derivatives **12-21**.

4.2.2.1. Biological effects in cell-free systems

The results obtained in *h*MAO inhibition studies showed that piperine (compound **22**), piperine derivatives **27-29**, **31**, **33**, **35-37** and CA derivatives **13**, **18-21** act as selective *h*MAO-B inhibitors, with IC_{50} values within the low micromolar or nanomolar ranges (**Tables 4.6 and 4.7**). Structure-activity-relationship studies identified the most favourable chemical modifications for potent and selective MAO-B inhibition (**Figure 4.15**), of which the insertion of an α-CN group was the most prominent feature. Esters were generally more active than piperidinyl amides, while secondary amides and carboxylic acids displayed poor or absent *h*MAO-B inhibitory activity. Benzyl derivatives were the most potent *h*MAO-B inhibitors, followed by phenethyl and phenyl derivatives. From the data obtained with α-cyanobenzyl derivatives (compounds **20**, **33** and **36**) and the parent α-unsubstituted analogues (compounds **15**, **24** and **28**), it was concluded that the combination of an α-CN and benzyl groups enhanced *h*MAO-B inhibition potency and selectivity (**Manuscripts V** and **VI**). Compounds with a benzodioxole group were generally more active towards *h*MAO-B than

the parent catechols (**Manuscripts IV, V** and **VI**). Within this compound libraries, the most potent *h*MAO-B inhibitors were piperine derivatives **27** (*h*MAO-B IC_{50} = 156±8 nM), **28** (*h*MAO-B IC_{50} = 167±11 nM), **31** (*h*MAO-B IC_{50} = 143±80 nM), **36** (*h*MAO-B IC_{50} = 47.1±8.0 nM) and **37** (*h*MAO-B IC_{50} = 99.2±8.2 nM) (**Tables 4.6 and 4.7**).

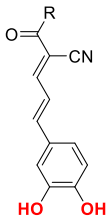
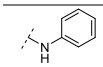
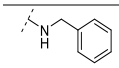
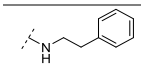
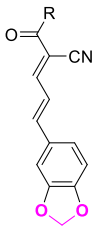
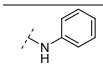
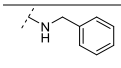
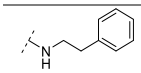
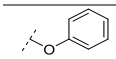
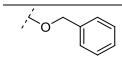
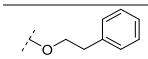
Table 4.6: *h*MAO inhibitory activities of compounds **12-16**, **23-29** and reference inhibitors.

	R	Compound	IC_{50} (μM)		SI[b]
			*h*MAO-A	*h*MAO-B	
		**12**	___[a]	___[a]	__
		**13**	___[a]	2.50±0.22	> 4[d]
		**14**	___[a]	___[a]	__
		**15**	___[a]	___[a]	__
		**16**	___[a]	___[a]	__
		**23**	___[a]	___[a]	__
		**22**	___[a]	1.05±0.08	> 10[d]
		**24**	___[a]	___[a]	__
		**25**	___[a]	___[a]	__
		**26**	___[a]	___[a]	__
		**27**	___[c]	0.156±0.008	> 64[d]
		**28**	4.24±0.56	0.167±0.011	25
		**29**	___[a]	0.448±0.043	> 22[d]
	(*R*)-(−)-Deprenyl[e]	__	20.1±1.9	0.0386±0.0043	522
	Rasagiline	__	3.65±0.31	147.3±249	24
	Safinamide	__	___[a]	0.0231±0.0026	> 433[d]
	Clorgyline[e]	__	0.00274±0.00047	2.21±0.26	0.00124

[a] Inactive at 10 μM considering an MAO-B inhibitory activity threshold of 50 %.
[b] SI: *h*MAO-B selectivity index = IC_{50}(*h*MAO-A)/IC_{50}(*h*MAO-B).
[c] Not soluble in phosphate buffer at concentrations higher than 10 μM.
[d] Values obtained under the assumption that the corresponding IC_{50} value against *h*MAO-A or *h*MAO-B is the highest concentration tested (10 μM).

Table 4.7: *h*MAO inhibitory activities of α-CN derivatives **17-21**, **30-37**.

	R	Compound	IC_{50} (μM)	SI[b]

			*h*MAO-A	*h*MAO-B	
		**17**	___[a]	___[a]	__
		**18**	___[a]	4.27±0.30	> 2[c]
		**19**	___[a]	4.55±0.31	> 2[c]
		**20**	___[a]	1.15±0.04	> 9[c]
		**21**	___[a]	4.38±0.51	> 2[c]
		**30**	___[a]	___[a]	__
		**31**	___[a]	0.143±0.080	> 70[c]
		**32**	___[a]	___[a]	__
		**33**	___[a]	0.471±0.008	> 21[c]
		**34**	___[a]	___[a]	__
		**35**	___[a]	0.215±0.038	>47[c]
		**36**	___[a]	0.0474±0.0042	> 211[c]
		**37**	___[a]	0.0992±0.0082	> 101[c]

[a] Inactive at 10 μM considering an MAO-B inhibitory activity threshold of 50 %.
[b] SI: *h*MAO-B selectivity index = IC_{50}(*h*MAO-A)/IC_{50}(*h*MAO-B).
[c] Values obtained under the assumption that the corresponding IC_{50} value against *h*MAO-A or *h*MAO-B is the highest concentration tested (10 μM).

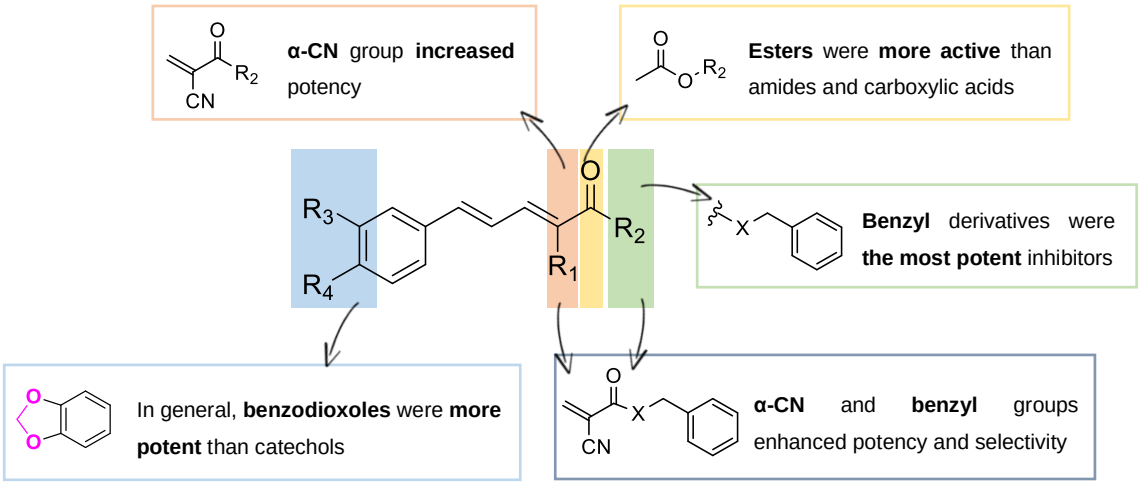


Figure 4.15: Preliminary structure-activity relationships obtained from *h*MAO-B inhibition studies with piperine- and CA-based libraries.

Kinetic studies with compounds **28**, **36** and **37** clearly showed that they act as competitive *h*MAO-B inhibitors (**Figure 4.16A**). Moreover, time-dependent inhibition studies indicated that compound **36** is a reversible inhibitor (**Figure 4.16B**) (**Manuscript VI**).

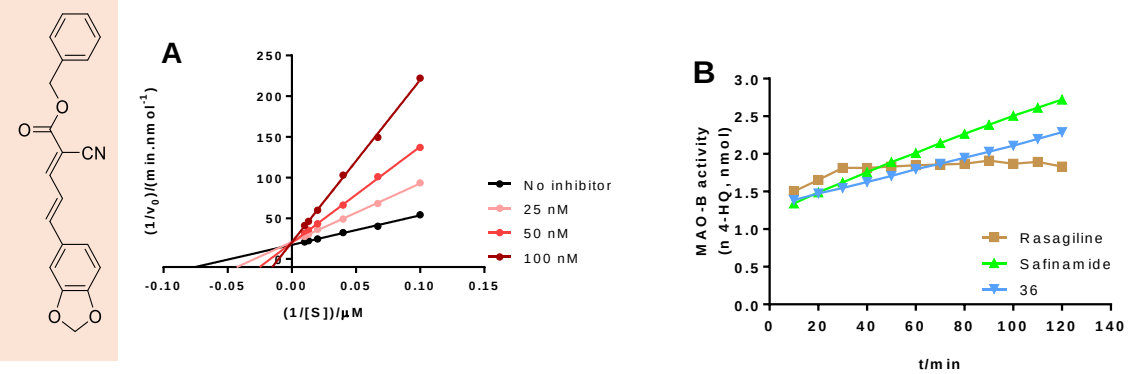


Figure 4.16: (**A**) Representative double reciprocal plot of the initial velocity of *h*MAO-B at increasing substrate concentrations (10-100 µM) in the absence or the presence of compound **36**. (**B**) Time-dependent inhibition of recombinant *h*MAO-B by reference drugs rasagiline and safinamide, and compound **36**.

The inhibitory activity of CA **11** and derivatives **12-21** towards COMT was also assessed in rat liver and brain homogenates. Preliminary results showed that compounds **12-21** were potent brain COMT inhibitors. The data acquired so far is being confirmed by other assays and will be patented.

In addition to MAO and COMT inhibition studies, the ability of compounds **11-37** to inhibit *ee*AChE and *eq*BChE were investigated. However, under our experimental conditions, none of the compounds inhibited both ChEs in the first screening at a concentration of 10 µM.

Following the preliminary screening towards neurotransmitter-metabolizing enzymes, the antioxidant activity of CA (compound **11**) and derivatives thereof **12-21** was assessed towards ROO• radicals using the ORAC assay. In general, all catechols presented remarkable ROO• radical scavenging activity. The antioxidant activity was enhanced with the insertion of an ethylenic group in the side chain of CA. On the other hand, α-CN groups and increased lipophilicity had a negative effect on ROO• radical scavenging in the ORAC assay (**Manuscript IV**). These observations were in line with the results obtained in DPV experiments at physiological pH. Accordingly, E_p values of compounds **12-16** ranged between 113 and 129 mV and were considerably lower than the obtained with CA (compound **11,** E_p = 168 mV). Therefore, the increased electron delocalization provided by the additional double bond shifted the peak potentials towards lower values, thereby increasing the reducing power of catechols. In contrast, α-CN

derivatives **17-21** presented E_p between 144 and 174 mV, being higher than the values obtained for non-substituted analogues **12-16** and similar to CA. The electron-withdrawing nature of α-CN reduced the stabilisation of the oxidized form (403) of compounds **17-21**, thereby promoting a positive shift in the peak potentials. Finally, since catechol amides **13-16** and **18-21** showed E_p values similar to the parent carboxylic acids, the redox properties of CA derivatives were preserved with carboxylic acid amidation (**Manuscript IV**). The effects of the chemical modifications of CA scaffold in the antioxidant activity are summarized in **Figure 4.17**.

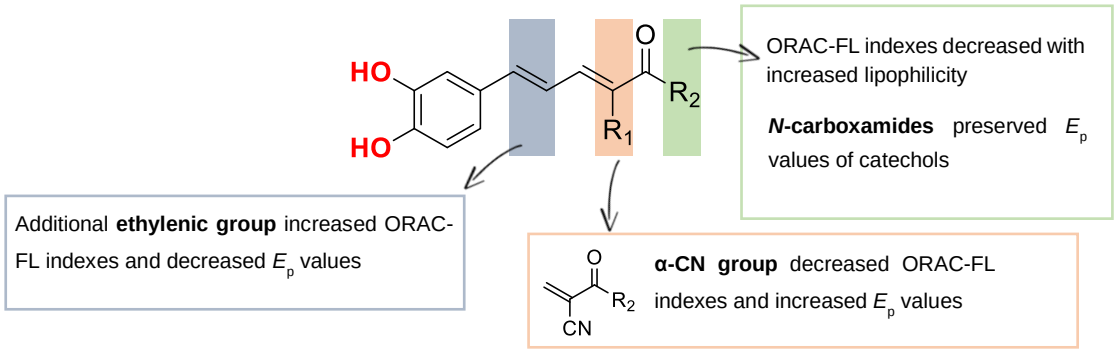


Figure 4.17: Preliminary structure-activity relationships obtained from ORAC assay and electrochemical assays with caffeic acid **11** and derivatives **12-21**.

4.2.2.2. Cytotoxicity in differentiated SH-SY5Y cells and Caco-2 cells

Subsequent studies were performed in two cell lines (SH-SY5Y cells and Caco-2 cells) with the compounds that displayed relevant biological effects in the preliminary screenings (CA derivatives **13, 18-21** and piperine derivatives **27**, **28**, **31**, **36** and **37, Tables 4.6 and 4.7**). Caffeic acid (compound **11**), catechols **12** and **17**, and piperine were also included in the cell-based studies to evaluate the effects of the chemical modifications in cytotoxicity, antioxidant activity and modulation of P-gp transport.

First, the cytotoxicity at 10 and 50 µM was assessed in differentiated SH-SY5Y cells. Caffeic acid (compound **11**) and carboxylic acids **12** and **17** did not exhibit cytotoxic effects at both tested concentrations. On the other hand, catechol amides **13, 18-21** showed safe cytotoxicity profiles at concentrations up to 10 µM, although moderate cytotoxic effects were detected at 50 µM (**Figure 4.18**; **Manuscript IV**).

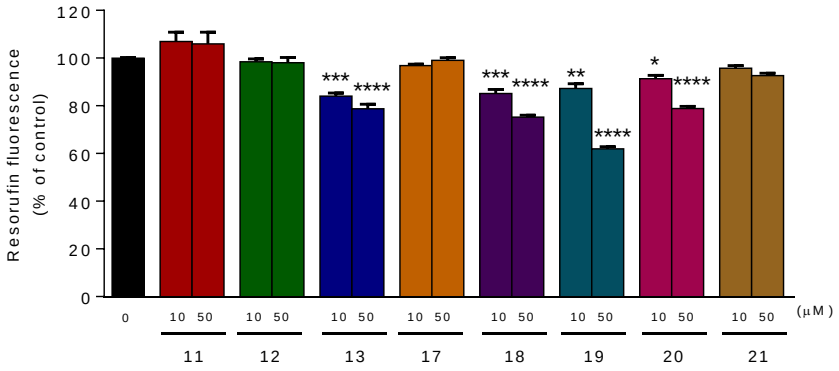


Figure 4.18: Cellular viability of differentiated SH-SY5Y cells after incubation with CA (compound **11**) and compounds 1**2, 13**, **17-21** at two concentrations (10 and 50 µM) for 24 h. Cellular viability was evaluated by measuring metabolic activity using the resazurin reduction assay. Statistical comparisons were made using one-way ANOVA followed by Kruskal-Wallis test. In all cases, *p* values lower than 0.05 were considered significant (* $p < 0.05$, ** $p < 0.01$, *** $p < 0.001$; **** $p < 0.0001$).

The toxicity observed at 50 µM was associated with the increased formation of RS, generated from the oxidation of the catechol group and in redox cycling processes mediated by the resulting *ortho*-quinones (404, 405). In fact, CA (compound **11**) and compounds **12-21** displayed reversible oxidative behaviours in CV experiments (**Manuscript IV**). Treatments of neuroblastoma cells with catechol amides **13**, **18-21** at 10 and 50 µM resulted in significant concentration-dependent increases in 2',7'-dichlorofluorescein (DCF) fluorescence indicating augmented intracellular oxidative stress (**Manuscript IV**).

Piperine derivatives **28**, **31**, **36** and **37** (**Tables 4.6 and 4.7**) exhibited a broader safety window than the tested CA derivatives in differentiated SH-SY5Y cells. The only exception was compound **27**, which presented marked cytotoxic effects at 50 µM (**Figure 4.19A, Manuscript VI**). The cytotoxicity of piperine derivatives **27**, **28**, **31**, **36** and **37** was also conducted in Caco-2 cells. In this case, treatment with the test compounds at 10 and 50 µM did not markedly affect cellular metabolic and lysosomal activities (**Figure 4.19B, Manuscript VI**).

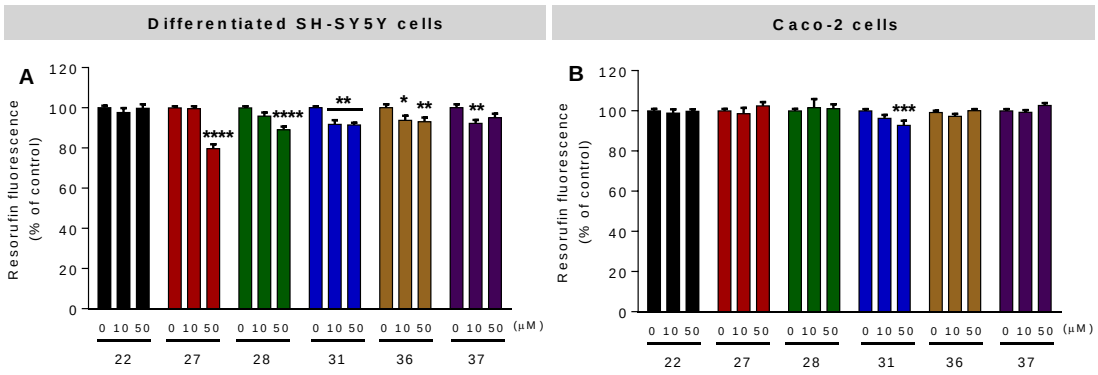
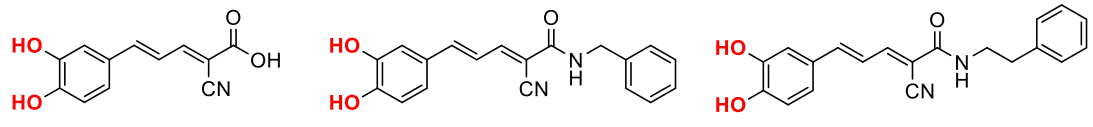


Figure 4.19: cellular viability of differentiated SH-SY5Y cells (**A**) and Caco-2 cells (**B**) after incubation with piperine (**22**) and compounds **27**, **28**, **31**, **36** and **37** at two different concentrations (10 μM and 50 μM) for 24 h. Cellular viability was evaluated by measuring metabolic activity using the resazurin reduction assay. Statistical comparisons were performed using the parametric method of two-way ANOVA, followed by the Dunnett's multiple comparisons test. In all cases, *p* values lower than 0.05 were considered significant (* $p < 0.05$, ** $p < 0.01$, *** $p < 0.001$, **** $p < 0.0001$ vs untreated cells).

4.2.2.3. Antioxidant activity of caffeic acid derivatives in SH-SY5Y cells

Based on the results obtained in the antioxidant, enzyme inhibition and cytotoxicity studies, compounds **20** and **21** (**Figure 4.20**) were proposed as the most promising CA derivatives. Therefore, these compounds were selected for the evaluation of the antioxidant activity against *t*-BHP in differentiated SH-SY5Y cells. Compound **17**, the parent α-CN carboxylic acid, was also tested to study the effect of the carboxylic acid amidation in the antioxidant efficiency of CA derivatives. Unlike compound **17**, CA derivatives **20** and **21** at non-toxic concentrations displayed noticeable cytoprotective properties against *t*-BHP-induced oxidative damage (**Figure 4.21**). Indeed, neuroblastoma cells pre-treated with catechol amides **20** and **21** showed cellular metabolic activity significantly higher than that of the *t*-BHP treatment alone ($p < 0.0001$) and similar to that of non-treated cells. Therefore, the carboxylic acid amidation with lipophilic groups may increase the compounds' ability to cross the cell membranes by passive diffusion, thereby improving the antioxidant efficiency of CA derivatives in cellular systems (**Manuscript IV**).



Compound **17**
Non-significant *h*MAO-B inhibition
ORAC-FL index = 4.9±0.1
E_p = 144 mV

Compound **20**
IC_{50} *h*MAO-B = 1.15±0.04 µM
ORAC-FL index = 2.8±0.2
E_p = 174 mV

Compound **21**
IC_{50} *h*MAO-B = 4.38±0.51 µM
ORAC-FL index = 3.0±0.1
E_p = 163 mV

Figure 4.20: chemical structures and biological effects of caffeic acid derivatives **20** and **21**.

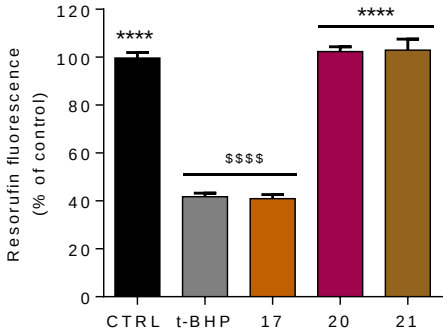


Figure 4.21: Neuroprotection against *t*-BHP-induced damage in differentiated SH-SY5Y cells by α-CN derivatives 1**7**, **20** and **21**. After a pre-treatment with the test compounds (10 µM) for 30 min, cells were exposed to *t*-BHP 200 µM for additional 24 h. Cellular viability was evaluated by the resazurin reduction assay. Results are expressed as the mean % of untreated controls ± SEM (n = 3). Statistical comparisons were performed using the one-way ANOVA followed by Dunnet's multiple comparison test. In all cases, p values lower than 0.05 were considered significant (**** $p < 0.0001$, compared with *t*-BHP; $^{\$\$\$\$}$ $p < 0.0001$, compared with non-treated cells).

In summary, the gathered data showed that compounds **20** and **21** are potent antioxidants and moderate MAO-B inhibitors. Although these compounds presented moderate toxicity at 50 µM, it is important to highlight that both antioxidant activity and MAO-B inhibition were observed at non-toxic concentrations.

4.2.2.4. Modulation of P-glycoprotein transport activity by piperine derivatives in Caco-2 cells

Considering that piperine was reported as a P-gp inhibitor (400), a preliminary evaluation of P-gp modulatory activity of piperine (compound **22**) and piperine-based *h*MAO-B inhibitors with safe cytotoxicity profiles (compounds **28**, **31**, **36** and **37**, **Figure**

4.22) was considered relevant. This study was performed in Caco-2 cells, a cellular model commonly used not only to assess the P-gp-mediated transport of drugs (406), but also to study the effect of new drug candidates in P-gp expression and/or activity (407, 408).

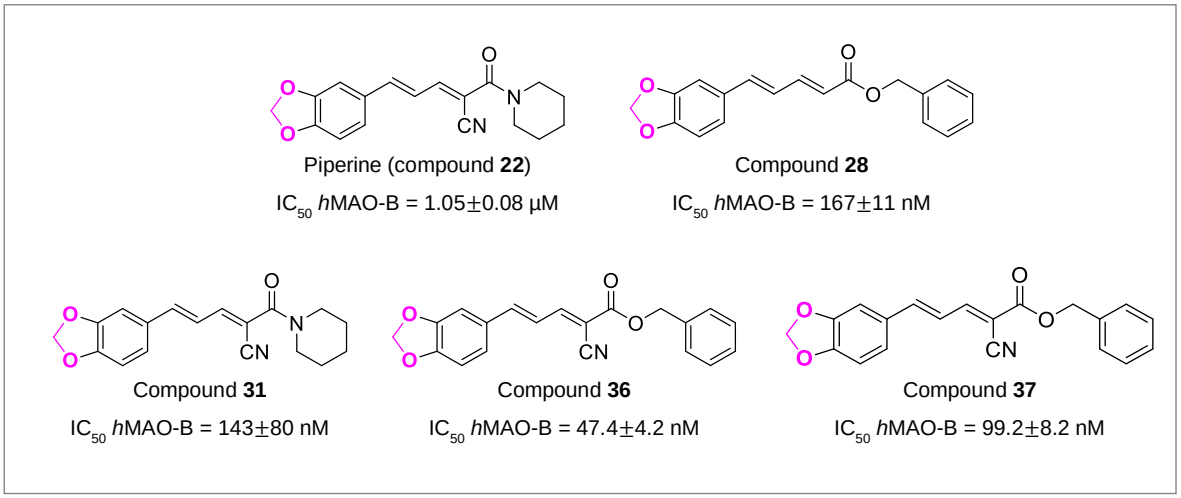


Figure 4.22: chemical structures and biological effects of piperine (compound **22**) and compounds **28, 31, 36** and **37**.

From the results obtained in the rhodamine 123 accumulation assay, it was concluded that compound **31** demonstrated potential for P-gp activation (**Figure 4.23**). Given the short incubation period with both the P-gp substrate and the test compounds, the increased P-gp activity observed with compound **31** is not associated with increased P-gp expression. On the other hand, compounds **36** and **37** significantly decreased P-gp transport activity indicating mild P-gp inhibition (**Figure 4.23**).

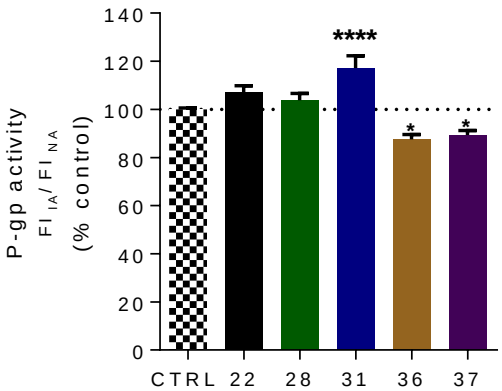


Figure 4.23: Evaluation of P-gp activity in Caco-2 cells exposed to compounds **22**, **28**, **31, 36** and **37** (10 µM) only during the incubation period with the fluorescent substrate (RHO 123, 5 µM). Results are presented as

mean ± SEM from at least three independent experiments, performed in triplicate. Statistical comparisons were made using the parametric method of one-way ANOVA, followed by the Dunnett's multiple comparisons test (****p < 0.0001 vs. control cells).

Drugs endowed with mild P-gp inhibitory activity can be valuable assets in PD combination therapy. Considering that several antiparkinsonian drugs (e.g.: L-DOPA, pergolide, pramipexole, bromocriptine) were described as P-gp substrates (342), mild P-gp inhibition could decrease the drug efflux in the capillary endothelial cells of the BBB, thereby improving the drug delivery into the brain and enabling a more sustained symptomatic relief (409).

Overall, the results obtained in **Manuscripts V** and **VI** provided valuable data concerning the development of non-toxic, piperine-based MAO-B inhibitors. Compounds **15** and **16** stood out as potent and selective *h*MAO-B inhibitors with mild P-gp inhibitory activity and safe cytotoxicity profile.

4.2.3. Targeting piperine and caffeic acid derivatives to michochondria

In addition to the low neurotransmitter levels observed in AD and PD (68), mitochondrial dysfunction is a prominent feature of NDs. Dysfunctional mitochondria are major contributors for the redox imbalance observed in NDs, since they are less efficient producers of ATP and more efficient producers of RS (7). Therefore, there is an increasing interest in developing of mitochondria-targeted agents able to mitigate mitochondrial oxidative damage (410).

An effective strategy commonly used to enhance the mitochondrial uptake of bioactive molecules is their conjugation with lipophilic TPP cations. Recently, our research group employed this approach to develop the first mitochondria-targeted antioxidants based on phenolic acids. The resulting compounds displayed strong antioxidant activity in cell-free and cell-based assays (297-300, 411) and acted as potent and noncompetitive ChE inhibitors (299). Together with the promising biological effects of piperine and CA derivatives, these observations prompted the design and development of four new mitochondria-targeted agents (**Manuscript VII**). Accordingly, compounds based on piperine and CA scaffolds were conjugated with TPP cations via four- or six-carbon alkyl chains (**Figure 4.24**). Preliminary biological screenings were then performed to assess their antioxidant properties and the inhibition of ChEs and MAOs. The ability of mitochondria-targeted agents to accumulate within mitochondria and their potential mitochondrial toxicity were also assessed.

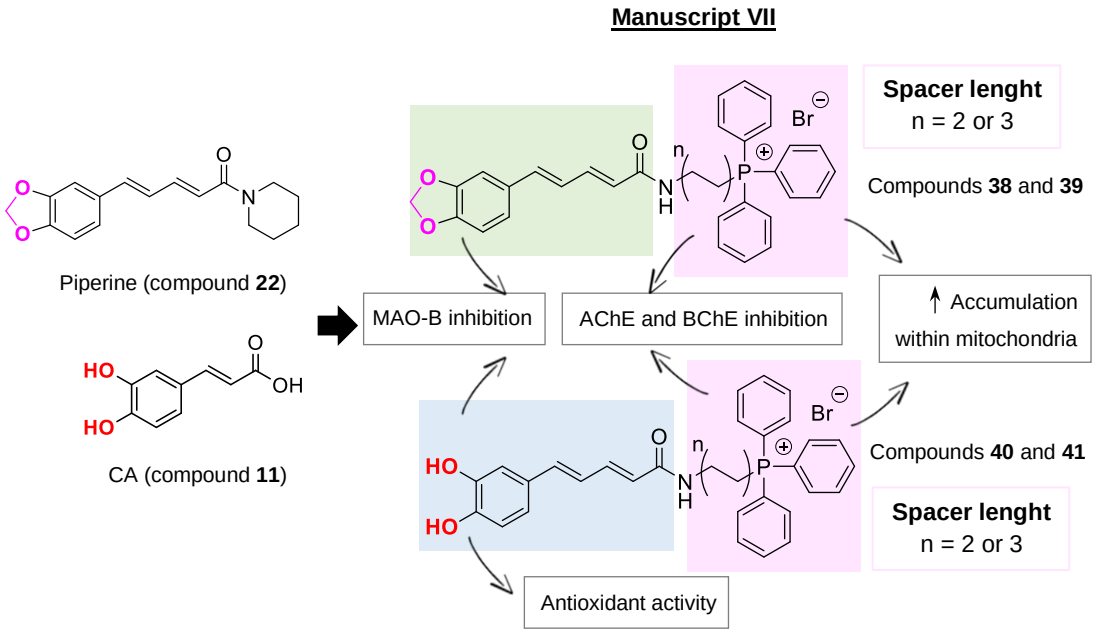


Figure 4.24: Drug design strategy used to obtain mitochondria-targeted agents based on the chemical scaffolds of piperine and caffeic acid.

4.2.3.1. Biological effects in cell-free systems

The data obtained in ChE inhibition studies indicated that compounds **38-41** inhibited both equine butyrylcholinesterase (*eq*BChE) and electric eel acetylcholinesterase (*ee*AChE), with higher selectivity towards the former (**Table 4.8**). Compounds **38-41** exhibited *ee*AChE IC_{50} values within the low micromolar range, while *eq*BChE IC_{50} values were within the nanomolar range. Catechols **40** and **41** were more active towards *ee*AChE than the parent benzodioxole derivatives, while the spacer length did not significantly affect *ee*AChE inhibition. On the other hand, *eq*BChE inhibition increased with the presence of a benzodioxole ring and/or longer alkyl chains (**Manuscript VII**).

Table 4.8: ChE (*ee*AChE and *eq*BChE) and *h*MAOs (*h*MAO-A and *h*MAO-B) inhibitory activities of piperine (compound **22**), compounds **38-41** and reference inhibitors.

Compound	IC_{50}/μM		SI (1)[b]	IC_{50}/μM		SI (2)[c]
	*ee*AChE	*eq*BChE		*h*MAO-A	*h*MAO-B	
22	___[a]	___[a]	___	___[a]	1.05±0.08	10[d]
38	6.39±0.28	0.0282±0.0014	226	0.888±0.022	12.4±1.9	0.07
39	5.74±0.32	0.0179±0.0009	314	1.23±0.13	4.64±0.29	0.26
40	2.23±0.12	0.0619±0.0042	36	5.17±0.54	13.5±1.1	0.38
41	2.14±0.06	0.0341±0.0029	62	2.17±0.28	10.9±0.7	0.20
Donepezil	0.0129±0.0008	2.50±0.07	0.0052	n.d.	n.d.	n.d.
R-(-)-Deprenyl	n.d.	n.d.	n.d.	20.1±1.9	0.0386±0.0043	522
Rasagiline	n.d.	n.d.	n.d.	3.65±0.31	147.3±249	24
Safinamide	n.d.	n.d.	n.d.	___[a]	0.0231±0.0026	433[d]
Clorgyline	n.d.	n.d.	n.d.	0.00274±0.00047	2.21±0.26	0.00124

[a] Inactive at 10 μM;
[b] SI (1): *eq*BChE selectivity index = IC_{50}(*ee*AChE)/IC_{50}(*eq*BChE).
[c] SI (2): *h*MAO-B selectivity index = IC_{50} (*h*MAO-A)/IC_{50} (*h*MAO-B).
[d] Values obtained under the assumption that the corresponding IC_{50} against *h*MAO-A or *h*MAO-B is the highest concentration tested (10 μM).
n.d.: not determined

Motivated by these promising results, the mechanism of *eq*BChE inhibition by six-carbon chain derivatives **39** and **41** was further evaluated. The Lineweaver-Burk plots of these compounds were consistent with a mixed-type inhibition mechanism (**Figure 4.25**), in which the inhibitor binds both the free enzyme and the enzyme-substrate binding complex at a site other than the active site. Data obtained from the Lineweaver-Burk plots were then replotted against the inhibitor concentration to determine the inhibition constants K_i and K_i'. Since K_i values of compounds **39** (K_i = 14.7 nM) and **41** (K_i = 23.3 nM) were lower than K_i' values (compound **39**: K_i' = 62.1 nM; compound **41**: K_i' = 69.7 nM), both inhibitors preferably bind to the free enzyme over the enzyme-substrate binding complex (**Manuscript VII**).

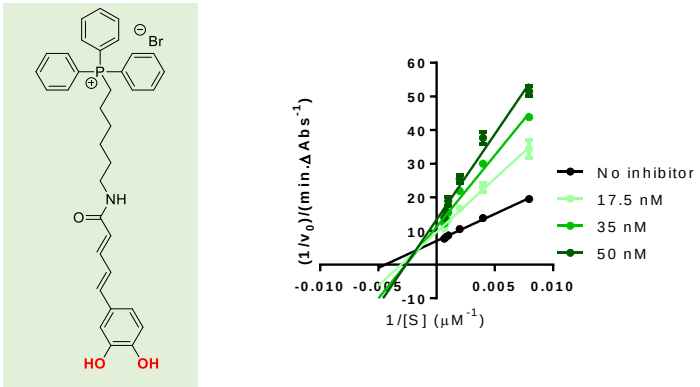


Figure 4.25: Representative double reciprocal plot of the initial velocity of *eq*BChE at increasing substrate concentrations (0.063 – 1.3 mM), in the absence or the presence of compound **41**.

In *h*MAO inhibition studies, piperine and compounds **39-41** presented dissimilar inhibitory profiles. While piperine acted as a moderate and selective *h*MAO-B inhibitor (**Manuscript V**), lipophilic TPP conjugates **39-41** displayed moderate inhibitory activity towards both *h*MAO isoforms with higher preference for *h*MAO-A (**Table 4.8**). The derivatives containing a benzodioxole ring were more potent *h*MAO-A and *h*MAO-B inhibitors than the corresponding catechols. A longer alkyl chain also favoured hMAO-B inhibition, while no correlation was found between *h*MAO-A inhibition and the spacer length (**Manuscript VII**).

Subsequent studies were performed to assess the antioxidant properties of compounds **38-41**. Benzodioxole derivatives **38** and **39** presented high E_p values in DPV studies (compound **38**: E_p = 942 mV, 1070 mV; compound **39**: E_p = 931 mV, 1083 mV), as a result from the absence of functional groups with recognized antioxidant activity (e.g.: phenols). These data were in line with the absence of $ROO^{\bullet}$ radical scavenging activity in ORAC assay (**Manuscript VII**).

On the other hand, compounds **40** and **41** showed similar electrochemical behavior to other catechols containing the same conjugated dienone system (compounds **12-16**; **subsection 4.2.2.1.**), both concerning the E_p values obtained and the reversibility of the electrochemical oxidation (**Manuscript VII**). Moreover, E_p values of compounds **40** and **41** (compound **40**: E_p = 125 mV; compound **41**: E_p = 144 mV) were considerably lower than those obtained with parent lipophilic TPP conjugates based on protocatechuic acid (E_p = 210-216 mV (299, 300)) and caffeic acid (164-174 mV (297, 411)). This behavior indicates a direct correlation between the reducing power of catechols and the increased electron delocalization between the aromatic ring and the carbonyl group.

4.2.3.2. Cytotoxicity in differentiated SH-SY5Y cells

Cytotoxicity studies were then conducted in differentiated SH-SY5Y cells with increasing concentrations of compounds **38-41**. Overall, the results indicated that lipophilic TPP conjugates **38-41** present safe cytotoxicity profiles at concentrations up to 12.5 µM, although they may affect cellular metabolism at higher concentrations (**Figure 4.26**). Compound **39** also presented significant lysosomal toxicity at concentrations above 12.5 µM.

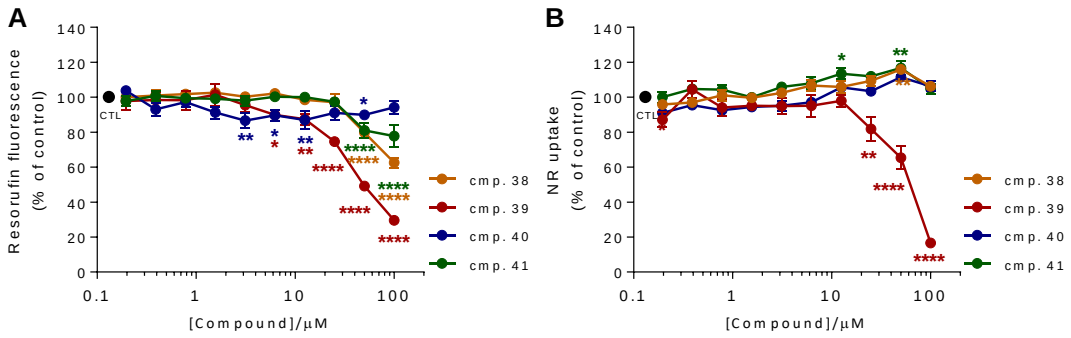


Figure 4.26: Cellular viability of differentiated SH-SY5Y neuroblastoma cells after a 24 h treatment with increasing concentrations of compounds **38-41** (0.20-100 µM). Cellular viability was evaluated using the resazurin reduction assay (**A**) and the NR uptake assay (**B**). Results are expressed as the mean % of untreated controls ± SEM (n = 3). Statistical comparisons were made using two-way ANOVA followed by Dunnet's multiple comparison test. In all cases, p values lower than 0.05 were considered significant (* $p < 0.05$, ** $p < 0.01$, *** $p < 0.001$, **** $p < 0.0001$ vs untreated cells).

The resazurin reduction assay showed that the substitution pattern of the aromatic ring and the alkyl spacer length affected the metabolic activity of compounds. Cell treatments with catechol derivatives (compounds **40** and **41**) led to lower decreases in resazurin reduction than benzodioxole derivatives (compounds **38** and **39**). In addition, compounds with four-carbon alkyl chains (compounds **38** and **40**) showed lower decreases in metabolic activity than the parent six-carbon alkyl derivatives (compounds **39** and **41**). The presence of hydrophobic elements (benzodioxole group, longer alkyl spacers) may have a negative effect on the safety window of TPP conjugates. Indeed, TPP conjugates with longer alkyl chains may exhibit a higher ability to inhibit the respiratory chain activity and decrease the mitochondrial membrane potential (294), thereby compromising cell viability. These trends demonstrate the interest of modulating the lipophilicity of TPP conjugates to obtain effective mitochondrial-targeted therapeutics with minimal cytotoxic effects.

Subsequent studies were performed to evaluate whether the decreased cellular metabolic activity observed in the presence of compounds **38**, **39** and **41** at high concentrations is associated with increased intracellular oxidative stress. To this end, DCF fluorescence was measured following the treatment of neuroblastoma cells with compounds **38-41** (**Figure 4.27A**). Then, the fluorescence was normalized with the number of metabolically viable cells (data taken from resazurin reduction assay) to calculate the ratio between the intracellular RS levels and metabolic activity (IRL/MA) (**Figure 4.27B**). Compared to non-treated cells, significant concentration-dependent increases in IRL/MA ratios were detected for all compounds. Therefore, the decreased metabolic activity

observed in the presence of compounds **38**, **39** and **41** at high concentrations may result from an increased generation of intracellular RS. This increment was particularly prominent with six-carbon chain derivatives (compounds **39** and **41**), reinforcing the negative impact of long hydrophobic alkyl linkers.

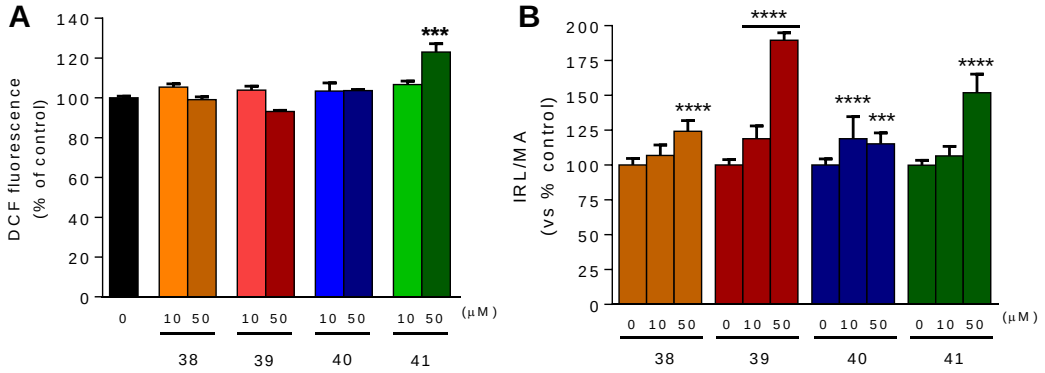


Figure 4.27: (A) Evaluation of intracellular oxidative stress levels in differentiated SH-SY5Y cells using the DCF fluorescence assay, after incubation for 24 h with compounds **38-41** at 10 and 50 μM. Results are expressed as DCF fluorescence (% of control) ± SEM (*n* = 3). Statistical comparisons were performed using the nonparametric method of Kruskal–Wallis (one-way ANOVA on ranks), followed by Dunn's *post hoc* test (**B**) Ratio between intracellular RS levels and metabolic activity (IRL/MA) at 10 and 50 μM. Statistical comparisons were performed using the parametric method of two-way ANOVA, followed by the Dunnett's multiple comparisons test. In all cases, *p* values lower than 0.05 were considered significant (* $p < 0.05$, ** $p < 0.01$, *** $p < 0.001$, **** $p < 0.0001$ vs untreated cells).

4.2.3.3. Mitochondrial accumulation, and glycolytic and mitochondrial oxidative phosphorylation fluxes

Since lipophilic TPP conjugates **38-41** were designed to exert their biological effects in mitochondria, their accumulation in the mitochondrial matrix was studied in isolated mouse liver mitochondria (MLM). The data obtained showed that all compounds accumulated within the mitochondrial matrix of energized MLM. The highest mitochondrial uptake was obtained with compound **41** (mitochondrial accumulation ratio = 1970)**,** the catechol derivative with a six-carbon alkyl chain. This compound was followed by compounds **38** and **40**, the four-carbon alkyl chain derivatives, which presented similar mitochondrial accumulation ratios (mitochondrial accumulation ratio = 1457). Finally, the lowest mitochondrial accumulation ration was observed with compound **39** (mitochondrial accumulation ratio = 1130), the benzodioxole derivatives with a six-carbon alkyl chain (**Manuscript VII**).

Then, the effects of piperine (compound **22**) and compounds **38-41** on glycolytic and mitochondrial oxidative phosphorylation fluxes were investigated. This evaluation was considered relevant, since mitochondrial toxicity is an important factor contributing to the failure of preclinical drug candidates and to the withdrawal of marketed drugs (412). A preliminary identification of mitochondrial liabilities may enable the development of effective and safe drug candidates (413), reducing the chances of drug attrition and focusing resources on safer compounds (412).

The analyses of glycolytic and mitochondrial oxidative phosphorylation fluxes were performed in differentiated SH-SY5Y cells, with non-toxic concentrations of the test compounds, using the Seahorse XF96 Extracellular Flux Analyzer technology. This method enables the measurement of oxygen consumption rate (OCR), an indicator of mitochondrial respiration, and extracellular acidification rate (ECAR), a parameter indirectly associated with glycolytic metabolism. Oxygen consumption rate (OCR) and ECARs were measured under basal conditions. In addition, OCR measurements were performed following sequential injections of oligomycin (OLIG, adenosine triphosphate (ATP) synthase inhibitor), carbonyl cyanide *p*-triflouromethoxyphenylhydrazone (FCCP, mitochondrial uncoupler), and rotenone and antimycin A (ROT/AA, inhibitors of complexes I and III, respectively) (414). Key parameters of mitochondrial function were then determined from OCR measurements, namely basal respiration, proton leak, maximal respiration, spare respiratory capacity and ATP production-linked respiration (**Figure 4.28**).

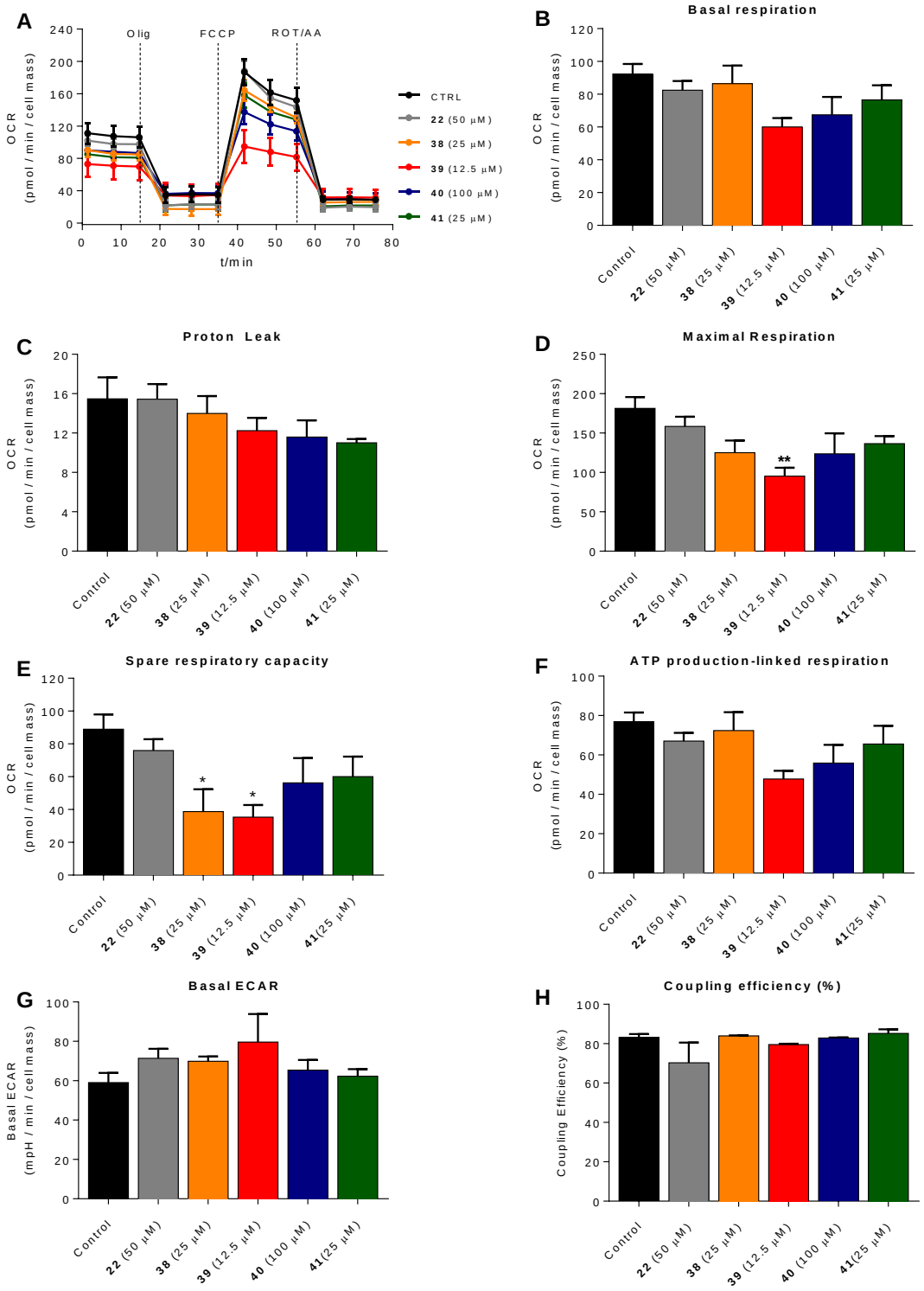


Figure 4.28: Effect of piperine (compound **22**) and TPP conjugates **38-41** at non-toxic concentrations on mitochondrial oxygen consumption. (**A**) Representative image of OCR measurements in differentiated SH-SY5Y cells treated with vehicle (Control) and non-toxic concentrations of compounds 22, **38-41** for 24 h using the Seahorse XF96 Extracellular Flux Analyzer. Several respiratory parameters were evaluated, namely (**B**) basal cellular respiration, (**C**) proton leak, (**D**) maximal respiration, (**E**) spare respiratory capacity, (**F**) ATP-linked respiration, (**G**) basal ECAR and (**H**) coupling efficiency. Data are expressed as pmol O_2/min/cell mass (measured by the sulforhodamine B assay) for OCR (**B-F**) and mpH/min/cell mass for ECAR (**G**). The results

are presented as mean ± SEM (n = 4). Statistical comparisons were performed using the parametric method of one-way ANOVA, followed by the Dunnett's multiple comparisons test. In all cases, p values lower than 0.05 were considered significant (* $p < 0.05$, ** $p < 0.01$ vs untreated cells).

Based on the results obtained, it was concluded that catechol derivatives (compounds **40** and **41**) did not significantly affect both glycolytic and mitochondrial oxidative phosphorylation fluxes of neuroblastoma cells. On the other hand, cell treatment with compound **39** significantly decreased maximal respiration (**Figure 4.28D**). Significant reductions in spare respiratory capacity were also observed with compounds **38** and **39** (**Figure 4.28E**). Spare respiratory capacity describes the ability of cells to produce energy in case of a sudden increase in energy demand, namely in response to cellular stress or increased workload (415). Therefore, benzodioxole derivatives **38** and **39** may decrease the ability of neuroblastoma cells to produce ATP under conditions of high energy demand.

In summary, catechols **40** and **41** were identified as the most promising lipophilic TPP conjugates. In addition to their remarkable antioxidant properties, these compounds acted as potent, mixed type *eq*BChE inhibitors and moderate *ee*AChE, *h*MAO-A and *h*MAO-B inhibitors. Compared to the parent benzodioxole derivatives, compounds **40** and **41** displayed safer cytotoxicity profiles in differentiated SH-SY5Y cells and did not significantly affect mitochondrial bioenergetics in the same cellular model.

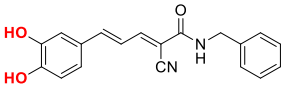
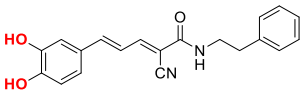
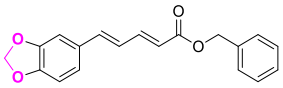
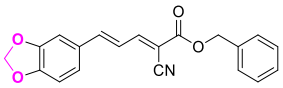
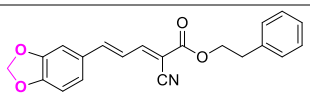
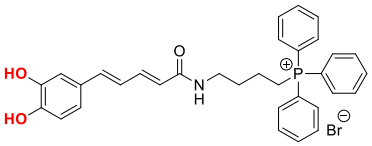
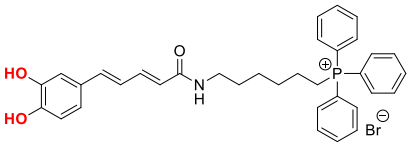
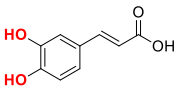
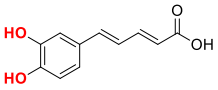
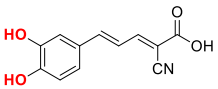
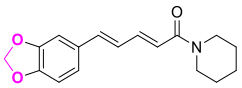
4.3. Evaluation of drug-like properties

The development of new drugs is a complex and time-consuming process with very low success rates, suffering from high attrition of drug candidates during all stages (416, 417). Poor pharmacokinetics caused by unfavourable drug-like properties are among the factors associated to the low *in vivo* efficacy of drug candidates, even if they present good *in vitro* potency (418). To address this issue, drug-like properties are being assessed in parallel with the biological screenings (418). In this context, the drug-like properties of the compounds with the most favourable biological and cytotoxicity profiles were evaluated (compounds **2**, **3**, **10**, **20**, **21**, **28**, **36**, **37**, **40** and **41**).

First, chromatographic hydrophobicity indexes (CHI) of compounds **20**, **21**, **28**, **36**, **37**, **40** and **41** were determined based on the retention times (t_R) observed in a fast gradient reverse-phase HPLC (**Table 4.9**). The CHI values of neutral molecules are directly correlated with the compounds' lipophilicity (419). Therefore, the measurements performed with catechols were carried out under acidic conditions (pH 2.3) to prevent phenol ionization. Benzodioxole derivatives were tested at physiological pH 7.4. To evaluate the

effect of the different structural modifications in lipophilicity, CA (compound **11**), catechols **12** and **17**, and piperine (compound **22**) were also included in this study.

Table 4.9: Retention times (t_R) obtained by LC/UV at pH 2.3 and 7.4 and calculated CHI parameters of CA (compound 11), CA derivatives **12**, **17**, **20**, **21**, piperine (compound 22), piperine derivatives **28**, **36** and **37**, and mitochondria-targeted antioxidants **40** and **41**.

Compound	Structure	pH 2.3		pH 7.4	
		t_R/min	CHI	t_R/min	CHI
20		9.68	60.3	---	---
21		9.89	63.8	---	---
28		---	---	12.46	102.1
36		---	---	12.11	96.7
37		---	---	12.37	100.8
40		8.20	34.4	---	---
41		8.38	37.2	---	---
11		7.84	30.4	---	---
12		8.25	37.1	---	---
17		8.43	40.0	---	---
22		---	---	10.61	73.4

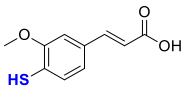
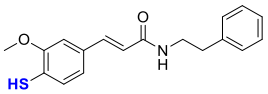
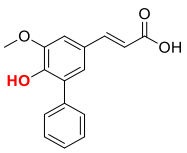
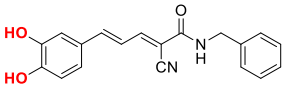
Catechols **11**, **12**, **17**, **20**, **21**, **40** and **41** displayed CHI values at pH 2.3 between 30.4 and 63.8. Chromatographic hydrophobicity indexes progressively increased with the insertion of an additional double bond (compound **12**), α-CN group (compound **13**), and benzyl or phenethyl amide groups (compounds **20** and **21**) (**Manuscript IV**). Surprisingly, lipophilic TPP conjugates **40** and **41** presented similar CHI values at pH 2.3 to the free carboxylic acid (compound **12**). In spite of the presence of lipophilic bulky groups in TPP, the positive charge of TPP cations may decrease the affinity towards the hydrophobic stationary phase (**Manuscript VII**).

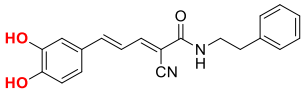
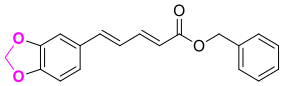
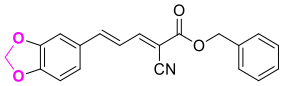
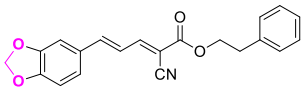
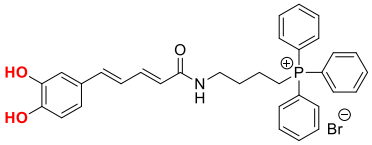
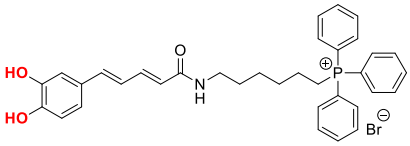
Piperine (compound **22**) and derivatives thereof presented CHI values at pH 7.4 between 73.4 and 100.8. Compounds **28**, **36** and **37** showed higher CHI values than piperine, suggesting that the isosteric replacement of the piperidinyl ring with benzyl and phenethyl ester groups increased lipophilicity (**Manuscript VI**).

The lipophilicity of FA derivatives **2**, **3** and **10** was estimated by their octanol-water partition coefficient (cLogP). While compounds **2** (cLogP = 1.97) presented a cLogP value below the limits suggested for CNS active drugs (cLogP = 2-5) (328), the value obtained for compounds **3** (cLogP =3.27) and **10** (cLogP = 2.76) were in line with the optimal range (**Manuscript III**).

Other physicochemical properties of the selected compounds were then predicted, namely molecular weight, topological polar surface area (TPSA in Å), number of hydrogen acceptors (HBA), number of hydrogen donors (HBD), number of rotatable bonds (RB) and logarithm of the ratio of the concentration of a drug in the brain and in the blood (LogBB) (**Table 4.10**).

Table 4.10: Predicted drug-like properties of FA derivatives **2**, **3** and **10**, CA derivatives **12**, **17**, **20**, **21**, piperine (compound **22**), piperine derivatives **28**, **36** and **37**, and mitochondria-targeted antioxidants **40** and **41**.

Compound	Structure	MW[a]	TPSA[a]	HBA[a]	HBD[a]	RB[a]	LogBB[a]
2		210.25	46.53	4	2	3	-0.9373
3		299.39	38.33	4	2	6	0.02948
10		270.28	66.76	4	2	4	-1.511
20		320.4	93.35	5	3	6	-0.8517

21		334.38	93.35	5	3	8	-0.8520
28		308.3	44.76	4	0	6	0.059
36		333.3	68.55	5	0	6	-0.194
37		347.4	68.55	5	0	7	-0.175
40		602.5	69.56	4	3	12	-0.784
41		630.6	69.56	4	3	14	-0.771
CNS$^+$ drugs		< 500[b]	< 90[b]	< 7[b]	< 3[b]	< 8[b]	> -1[b]

[a] Properties predicted using the Stardrop software. MW: molecular weight; TPSA: topological polar surface area; HBA: number of H-bond acceptor atoms; HBD: number of H-bond donor atoms; RB: number of rotatable bonds; logBB: logarithm of the ratio of the concentration of a drug in the brain and in the blood.
[b] Data from (327, 328, 336).

All the calculated parameters for piperine derivatives **28**, **36** and **37** fell within the optimal ranges of drugs able to act in CNS (**Manuscript VI**).

The predicted MW and number of RB of mitochondria-targeted antioxidants **40** and **41** exceeded the suggested guidelines for CNS drugs (MW < 500 g.mol^{-1}; RB < 8). The high MW (> 500 g.mol^{-1}) and high molecular flexibility (RB > 10) may also compromise the oral bioavailability of these compounds (331, 420). These results do not necessarily mean that derivatives **40** and **41** have poor bioavailability. Other groups have shown that related TPP derivatives accumulate within mitochondria in several tissues (brain, heart, liver) following long-term oral administration (301). Moreover, since compounds **40** and **41** exhibited LogBB values above -1, they are predicted to cross the BBB by passive diffusion and reach the CNS (**Manuscript VII**).

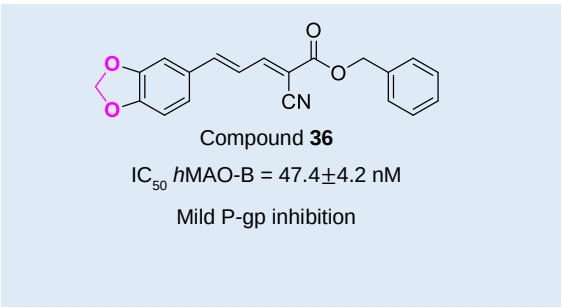
Catechol derivatives **20** and **21** presented TPSA values slightly above the suggested limits, which may hinder their ability to permeate cell membranes and move across the BBB (421). However, since their LogBB values were above -1, these compounds may still have access to the CNS.

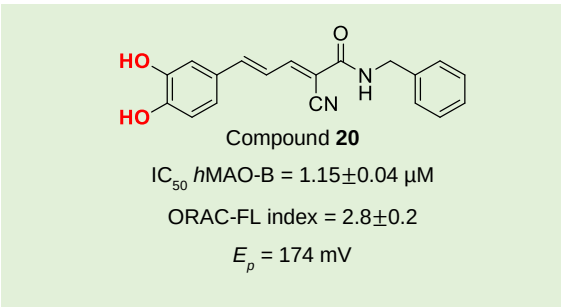
Concerning the FA derivatives, the values obtained for thiophenol **3** were in accordance with the reported limits of CNS drugs. On the other hand, compounds **2** and **10** presented LogBB values close to or below -1, suggesting that these compounds are less likely to act in the CNS.

With the exception of compounds **2** and **10**, the data suggests that the selected candidates presented favourable drug-like properties and are predicted to exert their pharmacological effects in the CNS.

4.4. Selection of drug candidates for lead optimization

In this Thesis, different approaches were explored in order to improve the pharmacological activity of three natural compounds (FA, CA and piperine). Following the development of structurally diverse compound libraries, the bioactivity and cytotoxicity profiles of all compounds were investigated. The gathered data discussed in the previous sections enabled the selection of three compounds for lead optimization (**Figure 4.29**), which may potentially lead to the discovery of innovative drug candidates for NDs in future drug discovery programs.





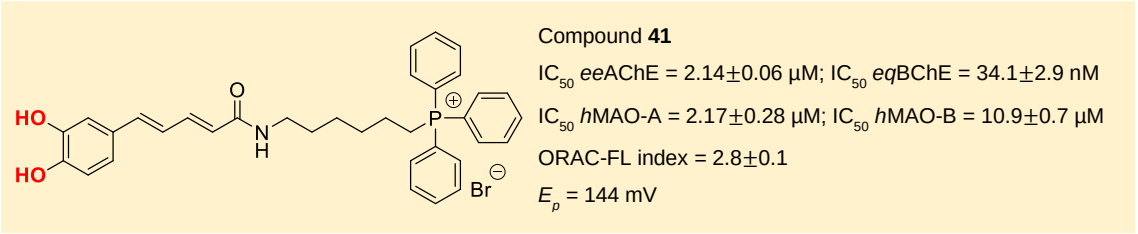


Figure 4.29: chemical structures and biological data of lead candidates.

Piperine derivative **36** was identified as the most potent and selective *h*MAO-B inhibitor among the series, displaying a competitive and reversible inhibition profile. It presented safe cytotoxicity profiles in two cell lines and mild P-gp inhibitory activity, along with favourable drug-like properties for brain penetration.

Caffeic acid derivative **20** is also proposed as a lead candidate. In addition to the outstanding antioxidant activity against lipophilic radicals in both cell-free and cell-based assays, compound **20** exhibited moderate *h*MAO-B inhibition.

Finally, mitochondria-targeted agent **41** combined ChE and MAO inhibition with antioxidant activity. It acted as a potent, mixed type *eq*BChE inhibitor with moderate inhibitory activities towards eeAChE, *h*MAO-A and *h*MAO-B. Compound **41** was well-tolerated by differentiated SH-SY5Y at concentrations up to 25 µM. Among the developed lipophilic TPP conjugates, compound **41** showed the highest mitochondria accumulation ratios, without significantly affecting mitochondrial bioenergetics in neuroblastoma cells at nontoxic concentrations. The antioxidant activity of compound **41** was not investigated in cellular models due to time restrictions. However, it displayed similar electrochemical behaviour to other structurally related catechols. The results obtained in the ORAC assay also indicated that compound **41** may act as a chain-breaking antioxidant against lipophilic radicals.

4.5. Conclusions and future perspectives

Overall, the work developed and the experimental results obtained within the scope of this Thesis led to the following conclusions:

- Structurally diverse libraries based on FA, CA and piperine were successfully obtained using synthetic methodologies and cost-effective start materials;

- The chemical modifications performed in the scaffolds of natural compounds modulated their pharmacological activity and cytotoxicity profile;

- Marked differences were observed in the antioxidant properties, reactivity and acidity of FA-based phenols and thiophenols. Thiophenols **2-6** reacted faster and more efficiently against synthetic radicals, displayed lower E_p values and were considerably more acidic than phenols **1**, **7-10**. On the other hand, phenols presented higher radical scavenging activity towards $ROO^{\bullet}$ radicals;

- The antioxidant profile of FA and compound **2** was not significantly enhanced with the insertion of 5-methoxy and 5-phenyl groups. Carboxylic acid amidation with lipophilic groups preserved the antioxidant profile of the parent compounds while improving their drug-likeness;

- Both thiophenols and phenols presented safe cytotoxicity profiles in differentiated SH-SY5Y cells. Compounds **2**, **3** and **10** also showed mild cytoprotective effects against inducers of oxidative stress (t-BHP, H_2O_2 and FeNTA);

- Structure-activity-relationship studies pointed out that benzyl ester, α-CN and benzodioxole groups are associated with increased *h*MAO-B inhibition. Piperine derivative **36** stands out as the most potent and selective *h*MAO-B inhibitor, exhibiting a competitive and reversible inhibition profile;

- Concerning the antioxidant properties of CA derivatives **12-21**, both $ROO^{\bullet}$ radical scavenging and E_p values were improved with the insertion of an ethylenic group, while α-CN group had a negative effect. Carboxylic acid amidation with lipophilic groups decreased $ROO^{\bullet}$ radical scavenging, although a preservation of E_p values was observed;

- Caffeic acid derivatives **13**, **28-31** at 10 µM did not markedly affect cellular viability of differentiated SH-SY5Y cells. However, moderate cytotoxic effects were detected at 50 µM, which may result from the deleterious effects of catechol redox chemistry. On the other hand, piperine derivatives **31**, **36** and **37** displayed safe cytotoxicity profiles at 10 and 50 µM in both neuroblastoma and adenocarcinoma cells;

- Caffeic acid derivatives **30** and **31** showed marked cytoprotective effects against *t*-BHP;

- Piperine derivative **31** demonstrated potential to act as a P-gp activator, while compounds **36** and **37** exhibited mild P-gp inhibition;

- Mitochondria targeted agents **38-41** acted as dual *ee*AChE/*eq*BChE inhibitors, showing higher selectivity towards the later. Longer alkyl chains favoured both *ee*AChE and *eq*BChE inhibition. The benzodioxole ring increased *eq*BChE inhibitory activity, while catechol groups were associated with higher *ee*AChE inhibition. Kinetic studies indicated that *eq*BChE inhibition by six-carbon chain derivatives **39** and **41** occurred through a mixed-type inhibition mechanism;

- Moderate *h*MAO-A and *h*MAO-B inhibition was also obtained with compounds **38-41** with slightly higher preference for *h*MAO-A;

- Lipophilic TPP conjugates containing a catechol moiety (compounds **40** and **41**) scavenged $ROO^{\bullet}$ radicals in the ORAC assay and showed similar electrochemical behaviour to other structurally related catechols;

- In cytotoxicity studies, mitochondria-targeted agents **38-41** did not significantly induce cytotoxic effects in differentiated SH-SY5Y cells at concentrations up to 12.5 μM, although cellular metabolic activity may be affected at higher concentrations. The presence of hydrophobic structural elements (six-carbon alkyl linkers, benzodioxole ring) was associated with decreased cellular metabolic activity. Compound **39** also exhibited significant lysosomal toxicity at concentrations ≥ 25 μM;

- The induction of intracellular oxidative stress may be a mechanism underlying the decreased cellular metabolic activity observed with compounds **38-41** at concentrations ≥ 25 μM. The most noticeable increments of intracellular oxidative stress were obtained with six-carbon chain derivatives, reinforcing the potential negative impact of hydrophobic structural elements;

- All lipophilic TPP conjugates were taken up by energized MLM. Compound **41** displayed the highest mitochondrial accumulation ratio;

- Mitochondria-targeted agents with a catechol moiety (compounds **40** and **41**) did not significantly affect glycolytic and mitochondrial oxidative phosphorylation fluxes of differentiated SH-SY5Y cells. In contrast, decreases in spare respiratory capacity and in maximal respiration were observed following treatment of neuroblastoma cells with benzodioxole derivatives **38** and **39**;

- Physicochemical properties of the most promising drug candidates were studied to predict their ability to act as effective CNS drugs;

- Compounds **20**, **36** and **41** were proposed as valid leads for future optimization and development of drug candidates for AD and PD;

Overall, the data obtained under the current Thesis endorse the chemical scaffolds of FA, CA and piperine as valid starting points for the development of neuroprotective agents. These findings also encourage the development of future projects, mainly related with lead optimization and evaluation of BBB permeability of the most promising compounds. Other main goals of future research include the evaluation of the antioxidant activity mitochondria-targeted agents **40** and **41** in cellular models, as well as the assessment of their inhibitory activities towards human ChEs. Cytotoxicity studies with all compounds developed in this work must also be performed in primary neuron cultures and in other cell lines, such as human hepatocellular carcinoma (HepG2) and rat embryonic cardiomyoblasts (H9c2).

The result presented in this Thesis significantly contributed to the field of drug discovery of CNS drugs, and may potentially lead to the development of new drug candidates for AD and PD.

CHAPTER V

References

1. Partridge L. Intervening in ageing to prevent the diseases of ageing. Trends Endocrinol Metab. 2014; 25(11): 555-7.
2. Jin K, Simpkins JW, Ji X, Leis M, Stambler I. The Critical Need to Promote Research of Aging and Aging-related Diseases to Improve Health and Longevity of the Elderly Population. Aging Dis. 2014; 6(1): 1-5.
3. Melo A, Monteiro L, Lima RM, Oliveira DM, Cerqueira MD, El-Bacha RS. Oxidative stress in neurodegenerative diseases: mechanisms and therapeutic perspectives. Oxid Med Cell Longev. 2011: 467180.
4. Perez-Hernandez J, Zaldivar-Machorro VJ, Villanueva-Porras D, Vega-Avila E, Chavarria A. A Potential Alternative against Neurodegenerative Diseases: Phytodrugs. Oxid Med Cell Longev. 2016: 8378613.
5. Fereshtehnejad SM, Vosoughi K, Heydarpour P, Sepanlou SG, Farzadfar F, Tehrani-Banihashemi A, et al. Burden of Neurodegenerative Diseases in the Eastern Mediterranean Region, 1990-2016: Findings from the Global Burden of Disease 2016 Study. Eur J Neurol. 2019.
6. Shook BC, Jackson PF. Adenosine A_{2A} Receptor Antagonists and Parkinson's Disease. ACS Chem Neurosci. 2011; 2(10): 555-67.
7. Wang X, Wang W, Li L, Perry G, Lee HG, Zhu X. Oxidative stress and mitochondrial dysfunction in Alzheimer's disease. Biochim Biophys Acta. 2014; 1842(8): 1240-7.
8. Moutinho M, Codocedo JF, Puntambekar SS, Landreth GE. Nuclear Receptors as Therapeutic Targets for Neurodegenerative Diseases: Lost in Translation. Annu Rev Pharmacol Toxicol. 2019; 59: 237-61.
9. Trippier PC, Jansen Labby K, Hawker DD, Mataka JJ, Silverman RB. Target- and mechanism-based therapeutics for neurodegenerative diseases: strength in numbers. J Med Chem. 2013; 56(8): 3121-47.
10. Wirdefeldt K, Adami HO, Cole P, Trichopoulos D, Mandel J. Epidemiology and etiology of Parkinson's disease: a review of the evidence. Eur J Epidemiol. 2011; 26 Suppl 1: S1-S58.
11. Ehret MJ, Chamberlin KW. Current Practices in the Treatment of Alzheimer Disease: Where is the Evidence After the Phase III Trials? Clin Ther. 2015; 37(8): 1604-16.
12. Gao H-M, Hong J-S. Why neurodegenerative diseases are progressive: uncontrolled inflammation drives disease progression. Trends Immunol. 2008; 29(8): 357-65.
13. Romero A, Egea J, Gonzalez-Munoz GC, Martin de Saavedra MD, del Barrio L, Rodriguez-Franco MI, et al. ITH12410/SC058: a new neuroprotective compound with potential in the treatment of Alzheimer's disease. ACS Chem Neurosci. 2014; 5(9): 770-5.
14. Jellinger KA. Basic mechanisms of neurodegeneration: a critical update. J Cell Mol Med. 2010; 14(3): 457-87.
15. Gan L, Cookson MR, Petrucelli L, La Spada AR. Converging pathways in neurodegeneration, from genetics to mechanisms. Nat Neurosci. 2018; 21(10): 1300-9.
16. Coppedè F. The potential of epigenetic therapies in neurodegenerative diseases. Front Genet. 2014; 5(220): 1-8.
17. Montanari S, Scalvini L, Bartolini M, Belluti F, Gobbi S, Andrisano V, et al. Fatty Acid Amide Hydrolase (FAAH), Acetylcholinesterase (AChE), and Butyrylcholinesterase (BuChE): Networked Targets for the Development of Carbamates as Potential Anti-Alzheimer's Disease Agents. J Med Chem. 2016; 59(13): 6387-406.
18. Zhao L, Cheng X, Zhong C. Implications of Successful Symptomatic Treatment in Parkinson's Disease for Therapeutic Strategies of Alzheimer's Disease. ACS Chem Neurosci. 2019; 10(2): 922-30.
19. Savelieff MG, Nam G, Kang J, Lee HJ, Lee M, Lim MH. Development of Multifunctional Molecules as Potential Therapeutic Candidates for Alzheimer's Disease, Parkinson's Disease, and Amyotrophic Lateral Sclerosis in the Last Decade. Chem Rev. 2019; 119(2): 1221-322.

20. Winblad B, Amouyel P, Andrieu S, Ballard C, Brayne C, Brodaty H, et al. Defeating Alzheimer's disease and other dementias: a priority for European science and society. The Lancet Neurology. 2016; 15(5): 455-532.
21. Bossy-Wetzel E, Schwarzenbacher R, Lipton SA. Molecular pathways to neurodegeneration. Nat Med. 2004; 10 Suppl: S2-9.
22. Piaceri I, Nacmias B, Sorbi S. Genetics of familial and sporadic Alzheimer's disease. Front Biosci (Elite Ed). 2013; 5: 167-77.
23. Morsy A, Trippier PC. Amyloid-Binding Alcohol Dehydrogenase (ABAD) Inhibitors for the Treatment of Alzheimer's Disease. J Med Chem. 2019; 62(9): 4252-64.
24. Davis M, O Connell T, Johnson S, Cline S, Merikle E, Martenyi F, et al. Estimating Alzheimer's Disease Progression Rates from Normal Cognition Through Mild Cognitive Impairment and Stages of Dementia. Curr Alzheimer Res. 2018; 15(8): 777-88.
25. Swomley AM, Butterfield DA. Oxidative stress in Alzheimer disease and mild cognitive impairment: evidence from human data provided by redox proteomics. Arch Toxicol. 2015; 89(10): 1669-80.
26. Bulic B, Pickhardt M, Mandelkow E. Progress and developments in tau aggregation inhibitors for Alzheimer disease. J Med Chem. 2013; 56(11): 4135-55.
27. Mattson MP. Pathways towards and away from Alzheimer's disease. Nature. 2004; 430(7000): 631-9.
28. Cheignon C, Tomas M, Bonnefont-Rousselot D, Faller P, Hureau C, Collin F. Oxidative stress and the amyloid beta peptide in Alzheimer's disease. Redox Biol. 2018; 14: 450-64.
29. Venkateshappa C, Harish G, Mahadevan A, Srinivas Bharath MM, Shankar SK. Elevated oxidative stress and decreased antioxidant function in the human hippocampus and frontal cortex with increasing age: implications for neurodegeneration in Alzheimer's disease. Neurochem Res. 2012; 37(8): 1601-14.
30. Mufson EJ, Counts SE, Perez SE, Ginsberg SD. Cholinergic system during the progression of Alzheimer's disease: therapeutic implications. Expert Rev Neurother. 2008; 8(11): 1703-18.
31. Kljakic O, Janickova H, Prado VF, Prado MAM. Cholinergic/glutamatergic co-transmission in striatal cholinergic interneurons: new mechanisms regulating striatal computation. J Neurochem. 2017; 142 Suppl 2: 90-102.
32. Agrawal M, Biswas A. Molecular diagnostics of neurodegenerative disorders. Front Mol Biosci. 2015; 2(54): 1-10.
33. Pepeu G, Grazia Giovannini M. The fate of the brain cholinergic neurons in neurodegenerative diseases. Brain Res. 2017; 1670: 173-84.
34. Shao X, Carpenter GM, Desmond TJ, Sherman P, Quesada CA, Fawaz M, et al. Evaluation of [^{11}C]N-Methyl Lansoprazole as a Radiopharmaceutical for PET Imaging of Tau Neurofibrillary Tangles. ACS Med Chem Lett. 2012; 3(11): 936-41.
35. Pocernich CB, Butterfield DA. Elevation of glutathione as a therapeutic strategy in Alzheimer disease. Biochim Biophys Acta. 2012; 1822(5): 625-30.
36. Yamin G. NMDA receptor-dependent signaling pathways that underlie amyloid beta-protein disruption of LTP in the hippocampus. J Neurosci Res. 2009; 87(8): 1729-36.
37. Portelius E, Price E, Brinkmalm G, Stiteler M, Olsson M, Persson R, et al. A novel pathway for amyloid precursor protein processing. Neurobiol Aging. 2011; 32(6): 1090-8.
38. Lee SJ, Nam E, Lee HJ, Savelieff MG, Lim MH. Towards an understanding of amyloid-beta oligomers: characterization, toxicity mechanisms, and inhibitors. Chem Soc Rev. 2017; 46(2): 310-23.
39. Zlokovic BV. Neurovascular pathways to neurodegeneration in Alzheimer's disease and other disorders. Nat Rev Neurosci. 2011; 12(12): 723-38.
40. Kumar A, Singh A, Ekavali. A review on Alzheimer's disease pathophysiology and its management: an update. Pharmacol Rep. 2015; 67(2): 195-203.
41. Goedert M. Alzheimer's and Parkinson's diseases: The prion concept in relation to assembled Aβ, tau, and α-synuclein. Science. 2015; 349(6248): 1255555.

42. Reddy PH. Amyloid beta, mitochondrial structural and functional dynamics in Alzheimer's disease. Exp Neurobiol. 2009; 218(2): 286-92.
43. Iqbal K, Liu F, Gong CX, Grundke-Iqbal I. Tau in Alzheimer disease and related tauopathies. Curr Alzheimer Res. 2010; 7(8): 656-64.
44. Iba M, Guo JL, McBride JD, Zhang B, Trojanowski JQ, Lee VM. Synthetic tau fibrils mediate transmission of neurofibrillary tangles in a transgenic mouse model of Alzheimer's-like tauopathy. J Neurosci. 2013; 33(3): 1024-37.
45. Zhang Z, Song M, Liu X, Kang SS, Kwon IS, Duong DM, et al. Cleavage of tau by asparagine endopeptidase mediates the neurofibrillary pathology in Alzheimer's disease. Nat Med. 2014; 20(11): 1254-62.
46. Mandelkow EM, Mandelkow E. Biochemistry and cell biology of tau protein in neurofibrillary degeneration. Cold Spring Harb Perspect Med. 2012; 2(7): a006247.
47. Ittner LM, Gotz J. Amyloid-beta and tau - a toxic pas de deux in Alzheimer's disease. Nat Rev Neurosci. 2011; 12(2): 65-72.
48. Lee VM, Goedert M, Trojanowski JQ. Neurodegenerative tauopathies. Annu Rev Neurosci. 2001; 24: 1121-59.
49. Melo TQ, Copray S, Ferrari MFR. Alpha-Synuclein Toxicity on Protein Quality Control, Mitochondria and Endoplasmic Reticulum. Neurochem Res. 2018; 43(12): 2212-23.
50. Zanforlin E, Zagotto G, Ribaudo G. The Medicinal Chemistry of Natural and Semisynthetic Compounds against Parkinson's and Huntington's Diseases. ACS Chem Neurosci. 2017; 8(11): 2356-68.
51. Elmabruk A, Das B, Yedlapudi D, Xu L, Antonio T, Reith MEA, et al. Design, Synthesis, and Pharmacological Characterization of Carbazole Based Dopamine Agonists as Potential Symptomatic and Neuroprotective Therapeutic Agents for Parkinson's Disease. ACS Chem Neurosci. 2019; 10(1): 396-411.
52. Sanchez-Danes A, Richaud-Patin Y, Carballo-Carbajal I, Jimenez-Delgado S, Caig C, Mora S, et al. Disease-specific phenotypes in dopamine neurons from human iPS-based models of genetic and sporadic Parkinson's disease. EMBO Mol Med. 2012; 4(5): 380-95.
53. Abeliovich A, Gitler AD. Defects in trafficking bridge Parkinson's disease pathology and genetics. Nature. 2016; 539(7628): 207-16.
54. Ryan BJ, Hoek S, Fon EA, Wade-Martins R. Mitochondrial dysfunction and mitophagy in Parkinson's: from familial to sporadic disease. Trends Biochem Sci. 2015; 40(4): 200-10.
55. Hernandez DG, Reed X, Singleton AB. Genetics in Parkinson disease: Mendelian versus non-Mendelian inheritance. J Neurochem. 2016; 139 Suppl 1: 59-74.
56. Antony PM, Diederich NJ, Kruger R, Balling R. The hallmarks of Parkinson's disease. FEBS J. 2013; 280(23): 5981-93.
57. Kalia LV, Lang AE. Parkinson's disease. Lancet. 2015; 386(9996): 896-912.
58. Zheng J, Zhang X, Zhen X. Development of Adenosine A_{2A} Receptor Antagonists for the Treatment of Parkinson's Disease: A Recent Update and Challenge. ACS Chem Neurosci. 2019; 10(2): 783-91.
59. Morales-Garcia JA, Susin C, Alonso-Gil S, Perez DI, Palomo V, Perez C, et al. Glycogen synthase kinase-3 inhibitors as potent therapeutic agents for the treatment of Parkinson disease. ACS Chem Neurosci. 2013; 4(2): 350-60.
60. Oertel W, Schulz JB. Current and experimental treatments of Parkinson disease: A guide for neuroscientists. J Neurochem. 2016; 139 Suppl 1: 325-37.
61. Dauer W, Przedborski S. Parkinson's disease: mechanisms and models. Neuron. 2003; 39(6): 889-909.
62. Swanson J, Posner M, Fusella J, Wasdell M, Sommer T, Fan J. Genes and attention deficit hyperactivity disorder. Curr Psychiatry Rep. 2001; 3(2): 92-100.
63. Brunelin J, Fecteau S, Suaud-Chagny M-F. Abnormal striatal dopamine transmission in schizophrenia. Curr Med Chem. 2013; 20(3): 397-404.
64. Dickson DW. Parkinson's disease and parkinsonism: neuropathology. Cold Spring Harb Perspect Med. 2012; 2(8).

65. Zhang G, Xia Y, Wan F, Ma K, Guo X, Kou L, et al. New Perspectives on Roles of Alpha-Synuclein in Parkinson's Disease. Front Aging Neurosci. 2018; 10: 370.
66. Borland MK, Trimmer PA, Rubinstein JD, Keeney PM, Mohanakumar K, Liu L, et al. Chronic, low-dose rotenone reproduces Lewy neurites found in early stages of Parkinson's disease, reduces mitochondrial movement and slowly kills differentiated SH-SY5Y neural cells. Mol Neurodegener. 2008; 3: 21.
67. Volpicelli-Daley LA, Gamble KL, Schultheiss CE, Riddle DM, West AB, Lee VMY. Formation of α-synuclein Lewy neurite-like aggregates in axons impedes the transport of distinct endosomes. Mol Biol Cell. 2014; 25(25): 4010-23.
68. Ramsay RR, Majekova M, Medina M, Valoti M. Key Targets for Multi-Target Ligands Designed to Combat Neurodegeneration. Front Neurosci. 2016; 10(375): 1-24.
69. Guzior N, Wieckowska A, Panek D, Malawska B. Recent development of multifunctional agents as potential drug candidates for the treatment of Alzheimer's disease. Curr Med Chem. 2015; 22(3): 373-404.
70. Macdonald IR, Rockwood K, Martin E, Darvesh S. Cholinesterase inhibition in Alzheimer's disease: is specificity the answer? J Alzheimers Dis. 2014; 42(2): 379-84.
71. von Bernhardi R, Eugenin J. Alzheimer's disease: redox dysregulation as a common denominator for diverse pathogenic mechanisms. Antioxid Redox Signal. 2012; 16(9): 974-1031.
72. Van Bulck M, Sierra-Magro A, Alarcon-Gil J, Perez-Castillo A, Morales-Garcia JA. Novel Approaches for the Treatment of Alzheimer's and Parkinson's Disease. Int J Mol Sci. 2019; 20(3): 719.
73. Huang L, Miao H, Sun Y, Meng F, Li X. Discovery of indanone derivatives as multi-target-directed ligands against Alzheimer's disease. Eur J Med Chem. 2014; 87: 429-39.
74. Wang Q, Liu Y, Zhou J. Neuroinflammation in Parkinson's disease and its potential as therapeutic target. Transl Neurodegener. 2015; 4: 19.
75. Tripathi RKP, Ayyannan SR. Monoamine oxidase-B inhibitors as potential neurotherapeutic agents: An overview and update. Med Res Rev. 2019: 1-104.
76. Woolf NJ, Butcher LL. Cholinergic systems mediate action from movement to higher consciousness. Behav Brain Res. 2011; 221(2): 488-98.
77. Greig NH, Utsuki T, Ingram DK, Wang Y, Pepeu G, Scali C, et al. Selective butyrylcholinesterase inhibition elevates brain acetylcholine, augments learning and lowers Alzheimer β-amyloid peptide in rodent. Proc Natl Acad Sci USA. 2005; 102(47): 17213-8.
78. Terry AV, Jr., Buccafusco JJ. The cholinergic hypothesis of age and Alzheimer's disease-related cognitive deficits: recent challenges and their implications for novel drug development. J Pharmacol Exp Ther. 2003; 306(3): 821-7.
79. Wilkinson DG, Francis PT, Schwam E, Payne-Parrish J. Cholinesterase inhibitors used in the treatment of Alzheimer's disease: the relationship between pharmacological effects and clinical efficacy. Drugs Aging. 2004; 21(7): 453-78.
80. Li F, Wang ZM, Wu JJ, Wang J, Xie SS, Lan JS, et al. Synthesis and pharmacological evaluation of donepezil-based agents as new cholinesterase/monoamine oxidase inhibitors for the potential application against Alzheimer's disease. J Enzyme Inhib Med Chem. 2016; 31(sup3): 41-53.
81. Contestabile A. The history of the cholinergic hypothesis. Behav Brain Res. 2011; 221(2): 334-40.
82. Du X, Wang X, Geng M. Alzheimer's disease hypothesis and related therapies. Transl Neurodegener. 2018; 7(2): 1-7.
83. Di Giovanni S, Borloz A, Urbain A, Marston A, Hostettmann K, Carrupt PA, et al. *In vitro* screening assays to identify natural or synthetic acetylcholinesterase inhibitors: thin layer chromatography versus microplate methods. Eur J Pharm Sci. 2008; 33(2): 109-19.
84. Colović MB, Krstić DZ, Lazarević-Pašti TD, Bondžić AM, Vasić VM. Acetylcholinesterase inhibitors: pharmacology and toxicology. Curr Neuropharmacol. 2013; 11(3): 315-35.
85. Okuda T, Haga T. High-affinity choline transporter. Neurochem Res. 2003; 28(3-4): 483-8.

86. Amenta F, Tayebati SK. Pathways of acetylcholine synthesis, transport and release as targets for treatment of adult-onset cognitive dysfunction. Curr Med Chem. 2008; 15(5): 488-98.
87. Prado MA, Reis RA, Prado VF, de Mello MC, Gomez MV, de Mello FG. Regulation of acetylcholine synthesis and storage. Neurochem Int. 2002; 41(5): 291-9.
88. Ferreira-Vieira TH, Guimaraes IM, Silva FR, Ribeiro FM. Alzheimer's disease: Targeting the Cholinergic System. Curr Neuropharmacol. 2016; 14(1): 101-15.
89. Scarpini E, Scheltens P, Feldman H. Treatment of Alzheimer's disease: current status and new perspectives. Lancet Neurol. 2003; 2(9): 539-47.
90. Pohanka M. Alpha7 nicotinic acetylcholine receptor is a target in pharmacology and toxicology. Int J Mol Sci. 2012; 13(2): 2219-38.
91. Reale M, Costantini E, Di Nicola M, D'Angelo C, Franchi S, D'Aurora M, et al. Butyrylcholinesterase and Acetylcholinesterase polymorphisms in Multiple Sclerosis patients: Implication in peripheral inflammation. Sci Rep. 2018; 8(1).
92. Mushtaq G, Greig NH, Khan JA, Kamal MA. Status of acetylcholinesterase and butyrylcholinesterase in Alzheimer's disease and type 2 diabetes mellitus. CNS Neurol Disord Drug Targets. 2014; 13(8): 1432-9.
93. Zhuang Q, Young A, Callam CS, McElroy CA, Ekici OD, Yoder RJ, et al. Efforts toward treatments against aging of organophosphorus-inhibited acetylcholinesterase. Ann N Y Acad Sci. 2016; 1374(1): 94-104.
94. Soreq H, Seidman S. Acetylcholinesterase - new roles for an old actor. Nat Rev Neurosci. 2001; 2(4): 294-302.
95. Gulcin I, Scozzafava A, Supuran CT, Koksal Z, Turkan F, Cetinkaya S, et al. Rosmarinic acid inhibits some metabolic enzymes including glutathione S-transferase, lactoperoxidase, acetylcholinesterase, butyrylcholinesterase and carbonic anhydrase isoenzymes. J Enzyme Inhib Med Chem. 2016; 31(6): 1698-702.
96. Anand P, Singh B. A review on cholinesterase inhibitors for Alzheimer's disease. Arch Pharm Res. 2013; 36(4): 375-99.
97. Li Q, Yang H, Chen Y, Sun H. Recent progress in the identification of selective butyrylcholinesterase inhibitors for Alzheimer's disease. Eur J Med Chem. 2017; 132: 294-309.
98. Carolan CG, Dillon GP, Khan D, Ryder SA, Gaynor JM, Reidy S, et al. Isosorbide-2-benzyl carbamate-5-salicylate, a peripheral anionic site binding subnanomolar selective butyrylcholinesterase inhibitor. J Med Chem. 2010; 53(3): 1190-9.
99. Lane RM, Potkin SG, Enz A. Targeting acetylcholinesterase and butyrylcholinesterase in dementia. Int J Neuropsychopharmacol. 2006; 9(1): 101-24.
100. Rao AA, Sridhar GR, Das UN. Elevated butyrylcholinesterase and acetylcholinesterase may predict the development of type 2 diabetes mellitus and Alzheimer's disease. Med Hypotheses. 2007; 69(6): 1272-6.
101. Kumar A, Pintus F, Di Petrillo A, Medda R, Caria P, Matos MJ, et al. Novel 2-pheynlbenzofuran derivatives as selective butyrylcholinesterase inhibitors for Alzheimer's disease. Sci Rep. 2018; 8(1): 4424.
102. Czarnecka K, Szymanski P, Girek M, Mikiciuk-Olasik E, Skibinski R, Kabzinski J, et al. Tetrahydroacridine derivatives with fluorobenzoic acid moiety as multifunctional agents for Alzheimer's disease treatment. Bioorg Chem. 2017; 72: 315-22.
103. Brus B, Kosak U, Turk S, Pislar A, Coquelle N, Kos J, et al. Discovery, biological evaluation, and crystal structure of a novel nanomolar selective butyrylcholinesterase inhibitor. J Med Chem. 2014; 57(19): 8167-79.
104. Wang Y, Guan XL, Wu PF, Wang CM, Cao H, Li L, et al. Multifunctional mercapto-tacrine derivatives for treatment of age-related neurodegenerative diseases. J Med Chem. 2012; 55(7): 3588-92.
105. Zemek F, Drtinova L, Nepovimova E, Sepsova V, Korabecny J, Klimes J, et al. Outcomes of Alzheimer's disease therapy with acetylcholinesterase inhibitors and memantine. Expert Opin Drug Saf. 2014; 13(6): 759-74.

106. Hampel H, Mesulam MM, Cuello AC, Farlow MR, Giacobini E, Grossberg GT, et al. The cholinergic system in the pathophysiology and treatment of Alzheimer's disease. Brain. 2018; 141(7): 1917-33.
107. Unzeta M, Esteban G, Bolea I, Fogel WA, Ramsay RR, Youdim MBH, et al. Multi-target directed donepezil-like ligands for Alzheimer's disease. Front Neurosci. 2016; 10: 205.
108. Seltzer B. Donepezil: a review. Expert Opin Drug Metab Toxicol. 2005; 1(3): 527-36.
109. Berk C, Sabbagh M. Broader considerations of higher doses of donepezil in the treatment of mild, moderate, and severe Alzheimer's disease. Int J Alzheimers Dis. 2012; 2012: 707468.
110. Camps P, Formosa X, Galdeano C, Gomez T, Munoz-Torrero D, Scarpellini M, et al. Novel donepezil-based inhibitors of acetyl- and butyrylcholinesterase and acetylcholinesterase-induced beta-amyloid aggregation. J Med Chem. 2008; 51(12): 3588-98.
111. Pourmand A, Shay C, Redha W, Aalam A, Mazer-Amirshahi M. Cholinergic symptoms and QTc prolongation following donepezil overdose. 2017; 35(9): 1386.e1-.e3.
112. Cummings JL, Geldmacher D, Farlow M, Sabbagh M, Christensen D, Betz P. High-dose donepezil (23 mg/day) for the treatment of moderate and severe Alzheimer's disease: drug profile and clinical guidelines. CNS Neurosci Ther. 2013; 19(5): 294-301.
113. Rodrigues Simões MC, Dias Viegas FP, Moreira MS, de Freitas Silva M, Riquiel MM, da Rosa PM, et al. Donepezil: an important prototype to the design of new drug candidates for Alzheimer's disease. Mini Reviews in Medicinal Chemistry. 2014; 14(1): 2-19.
114. Prvulovic D, Schneider B. Pharmacokinetic and pharmacodynamic evaluation of donepezil for the treatment of Alzheimer's disease. Expert Opin Drug Metab Toxicol. 2014; 10(7): 1039-50.
115. Mehta M, Adem A, Sabbagh M. New acetylcholinesterase inhibitors for Alzheimer's disease. Int J Alzheimers Dis. 2012; 2012: 728983.
116. Kandiah N, Pai M-C, Senanarong V, Looi I, Ampil E, Park KW, et al. Rivastigmine: the advantages of dual inhibition of acetylcholinesterase and butyrylcholinesterase and its role in subcortical vascular dementia and Parkinson's disease dementia. Clin Interv Aging. 2017; 12: 697-707.
117. Khoury R, Rajamanickam J, Grossberg GT. An update on the safety of current therapies for Alzheimer's disease: focus on rivastigmine. Ther Adv Drug Saf. 2018; 9(3): 171-8.
118. Huang F, Fu Y. A review of clinical pharmacokinetics and pharmacodynamics of galantamine, a reversible acetylcholinesterase inhibitor for the treatment of Alzheimer's disease, in healthy subjects and patients. Curr Clin Pharmacol. 2010; 5(2): 115-24.
119. Prvulovic D, Hampel H, Pantel J. Galantamine for Alzheimer's disease. Expert Opin Drug Metab Toxicol. 2010; 6(3): 345-54.
120. Jann MW, Shirley KL, Small GW. Clinical pharmacokinetics and pharmacodynamics of cholinesterase inhibitors. Clin Pharmacokinet. 2002; 41(10): 719-39.
121. Penner J, Rupsingh R, Smith M, Wells JL, Borrie MJ, Bartha R. Increased glutamate in the hippocampus after galantamine treatment for Alzheimer disease. Prog Neuropsychopharmacol Biol Psychiatry. 2010; 34(1): 104-10.
122. Rangel-Barajas C, Coronel I, Florán B. Dopamine Receptors and Neurodegeneration. Aging Dis. 2015; 6(5): 349-68.
123. Tritsch NX, Sabatini BL. Dopaminergic modulation of synaptic transmission in cortex and striatum. Neuron. 2012; 76(1): 33-50.
124. Lester DB, Rogers TD, Blaha CD. Acetylcholine-dopamine interactions in the pathophysiology and treatment of CNS disorders. CNS Neurosci Ther. 2010; 16(3): 137-62.
125. Jones DR, Moussaud S, McLean P. Targeting heat shock proteins to modulate α-synuclein toxicity. Ther Adv Neurol Disord. 2014; 7(1): 33-51.

126. Finberg JPM. Inhibitors of MAO-B and COMT: their effects on brain dopamine levels and uses in Parkinson's disease. J Neural Transm (Vienna). 2018; 126(4): 433-48.
127. Godar SC, Bortolato M. Gene-sex interactions in schizophrenia: focus on dopamine neurotransmission. Front Behav Neurosci. 2014; 8(71): 1-16.
128. Shook BC, Rassnick S, Wallace N, Crooke J, Ault M, Chakravarty D, et al. Design and characterization of optimized adenosine A(2)A/A(1) receptor antagonists for the treatment of Parkinson's disease. J Med Chem. 2012; 55(3): 1402-17.
129. Rusiecka I, Ruczyński J, Kozłowska A, Backtrog E, Mucha P, Kocić I, et al. TP10-Dopamine Conjugate as a Potential Therapeutic Agent in the Treatment of Parkinson's Disease. Bioconjug Chem. 2019; 30(3): 760-74.
130. Huleatt PB, Khoo ML, Chua YY, Tan TW, Liew RS, Balogh B, et al. Novel arylalkenylpropargylamines as neuroprotective, potent, and selective monoamine oxidase B inhibitors for the treatment of Parkinson's disease. J Med Chem. 2015; 58(3): 1400-19.
131. Wang YD, Bao XQ, Xu S, Yu WW, Cao SN, Hu JP, et al. A Novel Parkinson's Disease Drug Candidate with Potent Anti-neuroinflammatory Effects through the Src Signaling Pathway. J Med Chem. 2016; 59(19): 9062-79.
132. Youdim MB, Edmondson D, Tipton KF. The therapeutic potential of monoamine oxidase inhibitors. Nat Rev Neurosci. 2006; 7(4): 295-309.
133. Naoi M, Maruyama W, Inaba-Hasegawa K. Type A and B monoamine oxidase in age-related neurodegenerative disorders: their distinct roles in neuronal death and survival. Curr Top Med Chem. 2012; 12(20): 2177-88.
134. Vianello R, Domene C, Mavri J. The Use of Multiscale Molecular Simulations in Understanding a Relationship between the Structure and Function of Biological Systems of the Brain: The Application to Monoamine Oxidase Enzymes. Front Neurosci. 2016; 10: 327-
.
135. Binda C, Newton-Vinson P, Hubalek F, Edmondson DE, Mattevi A. Structure of human monoamine oxidase B, a drug target for the treatment of neurological disorders. Nat Struct Biol. 2002; 9(1): 22-6.
136. MacMillar S, Edmondson DE, Matsson O. Nitrogen kinetic isotope effects for the monoamine oxidase B-catalyzed oxidation of benzylamine and (1,1- 2H 2)benzylamine: Nitrogen rehybridization and CH bond cleavage are not concerted. J Am Chem Soc. 2011; 133(32): 12319-21.
137. Naoi M, Riederer P, Maruyama W. Modulation of monoamine oxidase (MAO) expression in neuropsychiatric disorders: genetic and environmental factors involved in type A MAO expression. J Neural Transm (Vienna). 2016; 123(2): 91-106.
138. Gealageas R, Devineau A, So PPL, Kim CMJ, Surendradoss J, Buchwalder C, et al. Development of Novel Monoamine Oxidase-B (MAO-B) Inhibitors with Reduced Blood-Brain Barrier Permeability for the Potential Management of Noncentral Nervous System (CNS) Diseases. J Med Chem. 2018; 61(16): 7043-64.
139. Nicotra A, Pierucci F, Parvez H, Senatori O. Monoamine oxidase expression during development and aging. Neurotoxicology. 2004; 25(1-2): 155-65.
140. Tong J, Meyer JH, Furukawa Y, Boileau I, Chang LJ, Wilson AA, et al. Distribution of monoamine oxidase proteins in human brain: implications for brain imaging studies. J Cereb Blood Flow Metab. 2013; 33(6): 863-71.
141. Finberg JPM, Rabey JM. Inhibitors of MAO-A and MAO-B in Psychiatry and Neurology. Front Pharmacol. 2016; 7: 340.
142. Gaweska H, Fitzpatrick PF. Structures and Mechanism of the Monoamine Oxidase Family. Biomol Concepts. 2011; 2(5): 365-77.
143. Edmondson DE, Binda C, Mattevi A. Structural insights into the mechanism of amine oxidation by monoamine oxidases A and B. Arch Biochem Biophys. 2007; 464(2): 269-76.
144. Finberg JP. Update on the pharmacology of selective inhibitors of MAO-A and MAO-B: focus on modulation of CNS monoamine neurotransmitter release. Pharmacol Ther. 2014; 143(2): 133-52.
145. Bortolato M, Chen K, Shih JC. Monoamine oxidase inactivation: from pathophysiology to therapeutics. Adv Drug Deliv Rev. 2008; 60(13-14): 1527-33.

146. Booysen HP, Moraal C, Terre'Blanche G, Petzer A, Bergh JJ, Petzer JP. Thio- and aminocaffeine analogues as inhibitors of human monoamine oxidase. Bioorg Med Chem. 2011; 19(24): 7507-18.
147. Binda C, Wang J, Pisani L, Caccia C, Carotti A, Salvati P, et al. Structures of human monoamine oxidase B complexes with selective noncovalent inhibitors: safinamide and coumarin analogs. J Med Chem. 2007; 50(23): 5848-52.
148. Hammuda A, Shalaby R, Rovida S, Edmondson DE, Binda C, Khalil A. Design and synthesis of novel chalcones as potent selective monoamine oxidase-B inhibitors. Eur J Med Chem. 2016; 114: 162-9.
149. Tzvetkov NT, Stammler HG, Neumann B, Hristova S, Antonov L, Gastreich M. Crystal structures, binding interactions, and ADME evaluation of brain penetrant *N*-substituted indazole-5-carboxamides as subnanomolar, selective monoamine oxidase B and dual MAO-A/B inhibitors. Eur J Med Chem. 2017; 127: 470-92.
150. Robakis D, Fahn S. Defining the Role of the Monoamine Oxidase-B Inhibitors for Parkinson's Disease. CNS Drugs. 2015; 29(6): 433-41.
151. Tong J, Rathitharan G, Meyer JH, Furukawa Y, Ang LC, Boileau I, et al. Brain monoamine oxidase B and A in human parkinsonian dopamine deficiency disorders. Brain. 2017; 140(9): 2460-74.
152. Krishna R, Ali M, Moustafa AA. Effects of combined MAO-B inhibitors and levodopa vs. monotherapy in Parkinson's disease. Front Aging Neurosci. 2014; 6: 180.
153. Weinreb O, Amit T, Bar-Am O, Youdim MBH. Rasagiline: A novel anti-Parkinsonian monoamine oxidase-B inhibitor with neuroprotective activity. Prog Neurobiol. 2010; 92(3): 330-44.
154. Helguera AM, Perez-Machado G, Cordeiro MN, Borges F. Discovery of MAO-B inhibitors - present status and future directions part I: oxygen heterocycles and analogs. Mini Rev Med Chem. 2012; 12(10): 907-19.
155. Tandarić T, Vianello R. Computational Insight into the Mechanism of the Irreversible Inhibition of Monoamine Oxidase Enzymes by the Antiparkinsonian Propargylamine Inhibitors Rasagiline and Selegiline. ACS Chem Neurosci. 2019; 10(8): 3532-42.
156. Schapira AH. Monoamine oxidase B inhibitors for the treatment of Parkinson's disease: a review of symptomatic and potential disease-modifying effects. CNS Drugs. 2011; 25(12): 1061-171.
157. Strydom B, Bergh JJ, Petzer JP. 8-Aryl- and alkyloxycaffeine analogues as inhibitors of monoamine oxidase. Eur J Med Chem. 2011; 46(8): 3474-85.
158. Prins LH, Petzer JP, Malan SF. Inhibition of monoamine oxidase by indole and benzofuran derivatives. Eur J Med Chem. 2010; 45(10): 4458-66.
159. Tipton KF, Boyce S, O'Sullivan J, Davey GP, Healy J. Monoamine oxidases: certainties and uncertainties. Curr Med Chem. 2004; 11(15): 1965-82.
160. Cattaneo C, Ferla RL, Bonizzoni E, Sardina M. Long-Term Effects of Safinamide on Dyskinesia in Mid- to Late-Stage Parkinson's Disease: A Post-Hoc Analysis. J Parkinsons Dis. 2015; 5(3): 475-81.
161. Blair HA, Dhillon S. Safinamide: A Review in Parkinson's Disease. CNS Drugs. 2017; 31(2): 169-76.
162. Fabbri M, Rosa MM, Abreu D, Ferreira JJ. Clinical pharmacology review of safinamide for the treatment of Parkinson's disease. Neurodegenerative Disease Management. 2015; 5(6): 481-96.
163. Learmonth DA, Kiss LE, Soares-da-Silva P. The chemistry of catechol-O-methyltransferase inhibitors. Int Rev Neurobiol: Academic Press Inc.; 2010. p. 119-62.
164. Lerner C, Jakob-Roetne R, Buettelmann B, Ehler A, Rudolph M, Rodriguez Sarmiento RM. Design of Potent and Druglike Nonphenolic Inhibitors for Catechol O-Methyltransferase Derived from a Fragment Screening Approach Targeting the S-Adenosyl-l-methionine Pocket. J Med Chem. 2016; 59(22): 10163-75.
165. Jatana N, Sharma A, Latha N. Pharmacophore modeling and virtual screening studies to design potential COMT inhibitors as new leads. J Mol Graph Model. 2013; 39: 145-64.

166. Bai HW, Shim JY, Yu J, Bao TZ. Biochemical and molecular modeling studies of the O-methylation of various endogenous and exogenous catechol substrates catalyzed by recombinant human soluble and membrane-bound catechol-O-methyltransferases. Chem Res Toxicol. 2007; 20(10): 1409-25.
167. Ma Z, Liu H, Wu B. Structure-based drug design of catechol-O-methyltransferase inhibitors for CNS disorders. Br J Clin Pharmacol. 2014; 77(3): 410-20.
168. Kiss LE, Soares-da-Silva P. Medicinal chemistry of catechol O-methyltransferase (COMT) inhibitors and their therapeutic utility. J Med Chem. 2014; 57(21): 8692-717.
169. Käenmäki M, Tammimäki A, Garcia-Horsman JA, Myöhänen T, Schendzielorz N, Karayiorgou M, et al. Importance of membrane-bound catechol-O-methyltransferase in L-DOPA metabolism: A pharmacokinetic study in two types of Comt gene modified mice. Br J Pharmacol. 2009; 158(8): 1884-94.
170. Silva T, Mohamed T, Shakeri A, Rao PP, Martinez-Gonzalez L, Perez DI, et al. Development of Blood-Brain Barrier Permeable Nitrocatechol-Based Catechol O-Methyltransferase Inhibitors with Reduced Potential for Hepatotoxicity. J Med Chem. 2016; 59(16): 7584-97.
171. Palma PN, Rodrigues ML, Archer M, Bonifacio MJ, Loureiro AI, Learmonth DA, et al. Comparative study of ortho- and meta-nitrated inhibitors of catechol-O-methyltransferase: interactions with the active site and regioselectivity of O-methylation. Mol Pharmacol. 2006; 70(1): 143-53.
172. Solla P, Cannas A, Marrosu F, Marrosu MG. Therapeutic interventions and adjustments in the management of Parkinson disease: role of combined carbidopa/levodopa/entacapone (Stalevo). Neuropsychiatr Dis Treat. 2010; 6: 483-90.
173. Bonifácio MJ, Palma PN, Almeida L, Soares-da-Silva P. Catechol-O-methyltransferase and its inhibitors in Parkinson's disease. CNS Drug Rev. 2007; 13(3): 352-79.
174. Haasio K. Toxicology and safety of comt inhibitors. Int Rev Neurobiol: Academic Press Inc.; 2010. p. 163-89.
175. von Kleist L, Michaelis S, Bartho K, Graebner O, Schlief M, Dreger M, et al. Identification of Potential Off-target Toxicity Liabilities of Catechol-O-methyltransferase Inhibitors by Differential Competition Capture Compound Mass Spectrometry. J Med Chem. 2016; 59(10): 4664-75.
176. Kiss LE, Ferreira HS, Torrao L, Bonifacio MJ, Palma PN, Soares-da-Silva P, et al. Discovery of a long-acting, peripherally selective inhibitor of catechol-O-methyltransferase. J Med Chem. 2010; 53(8): 3396-411.
177. Assal F, Spahr L, Hadengue A, Rubbia-Brandt L, Burkhard PR. Tolcapone and fulminant hepatitis. Lancet. 1998; 352(9132): 958.
178. Piccini P, Brooks DJ, Korpela K, Pavese N, Karlsson M, Gordin A. The catechol-O-methyltransferase (COMT) inhibitor entacapone enhances the pharmacokinetic and clinical response to Sinemet CR in Parkinson's disease. J Neurol Neurosurg Psychiatry. 2000; 68(5): 589-94.
179. Castro Caldas A, Teodoro T, Ferreira JJ. The launch of opicapone for Parkinson's disease: negatives versus positives. Expert Opin Drug Saf. 2018; 17(3): 331-7.
180. Bonifácio MJ, Torrão L, Loureiro AI, Palma PN, Wright LC, Soares-da-Silva P. Pharmacological profile of opicapone, a third-generation nitrocatechol catechol-O-methyl transferase inhibitor, in the rat. Br J Pharmacol. 2015; 172(7): 1739-52.
181. Learmonth DA, Palma PN, Vieira-Coelho MA, Soares-da-Silva P. Synthesis, biological evaluation, and molecular modeling studies of a novel, peripherally selective inhibitor of catechol-O-methyltransferase. J Med Chem. 2004; 47(25): 6207-17.
182. Pinheiro SD, Serrao MP, Silva T, Borges F, Soares-da-Silva P. Pharmacodynamic evaluation of novel Catechol-*O*-methyltransferase inhibitors. Eur J Pharmacol. 2019; 847: 53-60.
183. Fabbri M, Ferreira JJ, Lees A, Stocchi F, Poewe W, Tolosa E, et al. Opicapone for the treatment of Parkinson's disease: A review of a new licensed medicine. Mov Disord. 2018; 33(10): 1528-39.

184. Almeida L, Rocha JF, Falcao A, Palma PN, Loureiro AI, Pinto R, et al. Pharmacokinetics, pharmacodynamics and tolerability of opicapone, a novel catechol-O-methyltransferase inhibitor, in healthy subjects: prediction of slow enzyme-inhibitor complex dissociation of a short-living and very long-acting inhibitor. Clin Pharmacokinet. 2013; 52(2): 139-51.
185. Lees AJ, Ferreira J, Rascol O, Poewe W, Rocha JF, McCrory M, et al. Opicapone as Adjunct to Levodopa Therapy in Patients With Parkinson Disease and Motor Fluctuations: A Randomized Clinical Trial. JAMA Neurol. 2017; 74(2): 197-206.
186. Parashos SA, Wielinski CL, Kern JA. Frequency, reasons, and risk factors of entacapone discontinuation in Parkinson disease. Clin neuropharmacol. 2004; 27(3): 119-23.
187. Dasuri K, Zhang L, Keller JN. Oxidative stress, neurodegeneration, and the balance of protein degradation and protein synthesis. Free Radic Biol Med. 2013; 62: 170-85.
188. Gan L, Johnson JA. Oxidative damage and the Nrf2-ARE pathway in neurodegenerative diseases. Biochim Biophys Acta. 2014; 1842(8): 1208-18.
189. Sies H. Oxidative stress: a concept in redox biology and medicine. Redox Biol. 2015; 4: 180-3.
190. Uttara B, Singh AV, Zamboni P, Mahajan RT. Oxidative stress and neurodegenerative diseases: a review of upstream and downstream antioxidant therapeutic options. Curr Neuropharmacol. 2009; 7(1): 65-74.
191. Pizzino G, Irrera N, Cucinotta M, Pallio G, Mannino F, Arcoraci V, et al. Oxidative Stress: Harms and Benefits for Human Health. Oxid Med Cell Longev. 2017; 2017: 8416763.
192. Heck DE, Shakarjian M, Kim HD, Laskin JD, Vetrano AM. Mechanisms of oxidant generation by catalase. Ann N Y Acad Sci. 2010; 1203: 120-5.
193. Lushchak VI. Free radicals, reactive oxygen species, oxidative stress and its classification. Chem Biol Interact. 2014; 224: 164-75.
194. Weydert CJ, Cullen JJ. Measurement of superoxide dismutase, catalase and glutathione peroxidase in cultured cells and tissue. Nat Protoc. 2010; 5(1): 51-66.
195. Niedzielska E, Smaga I, Gawlik M, Moniczewski A, Stankowicz P, Pera J, et al. Oxidative Stress in Neurodegenerative Diseases. Mol Neurobiol. 2016; 53(6): 4094-125.
196. Lushchak VI. Environmentally induced oxidative stress in aquatic animals. Aquat Toxicol. 2011; 101(1): 13-30.
197. Pisoschi AM, Pop A. The role of antioxidants in the chemistry of oxidative stress: A review. Eur J Med Chem. 2015; 97: 55-74.
198. Wang Y, Branicky R, Noe A, Hekimi S. Superoxide dismutases: Dual roles in controlling ROS damage and regulating ROS signaling. J Cell Biol. 2018; 217(6): 1915-28.
199. Jomova K, Vondrakova D, Lawson M, Valko M. Metals, oxidative stress and neurodegenerative disorders. Mol Cell Biochem. 2010; 345(1-2): 91-104.
200. Day BJ. Catalase and glutathione peroxidase mimics. Biochem Pharmacol. 2009; 77(3): 285-96.
201. Kosenko E, Venediktova N, Kaminsky Y, Montoliu C, Felipo V. Sources of oxygen radicals in brain in acute ammonia intoxication *in vivo*. Brain Res. 2003; 981(1-2): 193-200.
202. Zámocký M, Gasselhuber B, Furtmüller PG, Obinger C. Molecular evolution of hydrogen peroxide degrading enzymes. Arch Biochem Biophys. 2012; 525(2): 131-44.
203. Sayre LM, Perry G, Smith MA. Oxidative stress and neurotoxicity. Chem Res Toxicol. 2008; 21(1): 172-88.
204. Moreira JD, Pernomian L, Gomes MS, Moreira RP, do Prado AF, da Silva CH, et al. Enhanced nitric oxide generation from nitric oxide synthases as the cause of increased peroxynitrite formation during acute restraint stress: Effects on carotid responsiveness to angiotensinergic stimuli in type-1 diabetic rats. European Journal of Pharmacology. 2016; 783: 11-22.
205. Tharmalingam S, Alhasawi A, Appanna VP, Lemire J, Appanna VD. Reactive nitrogen species (RNS)-resistant microbes: adaptation and medical implications. Biol Chem. 2017; 398(11): 1193-208.

206. Valko M, Leibfritz D, Moncol J, Cronin MT, Mazur M, Telser J. Free radicals and antioxidants in normal physiological functions and human disease. Int J Biochem Cell Biol. 2007; 39(1): 44-84.
207. Ungvari Z, Gupte SA, Recchia FA, Batkai S, Pacher P. Role of oxidative-nitrosative stress and downstream pathways in various forms of cardiomyopathy and heart failure. Curr Vasc Pharmacol. 2005; 3(3): 221-9.
208. Mironczuk-Chodakowska I, Witkowska AM, Zujko ME. Endogenous non-enzymatic antioxidants in the human body. Adv Med Sci. 2018; 63(1): 68-78.
209. Lobo V, Patil A, Phatak A, Chandra N. Free radicals, antioxidants and functional foods: Impact on human health. Pharmacogn Rev. 2010; 4(8): 118-26.
210. Mut-Salud N, Álvarez PJ, Garrido JM, Carrasco E, Aránega A, Rodríguez-Serrano F. Antioxidant Intake and Antitumor Therapy: Toward Nutritional Recommendations for Optimal Results. Oxid Med Cell Longev. 2016: 6719534.
211. Firuzi O, Miri R, Tavakkoli M, Saso L. Antioxidant therapy: current status and future prospects. Curr Med Chem. 2011; 18(25): 3871-88.
212. Wu JQ, Kosten TR, Zhang XY. Free radicals, antioxidant defense systems, and schizophrenia. Prog Neuropsychopharmacol Biol Psychiatry. 2013; 46: 200-6.
213. Awad MA, Aldosari SR, Abid MR. Genetic Alterations in Oxidant and Anti-Oxidant Enzymes in the Vascular System. Front Cardiovasc Med. 2018; 5: 107.
214. Demirkol O, Adams C, Ercal N. Biologically important thiols in various vegetables and fruits. J Agric Food Chem. 2004; 52(26): 8151-4.
215. Sen CK, Packer L. Thiol homeostasis and supplements in physical exercise. Am J Clin Nutr. 2000; 72(2 Suppl): 653s-69s.
216. Poole LB. The basics of thiols and cysteines in redox biology and chemistry. Free Radic Biol Med. 2015; 80: 148-57.
217. Güngör N, Ozyürek M, Güçlü K, Cekiç SD, Apak R. Comparative evaluation of antioxidant capacities of thiol-based antioxidants measured by different *in vitro* methods. Talanta. 2011; 83(5): 1650-8.
218. Zitka O, Skalickova S, Gumulec J, Masarik M, Adam V, Hubalek J, et al. Redox status expressed as GSH:GSSG ratio as a marker for oxidative stress in paediatric tumour patients. Oncol Lett. 2012; 4(6): 1247-53.
219. Owen JB, Butterfield DA. Measurement of oxidized/reduced glutathione ratio. Methods Mol Biol. 2010; 648: 269-77.
220. Rochette L, Ghibu S, Richard C, Zeller M, Cottin Y, Vergely C. Direct and indirect antioxidant properties of alpha-lipoic acid and therapeutic potential. Mol Nutr Food Res. 2013; 57(1): 114-25.
221. Teixeira J, Silva T, Andrade PB, Borges F. Alzheimer's disease and antioxidant therapy: how long how far? Curr Med Chem. 2013; 20(24): 2939-52.
222. Pocernich CB, Lange ML, Sultana R, Butterfield DA. Nutritional approaches to modulate oxidative stress in Alzheimer's disease. Curr Alzheimer Res. 2011; 8(5): 452-69.
223. Hernández-Camacho JD, Bernier M, López-Lluch G, Navas P. Coenzyme Q(10) Supplementation in Aging and Disease. Front Physiol. 2018; 9: 44.
224. Liu H-T, Huang Y-C, Cheng S-B, Huang Y-T, Lin P-T. Effects of coenzyme Q10 supplementation on antioxidant capacity and inflammation in hepatocellular carcinoma patients after surgery: a randomized, placebo-controlled trial. Nutr J. 2016; 15(1): 85-.
225. Carocho M, Ferreira IC. A review on antioxidants, prooxidants and related controversy: natural and synthetic compounds, screening and analysis methodologies and future perspectives. Food Chem Toxicol. 2013; 51: 15-25.
226. Chen W, Park SK, Yu W, Xiong A, Sanders BG, Kline K. Synthesis and screening of novel vitamin E derivatives for anticancer functions. Eur J Med Chem. 2012; 58: 72-83.
227. Kurutas EB. The importance of antioxidants which play the role in cellular response against oxidative/nitrosative stress: current state. Nutr J. 2016; 15(1): 71.
228. Raederstorff D, Wyss A, Calder PC, Weber P, Eggersdorfer M. Vitamin E function and requirements in relation to PUFA. Br J Nutr. 2015; 114(8): 1113-22.

229. Ziani K, Fang Y, McClements DJ. Encapsulation of functional lipophilic components in surfactant-based colloidal delivery systems: vitamin E, vitamin D, and lemon oil. Food Chem. 2012; 134(2): 1106-12.
230. Barros AI, Nunes FM, Goncalves B, Bennett RN, Silva AP. Effect of cooking on total vitamin C contents and antioxidant activity of sweet chestnuts (*Castanea sativa Mill.*). Food Chem. 2011; 128(1): 165-72.
231. Sadowska-Bartosz I, Bartosz G. Effect of antioxidants supplementation on aging and longevity. Biomed Res Int. 2014: 404680.
232. Leopoldini M, Russo N, Toscano M. The molecular basis of working mechanism of natural polyphenolic antioxidants. Food Chem. 2011; 125(2): 288-306.
233. Koch W. Dietary Polyphenols-Important Non-Nutrients in the Prevention of Chronic Noncommunicable Diseases. A Systematic Review. Nutrients. 2019; 11(5): 1039.
234. Benfeito S, Oliveira C, Soares P, Fernandes C, Silva T, Teixeira J, et al. Antioxidant therapy: Still in search of the 'magic bullet'. Mitochondrion. 2013; 13(5): 427-35.
235. Mota SI, Costa RO, Ferreira IL, Santana I, Caldeira GL, Padovano C, et al. Oxidative stress involving changes in Nrf2 and ER stress in early stages of Alzheimer's disease. Biochim Biophys Acta. 2015; 1852(7): 1428-41.
236. Dias V, Junn E, Mouradian MM. The role of oxidative stress in Parkinson's disease. J Parkinsons Dis. 2013; 3(4): 461-91.
237. Venkateshappa C, Harish G, Mythri RB, Mahadevan A, Bharath MM, Shankar SK. Increased oxidative damage and decreased antioxidant function in aging human *substantia nigra* compared to striatum: implications for Parkinson's disease. Neurochem Res. 2012; 37(2): 358-69.
238. Kim GH, Kim JE, Rhie SJ, Yoon S. The Role of Oxidative Stress in Neurodegenerative Diseases. Exp Neurobiol. 2015; 24(4): 325-40.
239. Gandhi S, Abramov AY. Mechanism of oxidative stress in neurodegeneration. Oxid Med Cell Longev. 2012: 428010.
240. Cobley JN, Fiorello ML, Bailey DM. 13 reasons why the brain is susceptible to oxidative stress. Redox Biol. 2018; 15: 490-503.
241. Ward RJ, Zucca FA, Duyn JH, Crichton RR, Zecca L. The role of iron in brain ageing and neurodegenerative disorders. Lancet Neurol. 2014; 13(10): 1045-60.
242. Kausar S, Wang F, Cui H. The Role of Mitochondria in Reactive Oxygen Species Generation and Its Implications for Neurodegenerative Diseases. Cells. 2018; 7(12): 274.
243. Smith RA, Hartley RC, Cocheme HM, Murphy MP. Mitochondrial pharmacology. Trends Pharmacol Sci. 2012; 33(6): 341-52.
244. Bhat AH, Dar KB, Anees S, Zargar MA, Masood A, Sofi MA, et al. Oxidative stress, mitochondrial dysfunction and neurodegenerative diseases: a mechanistic insight. Biomed Pharmacother. 2015; 74: 101-10.
245. Sheikh S, Safia, Haque E, Mir SS. Neurodegenerative Diseases: Multifactorial Conformational Diseases and Their Therapeutic Interventions. J Neurodegener Dis. 2013: 563481.
246. Collin F. Chemical Basis of Reactive Oxygen Species Reactivity and Involvement in Neurodegenerative Diseases. Int J Mol Sci. 2019; 20(10): 2407.
247. Sivitz WI, Yorek MA. Mitochondrial dysfunction in diabetes: from molecular mechanisms to functional significance and therapeutic opportunities. Antioxid Redox Signal. 2010; 12(4): 537-77.
248. Angelova PR, Abramov AY. Role of mitochondrial ROS in the brain: from physiology to neurodegeneration. FEBS Lett. 2018; 592(5): 692-702.
249. Jin H, Kanthasamy A, Ghosh A, Anantharam V, Kalyanaraman B, Kanthasamy AG. Mitochondria-targeted antioxidants for treatment of Parkinson's disease: preclinical and clinical outcomes. Biochim Biophys Acta. 2014; 1842(8): 1282-94.
250. Guo JD, Zhao X, Li Y, Li GR, Liu XL. Damage to dopaminergic neurons by oxidative stress in Parkinson's disease (Review). Int J Mol Med. 2018; 41(4): 1817-25.

251. Facecchia K, Fochesato LA, Ray SD, Stohs SJ, Pandey S. Oxidative toxicity in neurodegenerative diseases: role of mitochondrial dysfunction and therapeutic strategies. J Toxicol. 2011; 2011: 683728.
252. Cai Q, Tammineni P. Mitochondrial Aspects of Synaptic Dysfunction in Alzheimer's Disease. J Alzheimer's Dis. 2017; 57(4): 1087-103.
253. Federico A, Cardaioli E, Da Pozzo P, Formichi P, Gallus GN, Radi E. Mitochondria, oxidative stress and neurodegeneration. J Neurol Sci. 2012; 322(1-2): 254-62.
254. Johri A, Beal MF. Mitochondrial dysfunction in neurodegenerative diseases. J Pharmacol Exp Ther. 2012; 342(3): 619-30.
255. Barnham KJ, Masters CL, Bush AI. Neurodegenerative diseases and oxidative stress. Nature reviews Drug discovery. 2004; 3(3): 205-14.
256. Munoz P, Paris I, Sanders LH, Greenamyre JT, Segura-Aguilar J. Overexpression of VMAT-2 and DT-diaphorase protects substantia nigra-derived cells against aminochrome neurotoxicity. Biochim Biophys Acta. 2012; 1822(7): 1125-36.
257. Blesa J, Trigo-Damas I, Quiroga-Varela A, Jackson-Lewis VR. Oxidative stress and Parkinson's disease. Front Neuroanat. 2015; 9: 91.
258. Segura-Aguilar J, Paris I, Munoz P, Ferrari E, Zecca L, Zucca FA. Protective and toxic roles of dopamine in Parkinson's disease. J Neurochem. 2014; 129(6): 898-915.
259. Umek N, Geršak B, Vintar N, Šoštarič M, Mavri J. Dopamine Autoxidation Is Controlled by Acidic pH. Front Mol Neurosci. 2018; 11: 467.
260. Munoz P, Huenchuguala S, Paris I, Segura-Aguilar J. Dopamine oxidation and autophagy. Parkinsons Dis. 2012: 920953.
261. Zucca FA, Segura-Aguilar J, Ferrari E, Munoz P, Paris I, Sulzer D, et al. Interactions of iron, dopamine and neuromelanin pathways in brain aging and Parkinson's disease. Prog Neurobiol. 2017; 155: 96-119.
262. Meiser J, Weindl D, Hiller K. Complexity of dopamine metabolism. Cell Commun Signal. 2013; 11(1): 1-18.
263. Hwang O. Role of oxidative stress in Parkinson's disease. Exp Neurobiol. 2013; 22(1): 11-7.
264. Mousseau DD, Baker GB. Recent developments in the regulation of monoamine oxidase form and function: is the current model restricting our understanding of the breadth of contribution of monoamine oxidase to brain [dys]function? Curr Top Med Chem. 2012; 12(20): 2163-76.
265. Biasutto L, Mattarei A, La Spina M, Azzolini M, Parrasia S, Szabò I, et al. Strategies to target bioactive molecules to subcellular compartments. Focus on natural compounds. Eur J Med Chem. 2019; 181.
266. Mallajosyula JK, Kaur D, Chinta SJ, Rajagopalan S, Rane A, Nicholls DG, et al. MAO-B elevation in mouse brain astrocytes results in Parkinson's pathology. PLoS One. 2008; 3(2): e1616.
267. Solleiro-Villavicencio H, Rivas-Arancibia S. Effect of Chronic Oxidative Stress on Neuroinflammatory Response Mediated by CD4(+)T Cells in Neurodegenerative Diseases. Front Cell Neurosci. 2018; 12: 114.
268. Gelders G, Baekelandt V, Van der Perren A. Linking Neuroinflammation and Neurodegeneration in Parkinson's Disease. J Immunol Res. 2018: 4784268.
269. Kinney JW, Bemiller SM, Murtishaw AS, Leisgang AM, Salazar AM, Lamb BT. Inflammation as a central mechanism in Alzheimer's disease. Alzheimers Dement (N Y). 2018; 4: 575-90.
270. Subhramanyam CS, Wang C, Hu Q, Dheen ST. Microglia-mediated neuroinflammation in neurodegenerative diseases. Semin Cell Dev Biol. 2019; 94: 112-20.
271. de Vries HE, Witte M, Hondius D, Rozemuller AJ, Drukarch B, Hoozemans J, et al. Nrf2-induced antioxidant protection: a promising target to counteract ROS-mediated damage in neurodegenerative disease? Free Radic Biol Med. 2008; 45(10): 1375-83.
272. Surace MJ, Block ML. Targeting microglia-mediated neurotoxicity: the potential of NOX2 inhibitors. Cell Mol Life Sci. 2012; 69(14): 2409-27.

273. Butterfield DA, Swomley AM, Sultana R. Amyloid β-peptide (1-42)-induced oxidative stress in Alzheimer disease: importance in disease pathogenesis and progression. Antioxid Redox Signal. 2013; 19(8): 823-35.
274. Butterfield DA, Boyd-Kimball D. Oxidative Stress, Amyloid-β Peptide, and Altered Key Molecular Pathways in the Pathogenesis and Progression of Alzheimer's Disease. J Alzheimers Dis. 2018; 62(3): 1345-67.
275. Tönnies E, Trushina E. Oxidative Stress, Synaptic Dysfunction, and Alzheimer's Disease. J Alzheimers Dis. 2017; 57(4): 1105-21.
276. Rosini M, Simoni E, Milelli A, Minarini A, Melchiorre C. Oxidative stress in Alzheimer's disease: are we connecting the dots? J Med Chem. 2014; 57(7): 2821-31.
277. Roleira FM, Siquet C, Orru E, Garrido EM, Garrido J, Milhazes N, et al. Lipophilic phenolic antioxidants: correlation between antioxidant profile, partition coefficients and redox properties. Bioorg Med Chem. 2010; 18(16): 5816-25.
278. Teixeira J, Silva T, Benfeito S, Gaspar A, Garrido EM, Garrido J, et al. Exploring nature profits: development of novel and potent lipophilic antioxidants based on galloyl-cinnamic hybrids. Eur J Med Chem. 2013; 62: 289-96.
279. Garrido J, Gaspar A, Garrido EM, Miri R, Tavakkoli M, Pourali S, et al. Alkyl esters of hydroxycinnamic acids with improved antioxidant activity and lipophilicity protect PC12 cells against oxidative stress. Biochimie. 2012; 94(4): 961-7.
280. Silva T, Bravo J, Summavielle T, Remião F, Pérez C, Gil C, et al. Biology-oriented development of novel lipophilic antioxidants with neuroprotective activity. RSC Adv. 2015; 5(21): 15800-11.
281. Murphy MP. Targeting lipophilic cations to mitochondria. Biochim Biophys Acta. 2008; 1777(7-8): 1028-31.
282. Sheu SS, Nauduri D, Anders MW. Targeting antioxidants to mitochondria: a new therapeutic direction. Biochim Biophys Acta. 2006; 1762(2): 256-65.
283. Szeto HH. Mitochondria-targeted peptide antioxidants: novel neuroprotective agents. AAPS J. 2006; 8(3): E521-E31.
284. Fetisova EK, Avetisyan AV, Izyumov DS, Korotetskaya MV, Chernyak BV, Skulachev VP. Mitochondria-targeted antioxidant SkQR1 selectively protects MDR (Pgp 170)-negative cells against oxidative stress. FEBS Lett. 2010; 584(3): 562-6.
285. Guzman-Villanueva D, Weissig V. Mitochondria-Targeted Agents: Mitochondriotropics, Mitochondriotoxics, and Mitocans. Handb Exp Pharmacol. 2017; 240: 423-38.
286. He H, Li DW, Yang LY, Fu L, Zhu XJ, Wong WK, et al. A novel bifunctional mitochondria-targeted anticancer agent with high selectivity for cancer cells. Sci Rep. 2015; 5: 13543.
287. Smith RA, Murphy MP. Animal and human studies with the mitochondria-targeted antioxidant MitoQ. Ann N Y Acad Sci. 2010; 1201: 96-103.
288. Murphy MP, Hartley RC. Mitochondria as a therapeutic target for common pathologies. Nat Rev Drug Discov. 2018; 17(12): 865-86.
289. Porteous CM, Logan A, Evans C, Ledgerwood EC, Menon DK, Aigbirhio F, et al. Rapid uptake of lipophilic triphenylphosphonium cations by mitochondria in vivo following intravenous injection: implications for mitochondria-specific therapies and probes. Biochim Biophys Acta. 2010; 1800(9): 1009-17.
290. Zielonka J, Joseph J, Sikora A, Hardy M, Ouari O, Vasquez-Vivar J, et al. Mitochondria-Targeted Triphenylphosphonium-Based Compounds: Syntheses, Mechanisms of Action, and Therapeutic and Diagnostic Applications. Chem Rev. 2017; 117(15): 10043-120.
291. Abu-Gosh SE, Kolvazon N, Tirosh B, Ringel I, Yavin E. Multiple triphenylphosphonium cations shuttle a hydrophilic peptide into mitochondria. Mol Pharm. 2009; 6(4): 1138-44.
292. Murphy MP, Smith RA. Targeting antioxidants to mitochondria by conjugation to lipophilic cations. Annu Rev Pharmacol Toxicol. 2007; 47: 629-56.

293. Smith RA, Hartley RC, Murphy MP. Mitochondria-targeted small molecule therapeutics and probes. Antioxid Redox Signal. 2011; 15(12): 3021-38.
294. Trnka J, Elkalaf M, Anděl M. Lipophilic triphenylphosphonium cations inhibit mitochondrial electron transport chain and induce mitochondrial proton leak. PLoS One. 2015; 10(4): e0121837.
295. Kelso GF, Porteous CM, Coulter CV, Hughes G, Porteous WK, Ledgerwood EC, et al. Selective targeting of a redox-active ubiquinone to mitochondria within cells: antioxidant and antiapoptotic properties. J Biol Chem. 2001; 276(7): 4588-96.
296. Jameson VJA, Cochemé HM, Logan A, Hanton LR, Smith RAJ, Murphy MP. Synthesis of triphenylphosphonium vitamin E derivatives as mitochondria-targeted antioxidants. Tetrahedron. 2015; 71(44): 8444-53.
297. Teixeira J, Cagide F, Benfeito S, Soares P, Garrido J, Baldeiras I, et al. Development of a Mitochondriotropic Antioxidant Based on Caffeic Acid: Proof of Concept on Cellular and Mitochondrial Oxidative Stress Models. J Med Chem. 2017; 60(16): 7084-98.
298. Benfeito S, Oliveira C, Fernandes C, Cagide F, Teixeira J, Amorim R, et al. Fine-tuning the neuroprotective and blood-brain barrier permeability profile of multi-target agents designed to prevent progressive mitochondrial dysfunction. Eur J Med Chem. 2019; 167: 525-45.
299. Oliveira C, Cagide F, Teixeira J, Amorim R, Sequeira L, Mesiti F, et al. Hydroxybenzoic Acid Derivatives as Dual-Target Ligands: Mitochondriotropic Antioxidants and Cholinesterase Inhibitors. Front Chem. 2018; 6: 126.
300. Teixeira J, Oliveira C, Amorim R, Cagide F, Garrido J, Ribeiro JA, et al. Development of hydroxybenzoic-based platforms as a solution to deliver dietary antioxidants to mitochondria. Sci Rep. 2017; 7(1): 6842.
301. Smith RAJ, Porteous CM, Gane AM, Murphy MP. Delivery of bioactive molecules to mitochondria *in vivo*. Proc Natl Acad Sci USA. 2003; 100(9): 5407-12.
302. Liu W, Lang M, Youdim MBH, Amit T, Sun Y, Zhang Z, et al. Design, synthesis and evaluation of novel dual monoamine-cholinesterase inhibitors as potential treatment for Alzheimer's disease. Neuropharmacology. 2016; 109: 376-85.
303. Prati F, Cavalli A, Bolognesi ML. Navigating the Chemical Space of Multitarget-Directed Ligands: From Hybrids to Fragments in Alzheimer's Disease. Molecules. 2016; 21(4).
304. Proschak E, Stark H, Merk D. Polypharmacology by Design: A Medicinal Chemist's Perspective on Multitargeting Compounds. J Med Chem. 2019; 62(2): 420-44.
305. Geldenhuys WJ, Van Der Schyf CJ. Designing drugs with multi-target activity: The next step in the treatment of neurodegenerative disorders. Expert Opin Drug Discov. 2013; 8(2): 115-29.
306. Ramsay RR, Popovic-Nikolic MR, Nikolic K, Uliassi E, Bolognesi ML. A perspective on multi-target drug discovery and design for complex diseases. Clin Transl Med. 2018; 7(1): 3.
307. Zhou J, Jiang X, He S, Jiang H, Feng F, Liu W, et al. Rational Design of Multitarget-Directed Ligands: Strategies and Emerging Paradigms. J Med Chem. 2019.
308. Bolognesi ML. Polypharmacology in a single drug: Multitarget drugs. Curr Med Chem. 2013; 20(13): 1639-45.
309. Bansal Y, Silakari O. Multifunctional compounds: Smart molecules for multifactorial diseases. Eur J Med Chem. 2014; 76: 31-42.
310. Anighoro A, Bajorath J, Rastelli G. Polypharmacology: Challenges and opportunities in drug discovery. J Med Chem. 2014; 57(19): 7874-87.
311. Hargreaves RJ, Hoppin J, Sevigny J, Patel S, Chiao P, Klimas M, et al. Optimizing central nervous system drug development using molecular imaging. Clin Pharmacol Ther. 2015; 98(1): 47-60.
312. Gunn RN, Rabiner EA. Imaging in Central Nervous System Drug Discovery. Semin Nucl Med. 2017; 47(1): 89-98.
313. Hochman JH, Ha SN, Sheridan RP. Establishment of P-Glycoprotein Structure–Transport Relationships to Optimize CNS Exposure in Drug Discovery. Blood–Brain Barrier

in Drug Discovery: Optimizing Brain Exposure of CNS Drugs and Minimizing Brain Side Effects for Peripheral Drugs. First ed: John Wiley & Sons, Inc; 2015. p. 113-24.
314. Gribkoff VK, Kaczmarek LK. The need for new approaches in CNS drug discovery: Why drugs have failed, and what can be done to improve outcomes. Neuropharmacology. 2017; 120: 11-9.
315. Liu Q, Hou J, Chen X, Liu G, Zhang D, Sun H, et al. P-glycoprotein mediated efflux limits the transport of the novel anti-Parkinson's disease candidate drug FLZ across the physiological and PD pathological in vitro BBB models. PLoS One. 2014; 9(7): e102442.
316. Pardridge WM. Blood-brain barrier delivery. Drug Discov Today. 2007; 12(1-2): 54-61.
317. Warren KE. Beyond the blood: Brain barrier: The importance of central nervous system (CNS) pharmacokinetics for the treatment of CNS tumors, including diffuse intrinsic pontine glioma. Front Oncol. 2018; 8: 239.
318. Bors LA, Erdö F. Overcoming the blood-brain barrier. Challenges and tricks for CNS drug delivery. Sci Pharm. 2019; 87(1): 6.
319. Tang W, Fan W, Lau J, Deng L, Shen Z, Chen X. Emerging blood-brain-barrier-crossing nanotechnology for brain cancer theranostics. Chem Soc Rev. 2019; 48(11): 2967-3014.
320. Chen Y, Liu L. Modern methods for delivery of drugs across the blood-brain barrier. Adv Drug Deliv Rev. 2012; 64(7): 640-65.
321. Abbott NJ. Prediction of blood-brain barrier permeation in drug discovery from in vivo, in vitro and in silico models. Drug Discov Today Technol. 2004; 1(4): 407-16.
322. De Boer AG, Gaillard PJ. Strategies to improve drug delivery across the blood-brain barrier. Clin Pharmacokinet. 2007; 46(7): 553-76.
323. Rankovic Z. Designing CNS Drugs for Optimal Brain Exposure. Blood–Brain Barrier in Drug Discovery: Optimizing Brain Exposure of CNS Drugs and Minimizing Brain Side Effects for Peripheral Drugs: John Wiley & Sons, Inc.; 2015. p. 387-424.
324. Trippier PC. Selecting good 'drug-like' properties to optimize small molecule blood-brain barrier penetration. Curr Med Chem. 2016; 23(14): 1392-407.
325. Rankovic Z. CNS drug design: balancing physicochemical properties for optimal brain exposure. J Med Chem. 2015; 58(6): 2584-608.
326. Leeson PD, Davis AM. Time-related differences in the physical property profiles of oral drugs. J Med Chem. 2004; 47(25): 6338-48.
327. Pajouhesh H, Lenz GR. Medicinal Chemical Properties of Successful Central Nervous System Drugs. NeuroRx. 2005; 2(4): 541-53.
328. Hitchcock SA, Pennington LD. Structure-brain exposure relationships. J Med Chem. 2006; 49(26): 7559-83.
329. Wager TT, Hou X, Verhoest PR, Villalobos A. Moving beyond rules: the development of a central nervous system multiparameter optimization (CNS MPO) approach to enable alignment of druglike properties. ACS Chem Neurosci. 2010; 1(6): 435-49.
330. Waring MJ. Lipophilicity in drug discovery. Expert Opin Drug Discov. 2010; 5(3): 235-48.
331. Arnott JA, Planey SL. The influence of lipophilicity in drug discovery and design. Expert Opin Drug Discov. 2012; 7(10): 863-75.
332. Leeson PD. Molecular inflation, attrition and the rule of five. Adv Drug Deliv Rev. 2016; 101: 22-33.
333. Kelder J, Grootenhuis PDJ, Bayada DM, Delbressine LPC, Ploemen JP. Polar molecular surface as a dominating determinant for oral absorption and brain penetration of drugs. Pharm Res. 1999; 16(10): 1514-9.
334. Lobell M, Hendrix M, Hinzen B, Keldenich J, Meier H, Schmeck C, et al. In silico ADMET traffic lights as a tool for the prioritization of HTS hits. ChemMedChem. 2006; 1(11): 1229-36.
335. Clark DE. Rapid calculation of polar molecular surface area and its application to the prediction of transport phenomena. 2. Prediction of blood-brain barrier penetration. J Pharm Sci. 1999; 88(8): 815-21.

336. Vilar S, Chakrabarti M, Costanzi S. Prediction of passive blood-brain partitioning: straightforward and effective classification models based on in silico derived physicochemical descriptors. J Mol Graph Model. 2010; 28(8): 899-903.
337. Muehlbacher M, Spitzer GM, Liedl KR, Kornhuber J. Qualitative prediction of blood-brain barrier permeability on a large and refined dataset. J Comput Aided Mol Des. 2011; 25(12): 1095-106.
338. Alavijeh MS, Chishty M, Qaiser MZ, Palmer AM. Drug metabolism and pharmacokinetics, the blood-brain barrier, and central nervous system drug discovery. NeuroRx. 2005; 2(4): 554-71.
339. Miller DS, Bauer B, Hartz AMS. Modulation of P-glycoprotein at the blood-brain barrier: opportunities to improve central nervous system pharmacotherapy. Pharmacol Rev. 2008; 60(2): 196-209.
340. De Lange ECM, vd Berg DJ, Bellanti F, Voskuyl RA, Syvänen S. P-glycoprotein protein expression versus functionality at the blood-brain barrier using immunohistochemistry, microdialysis and mathematical modeling. Eur J Pharm Sci. 2018; 124: 61-70.
341. McCaffrey G, Staatz WD, Sanchez-Covarrubias L, Finch JD, Demarco K, Laracuente M-L, et al. P-glycoprotein trafficking at the blood-brain barrier altered by peripheral inflammatory hyperalgesia. J Neurochem. 2012; 122(5): 962-75.
342. Bartels AL. Blood-brain barrier P-glycoprotein function in neurodegenerative disease. Curr Pharm Des. 2011; 17(26): 2771-7.
343. Davison EK, Brimble MA. Natural product derived privileged scaffolds in drug discovery. Curr Opin Chem Biol. 2019; 52: 1-8.
344. Rodrigues T, Reker D, Schneider P, Schneider G. Counting on natural products for drug design. Nat Chem. 2016; 8(6): 531-41.
345. Koehn FE, Carter GT. The evolving role of natural products in drug discovery. Nat Rev Drug Discov. 2005; 4(3): 206-20.
346. Lachance H, Wetzel S, Kumar K, Waldmann H. Charting, navigating, and populating natural product chemical space for drug discovery. J Med Chem. 2012; 55(13): 5989-6001.
347. Harvey AL. Natural products in drug discovery. Drug Discov Today. 2008; 13(19-20): 894-901.
348. Bharate SS, Mignani S, Vishwakarma RA. Why Are the Majority of Active Compounds in the CNS Domain Natural Products? A Critical Analysis. J Med Chem. 2018; 61(23): 10345-74.
349. Schneider G. Automating drug discovery. Nat Rev Drug Discov. 2018; 17(2): 97-113.
350. Basu S, Ellinger B, Rizzo S, Deraeve C, Schürmann M, Preut H, et al. Biology-oriented synthesis of a natural-product inspired oxepane collection yields a small-molecule activator of the Wnt-pathway. Proc Natl Acad Sci USA. 2011; 108(17): 6805-10.
351. Lee DS, Woo JY, Ahn CB, Je JY. Chitosan-hydroxycinnamic acid conjugates: preparation, antioxidant and antimicrobial activity. Food Chem. 2014; 148: 97-104.
352. Taofiq O, González-Paramás AM, Barreiro MF, Ferreira ICFR. Hydroxycinnamic Acids and Their Derivatives: Cosmeceutical Significance, Challenges and Future Perspectives, a Review. Molecules. 2017; 22(2): 281.
353. Macoy DM, Kim WY, Lee SY, Kim MG. Biosynthesis, physiology, and functions of hydroxycinnamic acid amides in plants. Plant Biotechnol Rep. 2015; 9(5): 269-78.
354. Razzaghi-Asl N, Garrido J, Khazraei H, Borges F, Firuzi O. Antioxidant properties of hydroxycinnamic acids: a review of structure-activity relationships. Curr Med Chem. 2013; 20(36): 4436-50.
355. Makila L, Laaksonen O, Alanne AL, Kortesniemi M, Kallio H, Yang B. Stability of Hydroxycinnamic Acid Derivatives, Flavonol Glycosides, and Anthocyanins in Black Currant Juice. J Agric Food Chem. 2016; 64(22): 4584-98.
356. Son S, Lewis BA. Free radical scavenging and antioxidative activity of caffeic acid amide and ester analogues: Structure-activity relationship. J Agric Food Chem. 2002; 50(3): 468-72.

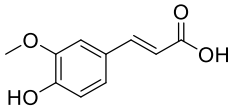
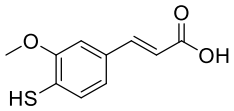
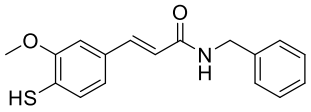
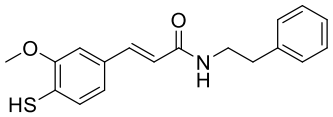
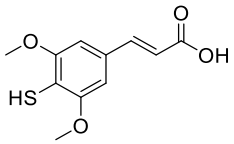
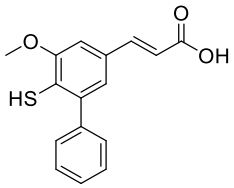
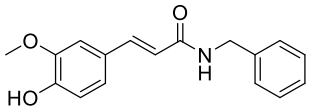
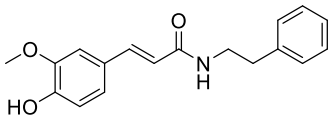
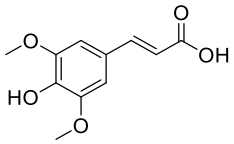
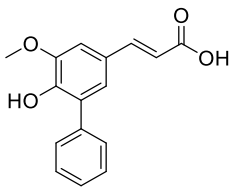
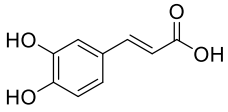
357. Consoli GML, Galante E, Daquino C, Granata G, Cunsolo F, Geraci C. Hydroxycinnamic acid clustered by a calixarene platform: radical scavenging and antioxidant activity. Tetrahedron Lett. 2006; 47(37): 6611-4.
358. Siquet C, Paiva-Martins F, Lima JL, Reis S, Borges F. Antioxidant profile of dihydroxy- and trihydroxyphenolic acids - a structure-activity relationship study. Free Radic Res. 2006; 40(4): 433-42.
359. El-Seedi HR, El-Said AM, Khalifa SA, Goransson U, Bohlin L, Borg-Karlson AK, et al. Biosynthesis, natural sources, dietary intake, pharmacokinetic properties, and biological activities of hydroxycinnamic acids. J Agric Food Chem. 2012; 60(44): 10877-95.
360. Gaspar A, Garrido EM, Esteves M, Quezada E, Milhazes N, Garrido J, et al. New insights into the antioxidant activity of hydroxycinnamic acids: Synthesis and physicochemical characterization of novel halogenated derivatives. Eur J Med Chem. 2009; 44(5): 2092-9.
361. Wrigstedt P, Kylli P, Pitkanen L, Nousiainen P, Tenkanen M, Sipila J. Synthesis and antioxidant activity of hydroxycinnamic acid xylan esters. J Agric Food Chem. 2010; 58(11): 6937-43.
362. Balasundram N, Sundram K, Samman S. Phenolic compounds in plants and agri-industrial by-products: Antioxidant activity, occurrence, and potential uses. Food Chem. 2006; 99(1): 191-203.
363. Kylli P, Nousiainen P, Biely P, Sipila J, Tenkanen M, Heinonen M. Antioxidant potential of hydroxycinnamic acid glycoside esters. J Agric Food Chem. 2008; 56(12): 4797-805.
364. Silva T, Oliveira C, Borges F. Caffeic acid derivatives, analogs and applications: A patent review (2009-2013). Expert Opin Ther Pat. 2014; 24(11): 1257-70.
365. Andjelković M, Van Camp J, De Meulenaer B, Depaemelaere G, Socaciu C, Verloo M, et al. Iron-chelation properties of phenolic acids bearing catechol and galloyl groups. Food Chem. 2006; 98(1): 23-31.
366. Teixeira J, Gaspar A, Garrido EM, Garrido J, Borges F. Hydroxycinnamic acid antioxidants: an electrochemical overview. Biomed Res Int. 2013; 2013(251754): 1-13.
367. Sgarbossa A, Giacomazza D, di Carlo M. Ferulic Acid: A Hope for Alzheimer's Disease Therapy from Plants. Nutrients. 2015; 7(7): 5764-82.
368. Fazary AE, Ju YH. Feruloyl esterases as biotechnological tools: current and future perspectives. Acta Biochim Biophys Sin (Shanghai). 2007; 39(11): 811-28.
369. Brand-Williams W, Cuvelier ME, Berset C. Use of a free radical method to evaluate antioxidant activity. LWT - Food Sci Technol. 1995; 28(1): 25-30.
370. Firuzi O, Giansanti L, Vento R, Seibert C, Petrucci R, Marrosu G, et al. Hypochlorite scavenging activity of hydroxycinnamic acids evaluated by a rapid microplate method based on the measurement of chloramines. J Pharm Pharmacol. 2003; 55(7): 1021-7.
371. Kanski J, Aksenova M, Stoyanova A, Butterfield DA. Ferulic acid antioxidant protection against hydroxyl and peroxyl radical oxidation in synaptosomal and neuronal cell culture systems in vitro: structure-activity studies. J Nutr Biochem. 2002; 13(5): 273-81.
372. Ojha S, Javed H, Azimullah S, Abul Khair SB, Haque ME. Neuroprotective potential of ferulic acid in the rotenone model of Parkinson's disease. Drug Des Devel Ther. 2015; 9: 5499-510.
373. Zhang Y, Cui L, Zhang Y, Cao H, Wang Y, Teng T, et al. Ferulic acid inhibits the transition of amyloid-β 42 monomers to oligomers but accelerates the transition from oligomers to fibrils. J Alzheimer's Dis. 2013; 37(1): 19-28.
374. Ono K, Hirohata M, Yamada M. Ferulic acid destabilizes preformed β-amyloid fibrils *in vitro*. Biochem Biophys Res Commun. 2005; 336(2): 444-9.
375. Sultana R, Ravagna A, Mohmmad-Abdul H, Calabrese V, Butterfield DA. Ferulic acid ethyl ester protects neurons against amyloid β-peptide(1-42)-induced oxidative stress and neurotoxicity: Relationship to antioxidant activity. J Neurochem. 2005; 92(4): 749-58.
376. Perluigi M, Joshi G, Sultana R, Calabrese V, De Marco C, Coccia R, et al. In vivo protective effects of ferulic acid ethyl ester against amyloid-beta peptide 1-42-induced oxidative stress. J Neurosci Res. 2006; 84(2): 418-26.

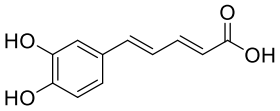
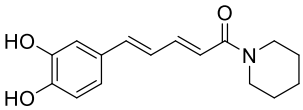
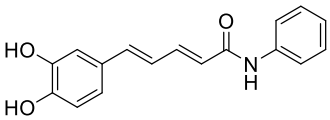
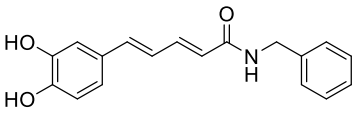
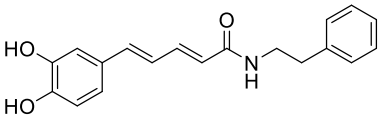
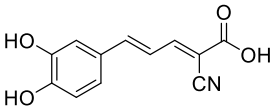
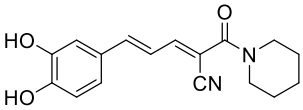
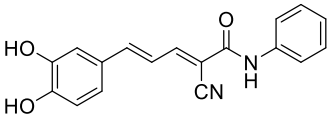
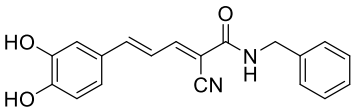
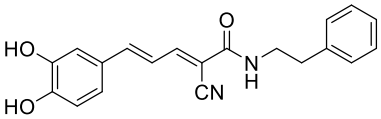
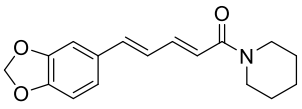
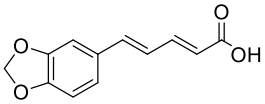
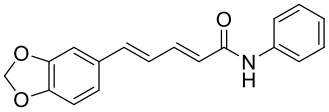
377. Masuda T, Yamada K, Akiyama J, Someya T, Odaka Y, Takeda Y, et al. Antioxidation mechanism studies of caffeic acid: identification of antioxidation products of methyl caffeate from lipid oxidation. J Agric Food Chem. 2008; 56(14): 5947-52.
378. Farhoosh R, Johnny S, Asnaashari M, Molaahmadibahraseman N, Sharif A. Structure-antioxidant activity relationships of *o*-hydroxyl, *o*-methoxy, and alkyl ester derivatives of *p*-hydroxybenzoic acid. Food Chem. 2016; 194: 128-34.
379. Borges F, Lima JLFC, Pinto I, Reis S, Siquet C. Application of a potentiometric system with data-analysis computer programs to the quantification of metal-chelating activity of two natural antioxidants: Caffeic acid and ferulic acid. Helv Chim Acta. 2003; 86(9): 3081-7.
380. Iglesias J, Pazos M, Andersen ML, Skibsted LH, Medina I. Caffeic acid as antioxidant in fish muscle: Mechanism of synergism with endogenous ascorbic acid and α-tocopherol. J Agric Food Chem. 2009; 57(2): 675-81.
381. Sørensen ADM, Durand E, Laguerre M, Bayrasy C, Lecomte J, Villeneuve P, et al. Antioxidant properties and efficacies of synthesized alkyl caffeates, ferulates, and coumarates. J Agric Food Chem. 2014; 62(52): 12553-62.
382. Sul D, Kim HS, Lee D, Joo SS, Hwang KW, Park SY. Protective effect of caffeic acid against beta-amyloid-induced neurotoxicity by the inhibition of calcium influx and tau phosphorylation. Life Sci. 2009; 84(9-10): 257-62.
383. Tsai CF, Kuo YH, Yeh WL, Wu CYJ, Lin HY, Lai SW, et al. Regulatory effects of caffeic acid phenethyl ester on neuroinflammation in microglial cells. Int J Mol Sci. 2015; 16(3): 5572-89.
384. Barros Silva R, Santos NAG, Martins NM, Ferreira DAS, Barbosa F, Oliveira Souza VC, et al. Caffeic acid phenethyl ester protects against the dopaminergic neuronal loss induced by 6-hydroxydopamine in rats. Neuroscience. 2013; 233: 86-94.
385. Rahman T, Rahmatullah M. Proposed structural basis of interaction of piperine and related compounds with monoamine oxidases. Bioorg Med Chem Lett. 2010; 20(2): 537-40.
386. Mao QQ, Huang Z, Ip SP, Xian YF, Che CT. Protective effects of piperine against corticosterone-induced neurotoxicity in PC12 cells. Cell Mol Neurobiol. 2012; 32(4): 531-7.
387. Liu J, Chen M, Wang X, Wang Y, Duan C, Gao G, et al. Piperine induces autophagy by enhancing protein phosphotase 2A activity in a rotenone-induced Parkinson's disease model. Oncotarget. 2016; 7(38): 60823-43.
388. Chonpathompikunlert P, Wattanathorn J, Muchimapura S. Piperine, the main alkaloid of Thai black pepper, protects against neurodegeneration and cognitive impairment in animal model of cognitive deficit like condition of Alzheimer's disease. Food Chem Toxicol. 2010; 48(3): 798-802.
389. Lee SA, Hong SS, Han XH, Hwang JS, Oh GJ, Lee KS, et al. Piperine from the fruits of Piper longum with inhibitory effect on monoamine oxidase and antidepressant-like activity. Chem Pharm Bull (Tokyo). 2005; 53(7): 832-5.
390. Cagide F, Reis J, Gaspar A, Borges F. Accelerating lead optimization of chromone carboxamide scaffold throughout microwave-assisted organic synthesis. Tetrahedron Lett. 2011; 52(48): 6446-9.
391. Chen G, Zhang Y, Liu X, Fang Q, Wang Z, Fu L, et al. Discovery of a New Inhibitor of Myeloid Differentiation 2 from Cinnamamide Derivatives with Anti-Inflammatory Activity in Sepsis and Acute Lung Injury. J Med Chem. 2016; 59(6): 2436-51.
392. Vashisth P, Kumar N, Sharma M, Pruthi V. Biomedical applications of ferulic acid encapsulated electrospun nanofibers. Biotechnol Rep (Amst). 2015; 8: 36-44.
393. Mancuso C, Santangelo R. Ferulic acid: pharmacological and toxicological aspects. Food Chem Toxicol. 2014; 65: 185-95.
394. Zhao Z, Moghadasian MH. Chemistry, natural sources, dietary intake and pharmacokinetic properties of ferulic acid: A review. Food Chem. 2008; 109(4): 691-702.
395. Wu WM, Lu L, Long Y, Wang T, Liu L, Chen Q, et al. Free radical scavenging and antioxidative activities of caffeic acid phenethyl ester (CAPE) and its related compounds in solution and membranes: A structure-activity insight. Food Chem. 2007; 105(1): 107-15.

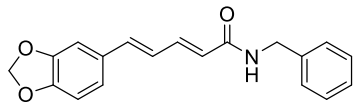
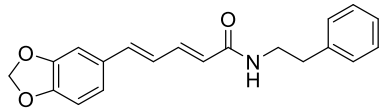
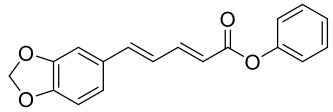
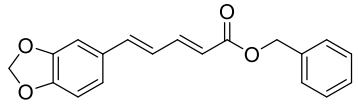
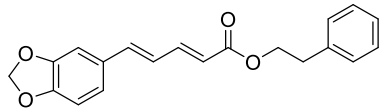
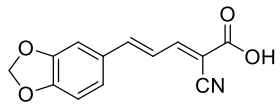
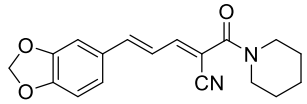
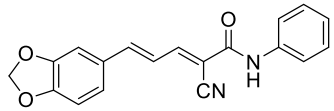
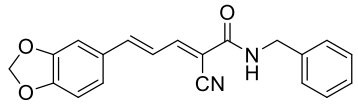
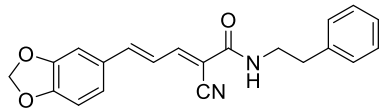
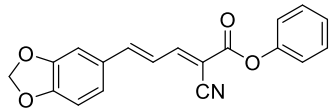
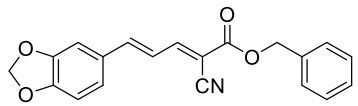
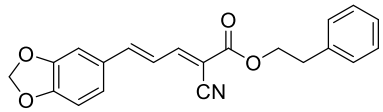
396. Andreasen MF, Landbo AK, Christensen LP, Hansen A, Meyer AS. Antioxidant effects of phenolic rye (*Secale cereale* L.) extracts, monomeric hydroxycinnamates, and ferulic acid dehydrodimers on human low-density lipoproteins. J Agric Food Chem. 2001; 49(8): 4090-6.
397. Menezes JC, Kamat SP, Cavaleiro JA, Gaspar A, Garrido J, Borges F. Synthesis and antioxidant activity of long chain alkyl hydroxycinnamates. Eur J Med Chem. 2011; 46(2): 773-7.
398. Li Y, Dai F, Jin XL, Ma MM, Wang YH, Ren XR, et al. An effective strategy to develop active cinnamic acid-directed antioxidants based on elongating the conjugated chains. Food Chem. 2014; 158: 41-7.
399. Schaich KM, Tian X, Xie J. Hurdles and pitfalls in measuring antioxidant efficacy: A critical evaluation of ABTS, DPPH, and ORAC assays. J Funct Foods. 2015; 14: 111-25.
400. Bhardwaj RK, Glaeser H, Becquemont L, Klotz U, Gupta SK, Fromm MF. Piperine, a major constituent of black pepper, inhibits human P-glycoprotein and CYP3A4. J Pharmacol Exp Ther. 2002; 302(2): 645-50.
401. Kong LD, Cheng CH, Tan RX. Inhibition of MAO A and B by some plant-derived alkaloids, phenols and anthraquinones. J Ethnopharmacol. 2004; 91(2-3): 351-5.
402. Backstrom R, Honkanen E, Pippuri A, Kairisalo P, Pystynen J, Heinola K, et al. Synthesis of some novel potent and selective catechol O-methyltransferase inhibitors. J Med Chem. 1989; 32(4): 841-6.
403. Abreu R, Falcão S, Calhelha RC, Ferreira ICFR, Queiroz MJRP, Vilas-Boas M. Insights in the antioxidant activity of diarylamines from the 2,3-dimethylbenzo[b]thiophene through the redox profile. J Electroanal Chem. 2009; 628(1-2): 43-7.
404. Rodriguez CE, Shinyashiki M, Froines J, Yu RC, Fukuto JM, Cho AK. An examination of quinone toxicity using the yeast *Saccharomyces cerevisiae* model system. Toxicology. 2004; 201(1-3): 185-96.
405. Siraki AG, Chan TS, O'Brien PJ. Application of quantitative structure-toxicity relationships for the comparison of the cytotoxicity of 14 *p*-benzoquinone congeners in primary cultured rat hepatocytes versus PC12 cells. Toxicol Sci. 2004; 81(1): 148-59.
406. Faassen F, Vogel G, Spanings H, Vromans H. Caco-2 permeability, P-glycoprotein transport ratios and brain penetration of heterocyclic drugs. Int J Pharm. 2003; 263(1-2): 113-22.
407. Silva R, Carmo H, Dinis-Oliveira R, Cordeiro-da-Silva A, Lima SC, Carvalho F, et al. *In vitro* study of P-glycoprotein induction as an antidotal pathway to prevent cytotoxicity in Caco-2 cells. Arch Toxicol. 2011; 85(4): 315-26.
408. Gameiro M, Silva R, Rocha-Pereira C, Carmo H, Carvalho F, Bastos ML, et al. Cellular Models and *In Vitro* Assays for the Screening of modulators of P-gp, MRP1 and BCRP. Molecules. 2017; 22(4): 1-48.
409. Müller T. ABCB1: is there a role in the drug treatment of Parkinson's disease? Expert Opin Drug Metab Toxicol. 2018; 14(2): 127-9.
410. Murphy MP. Understanding and preventing mitochondrial oxidative damage. Biochem Soc Trans. 2016; 44(5): 1219-26.
411. Teixeira J, Soares P, Benfeito S, Gaspar A, Garrido J, Murphy MP, et al. Rational discovery and development of a mitochondria-targeted antioxidant based on cinnamic acid scaffold. Free Radic Res. 2012; 46(5): 600-11.
412. Zhang H, Yu P, Ren JX, Li XB, Wang HL, Ding L, et al. Development of novel prediction model for drug-induced mitochondrial toxicity by using naïve Bayes classifier method. Food Chem Toxicol. 2017; 110: 122-9.
413. Will Y, Dykens J. Mitochondrial toxicity assessment in industry-a decade of technology development and insight. Expert Opin Drug Metab Toxicol. 2014; 10(8): 1061-7.
414. Kalyanaraman B, Cheng G, Hardy M, Ouari O, Lopez M, Joseph J, et al. A review of the basics of mitochondrial bioenergetics, metabolism, and related signaling pathways in cancer cells: Therapeutic targeting of tumor mitochondria with lipophilic cationic compounds. Redox Biol. 2018; 14: 316-27.

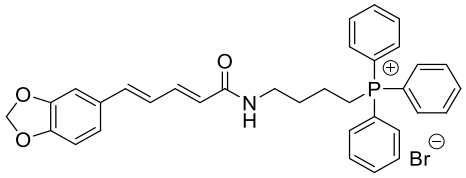
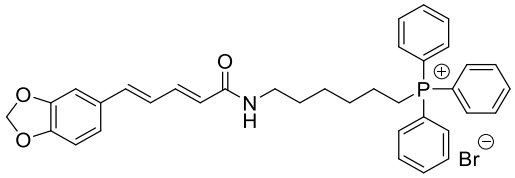
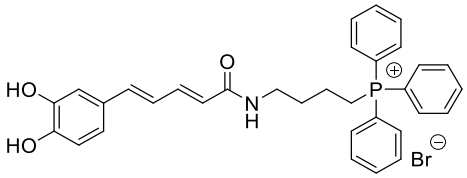
415. Desler C, Hansen TL, Frederiksen JB, Marcker ML, Singh KK, Juel Rasmussen L. Is there a link between mitochondrial reserve respiratory capacity and aging? J Aging Res. 2012: 192503.
416. Meanwell NA. Improving drug candidates by design: a focus on physicochemical properties as a means of improving compound disposition and safety. Chem Res Toxicol. 2011; 24(9): 1420-56.
417. Meanwell NA. Improving Drug Design: An Update on Recent Applications of Efficiency Metrics, Strategies for Replacing Problematic Elements, and Compounds in Nontraditional Drug Space. Chem Res Toxicol. 2016; 29(4): 564-616.
418. Di L, Kerns EH, Carter GT. Drug-like property concepts in pharmaceutical design. Curr Pharm Des. 2009; 15(19): 2184-94.
419. Valko K, Bevan C, Reynolds D. Chromatographic Hydrophobicity Index by Fast-Gradient RP-HPLC: A High-Throughput Alternative to log P/log D. Anal Chem. 1997; 69(11): 2022-9.
420. Tian S, Li Y, Wang J, Zhang J, Hou T. ADME evaluation in drug discovery. 9. Prediction of oral bioavailability in humans based on molecular properties and structural fingerprints. Mol Pharm. 2011; 8(3): 841-51.
421. Lagorce D, Douguet D, Miteva MA, Villoutreix BO. Computational analysis of calculated physicochemical and ADMET properties of protein-protein interaction inhibitors. Sci Rep. 2017; 7: 46277.

ANNEX

Thesis notation	Manuscript notation	Manuscript	Structure
1	**II**	**FA**	
	III	**FA (1)**	
2	**II**	**TFA**	
	III	**TFA (2)**	
3	**III**	**3**	
4	**III**	**4**	
5	**III**	**5**	
6	**III**	**6**	
7	**III**	**7**	
8	**III**	**8**	
9	**III**	**9**	
10	**III**	**10**	
11	**IV**	**CA (1)**	

12	**IV**	**2**	
13	**IV**	**3**	
14	**IV**	**4**	
15	**IV**	**5**	
16	**IV**	**6**	
17	**IV**	**7**	
18	**IV**	**8**	
19	**IV**	**9**	
20	**IV**	**10**	
21	**IV**	**11**	
22	**IV**	**12**	
	V	**1**	
	VI	**1**	
	VII	**1**	
23	**IV**	**13**	
	V	**2**	
	VI	**2**	
	VII	**12**	
24	**IV**	**14**	
	V	**3**	
	VI	**3**	

25	IV	15	
	V	4	
	VI	4	
26	IV	16	
	VI	5	
27	V	6	
	VI	6	
28	V	7	
	VI	7	
29	VI	8	
30	VI	9	
31	VI	10	
32	VI	11	
33	VI	12	
34	VI	13	
35	VI	14	
36	VI	15	
37	VI	16	

38	**VII**	**2**	
39	**VII**	**3**	
40	**VII**	**4**	
41	**VII**	**5**	